Cranfield University

ALEXANDER ELLERY

Systems design & control of a freeflying space robotic manipulator system (ATLAS) for in-orbit satellite servicing operations

College of Aeronautics

PhD Thesis

1996

Cranfield University (formerly Institute of Technology)
College of Aeronautics
Department of Aerospace Science

PhD Thesis*
(1996)

ALEXANDER ELLERY

Systems design & control of a freeflying space robotic manipulator system (ATLAS) for in-orbit satellite servicing operations

Supervisors: *Tom Bowling*
John Lewis

Date of submission: 2 August 1996

* "This thesis is submitted in fulfilment of the requirements for the Degree of Doctor of Philosophy (PhD)"

TABLE OF CONTENTS

LIST OF FIGURES

There are in addition mumerous illustrative sketches, tables and graphs embedded in the text

Nomenclature

A_i=4x4 Denavit-Hartenburg matrix

$\mathbf{a} = (a_x a_y a_z)^T$ =approach vector perpendicular to end effector palm (turn) for i=n

$F_{ext} = F_{eff} = (f_{ext} n_{ext})^T = (f_x^{ext} f_y^{ext} f_z^{ext} n_x^{ext} n_y^{ext} n_z^{ext})^T$ =generalised external cartesian forces with respect to end effector

F_{ci} =total force on link i centre of mass with respect to base coordinates

F_T =total forces acting at manipulator base $(x_0 y_0 z_0)$ with respect to base coordinates

F_0 =total force acting at manipulator base with respect to inertial coordinates

f_i =force on link i due to link i-1 at $(x_{i-1} y_{i-1} z_{i-1})$ to support outboard links

$I_i = R_i^0 I_{ci} R_0^i$ =inertia matrix of link i with respect to base coordinates

$I_{ci} = \mathrm{diag}(I_{ix} I_{iy} I_{iz})$ =inertia matrix of link i with respect to own principal link coordinates

J=nxn Jacobian matrix relating joint angle rates to end effector rates

$\dot{J}$=nxn time differential of Jacobian matrix

$l_i = r_i + s_i = (p_i - p_{i-1})$ =length of link i from $(x_{i-1} y_{i-1} z_{i-1})to(x_i y_i z_i)$ with respect to base coordinates

m_i=mass of body i

m_0=mass of satellite platform mounting

$m_T = \sum_{i=0}^{n+1} m_i$ = total mass of robot/spacecraft system

n=number of serial robotic links; n+1 indicates payload

$\mathbf{n} = (n_x n_y n_z)^T$ =normal vector perpendicular to end effector finger grip (tilt) for i=n

n_i =moment on link i due to due to link i-1 at $(x_{i-1} y_{i-1} z_{i-1})$ to support outboard links

N_{ci} =total moment about link i centre of mass with respect to base coordinates

N_r =total torque about centre of mass of spacecraft bus with respect to inertial coordinates

N_T =total moments on acting at manipulator base $(x_0 y_0 z_0)$ with respect to base coordinates

N_0 =total moments acting at manipulator base with respect to inertial coordinates

$\mathbf{p} = (p_x p_y p_z)^T$ =cartesian position vector of end effector with respect to base coordinates $(x_0 y_0 z_0)$

p_{ci} =location of centre of mass of link i with respect to base coordinates

p^* =position of end effector with respect to inertial coordinates $(x_* y_* z_*)$

p_{ci}^* =position of centre of mass of link i with respect to inertial coordinates

p_{cm}^* =location of centre of mass of total robot/spacecraft system with respect to inertial coordinates

q=generalised Cartesian position coordinates

$\dot{q} = (v w)^T$=generalised cartesian velocity of end effector with respect to base coordinates

$\ddot{q} = (\dot{v} \dot{w})^T$=generalised cartesian acceleration of end effector with respect to base coordinates

$R_i = (n_i s_i a_i) = 3x3$ direction cosine matrix

$r_i = (p_{i-1} - p_{ci})$ =position of link i centre of mass from $(x_{i-1} y_{i-1} z_{i-1})$ with respect to base coordinates

R_0 =attitude of spacecraft with respect to inertial coordinates

r_{c0} =position of spacecraft body centre of mass with respect to inertial coordinates

$r_{ci} = (p_{ci} - p_{ci+1})$ =distance between centres of mass of adjacent links with respect to base coordinates

$s = (s_x s_y s_z)^T = a \times n$ =slide vector parallel to end effector finger grip (twist) for i=n

$-s_i = (p_i - p_{ci})$ =position of link i centre of mass from $(x_i y_i z_i)$ with respect to base coordinates

s_0 =position vector of base of manipulator with respect to spacecraft body centre of mass

$v_i = \frac{dp_i}{dt}$ =linear velocity of joint i with respect to base coordinates

$\dot{v}_i = \frac{d^2 p_i}{dt^2}$ =linear acceleration of joint with respect to base coordinates

$v_{ci} = \frac{dp_{ci}}{dt}$ =linear velocity of link i centre of mass with respect to base coordinates

$\dot{v}_{ci} = \frac{d^2 p_{ci}}{dt^2}$ =linear acceleration of link i centre of mass with respect to base coordinates

v^* =linear velocity of end effector with respect to inertial coordinates

$\dot{v}^*$ =linear acceleration of end effector with respect to inertial coordinates

w_i =angular velocity of joint i with respect to base coordinates

$\dot{w}_i$ =angular acceleration of joint i with respect to base coordinates

z_{i-1} =rotational axis of joint i

$\theta = (\theta_1 \ldots \theta_n)^T$ =joint angle displacements

$\dot{\theta} = (\dot{\theta}_1 \ldots \dot{\theta}_n)^T$ =joint angle rates

$\ddot{\theta} = (\ddot{\theta}_1 \ldots \ddot{\theta}_n)^T$ =joint accelerations

$\tau = (\tau_1 \ldots \tau_n)^T$ =joint torques

ABSTRACT

This thesis is concerned with a freeflyer robotic spacecraft for in-orbit satellite servicing employing a dedicated attitude control system, ATLAS (Advanced TeLerobotic Actuation System). It adopts a unique control system design to alleviate the reaction coupling between the spacecraft mounting and the manipulator such that control of both the spacecraft attitude and manipulator kinematics may be effected in real-time using present-day space-rated electronics. It has been found that very few additional computations are required to compensate the coupling problem over standard terrestrial resolved motion robot control algorithms and standard spacecraft attitude control techniques. A mathematical proof of the concept is outlined. The technique is also extended for dual-arm operation. Two manipulator arms are necessary for EVA-equivalence to afford maximum flexibility. Mutual collision possibilities will be eliminated by incorporating a modified Zambesi bridge via interrupt software whereby each manipulator is restricted to operations within its own quadrant. This eases the computational burden of monitoring arm-to-arm collisions in the open chain mode with little loss of flexibility. Closed chain mode is shown to be similar to the open chain mode but with the addition of certain kinematic and force constraints. Each arm must be capable of operating independently or cooperatively, necessitating a hierarachical control architecture which is compatible with the NASREM control architecture. Given that the single arm freeflyer is the baseline of this thesis and that dual arm configurations are merely extensions of this, a simulation program of the techniques outlined has been constructed to output some of the parameters of interest. Consideration is also given to the possible commercial impact of such a system.

Chapter 1

INTRODUCTION

Space robotics applications can be justified at all levels of the space industry. Recently, space robotics has become a burgeoning field of study unifying the disciplines of astronautics and robotics mainly due to the focus provided by the International Space Station programme. In many respects, this is only proper. Quite apart from the historical coincidences of both disciplines' development, both can benefit each other in a uniquely symbiotic relationship. The year 1957 saw the launch of the world's first spacecraft, Sputnik 1 into Earth orbit, while 1961 saw the launch of the first industrial production robot Unimate by Unimation; 1969 saw both the first landing of men on the Moon marking the height of manned space exploration, and the development of the Stanford robot arm which evolved into the Unimate PUMA robot which became the workhorse standard of robotics. Notwithstanding these parallel developments, robotics provides a means to effectively explore and commercialise space, while the space environment provides a unique impetus and applications arena for pioneering robotics and automation research. Automated robotic spacecraft are not new, eg. the planetary rover explorers and probes. The first US planetary mission was the Mariner Venus flyby in 1962 and the USSR sent 23 robotic missions to the inner planets from 1965 to 1984. Lunokhod 1 and 2 (1970 and 1973) were teleoperated lunar rover vehicles controlled from Earth by 4-5 man teams. Voyager 2 provided the spectacular Grand Tour of the outer solar system: Jupiter (1979), Saturn (1981), Uranus (1986) and Neptune (1981).The seven missions of the US lunar Surveyor series between 1966 and 1968 was essential for the success of the Apollo 11 lunar landing. The two Viking landers on Mars (1975) were the first space missions to utilise articulated remote manipulators to dig Martian soil up to 2.5m from the landers.

The commercial motive for robotic spacecraft and their future central role in space activities is comparatively new, particularly for general Earth orbit operations which are presently dominated by manned missions. There is little dispute that manned spaceflight affords a flexibility of space operations that are unattainable in unmanned missions. However a robotic capability would enable some of this flexibility to be retained in unmanned missions without human endurance limitations of bone decalcification and muscle atrophy. This is not to say that such robotic capabilities could replace men in space - the issue is one of complementation. For example, the SARSAT system could be extended to encompass a space-based distress system such as astronaut rescue in utilising a robotic freeflyer as the executive component to overcome the tight Space Shuttle rescue launch windows that would be involved in any such rescue mission. There is little doubt that robotic and automated systems in space will contribute considerably to the future commercialisation of the space environment. Indeed, it may be considered that the true commercial utilisation of space relies on two major capabilities: advances in inexpensive re-usable space transportation from Earth to reduce launch costs presently ~$10,000/kg, and the development of remote complex manipulation for in-orbit activities. The time is indeed ripe for the introduction of remote manipulation technology into space. Spacecraft are now being designed to be serviceable in-orbit. Advances in CCD sensor technology motivated by remote earth observation satellite and astronomical satellite applications may be utilised for advanced robotic vision. The presently available communications infrastructure, eg.

EDRS/TDRSS (European Data Relay System/Telemetry & Data Relay Satellite System), may be flexibly exploited by robotic spacecraft in Earth orbit. The next stage in the evolution of space infrastructure lies in the development of a permanent human presence in space together with robotic manipulators which will be essential both for in-orbit truss assembly and construction and for servicing tasks. Furthermore, any future proposed attempt to return to the Moon or any other of the planets will rely extensively on unmanned robotic precursor missions.

In 1985, the NASA Advanced Technology Advisory Committee made recommendations to the US Congress Committee on Science & Technology to develop a permanently manned Space Station and highlighted the critical role to be played by robotics and automation. The reasoning behind their report and the emphasis on robotics and automation was that such capabilities would considerably reduce the cost of future space programmes by providing the basis for the development of a spaceflight infrastructure. The development of a robotics and automation capability was seen as critical for all areas of space exploration, global information technology, space utilisation and space industrialisation. It was consequently expected that robotics and automation would play a central role in the Space Station Freedom programme as a small step towards the expansion of a highly underdeveloped technology applications area ripe for exploitation. Greater autonomy would increase flexibility of space operations and so increase responsiveness to innovation and reduce human exposure to hazard, reduce reliance on ground support and so reduce operational costs and extend the capabilities of unmanned missions, and improved reliability and improved productivity would increase the probability of mission success and mission efficiency. The report recommended that the robotics and automation development budget should comprise no less than 10% of the total Space Station cost. Futhermore, the robotics and automation programme would benefit US technology in general, and consequently the US economy. The following recommendations were made [Cohen & Erickson 1985]:

1. Automation & Robotics should be a significant element of the Space Station programme.
2. The initial Space Station should be designed to accomodate the evolution and growth in Automation & Robotics technology.
3. The initial Space Station should utilise significant elements of Automation & Robotics technology.
4. The criteria for the incorporation of Automation & Robotics technology should be developed and promulgated.
5. Verification of the performances of automated equipment should be stressed, including terrestrial and space demonstrations to validate technology for Space Station use.
6. Maximum use should be made of technology developed for industry and the Government.
7. Automation & Robotics techniques should be used to enhance NASA's management capability.
8. NASA should provide measures and assessments to verify the inclusion of Automation & Robotics in the Space Station.
9. The initial Space Station should utilise as much Automation & Robotics technology as time and resources permit.

10. An evolutionary Space Station would achieve in stages a very high level of advanced automation.
11. An aggressive programme of long range technology advancement should be pursued, recognising areas in which NASA must lead, provide leverage for, or exploit developments.
12. A vigorous programme of technology transfer to US industries and R&D communities should be pursued.
13. Satellites and their payloads accessible from the Space Station should be designed as to be serviced and repaired by robots.

The introduction of robotics to the space environment was seen as a means to increase productivity in space for both commerce and research and, through technology transfer to earth-based industries thereby increasing productivity on Earth. The ability to deploy, construct, inspect, repair and retrieve space systems may be considered to be a primary requisite for future expansion into the space environment. To this end, NASA had devoted ~$25M/y for the development of automation & robotics technology for space missions. It has been estimated that NASA could save $5B/y by 2000AD if such research was pursued with vigour [Freitas & Gilbreath 1980]. Specifically, NASA began work on two specific proposals to support the Space Station Freedom programme: the Orbital Maneovering Vehicle (OMV) and the Flight Telerobotic Servicer (FTS). The OMV was an off-the-shelf spacecraft bus module designed for docking operations for bolt-on payloads particularly robot manipulators: it had dimensions of 94cm thickness and 4.52m diameter, ie. disk shaped for maneouverability, with a mass of 4761kg of which 3039kg was N_2O_4/MMH propellant. FTS was a dedicated freeflyer robotic spacecraft with two seven degree of freedom manipulator arms and a third simpler arm designed for spacecraft retrieval in low Earth orbit (LEO). The spacecraft bus was hexagonal in shape with two cameras for stereoscopic imaging. Although both programmes have since been cancelled due to budgetary constraints, research into Robotics & Automation is still a priority for NASA [Weisbin & Montemerlo 1992]. Indeed, NASA's new Ranger project presently under development is a dual arm freeflying telerobotics flight experiment for in-orbit validation of robotic technologies relating to satellite servicing to be operated in conjunction with an underwater unit in a ground based neutral bouyancy environment.

1.1 ROBOTIC SYSTEMS FOR SPACE APPLICATION:

Space robotics applications may be divided into three categories: extravehicular servicers (freeflyers), intravehicular science payload servicers and planetary surface rovers [Lavery 1994]. Much of the US and elsewhere have used the International Space Station Freedom programme as a focus for their robotics and automation research particularly concerning in-orbit servicing repair and assembly. It is likely that the Space Station despite its problems will be forthcoming in some form or other and it will require robotic capabilities.

The US Space Shuttle Remote Manipulator System (RMS) which first flew in November 1981 has had 22+ missions to its credit including the capture of the Solar Maximum satellite, the recovery of LDEF (Long Duration Exposure Facility) and Eureca (EUopean REtrievable CArrier), and the capture of Intelsat VI. It was designed by the Canadian Space Agency with Spar Aerospace as the prime contractor and is at present the only operational space manipulator. It has been designed as fail-safe with

redundant systems and built-in test circuitry such that crew safety would not be jeopardised [Hedley 1986]. Closed circuit TV cameras with pan, tilt and zoom capabilities and light assemblies are mounted at the elbow and at the end effector. Its mass is 480kg with a reach of 15m, and a payload capacity in excess of 30 tonnes. It is constructed from graphite carbon composite booms with Ti and Al alloy joints for high stiffness. Boom stiffness ~10^9 kg/cm^2. Although it has over 15,000 parts it is designed for a lifetime of 100 shuttle missions without maintenance, ie. 10y. It is capable of ~5cm and 1^o position/orientation accuracy with an unloaded tip velocity of 0.6m/s and a maximum end effector torque of 300Nm. It is however based on 1970's technology and is capable only of simple positioning and retrieval tasks ("fly-swatting"). However, it has demonstrated the potential of robot manipulation in space. The US/Canada have concentrated their research effort for the Space Station on their Mobile Servicing System (MMS) designed by the Canadian Space Agency with Spar Aerospace as the prime contractor. The Canadian robotics contribution amounts to ~$1.3B. The MMS provides the basis for the Space Station Remote Manipulator System (SSRMS) for handling large payloads including the US Space Shuttle for berthing and deberthing. It is based on the Shuttle RMS but is three times stronger. The smaller Special Purpose Dextrous Manipulator (SPDM) serves as a "bolt-on" front end for more intricate EVA-type operations such as ORU (Orbital Replacement Unit)-changeout. The SSRMS has 7 degrees-of-freedom with a reach of 15m (same as the Shuttle RMS) and a positioning accuracy of 0.5m. Its mass is 1.7 tonnes and has a payload capacity of ~160 tonnes and operates on guide rails for additional mobility. It has end effectors at both ends to enable it to move around hand-over-hand along any truss structure. The SPDM has a mass of ~1.2 tonnes with an average operational power requirement of 1.4kW. It comprises a body with two 7 degree-of-freedom dextrous arms. The body can be attached to the SSRMS end effector and all joints are offset for maximum dexterity. Cameras with lights are mounted on each forearm boom and within each end effector. It has a reach of 2m and a tip positioning accuracy of 0.024m and 1^o and maximum velocities of 0.075m/s and 2.5^o/s. A mobile remote servicer base system provides a portable work platform with EVA support equipment, ORU pallets, propulsion module attachment system, tool carrier, cameras and lights. It also provides power and data links to the mounted system. It has a mass of ~2 tonnes and an average power requirement of 740W. Both manipulators are designed to be ORU compatible. Both large manipulator and small dual-manipulator can be mounted onto this base.

The Japanese experimental module (JEM) of the Space Station is also to have its own dedicated manipulators with 6 degrees of freedom. A single main arm of 9.7m length, 370kg mass with a payload capacity of 7 tonnes and maximum speed of 0.05m/s would be used for large payloads. A smaller arm of 1.6m length, 120kg mass, with a payload capacity of 300kg and maximum tip speed of 0.1m/s will be used for smaller payloads. Indeed, in support of their space robotics programme, Japan's NASDA (National Space Development Agency) have been designing and constructing their Experimental Test Satellite, ETS-VII to be launched in 1997 into a 550 km orbit at 35^o inclination to test a manipulator in space teleoperated from the ground to demonstrate automated rendezvous and docking tasks such as fuel transfer, battery exchange and grappling of objects. The ETS-VII manipulator is a 6 degree-of-freedom design of mass ~80kg mounted onto the ~2 tonne satellite platform and powered by large symmetric solar arrays.

ESA are also committed to robotics in the space environment and this may be regarded as a major component in Europe's thrusting research into information technology such as ESPRIT. ESA has a number of space robotic programmes with the International Space Station Freedom providing the focus. The European contribution will to be the Columbus Attached Module. Many studies have been done: the BIAS (Bi-Arm Servicer) was conceived as a smart front end to a larger manipulator for fine manipulation tasks; MTSU (Man-Tended Servicing Unit) was a manned small pressurised maneouvering vehicle equipped with manipulator arms to be teleoperated from inside the chamber (now cancelled), IRAS (Interactive Remote Automation & Robotic Servicing) system for investigation into task-oriented telerobotics; EMATS (Experiment Manipulation And Transportation System) comprised two 6 degree-of-freedom robot arms mounted onto a 2 degree-of-freedom mobile gantry carriage to provide the IVA system for servicing and experimentation within the Columbus Attached Laboratory; ERA (European Robotic Arm) is a 10m long 7 degree-of-freedom manipulator with end effectors at both ends to enable it to walk along truss structures using the two end effectors as legs - it evolved from HERA (HErmes Robot Arm) after the cancellation of the Hermes spaceplane and now has a role in external servicing the Columbus laboratory of the European space station module, as well as for general equipment exchange, outer surface inspection and to provide support for EVA astronauts. ROTEX (space RObot Technology EXperiment) was the most extensive robotic experiment in space by ESA [Hirzinger 1987, 1993]. It flew on the Spacelab D2 mission in 1993 as one of the rack experiments to provide basic knowledge on microgravity robotics. ESA's Spacelab is a manned laboratory that flies in the US space Shuttle payload bay. It has been used extensively to perform microgravity experiments of various kinds including materials and life science. For ROTEX, a 20kHz AC power supply connected all sensors and actuator systems. In addition, D2 experiments included telescience nodes for microgravity investigations of single crystal growth of various semiconductor materials using zone melting techniques. The ROTEX comprised a 6 degree-of-freedom multisensory gripper with 15 sensory components sealed inside a working cell of an experiment rack. With 400 mechanical components, it represented one of the most complex robot grippers ever built. The sensory suite included a lockable force-torque sensor, 9 triangulation-based laser range finders for 0-50cm ranges, a 32-element conductive rubber tactile array in each finger, a pair of CCD cameras for stereo images mounted into the gripper. The design philosophy was fundamentally based on using minimally sized modularly exchangeable sensors with the integration of the electronics into the sensors. ROTEX could carry its own mass ~10kg as payload compared with most industrial manipulators which are restricted to ~20:1 robot mass-to-payload mass ratio. One of the tasks performed successfully by the manipulator was an ORU-exchange type operation with bayonet connectors as well as grasping a free-floating object. These operations were performed by both astronauts and from the ground in teleoperative modes and automated modes. Fast switching between different operational modes was demonstrated to be a powerful tool for remote manipulation. Finally, de Peuter (1993) proposed a dedicated robotic satellite system for operation in GEO (geostationary equatorial orbit) as a service for comsats. Such a system would provide commercial services such as satellite inspection, mechanical assistance to faulty deployment mechanisms and re-orbiting satellites into graveyard orbits at EOL (end of life). The fuel penalty of a GEO satellite to boost into a graveyard orbit is equivalent to 6 months further operational life. With the GSV (Geosynchronous Servicing Vehicle) operating, no such fuel penalty is necessary. This

would provide the "bread-and-butter" revenue for the GSV for its 15y lifetime. During such a lifetime, it was envisaged that there was a potential market for 25 re-orbiting missions, 10 inspections, 3 mechanical interventions and 2 dead satellite removals. The GSV would have a mass of 4.2 tonnes (dry mass 1.2 tonnes) giving a delta-v of 3.7km/s. It would be operated from a dedicated portable ground station colocated with the customer's main ground station via a low gain S-band antenna with wide lobes to maintain communications links even in the event of obstruction.

Even with the replacement of the original Space Station Freedom with the Alpha-Mir Space Station, robotic systems will continue to have a vital role to play in the space environment, and indeed such systems may be adapted comparatively straight-forwardly to other projects if required (eg. the Hermes Robotic Arm HERA became the External Robotic Arm ERA for the European Columbus module of the Space Station). The cancellation of FTS in the early stages of the Space Station programme was an indication of short-sightedness on the behalf of NASA when under budgetary pressure, since its role was seen as in support of Space Station Freedom alone, rather than as a generic capability in space. The Alpha-Mir space station is expected to be launched in 1997 to become fully operational in 2002 with a permanent crew of 6. It is currently envisaged to comprise of 7 laboratory modules, two crew compartments and two supply modules to give an enclosed pressurised volume of 11,311m^3 in a mass of 420 tonnes. Included will be ESA's Columbus module. Around $12.2B had been spent in 1995 on the original Freedom and it has been estimated that Alpha will cost a further $15.3B to complete in 2002.

Although much of space robotic activities have centred around Space Station Freedom/Alpha-Mir, space robotic systems are also consistent with the UK's rejection of manned spaceflight yet it achieves some of the capabilities peculiar to manned spaceflight.

1.2. LITERATURE REVIEW:

The tools of both robotic and spacecraft dynamics have an unparalled pedigree. Indeed their development reflects the history of science and the scientific method itself. The fundamental science of mechanics was developed by those great minds who in the process gave birth to modern science as natural philosophy: Galileo Galilei (1564-1642), Johann Kepler (1571-1630), Isaac Newton (1642-1729), Gottfried Leibnitz (1646-1716), Leonhard Euler (1707-1783), Jean D'Alembert (1717-1783), Joseph Lagrange (1736-1813), Pierre Laplace (1749-1827) and William Hamilton (1805-1865) - all made fundamental contributions that laid the foundations of mechanics and established a unique relationship between empirical science as a universal description of the world and mathematics as the language of science.

Space robotics may be regarded as a specialised application of mechanics. Space introduces a complicating factor to robotic systems that is not apparent on Earth - the manipulator base is not fixed in space and so reference coordinates are no longer fixed with respect to the spacecraft. This introduces a high degree of dynamic complexity. This effect will be significant as it has been suggested that the mass of a space manipulator payload may comprise up to 1/3 the mass of the spacecraft bus mounting [Vafa & Dubowsky 1990]. The motion of the manipulator will generate reaction forces and moments on the interceptor platform at the spacecraft mounting/manipulator

coupling point. This will induce translational and rotational motion of the satellite platform in response to the manipulator movements. If no compensation is made for the motion of the interceptor mount, the robot end effector will not attain its target since the coupling has a significant effect on the manipulator kinematics, dynamics and control. Feedforward thruster control may be utilised to compensate for the motion of the mount, but this introduces undesirable and prohibitively excessive expenditure of fuel as well as generating exhaust plumes which may be detrimental to sensor operation. In addition, they are difficult to control proportionally since they operate in pulse mode.

Most solutions to the moving platform problem discussed in the literature involve a considerable computational burden for the control of such systems in space. A 6 degree-of-freedom robot mounted onto a 6 degree-of-freedom platform generates a 12 degree-of-freedom system controlled by only 6 joints inputs. The system is redundant since both vehicle and manipulator have more controllable states than are necessary to specify the motion of the end effector. They do not generate closed form solutions for position/orientation due to their inherent redundancy. Longman (1988) considered this form of "kinetic" position control of a satellite with a 3 degree-of-freedom manipulator model and found that an infinite number of solutions exist to the inverse kinematics due to this redundancy. The solutions are a function of the history of manipulator motion rather than joint angle configuration alone. Solutions can be obtained but usually involve the introduction of selective cyclic "coning" motions superimposed on the desired manipulator trajectory to maintain constant spacecraft attitude without employing dedicated attitude control actuators [Vafa & Dubowsky 1990]. This "coning" motion is equivalent to using spinning wheels within the spacecraft. The coning motions may also introduce possible collision hazards with target satellite appendages which would require complex path planning to avoid. Overcoming this by using small cyclic motions to eliminate non-negligible nonlinear terms introduces the requirement for many cycles for even small changes in spacecraft attitude. Vafa (1990) used a Virtual Manipulator approach to derive the conservation of angular momentum in relative joint coordinates. Only the end effector trajectory was controlled whilst the satellite attitude was allowed to be arbitrary. Clearly this is not desirable since the spacecraft bus will have components and subsystems that have their own specific pointing requirements. Another formulation is to find the generalised Jacobian matrix J* by applying applied momentum constraints to a complete free-floating spacecraft/manipulator to account for platform translation and rotation by relating end effector velocities to joint and platform velocities [Umetani & Yoshida 1989, Papadopoulos & Dubowsky 1991]. Such free-floating systems are defined by their lack of a dedicated spacecraft attitude control system. The generalised Jacobian due its dynamic nature is complex to compute with a complexity of $O(n^2)$ and so not conducive to real-time operation [Masutani, Mujazaki & Arimoto 1989]. Xu (1993) introduced a dynamic coupling coefficient to quantify the relation between the end effector velocity (subscript "eff") and base velocity (subscript "o"):

$$\begin{pmatrix} v_0 \\ w_0 \end{pmatrix} = P \begin{pmatrix} v_{eff} \\ w_{eff} \end{pmatrix}.$$

This dynamic factor P is similar to the generalised Jacobian and may be reduced to a single value $w = \det(P^T P)$ to quantify the coupling effect. Evidently attitude control would reduce this coupling effect by making $w_0=0$. However this was only an

analytical factor to characterise the coupling rather than having any application for control purposes. Masutani, Mujazaki & Arimoto (1989) found that the generalised Jacobian is comprised of the conventional Jacobian of computational complexity of O(n) with additional terms dependent on the masses, inertias and geometric structures of each link which generate the additional complexity. The conventional Jacobian could be used to derive a transposed Jacobian which yielded satisfactory results when the platform-manipulator mass ratios were in excess of ~5. This however, limits the applicability of the formulation where it is conceivable that freeflyer robotic systems will have mass ratios <1.

Hence, these solutions are less than ideal since the computational power of space-rated microprocessors is a limited and valuable resource and the requirement for real-time operation is strict. Space system computer technology lags terrestrial computer technology by ~10-15y. Present day space rated processors are of the 8086 variety while terrestrial technology has the Pentium processor commercially available. Surprisingly, although the motivation for this time lag is reliability (as evidenced by a proven track record of Earth operation), this can and does often lead to reduced performance, increased design costs and delayed launches. Spacecraft now tend to be designed with subsystem-dedicated computers interconnected across a vehicle wide databus. As well as providing a degree of functional redundancy this suggests that a piecewise approach to the problem is more suitable for a distributed computer system implementation. Finally and most importantly, it has been found that freefloating systems are subject to unpredictable dynamic singularities in their manipulator workspaces due to the attitude motion of the platform at which point they become unstable [Papadopoulos & Dubowsky 1989]. Indeed dynamic singularities are characteristic of freefloating systems and are functions of the mass and inertia of the composite spacecraft/manipulator system. These singular joint configurations cannot be mapped into unique points in the workspace since the generalised Jacobian is a dynamic function rather than being kinematic, and spacecraft attitude coordinates do not map uniquely to end effector coordinates. Hence, these singularities cannot be predicted from the kinematic configuration alone since they are functions of the history of the end effector path also, ie. points in a workspace may become singular depending on the path taken to reach it. Any control system which uses inverse generalised Jacobian techniques for freefloating systems will encounter such singularities within the workspace. Although the bidirectional approach attempts to alleviate the problem of freefloating systems, this method is computationally intensive since the scheme relegates the problem to the path planning algorithms higher up the control heirarchy by using the extra degrees of freedom for path planning [Nakaruma & Mukherjee 1989]. They used a bidirectional search to map between the original state and final desired configuration using the generalised Jacobian to avoid excessive joint torques, for obstacle avoidance or for re-orientation of attitude. Nenchev, Umetani & Yoshida (1992) used a Moore-Penrose pseudo-inverse version of the generalised Jacobian $(J^*)^+$ to overcome the dynamic singularities problem by using the redundant degrees of freedom. It allowed change of spacecraft attitude whilst keeping the position/orientation of the end effector fixed with respect to the inertial reference frame to provide greater flexibility of operation.

Joint angular velocity, $\dot{\theta} = (J^*)^+ \dot{q}$ where $\dot{q}$ = generalised cartesian velocity

However, this formulation is even more complex than the generalised Jacobian technique. Dubowksy, Vance & Torres (1990) noted that excessive spacecraft motions may occur which cannot be accounted for in path planning and so adapted standard robotic minimum-time optimal trajectory generation to limit joint torques and attitude rates to within specified bounds. Control schemes have been devised which switch between different coordinated modes of control. This involves control of the platform/manipulator being switched from the freefloating formulation to a redundancy formulation for the control of the platform alone whenever dynamic singularites are encountered [Papadopoluos & Dubowsky 1991, Spofford & Akin 1988]. However, switching is characteristic of variable structure control schemes and these tend to suffer from "chattering" induced by the switching. This is clearly undesirable for a space-borne manipulator which operates in an undamped medium. In conclusion then, freefloating systems are subject to certain constraints not encountered in terrestrial robotics (Papadopoulos & Dubowsky 1990):
(a) spacecraft orientation is required to derive the generalised Jacobian;
(b) dynamic properties affect the kinematics;
(c) dynamic singularities occur in the workspace;
(d) nonholonomic redundancy imply path dependency of joint angle configuration.
All such schemes which leave spacecraft attitude uncontrolled cannot cope with the input dynamics of target acquisition in real-time using present-day and near-future space-rated computational hardware.

Longman, Lindberg & Zedd (1987) and Lindberg, Longman & Zedd (1986) applied classical dynamics techniques to the Remote Manipulator Servicer mounted onto the Space Shuttle. They used two models of the manipulator: one with a prismatic elbow joint and one with a revolute elbow joint. These two papers marked the first detailed analysis of the space robot problem. They decoupled the translation and rotation components of the combined RMS/Shuttle system. They calculated the total reaction moment on the Space Shuttle due to the motion of the RMS using the Newton-Euler method referenced to inertial coordinates. This provided the basis for a feedforward compensation component to be input to the Shuttle's dedicated attitude control system (comprising orthogonal reaction wheels) to compensate for the torques applied to the Shuttle at the base of the arm. Further, they reformulated the position kinematics to include dynamic variables by the application of equilibrium constraints derived fom the definition of the system centre of mass. They found that for the Shuttle/RMS system, reaction wheels were insufficient to effect reaction moment compensation of 34Nms, suggesting that CMG's might be within the required performance bounds. It is important to note that these formulations were manipulator geometry specific rather than generalised. It was not evident how the scheme may be applicable beyond the manipulator geometries chosen. Walker & Wee (1991a,b) analysed a single arm 15 degree-of-freedom space robot system with orthogonal reaction wheels and found that such a system comprises a 9 degree-of-freedom invertible portion including manipulator joint angles and base orientation and a 6 degree-of-freedom component including the base position and reaction wheel positions. The reaction wheel dynamics were incorporated to eliminate reaction wheel position, and base translation was eliminated by application of the conservation of linear momentum. Once again, it was quite complex in its approach by globalising the dynamics and control of the whole system.

Some workers have considered two arm systems since these offer more realistic models of future robotic systems. Yoshida et al (1991) extended their generalised Jacobian approach to consider dual arm coordination whilst mounted onto a space platform. Their generalised Jacobian was a composite 18x18 element matrix even larger than the original 6x6 generalised Jacobian required for a single arm.. To provide coordinated control they suggested that whilst one arm was used for task operations, the other arm should be moved in compensatory mode to keep the satellite attitude stable and minimise the total torques applied to the spacecraft mount. Quite apart from the excessive computational overhead of the 18x18 Jacobian, the use of a manipulator as a stabiliser is wasteful of costly hardware since it effectively reduces (operationally-speaking) the dual arm system to a single arm system as well as imposing possible collision problems. The appropriateness of two arms derives from its operational capabilities rather than any other factor. Murphy, Wen & Saridis (1991) also considered a two-armed robot mounted onto a satellite platform. They derived a set of closed form Newton-Euler equations for both manipulators. Once again, their formulation involved an 18x18 Jacobian transpose matrix precluding the formulation from real-time operation.

In conclusion, it appears that once the generalised Jacobian method had been developed, many workers in this field built on it to develop ever more fanciful control algorithms without considering the realities of the situation regarding limited computational resources in space and the inherent disadvantages of the generalised Jacobian. Although many of these techniques are elegant and yield interesting and useful insights to the problem, they are not implementable on available space-rated hardware.

1.3. IN-ORBIT OPERATIONS:

This thesis is concerned with one application of robotics which is in fact highly general in the form of a telerobotic interceptor spacecraft dedicated to in-orbit servicing, inspection, repair and maintenance of operational satellites in Earth orbit, be they Earth observation, telecommunications, global navigation, scientific or meteorological satellites. A freeflying telerobotic spacecraft is a natural evolution from astronaut EVA (extravehicular activity) and the Shuttle-attached manipulator. In EVA the astronaut acts directly as the manual worker for small activities while the Shuttle RMS operates for heavier duties with the Shuttle providing a stable platform (due to its high mass - the reaction control system is switched off when the RMS is deployed). A freeflying teleoperated system can be remotely controlled from the ground to provide great flexibility. It would provide a natural testbed for general automated facilities in space for construction, processing and experimentation. The manipulator system represents the spacecraft payload mounted onto the spacecraft bus platform. The robotic interceptor is likely to become the workhorse for such activities in space in the future. Such a capability has considerable immediate commercial application by opening up hitherto underutilised markets. Indeed, the US Civil Space Policy of 1978 stated categorically that increased participation for private enterprises should be stimulated. There is little doubt that certain space activities have generated commercial successes: Intelsat/Inmarsat (telecommunications), BSkyB (television), Spot Image (remote sensing), Arianespace (launchers). Robotic in-orbit servicing will be no exception. Spacecraft system redundancy is no longer sufficient to ensure reliability in spacecraft due to cost constraints. Redundancy imposes launch mass penalties and trade-off

studies for individual systems indicate that there is a limit to which redundancy is cost-effective at which point maintainability should be implemented. Particularly for long-life Earth-oriented missions, in-orbit exchange of parts is a necessary precursor to success. No small number of cases have been documented whereby satellites have failed to function properly in orbit - between 1962 and 1983, there have been ~2500 spacecraft failures of one kind or another. The majority of failures occur within the first few weeks or months of operational service due to infant mortality, and in the latter years of operational service due to propellant or battery lifetime limitations.

There are exceptions however: the European EXOSAT launched in 1983 malfunctioned in 1986 with a permanent loss of attitude control. EXOSAT had been designed with a degree of onboard reprogramming flexibility. The AOCS (attitude & orbit control system) sensor processing and control algorithms were implemented in a 16k microprocessor. Software was parametrised such that the code was contained in ROM with parameter values in RAM. This allowed the updating of parameters. Some of the 40k applications software which were not in constant use was stored in a ground library which could be uploaded as required into the spaceborne computer for operational execution allowing newly developed programs to be uploaded if required. Regardless of this operational flexibility, EXOSAT was plagued with problems concerning its AOCS. The drift bias circuitry of the gyros which was used to compensate for the inherent gyro drift regularly experienced jumps during passage through the Van Allan radiation belts due to electrostatic discharge of accumulated charge. Unfortunately during radiation belt passage the star tracker was closed down and so was unable to provide closed loop control. An onboard program was developed and uploaded to reset the drift bias levels when jumping occurred. The hardwired safety mode circuits of the AOCS was also problematic. One of the two redundant safety modes started to trigger spuriously during perigee and was disabled from the ground. This was followed by one of the 4 gyros intermittently registering failure incorrectly and was automatically deselected by the remaining safety mode. Unfortunately later a second gyro actually failed catastrophically and was switched out automatically by the failure mode leaving only two gyros operational. The only way to reactivate the incorrectly diagnosed failed gyro was to disable the remaining safety mode circuit and replace it in software. This was used successfully for the rest of the mission. Another AOCS problem was a spurious thruster-on condition which resulted in the automatic activation of the opposing thruster to counteract the rotation. However due to a thruster imbalance the satellite spun up until the threshold rate should have triggered one of the safety mode circuits. This would have resulted in automatic switching to a redundant propulsion system but with the disabling of both hardwired safety mode circuits this did not occur. A means was developed exploiting the sensors used to detect pressure changes in the propellant tanks to detect the thruster-on condition and so invoke automatic switching to the redundant propulsion system but not until after much fuel loss. These events show the flexibility of augmenting ROM based systems with RAM which can replace ROM processes if necessary through applications software uploaded into RAM.

Some faults may be corrected in this way either fully or partially from the ground by uploading such software changes (workarounds), but hardware faults cannot be corrected except by re-routing often leading to suboptimal operation and degraded performance. Some faults can be corrected through software: OAO-A2 lost its star

tracker due to debris spoofing it; OAO-C lost attitude control causing excess momentum build up and excess spin rates; ATS-6 lost its star sensor due to debris spoofing and lost a momentum wheel actuator; NOAA-6 set about tumbling after hydrazine venting. In all these failures, software corrections allowed re-establishment of the spacecraft mission. Attitude control failure corrections were possible due to the existence of redundant thrusters. Such workarounds and reconfiguring require extensive ground support with dynamic simulations for software update validation. Validated software is the uploaded to the spacecraft via the communications link (assuming that it hasn't been compromised). Although these software corrections often work quite well, they are not inexpensive solutions to the problems. The Hipparcus satellite was launched into the wrong orbit due to a fault in the apogee kick motor requiring extensive changes to the mission. Galileo which was launched to Jupiter in 1990 has a high gain antenna which failed to deploy fully and the science mission return has consequently degraded by 30%. Some workarounds have been quite spectacular: Olympus, an ESA experimental telecommunications satellite of 2.6 tonnes was launched in 1989 to test EDRS technologies. In 1991 it went out of control and its fuel froze but the ground team was able to retrieve it and put it back into operation. However, workarounds can correct only ~17% of all failures. Loss of attitude sensing or control appears to be a ubiquitous problem. For a satellite operating a valuable service or function, this may be unacceptable (particularly for military satellites). Military reconnaissance satellites are critical for political stability in the modern volatile world that has emerged since the cessation of the Cold War. They are the only means by which reliable control of disarmament and military activities may be monitored throughout the world. Their extensive use in the Gulf War is a testament to their absolute importance. Most failures occur due to environmental conditions, excess load beyond design tolerance or through random failures. Design failures account for ~25% of all faults, environmental failures for ~21%, random failures for ~30%, software failures for ~5% while ~19% of all failures result from unknown origin. A dedicated robotic interceptor satellite for in-orbit servicing would alleviate these eventualities through maintenance and servicing and effectively increase the overall reliability of all accessible space systems as part of a post-commissioning service package to the customer.

The cost of space hardware has grown to the extent that spacecraft are being designed in modular fashion to be serviceable in-orbit despite the mass penalties. Orbital replacement units (ORU) are such modules which serve as containment packages for equipment which may be replaced. For low levels of repair at component level, a high number of interfaces need to be broken and rejoined implying long time periods to perform as well as simulate prior to operation. On the other hand, higher standardisation of replaceable modules at subsystem level implies that higher masses have to be transported to the worksite for replacement. However, standardisation minimises the number and variety of tools that are required to be transported to orbit, minimisation of training and simulation requirements for different scenarios and minimisation of task execution. Availability of spare standard modules reduces unplanned down-time. Finally, modularity substantially reduces costs during integration and test phases prior to launch. If standardisation can be made at a sufficiently low level such as for common PCB's and electronics boxes (eg. power supplies and conditioning) further advantages are gained. However, at no point should standardisation resolve down to component level as this impairs flexibility of design

and probably escalates costs in the long run. Hence, although interface standardisation is at the modular level, it would be desirable to extend it to electronics box level. Such ORU's, since they are usually of low mass (~50-500 kg) can be carried as piggyback payloads at low cost on scheduled launches. Reliability and maintainability are related concepts - system operational availability (a measure of system performance) and cost are both cubic functions of reliability and maintainability such that they initially increase very rapidly before tailing off due to the decreasing return on investment [Sepehri 1987]. It is desirable to increase operational availability within cost restraints. This requires a mixed approach since:

Availability, A=(MTBF/(MTBF+MTTR+MTFS)

where MTBF=mean time between failures and reflects reliability

MTTR=mean time to repair and reflects maintainability

MTFS=mean time for supply and reflects logistic capability

The optimal cost is attained when an incremental change in reliability equates to an incremental change in maintainability for a given total investment. At present, MTFS is very large since it is subject to long delays due to long launch preparation times, advanced launch bookings, astronaut training, launch delays, turnaround times, etc. The HST had to wait three-and-a-half years after its launch before it was repaired. Only a dedicated in-orbit robotic system can reduce this parameter. Furthermore, since one of the purposes of robotics is to remove the human from the hostile environment, the system itself must have a high availablity and be capable of self-repair and self-reconfiguration - sending a human to a remote hostile environment to repair a robotic system defeats the object of the system. The system should therefore be highly modular, highly redundant, highly maintainable and accessible. Fault tolerance implies the necessity of cross-strapping all arm control units and employing redundant power switch units for arm power switching to reinforce the cross-strapping redundancy. Backup joint electronics units and redundant force-torque sensor cross-strap switch ensure safety-critical redundancy for joint control.

Ageing satellites could be upgraded with more modern systems as technology proceeds, re-orbited from orbit degradation and resupplied with consumables such as propellant, batteries or cryogens to function beyond their design lifetimes (possibly up to 2-3 decades for comsats and 5-10y for scientific and Earth observation satellites), enhancing their profitability and usefulness by eliminating these restrictions. Warships have a 10y development schedule typical of spacecraft, but every 7-10y such ships undergo a major overhaul lasting ~18 months for upgradings.

The UK/US/NL IRAS satellite was fundamentally limited by its He cryogen coolant supply and its ESA successor ISO is similarly limited to 18 months operational life. Passive radiant cooling is limited to above 50K and they restrict spacecraft orbits to ensure that the radiators are not exposed to solar energy. ISO will supplement the sky survey of IRAS through detailed observations of selected sources between 2.5 and 200μ using an infrared Richey-Chretien telescope and 4 scientific instruments (infrared camera, infrared photopolarimeter, and short wave and long wave spectrometers). For maximum sensitivity the telescope and instruments require cooling. The telescope is enclosed in an He-cooled cryostat with the 4 instruments mounted behind the primary mirror. The cryogen tank contains 2286l of liquid He at a temperature of 1.8K and its evaporation limits the lifetime to 18 months. ISO will be in a 70,600x1000km eccentric orbit with a period of 24h of which only 16h lie outside the Earth's radiation belts to

allow observation. Hence the real-time observation schedule must be planned to maximise the overall efficiency of the mission. The number of candidate sources is large (planetary atmospheres, cometary detection at ~5AU, protostar and planetary accretion processes, red giant outflows, supernova remnants, galactic star forming regions, brown dwarf detection, etc.) and the observing time short. Astronomers would value extremely highly the potential for cryogenic refuelling. Furthermore, liquid He is expected to become increasingly used on comsats for cooling to improve their signal-to-noise ratios by reducing thermal dark currents.

Consumable replenishment (eg. fuel, cryogenic fluid, batteries, etc) essentially spreads fixed cost overheads over longer operational periods. In fact, the cost parameter of a communications satellite is given by [Bargellini 1978]:
(Launch cost+spacecraft cost)/(number years of service x number telephone circuits).
Hence, increasing the lifetime directly reduces the cost parameter in linear fashion. Russel & Price (1990) declared that the largest costs for GEO comsats are hardware and transport. To reduce these costs, it is desirable to maximise the payloads fraction, but this is subject to a limit. This limit can be curtailed by refuelling propellant and replacing worn-out batteries since when this is needed, the other systems are usually still functional. This effectively converts the fuel mass which has no direct earning capacity to payload mass and higher revenues without increasing spacecraft mass. Refuelling in particular increases the spacecraft net present value by up to $24.4M and increases the internal rate of return up to 8.3%. Furthermore, the present constraint of introducing redundancy into spacecraft systems increases costs. The advent of in-orbit servicing capability effectively makes the redundancy of certain mission subsystems as obsolete, thereby significantly reducing satellite construction and design costs. Indeed redundancy of some subsystems is virtually impossible (eg. the propulsion subsystem). Module replacement is much cheaper than satellite replacement which now have cost ranges of ~$200M-$600M and a refuelling capability enables a reduction in fuel mass allowing more payload.

Fewer satellite launches would slow down the ever-increasing problem of crowding and consequent space debris generation. In around 20y, there are ~7,000 trackable objects in Earth orbit. Space debris is becoming a serious hazard to operational spacecraft: only 5% of ~1000 spacecraft presently in orbit are operational. It has been estimated that ~28% of debris objects result from discarded shrouds, ejectiles, etc. Around 21% are dead payloads which are intact or near intact while 45% are large fragments resulting from around 100 satellite breakups (40% deliberate, 15% propulsion malfunctions, 45% unknown). An average mission produces 3 pieces of trackable debris. A robotic interceptor satellite could alleviate this problem by salvaging the larger pieces of redundant hardware that pose such a threat to operational spacecraft either for return to Earth (eg. as in the case of LDEF), for controlled re-entry disposal, or into new graveyard orbits in a cost-effective and practical manner. For objects without grapple fixtures highly compliant cushioned pads could be used [French & Boyce 1985]. The Soviet nuclear reactor powered Cosmos 954 incident which re-entered the Earth's atmosphere and spread nuclear debris over a remote area of Canada necessitating an expensive clean-up operation illustrates the need for retrieval particularly concerning nuclear powered spacecraft. Both the US Space Shuttle and the Russian Buran may provide the capability for LEO retrieval and return. Although satellite retrieval for salvage is unlikely to be cost effective propellant

scavanging is a potentially useful operation. Some satellites however are designed for retrieval and return to Earth, eg. LDEF (Long Duration Exposure Facility), Eureca. Finally, in-orbit satellite insurance premium rates may be reduced by the existence of such a robotic servicer. Satellite compatibility for robotic servicing such as number and ease of access to replacement modules, accessibility and number of grappling and docking fixtures, existence of detailed and accurate CAD databases for subsystems and components, would in effect increase spacecraft reliability. Indeed, it has been estimated that serviceability could reduce the in-orbit post-launch operational fraction of insurance costs by ~50% [Russel & Price 1990].

At present, all in-orbit operations are performed by astronauts in EVA (extravehicular activity) with a limited degree of assistance from teleoperated manipulators if at all. This is both costly and hazardous. Indeed, modern satellites are being designed to be serviced during such in-orbit operations. EVA tasks are restricted by access, risk and complexity, and trade studies comparing EVA against other alternative techniques are usually performed to assess payload mass limitations, reaction time requirements, performance time, astronaut workload and reliability. Other constraints include translation to the worksite (usually the cargo bay), equipment transfer to and from the cargo bay, lighting and tool logistics. Nearly all tasks require foot restraints and handholds, and loose objects require tethers to attach points. All EVA tasks exceeding 30 minutes must be tested in the neutral bouyancy tank which involve the design and construction of mockups and extensive task testing followed by astronaut crew training. Crew training includes KC-135 simulated-zero-g parabolic flight (30s weightlessness) for donning the EMU. NASA has three underwater neutral bouyancy training simulators, the largest and most used are at NASA Marshall Spaceflight Centre in Huntsville, Alabama and NASA Johnson Space Centre in Houston, Texas.

Hazards are imposed by a hostile, radiation-filled vacuum and the possibility of spacesuit rupture due to snagging, micrometeoroid or debris impacts, exposure to cryogenic fuels such as LOX/LOH or corrosive fuels such as hydrazine or ammonia if operating near fuel tanks or lines or near cryogenically cooled sensors. The probability of micrometeroid or debris penetration of the EMU during a single 2 man 6h EVA has been estimated to be 0.0006 which, although small, is finite. Accidental RCS thruster activation is another remote possibility which could cause unexpected impact on the astronaut and/or exposure to hot gases.

Furthermore there is a long lead time between failure and the contingency repair operation due to extensive preparations required and launch schedule contracts - the Hubble Space Telescope (HST) repair mission occurred $3\frac{1}{2}$y after its launch. The cost is also phenomenal. It has been quoted that the cost of EVA alone is ~$70,000/man-hour, but actual costs suggest that additional and hidden factors dominate, the cost of launch itself being probably the largest single factor and estimates of a single Shuttle flight have been estimated at costing ~$1B - most of this cost is not passed to the customer but subsidised by NASA. The Intelsat VI repair operation in 1992 was estimated to have cost the insurers around $150M [Williamson 1992]. The cost of the more complex repair of the $2B Hubble Space Telescope in 1993 was much greater at $700M, almost three-quarters the cost of the $1B Mars Observer probe lost in 1993. Errors are costly in the space business. Robotic remote execution of these activities would greatly relieve astronauts from hazardous and repetitive tasks and reduce their

workload allowing them to concentrate their valuable resources on tasks requiring beyond state-of-the-art machine intelligence such as scientific investigation and experiments. Furthermore, a dedicated robotic system capable of reasonably complex manipulation tasks would provide greater flexibility in task execution and enhanced performance, safety, cost-effectiveness and greater reliabilty for mission success. Finally, only low inclination LEO is accessible to astronauts as the Eastern Test Range at Vandenberg AFB will no longer support Shuttle operation for polar orbit. LEO satellites are estimated to fail at a rate ~40-50% higher than those in GEO. High inclination polar orbits (the preferred orbit for earth observation satellites) are inaccessible as are high orbits >500km altitude. High inclination (polar) orbit is the operational orbit for Earth observation and this orbit is likely to become increasingly populated with such satellites. Although there is a recent trend to place communications satellites into LEO for mobile communications, the majority of comsats still reside at the geostationary altitudes ~36,000km which are presently inaccessible to astronauts and also pose increased radiation hazard than LEO.

In summary, the need for robotic servicing in space has been outlined. The next problem concerns the type of robotic manipulation adopted by the robotic servicer spacecraft.

1.4 IN-ORBIT SERVICING

General purpose manipulation represents the most varied and diverse sets of tasks that may be performed in space. Nitzan et al (1985) divided robotic manipulation tasks into 4 categories:
(i) material handling;
(ii) parts fabrication;
(iii) inspection;
(iv) assembly.
Material handling (ie. transport) represents the simplest application. Parts fabrication represents the commonest use of robots in industry with half being used for welding, mostly spot welding. Assembly represents the most complex application of robot manipulators and it is this that most space-based robotic devices will be concerned with. This thesis is specifically concerned with in-orbit servicing, maintenance and repair of spacecraft, with truss assembly and construction and astronaut rescue and retrieval being regarded as secondary functions. Retrieval of spacecraft is unlikely to be economic, but complex major failures to expensive satellites may require return to Earth for refurbishment. Broadly, in-orbit operations may be defined as:
(i) construction operations involving in-orbit assembly;
(ii) maintenance operations including routine calibration of equipment;
(iii) repair functions to meet mission objectives in the face of failure or damage to equipment;
(iv) routine servicing by replenishment of expendables or installation of upgraded equipment [Seidman 1992].
Elfving (1990) and Schroer (1990) highlighted a series of reference tasks:
(i) RT1 - assembly of trusses;
(ii) RT2 - mating of connectors;
(iii) RT3 - exchange of ORU equipment box;
(iv) RT4 - removal of thermal blanket/panels;
(v) RT5 - operation of power tools;

(vi) RT6 - local inspection by sensors for faults.
Observe and inspect spacecraft, subsystems or components for flaws, defects, etc due to thermal stresses or micrometeoroid damage - inspection constitutes the first phase of any servicing activity. Inspection is particularly man-intensive and monotonous so it is well suited for automation. Terrestrial NDT is usually performed using ultrasonic techniques because they provide good depth capabilities, but space inspection would have to use other techniques: eddy current systems have little depth penetration and are limited to surface defects; the other alternative is X-ray radiography which has good depth capabilities, but has a high initial cost. In-orbit transportation of spacecraft for retrieval is also a critical capability and the in-orbit servicing process starts with grappling objects and docking fixtures on spacecraft. This may involve passivating tumbling about three rotational axes by momentum nullification through momentum exchange via the dual-spin turn for instance [Kaplan 1976]. All the more complex manipulation tasks will require certain basic capabilities: opening and closing access panels, doors and covers; operating mechanical connections such as latches, bolts, cranks, screws, plugs etc and operating electrical connections such as connectors, soldering, replacing faulty PCB's, etc. "Legged" locomotion on space truss structures is another potential capability. Dual grippers enable the robot to attach itself to threaded holes in the truss with walking accomplished by alternate grasping and releasing of the nodes by the grippers and swinging the arms from one node to the next. This requires sufficient span between the two grippers. The end effector must be able to grip to the nodes firmly as the robot platform shifts from one end effector to the other for support.

Fluid connector interchange represents a complex manipulation problem by virtue of the fact that it involves fluids and flexible elements [Abidi & Gonzalez 1990]. The mating elements in both cases must be within the FOV of any camera mounted on the arm so that guiding targets are visible. The requirement is to mate and demate a fluid connector. The alignment /locking mechanism comprises a nozzle to be inserted into a receptacle mounted on the target satellite. The nozzle and receptacle are essentially male and female BNC connectors. The nozzle is cylindrical with two steel pins located 180^{o} apart extending 0.5in. It has a flat parallelepiped end acting as an attachment point for the robot end effector. The nozzle is 4.75in long with inner and outer diameters of 1.25in and 1.75in respectively. The receptacle has a flared rim with inner and outer diameters of 2in and 2.9in respectively. It has 2 V-notches 180^{o} apart in its rim leading into 2 grooves that lock the nozzle into position once it is inserted. The robot picks up the nozzle and locates the receptacle. The robot arm inserts the nozzle with the flared rim guiding the receptacle by generating corrective forces on the nozzle. As the nozzle is inserted, the pins enter the V-notches which align the nozzle. When the nozzle reaches the bottom of the V-notches, the robot then rotates the nozzle 15^{o} clockwise which allows the pins to enter the grooves in the receptacle.

Now some real examples of in-orbit servicing missions are considered. In manual assembly sequences, line balance is achieved according to defining manual worker division of labour with similar timescales. A similar approach is valid for EVA tasks. In contrast, for robotic machines whose performance is different from humans, the assembly sequence musty be defined differently. However, initially in-orbit tasks will be performed by human operators through teleoperation so EVA sequences are of direct relevance to robotic assembly until automation has been achieved.

1.4.1 Solar Maximum Repair Mission (1984)

The STS 41-C Solar Maximum Mission in April 1984 has become a standard for space robotics and in situ servicing. Simpler EVA's had been performed such as the STS-37 mission when the two astronauts successfully manually freed a stuck antenna on the Gamma Ray Observatory satellite. The satellite would have had to have been returned to Earth otherwise. However, the Solar Maximum Repair mission was significantly more complex. The intention was to demonstrate the feasibility of in-orbit repair of satellites to justify the manned space station concept as a maintenance base. The original space station architecture was to have a central set of habitation and laboratory modules with several unmanned co-orbiting platforms to be periodically visited by astronauts. The platforms would enable microgravity experiments to be performed without interference from crew movements. Such an architecture would require extensive EVA.

The Solar Maximum satellite was based on NASA's standard Multimission Modular Spacecraft (MMS). In general, the MMS comprises 4 separate modules weighing ~225kg each: the Attitude Control Subsystem (ACS), the Communications & Data Handling Module, the Modular Power System, and the Propulsion Module. Each is externally a 1.4x1.4x0.5m box with the exception of the Propulsion Module which being optional was not installed on the Solar Max satellite. Each module is fastened to the spacecraft with two 2cm hex bolts requiring 135Nm torque for removal/installation. The Attitude Control Subsystem of the Solar Maximum satellite failed after 9 months of its 2y operational life suffering a loss of yaw and pitch control rendering the $235M spacecraft unable to point to solar flare locations on the Sun. Curiously, one of the astronauts attempted to capture the satellite manually using an MMU, but caught it by a solar array setting it tumbling. Only after the ground crew uploaded software corrections was the spacecraft detumbled to ~0.1m/s and retrieved by the RMS. This illustrates the difficulties in capturing bodies under irregular motion even by human action. The total EVA took two EVA's of two astronauts each. This operation has all the major features characteristic of satellite repair and it cost $77M. Two major repairs were required: replacement of the satellite's attitude control ORU module - this ORU exchange was a designed for servicing task [Davis 1987]; the electronics box exchange however was not designed for servicing [Adams et al 1987]. The third operation was to install a Be-Cu deflector baffle near the propane exhaust port to eliminate plasma interference of the X-ray polychromator. This operation took only a few minutes to complete.

(1) MMS ACS exchange:

Two astronauts, one riding the RMS foot restraint operated by a third astronaut replaced the MMS ACS using the EVA MST (Modular Servicing Tool) powered by Ag-Zn MMU battery to clamp to the ORU and allow tightening and loosening of the bolts. The MST is a power tool comprising a 2cm hex socket with 135Nm torque capability to turn the 2 MMS bolts on two opposite vertices of the MMS outer face. Prior to this, the removable panel covering the MMS module had to be removed. The single blind-mate connector for electrical interface on the module mates perefectly when the two bolts are fastened. This procedure took 35 minutes for EVA, 15 minutes by laboratory teleoperation and 40 minutes by laboratory automation.

ORU module exchange is likely to be highly structured since all objects will probably have known dimensions, locations, masses, moments of inertia and positions of grapple fixtures. The procedure has been performed both teleoperatively and autonomously in the laboratory. Bronez, Clarke & Quinon (1986) characterised the robotic in-orbit servicing task of the ORU exchange:
1. Isolate the old module.
2. Open and disconnect the thermal interface blankets and secure.
3. Acquire the power tool.
4. Latch the power tool to the old module captive bolts and loosen the bolts with the power tool while holding the cover: (a) stow power tool; (b) remove and stow the cover; (c) release the old module retention clamps.
5. Detach the old module.
6. Stow the old module to the robotic spacecraft bus (for controlled re-enty disposal or for return to Earth for refurbishment and subsequent re-use).
7. Find the replacement module.
8. Orient the new module for insertion.
9. Install the new module to the spacecraft: (a) tighten the module retention clamps; (b) acquire the cover; (c) acquire the power tool; (d) tighten the captive bolts with the power tool; (e) test the bolts; (f) stow the power tool; (g) release and grasp thermal blanket, then drape and fasten the blanket.
10. Inspect and wait for the new module checkout.

Backes & Tso (1990) subdivided the single arm autonomous ORU changeout sequence into subtasks. One of these subtasks, the dual-pin insertion/removal subtask required a decision-making strategy with compliant control to prevent jamming. They used a stiffness-type outer force control loop which modified the position trajectory. The subtasks used the RCCL (Robot Control C Library) and all were used more than once during the ORU changeout. The bolt was assumed to be located at the centre of the lug. The ORU exchange programme used subtask components to first unscrew the two bolts on the two opposite vertices of the outer face of the ORU. Then the ORU was changed out on unlatching them.

The Bolt sequence to turn the bolts with repeated 60^{o} turns:
1. Grapple-lug-acquisition subtask to locate the lug position;
2. Angled-bolt-seating subtask to set the socket onto the bolt;
3. Bolt-turning subtask about tool z-axis by 60^{o};
4. Compliant-move subtask along tool -z-axis to position above bolt to reduce contact forces;
5. Guarded-move subtask rotation of -60^{o} about tool z-axis to return tool twist;
6. Vertical-bolt-seating subtask to seat the socket onto the bolt;
7. Repeat 3-6 until desired tool turn is attained;
8. Compliant-move subtask along tool-z axis to position above bolt and reduce contact forces.

The ORU changeout sequence was as follows with ORU replacement following a similar pattern:
1. Grapple-lug-acquisition subtask to locate lug position;
2. Guarded-move subtask to mounting region;

3. Move-to-touch subtask at 4mm/s to contact between fingers and lug until the forces lie between the backoff force of 1N and the threshold force of 5N;
4. Level subtask to match finger surfaces on lug surface by reducing moments;
5. Compliant-grasp subtask to grapple ORU by closing the fingers to 60 psi;
6. Dual-pin insertion/removal subtask to remove the two-pin ORU from two-holed mount interface;
7. Guarded-move suntask to insertion point on stow platform;
8. Move-to-touch subtask at 4mm/s to contact between ORU pins and stowage holes until the forces lie between the backoff force of 1N and the threshold force of 5N;
9. Dual-pin-insertion/removal subtask to insert the two-pin ORU into the two-holed stowage interface;
10. Compliant-ungrasp subtask to release ORU by opening fingers;
11. Compliant-move subtask to move away from ORU by reducing the contact forces.

As can be seen, the ORU exchange task is a fairly complicated though well characterised task. Bruhm (1987) declared that the sensitivity of the single arm to disturbing forces due to the lever arm between the ORU centre of mass to the grapple points is high. Positioning/orientation errors arising from this may be as much as ~3-5 times higher than for the unloaded arm. The use of two arms significantly reduces the maximum compliance values.

(2) Main electronics box (MEB) exchange:

The Solar Maximum Repair Mission astronauts followed a 31 page document to replace the Chronograph/polarimeter main elecronics box using EVA hand tools and 3 Ni-Cd battery powered screw-drivers, one with an allen drive for retaining-cap screws, one with an allen drive with a screw capture shroud, and one with a slotted driver blade. Other EVA tools included the MEB hinge assembly, panel support bracket, electrical connector removal tool, electrical connector installation tool, Essex ratchet, and an assortment of simple tools such as cutters and tape. The MEB hinge assembly and panel support bracket were both unique tools designed specifically for the SMM repair. The task involved 13 steps:

(i) cutting the plastic Kapton tape holding the thermal blankets;
(ii) folding, unfolding and taping the thermal blankets;
(iii) installing the MEB panel hinge assembly;
(iv) removing 14x MEB panel 10-32 non-capture screws and re-installing 4x10-32 captive cap crews;
(v) installing the panel support bracket;
(vi) removing 22x4-40 slotted head connector screws;
(vii) removing 11 subminiature electrical connectors;
(viii) cutting the plastic tie wraps holding the wiring harness;
(ix) removing the MEB from the hinge assembly and reinstalling the new MEB onto the hinge aasembly;
(x) reinserting the connectors using a 3 sided guide and a pair of spring clips at each end of each connector;
(xi) removing the velcro straps from the thermal blankets;
(xii) using the velcro straps as cable ties;
(xiii) replacing the thermal blankets and sealing using tape.

This procedure took 2h of EVA compared with the neutral bouyancy simulation time of 3.5h. The remote MEB repair sequence in the lab was only possible using dual manipulators as some operations required parallel execution while others required

sequential execution using both arms. Laboratory dual arm teleoperation took 3h - automation of the task has yet to be attempted and it is unlikely to be feasible for the foreseeable future, although task sequence planning has been generated and simulated [Sanderson et al 1988]. This was the most difficult operation. In remote laboratory teleoperation, handling the thermal blanket and cutting tape were the most difficult processes while the removal of the connector crews and reinstalling the electrical connectors were much quicker in teleoperation than in EVA (38min versus 60min, and 27min versus 55min respectively). The handling of flexible extended objects then appears to require complex manipulation capabilities. All in all, the total EVA time was 7h. The total cost was estimated at $77M, though this must be a gross underestimate since both the cost of the Space Shuttle launch and the 1y neutral bouyancy training for the astronauts would exceed this.

Since the Solar Maximum Repair mission, several major repair or retrieval missions have been undertaken. Palapa B2 and Westar 6 C band communications satellites were both retrieved with 2 EVA's and boarded the STS-51A Shuttle after the upper stages failed in 1984. Both satellites were outside rendezvous capability necessitating their use of onboard hydrazine to circularise their orbits and alter their orbital parameters. Similarly a series of despin attitude maneovres enabled the astronauts to berth them and return them to Earth for reconditioning and relaunch in November 1984. Syncom satellite repair in September 1985 required two EVA's (STS-51D) which failed to activate the satellite time sequencer. The Challenger disaster effectively ceased all Shuttle operations for several years. The STS-49 4.5 tonne dual spin Intelsat VI reboost in May 1992 required 4 EVA's with 3 astronauts the longest EVA being 8.5h in duration during the Intelsat VI capture. This satellite was launched in 1990 and could not achieve operational orbit because the Titan second stage failed to separate the satellite. The satellite perigee kick motor seperated the satellite from the Titan by ground control command and was boosted to a stable orbit. This necessitated the addition of a new propulsion unit to place the satellite into its GEO orbit. Curiously due to its subsequent highly accurate placement in GEO the savings in propellant suggest that the satellite may have an operational lifetime of 15y. STS-49 was also the mission on which two EVA astronauts demonstrated the feasibility of constructing a 15x15 ft truss structure. The Eureca satellite was retrieved with 1 EVA in June 1993 (STS-57). The STS-61 Hubble Space Telescope (HST) repair in December 1993 required 5 EVA's. HST was designed to be serviced from the Space Station with 2 two-hour EVA's every 22 months.

1.4.2 HST (Hubble Space Telescope) Repair Mission (1993)

Towards the end of 1993, three-and-a half years after its launch into orbit, the 11 tonne Richey-Crethien design HST Hubble Space Telescope) was repaired during one of the most ambitious and hazardous in-orbit repair missions undertaken to enable it to continue it 15y life. The scientific instrument modules had been designed so that they could be removed and replaced by EVA as technology advanced but unfortunately not the mirrors of the telescope. HST has a stiff pointing requirement of 0.01 arcsec accomplished by its combination of 6 rate gyro assemblies, 3 fixed head star trackers, 4 gas bearing reaction wheels for attitude control and magnetorquers for momentum dumping of gravity gradient torque accumulation. Details of its design are outlined by Wojtalik (1987). It has 1.4×10^5 times the light gathering power of the human eye and

can image objects that are 25 times fainter than terrestrial telescopes expanding the optically visible universe by 350 times.

Although the HST was specifically designed to be maintained in-orbit NASA's public image had taken a severe blow when it was found that the HST 2.4m main mirror was incorrectly shaped causing spherical aberration. Rather than focussing 70% of the incident light to its 0.1arcsec radius resolution limit, it was focussing only 15%. This 70% was specified as the minimum scientific requirement set by the point spread function of a typical star. NASA's Space Shuttle Endeavour was selected as the newest shuttle with its superior fuel reserves to reach the high orbit of 310x297nm imposed by the requirement for minimal interference from the Earth. A crew of 7 were selected totalling an experience of 16 space missions. The commander was Col Richard Covey USAF with Cdr Kenneth Bowersox USN as the pilot. The payload commander was Dr Storey Musgrave who had helped plan the EVA for the STS-49 Intelsat VI repair mission. He with Dr Jeffrey Hoffman formed the first EVA team. Lt Col Thomas Allers USAF was one of the three-man EVA team who had repaired Intelsat VI and with Kathy Thornton formed the second EVA team. ESA astronaut Dr Claude Nicollier was the mission specialist to operate the RMS in support of the EVA team. They were prepared for the mission by 400h training in the neutral bouyancy tank at MSFC (Marshall Spaceflight Centre at Huntsville) and JSC (Johnson Space Centre at Florida). The mission was to last 10 days with 5 EVA excursions averaging over 7h each. Besides installing the corrective optics, other replacements were to be installed. Two of the 6 Goddard /Lockheed/Fairchild DF-224 coprocessor memory units had failed and three of the 6 rate sensing gyros had failed. The solar arrays also suffered thermal shock during the day-night terminator crossing causing spacecraft vibrations and so required replacement. Prior to EVA, the cabin pressure in the Shuttle was reduced from 14.7psi to 10.2psi to reduce pre-breathe periods. The HST was grappled by the RMS and berthed in the payload bay. The first EVA lasted 7h 54min and the EVA team successfully replaced 3 rate gyros. The second EVA involved replacing the two solar arrays. The third EVA also involved the RMS for the installation of the corrective optics and DF-224 coprocessors. Finally, the fourth and fifth EVA had the EVA team replace the solar array drive electronics. All in all, the whole mission involved a total of 35h 28min EVA, and Allers had broken the US record for accumulated EVA time with 29h 40min. The total cost of the mission was $700M. HST was corrected to achieve its original performance helping to revamp NASA's somewhat tarnished image since the recent loss of the Mars Observer probe.

The need for in-orbit servicing has been demonstrated and the complexity of potential tasks that are required has been outlined. Performance of such tasks robotically rather than by EVA would be a considerable asset to space missions in 1993.

1.5 MAN-MACHINE INTERFACE:

Most machines act as energy transformers to extend human capabilities. The robot however is a machine that is designed ultimately to reproduce human capabilities particularly for undesirable tasks such as in potentially lethal, harmful or hazardous environments or for strenuous or dull tasks. Repetitive and dull tasks are particularly suited to the machine since machines do not tire or become inattentive. They are ideally suited to tasks like monitoring and diagnosing multiple complex systems, and for fault detection and correction. Humans are suited to flexible pattern recognition in

high noise and uncertain environments involving multiple sense stimuli and for reacting in response to unexpected occurrences, whilst machines are suited to consistent, routine, repetitive and precise operations over long periods of time. Humans can make inductive decisions and utilise generalisations from past experience. However, onboard automated fault monitoring and diagnosis can provide good real-time aid in such human functions. Manual tasks that can be performed prescriptively by detailed procedures (algorithms) are suitable for automation to reduce the human workload. Tasks which exceed human capabilities due to a required high rate, high accuracy, repeatability and consistency should also be automated. The reasons for autonomy are multitudinous. Human error can also often lead to accidents - accidents are not only unacceptable to the public, they also represent considerable costs. Fatigue alone can cause up to ~30% of operator error in completed operations in space performed by astronauts. Astronauts in particular are susceptible to hiding fatigue or difficulties due to their perceived self image. Pilot error is the cause of 65% of airline accidents and non-pilot personnel generally were involved in 44% of all air-related accidents in 1980. The accident rate is around 3.25 accidents per 100,000 hours. This does not however account for the avoidance of accidents through human reaction and judgement to unexpected events [Chambers & Nagel 1985]. The majority of errors are resultant from misinterpretation of information, though this can be minimised by effective displays in man-machine interfaces. The need is for information management to avoid information overload.

Nevins (1985) classified tasks as deterministic or non-deterministic: deterministic tasks are those driven by geometry, eg. peg-in-hole task; non-deterministic tasks are those which require skill and involve not-well-understood process models, eg. data interpretation. Non-deterministic require either human intervention or a high degree of machine intelligence with adaptive learning capability. Deterministic tasks may be pre-programmed but may require adaptive capabilities. The Robot Institute of America defines a robot as: "A reprogrammable, multifunctional manipulator designed to move materials, parts, tools or specialised devices through variable programmed motions for the performance of a variety of tasks". This definition is a little narrow and refers specifically to industrial robots which have limited capabilities. The Japanese Industrial Robot Association went further and classified robots into a series of classes based on their capabilities:

Class 1 - teleoperated robots
Class 2 - fixed sequence robots
Class 3 - variable sequence robots
Class 4 - teach-playback robots
Class 5- computerised numerically controlled robots
Class 6 - adaptive/intelligent robots

Class 6 is in fact more properly subdivided into two categories:

(a) adaptively controlled robots
(b) autonomous robots employing artificial intelligence methods

A robot may be defined as [Nitzan et al 1985]:

"A general purpose machine manipulator that can perform a variety of difficult tasks in remote hostile conditions not necessarily known a priori by using an intelligent control system that observes the environment and takes appropiate autonomous actions to suit that environment and those task objectives". This corresponds to Class 6 of the Japanese classification of robots and is partially realisable to a certain degree using

today's technology and it is to this definition that space robotics should be working to attain.

Planetary surfaces are highly unstructured and susceptible to uncertainties which must be accomodated in real-time. Such longer range missions will require a high degree of intelligent automation for autonomy since human intervention will be limited to higher control levels with longer time constants. Pre-programmed sequences have all ready been used on spacecraft for autonomous execution, eg. Viking lander on Mars. Autonomy in space has three main advantages over manual task execution by EVA and teleoperation [Erickson 1987]: firstly, automated robots generate lower costs and improved productivity; secondly, increased flexibility and availability due to higher precision and quality; thirdly and most importantly, there is greater safety due to reduced hazards to humans. Robots with powerful onboard machine intelligence will be able to do many operations in space autonomously, and have the advantage that they can be given perceptual abilities beyond those of humans (eg. infra-red vision for inspection tasks). Modern technology has endowed mankind with the tools to use a multitude of senses beyond our natural five. The central point is that autonomy imposes a heavy reliance on sensory data to deal with an uncertain and changing environment. The general conclusion is: "Remote systems require the ability to do autonomous operations to be effective" [Heer 1979].

NASA has developed an evolutionary strategy of direct teleoperated systems gradually being replaced by increasing autonomy with human supervision as new technologies become available. During the late 1980's NASA had developed a baseline computational architecture to support space robotic systems and this envisaged gradual evolution from teleoperative mode towards autonomy (NASREM) [Albus, McCain & Lumia 1987]. The first phase of evolution is that of the "intelligent aid" whereby automatic control of individual subsystems would be achieved. The "intelligent apprentice" stage follows when automatic control of multiple subsystems has been achieved. Next comes the "intelligent assistant" characterised by hierarchical control of multiple subsystems and finally the "intelligent accomplice" will be characterised by automated distributed control of multiple subsystems. At all stages, humans will have top-level authority, responsibility and control. This evolution towards autonomy will result in major reductions in ground segment costs which can be as high as ~60% of space mission lifecycle costs [Wertz & Larson 1991]. The communication time delay, bandwidth limitations and human performance limits will contribute to this evolution. Teleoperation requires high information flows and will force the use of computational techniques to be employed remotely. It will also have to compete with the bandwidth requirements of other missions particularly from remote sensing satellites - currently $\sim 10^{12}$ bits per day are transmitted to Earth from space and this will increase in the near future. All projects proposed in Europe expect to remain in teleoperated mode for the forseeable future.

Teleoperation may be defined thus: "A teleoperator is a robotic device having video and/or other sensors, manipulator arms with some mobility capability which is remotely controlled over a telecommunications channel by a human operator. This human operator can be a direct man-in-the-loop controller who observes a video display of the teleoperator and with a joystick or analogous device continuously controls the position of the teleoperator vehicle, its arm or its sensor orientation. Alternatively the

teleoperator can employ a computer endowed with a modicum of artificial intelligence capable of executing simple control functions automatically through local force or proximity sensing; in this case the remote human operator shares and trades control with the computer" [Bejczy 1979]. The aim of teleoperation is to use a master/slave robot system such that a human operator (HO) uses the master device to control the slave manipulator within a remote environment (usually hostile) to perform work, ie. teleoperation is a cybernetic man-machine interface system designed to augment and project human senses and dexterity across physical distances [Bejczy 1980]. Indeed Arbib (1976) advocated that the goal of artificial intelligence is to enable the machine to cooperate with humans in a symbiotic fashion such that the machine enables humans to perform more tasks more intelligently.

Teleoperation for space missions are characterised by the remoteness of the operations environment. This generates time delays in the round-trip signal transmission and so in the control loop. Teleoperation to GEO involves ~0.5s time delay due to the time for the command to reach and return from the spacecraft, a ~0.8s delay for the modulation-demodulation of the signal (usually), plus ~0.2s delay due to limited human reaction speed, ie. all in all, the communication delay may be as high as ~1.5s for GEO. The problem of eclipse in LEO from the ground station suggests the necessity of a network of ground stations for continuous communication (prohibitively costly). However, the requirement for continuous communication during manipulative operation with the ground may be maintained using TDRSS/EDRS relay in GEO. Since this introduces a GEO time delay for the communications link of the robotic freeflyer spacecraft in LEO, this may be regarded as a standard time delay. If such space missions extend to beyond GEO, the communication time delay will increase to beyond tolerable levels necessitating the use of onboard decision-making capabilities, ie. autonomy. Some of these problems may be alleviated by using space-based HO's, ie. astronauts (eg. the Shuttle mission specialist operates the RMS). However, astronauts "on-site" are expensive and require a manned launcher. The Space Shuttle astronauts often perform in-orbit servicing tasks but Shuttle flights are not scheduled to coincide with the time constraints of any particular servicing requirement or worksite. For maximum flexibility, the robotic spacecraft must be operated from the ground. The maximum time delay for efficient teleoperation is ~0.2s [Korf 1982]. When longer transmission delays occur, move-and-wait strategies are usually adopted by the operator. More than 1 sec delay seriously degrades performance to the extent that move-and-wait strategies must be adopted automatically. This makes the capture of a moving target virtually impossible and prevents the operator from avoiding possible damage to the target or the manipulator [ESA 1986]. As the time delay increases, so the time for task completion increases - an adequate robot technology requires at least 80% usage time to be generally economic in the industrial environment and this provides a useful yardstick when applying robotics to other environments such as space: move-and-wait strategies are highly inefficient in terms of manipulator operation. Teleoperation can be performed in time scales ~3-5x those of human manipulation on Earth using EVA gloves [Andre et al 1990].

Predictive computer graphics pre-views can considerably improve tracking performance under conditions of transmission time delays between a remote site and the operator station [Stark et al 1987]. Predictive displays involve heuristic synthetic models represented graphically to simulate the robot and the target motions in real-

time. They operate by simulation of the task environment and simulation of the effects of operator actions. The predicted effects are displayed to the operator and are continuously updated to correspond to the delayed actual sensory data at the remote site. Hence they provide both previews of action and predictions of the environment. The 3D graphics models of the manipulators and objects are overlayed over the 2D scene TV images. The overlap may be wire-frame or solid-polygonal models with varying degrees of transparency. A CAD/CAM model is often used for such superposition. Calibration between the images is performed using the manipulator geometry as the calibration fixture and the cameras are modelled as ideal pin-hole image formation processes. The human operator can correlate the model to the video image and bring the two into alignment by superimposing the vertices of the model to their equivalent vertices on the image. Several prediction algorithms are available and Smith's control algorithm is a popular one and assumes a stationary target [Delpech & Manrrette 1985]. These predictive displays reduce the effects of time delays dramatically and reduce the total teleoperation time, but they do limit the manipulator speed of operation to a degree. Sato et al (1993) suggested using automatic velocity reduction from the operator to the robot controller such that the simulator performs like a slow motion action film to slow down the trajectory transmitted to the robot spacecraft.

Shared control for advanced telerobotic operation with a mixture of automation and teleoperation is desirable. The well-structured nature of many robot motion segments such as pick-and-place, tool exchange and subsystem control (eg. TV tracking of the task) are executed repeatedly in all teleoperations and impose a burden on the human operator (HO). This introduces the opportunity for high degrees of autonomy for such tasks through pre-progamming, automatic control and object-level languages. This may be enabled by the fact that target spacecraft are man-made and deterministic in structure and CAD/CAM models of high accuracy should be available. Automatic control of camera position and orientations based on manipulator and camera positions would significantly reduce the operator's workload since continuous work on the task is possible without interruption for camera adjustment. For override to alter requirements, the teleoperator may use object-level languages (possibly spoken) to specify the aim of the task or camera requirements which is automatically decomposed into motion-level procedures and automated control routines [Sati & Hirai 1987]. Supervisory telerobotic control may be maintained whereby remote devices operate in autonomous mode and only interacts with the HO for high-level instructions or when it encounters a problem that it cannot handle. Pin et al (1992) suggested that the ultimate goal of the intelligent machine is to support humans in the efficient accomplishment of increasingly complex tasks, and that former man-machine interfaces were characterised by a static allocation of tasks to the human and to the machine based on rigid, a priori capability characteristics. They regard this as limiting. Only through dynamic allocation of tasks based on changing skills, intellectual capabilities and performance of the human such as including the effects of fatigue will man-machine interfaces become effective. This forms the basis of a dynamic symbiotic relationship between humans and the machine or synergistic man-machine interface. This dynamic process allows the man-machine symbiont to cope with a changing environment, causing the resources most appropriate for performing a subtask to be assigned that subtask while the other monitors it. This essentially optimises the division of labour between man and machine. This requires the system to:

(i) acquire new knowledge over time through experience and observation;
(ii) evaluate current capabilities based on the current state of the environment and the skills of the system's components;
(iii) dynamically optimise the allocation of tasks between the human and the machine based on current capabilities.
This chapter provides the backdrop to robotic servicing in space.

1.6 THESIS SUMMARY:

This thesis is a mechatronics eye view of robotic spacecraft through a particular implementation of a freeflying spacecraft called ATLAS (Advanced TeLerobotic Actuation System). ATLAS is a dual manipulator configuration spacecraft designed to be teleoperated from the ground via a TDRS/EDRS communications link to service satellites in orbit. It is important to note that the techniques presented are completely general and that ATLAS in this respect serves merely as an example application. The other side of the coin is that ATLAS is perceived to be a potentially useful and economically viable space system and so this thesis is also in part a proposal and systems design.

Chapter 2 is the beginning of the survey of robotics techniques. This chapter is concerned with robot kinematics and the problem of defining joint angles, joint angle rates, and joint angle accelerations that correspond to those variables as defined at the end effector. The trajectory is generally defined in terms of the end effector motion while control is implemented at the joints. This is fundamentally a trigonometric problem that is based on the geometry of the robotic manipulator. The inverse position kinematics is particularly important as the velocity and acceleration kinematics are ultimately dependent on it.

Chapter 3 is concerned with robot dynamics so that given the solution to the kinematics problem (ie. finding the joint variables from the end effector variables) it is possible to calculate the joint motor actuator torques to produce those joint variables and thereby track the required cartesian trajectory of the end effector. The Newton-Euler method is explored as a recursive method to yield rapid outputs.

Chapter 4 is concerned with trajectory generation such that given a start point and a finish point in end effector coordinates it is possible to generate a trajectory between them by computing intermediate "knot" points along the cartesian path. This provides the means to determine the position, velocity and acceleration profile of the end effector. The inverse solutions are then computed at each knot point to yield those trajectories. Joint interpolation routines are then introduced which may be used to interpolate each joint trajectory between each inverse solution. The issue of computational resources is then explored.

Chapter 5 is concerned with robot control methodologies. It concerns both position and force control to reduce the error between specified desired behaviour and the actual behaviour. It is generally considered that the robot problem is precisely the control problem and for this reason it is given a substantial hearing. The control laws essentially utilise the techniques introduced in previous chapters: the kinematic conversion and the dynamics algorithms are employed to provide the inputs to the

control law. Force feedback is particularly important as it provides the means to manipulate to within precise bounds.

Chapter 6 is the meat of the thesis. This chapter is the central core of the whole approach adopted in this thesis. It derives from first principles the modifications required to the robotic techniques of the preceding chapters to operate in a zero-gravity environment. The approach is that of the mathematical proof through a series of well defined steps. As such it provides a rigour unobtainable from a computer model and validation will ultimately only be tested in hardware implementation. This chapter is virtually all completely original and represents the first (to the author's knowledge) comprehensive series of methodologies and techniques that are completely generally applicable to the space robot control problem. The same methodology is applied to the case of a dual manipulator system.

Chapter 7 represents an introduction to the example ATLAS robotic freeflyer spacecraft. This chapter provides an overall systems overview of the proposed ATLAS freeflyer robotic servicer including the spacecraft bus as well as the total robotic payload complement. It is the result of consideration of the various spacecraft subsystems and their trade offs in impacting the mission design. It is stressed that the systems design and tradeoffs are not trivial matters for a robotic servicer, particularly concerning problems of logistics and resupply.

Chapter 8 is concerned with the space mission profile and the spacecraft bus attitude control system. The mission profile discusses the orbital aspects of the spacecraft mission. The attitude control system is one of the central components of the spacecraft in dominating the spacecraft bus design and it is this component with which the robot control system interacts most strongly. Hence it is the only spacecraft subsystem covered in any detail.

Chapter 9 sets the economic, political and legal scene in which ATLAS operates. Its central thrust is to show that the ATLAS concept has the potential to be highly profitable. However its commercial attractiveness depends on the degree of state support during the earlier years of development. The legal environment also imposes constraints on the type of operations that may or may not be conducted.

Chapter 10 considers the simulation program which was written to derive data concerning the performance of the control techniques of Chapter 6. It utilised data from the other chapters including Chapter 7 for the program parameters derived for the ATLAS robotic freeflyer to obtain realistic results rather than adopting uncritical assumptions.

Chapter 11 concludes the thesis. A simulation of a space-based manipulator system (based on the ATLAS system) provides some indication of the required power outputs and the reaction torques generated on the spacecraft mounting platform by the manipulator movements. Force control as expected substantially affects the requirements in both cases. A brief mention is made of wider issues concerning robotic spacecraft and the proposed ATLAS robotic freeflyer in particular.

Chapter 2

ROBOT KINEMATIC CONTROL

Most machines (defined as transducer devices used to apply mechanical power) are kinematic chains such that they comprise paired links between which there is relative motion at the joint. Indeed most are reducible to one of two kinematic chains: the four-bar chain and the slider-crank chain. The four-bar chain comprises 4 rigid bodies connected in a closed chain by pivots, eg. the human knee. The slider-crank is in fact a special case of the four-bar chain with one of the 4 members replaced by the slider. A complete revolution of the crank causes a reciprocating motion of the slider, eg. the single slider-crank chain forms the basis of the simple reciprocating engine:

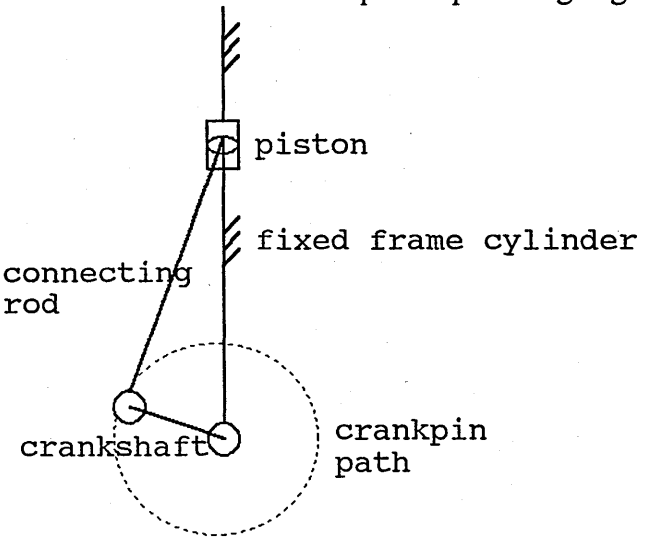

If the mating elements are in contact across a surface then the joint is a lower pair such as those characterising linkages; if the mating elements contact at a point or line then the joint is a higher pair such as those characterising gears. Robotic manipulators are serial multiple-link kinematic chains that are powered by motors at the lower-pair joints between the links. The robot manipulator is unique in all of Man's technological creations in that it is a general purpose tool. When used with advanced sensors and an information processing computer, the resultant system embodies all the characteristics that mark Man from the rest of the animal kingdom: binocular vision for high resolution data processing, complex symbol manipulation and information transmission, and opposable fingered gripping hand and tool use for complex manipulation to change the state of the environment.

A robot manipulator must have 6 joints to provide the 6 orthogonal degrees of freedom (DOF) in position and orientation required to produce any arbitrary position and orientation within a given workspace. For a general configuration 6 DOF robot, there are 6^6 =46656 different kinematic chain configurations possible. By decoupling the first 3 DOF into arm positioning variables and the final 3 DOF into an orienting spherical wrist where the 3 intersecting wrist axes are oriented at 0^o or 90^o to each other, there exist 20 arm and 12 wrist configurations which allow closed form analytic solutions to the inverse kinematics problem. This effectively allows the decomposition of a 6 DOF problem into two 3 DOF computations, one for the arm position and the other for wrist orientation. By eliminating degenerate, equivalent and planar configurations, 12 arm configurations and 5 wrist configurations are possible [Wang &

Lien 1988]. There 6 different lower pair joints (revolute, prismatic, cylindrical, spherical, screw and planar), but only revolute and prismatic joints are used in robotic manipulators whereby the two surfaces slide over each other while remaining in contact, so that each joint has one degree of freedom. The other joint types are merely implementations to achieve the same function (eg. the screw joint to provide translational motion through rotary motion) or provide additional degrees of freedom in their function (eg. the spherical joint which allows three degrees of freedom). From these two types of joint there are 4 common arm configurations and 2 common wrist configurations when neighbouring joint axes are either parallel or perpendicular to each other. The spherical wrist enables derivation of its position from the position of the end effector directly.

1. $R\perp R\|R$ (revolute configuration) - this comprises ~25% of industrial robots, eg. PUMA 560/600.

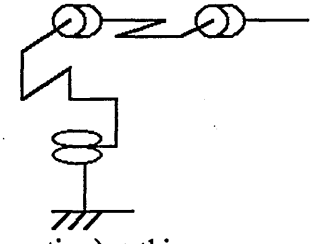

2. $R\perp R\perp L$ (spherical configuration) - this corresponds to ~13% of industrial robots, eg. Stanford arm.

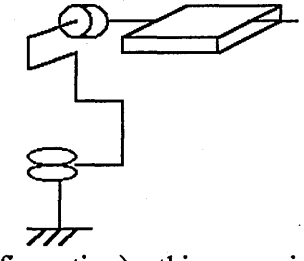

3. $R\|L\perp L$ (cylindrical configuration) - this comprises ~47% of industrial robots

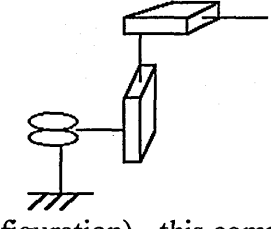

4. $L\perp L\perp L$ (cartesian configuration) - this comprises ~14% of industrial robots

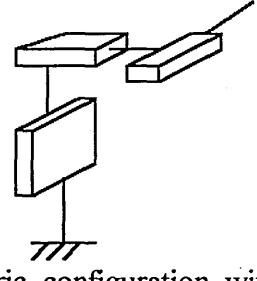

The $R\perp R\|R$ geometric configuration with all revolute joints yields the maximum workspace. It also allows a simple sequence of motions to perform the basic human arm motions of lift in the vertical direction, sweep along the horizontal direction and reach in the line of sight as well as motion in a spherical workspace. The wrist configuration requires all 3 neighbouring wrist axes to intersect at a point and are perpendicular or parallel to each other. Each wrist joint is a revolute joint and the 2 forms are: ZYZ Euler angle sequence or YXZ roll-pitch-yaw sequence, eg. Unimation

PUMA 560/600 has RRR arm and Euler configuration wrist while the Cincinatti Milacron T^3 has RRR arm and a RPY configuration wrist. The Euler angle sequence bears direct relations with the twist-turn-tilt motions commonly exhibited by human wrist actions and is the commonest convention. The human wrist very rarely engages in yaw motions and the ZYZ wrist double roll provides great flexibility in anthromorphic tasks. The roll axis also provides redundancy for rotary tools. Furthermore, the ZYZ wrist tends to be more compact than the RPY wrist.

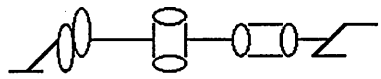

In terms of the kinematic formulation, a 6 DOF robot comprises 6 sequential links and 6 joints with the last 2 links having zero length and mass - the wrist parameters characterising the last 3 joints are lumped into the last link. This spherical wrist then enables the derivation of the end effector position directly from the wrist position/orientation. The end effector/tool parameters are usually lumped with the wrist into the final link. The end effector is usually a dextrous multifunctional gripper (either 2 parallel jaw gripper or 3-fingered hand) which in fact offer additional degrees of freedom beyond the manipulators' normal 6 DOF (degrees of freedom). In addition, specialised tools, eg. capture tools, ORU replacement tools, connector engagement tools, etc may be replaced in substitution to the end effector. Such tools could be stored in a carousel mounted onto the spacecraft lower assembly [Elfving 1990].

The robot control problem may be characterised in the statement that task requirements are normally specified in terms of cartesian world coordinates describing the motion and trajectory of the end effector, while control and commanding of the robot actuators is performed at the joints by motor torque generation. The desired motion of the end effector is specified as a trajectory in cartesian coordinates whilst the control system requires inputs in joint coordinates. Furthermore, proprioceptive sensors generate data concerning the actual state of the environment at joint level. This implies a requirement for expressing the kinematic variables of position, velocity and acceleration in both end effector cartesian coordinates and the equivalent joint coordinates. Hence, the robot control problem comprises 3 separate computational problems:

(i) the determination of the desired trajectory in cartesian world coordinates;

(ii) the transformation of the cartesian trajectory into equivalent body (joint) coordinates;

(iii) the generation of the motor torque commands to realise the trajectory.

For smooth straight line trajectories, several joint motors must be driven simultaneously at different rates in a coordinated fashion to generate steady hand (end effector) motion. The relationship between joint kinematic variables and cartesian end effector kinematic variables is given by complex trigonometric transformations. This defines resolved motion control whereby given the end effector cartesian kinematic variables, we need to find the equivalent inverse joint kinematic variables in order to drive the joint actuators.

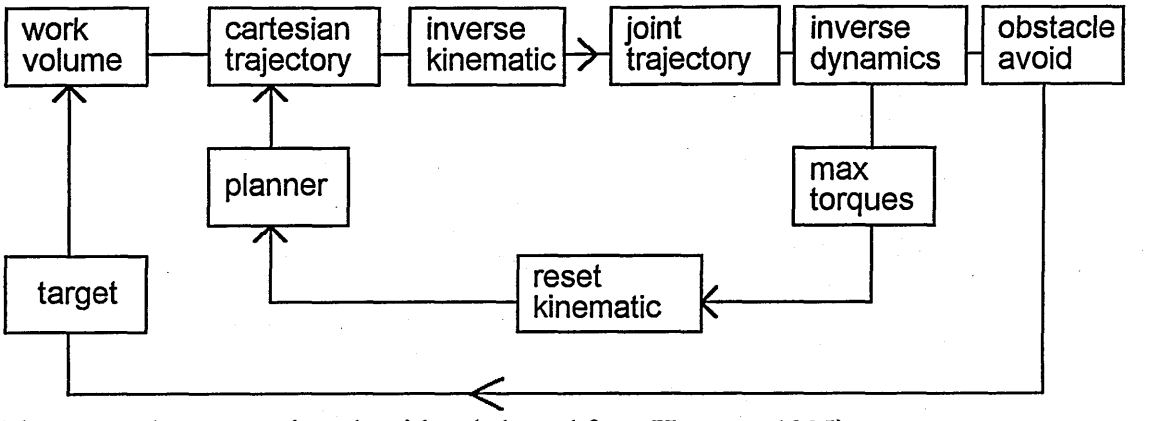

Fig 2.1. Path construction algorithm (adapted from Hamman 1985)

Kawato et al (1988) suggested that these are precisely the computations that are carried out neurally in the human brain in voluntary movement and this provides an illustrative example of the robot control algorithm as a whole. Areas 2,5 and 7 of the sensory-association cortex perform coordinate transformation and the generation of motor commands. Area 2 produces motor torque commands while areas 5 and 7 provide the cartesian trajectory and their transformation into joint coordinates. The parietal-association cortex receives visual and sensory information about the world. Neural circuits are capable of computing the nonlinear transformation and the inverse dynamics model of the musculoskeletal system through motor learning. This motor learning provides a nonlinear mapping between the torque input and the trajectory output by cross-correlation. Now we consider the transformation between cartesian and joint coordinates of kinematic variables which is central to robotics.

2.1 RESOLUTION OF POSITION COORDINATES

The direct kinematics problem is concerned with the transformation of joint coordinate angles (angular rates and angular accelerations) into the equivalent cartesian coordinates (velocities and accelerations) of the end effector. The inverse kinematics problem is to find the joint coordinate angles (angular rates and angular accelerations) that correspond to a given set of cartesian coordinates (velocities and accelerations) of the end effector. It is the inverse kinematics relation that is required by the control system. It is assumed that the manipulator base coincides with world coordinates from which all tasks are referred (a possible alternative world coordinates system may be defined at the workpiece). It is considered that such actor-oriented reference coordinate frames are natural for describing events relative to the robot.

2.1.1 Forward Position Kinematics Solution:

Robotic links are characterised by two parameters ("i" subscript signifies joint number counted consecutively from the base of the manipulator): link length a_i (common normal distance between joint axes z_{i-1} and z_i) and offset link twist angle α_i (angle between axes z_{i-1} and z_i perpendicular to a_i). These 2 parameters determine the link structure. Joints are characterised by two parameters: offset distance d_i (distance between 2 joint axis normals x_{i-1} and x_i) and joint angle θ_i (angle between normals perpendicular to joint axes z_{i-1} and z_i). These 2 parameters determine the relative

positioning of each link. For prismatic joints, a_i is variable and θ_i is constant while for revolute joints, θ_i is variable and a_i is constant. For both joints d_i and α_i are constant parameters of the link and joint and define the geometry of the robot manipulator.

Coordinate frames are assigned to each link at the intersection of the common normal at the joint axis. Base coordinates represent the coodinate frame at the origin of link 1. Hand coordinates represent the coordinate frame at the end effector. By convention, coordinate frames are designated by [Paul 1981, Paul et al 1981a,b]:
(i) z_{i-1} axis of joint i lies parallel to the rotation axis of joint i;
(ii) x_i axis of joint i is perpendicular to the z_{i-1} axis and points away from it;
(iii) y_i axis of joint i satisfies a right-hand coordinate system contraint.

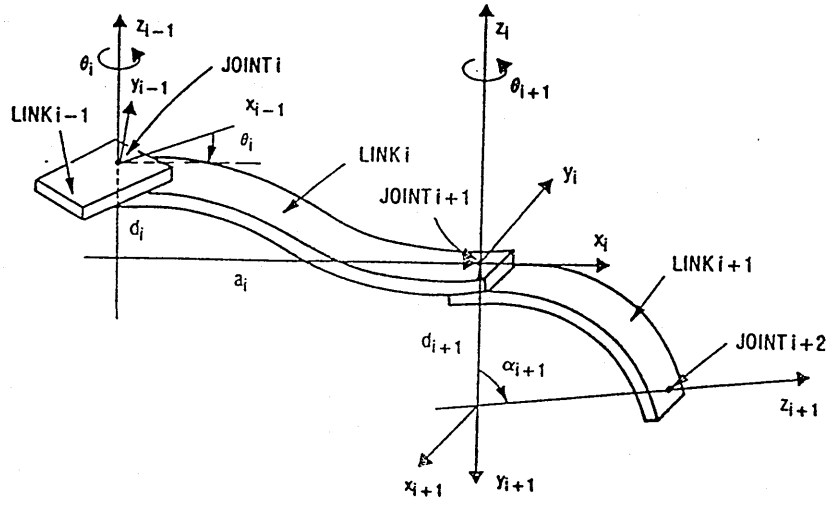

Fig 2.2. Robot link and joint kinematic variables [from Paul 1981]

For virtually all control operations, kinematic transformation has to be performed before any other transformations. The Denavit-Hartenberg (DH) 4x4 homogeneous "A" matrix transforms between each coordinate reference frame assigned to each link at each joint sequentially from the base of the manipulator $(x_0y_0z_0)$ to the end effector $(x_ny_nz_n)$ through each link [Denavit & Hartenberg 1955; Paul, Shimano & Meyer 1981]. The 4x4 DH matrix incorporates all link parameters in the position vector submatrix and contains a 3x3 direction cosine matrix and floating row. Successive multiplication of these coordinate frames will yield the required coordinates of the manipulator end effector with respect to base (world) coordinates.
The DH matrix that represents this sequence of events is constructed thus:
(i) rotate through θ_i about the z_{i-1} axis to align the x_{i-1} axis with the x_i axis: $\mathrm{Rot}(z_{i-1},\theta_i)$
(ii) translate by d_i along the z_{i-1} axis to coincide x_{i-1} and x_i axes: $\mathrm{Trans}(0,0,d_i)$
(iii) translate by a_i along the x_i axis to coincide the two coordinate frame origins: $\mathrm{Trans}(a_i,0,0)$
(iv) rotate through α_i about the x_i axis to coincide the two coordinate frames completely: $\mathrm{Rot}(x_i,\alpha_i)$
The DH "A"-matrix that represents this sequence of events has the form:

$$A_i^{i-1} = \mathrm{Rot}(z_{i-1},\theta_i)\mathrm{Trans}(0,0,d_i)\mathrm{Trans}(a_i,0,0)\mathrm{Rot}(x_i,\alpha_i)$$

$$= \begin{pmatrix} \cos\theta_i & -\sin\theta_i & 0 & 0 \\ \sin\theta_i & \cos\theta_i & 0 & 0 \\ 0 & 0 & 1 & 0 \\ 0 & 0 & 0 & 1 \end{pmatrix} \begin{pmatrix} 1 & 0 & 0 & 0 \\ 0 & 1 & 0 & 0 \\ 0 & 0 & 1 & d_i \\ 0 & 0 & 0 & 1 \end{pmatrix} \begin{pmatrix} 1 & 0 & 0 & a_i \\ 0 & 1 & 0 & 0 \\ 0 & 0 & 1 & 0 \\ 0 & 0 & 0 & 1 \end{pmatrix} \begin{pmatrix} 1 & 0 & 0 & 0 \\ 0 & \cos\alpha_i & -\sin\alpha_i & 0 \\ 0 & \sin\alpha_i & \cos\alpha_i & 0 \\ 0 & 0 & 0 & 1 \end{pmatrix}$$

$$= \begin{pmatrix} \cos\theta_i & -\cos\alpha_i \sin\theta_i & \sin\alpha_i \sin\theta_i & a_i \cos\theta_i \\ \sin\theta_i & \cos\alpha_i \cos\theta_i & -\sin\alpha_i \cos\theta_i & a_i \sin\theta_i \\ 0 & \sin\alpha_i & \cos\alpha_i & d_i \\ 0 & 0 & 0 & 1 \end{pmatrix}$$

This is the DH matrix for a revolute or prismatic joint. In both cases, the link structure parameters a_i and α_i are constant. For a prismatic joint θ_i is constant and d_i is variable; for a revolute joint d_i is constant and θ_i is variable. This matrix transforms a point P_{i-1} to point P_i: $P_i = A_i^{i-1} P_{i-1}$. This 4x4 matrix may be partitioned into two submatrices which represent the rotational and translational components:

$$A_i^{i-1} = \begin{pmatrix} R_i & p_i \\ 0 & 1 \end{pmatrix}$$

where $R_i = \begin{pmatrix} \cos\theta_i & -\sin\theta_i \cos\alpha_i & \sin\theta_i \sin\alpha_i \\ \sin\theta_i & \cos\theta_i \cos\alpha_i & -\cos\theta_i \sin\alpha_i \\ 0 & \sin\alpha_i & \cos\alpha_i \end{pmatrix}$ and $p_i = \begin{pmatrix} a_i \cos\theta_i \\ a_i \sin\theta_i \\ d_i \end{pmatrix}$

The DH formulation provides a means of relating joint coordinates for the servo control system to cartesian coordinates for task characterisation, and this relation is nonlinear. The elements of these matrices are complex trigonometric functions. For a 6 DOF robot manipulator, 6 DH "A" matrices, one for each link, are required to transform from base coordinates to hand coordinates (direct kinematics problem). Base coordinates are the body (world) coordinates lying at the base of the manipulator.

The final matrix (sometimes called the T-matrix) has the form (n defines the number of degrees of freedom) with generalised position coordinates:

$$q = T_{0n} = f(\theta) = \sum_{i=1}^{n} A_i(\theta) = A_1^0 \ldots A_n^{n-1} = \begin{pmatrix} x_6 & y_6 & z_6 & p_6 \\ 0 & 0 & 0 & 1 \end{pmatrix} = \begin{pmatrix} n & s & a & p \\ 0 & 0 & 0 & 1 \end{pmatrix}$$

where

$$\begin{aligned} n &= (n_x n_y n_z)^T \\ s &= (s_x s_y s_z)^T \\ a &= (a_x a_y a_z)^T \\ p &= (p_x p_y p_z)^T \end{aligned} \qquad (2.1)$$

where **n**= normal vector perpendicular to the fingers at the end effector (tilt);

s=slide vector parallel to the finger grip direction of the end effector (twist);

a= approach vector perpendicular to the palm of the end effector (turn);

p=position vector of the hand with respect to base coordinates (sweep, reach, lift).

An alternative form represents the rotational 3x3 and translational 3x1 components separately - it is this representation that is used in Chapter 6 for application to the space environment as the translational and rotational components are treated separately:

Generalised position coordinates:

$$q = T_{0n} = \sum_{i=1}^{n} R_i p_i \qquad (2.2)$$

Note that $R_n^0=(x_6, y_6, z_6)=(\mathbf{n\ s\ a})$

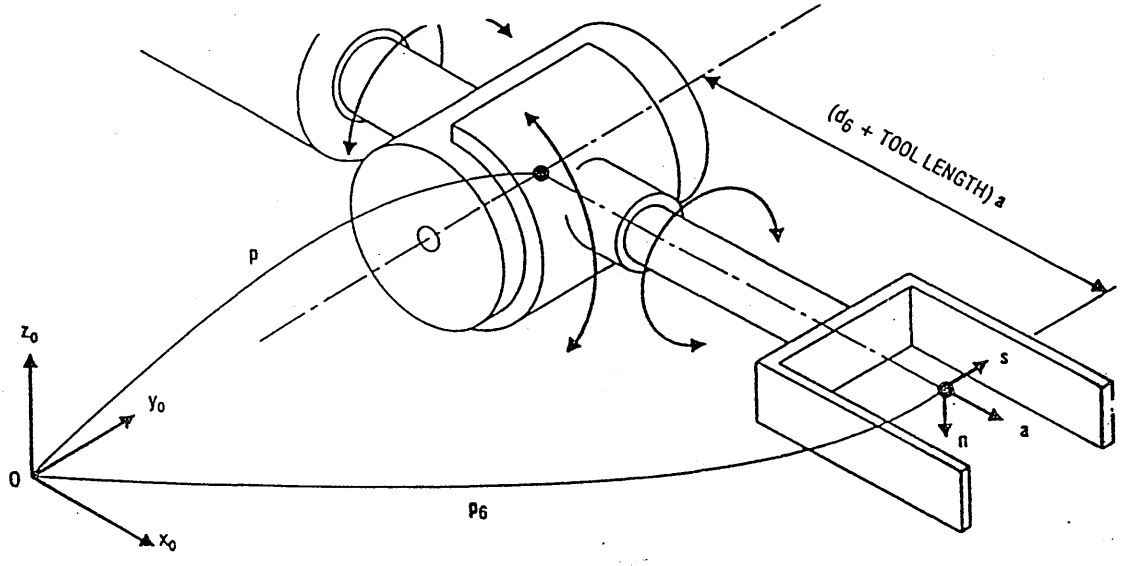

Fig 2.3 Hand coordinates with respect to base coordinates [from Fu, Gonzalez & Lee 1987]

A robot manipulator geometry derived from the Unimate PUMA 560/600 has been selected as the test case because:
(i) it represents a generalised 6 DOF configuration of revolute joints;
(ii) it yields closed form analytic solutions to the inverse kinematics problem;
(iii) the PUMA is widespread and has been the workhorse for robotics research for many years (though this place is now being eroded by the Cincinnatti Milacron T3);
(iv) it is anthromorphic being based on the human arm geometry facilitating manoeuvrability and flexibility of operation (though the human upper arm has 3 degrees of freedom at the shoulder through a ball joint).
The author also suggests that a 6 DOF manipulator system is more appropriate for space application than a redundant design since a spacecraft mounting already possesses inherent redundancy by virtue of the 6 DOF of the mounting platform. Furthermore, additional links on the manipulator arm imposes additional and unnecessary mass penalties.

The matrix representation of rotation in the DH matrix has 9 elements in the 3x3 R-submatrix representation. They are not generalised independent coordinates. However, an Euler angle set can provide such a representation describing the orientation of a rigid body target with respect to a world reference frame. Several possibilities exist according to the rotation sequence, but the RPY sequence is popular and is intuitively straight forward. It is used for aerospace vehicles to describe their orientations about reference principal coordinate axes. For roll R about the x axis, pitch P about the y axis and yaw Y about the z axis:

$$R_{ypr} = \begin{pmatrix} cR & -sR & 0 \\ sR & cR & 0 \\ 0 & 0 & 1 \end{pmatrix}\begin{pmatrix} cP & 0 & sP \\ 0 & 1 & 0 \\ -sP & 0 & cP \end{pmatrix}\begin{pmatrix} 1 & 0 & 0 \\ 0 & cY & -sY \\ 0 & sY & cY \end{pmatrix} = \begin{pmatrix} cRcP & cRsPsY - sRcY & cRsPcY + sRsY \\ sRcP & sRsPsY + cRcY & sRsPcY - cRsY \\ -sP & cPsY & cPcY \end{pmatrix}$$

Equating these to the (n s a) rotational submatrix:

$n_x = \cos R \cos P$

$n_y = \sin R \cos P$

$n_z = -\sin P$

$s_x = \cos R \sin P \sin Y - \sin R \cos Y$

$s_y = \sin R \sin P \sin Y + \cos R \cos Y$

$s_z = \cos P \sin Y$

$a_x = \cos R \sin P \cos Y + \sin R \sin Y$

$a_y = \sin R \sin P \cos Y - \cos R \sin Y$

$a_z = \cos P \cos Y$

Solutions are given by:

$P = -\sin^{-1}(n_z)$

$R = \cos^{-1}(n_x / \cos P)$

$Y = \cos^{-1}(a_z / \cos P)$

However, these solutions are ill-conditioned because $\cos\theta = \cos(-\theta)$ and $\sin^{-1}\theta = 0$ when $\theta = 0$ or 180. To use the $\tan^{-1}$ function, rearrange the equation equating (n s a) to RPY angles:

$$\begin{pmatrix} n_x & s_x & a_x \\ n_y & s_y & a_y \\ n_z & s_z & a_z \end{pmatrix} = \begin{pmatrix} cR & -sR & 0 \\ sR & cR & 0 \\ 0 & 0 & 1 \end{pmatrix}\begin{pmatrix} cP & 0 & sP \\ 0 & 1 & 0 \\ -sP & 0 & cP \end{pmatrix}\begin{pmatrix} 1 & 0 & 0 \\ 0 & cY & -sY \\ 0 & sY & cY \end{pmatrix}$$

$$\begin{pmatrix} cR & sR & 0 \\ -sR & cR & 0 \\ 0 & 0 & 1 \end{pmatrix}\begin{pmatrix} n_x & s_x & a_x \\ n_y & s_y & a_y \\ n_z & s_z & a_z \end{pmatrix} = \begin{pmatrix} cP & 0 & sP \\ 0 & 1 & 0 \\ -sP & 0 & cP \end{pmatrix}\begin{pmatrix} 1 & 0 & 0 \\ 0 & cY & -sY \\ 0 & sY & cY \end{pmatrix}$$

$$\begin{pmatrix} cRn_x + sRn_y & cRs_x + sRs_y & cRa_x + cRa_y \\ -sRn_x + cRn_y & -sRs_x + cRs_y & -sRa_x + cRa_y \\ n_z & s_z & a_z \end{pmatrix} = \begin{pmatrix} cP & sPsY & sPcY \\ 0 & cY & -sY \\ -sP & cPsY & cPcY \end{pmatrix}$$

Hence, $-sRn_x + cRn_y = 0 \rightarrow -sRn_x = -cRn_y$

$\rightarrow sR/cR = (n_y / n_x) \rightarrow R = \tan^{-1}(n_y / n_x)$

Similarly, $\tan P = sP/cP \rightarrow P = \tan^{-1}\left(\frac{-n_z}{cRn_x + sRn_y}\right)$

and $\tan Y = sY/cY \rightarrow Y = \tan^{-1}\left(\frac{sRa_x - cRa_y}{-sRs_x + cRs_y}\right)$

The following parameters are similar to those of the PUMA 560/600 which is modelled on the human arm geometry except that the link lengths are slightly longer for a larger workspace, there is no offset at the elbow and the elbow joint ranges have been reversed to favour the elbow down configuration over the elbow up configuration (the elbow up configuration may obscure the workspace) [Lee & Zeigler 1984].

Joint:	Variable:	α_i(º):	a_i(m):	d_i(m):	Range(º):	Range midpoint,β_i(º):
1	θ_1	-90	0	0	-160 to 160	0
2	θ_2	0	0.5	0.25	-45 to 225	90
3	θ_3	90	0	0	-225 to -45	-90
4	θ_4	-90	0	0.5	-110 to 170	30
5	θ_5	90	0	0	-100 to 100	0
6	θ_6	0	0	0.2	-266 to 266	0

For a freeflyer space robot system, these restrictions on joint angles would be much less severe due to the requirement for flexible operations. Conceptually, the robot manipulator workspaces must cover both the forward region of space and the overhead region of space. This coverage of two regions allows constraints to be placed on the spacecraft design which would otherwise be difficult to constrain.

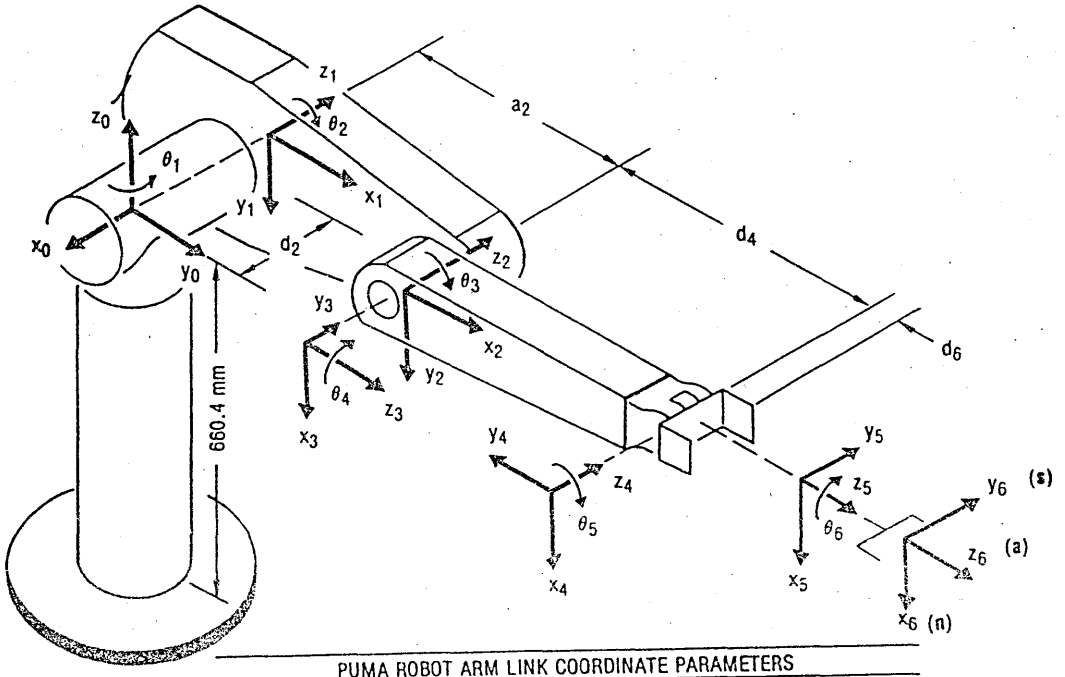

PUMA ROBOT ARM LINK COORDINATE PARAMETERS

JOINT i	ϑ_i	α_i	a_i	d_i	RANGE
1	90	−90	0	0	−160 to +160
2	0	0	432 mm	149.5 mm	−225 to +45
3	90	90	0	0	−45 to +225
4	0	−90	0	432.0	−110 to +170
5	0	90	0	0	−100 to +100
6	0	0	0	56.5	−266 to +266

2.4 PUMA 560/600 kinematic configuration [from Lee 1982]

Using these parameters in the DH matrix scheme,

$$A_1^0 = \begin{pmatrix} c_1 & 0 & -s_1 & 0 \\ s_1 & 0 & c_1 & 0 \\ 0 & -1 & 0 & 0 \\ 0 & 0 & 0 & 1 \end{pmatrix}, A_2^1 = \begin{pmatrix} c_2 & -s_2 & 0 & a_2c_2 \\ s_2 & c_2 & 0 & a_2s_2 \\ 0 & 0 & 1 & d_2 \\ 0 & 0 & 0 & 1 \end{pmatrix}, A_3^2 = \begin{pmatrix} c_3 & 0 & s_3 & 0 \\ s_3 & 0 & -c_3 & 0 \\ 0 & 1 & 0 & 0 \\ 0 & 0 & 0 & 1 \end{pmatrix},$$

$$A_4^3 = \begin{pmatrix} c_4 & 0 & -s_4 & 0 \\ s_4 & 0 & c_4 & 0 \\ 0 & -1 & 0 & d_4 \\ 0 & 0 & 0 & 1 \end{pmatrix}, A_5^4 = \begin{pmatrix} c_5 & 0 & s_5 & 0 \\ s_5 & 0 & -c_5 & 0 \\ 0 & 1 & 0 & 0 \\ 0 & 0 & 0 & 1 \end{pmatrix}, A_6^5 = \begin{pmatrix} c_6 & -s_6 & 0 & 0 \\ s_6 & c_6 & 0 & 0 \\ 0 & 0 & 1 & d_6 \\ 0 & 0 & 0 & 1 \end{pmatrix} \quad (2.3)$$

where $s_i = \sin\theta_i$ and $c_i = \cos\theta_i$.

The parameters are measured from the principal axes of the links through their respective centres of mass. Link 0 is the stationary pillar link bolted to a platform. Coordinates (x_i, y_i, z_i) are associated with joint i-1 so that z_{i-1} is the axis of rotation for joint i. If an end effector or tool is used whose origin or axes do not coincide with the coordinate system of link 6, the tool must be related by a constant transform E to link 6. It is assumed generally that the tool origin does coincide with the link origin and its dimensions are included in the d_6 end effector term in A_6^5.

To exploit the structure of the equations and avoid the extraneous computations of "0's" and "1's" in the floating row [Roth 1985], the usual procedure is to partition the computation into two parts, each of which is performed by hand, leaving the computer to do the final number-crunching in multiplying the two resultant matrices:

$T_{0n} = T_1T_2 = A_3^0A_6^4 = (A_1^0A_2^1A_3^2)(A_4^3A_5^4A_6^5)$

For the first three matrix multiplications:

$$T_1 = A_3^0 = \begin{pmatrix} c_1c_{23} & -s_1 & c_1s_{23} & a_2c_1c_2 - s_1d_2 \\ s_1c_{23} & c_1 & s_1s_{23} & a_2s_1c_2 + c_1d_2 \\ -s_{23} & 0 & c_{23} & -a_2s_2 \\ 0 & 0 & 0 & 1 \end{pmatrix} \text{ where } \begin{matrix} s_{ij} = c_js_i + c_is_j \\ c_{ij} = c_ic_j - s_is_j \end{matrix}$$

The last three matrix multiplications:

$$T_2 = A_6^4 = \begin{pmatrix} c_4c_5c_6 - s_4s_6 & -c_4c_5s_6 - s_4c_6 & c_4s_5 & c_4s_5d_6 \\ s_4c_5c_6 + c_4s_6 & -s_4c_5s_6 + c_4c_6 & s_4s_5 & s_4s_5d_6 \\ -c_6s_5 & s_5s_6 & c_5 & c_5d_6 + d_4 \\ 0 & 0 & 0 & \end{pmatrix}$$

Hence, $T_{0n} = T_1T_2 = A_n^0 = \begin{pmatrix} n_x & s_x & a_x & p_x \\ n_y & s_y & a_y & p_y \\ n_z & s_z & a_z & p_z \\ 0 & 0 & 0 & 1 \end{pmatrix}$

where $p_x = c_1[d_6(c_{23}c_4s_5 + s_{23}c_5) + s_{23}d_4 + a_2c_2] - s_1(s_4s_5d_6 + d_2)$

$p_y = s_1[d_6(c_{23}c_4s_5 + s_{23}c_5) + s_{23}d_4 + a_2c_2] + c_1(s_4s_5d_6 + d_2)$

$p_z = d_6[c_{23}c_5 - s_{23}c_4s_5] + c_{23}d_4 - a_2s_2$

$n_x = c_1[c_{23}(c_4c_5c_6 - s_4s_6) - s_{23}c_6s_5] - s_1(s_4c_5c_6 + c_4s_6)$

$$
\begin{aligned}
n_y &= s_1[c_{23}(c_4c_5c_6 - s_4s_6) - s_{23}s_5c_6] + c_1(s_4c_5c_6 + c_4s_6)\\
n_z &= -s_{23}(c_4c_5c_6 - s_4s_6) - c_{23}c_6s_5\\
s_x &= -c_1[c_{23}(c_4c_5s_6 + s_4c_6) - s_{23}s_5s_6] + s_1(s_4c_5s_6 - c_4c_6)\\
s_y &= -s_1[c_{23}(c_4c_5s_6 + s_4c_6) - s_{23}s_5s_6] + c_1(c_4c_6 - s_4c_5s_6)\\
s_z &= s_{23}(c_4c_5s_6 + s_4c_6) + c_{23}s_5s_6\\
a_x &= c_1(c_{23}c_4s_5 + s_{23}c_5) - s_1s_4s_5\\
a_y &= s_1(c_{23}c_4s_5 + c_5s_{23}) + c_1s_4s_5\\
a_z &= -s_{23}c_4s_5 + c_{23}c_5
\end{aligned}
\qquad (2.4)
$$

To check that the forward kinematics solution is correct, the stowed configuration has joint angles $\theta_1 = 90, \theta_2 = 90, \theta_3 = 90, \theta_4 = \theta_5 = \theta_6 = 0$ yielding

$p_x = -d_2, p_y = d_4 + d_6, p_z = -a_2$ and $R_6^0 = I_3$ as expected.

2.1.2 Inverse Position Kinematics Solution:

The inverse solution is to find the joint angles θ for given cartesian variables q, ie. $\theta = f^{-1}(q)$. This is the information required for the robot control system. To find the inverse solution of joint angles corresponding to a particular end effector configuration in cartesian space it is necessary to decouple the angular components of the wrist from the position components of the arm. For a six degree of freedom manipulator with six joints employing a spherical wrist where the last three orienting degrees of freedom intersect, closed form analytic solutions are possible. The position of the wrist subassembly may be found to separate the wrist orientation from the arm positioning assembly since the wrist contributes a distance d_6 in the direction of the approach vector to the final position of the end effector:

$$
\begin{pmatrix} p_x \\ p_y \\ p_z \end{pmatrix} = \begin{pmatrix} p_x^{arm} \\ p_y^{arm} \\ p_y^{arm} \end{pmatrix} + \begin{pmatrix} p_x^{wrist} \\ p_y^{wrist} \\ p_z^{wrist} \end{pmatrix} = \begin{pmatrix} p_x^{arm} \\ p_y^{arm} \\ p_z^{arm} \end{pmatrix} + d_6 \begin{pmatrix} a_x \\ a_y \\ a_z \end{pmatrix}
$$

$$
\begin{pmatrix} p_x^{arm} \\ p_y^{arm} \\ p_z^{arm} \end{pmatrix} = \begin{pmatrix} p_{4x}^0 \\ p_{4y}^0 \\ p_{4z}^0 \end{pmatrix} = \begin{pmatrix} p_x \\ p_y \\ p_z \end{pmatrix} - \begin{pmatrix} p_x^{wrist} \\ p_y^{wrist} \\ p_z^{wrist} \end{pmatrix} = \begin{pmatrix} p_x \\ p_y \\ p_z \end{pmatrix} - d_6 \begin{pmatrix} a_x \\ a_y \\ a_z \end{pmatrix} = \begin{pmatrix} c_1(a_2c_2 + d_4s_{23}) - d_2s_1 \\ s_1(a_2c_2 + d_4s_{23}) + d_2c_1 \\ d_4c_{23} - a_2s_2 \end{pmatrix} \qquad (2.5)
$$

For solutions to the inverse kinematic problem, a well-balanced trigonometric function is required: cosines and sines are often undefined or multivalued, so the arctangent is used with proper quadrants.

$\theta = \tan^{-1}(y/x)$ 0<theta<90 for x>0 & y>0

90<theta<180 for x<0 & y>0

-180<theta<-90 for x<0 & y<0

-90<theta<0 for x>0 & y<0

The position of the arm is determined by the first three positioning links d_2 ,a_2 ,d_4 and the first 3 joint angles $\theta_1, \theta_2, \theta_3$ [Lee & Ziegler 1984; Lee 1982; Fu Gonzalez & Lee 1987].

To find θ_1:

$$
-s_1p_x^{arm} + c_1p_y^{arm} = -s_1\{c_1(a_2c_2 + d_4s_{23}) - d_2s_1\} + c_1\{s_1(a_2c_2 + d_4s_{23}) + d_2c_1\} = d_2
$$

Let $p_x^{arm} = r\cos\varphi, p_y^{arm} = r\sin\varphi$ where $r = \sqrt{(p_x^{arm})^2 + (p_y^{arm})^2}$ and $\varphi = \tan^{-1}\left(p_y^{arm}/p_x^{arm}\right)$

Substitute:

Substitute:

$-(r\cos\varphi)s_1 + (r\sin\varphi)c_1 = d_2$

$\sin\varphi c_1 - \cos\varphi s_1 = d_2 / r \rightarrow \sin(\varphi - \theta_1) = d_2 / r$

Now, $\cos(\varphi - \theta_1) = \sqrt{1 - \sin^2(\varphi - \vartheta_1)} = \sqrt{1 - (d_2 / r)^2}$

ie. $\tan(\varphi - \theta_1) = \frac{d_2/r}{\sqrt{1-(d_2/r)^2}} \rightarrow \theta_1 = \varphi - \tan^{-1}\left[\frac{d_2/r}{\sqrt{1-(d_2/r)^2}}\right] = \varphi - \tan^{-1}\left[\frac{d_2}{\sqrt{r^2-d_2^2}}\right]$

Now, $\tan\varphi = r\sin\varphi / r\cos\varphi = p_y^{arm} / p_x^{arm}$

Hence, $\theta_1 = \tan^{-1}\left(\frac{p_y^{arm}}{p_x^{arm}}\right) - \tan^{-1}\left[\frac{d_2}{\pm\sqrt{(p_x^{arm})^2+(p_y^{arm})^2-d_2^2}}\right]$ (2.6)

The "+" indicates the right arm shoulder configuration and the "-" indicates the left arm shoulder configuration.

To find θ_2:

$c_1 p_x^{arm} + s_1 p_y^{arm} = c_1\{c_1(a_2c_2 + d_4s_{23}) - d_2s_1\} + s_1\{s_1(a_2c_2 + d_4s_{23}) + d_2c_1\} = a_2c_2 + d_4s_{23}$

Let $A = c_1 p_x^{arm} + s_1 p_y^{arm} = a_2c_2 + d_4s_{23} \rightarrow s_{23} = \left(\frac{A - a_2c_2}{d_4}\right)$

Similarly, $p_z^{arm} = d_4c_{23} - a_2s_2 \rightarrow c_{23} = \left(\frac{p_z^{arm} + a_2s_2}{d_4}\right)$

Now, $c_{23}^2 + s_{23}^2 = 1$: $(p_z^{arm} + a_2s_2)^2 + (A - a_2c_2) = d_4^2$

This yields, $-s_2 p_z^{arm} + c_2 A = \frac{A^2 + (p_z^{arm})^2 + a_2^2 - d_4^2}{2a_2} = B$

Let $p_z^{arm} = r\cos\varphi, A = r\sin\varphi$ where $r = \sqrt{A^2 + (p_z^{arm})^2}$ and $\varphi = \tan^{-1}\left(\frac{A}{p_z^{arm}}\right)$

Substitute: $(r\sin\varphi)c_2 - (r\cos\phi)s_2 = B \rightarrow \sin(\varphi - \theta_2) = B / r$

Now, $\cos(\varphi - \theta_2) = \sqrt{1 - (B/r)^2}$

ie. $\tan(\varphi - \theta_2) = \frac{B/r}{\sqrt{1-(B/r)^2}} \rightarrow \theta_2 = \varphi - \tan^{-1}\left[\frac{B}{\sqrt{r^2-B^2}}\right]$

Now, $\varphi = \tan^{-1}\left(\frac{A}{p_z^{arm}}\right)$

Hence, $\theta_2 = \tan^{-1}\left(\frac{A}{p_z^{arm}}\right) - \tan^{-1}\left[\frac{B}{\pm\sqrt{A^2+(p_z^{arm})^2-B^2}}\right]$ (2.7)

The "+" corresponds to the elbow down configuration ($\theta_3 - \theta_2 > 0$) such that the elbow lies below the wrist, and the "-" corresponds to the elbow "up" configuration ($\theta_3 - \theta_2 < 0$) such that the elbow is above the wrist. The elbow down configuration is preferred since the elbow up configuration could obscure the workspace.

To find θ_3:

$\tan(\theta_2 + \theta_3) = s_{23} / c_{23} = \left[\frac{A - a_2c_2}{p_z^{arm} + a_2s_2}\right]$

$\theta_3 = \{\tan^{-1}\left[\frac{A - a_2c_2}{p_z^{arm} + a_2s_2}\right]\} - \theta_2$ (2.8)

To find $\theta_4, \theta_5, \theta_6$ for the wrist joints, the rotational components of the DH matrix formulation are used [Hollerbach & Sahar 1983, Wang & Lien 1988]:

$R_6^0 = R_3^0 R_6^3 = R_{arm}^0 R_{wrist}^{arm}$

$R_6^3 = (R_3^0)^{-1} R_6^0 = (R_3^0)^T R_6^0$ where $R_6^0 = (nsa)$

Now, $(R_3^0)^{-1} = (R_3^0)^T = \begin{pmatrix} c_1c_{23} & s_1c_{23} & -s_{23} \\ -s_1 & c_1 & 0 \\ c_1s_{23} & s_1s_{23} & c_{23} \end{pmatrix}$

Hence, $R^{arm}_{wrist} = \begin{pmatrix} c_1c_{23} & s_1c_{23} & -s_{23} \\ -s_1 & c_1 & 0 \\ c_1s_{23} & s_1s_{23} & c_{23} \end{pmatrix} \begin{pmatrix} n_x & s_x & a_x \\ n_y & s_y & a_y \\ n_z & s_z & a_z \end{pmatrix} = \begin{pmatrix} n^w_x & s^w_x & a^w_x \\ n^w_y & s^w_y & a^w_y \\ n^w_z & s^w_z & a^w_z \end{pmatrix}$

where

$$n^w_x = c_1c_{23}n_x + s_1c_{23}n_y - s_{23}n_z$$
$$n^w_y = -s_1n_x + c_1n_y$$
$$n^w_z = c_1s_{23}n_x + s_1s_{23}n_y + c_{23}n_z$$
$$s^w_x = c_1c_{23}s_x + s_1c_{23}s_y - s_{23}s_z$$
$$s^w_y = -s_1s_x + c_1s_y$$
$$s^w_z = c_1s_{23}s_x + s_1s_{23}s_y + c_{23}s_z$$
$$a^w_x = c_1c_{23}a_x + s_1c_{23}a_y - s_{23}a_z$$
$$a^w_y = -s_1a_x + c_1a_y$$
$$a^w_z = c_1s_{23}a_x + s_1s_{23}a_y + c_{23}a_z$$

Equating these values to R^3_6:

$$R^3_6 = \begin{pmatrix} c_4c_5c_6 - s_4s_6 & -c_4c_5s_6 - s_4c_6 & c_4s_5 \\ s_4c_5c_6 + c_4s_6 & -s_4c_5s_6 + c_4c_6 & s_4s_5 \\ -c_6s_5 & s_5s_6 & c_5 \end{pmatrix} = \begin{pmatrix} n^w_x & s^w_x & a^w_x \\ n^w_y & s^w_y & a^w_y \\ n^w_z & s^w_z & a^w_z \end{pmatrix}$$

Now, $\tan\theta_4 = \frac{s_4s_5}{c_4s_5} = \frac{a^w_y}{a^w_x} \rightarrow \theta_4 = \tan^{-1}\left(\frac{-s_1a_x + c_1a_y}{c_{23}(c_1a_x + s_1a_y) - s_{23}a_z}\right)$ (2.9)

Now, $(c_4s_5)^2 + (s_4s_5)^2 = s_5^2 \rightarrow \sin\theta_5 = \sqrt{(a^w_x)^2 + (a^w_y)^2}$ and $\cos\theta_5 = a^w_z$

ie. $\theta_5 = \tan^{-1}\left[\frac{\sqrt{(c_1c_{23}a_x + s_1c_{23}a_y - s_{23}a_z)^2 + (-s_1a_x + c_1a_y)^2}}{s_{23}(c_1a_x + s_1a_y) + c_{23}a_z}\right]$ (2.10)

Now, $\tan\theta_6 = \frac{s_5s_6}{s_5c_6} = -\frac{s^w_z}{n^w_z} \rightarrow \theta_6 = \tan^{-1} - \left(\frac{s_{23}(c_1s_x + s_1s_y) + c_{23}s_z}{s_{23}(c_1n_x + s_1n_y) + c_{23}n_z}\right)$ (2.11)

This completes the analytic solution to the inverse kinematics problem. Alternatively, numerical techniques are available to solve the inverse kinematics, eg. the Newton-Raphson iteration method:

$q_{k+1} = q_k - f(q_k)/f'(q_k)$ or $\theta_{k+1} = \theta_k - J^{-1}(\theta_k)q_k$ where $q_k = f(\theta_k)$

This method requires the selection of an initial seed estimate and the number of iterations depends on the accuracy of this initial estimate. Usually 4 iterations are sufficient to reach an accuracy of <0.1mm. Numerical methods are much more complex than the closed form analytic solution since they involve inversion of the Jacobian matrix and a close estimate for the initial seed. Being an interpolation approximation, it is also subject to divergence if the initial seed is not sufficiently close to the solution.

2.1.3 Manipulator Workspace

The robot workspace is defined as the region which may be reached by the centre of the manipulator hand. The dextrous primary workspace is defined as the volume within which every point is reachable by the hand at any orientation, ie. the arm must be able

to deliver the wrist subassembly to any point within that sphere. The secondary workspace is reachable from limited directions due to singularities in that workspace: $W_T^{primary}(H) \subset W_T^{secondary}(H)$ [Kumar & Waldron 1981]. At singular points, the end effector loses one or more degrees of freedom since the kinematic equations become linearly dependent or certain solutions become undefined [Featherstone 1983]. One example is when the wrist lies above or below the shoulder such that it is parallel to the z_0 axis of base coordinates. Singular configurations must be avoided as the velocities required to move the end effector become effectively infinite. The solution is to ensure that singular configurations are forbidden within the controller. Wang & Lee (1983,1984) derived a recursive formula for determining the manipulator workspace volume $W_k(H)$ with $H(x_k, y_k, z_k)$ where H denotes the centre of the manipulator hand and $W_k(H)$ denotes the reachable workspace generated by point H by turning all revolute joints k...n within their permitted ranges whilst holding the axis k as fixed. This represents a circle with its centre at the origin of the coordinate frame k:

$$x_k = r_k \cos\theta_k$$
$$y_k = r_k \sin\theta_k \quad \text{and} \quad \begin{pmatrix} x \\ y \\ z \\ 1 \end{pmatrix}_k^* = A_{k+1} \begin{pmatrix} x \\ y \\ z \\ 1 \end{pmatrix}_{k+1}$$
$$z_k = z_k^*$$

with θ_k =total permitted range of revolution of joint k

$r_k = \sqrt{(x_k^*)^2 + (y_k^*)^2}$

β_k =location angle of midrange point of joint k

$A_k = \text{Rot}(x_k,\alpha_k)\text{Trans}(a_k,0,0)\text{Trans}(0,0,d_k)\text{Rot}(z_{k-1},\beta_k) =$

$$\begin{pmatrix} 1 & 0 & 0 & a_k \\ 0 & c\alpha_k & s\alpha_k & d_k s\alpha_k \\ 0 & -s\alpha_k & c\alpha_k & d_k c\alpha_k \\ 0 & 0 & 0 & 1 \end{pmatrix} \begin{pmatrix} c\beta_k & -s\beta_k & 0 & 0 \\ s\beta_k & c\beta_k & 0 & o \\ 0 & 0 & 1 & 0 \\ 0 & 0 & 0 & 1 \end{pmatrix} = \begin{pmatrix} c\beta_k & -s\beta_k & 0 & a_k \\ c\alpha_k s\beta_k & c\alpha_k c\beta_k & s\alpha_k & d_k s\alpha_k \\ -s\alpha_k s\beta_k & -s\alpha_k c\beta_k & c\alpha_k & d_k c\alpha_k \\ 0 & 0 & 0 & 1 \end{pmatrix}$$

Initial conditions for joint n are given by: $x_n = r_n \cos\theta_n$ with $r_n = \sqrt{a_n^2 + (d_n \sin\alpha_n)^2}$

$y_n = r_n \sin\theta_n$

$z_n = d_n \cos\alpha_n$

The total workspace of an n-jointed manipulator $= W_T(H) = \sum_{i=1}^{n} A_i^{i+1}\{W_n(H)\}$ [Gupta & Roth 1982]. For the PUMA 560/600, the workspace volume $W_T(H)=3.94\ m^3$. For any given manipulator, a constant volume index may be defined: $VI=W_T/(l_1+...+l_n)^3$. For the PUMA 560/600, VI=3.944/2.744=1.44. There exists a theoretical maximum such that the manipulator workpace is a sphere of radius L^3 where $L=(l_1+...+l_n)$ at the first joint, ie. $VI_{max} = {}^{4\pi L^3/3}/_{L^3} \approx 4.2$. This generates a normalised index, $NVI=VI/VI_{max}$. For a PUMA 560/600, NVI=1.44/4.2=0.34. Joint limits reduce the ideal unlimited workspace by 34%. For most industrial robots, at least two of the positioning links are coplanar. For maximum workspace, the coplanar links should have the same dimensions: $a_2/d_4=1$. Offsets do not contribute to the workspace volume and so should be reduced - in this formulation, the elbow offset of the industrial PUMA 560/600 model has been eliminated. Furthermore, increasing the wrist size d_6 increases the total workspace but reduces the primary workspace, so a small wrist enhances dexterity. The workspace is bounded by concentric spheres of radii R_i-d_6 and R_0-d_6 where $R_i = a_2 - d_4$ and $R_0 = a_2 + d_4$. The concentric spheres of radii R_i and R_0 define the

workspace of the wrist point. The surface of the sphere of radius d_6 within the region between the concentric spheres defines all possible approach angles to that point [Hanson et al 1983].

2.2 RESOLUTION OF VELOCITY COORDINATES

The Jacobian matrix is important and is the fundamental component of resolved rate, resolved acceleration and resolved force control schemes and itself relies on the joint solution given by the inverse position kinematics solution.

2.2.1 Forward Differential Kinematics Solution

The differential kinematics relating joint velocities to cartesian end effector velocities is determined by a square matrix of partial differential terms - the Jacobian matrix. The **nxn** Jacobian matrix J(θ) specifies how the end effector velocities may be linearly transformed into joint rates [Whitney 1969]:

From the kinematic analysis: $q = f(\theta) = \sum_{i=1}^{n} R_i p_i$

By differentiating: $\dot{q} = J(\theta)\dot{\theta}$ where $J(\theta) = \partial f(\theta)/\partial\theta$

Hence, $\dot{q} = \frac{d}{dt}\sum_{i=1}^{n} R_i p_i = \sum_{i=1}^{n} \dot{R}_i p_i$ since $\dot{p}_i = 0$ (2.12)

Now, $\dot{R}_i^{i-1} = \frac{\partial R_i^{i-1}}{\partial \theta_i}.\dot{\theta}_i$

So, $\dot{R}_i^0 = \frac{d}{dt}\sum_{k=1}^{i} R_i^{i-1} = \sum_{k=1}^{i} \frac{\partial R_i^0}{\partial \theta_k}\dot{\theta}_k$

Substitute, $\dot{q} = \left(\sum_{i=1}^{n}\sum_{k=1}^{i} \frac{\partial R_i^0}{\partial \theta_k} p_i\right)\dot{\theta}_k$

$\rightarrow \dot{q} = J(\theta)\dot{\theta}_k$ where $J(\theta) = \sum_{i=1}^{n}\sum_{k=1}^{i} \frac{\partial R_i^0}{\partial \theta_k} p_i$ (2.13)

A more convenient and efficient formulation of the Jacobian matrix may be derived from the Newton-Euler dynamics equations as cross product relations [Whitney 1972, Orin & Schrader 1984]. From the forward Newton-Euler dynamics formulation (see Chapter 3), the linear and angular velocity of the end effector, $\dot{q} = \begin{pmatrix} v_i \\ w_i \end{pmatrix}$ are given by:

$$w_i = w_{i-1} + z_{i-1}\dot{\theta}_i = \sum_{j}^{i} z_{j-2}\dot{\theta}_{j-1} + z_{i-1}\dot{\theta}_i = \sum_{j=1}^{i} z_{j-1}\dot{\theta}_j$$

$$v_i = v_{i-1} + w_i \times l_i = \left(\sum_{j=1}^{i} z_{j-2}\dot{\theta}_{j-1}\right) \times l_{j-1} + z_{i-1}\dot{\theta}_i \times l_i = \sum_{j=1}^{i} (z_{j-1} \times l_j)\dot{\theta}_j$$

where z_{i-1}=unit vector along axis of motion of joint i

$l_i = (p_i - p_{i-1})$=position of link i with respect to base coordinates

Hence, at the end effector:

$$w_n = \sum_{i=1}^{n} z_{i-1}\dot{\theta}_i$$

$$v_n = \sum_{i=1}^{n} (z_{i-1} \times l_i)\dot{\theta}_i$$

or alternatively,

$$\begin{pmatrix} v_n \\ w_n \end{pmatrix} = \begin{pmatrix} \sum_{i=1}^{n} (z_{i-1} \times l_i) \\ \sum_{i=1}^{n} z_{i-1} \end{pmatrix}\dot{\theta}_i$$

such that $J(\theta) = \begin{pmatrix} z_{i-1} \times p_i^{i-1} \\ z_{i-1} \end{pmatrix}$ (2.14)

To apply and calculate the Jacobian matrix from the kinematic equations, the kinematics may be reformulated from the end effector to the base - the normal formulation from the base to the end effector requires the calculation of the Jacobian at each joint in terms of all preceding links and this is wasteful [Orin & Schrader 1984]. For resolved rate control, only the Jacobian for the end effector coordinate system is required and allows advantage to be taken of the kinematic simplicity of the wrist.

Hence, $J = (J_1 \ldots J_n)$ so $J = \begin{pmatrix} z_0 \times p_6^0 & z_1 \times p_6^1 & z_2 \times p_6^2 & z_3 \times p_6^3 & z_4 \times p_6^4 & z_5 \times p_6^5 \\ z_0 & z_1 & z_2 & z_3 & z_4 & z_5 \end{pmatrix}$

for a 6-link manipulator.

For the PUMA 560/600-type structure adopted here:

$$p_6^0 = \begin{pmatrix} c_1[d_6(c_{23}c_4s_5 + s_{23}c_5) + s_{23}d_4 + a_2c_2] - s_1(s_4s_5d_6 + d_2) \\ s_1[d_6(c_{23}c_4s_5 + s_{23}c_5) + s_{23}d_4 + a_2c_2] + c_1(s_4s_5d_6 + d_2) \\ d_6(c_{23}c_5 - s_{23}c_5) + c_{23}d_4 - a_2s_2 \end{pmatrix} \qquad z_0 = \begin{pmatrix} 0 \\ 0 \\ 1 \end{pmatrix}$$

$$p_6^1 = \begin{pmatrix} c_{23}(c_4s_5d_6) + s_{23}(c_5d_6 + d_4) + a_2c_2 \\ s_{23}(c_4s_5d_6) - c_{23}(c_5d_6 + d_4) + a_2s_2 \\ s_4s_5d_6 + d_2 \end{pmatrix} \qquad z_1 = \begin{pmatrix} -s_1 \\ c_1 \\ 0 \end{pmatrix}$$

$$p_6^2 = \begin{pmatrix} c_3(c_4s_5d_6) + s_3(c_5d_6 + d_4) \\ s_3(c_4s_5d_6) - c_3(c_5d_6 + d_4) \\ s_4s_5d_6 \end{pmatrix} \qquad z_2 = \begin{pmatrix} -s_1 \\ c_1 \\ 0 \end{pmatrix}$$

$$p_6^3 = \begin{pmatrix} c_4s_5d_6 \\ s_4s_5d_6 + d_4 \\ c_5d_6 \end{pmatrix} \qquad z_3 = \begin{pmatrix} c_1s_{23} \\ s_1s_{23} \\ c_2 \end{pmatrix}$$

$$p_6^4 = \begin{pmatrix} s_5d_6 \\ -c_5d_6 \\ 0 \end{pmatrix} \qquad z_4 = \begin{pmatrix} -(c_1c_{23}s_4 + s_1c_4) \\ (c_1c_4 - s_1c_{23}c_4) \\ s_{23}s_4 \end{pmatrix}$$

$$p_6^5 = \begin{pmatrix} 0 \\ 0 \\ d_6 \end{pmatrix} \qquad z_5 = \begin{pmatrix} c_1(c_{23}c_4s_5 + s_{23}c_5) - s_1s_4s_5 \\ s_1(c_{23}c_4s_5 + s_{23}c_5) + c_1s_4s_5 \\ -s_{23}c_4s_5 + c_{23}c_5 \end{pmatrix}$$

Hence, $J = \begin{pmatrix} J_{11} & J_{21} & J_{31} & J_{41} & J_{51} & J_{61} \\ J_{12} & J_{22} & J_{32} & J_{42} & J_{52} & J_{62} \\ J_{13} & J_{23} & J_{33} & J_{43} & J_{53} & J_{63} \\ J_{14} & J_{24} & J_{34} & J_{44} & J_{54} & J_{64} \\ J_{15} & J_{25} & J_{35} & J_{45} & J_{55} & J_{65} \\ J_{16} & J_{26} & J_{36} & J_{46} & J_{56} & J_{66} \end{pmatrix}$

where

$J_{11} = -s_1[d_6(c_{23}c_4s_5 + s_{23}c_5) + s_{23}d_4 + a_2c_2] - c_1(s_4s_5d_6 + d_2)$

$J_{12} = c_1[d_6(c_{23}c_4s_5 + s_{23}c_5) + s_{23}d_4 + a_2c_2] - s_1(s_4s_5d_6 + d_2)$

$$
\begin{aligned}
&J_{13} = 0, J_{14} = 0, J_{15} = 0, J_{16} = 1\\
&J_{21} = c_1(s_4 s_5 d_6 + d_2)\\
&J_{22} = s_1(s_4 s_5 d_6 + d_2)\\
&J_{23} = -s_1[s_{23} c_4 s_5 d_6 - c_{23}(c_5 d_6 + d_4) + a_2 s_2] - c_1[c_{23} c_4 s_5 d_6 + s_{23}(c_5 d_6 + d_4) + a_2 c_2]\\
&J_{24} = -s_1, J_{25} = c_1 J_{26} = 0\\
&J_{31} = c_1 s_4 s_5 d_6\\
&J_{32} = s_1 s_4 s_5 d_6\\
&J_{33} = -s_1[s_3 c_4 s_5 d_6 - c_3(c_5 d_6 + d_4)] - c_1[c_3 c_4 s_5 d_6 + s_3(d_4 + c_5 d_6)]\\
&J_{34} = -s_1, J_{35} = c_1, J_{36} = 0\\
&J_{41} = s_1 s_{23}(d_6 c_5 + d_4) - d_6 c_{23} s_4 s_5\\
&J_{42} = d_6 c_{23} c_4 s_5 - c_1 s_{23}(d_6 c_5 + d_4)\\
&J_{43} = d_6 s_{23}(c_1 s_4 s_5 - s_1 c_4 s_5)\\
&J_{44} = c_1 s_{23}, J_{45} = s_1 s_{23}, J_{46} = c_{23}\\
&J_{51} = s_{23} s_4 c_5 d_6\\
&J_{52} = s_{23} s_4 s_5 d_6\\
&J_{53} = d_6[c_5(c_1 c_{23} s_4 + s_1 c_4) + s_5(s_1 c_{23} s_4 - c_1 c_4)]\\
&J_{54} = -(c_1 c_{23} s_4 + s_1 c_4)\\
&J_{55} = c_1 c_4 - s_1 c_{23} s_4\\
&J_{56} = s_{23} s_4\\
&J_{61} = d_6[s_1(c_{23} c_4 s_5 + c_5 s_{23}) + c_1 s_4 s_5]\\
&J_{62} = -d_6[c_1(c_{23} c_4 s_5 + s_{23} c_5) - s_1 s_4 s_5]\\
&J_{63} = 0\\
&J_{64} = c_1(c_{23} c_4 s_5 + s_{23} c_5) - s_1 s_4 s_5\\
&J_{65} = s_1(c_{23} c_4 s_5 + s_{23} c_5) + c_1 s_4 s_5\\
&J_{66} = -s_{23} c_4 s_5 + c_{23} c_5
\end{aligned}
\tag{2.15}
$$

Hence, we have resolution of the velocity coordinates between the end effector cartesian coordinates and the joint coordinates:

$$
\begin{pmatrix} v_x \\ v_y \\ v_z \\ w_x \\ w_y \\ w_z \end{pmatrix} = J \begin{pmatrix} \dot{\theta}_1 \\ \dot{\theta}_2 \\ \dot{\theta}_3 \\ \dot{\theta}_4 \\ \dot{\theta}_5 \\ \dot{\theta}_6 \end{pmatrix} \tag{2.16}
$$

This is a statement of the forward differential kinmatics problem. Paul (1981) used a differential translation and rotation method derived directly from the DH kinematic equations to compute the Jacobian as:

$$
J_i = \begin{pmatrix} p_x^i n_y^i - p_y^i n_x^i \\ p_x^i s_y^i - p_y^i s_x^i \\ p_x^i a_y^i - p_y^i a_x^i \\ n_z^i \\ s_z^i \\ a_z^i \end{pmatrix}_i \quad \text{for revolute joints;} \qquad J_i = \begin{pmatrix} n_z^i \\ s_z^i \\ a_z^i \\ 0 \\ 0 \\ 0 \end{pmatrix}_i d_i \quad \text{for prismatic joints}
$$

where i defines the Jacobian matrix column

However, the method is marginally computationally more expensive than the Whitney's cross product method [Hollerbach & Sahar 1983; Orin & Schrader 1984]:

DH formulation: 30n-25 multiplications
15n-25 additions
2n trigonometric functions

Cross product formulation: 30n-55 multiplications
15n-38 additions
2n-2 trigonometric functions

The advantage of Paul's method lies in that if the joint angles are not available, but the cartesian coordinates of each link are available, then the Jacobian can be calculated. However, although the end effector coordinates will be available, it is unlikely that the cartesian coordinates of the other joints will be available without the joint solutions.

2.2.2 Inverse Differential Kinematics Solution

For the inverse velocity kinematics, we require the differential change in joint angles expressed in terms of the cartesian linear and angular velocities of the end effector. The unique inverse solution may be found by inverting the Jacobian matrix: $\dot{\theta} = J^{-1}\dot{q}$. The Jacobian matrix is difficult to invert analytically so numerical techniques are usually used. Such numerical techniques usually involve Gaussian elimination. The numerical inversion is generally regarded as a computational bottleneck and the Jacobian can become singular at certain configurations. At this point the matrix loses its full rank, ie. the manipulator loses a degree of freedom and cannot contribute to moving the end effector position. At these unstable singular positions, infinite joint velocities are required to move the end effector through infinitesimal motions and no inverse exists. Physically, the end effector velocity is parallel to ther motion of two separate joints and the joints become degenerate. Singular positions may be found by solving det|J|=0. These points may then be avoided by storing lookup tables within the arm control system, or alternatively, additional joints in a kinematically redundant configuration may be introduced to give the extra degrees of freedom to overcome the singularities. Paul et al (1981b) avoided using the Jacobian altogether by directly differentiating the inverse joint angle kinematics solution to give differential joint coordinates in terms of the end effector velocity, thereby avoiding the Jacobian singularity problem. The method involves differentiating the inverse position kinematics solution directly to give for the modified PUMA 560/600 model which are quoted without proof:

$$\dot{\theta}_1 = \frac{c_1 v_y^{wrist} - s_1 v_x^{wrist}}{c_1 p_x^{wrist} + s_1 p_y^{wrist}}, \quad \dot{\theta}_2 = \frac{c_2 \dot{A} - s_2 v_z^{wrist}}{c_2 p_z^{wrist} + s_2 A} \tag{2.17}$$

$$A = c_1 p_x^{wrist} + s_1 p_y^{wrist}$$

where

$$\dot{A} = c_1 (v_x^{wrist} + p_y^{wrist}) + s_1 (v_y^{wrist} - p_x^{wrist})$$

$$\dot{\theta}_3 = \frac{a_2^2 \dot{\theta}_2 + a_2 c_2 (v_z^{wrist} - A\dot{\theta}_2) + a_2 s_2 (p_z^{wrist} \dot{\theta}_2 + \dot{A}) + p_z^{wrist} \dot{A} - A v_z^{wrist}}{d_4^2} - \dot{\theta}_2 \tag{2.18}$$

$$\dot{\theta}_4 = \frac{c4.sd4 - s4.cd4}{(c4)^2 + (s4)^2} \tag{2.19}$$

where

$$c4 = c_{23}[(c_1 a_x + s_1 a_y) - s_{23} a_z]$$

$$s4 = -s_1 a_x + c_1 a_y$$

$$cd4 = c_{23}[s_1(-a_x + \dot{a}_y) + c_1(\dot{a}_x + a_y) - a_z] - s_{23}[c_1 a_x + s_1 a_y - \dot{a}_z]$$

$$sd4 = -c_1 a_x - s_1 a_y - s_1 \dot{a}_x + c_1 \dot{a}_y$$

$$\dot{\theta}_5 = \frac{c5.sd5 - s5.cd5}{(c5)^2 + (s5)^2} \qquad (2.20)$$

where

$$c5 = s_{23}(c_1 a_x + s_1 a_y) + c_{23} a_z$$

$$s5 = \sqrt{[c_{23}(c_1 a_x + s_1 a_y) - s_{23} a_z]^2 + [-s_1 a_x + c_1 a_y]^2} = 1$$

$$cd5 = s_{23}[s_1(-a_x + \dot{a}_y) + c_1(a_y + \dot{a}_x) - a_z] - c_{23}[c_1 a_x + s_1 a_y + \dot{a}_z]$$

$$sd5 = 0$$

$$\dot{\theta}_6 = \frac{c6.sd6 - s6.cd6}{(c6)^2 + (s6)^2} \qquad (2.21)$$

where

$$c6 = s_{23}(c_1 n_x + s_1 n_y) + c_{23} n_z$$

$$s6 = s_{23}(c_1 s_x + s_1 s_y) + c_{23} s_z$$

$$cd6 = s_{23}[s_1(-n_x + \dot{n}_y) + c_1(n_y + \dot{n}_x) - n_z] - c_{23}[c_1 n_x + s_1 n_y - \dot{n}_z]$$

$$sd6 = s_{23}[s_1(-s_x + \dot{s}_y) + c_1(s_y + \dot{s}_x) - s_z] - c_{23}[c_1 s_x + s_1 s_y - \dot{s}_z]$$

with $$\dot{R} = (\dot{n}\dot{s}\dot{a}) = (nsa)\begin{pmatrix} 0 & -w_z & w_y \\ w_z & 0 & -w_x \\ -w_y & w_x & 0 \end{pmatrix}$$

so that:

$$\dot{n}_x = s_x w_x - a_y w_y \qquad \dot{s}_x = -n_x w_z + a_x w_x \qquad \dot{a}_x = n_x w_y - s_x w_x$$

$$\dot{n}_y = s_y w_z - a_y w_y \qquad \dot{s}_y = -n_y w_z + a_y w_x \qquad \dot{a}_y = n_y w_y - s_y w_x$$

$$\dot{n}_z = s_z w_x - a_z w_y \qquad \dot{s}_z = -n_z w_z + a_z w_x \qquad \dot{a}_z = n_z w_y - s_z w_x$$

This technique offers the inverse joint solution and a similar technique may be applied for resolved acceleration control, but the formulations (particularly for resolved acceleration control) are so complex that little is gained in terms of computational advantage. The technique is also manipulator specific restricting its application. The Jacobian need be inverted only once for both resolved rate and resolved acceleration control. Furthermore, the Jacobian itself is explicitly required for force control. One possible utilisation of the analytic solution to the inverse kinematics is for overcoming points when the Jacobian becomes singular.

2.2.3 Manipulator Redundancy

Although manipulator redundancy has not been employed in this study due to the additional mass penalty incurred by additional links, actuators and drive mechanisms, manipulators that are nonredundant with respect to certain tasks may become redundant for other tasks - this situation can occur in dual arm manipulation. Redundancy increases the reachability of points in the workspace particularly if

environmental constraints are present and enables points to be reached with smaller joint movements than nonredundant manipulators. Furthermore, the redundant degrees of freedom may be used to generate joint motion to overcome possible singular positions.

Resolved motion control uses a Jacobian matrix. In general J is an mxn matrix. If m=n, then the rank of J is n generating a square matrix which is invertible giving a unique solution for joint rates. However, if m<n, then m generates an infinite number of solutions: more degrees of freedom exist than are required for the task. This underdetermination arises from the fact that there are fewer rows than columns. Since J is no longer square, J^{-1} does not exist. Similarly, the transformation from cartesian coordinates to joint coordinates have no closed form solution. However, it can be expressed as roots of a polynomial of degree 2^n with constraints to reduce the multivalue problem. Iterative root finding may be time consuming and is approximate only. The way to solve the Jacobian is to make the Jacobian square by adding constraints to the joint variables. There exists a generalised pseudo-inverse Jacobian which provides a useful least squares solution such that:

$\dot{\theta} = J^{+}\dot{q}$

The generalised inverse is given by [Whitney 1969]:

Error to be minimised: $e = \lambda^{T}(\dot{q} - J\dot{\theta})$ where λ =Lagrange multiplier vector

This is minimised with respect to $\dot{\theta}$:

$$\left.\begin{array}{l}\dot{\theta} = J^{T}\lambda \\ \dot{q} = J\dot{\theta}\end{array}\right\} \rightarrow \dot{q} = JJ^{T}\lambda \rightarrow \lambda = (JJ^{T})^{-1}\dot{q}$$

Now, $\dot{\theta} = J^{T}\lambda \rightarrow \dot{\theta} = J^{T}(JJ^{T})^{-1}\dot{q}$ where $J^{+} = J^{T}(JJ^{T})^{-1}$

This is the Moore-Penrose pseudoinverse which satisfies the following properties [Liegeois 1977, Klein & Huang 1983]:

$(i) JJ^{+}J = J^{+}$;

$(ii) J^{+}JJ^{+} = J$;

$(iii)(J^{+}J)^{T} = J^{+}J$;

$(iv)(JJ^{+})^{T} = JJ^{+}$

This pseudoinverse is complex to compute being of order n^3 and yields a minimum Euclidean norm least squares solution. This minimum norm property minimises the product $\dot{\theta}^{T}\dot{\theta}$ which is closely related to the kinetic energy function and associated actuator power requirements. Similarly, singularities at which high joint velocities occur are avoided due to the tendency of the function to reduce such joint velocities. It is possible to modify the basic Moore-Penrose pseudoinverse to optimise additional position-dependent performance criteria in a least squares manner (the "null space vector"):

$\dot{\theta} = J^{+}\dot{q} + \alpha(I - J^{+}J)\frac{\partial g(\theta)}{\partial \theta}$ where α =scalar gain constant

$g(\theta)$ =minimised performance index

Different workers have proposed different schemes for $g(\theta)$ whereby secondary criteria are satisfied as well as the primary criterion of trajectory tracking:

(a) $g(\theta)$ represents a position dependent restriction to actuator angle limits and the extra degrees of freedom are used to optimise joint angle availability [Liegeois 1977]:

$$g = \sum_{i=1}^{n}\left(\frac{\theta_i - \theta_{ci}}{\delta\theta_i}\right) \text{ where } \theta_{ci} = \frac{\beta}{2} = (\theta_i^{min} + \theta_i^{max})/2 = \text{midpoint of joint angle}$$

$$\delta\theta_i = \text{maximum allowable drift}$$

(b) $g(\theta)$ represents a manipulability index such that g is maximised and singularites where w=0 are avoided [Klein & Huang 1983]:

$$g(\theta) = -w(\theta) = -\sqrt{\det JJ^T}$$

Unfortunately, any scheme involving the pseudoinverse generates a relation between end effector velocity and joint angle velocity which is not integrable. The path generated becomes nonconservative such that a closed path in x does not yield a closed path in $\dot{\theta}$. After a number of cycles around a closed path in x, a drift will occur generating unpredictable states for $\dot{\theta}$. Baillieuil (1985) introduced an extended Jacobian for redundant formulations to introduce conservative motion by adding an n-row vector to the mxn Jacobian to make the extended Jacobian square. This imposed limitations on the number of possible configurations of the manipulator corresponding to any set of cartesian coordinates. Hollerbach & Suh (1987) examined the effects of various optimisation techniques used in redundant formulations and they found that only the kinematic unweighted Moore-Penrose pseudoinverse is globally stable and that the extended Jacobian technique experienced instabilities at trajectory extremes and for longer trajectories. Stability problems occurred for dynamic formulations such as torque constraints and inertia weightings due to whiplash effects generated from conflicting requirements. This suggests that attempts to modify the Moore-Penrose pseudoinverse dynamically are detrimental and that kinematic formulations with the pseudoinverse only should be used.

Some of the advantages of redundant joints may be retained without the large increase in computational control complexity. An additional rotary joint may be included near the elbow joint on link a_2 of the PUMA 560/600 manipulator configuration. This joint may be locked at 0^o to yield the elbow up/down configuration or locked at 90^o about the x_2 axis to rotate the z_2 axis to produce a sideways elbows out/in configuration (with elbow out being utilised rather than elbow in which might obstruct the workspace). This provides the flexibility of the redundant joint by introducing two possible configurations of the elbow (similar to a human arm) such as for obstacle avoidance but by restricting the manipulator to one or other configuration (elbow down or elbow out), the pseudoinverse is not required. The kinematic formulation need only be changed by replacing the link rotation matrix R_3 with

$$R'_3 = \begin{pmatrix} c_3 & -s_3 & 0 \\ s_3 & c_3 & 0 \\ 0 & 0 & -1 \end{pmatrix} \text{ to rotate } (x_2, y_2, z_2) \text{ into } (x_3, -z_3, -y_3).$$

2.3 RESOLUTION OF ACCELERATION COORDINATES

Resolved acceleration control specifies how end effector accelerations are transformed to joint coordinates [Luh, Walker & Paul 1980]:

$$\ddot{q} = J\ddot{\theta} + \dot{J}\dot{\theta} \text{ or } \ddot{\theta} = J^{-1}(\ddot{q} - \dot{J}\dot{\theta}) \qquad (2.22)$$

Although this has always in the past been performed numerically, analytic solutions to $\dot{J}$ which represents the nonlinear components to acceleration are derived for the first time here using the Newton-Euler dynamics formulation for $\dot{w}_i, \dot{v}_i$ similar to Whitney's cross product dynamics method of finding the Jacobian (see Chapter 3):

$$\dot{w}_i = \dot{w}_{i-1} + z_{i-1}\ddot{\theta}_i + w_{i-1} \times (z_{i-1}\dot{\theta}_i) = \sum_{j=1}^{i} z_{j-1}\ddot{\theta}_j + \sum_{j=1}^{i}(\sum_{k=1}^{j-1} z_{k-1}\dot{\theta}_k) \times \sum_{j=1}^{i} z_{j-1}\dot{\theta}_j$$

$$\dot{v}_i = \dot{v}_{i-1} + \dot{w}_i \times l_i + w_i \times (w_i \times l_i) = \sum_{j=1}^{i} \dot{w}_j \times l_j + \sum_{j=1}^{i} w_j \times (w_j \times l_j)$$

$$= \left[\sum_{j=1}^{i} z_{j-1}\ddot{\theta}_j + \sum_{j=1}^{i} w_{j-1} \times z_{j-1}\dot{\theta}_j\right] \times l_j + \left[\sum_{j=1}^{i}\sum_{k=1}^{j} z_{k-1}\dot{\theta}_k \times \left(\sum_{k=1}^{j} z_{k-1}\dot{\theta}_k \times l_j\right)\right]$$

$$= \sum_{j=1}^{i}(z_{j-1} \times l_j)\ddot{\theta}_j + \sum_{j}^{i}\left[\sum_{k=1}^{j-1} z_{k-1}\dot{\theta}_k \times z_{j-1}\dot{\theta}_j\right] \times l_j + \sum_{j=1}^{i}\left[\sum_{k=1}^{j} z_{k-1}\dot{\theta}_k \times \left(\sum_{k=1}^{i} z_{k-1}\dot{\theta}_k \times l_j\right)\right]$$

At the end effector, these equations become:

$$\dot{w}_n = \sum_{i=1}^{n} z_{i-1}\ddot{\theta}_i + \sum_{i=1}^{n}\left(\sum_{k=1}^{i} z_{k-2}\dot{\theta}_{k-1}\right) \times z_{i-1}\dot{\theta}_i$$

$$\dot{v}_n = \sum_{i=1}^{n}(z_{i-1} \times l_i)\ddot{\theta}_i + \sum_{i=1}^{n}\left(\sum_{k=1}^{i} z_{k-2} \times z_{i-1} \times l_i\right)\dot{\theta}_k\dot{\theta}_i + \sum_{i=1}^{n}\left[\sum_{k=1}^{i} z_{k-1}\dot{\theta}_k \times \left(\sum_{k=1}^{i} z_{k-1}\dot{\theta}_k \times l_i\right)\right]$$

Or an alternative formulation:

$$\begin{pmatrix}\dot{v}_n \\ \dot{w}_n\end{pmatrix} = \begin{pmatrix}\sum_{i=1}^{n} z_{i-1} \times l_i \\ \sum_{i=1}^{n} z_{i-1}\end{pmatrix}\ddot{\theta}_i + \begin{pmatrix}\sum_{i=1}^{n}\left[\sum_{k=1}^{i} z_{k-2} \times z_{i-1} \times l_i\right]\dot{\theta}_{k-1} + \left[\sum_{k=1}^{i} z_{k-1}\dot{\theta}_k \times \left(\sum_{k=1}^{i} z_{k-1}\dot{\theta}_k \times l_i\right)\right] \\ \sum_{i=1}^{n}\left[\sum_{k=1}^{i} z_{k-2} \times z_{i-1}\right]\dot{\theta}_{k-1}\end{pmatrix}\dot{\theta}_i \tag{2.23}$$

This is consistent with $\ddot{q} = J\ddot{\theta} + \dot{J}\dot{\theta}$ and represents the problem statement of the forward acceleration kinematics solution in analytic form. For the PUMA-type configuration being adopted:

$$\dot{J} = \begin{pmatrix}\dot{J}_1 & \dot{J}_2 & \dot{J}_3 & \dot{J}_4 & \dot{J}_5 & \dot{J}_6\end{pmatrix}$$

where:

$$\dot{J}_1 = \begin{pmatrix} z_0\dot{\theta}_1 \times (z_0\dot{\theta}_1 \times p_6^0) \\ 0 \end{pmatrix}; \dot{J}_2 = \begin{pmatrix} z_0\dot{\theta}_1 \times z_1 \times p_6^1 + (z_0\dot{\theta}_1 + z_1\dot{\theta}_2) \times [(z_0\dot{\theta}_1 + z_1\dot{\theta}_2) \times p_6^1 \\ z_0\dot{\theta}_1 \times z_1 \end{pmatrix};$$

$$\dot{J}_3 = \begin{pmatrix} (z_0\dot{\theta}_1 + z_1\dot{\theta}_2) \times z_2 \times p_6^2 + (z_0\dot{\theta}_1 + z_1\dot{\theta}_2 + z_2\dot{\theta}_3) \times [(z_0\dot{\theta}_1 + z_1\dot{\theta}_2 + z_2\dot{\theta}_3) \times p_6^2] \\ (z_0\dot{\theta}_1 + z_1\dot{\theta}_2) \times z_2 \end{pmatrix}$$

The rest of the differential Jacobian columns are derived similarly. This may be resolved into the differential Jacobian matrix elements as:

$$\dot{J}=\begin{pmatrix} \dot{J}_{11} & \dot{J}_{21} & \dot{J}_{31} & \dot{J}_{41} & \dot{J}_{51} & \dot{J}_{61} \\ \dot{J}_{12} & \dot{J}_{22} & \dot{J}_{32} & \dot{J}_{42} & \dot{J}_{52} & \dot{J}_{62} \\ \dot{J}_{13} & \dot{J}_{23} & \dot{J}_{33} & \dot{J}_{43} & \dot{J}_{53} & \dot{J}_{63} \\ \dot{J}_{14} & \dot{J}_{24} & \dot{J}_{34} & \dot{J}_{44} & \dot{J}_{54} & \dot{J}_{64} \\ \dot{J}_{15} & \dot{J}_{25} & \dot{J}_{35} & \dot{J}_{45} & \dot{J}_{55} & \dot{J}_{65} \\ \dot{J}_{16} & \dot{J}_{26} & \dot{J}_{36} & \dot{J}_{46} & \dot{J}_{56} & \dot{J}_{66} \end{pmatrix}$$

$$\dot{J}_{11}=-p_{6x}^{0}\dot{\theta}_1;\dot{J}_{12}=-p_{6y}^{0}\dot{\theta}_1;\dot{J}_{13}=\dot{J}_{14}=\dot{J}_{15}=\dot{J}_{16}=0;$$

$$\dot{J}_{21}=-s_1\dot{\theta}_1(s_4s_5d_6+d_2)-c_1\dot{\theta}_2(s_1\dot{\theta}_2p_{6y}^{1}+c_1\dot{\theta}_2p_{6x}^{1})-\dot{\theta}_1(s_1\dot{\theta}_2p_{6z}^{1}+\dot{\theta}_1p_{6x}^{1})$$

$$\dot{J}_{22}=c_1\dot{\theta}_1(s_4s_5d_6+d_2)-s_1\dot{\theta}_2(s_1\dot{\theta}_2p_{6y}^{1}+c_1\dot{\theta}_2p_{6x}^{1})+\dot{\theta}_1(c_1\dot{\theta}_2p_{6z}^{1}-\dot{\theta}_1p_{6y}^{1})$$

$$\dot{J}_{23}=s_1\dot{\theta}_1p_{6x}^{1}-c_1\dot{\theta}_1p_{6y}^{1}-s_1\dot{\theta}_2(s_1\dot{\theta}_2p_{6z}^{1}+\dot{\theta}_1p_{6x}^{1})-c_1\dot{\theta}_2(c_1\dot{\theta}_2p_{6z}^{1}-\dot{\theta}_1p_{6y}^{1})$$

$$\dot{J}_{24}=-c_1\dot{\theta}_1;\ \dot{J}_{25}=-s_1\dot{\theta}_1;\ \dot{J}_{26}=0$$

$$\dot{J}_{31}=-s_1\dot{\theta}_1(s_4s_5d_6)+c_1(\dot{\theta}_2+\dot{\theta}_3)[-s_1(\dot{\theta}_2+\dot{\theta}_3)p_{6y}^{2}-c_1(\dot{\theta}_2+\dot{\theta}_3)p_{6x}^{2}]$$
$$-\dot{\theta}_1[s_1(\dot{\theta}_2+\dot{\theta}_3)p_{6z}^{2}+\dot{\theta}_1p_{6x}^{2}]$$

$$\dot{J}_{32}=c_1\dot{\theta}_1(s_4s_5d_6)+s_1(\dot{\theta}_2+\dot{\theta}_3)[-s_1(\dot{\theta}_2+\dot{\theta}_3)p_{6y}^{2}-c_1(\dot{\theta}_2+\dot{\theta}_3)p_{6x}^{2}]$$
$$+\dot{\theta}_1[c_1(\dot{\theta}_2+\dot{\theta}_3)p_{6z}^{2}-\dot{\theta}_1p_{6y}^{2}]$$

$$\dot{J}_{33}=-c_1\dot{\theta}_1p_{6y}^{2}-s_1\dot{\theta}_1p_{6x}^{2}-s_1(\dot{\theta}_2+\dot{\theta}_3)[s_1(\dot{\theta}_2+\dot{\theta}_3)p_{6z}^{2}+\dot{\theta}_1p_{6x}^{2}]$$
$$-c_1(\dot{\theta}_2+\dot{\theta}_3)[c_1(\dot{\theta}_2+\dot{\theta}_3)p_{6z}^{2}-\dot{\theta}_1p_{6y}^{2}]$$

$$\dot{J}_{34}=-c_1\dot{\theta}_1;\ \dot{J}_{35}=-s_1\dot{\theta}_1;\ \dot{J}_{36}=0$$

$$\dot{J}_{41}=c_{23}[s_1(\dot{\theta}_2+\dot{\theta}_3)+c_1\dot{\theta}_1]c_5d_6+c_{23}(\dot{\theta}_2+\dot{\theta}_3)(s_4s_5d_6+d_4)$$
$$+a_{3y}[a_{3x}(s_4s_5d_6+d_4)-a_{3y}(c_4s_5d_6)]-a_{3z}[a_{3z}(c_4s_5d_6)-a_{3x}(c_5d_6)]$$

$$\dot{J}_{42}=-c_{23}[c_1(\dot{\theta}_2+\dot{\theta}_3)-s_1\dot{\theta}_1]c_5d_6-c_{23}(\dot{\theta}_2+\dot{\theta}_3)(c_4s_5d_6)$$
$$+a_{3z}[a_{3y}(c_5d_6)-a_{3z}(s_4s_5d_6+d_4)]-a_{3x}[a_{3x}(s_4s_5d_6+d_4)-a_{3y}(c_4s_5d_6)]$$

$$\dot{J}_{43}=c_{23}[c_1(\dot{\theta}_2+\dot{\theta}_3)-s_1\dot{\theta}_1](s_4s_5d_6+d_4)-c_{23}[s_1(\dot{\theta}_2+\dot{\theta}_3)+c_1\dot{\theta}_1](c_4s_5d_6)$$
$$+a_{3x}[a_{3z}(c_4s_5d_6)-a_{3x}(c_5d_6)]-a_{3y}[a_{3y}(c_5d_6)-a_{3z}(s_4s_5d_6+d_4)]$$

$$\dot{J}_{44}=c_1c_{23}(\dot{\theta}_2+\dot{\theta}_3)-s_1c_{23}\dot{\theta}_1;\ \dot{J}_{45}=s_1c_{23}(\dot{\theta}_2+\dot{\theta}_3)+c_1c_{23}\dot{\theta}_1;\ \dot{J}_{46}=-c_{23}(\dot{\theta}_2+\dot{\theta}_3)$$

$$\dot{J}_{51}=c_5d_6\{z_{4y}[-s_1(\dot{\theta}_2+\dot{\theta}_3)+c_1c_{23}\dot{\theta}_4]-z_{4x}[c_1(\dot{\theta}_2+\dot{\theta}_3)+s_1c_{23}\dot{\theta}_4]\}$$
$$+d_6[a_{4y}(a_{4y}s_5-a_{4x}c_5)-a_{4z}a_{4z}s_5]$$

$$\dot{J}_{52}=s_5d_6\{z_{4y}[-s_1(\dot{\theta}_2+\dot{\theta}_3)+c_1c_{23}\dot{\theta}_4]-z_{4x}[c_1(\dot{\theta}_2+\dot{\theta}_3)+s_1c_{23}\dot{\theta}_4]\}$$
$$+d_6[a_{4z}a_{4z}c_5-a_{4x}(a_{4y}s_5-a_{4x}c_5)]$$

$$\dot{J}_{53}=-c_5d_6\{z_{4z}[c_1(\dot{\theta}_2+\dot{\theta}_3)+s_1c_{23}\dot{\theta}_4]-z_{4y}[\dot{\theta}_1+c_{23}\dot{\theta}_4]\}$$
$$-s_5d_6\{z_{4z}[s_1(\dot{\theta}_2+\dot{\theta}_3)-c_1c_{23}\dot{\theta}_4]+z_{4x}[-s_1(\dot{\theta}_2+\dot{\theta}_3)+c_1c_{23}\dot{\theta}_4]\}$$
$$+d_6[a_{4z}(a_{4x}s_5-a_{4y}c_5)]$$

$$\dot{J}_{54}=z_{4z}[c_1(\dot{\theta}_2+\dot{\theta}_3)+s_1c_{23}\dot{\theta}_4]-z_{4y}[\dot{\theta}_1+c_{23}\dot{\theta}_4]$$

$$\dot{J}_{55}=z_{4z}[s_1(\dot{\theta}_2+\dot{\theta}_3)-c_1c_{23}\dot{\theta}_4]+z_{4x}[-s_1(\dot{\theta}_2+\dot{\theta}_3)+c_1c_{23}\dot{\theta}_4]$$

$$\dot{J}_{56} = z_{4y}[-s_1(\dot{\theta}_2+\dot{\theta}_3)+c_1c_{23}\dot{\theta}_4]-z_{4x}[c_1(\dot{\theta}_2+\dot{\theta}_3)+s_1c_{23}\dot{\theta}_4]$$

$$\dot{J}_{61} = d_6\{-z_{5z}\{-s_1(\dot{\theta}_2+\dot{\theta}_3)+c_1c_{23}\dot{\theta}_4+z_{4x}\dot{\theta}_5]+z_{5x}[\dot{\theta}_1+c_{23}\dot{\theta}_4+z_{4z}\dot{\theta}_5]\}+d_6a_{5x}a_{5z}$$

$$\dot{J}_{62} = -d_6\{z_{5z}[c_1(\dot{\theta}_2+\dot{\theta}_3)+s_1c_{23}\dot{\theta}_4+z_{4y}\dot{\theta}_5]-z_{5y}[\dot{\theta}_1+c_{23}\dot{\theta}_4+z_{4z}\dot{\theta}_5]\}+d_6a_{5y}a_{5z}$$

$$\dot{J}_{63} = -d_6(a_{5x}a_{5x}+a_{5y}a_{5y})$$

$$\dot{J}_{64} = z_{5z}[c_1(\dot{\theta}_2+\dot{\theta}_3)+s_1c_{23}\dot{\theta}_4+z_{4y}\dot{\theta}_5]-z_{5y}[\dot{\theta}_1+c_{23}\dot{\theta}_4+z_{4z}\dot{\theta}_5]$$

$$\dot{J}_{65} = -z_{5z}[-s_1(\dot{\theta}_2+\dot{\theta}_3)+c_1c_{23}\dot{\theta}_4+z_{4x}\dot{\theta}_5]+z_{5x}[\dot{\theta}_1+c_{23}\dot{\theta}_4+z_{4z}\dot{\theta}_5]$$

$$\dot{J}_{66} = z_{5y}[-s_1(\dot{\theta}_2+\dot{\theta}_3)+c_1c_{23}\dot{\theta}_4+z_{4x}\dot{\theta}_5]-z_{5x}[c_1(\dot{\theta}_2+\dot{\theta}_3)+s_1c_{23}\dot{\theta}_4+z_{4y}\dot{\theta}_5] \qquad (2.24)$$

with $\begin{pmatrix} a_{3x} \\ a_{3y} \\ a_{3z} \end{pmatrix} = \begin{pmatrix} -s_1(\dot{\theta}_2+\dot{\theta}_3)+c_1s_{23}\dot{\theta}_4 \\ c_1(\dot{\theta}_2+\dot{\theta}_3)+s_1s_{23}\dot{\theta}_4 \\ \dot{\theta}_1+c_{23}\dot{\theta}_4 \end{pmatrix}; \begin{pmatrix} a_{4x} \\ a_{4y} \\ a_{4z} \end{pmatrix} = \begin{pmatrix} a_{3x}+z_{4x}\dot{\theta}_5 \\ a_{3y}+z_{4y}\dot{\theta}_5 \\ a_{3z}+z_{4z}\dot{\theta}_5 \end{pmatrix}; \begin{pmatrix} a_{5x} \\ a_{5y} \\ a_{5z} \end{pmatrix} = \begin{pmatrix} a_{4x}+z_{5x}\dot{\theta}_6 \\ a_{4y}+z_{5y}\dot{\theta}_6 \\ a_{4z}+z_{5z}\dot{\theta}_6 \end{pmatrix}$

Hence $\dot{J}$ may be computed analytically rather than numerically. The inverse solution which is required by the servocontroller is found by numerically inverting the Jacobian:

$$\ddot{\theta} = J^{-1}(\ddot{q}-\dot{J}\dot{\theta}) = J^{-1}(\ddot{q}-\alpha)$$

where $\begin{pmatrix} \alpha_x \\ \alpha_y \\ \alpha_z \\ \alpha_\alpha \\ \alpha_\beta \\ \alpha_\gamma \end{pmatrix} = \dot{J}\begin{pmatrix} \dot{\theta}_1 \\ \dot{\theta}_2 \\ \dot{\theta}_3 \\ \dot{\theta}_4 \\ \dot{\theta}_5 \\ \dot{\theta}_6 \end{pmatrix}$ (2.25)

2.4 RESOLUTION OF STATIC FORCE COORDINATES

Although force is not a kinematic variable, cartesian static external forces and torques at the end effector may be transformed directly into their joint torque equivalents by the Jacobian transpose [Paul 1981; Whitney 1977]. This stipulates a requirement for the explicit calculation of the Jacobian matrix. Force feedback is a critical part of the robot control structure and is required to correct errors in position to allow the manipulator to accomodate the physical constraints of the task which usually require high degrees of positioning accuracy between mating parts, eg. insertion tasks. Force control effectively reduces the required positioning accuracy to perform a task: there will always be random fluctuations in final positioning which need to be accounted for. Small variations in relative position will generate large contact forces when parts interact providing a natural mechanism of amplifying small position errors at hand level. Much manipulation involves contact forces encountered at the end effector rather than just positioning and so force sensing and control is a fundamental requirement for any robot working in a variable structure environment. Indeed, Paul (1987) stated that manipulation comprises of a series of collisions between object and manipulator. The three types of manipulator motion are therefore: motion in freespace, contact, and force exertion. Force sensors may be mounted on the joints or the wrist [Shimano & Roth 1975]. Joint sensors measure motor torque currents directly at the joints but they limit the accuracy of the force coefficients at the end effector due to

uncertainties in joint friction and damping making this method unsuitable when small hand force resolution <1N are required. Such inaccuracies are intolerable for precise assembly tasks. Furthermore, it is time consuming to convert from joint torques to cartesian hand forces and moments since it involves inversion of the J^T matrix - a major problem with force feedback is that even short delays in computation can cause instability [Whitney 1987]. Hence, wrist sensors such as the Scheinmann wrist should be used since they eliminate motor torque and dynamic link effects by measuring forces directly at hand level to high resolution. The wrist sensor should be mounted as close to the hand as possible. Mounting at the gripper fingers itself is not practical as the sensor will experience noise problems and wear-and-tear. The application of signal processing, filtering and estimation for prediction is required for noise handling, and this is too time consuming for the servocontrol loop level.

The resolution of force coordinates is based on virtual work arguments. Virtual work is performed when a real force moves through a virtual displacement. The principle of virtual work is one of the two cornerstones underlying structural analysis (the other being the principle of equilibrium). It states that a rigid body in equilibrium will have zero net work done by a system of forces acting on it through an arbitrary displacement. Hence, between any two coordinate frames, the virtual work done by any applied force is the same [Paul 1981]:

$dW_i = dW_{ext}$ or equivalently $F_i^T dx_i = F_{ext}^T dx_{ext}$ where F=generalised force vector

Since the generalised force vector at the joints are of revolute form they represent the joint torques:

$\tau_i^T dx_i = F_{eff}^T dx_{eff}$ for revolute jointed manipulator where $F_i = \tau_i$

The external forces acting on the manipulator (subscript "ext") are assumed to be precisely coincident with those forces measured by the wrist force sensor (subscript "eff").

Now, $dx_{eff} = v_{eff} = J\theta_i = Jv_i$:

Hence, $\tau_i^T v_i = F_{eff}^T J v_i$

ie. $\tau = J^T F_{ext}$ where $F_{ext} = (f_x^{ext} f_y^{ext} f_z^{ext} n_x^{ext} n_y^{ext} n_z^{ext})^T$ (2.26)

$$\tau = (\tau_1 \tau_2 \tau_3 \tau_4 \tau_5 \tau_6)^T$$

$$J^T = \begin{pmatrix} J_{11} & J_{12} & J_{13} & J_{14} & J_{15} & J_{16} \\ J_{21} & J_{22} & J_{23} & J_{24} & J_{25} & J_{26} \\ J_{31} & J_{32} & J_{33} & J_{34} & J_{35} & J_{36} \\ J_{41} & J_{42} & J_{43} & J_{44} & J_{45} & J_{46} \\ J_{51} & J_{52} & J_{53} & J_{54} & J_{55} & J_{56} \\ J_{61} & J_{62} & J_{63} & J_{64} & J_{65} & J_{66} \end{pmatrix}$$

This enables force control to be implemented explicitly at hand level within the servo-controller.

Chapter 3

ROBOT DYNAMICS

Although space robotics *per se* has only recently been considered in the literature, multi-body dynamics in space has attracted interest for some years due to its highly complex nature and applicability to orbiting spacecraft. Hooker & Margulies (1965) first considered the dynamics formulation of multibody systems in space. They found that for n rigid bodies connected by rotational joints in an arbitrary open topological tree configuration (ie. no closed loops), any rotational motion of the bodies produced a relative translation with respect to each other. They introduced the notion of connection barycentre which they defined as the composite centre of mass of each body obtained by loading each joint of the body with the total residual mass of the system connected to that joint, ie. the mass distribution is represented by the total mass of inboard links Mu_i acting on the inboard joint i and the total mass of outboard links $M(1-u_{i+1})$ acting on the outboard joint i+1 to form an augmented body.
The barycentric vector from the i^{th} barycentre to i^{th} body centre of mass:

$c_i = r_i u_i + s_i(1-u_{i+1})$ where $u_i = \sum_{j=0}^{i-1} \frac{m_j}{M_T}$ for i=0....n

M_T=total mass of all links
r_i=link vector from joint i-1 to link i centre of mass
s_i=link vector from link i centre of mass to joint i

They used the barycentric concept to derive the inertia dyadics for the Newton-Euler dynamics equations to describe the attitude equations of the system. Hooker (1970) extended the barycentric approach by eliminating the constraint torques for the n body attitude equations using the Lagrangian method, reducing the number of equations from 3n to r where r=number of rotational degrees of freedom of the multibody system. This method is not really suitable for robotic application since it requires recomputation of the barycentres whenever any payload is acquired or released, generating high computational overheads and is restricted to open chain configurations.

Ho (1977) stated that Hooker later abandoned the barycentric approach in favour of the direct path method advocated by Ho. This method involves determining the contribution of the motion of each body singly to coefficient matrices of the overall dynamic equations describing the system. The direct path is a vectorial path from the main reference body 0 to each separate body j centre of mass comprising the system. The motion of each body influences the motion of the whole system. Since linear and angular positions, velocities and accelerations are related to the other bodies and to the reference coodinates kinematically, these direct path vectors transform the influence of the motion of one body to the other bodies. However, for revolute robots, this method is inappropiate since almost inevitably, more than one link motion is required to move to attain any particular point in space. Jerkovsky (1978) adapted the direct path method by introducing the concept of path matrices and reference matrices which describe the particular topology of the system.

Path matrix, $\pi_{ij} = \begin{cases} 1 \\ 0 \end{cases}$ 1 signifies body j between body 1 and body i, 0 otherwise

Reference matrix, $\rho_{ij} = \begin{cases} 1 \\ - \\ 0 \end{cases}$ 1 if i=j,-1 if body i referred to body j, 0 otherwise

and $\rho\pi = \pi\rho = I$.

He derived the primitive equations of motion for each body separately considering them to be free bodies. By converting inertial velocities to relative velocities using linear operators, he was able then to apply the constraints of motion to the system equations. Hughes (1979) suggested that the direct path method is superior to the barycentric approach. However, the method is unsuitable for closed chain configurations whose inertial velocities cannot be expressed as independent sets of relative velocities for each body. These methods are very general and may be applied to multiple degree-of-freedom joints as well as for forward dynamic analysis for simulation. However, generality is not an issue for space robotic control which only require inverse dynamics solutions where each actuator has only a single degree of freedom, and efficient equations have been developed for these problems. Robot dynamics is concerned with relating joint motions (position, velocity, acceleration) to the required forces and torques to achieve those motions. The required actuator joint torques are computed to enforce tracking of the prescribed trajectory. The torques are fedforward to the joint servos to provide fast response without instability.

Generally speaking, two main approaches exist for the description of the dynamics of robots: the Lagrange-Euler technique and the Newton-Euler technique (excluding more exotic techniques such as characterising robot dynamics as a Kalman filter problem [Rodriguez 1987]) and these two formulations are in fact equivalent [Silver 1982]. Both generate a set of 6 coupled second order nonlinear differential equations in position, velocity and acceleration. The Lagrange-Euler technique yields highly structured equations highly suited to control analysis in the state space form by decomposing the complex system into a set of smaller systems [Bejczy & Tarn 1986].

Generalised force, $\tau_i = \frac{d}{dt}\left(\frac{\partial L}{\partial \dot{\theta}_i}\right) - \left(\frac{\partial L}{\partial \theta_i}\right)$ where L=T-V=Lagrangian

T=kinetic energy=$\frac{1}{2}$mvv + $\frac{1}{2}$wIw

V=potential energy=0 in zero-gravity

ie. $\tau = \frac{d}{dt}\left(\frac{\partial T}{\partial \dot{\theta}}\right) - \left(\frac{\partial T}{\partial \theta}\right)$

where $T = \frac{1}{2}\dot{\theta}^T D(\theta)\dot{\theta}$=Kinetic Energy which forms the Routhian and Hamiltonian functions where $D(\theta)$=inertia matrix. The Lagrange-Euler method yields the general form of the dynamics [Walker & Orin 1982]:

$$\tau_i = \sum_{k=1}^{n} D_{ik}(\theta)\ddot{\theta}_k + \sum_{k=1}^{n}\sum_{m=1}^{n} H_{ikm}(\theta,\dot{\theta}) + G_i(\theta) + B_i\dot{\theta}_i \qquad (3.1)$$

$D(\theta)$ represents the symmetric positive definite ***nxn*** mass/inertia matrix whereby the diagonals represent joint inertias and off-diagonals the inertial coupling between joints, $H(\theta,\dot{\theta})$ represents the ***nx1*** vector of coriolis and centrifugal forces, $G(\theta)$ represents the ***nx1*** gravity loading vector, and B represents the actuator viscous damping coefficient. H and G represent the nonlinear terms, and viscous damping is usually neglected to a first approximation. Terms involving $\dot{\theta}_i^2$ are the centrifugal components while terms involving $\dot{\theta}_i\,\dot{\theta}_j$ are the coriolis components. The Lagrangian equations are

thus coupled and highly nonlinear. Hamman (1985) considered that the space environment exerts special conditions on manipulator dynamics. Based on ESA contract report, ESA CR(P) 2048, he outlined low gravity, low end effector speed (and so low centrifugal and coriolis forces) but strong inertial cross coupling to be peculiar to space robots. The advantage of microgravity entails that actuator torques are available for robot motion without the need to support the weight of the manipulator or payload [Lumia & Wavering 1989]. Motion trajectories comprise of an acceleration phase, a constant velocity phase and a deceleration phase. Inertial cross-coupling occurs when the manipulator changes configuration. If the constant velocity phase is short compared with the acceleration/deceleration phases (eg. for near time-optimal bang-bang maneouvres) then the inertial cross coupling will be significant over most of the trajectory. The net moment of inertia opposes the acceleration at one joint due to the effective stiffness of the other joints and loads. Coupling is especially dominant for the positioning links over those of the wrist due to their higher moments of inertia. Coriolis and centrifugal terms are significant and dominate at high velocity phases becoming insignificant near the goal point when joint velocities are decreasing [Kosha & Kanade 1988]. These terms become small only when the joints are driven slowly and generally their neglect will generate significant errors in joint torque generation. However, the gravity term even for terrestrial manipulators is small. The average execution time for the Lagrangian formulation is ~8 sec for the Stanford manipulator on a PDP11/45 - clearly this is not suitable for real-time control and is suitable only for modelling analysis. It is conceivable that future control systems may be implemented on parallel systolic computer hardware architectures allowing real time control but this is not likely for space systems in the near future.

Khatib (1987) suggested casting all the Lagrange-Euler dynamics in end effector (operational space) coordinates:

Generalised cartesian force, $F = \lambda(q)\ddot{q} + \mu(q,\dot{q}) + p(q)$

Since $\tau = J^T F = D(\theta)\ddot{\theta} + C(\theta,\dot{\theta}) + G(\theta)$:

$$F = \lambda(\theta)\ddot{\theta} + J^{-T}C(\theta,\dot{\theta}) + J^{-T}G(\theta) \quad \text{where} \quad \lambda(\theta) = J^{-T}(\theta)D(\theta)$$

According to this formulation:

$$\lambda(x) = J^{-T}(\theta)D(\theta)J^{-1}(\theta)$$

$$\mu(x,\dot{x}) = J^{-T}(\theta)C(\theta,\dot{\theta}) - \lambda(\theta)\dot{J}(\theta)\dot{\theta}$$

$$p(x) = J^{-T}(\theta)G(\theta)$$

$$F = J^{-T}(\theta)\tau$$

Although this formulation allows the specification of the control law in end effector and task coordinates, eg. $\ddot{q} = \ddot{q}^d + K_p(q^d - q) + K_v(\dot{q}^d - \dot{q})$, its extreme complexity exceeds that of the Lagrange-Euler formulation in joint coordinates (K_p and K_V are position and velocity control gains respectively; superscript "d" indicates desired variable value, and unsuperscripted variable indicates actual variable value as measured by sensors).

Kane & Levinson (1980) compared several dynamics formulations for multibody systems in terms of equation simplicity and difficulty of derivation. They found that the Newton-Euler methods are much more efficient computationally than Langrangian

approaches. They introduced their own formulation of generating partial velocities which linearise the kinematics to give generalised velocities and enabled the derivation of generalised forces by serial approximation. They later adapted those equations specifically for robotics applications [Kane & Levinson 1983] which formed the basis of Konigstein et al's (1989) approach to the Newton-Euler type of computed torque control of a two-armed space robot using Kane's equations for rate and acceleration resolution with momentum constraints. This approach exploited the purely closed chain kinematic configuration without considering the contact interaction forces. Kane's equations involve serial approximations whereas the classical Newton-Euler method is exact. Nagashima & Nakaruma (1992) suggested that the Newton-Euler dynamics method of computation offers the most efficient technique for space-based robotics due to the recursive nature of those equations.

Luh, Walker & Paul (1980) derived a Newton-Euler formulation for robot mechanisms where D'Alembert's principle is applied to each link sequentially. This method was found to be extremely efficient with a linear computational complexity of O(n) where n=number of links. They further reduced the computational requirement by referring all link parameters to their own coordinate systems rather than in base reference coordinates. However, for space-based manipulators, the total reaction moment on the mounting platform is required for control purposes which necessitates the Newton-Euler computation to be performed in base reference coordinates as well but this does increases the computational overhead only marginally. Hollerbach (1980) derived a recursive formulation for the Lagrangian dynamics method to reduce the computational overheads associated with the formulation. Since Coriolis and centrifugal forces are significant at moderate speeds of motion, they cannot be ignored. He derived a series of forward recursive equations of velocities and accelerations from the base to the end effector and backward recursive equations of forces from the end effector to the base for real-time Lagrange-Euler computation but this destroyed the structure of the LE approach. He also used 3x3 rotation matrices and vectors rather than the usual 4x4 homogeneous matrices to reduce unnecessary computation. This reduced the complexity of the Lagrangian method from $O(n^4)$ to O(n). Silver (1982) later showed through tensor methods that the Newton-Euler and Lagrangian recursive formulations were equivalent since the 9 element time derivative of the 3x3 rotational matrix of the Lagrangian equates to the 3 element angular velocity components of the Newton-Euler formulation. However, the Newton-Euler method remains 60% more efficient than the recursive Lagrangian method. Hence this is the algorithm of choice for deriving the robot dynamics.

The Newton-Euler technique explicitly states all constraint forces and moments and generates a set of recursive equations [Orin et al 1979; Luh, Walker & Paul 1980]. It is stipulated here that all dynamics equations and variables are referred to base coordinates in addition to their own link coordinates for reasons that are elaborated in Chapter 6. Although this means that the moments of inertia of each link changes as the arm configuration changes, this does not disadvantage the scheme with excessive computation. Kinematic information is propagated from the base to the hand and dynamic information is propagated back from the hand to the base. Such a recursive structure lends itself to implementation using a pipelined microprocessor architecture reducing the number of wires inside the robot arm. Newton's laws of motion are applied through D'Alembert's principle to each link in turn: "For any body, the

algebraic sum of imaginary external forces and forces resisting motion in any direction for equilibrium is zero".

The forward recursive equations derive the velocities and accelerations of each link at its joint $\begin{pmatrix} v_i \\ w_i \end{pmatrix}$ and $\begin{pmatrix} \dot{v}_i \\ \dot{w}_i \end{pmatrix}$, the velocities of each link centre of mass (subscript ci), and the forces at each link centre of mass $\begin{pmatrix} F_{ci} \\ N_{ci} \end{pmatrix}$:

$$
\begin{aligned}
w_i &= w_{i-1} + z_{i-1}\dot{\theta}_i \\
\dot{w}_i &= \dot{w}_{i-1} + z_{i-1}\ddot{\theta}_i + w_{i-1} \times (z_{i-1}\dot{\theta}_i) \\
v_i &= v_{i-1} + w_i \times l_i \\
\\
\dot{v}_i &= \dot{v}_{i-1} + \dot{w}_{i-1} \times l_i + w_i \times (w_i \times l_i) \\
v_{ci} &= v_i + w_i \times (-s_i) \\
\dot{v}_{ci} &= \dot{v}_i + \dot{w}_i \times (-s_i) + w_i \times (w_i \times (-s_i)) \\
F_{ci} &= m_i \dot{v}_{ci} \\
N_{ci} &= I_i \dot{w}_i + w_i \times (I_i w_i)
\end{aligned}
\qquad (3.2)
$$

The backward recursive equations are:

$$
\begin{aligned}
f_i &= f_{i+1} + F_{ci} - m_i g \\
\\
n_i &= n_{i+1} + N_{ci} + l_i \times f_{i+1} + (l_i - s_i) \times F_{ci} \\
\\
\tau_i &= n_i^T z_{i-1} + b_i \dot{\theta}_i
\end{aligned}
\qquad (3.3)
$$

where z_{i-1}=rotational axis of joint i

l_i=length of link i

s_i=position of linki centre of mass from joint i

m_i=mass of link i

F_{ci}=total force on link i centre of mass

N_{ci}=total moment about link i centre of mass

I_i=inertia matrix of link i

f_i=force on link i due to link i-1

n_i=moment on link i due to link i-1

w_i=angular velocity of joint i

$\dot{w}_i$=angular acceleration of joint i

v_i=linear velocity of joint i

$\dot{v}_i$=linear acceleration of joint i

v_{ci}=linear velocity of link i centre of mass

$\dot{v}_{ci}$=linear acceleration of link i centre of mass

τ_i=actuator torque on joint i

b_i=viscous friction on joint i

This formulation generates the joint torques required to provide the stipulated end effector positions, velocities, and accelerations.

3.1 DERIVATION OF NEWTON-EULER DYNAMICS

Consider a fixed inertial frame of reference with origin O_{XYZ} coincident with the origin of a rotating frame O_{xyz} with a vector **r** to point P [Fu, Gonzalez & Lee 1987]:

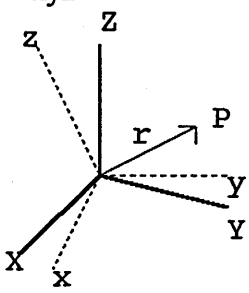

r=XI+YJ+ZK from the fixed frame and **r**=xi+yj+zk from the rotating frame.

From the fixed frame: $\frac{dr}{dt} = \dot{X}I + \dot{Y}J + \dot{Z}K$ - this is the velocity of P relative to O_{XYZ}

From the rotating frame: $\frac{\delta r}{\delta t} = \dot{x}i + \dot{y}j + \dot{z}k$ - this is the velocity of P relative to O_{xyz}.

Now, $\frac{dr}{dt} = \dot{x}i + \dot{y}j + \dot{z}k + x\frac{di}{dt} + y\frac{dj}{dt} + z\frac{dk}{dt}$

where $\frac{di}{dt} = w_z j - w_y k = w \times i; \frac{dj}{dt} = w_x k - w_z i = w \times j; \frac{dk}{dt} = w_y i - w_x j = w \times k$:

Hence, $\frac{dr}{dt} = \frac{\delta r}{\delta t} + x(w \times i) + y(w \times j) + z(w \times k)$

If **r** is fixed in the rotating frame, $\frac{\delta r}{\delta t} = 0 \rightarrow \frac{dr}{dt} = w \times r$

Acceleration with respect to the fixed reference frame is found by differentiation:

$$\frac{d^2r}{dt^2} = \frac{d}{dt}\left(\frac{\delta r}{\delta t} + w \times r\right) = \frac{d}{dt}\left(\frac{\delta r}{\delta t}\right) + \frac{d}{dt}(w \times r) = \left(\frac{\delta^2 r}{\delta t^2} + w \times \frac{\delta r}{\delta t}\right) + w \times \frac{dr}{dt} + \frac{dw}{dt} \times r$$

$$= \frac{\delta^2 r}{\delta t^2} + w \times \frac{\delta r}{\delta t} + w \times \left(\frac{\delta r}{\delta t} + w \times r\right) + \frac{dw}{dt} \times r = \frac{\delta^2 r}{\delta t^2} + 2w \times \frac{\delta r}{\delta t} + w \times (w \times r) + \frac{dw}{dt} \times r$$

Now, $\dot{w} = \frac{\delta w}{\delta t} + w \times w = \frac{\delta w}{\delta t}$:

$$\frac{d^2r}{dt^2} = \frac{\delta^2 r}{\delta t^2} + 2w \times \frac{\delta r}{\delta t} + \dot{w} \times r + w \times (w \times r)$$

This is the Coriolis theorem: the first term represents the acceleration of the point with respect to the rotating frame O_{xyz}.; the second term represents the Coriolis acceleration perpendicular to the trajectory path; the third term represents the rate of change of angular velocity; and the fourth term represents the centrifugal acceleration towards the axis of revolution.

Now, consider translating the rotating coordinate system such that the origin of O_{xyz} is displaced by a vector **h** with respect to O_{XYZ}:

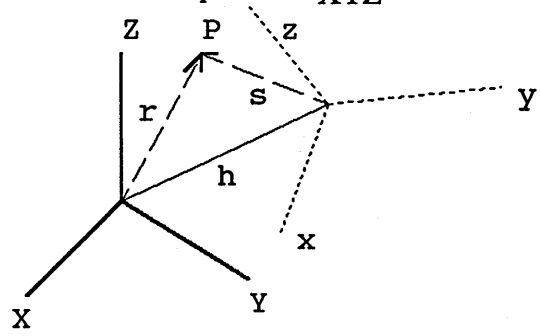

Now, **r**=**s**+**h**

From a fixed frame of reference O_{XYZ} , the velocity of P is $v = \frac{dr}{dt} = \frac{ds}{dt} + \frac{dh}{dt} = v_s + v_h$

where v_S=velocity of P relative to O_{xyz}, and v_h=velocity of O_{xyz} relative to O_{XYZ}.

Now, $\frac{ds}{dt} = \frac{\delta s}{\delta t} + w \times s$, so relative to the fixed coordinate system O_{XYZ} :

$v = (\frac{\delta s}{\delta t} + w \times s) + \frac{dh}{dt}$ and $\dot{v} = \frac{d^2r}{dt^2} = \frac{d^2s}{dt^2} + \frac{d^2h}{dt^2} = \frac{\delta^2 s}{\delta t^2} + 2w \times \frac{\delta s}{\delta t} + \dot{w} \times s + w \times (w \times s) + \frac{d^2h}{dt^2}$

3.1.1 Link Kinematics

These results are now applied to the link kinematics [Luh Walker & Paul 1980; McInnis & Lin 1986; de Silva 1991]. Link kinematics define the required information for the Newton-Euler dynamics formulation with respect to base reference coordinates $(x_0 y_0 z_0)$. The centroid of each link i is assumed to be located along the line segment connecting joint i-1 and i, ie. each link is a body of revolution about its central axis of symmetry.

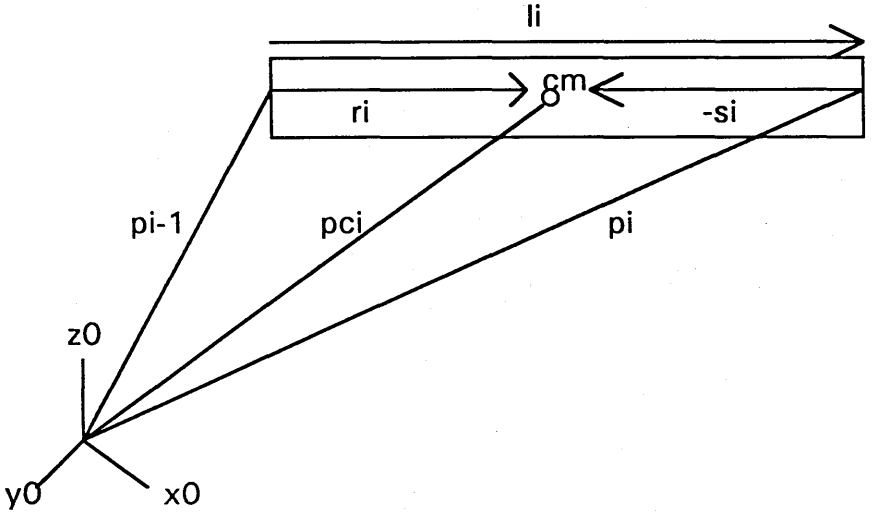

Some preliminary definitions follow:

$(x_i y_i z_i)$ defines the coordinate system at joint i where z_{i-1} is the axis of rotation of link i; $(x_0 y_0 z_0)$ defines the base reference coordinate system; $(x_6 y_6 z_6)=(nsa)$ defines the hand coordinate system.

v_i^0 =linear velocity of moving coordinate system $(x_i y_i z_i)$ with respect to base reference coordinates $(x_0 y_0 z_0)$;

w_i^0=angular velocity of moving coordinate system $(x_i y_i z_i)$ with respect to base reference coordinates $(x_0 y_0 z_0)$;

v_i^{i-1} =linear velocity of coordinate system $(x_i y_i z_i)$with respect to coordinate system $(x_{i-1} y_{i-1} z_{i-1})$

w_i^{i-1}=angular velocity of coordinate system $(x_i y_i z_i)$ with respect to coordinate system $(x_{i-1} y_{i-1} z_{i-1})$.

By definition: $l_i = p_i - p_{i-1} \rightarrow p_i = l_i + p_{i-1}$ where l_i=position from the origin of the i frame with respect to the i-1 frame.

Now, $v_i^0 = v_{i-1}^0 + \frac{\delta l_i}{\delta t} + w_{i-1}^0 \times l_i$

$$\dot{v}_i^0 = \dot{v}_{i-1}^0 + \frac{\delta^2 l_i}{\delta t^2} + 2w_{i-1}^0 \times \frac{\delta l_i}{\delta t} + \dot{w}_{i-1}^0 \times l_i + w_{i-1}^0 \times (w_{i-1}^0 \times l_i)$$

Furthermore, $w_i^0 = w_{i-1}^0 + w_i^{i-1}$

$$\dot{w}_i^0 = \dot{w}_{i-1}^0 + \dot{w}_i^{i-1}$$

$$\rightarrow \dot{w}_i^0 = \dot{w}_{i-1}^0 + \frac{\delta w_i^{i-1}}{\delta t} + w_{i-1}^0 \times w_i^{i-1} \text{ since } \dot{w}_i^{i-1} = \frac{\delta w_i^0}{\delta t} + w_{i-1}^0 \times w_i^0$$

For a rotational joint the coordinate system $(x_i y_i z_i)$ has angular velocity w_i^{i-1} about the z_{i-1} axis in the $(x_{i-1} y_{i-1} z_{i-1})$ coordinate system. Hence, relative to link i-1 coordinates $(x_{i-1} y_{i-1} z_{i-1})$:

$$\left.\begin{aligned} w_i^{i-1} &= z_{i-1}\dot{\theta}_i \\ \frac{\delta w_i^{i-1}}{\delta t} &= z_{i-1}\ddot{\theta}_i \end{aligned}\right\} \text{for revolute joints, and} \quad \left.\begin{aligned} w_i^{i-1} &= 0 \\ \frac{\delta w_i^{i-1}}{\delta t} &= 0 \end{aligned}\right\} \text{for prismatic joints.}$$

Hence, referred to base coordinates $(x_0 y_0 z_0)$:

$$\begin{aligned} w_i^0 &= w_{i-1}^0 + z_{i-1}\dot{\theta}_i \quad \text{for a revolute joint} \\ &= w_{i-1}^0 \quad \text{for a prismatic joint} \\ \dot{w}_i^0 &= \dot{w}_{i-1}^0 + z_{i-1}\ddot{\theta}_i + w_{i-1}^0 \times (z_{i-1}\dot{\theta}_i) \quad \text{for a revolute joint} \\ &= \dot{w}_{i-1}^0 \quad \text{for a prismatic joint} \end{aligned}$$

Similarly, relative to link i-1 coordinates $(x_{i-1} y_{i-1} z_{i-1})$:

$$\left.\begin{aligned} \frac{\delta l_i}{\delta t} &= w_i^{i-1} \times l_i \\ \frac{\delta^2 l_i}{\delta t^2} &= \frac{\delta w_i^{i-1}}{\delta t} \times l_i + w_i^{i-1} \times \frac{\delta l_i}{\delta t} = \frac{\delta w_i^{i-1}}{\delta t} \times l_i + w_i^{i-1} \times (w_i^{i-1} \times l_i) \end{aligned}\right\} \text{for revolute joints;}$$

$$\left.\begin{aligned} \frac{\delta l_i}{\delta t} &= z_{i-1}\dot{\theta}_i \\ \frac{\delta^2 l_i}{\delta t^2} &= z_{i-1}\ddot{\theta}_i \end{aligned}\right\} \text{for prismatic joints;}$$

Hence referred to base coordinates $(x_0 y_0 z_0)$:

$$\begin{aligned} v_i^0 &= v_{i-1}^0 + w_{i-1}^0 \times l_i + w_i^{i-1} \times l_i = v_{i-1}^0 + w_i^0 \times l_i \quad \text{for a revolute joint} \\ &= v_{i-1}^0 + z_{i-1}\dot{\theta}_i + w_i^0 \times l_i \quad \text{for a prismatic joint} \end{aligned}$$

For the centre of mass of a link: $v_{ci} = v_i^0 + w_i^0 \times (-s_i)$ since $p_{ci} = p_i - s_i$

Now, $\dot{v}_i^0 = \dot{v}_{i-1}^0 + \frac{\delta^2 l_i}{\delta t^2} + \dot{w}_{i-1}^0 \times l_i + 2w_{i-1}^0 \times \frac{\delta l_i}{\delta t} + w_{i-1}^0 \times (w_{i-1}^0 \times l_i)$

Using the following relations: (axb)xc=b(a.c)-a(b.c)

ax(bxc)=b(a.c)-c(a.b)

and $\frac{\delta^2 l_i}{\delta t^2} = \frac{\delta w_i^{i-1}}{\delta t} \times l_i + w_i^{i-1} \times w_i^{i-1} \times (w_i^{i-1} \times l_i)$; $\frac{\delta w_i^{i-1}}{\delta t} = z_{i-1}\ddot{\theta}_i \times l_i$; $\frac{\delta l_i}{\delta t} = w_i^{i-1} \times l_i$;

we have: $\frac{\delta^2 l_i}{\delta t^2} + w_i^0 \times l_i = w_{i-1}^0 \times (w_{i-1}^0 \times l_i) + w_i^0 \times l_i - (w_{i-1}^0 \times w_i^{i-1}) \times l_i = \dot{w}_i^0 \times l_i$

$$2w_{i-1}^0 \times \frac{\delta l_i}{\delta t} = 2[w_i^{i-1}(w_{i-1}^0 . l_i) - l_i(w_{i-1}^0 . w_i^{i-1})] = 0$$

$$\begin{aligned} w_{i-1}^0 \times (w_{i-1}^0 \times l_i) &= w_i^0 \times (w_i^0 \times l_i) - w_i^{i-1}(w_i^{i-1} . l_i) - l_i(w_i^{i-1} . w_i^{i-1}) \\ &= w_i^0 \times (w_i^0 \times l_i) \end{aligned}$$

Hence,

$\dot{v}_i^0 = \dot{v}_{i-1}^0 + \dot{w}_i^0 \times l_i + w_i^0 \times (w_i^0 \times l_i)$ for a revolute joint

$\dot{v}_i^0 = \dot{v}_{i-1}^0 + z_{i-1}\ddot{\theta}_i + w_i^0 \times l_i + 2w_i^0 \times (z_{i-1}\dot{\theta}_i) + w_i^0 \times (w_i^0 \times l_i)$ for a prismatic joint

$\dot{v}_{ci}^0 = \dot{v}_i^0 + \dot{w}_i^0 \times (-s_i) + w_i^0 \times (w_i^0 \times -s_i)$

3.1.2 Link Dynamics

Next, the forces and torques need to be calculated:

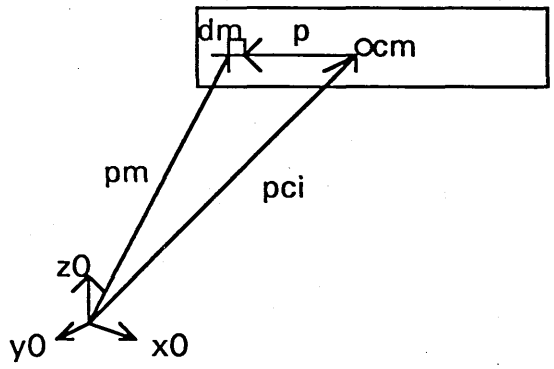

The total angular momentum about the base reference point is the sum of angular moments of all rigid bodies composing the manipulator (assuming zero or negligible gravity):

$H_0 = \int_L p_m \times \frac{dp_m}{dt} dm = \sum_{i=1}^{n} \int_i (p_m \times \frac{dp_m}{dt}) dm$ at any mass element dm .

Now, $p_m = p_{ci} + p$: $H_0 = \sum_{i=1}^{n} \int (p_{ci} \times \frac{dp_{ci}}{dt}) dm + \sum_{i=1}^{n} \int (p \times \frac{dp}{dt}) dm$ where $v_{ci} = \frac{dp_{ci}}{dt}$

Now, $\frac{^0dp}{dt}$ in reference coordinates is related to $\frac{^idp}{dt}$ in link coordinates by:

$\frac{^0dp}{dt} = \frac{^idp}{dt} + w_i \times p$ where w_i=angular velocity of link i centre of mass from base reference coordinates.

ie. $H_0 = \sum_{i=1}^{n} \left[m_i p_{ci} \times \frac{dp_{ci}}{dt} + \int p \times (\frac{^idp}{dt} + w_i \times p) dm \right]$

The position of the centre of mass of each link is fixed with respect to link coordinates so $\int p dm = 0$ so: $H_0 = \sum_{i=1}^{n} m_i p_{ci} \times \frac{dp_{ci}}{dt} + \int p \times (w_i \times p) dm = \sum_{=1}^{n} m_i p_{ci} \times \frac{dp_{ci}}{dt} + I_{ci} w_i$

where $I_{Ci} = \int_V rr.dm = mk^2$ =moment of inertia of body i about its own centre of mass; k=radius of gyration.

eg. moment of inertia of a rod about an axis through its mass centre, $I_{rod} = \frac{2}{3} ml^2$

moment of inertia of a disc about its central axis, $I_{disc} = \frac{1}{2} mr^2$

moment of inertia of a sphere about a diameter, $I_{sphere} = \frac{2}{5} mr^2$

moment of inertia of a uniform block about one central face-parallel axis, $I_{block} = \frac{1}{3} m[(\frac{l_1}{2})^2 + (\frac{l_2}{2})^2]$

Assuming that the links are bodies of revolution and are symmetric about their central axes and have a uniform mass distribution:

$$I_{ci} = diag(J) = \begin{pmatrix} I_{ix} & 0 & 0 \\ 0 & I_{iy} & 0 \\ 0 & 0 & I_{iz} \end{pmatrix} \text{ where } \begin{matrix} I_{ix} = I_{iy} = 0.5 m_i r^2 \\ I_{iz} = 0.67 m_i l^2 \end{matrix}$$

Now for revolute joints, p_{ci} is constant: $H_0 = \sum_{i=1}^{n} I_{ci} w_i$

By definition, moments are the rate of change of angular momentum and $N_0 = \sum_{i=1}^{n} N_{ci}$:

$N_0 = \dot{H}_0 = \frac{d}{dt} \int_L p_m \times \frac{^0dp_m}{dt} dm = \int_L p_m \times dF$ where $dF = \frac{^0d^2p_m}{dt^2}.dm$

Hence, $N_0 = \sum_{i=1}^{n}\left[m_i p_{ci} \times \frac{d^2 p_{ci}}{dt^2} + \frac{d(I_{ci} w_i)}{dt} + w_i \times (I_{ci} w_i)\right]$

Now, $\frac{d^2 p_{ci}}{dt^2} = 0$ since p_{ci} is constant with respect to its own coordinates:

$$N_0 = \sum_{i=1}^{n}\left[I_{ci}\dot{w}_i + w_i \times (I_{ci} w_i)\right]$$

The first term is the rate of change of angular momentum relative to base reference coordinates and the second term is the rate of change of angular momentum relative to a body-corotational reference frame.

Similarly, $F_0 = \sum_{i=1}^{n} F_{ci} = \sum_{i=1}^{n} m_i \frac{d^2 p_{ci}}{dt^2}$ where $\dot{v}_{ci} = \frac{d^2 p_{ci}}{dt^2}$

At each link: $F_{ci} = m_i \dot{v}_{ci}$ and $N_{ci} = I_{ci}\dot{w}_i + w_i \times (I_{ci} w_i)$

For the backward recursion of forces and torques assuming that gravity is negligible, we have at the centre of mass of each link:

$F_{ci} = f_i - f_{i+1}$ where f_i=force due to link i-1

f_{i+1}=force due to link i+1

$\rightarrow f_i = F_{ci} + f_{i+1} = m_i \dot{v}_{ci} + f_{i+1}$

Similarly, $N_{ci} = n_i - n_{i+1} - r_i \times f_i - s_i \times f_{i+1}$

Note that f_{n+1} and n_{n+1} represent external forces and torques on the manipulator hand.

Now,

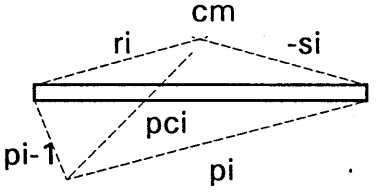

$r_i = p_{ci} - p_{i-1}$

$-s_i = p_{ci} - p_i$

$l_i = r_i - s_i = p_i - p_{i-1}$

Hence, $N_{ci} = n_i - n_{i+1} - p_{ci} \times f_i + p_{i-1} \times l_i + p_{ci} \times f_{i+1} - p_i \times f_{i+1}$

Now, $n_i - n_{i+1} + (p_{i-1} - p_{ci}) \times F_{ci} - l_i \times f_{i+1}$

$= n_i - n_{i+1} - p_{ci} \times f_i + p_{i-1} \times f_i + p_{ci} \times f_{i+1} - p_i \times f_{i+1}$

Hence, $N_{ci} = n_i - n_{i+1} + (p_{i-1} - p_{ci}) \times F_{ci} - l_i \times f_{i+1}$

or $N_{ci} = n_i - n_{i+1} - (l_i - s_i) \times F_{ci} - l_i \times f_{i+1}$

$\rightarrow n_i = N_{ci} + n_{i+1} + (l_i - s_i) \times F_{ci} + l_i \times f_{i+1}$

The torque at joint i produces a rotation of θ_i of coordinates $(x_i y_i z_i)$ about the z_{i-1} axis (for revolute joints), so $\tau_i = z_{i-1} n_i$ or $\tau_i = z_{i-1} n_i + b_i \dot{\theta}_i$ if viscous damping is included. Other slightly different formulations exist, but they offer no computational advantage, eg. de Silva (1991). Hence, from the joint kinematic variables, the joint torques may be computed.

3.1.3 Link Referenced Formulation

The drawback of these recursive equations is that all link inertia matrices are referenced to base coordinates, ie. they will change as the robot arm configuration

changes. By referring all variables to their own link coordinates, the moments of inertia of each link are referred with respect to their own principal axis coordinates, and so will be invariant: $I_{ci} = R_0^i(R_i^0 I_{ci} R_0^i)R_i^0$ since the inverse of the 3x3 R-submatrix of the 4x4 DH "A" matrix is its transpose.

$$\text{ie. } \begin{pmatrix} N_{cix} \\ N_{ciy} \\ N_{ciz} \end{pmatrix} = \begin{pmatrix} I_{cix} & 0 & 0 \\ 0 & I_{ciy} & 0 \\ 0 & 0 & I_{ciz} \end{pmatrix} \begin{pmatrix} \dot{w}_{ix} \\ \dot{w}_{iy} \\ \dot{w}_{iz} \end{pmatrix} + \begin{pmatrix} w_{ix} \\ w_{iy} \\ w_{iz} \end{pmatrix} \times \left[\begin{pmatrix} I_{cix} & 0 & 0 \\ 0 & I_{ciy} & 0 \\ 0 & 0 & I_{ciz} \end{pmatrix} \begin{pmatrix} w_{ix} \\ w_{iy} \\ w_{iz} \end{pmatrix} \right]$$

$$= \begin{pmatrix} I_{cix}\dot{w}_{ix} + (I_{ciz} - I_{ciy})w_{iy}w_{iz} \\ I_{ciy}\dot{w}_{iy} + (I_{ix} - I_{iz})w_{ix}w_{iy} \\ I_{ciz}\dot{w}_{iz} + (I_{iy} - I_{iz})w_{ix}w_{iy} \end{pmatrix}$$

To transform all dynamics variables back into their own link coordinates the inverse of the rotation matrix is required:

$$R_{i-1}^i = (R_i^{i-1})^T = \begin{pmatrix} c\theta_i & s\theta_i & 0 \\ -c\alpha s\theta_i & c\alpha c\theta_i & s\alpha \\ s\alpha s\theta_i & -s\alpha c\theta_i & c\alpha \end{pmatrix}$$ which transforms $(x_i y_i z_i)$ to $(x_{i-1} y_{i-1} z_{i-1})$.

so that the Newton-Euler equations now become:

$$R_0^i w_i = R_0^i(w_{i-1} + z_{i-1}\dot{\theta}_i) = R_{i-1}^i(R_0^{i-1}w_i + R_0^{i-1}z_{i-1}\dot{\theta}_i) = R_{i-1}^i(R_0^{i-1}w_i + z_0\dot{\theta}_i)$$

$$R_0^i \dot{w}_i = R_{i-1}^i(R_0^{i-1}\dot{w}_{i-1} + R_0^{i-1}z_{i-1}\ddot{\theta}_i + R_0^{i-1}w_i \times R_0^{i-1}z_{i-1}\dot{\theta}_i)$$

$$= R_{i-1}^i(R_0^{i-1}\dot{w}_{i-1} + z_0\ddot{\theta}_i + R_0^{i-1}w_{i-1} \times z_0\dot{\theta}_i)$$

$$R_0^i \dot{v}_i = R_{i-1}^i R_0^{i-1}\dot{v}_{i-1} + (R_0^i \dot{w}_i \times R_0^i l_i) + R_0^i w_i \times [(R_0^i w_i) \times (R_0^i l_i)]$$

$$R_0^i \dot{v}_{ci} = R_0^i \dot{v}_i + R_0^i \dot{w}_i \times R_0^i s_i + R_0^i w_i \times [(R_0^i w_i) \times (R_0^i s_i)]$$

$$R_0^i F_{ci} = m_i R_0^i \dot{v}_{ci}$$

$$R_0^i N_{ci} = I_{ci} R_0^i \dot{w}_i + R_0^i w_i \times (I_{ci} R_0^i w_i)$$

$$R_0^i f_i = R_{i+1}^i R_0^{i+1} f_{i+1} + R_0^i F_{ci}$$

$$R_0^i n_i = R_{i+1}^i [R_0^{i+1} n_{i+1} + R_0^i l_i \times R_0^{i+1} f_{i+1}] + [R_0^i l_i + R_0^i s_i] \times R_0^i F_{ci} + R_0^i N_{ci}$$

$$\tau_i = (R_{i-1}^i z_0)^T (R_0^i n_i) \qquad \text{where } z_0 = (001)^T$$

These equations are necessary to derive link-referenced joint motor torques for the robot controller but the formulation for space manipulators followed in Chapter 6 requires the dynamics equations to be referred to base coordinates also.

3.2 NEWTON-EULER DYNAMICS OF A PUMA 560/600 MANIPULATOR:

For the sake of simplicity, the recursive scheme is applied assuming that the link geometries are formed as bodies of revolution about their central axes of symmetry. The forward recursion is performed from link 1 to link n, whilst the backward recursion is performed from link n to link 1 via iterative loops. The following section applies the Newton Euler method to the PUMA 560/600 geometry particularly concerning supplying initial conditions for the recursion.

3.2.1 Forward Recursion:

The forward recursion is performed by a recursive loop algorithm from i=1 to n. To find $w_i = w_{i-1} + z_{i-1}\dot{\theta}_i$ and $\dot{w}_i = \dot{w}_{i-1} + z_{i-1}\ddot{\theta}_i + w_{i-1} \times z_{i-1}\dot{\theta}_i$ with respect to base coordinates. From the DH matrix formulation:

$$\begin{pmatrix} z_{0x} \\ z_{0y} \\ z_{0z} \end{pmatrix} = \begin{pmatrix} 0 \\ 0 \\ 1 \end{pmatrix}; \quad \begin{pmatrix} z_{1x} \\ z_{1y} \\ z_{1z} \end{pmatrix} = \begin{pmatrix} -s_1 \\ c_1 \\ 0 \end{pmatrix}; \quad \begin{pmatrix} z_{2x} \\ z_{2y} \\ z_{2z} \end{pmatrix} = \begin{pmatrix} -s_1 \\ c_1 \\ 0 \end{pmatrix}; \quad \begin{pmatrix} z_{3x} \\ z_{3y} \\ z_{3z} \end{pmatrix} = \begin{pmatrix} c_1 s_{23} \\ s_1 s_{23} \\ c_{23} \end{pmatrix};$$

$$\begin{pmatrix} z_{4x} \\ z_{4y} \\ z_{4z} \end{pmatrix} = \begin{pmatrix} -(c_1 c_{23} s_4 + s_1 c_4) \\ c_1 c_4 - s_1 c_{23} s_4 \\ s_{23} s_4 \end{pmatrix}; \quad \begin{pmatrix} z_{5x} \\ z_{5y} \\ z_{5z} \end{pmatrix} = \begin{pmatrix} a_x \\ a_y \\ a_z \end{pmatrix}$$

The initial conditions for a stationary base are:

$$\begin{pmatrix} w_{0x} \\ w_{0y} \\ w_{0z} \end{pmatrix} = \begin{pmatrix} \dot{w}_{0x} \\ \dot{w}_{0y} \\ \dot{w}_{0z} \end{pmatrix} = \begin{pmatrix} 0 \\ 0 \\ 0 \end{pmatrix}$$

Whence:

$$\begin{pmatrix} w_{ix} \\ w_{iy} \\ w_{iz} \end{pmatrix} = \begin{pmatrix} w_{i-1x} \\ w_{i-1y} \\ w_{i-1z} \end{pmatrix} + \begin{pmatrix} z_{i-1x} \\ z_{i-1y} \\ z_{i-1z} \end{pmatrix}\dot{\theta}_i$$

$$\begin{pmatrix} \dot{w}_{ix} \\ \dot{w}_{iy} \\ \dot{w}_{iz} \end{pmatrix} = \begin{pmatrix} \dot{w}_{i-1x} \\ \dot{w}_{i-1y} \\ \dot{w}_{i-1z} \end{pmatrix} + \begin{pmatrix} z_{i-1x} \\ z_{i-1y} \\ z_{i-1z} \end{pmatrix}\ddot{\theta}_i + \begin{pmatrix} w_{i-1y}z_{i-1z} - w_{i-1z}z_{i-1y} \\ w_{i-1z}z_{i-1x} - w_{i-1x}z_{i-1z} \\ w_{i-1x}z_{i-1y} - w_{i-1y}z_{i-1x} \end{pmatrix}\dot{\theta}_i$$

To find $\dot{v}_i = \dot{v}_{i-1} + \dot{w}_i \times l_i + w_i \times (w_i \times l_i)$ and $\dot{v}_{ci} = \dot{v}_i + \dot{w}_i \times s_i + w_i \times (w_i \times s_i)$ with respect to base coordinates. From the DH matrix formulation, l_i is in base coordinates:

$$\begin{pmatrix} l_{1x} \\ l_{1y} \\ l_{1z} \end{pmatrix} = \begin{pmatrix} p_{1x} \\ p_{1y} \\ p_{1z} \end{pmatrix} = \begin{pmatrix} 0 \\ 0 \\ 0 \end{pmatrix} \text{ and } \begin{pmatrix} s_{1x} \\ s_{1y} \\ s_{1z} \end{pmatrix} = \begin{pmatrix} 0 \\ 0 \\ 0 \end{pmatrix};$$

$$\begin{pmatrix} l_{2x} \\ l_{2y} \\ l_{2z} \end{pmatrix} = \begin{pmatrix} p_{2x} - p_{1x} \\ p_{2y} - p_{1y} \\ p_{2z} - p_{1z} \end{pmatrix} = \begin{pmatrix} a_2 c_1 c_2 - s_1 d_2 \\ a_2 s_1 c_2 + c_1 d_2 \\ -a_2 s_2 \end{pmatrix} \text{ and } \begin{pmatrix} s_{2x} \\ s_{2y} \\ s_{2z} \end{pmatrix} = -\frac{1}{2}\begin{pmatrix} a_2 c_1 c_2 - s_1 d_2 \\ a_2 s_1 c_2 + c_1 d_2 \\ -a_2 s_2 \end{pmatrix};$$

$$\begin{pmatrix} l_{3x} \\ l_{3y} \\ l_{3z} \end{pmatrix} = \begin{pmatrix} p_{3x} - p_{2x} \\ p_{3y} - p_{2y} \\ p_{3z} - p_{2z} \end{pmatrix} = \begin{pmatrix} 0 \\ 0 \\ 0 \end{pmatrix} \text{ and } \begin{pmatrix} s_{3x} \\ s_{3y} \\ s_{3z} \end{pmatrix} = \begin{pmatrix} 0 \\ 0 \\ 0 \end{pmatrix} \text{ since } p_2 = p_3;$$

$$\begin{pmatrix} l_{4x} \\ l_{4y} \\ l_{4z} \end{pmatrix} = \begin{pmatrix} p_{4x} - p_{3x} \\ p_{4y} - p_{3y} \\ p_{4z} - p_{3z} \end{pmatrix} = \begin{pmatrix} a_2 c_1 c_2 - s_1 d_2 + d_4 c_1 s_{23} \\ a_2 s_1 c_2 + c_1 d_2 + d_4 s_1 s_{23} \\ -a_2 s_2 + d_4 c_{23} \end{pmatrix} - \begin{pmatrix} p_{3x} \\ p_{3y} \\ p_{3z} \end{pmatrix} = \begin{pmatrix} d_4 c_1 s_{23} \\ d_4 s_1 s_{23} \\ d_4 c_{23} \end{pmatrix}$$

and $\begin{pmatrix} s_{4x} \\ s_{4y} \\ s_{4z} \end{pmatrix} = -\frac{1}{2}\begin{pmatrix} d_4 c_1 s_{23} \\ d_4 s_1 s_{23} \\ d_4 c_{23} \end{pmatrix}$;

$\begin{pmatrix} l_{5x} \\ l_{5y} \\ l_{5z} \end{pmatrix} = \begin{pmatrix} p_{5x} - p_{4x} \\ p_{5y} - p_{4y} \\ p_{5z} - p_{4z} \end{pmatrix} = \begin{pmatrix} s_{5x} \\ s_{5y} \\ s_{5z} \end{pmatrix} = \begin{pmatrix} 0 \\ 0 \\ 0 \end{pmatrix}$ since $p_5 = p_4$;

$\begin{pmatrix} l_{6x} \\ l_{6y} \\ l_{6z} \end{pmatrix} = \begin{pmatrix} p_{6x} - p_{5x} \\ p_{6y} - p_{5y} \\ p_{6z} - p_{5z} \end{pmatrix} = \begin{pmatrix} d_6 a_x \\ d_6 a_y \\ d_6 a_z \end{pmatrix}$ and $\begin{pmatrix} s_{6x} \\ s_{6y} \\ s_{6z} \end{pmatrix} = -\frac{1}{2}\begin{pmatrix} d_6 a_x \\ d_6 a_y \\ d_6 a_z \end{pmatrix}$.

The initial conditions for a stationary base are:

$$\begin{pmatrix} v_{0x} \\ v_{0y} \\ v_{0z} \end{pmatrix} = \begin{pmatrix} \dot{v}_{0x} \\ \dot{v}_{0y} \\ \dot{v}_{0z} \end{pmatrix} = \begin{pmatrix} \dot{v}_{c0x} \\ \dot{v}_{c0y} \\ \dot{v}_{c0z} \end{pmatrix} = \begin{pmatrix} 0 \\ 0 \\ 0 \end{pmatrix},$$

Hence,

$$\begin{pmatrix} \dot{v}_{ix} \\ \dot{v}_{iy} \\ \dot{v}_{iz} \end{pmatrix} = \begin{pmatrix} \dot{v}_{i-1x} \\ \dot{v}_{i-1y} \\ \dot{v}_{i-1z} \end{pmatrix} + \begin{pmatrix} \dot{w}_{iy}.l_{iz} - \dot{w}_{iz}.l_{iy} \\ \dot{w}_{iz}.l_{ix} - \dot{w}_{ix}.l_{iz} \\ \dot{w}_{ix}.l_{iy} - \dot{w}_{iy}.l_{ix} \end{pmatrix} + \begin{pmatrix} w_{iy}(w_{ix}.l_{iy} - w_{iy}.l_{ix}) - w_{iz}(w_{iz}.l_{ix} - w_{ix}.l_{iz}) \\ w_{iz}(w_{iy}.l_{iz} - w_{iz}.l_{iy}) - w_{ix}(w_{ix}.l_{iy} - w_{iy}.l_{ix}) \\ w_{ix}(w_{iz}.l_{ix} - w_{ix}.l_{iz}) - w_{iy}(w_{iy}.l_{iz} - w_{iz}.l_{iy}) \end{pmatrix}$$

$$\begin{pmatrix} \dot{v}_{cix} \\ \dot{v}_{ciy} \\ \dot{v}_{ciz} \end{pmatrix} = \begin{pmatrix} \dot{v}_{ix} \\ \dot{v}_{iy} \\ \dot{v}_{iz} \end{pmatrix} + \begin{pmatrix} \dot{w}_{iy} s_{iz} - \dot{w}_{iz} s_{iy} \\ \dot{w}_{iz} s_{ix} - \dot{w}_{ix} s_{iz} \\ \dot{w}_{ix} s_{iy} - \dot{w}_{iy} s_{ix} \end{pmatrix} + \begin{pmatrix} w_{iy}(w_{ix} s_{iy} - w_{iy} s_{ix}) - w_{iz}(w_{iz} s_{ix} - w_{ix} s_{iz}) \\ w_{iz}(w_{iy} s_{iz} - w_{iz} s_{iy}) - w_{ix}(w_{ix} s_{iy} - w_{iy} s_{ix}) \\ w_{ix}(w_{iz} s_{ix} - w_{ix} s_{iz}) - w_{iy}(w_{iy} s_{iz} - w_{iz} s_{iy}) \end{pmatrix}$$

The inertia matrix must be referenced to base coordinates in the formulation used for space manipulators such that $I_i^0 = R_i^0 I_{ci} R_0^i$ where $R_0^i = (R_i^0)^T$ and $R_i^0 = (x_i y_i z_i)$. From the DH formulation:

$\begin{pmatrix} x_{1x} \\ x_{1y} \\ x_{1z} \end{pmatrix} = \begin{pmatrix} c_1 \\ s_1 \\ 0 \end{pmatrix}$; $\begin{pmatrix} y_{1x} \\ y_{1y} \\ y_{1z} \end{pmatrix} = \begin{pmatrix} 0 \\ 0 \\ -1 \end{pmatrix}$; $\begin{pmatrix} z_{1x} \\ z_{1y} \\ z_{1z} \end{pmatrix} = \begin{pmatrix} -s_1 \\ c_1 \\ 0 \end{pmatrix}$;

$\begin{pmatrix} x_{2x} \\ x_{2y} \\ x_{2z} \end{pmatrix} = \begin{pmatrix} c_1 c_2 \\ s_1 c_2 \\ -s_2 \end{pmatrix}$; $\begin{pmatrix} y_{2x} \\ y_{2y} \\ y_{2z} \end{pmatrix} = \begin{pmatrix} -c_1 s_2 \\ -s_1 s_2 \\ -c_2 \end{pmatrix}$; $\begin{pmatrix} z_{2x} \\ z_{2y} \\ z_{2z} \end{pmatrix} = \begin{pmatrix} -s_1 \\ c_1 \\ 0 \end{pmatrix}$;

$\begin{pmatrix} x_{3x} \\ x_{3y} \\ x_{3z} \end{pmatrix} = \begin{pmatrix} c_1 c_{23} \\ s_1 s_{23} \\ -s_{23} \end{pmatrix}$; $\begin{pmatrix} y_{3x} \\ y_{3y} \\ y_{3z} \end{pmatrix} = \begin{pmatrix} -s_1 \\ c_1 \\ 0 \end{pmatrix}$; $\begin{pmatrix} z_{3x} \\ z_{3y} \\ z_{3z} \end{pmatrix} = \begin{pmatrix} c_1 s_{23} \\ s_1 s_{23} \\ c_{23} \end{pmatrix}$;

$\begin{pmatrix} x_{4x} \\ x_{4y} \\ x_{4z} \end{pmatrix} = \begin{pmatrix} c_1 c_{23} c_4 - s_1 s_4 \\ s_1 c_{23} c_4 + c_1 s_4 \\ -s_{23} c_4 \end{pmatrix}$; $\begin{pmatrix} y_{4x} \\ y_{4y} \\ y_{4z} \end{pmatrix} = \begin{pmatrix} -c_1 s_{23} \\ -s_1 s_{23} \\ -c_{23} \end{pmatrix}$; $\begin{pmatrix} z_{4x} \\ z_{4y} \\ z_{4z} \end{pmatrix} = \begin{pmatrix} -c_1 c_{23} s_4 - s_1 c_4 \\ -s_1 c_{23} s_4 + c_1 c_4 \\ s_{23} s_4 \end{pmatrix}$;

$$\begin{pmatrix} x_{5x} \\ x_{5y} \\ x_{5z} \end{pmatrix} = \begin{pmatrix} c_5(c_1c_{23}c_4 - s_1s_4) - c_1s_{23}s_5 \\ c_5(s_1c_{23}c_4 + c_1s_4) - s_1s_{23}s_5 \\ -s_{23}c_4c_5 - c_{23}s_5 \end{pmatrix}; \quad \begin{pmatrix} y_{5x} \\ y_{5y} \\ y_{5z} \end{pmatrix} = \begin{pmatrix} -c_1c_{23}s_4 - s_1c_4 \\ -s_1c_{23}s_4 + c_1c_4 \\ s_{23}s_4 \end{pmatrix};$$

$$\begin{pmatrix} z_{5x} \\ z_{5y} \\ z_{5z} \end{pmatrix} = \begin{pmatrix} s_5(c_1c_{23}c_4 - s_1s_4) + c_1c_5s_{23} \\ s_5(s_1c_{23}c_4 + c_1s_4) + s_1c_5s_{23} \\ -s_{23}c_4s_5 + c_{23}c_5 \end{pmatrix};$$

$$\begin{pmatrix} x_{6x} \\ x_{6y} \\ x_{6z} \end{pmatrix} = \begin{pmatrix} n_x \\ n_y \\ n_z \end{pmatrix}; \quad \begin{pmatrix} y_{6x} \\ y_{6y} \\ y_{6z} \end{pmatrix} = \begin{pmatrix} s_x \\ s_y \\ s_z \end{pmatrix}; \quad \begin{pmatrix} z_{6x} \\ z_{6y} \\ z_{6z} \end{pmatrix} = \begin{pmatrix} a_x \\ a_y \\ a_z \end{pmatrix}$$

$$\begin{pmatrix} I_{c3x} \\ I_{c3y} \\ I_{c3z} \end{pmatrix} = \begin{pmatrix} I_{c5x} \\ I_{c5y} \\ I_{c5z} \end{pmatrix} = \begin{pmatrix} 0 \\ 0 \\ 0 \end{pmatrix}$$ since links 3 and 5 are fictitious links.

Hence,

$$\begin{pmatrix} I^0_{ixx} & I^0_{ixy} & I^0_{ixz} \\ I^0_{iyx} & I^0_{iyy} & I^0_{iyz} \\ I^0_{izx} & I^0_{izy} & I^0_{izz} \end{pmatrix} = \begin{pmatrix} x_{ix} & y_{ix} & z_{ix} \\ x_{iy} & y_{iy} & z_{iy} \\ x_{iz} & y_{iz} & z_{iz} \end{pmatrix} \begin{pmatrix} I_{cix} & 0 & 0 \\ 0 & I_{ciy} & 0 \\ 0 & 0 & I_{ciz} \end{pmatrix} \begin{pmatrix} x_{ix} & x_{iy} & x_{iz} \\ y_{ix} & y_{iy} & y_{iz} \\ z_{ix} & z_{iy} & z_{iz} \end{pmatrix}$$

such that $I^0_{ixx} = I_{cix}x^2_{ix} + I_{ciy}y^2_{ix} + I_{ciz}z^2_{ix}$;

$I^0_{iyx} = I^0_{ixy} = I_{cix}x_{ix}x_{iy} + I_{ciy}y_{ix}y_{iy} + I_{ciz}z_{ix}z_{iy}$;

$I^0_{izx} = I^0_{ixz} = I_{cix}x_{ix}x_{iz} + I_{ciy}y_{ix}y_{iz} + I_{ciz}z_{ix}z_{iz}$;

$I^0_{iyy} = I_{cix}x^2_{iy} + I_{ciy}y^2_{iy} + I_{ciz}z^2_{iy}$;

$I^0_{izy} = I^0_{iyz} = I_{cix}x_{iy}x_{iz} + I_{ciy}y_{iy}y_{iz} + I_{ciz}z_{iy}z_{iz}$;

$I^0_{izz} = I_{cix}x^2_{iz} + I_{ciy}y^2_{iz} + I_{ciz}z^2_{iz}$.

From this we can calculate the forward forces and moments about each link centre of mass in turn:

$$N_{ci} = I^0_i \dot{w}_i + w_i \times I^0_i w_i$$

$$F_{ci} = m_i \dot{v}_{ci}$$

$$\begin{pmatrix} N_{cix} \\ N_{ciy} \\ N_{ciz} \end{pmatrix} = \begin{pmatrix} I^0_{ixx} & I^0_{ixy} & I^0_{ixz} \\ I^0_{iyx} & I^0_{iyy} & I^0_{iyz} \\ I^0_{izx} & I^0_{izy} & I^0_{izz} \end{pmatrix} \begin{pmatrix} \dot{w}_{ix} \\ \dot{w}_{iy} \\ \dot{w}_{iz} \end{pmatrix} + \begin{pmatrix} 0 & -w_{iz} & w_{iy} \\ w_{iz} & 0 & -w_{ix} \\ -w_{iy} & w_{ix} & 0 \end{pmatrix} \begin{pmatrix} I^0_{ixx} & I^0_{ixy} & I^0_{ixz} \\ I^0_{iyx} & I^0_{iyy} & I^0_{iyz} \\ I^0_{izx} & I^0_{izy} & I^0_{izz} \end{pmatrix} \begin{pmatrix} w_{ix} \\ w_{iy} \\ w_{iz} \end{pmatrix} \quad (3.4)$$

such that

$$N_{cix} = I^0_{ixx}\dot{w}_{ix} + I^0_{ixy}\dot{w}_{iy} + I^0_{ixz}\dot{w}_{iz} - w_{iz}(I^0_{iyx}w_{ix} + I^0_{iyy}w_{iy} + I^0_{iyz}w_{iz}) + w_{iy}(I^0_{izx}w_{ix} + I^0_{izy}w_{iy} + I^0_{izz}w_{iz})$$

$$N_{ciy} = I^0_{iyx}\dot{w}_{ix} + I^0_{iyy}\dot{w}_{iy} + I^0_{iyz}\dot{w}_{iz} + w_{iz}(I^0_{ixx}w_{ix} + I^0_{ixy}w_{iy} + I^0_{ixz}w_{iz}) - w_{ix}(I^0_{izx}w_{ix} + I^0_{izy}w_{iy} + I^0_{izz}w_{iz})$$

$$N_{ciz} = I^0_{izx}\dot{w}_{ix} + I^0_{izy}\dot{w}_{iy} + I^0_{izz}\dot{w}_{iz} - w_{iy}(I^0_{ixx}w_{ix} + I^0_{ixy}w_{iy} + I^0_{ixz}w_{iz}) + w_{ix}(I^0_{iyx}w_{ix} + I^0_{iyy}w_{iy} + I^0_{iyz}w_{iz})$$

Similarly,

$$\begin{pmatrix} F_{cix} \\ F_{ciy} \\ F_{ciz} \end{pmatrix} = m_i \begin{pmatrix} \dot{v}_{cix} \\ \dot{v}_{ciy} \\ \dot{v}_{ciz} \end{pmatrix}$$ where $m_3 = m_5 = 0$ and $m_2 = m_1' + m_2'$ (composite link) (3.5)

since links 3 and 5 are fictitious and m_2 is composite.

3.2.2 Backward Recursion

The backward recursion proceeds from the end effector towards the base to find the joint torques and is performed by a recursive loop algorithm from i=n to 1.

$$f_i = F_{ci} + f_{i+1}$$

$$n_i = N_{ci} + n_{i+1} + (l_i + s_i) \times F_{ci} + l_i \times f_{i+1}$$

Let $\begin{pmatrix} f_{ext} \\ n_{ext} \end{pmatrix} = \begin{pmatrix} f_7 \\ n_7 \end{pmatrix} = \begin{pmatrix} 0 \\ 0 \end{pmatrix}$ since external forces and moments are dealt with separately and explicitly through the Jacobian transpose.

$$\begin{pmatrix} f_{ix} \\ f_{iy} \\ f_{iz} \end{pmatrix} = \begin{pmatrix} F_{cix} \\ F_{ciy} \\ F_{ciz} \end{pmatrix} + \begin{pmatrix} f_{i+1x} \\ f_{i+1y} \\ f_{i+1z} \end{pmatrix} \tag{3.6}$$

$$\begin{pmatrix} n_{ix} \\ n_{iy} \\ n_{iz} \end{pmatrix} = \begin{pmatrix} N_{cix} \\ N_{ciy} \\ N_{ciz} \end{pmatrix} + \begin{pmatrix} n_{i+1x} \\ n_{i+1y} \\ n_{i+1z} \end{pmatrix} + \begin{pmatrix} 0 & -l_{iz} & l_{iy} \\ l_{iz} & 0 & -l_{ix} \\ -l_{iy} & l_{ix} & 0 \end{pmatrix} \begin{pmatrix} f_{i+1x} \\ f_{i+1y} \\ f_{i+1z} \end{pmatrix} + \begin{pmatrix} 0 & -(l_i + s_i)_z & (l_i + s_i)_y \\ (l_i + s_i)_z & 0 & -(l_i + s_i)_x \\ -(l_i + s_i)_y & (l_i + s_i)_x & 0 \end{pmatrix} \begin{pmatrix} F_{cix} \\ F_{ciy} \\ F_{ciz} \end{pmatrix}$$

such that

$$\begin{aligned} n_{ix} &= N_{cix} + n_{i+1x} + f_{i+1z} l_{iy} - f_{i+1y} l_{iz} + F_{ciz}(l_{iy} + s_{iy}) - F_{ciy}(l_{iz} + s_{iz}) \\ n_{iy} &= N_{ciy} + n_{i+1y} + f_{i+1x} l_{iz} - f_{i+1z} l_{ix} + F_{cix}(l_{iz} + s_{iz}) - F_{ciz}(l_{ix} + s_{ix}) \\ n_{iz} &= N_{ciz} + n_{i+1z} + f_{i+1y} l_{ix} - f_{i+1x} l_{iy} + F_{ciy}(l_{ix} + s_{ix}) - F_{cix}(l_{iy} + s_{iy}) \end{aligned} \tag{3.7}$$

To find the input torques, the input torque at joint i is the projection of n_i onto the z_{i-1} axis:

$$\tau_i = n_i^T . z_{i-1} = \begin{pmatrix} n_{ix} & n_{iy} & n_{iz} \end{pmatrix} \begin{pmatrix} z_{i-1x} \\ z_{i-1y} \\ z_{i-1z} \end{pmatrix} = (n_{ix} z_{i-1x} + n_{iy} z_{i-1y} + n_{iz} z_{i-1z}) \tag{3.8}$$

If any payload for a space manipulator system is included, F_{c7} and N_{c7} must be added into the formulation of Chapter 6:

$$F_{c7} = m_7 \dot{v}_{c7} \quad \text{where} \quad \dot{v}_{c7} = \dot{v}_6 + \dot{w}_6 \times r_7 + w_6 \times (w_6 \times r_7)$$

$$N_{c7} = I_7^0 \dot{w}_6 + w_6 \times (I_7^0 w_6) \quad \text{where} \quad I_7^0 = R_6^0 I_7 R_0^6$$

The orientation of the object with respect to the end effector is invariant so $w_7^7 = \dot{w}_7^7 = 0$ so end effector variables are applicable with respect to the target object. Furthermore, the spacecraft moment of inertia will in general not have zero off-diagonals when referred to the end effector frame.

This completes the recursive dynamics formulation for the PUMA 560/600 and it allows the computation of the joint torques given the kinematic joint variables.

3.3 COLLISION/CAPTURE DYNAMICS

Iwata et al (1991) and Yoshida et al (1992) have considered the problem of collisions with a manipulator end effector and a payload in space. The robot receives momentum from the object. A force acts on the collision points on the end effector for a very short time to cause a momentum distribution change between the colliding objects. The behaviour of the impacting body is dependent on the elasticity of the impacting objects. Newton's law of restitution states that when two bodies collide, their relative parting

velocities in the direction of the common normal at the point of impact is -e x relative approach velocity whereby 0<e<1: $v_f - u_f = -e(v_i - u_i)$. For an inelastic collision, the bodies adhere and e=0; for an elastic collision, the bodies rebound and e=1. Assuming inelastic rigid body collisions, the total system momentum is conserved before and after collision, ie. momentum is lost from the payload to the spacecraft end effector (subscript "obj" refers to the target; subscript "s/c" refers to the spacecraft; subscript "eff" refers to the end effector; and subscript "com" refers to the composite body):

$m_{obj}v_{obj} + m_{s/c}v_{eff} = (m_{obj} + m_{s/c})v$

$I_{obj}w_{obj} + I_{s/c}w_{s/c} = I_{com}w$

Assume that the final velocity of the composite object in inertial space is zero, ie. the manipulator brings the object to rest: $\begin{pmatrix} v \\ w \end{pmatrix} = 0$.

Impulse, $\int_{t_0}^{t_f} F.dt = m\int_{t_0}^{t_f} \frac{dv}{dt}.dt = m\delta v$

$$\rightarrow \begin{matrix} m_{obj}\delta v = f_{ext}\delta t \\ I_{obj}\delta w = n_{ext}\delta t \end{matrix} \quad \text{where} \quad \begin{matrix} \delta v = v_{obj} - v = v_{obj} \\ \delta w = w_{obj} - w = w_{obj} \end{matrix}$$

ie.
$$\begin{matrix} f_{ext} = m_{obj}v_{obj}/\delta t \\ n_{ext} = I_{obj}w_{obj}/\delta t \end{matrix} \qquad (3.9)$$

External forces and moments introduce a problem for space manipulators - the need to express the external forces and moments at the end effector with respect to their reactive effects on the manipulator base point (see Chapter 6). Now, the virtual work done by applied force is constant [Paul 1981] - subscript "0" signifies base referenced variables and subscript "eff" signifies end effector referenced variables:

$\delta W_0 = \delta W_{eff} \rightarrow F_0^T dq_0 = F_{eff}^T dq_{eff} \rightarrow F_0^T v_0 = F_{eff}^T v_{eff}$

The question is to find the relationship between v_0 and v_{eff} which is defined by the matrix N. The Jacobian J transforms the end effector velocities to each joint rate by propagating the end effector velocities to the required joint coordinates and summing the contributions to the end effector velocities by each joint's motion. A similar principle may be applied to the problem of determining the transform from the end effector velocities to the robot base. The total effect of the end effector velocities on the base may then be determined and so allow the explicit calculation of the external forces reaction effect on the base:

$\begin{pmatrix} v_{eff} \\ w_{eff} \end{pmatrix} = N\begin{pmatrix} v_0 \\ w_0 \end{pmatrix}$ where $N = \begin{pmatrix} z_n \times l_n & 0 \\ 0 & z_n \end{pmatrix}$ using a cross product formulation

Now, $F_0^T v_0 = F_{eff}^T N v_0 \rightarrow F_0^T = F_{eff}^T N \rightarrow F_0^T = N^T F_{eff}$

where $N^T = \begin{pmatrix} 0 & z_n \times l_n \\ z_n & 0 \end{pmatrix}$

For a PUMA 560/600,

$\begin{pmatrix} z_{6x} \\ z_{6y} \\ z_{6z} \end{pmatrix} = \begin{pmatrix} a_x \\ a_y \\ a_y \end{pmatrix}$ and $\begin{pmatrix} l_{6x} \\ l_{6y} \\ l_{6z} \end{pmatrix} = \begin{pmatrix} p_x \\ p_y \\ p_z \end{pmatrix}$ so $a \times p = \begin{pmatrix} 0 & -a_z & a_y \\ a_z & 0 & a_x \\ -a_z & a_x & 0 \end{pmatrix}\begin{pmatrix} p_x \\ p_y \\ p_z \end{pmatrix}$:

Explicitly, we have:

$$\begin{pmatrix} F_{cn+1} \\ N_{cn+1} \end{pmatrix} = \begin{pmatrix} f_x^0 \\ f_y^0 \\ f_z^0 \\ n_x^0 \\ n_y^0 \\ n_z^0 \end{pmatrix} = \begin{pmatrix} (a_y p_z - a_z p_y) n_x^{eff} \\ (a_z p_x - a_x p_z) n_y^{eff} \\ (a_x p_y - a_y p_x) n_z^{eff} \\ a_x f_x^{eff} \\ a_y f_y^{eff} \\ a_z f_z^{eff} \end{pmatrix} \tag{3.10}$$

This represents $\begin{pmatrix} F_{c7} \\ N_{c7} \end{pmatrix}$ for the forward dynamics for modelling impacts with a 6 dgree of freedom manipulator. The force sensor at the end effector measures impulses at the end effector which is divided by δt in order to obtain the end effector forces and torques.

Chapter 4

PLANNING OF MANIPULATOR TRAJECTORIES

Trajectory planning is the process of specifying the desired time dependent smooth path trajectory for the robot end effector to track from an initial location to a final desired location. It comprises 4 steps:
(i) compute a series of points in cartesian space;
(ii) convert to joint space via the inverse kinematics;
(iii) quadratic spline fit to join the joint space points;
(iv) check the actuator input violations via the dynamics formulation.
The end effector is moved through a series of "knot/interpolation points" on a straight line cartesian path, ie. trajectory generation algorithm is given by:

$t = t_0$

loop: wait for next control interval

$t = \delta t$ where δt=control sampling interval

H(t)=hand path position function at time t

J(t)=joint solution corresponding to F(t)

if $t = t_f$ the exit

return to loop.

The time to move between point j and j+1 is defined as $T_j = t_f - t_0$. For accurate tracking, position, velocity and acceleration at hand level must be controlled so that no deviation from a staight line trajectory occurs. Paul (1979) formulated a series of uniform motions in matrix form between cartesian knot points: one straight line translation with constant linear velocity with respect to the base and two rotations with constant angular velocity. One rotation rotated the approach vector to align the tool, and another rotation rotated the orientation vector of the tool about the tool axis. At the initial and final positions, the linear and angular velocities are zero (at rest). Taylor (1979) developed a more efficient technique by using a quaternion formulation to represent rotation rather than 3x3 rotation matrices to reduce storage requirements and the number of primitive operations. In addition, he reduced the number of interpolation points by employing tracking to ensure that the end effector remained within a "deadband" region about the desired points. This method is not adopted here since the matrix representation is used for other computations and is generally employed. The inverse transform at each knot point must be performed at a rate sufficiently high to drive the joints to track in real-time accurately, yet avoiding the structural resonant frequency of the manipulator to maintain servo stability. Paul (1979) found that the driving frequency should be 8 times the resonant frequency. For the Unimate PUMA 560/600, $f_{resonant}$~8Hz implies a sampling frequency of 60 Hz giving a sample interpolation point every 16 ms. High sampling rate is particularly important for force control to yield desirable dynamic performance.

There is some evidence for straight line linear path planning in human cognition [Shepard 1984]. Surface optical information about bodies is constrained by the geometric lines of perspective. Similarly the relative motion of rigid objects are also constrained by kinematic geometry. Although an infinite number of paths exist through which an object may be moved and/or rotated from a position A to a position B, the simplest motion is given through Chasles theorem. A unique axis exists such that an object may be moved from A to B by a rotation about that axis with a simultaneous

translation along that axis to generate a minimal 6 degree of freedom helical twist in 3D space (including the limiting cases of circular or rectilinear motion).

4.1 CARTESIAN TRAJECTORY GENERATION

The trajectory is characterised by a sequence of cartesian task positions/orientations represented by pairs of points j and j+1 expressed in DH matrix form in a time interval $[0,T_j]$:

$$T_{06j} = C_j(t)H_j^j \quad \text{and} \quad T_{06j+1} = C_{j+1}(t)H_{j+1}^{j+1} \text{ where } H = \begin{pmatrix} n & s & a & p \\ 0 & 0 & 0 & 1 \end{pmatrix}$$

$$C(t) = \begin{pmatrix} 1 & -w_z & w_y & v_x \\ w_z & 1 & -w_x & v_y \\ -w_y & w_x & 1 & v_z \\ 0 & 0 & 0 & 1 \end{pmatrix} \delta t$$

C(t) represents the time-dependent transform matrix of the moving working coordinate frame with respect to base coordinates. If H_j is represented with respect to j+1 coordinates:

$T_{06j} = C_{j+1}(t)H_j^{j+1} \rightarrow H_j^{j+1} = [C_{j+1}(t)]^{-1}T_{06j}$

The motion between any points j and j+1 is from $T_{06j} = C_{j+1}(t)H_j^{j+1}$ to $T_{06j+1} = C_{j+1}(t)H_{j+1}^{j+1}$. Motion from j to j+1 is expresed in terms of a drive function D(h) where h=t/T where t=elapsed time and T=total move time:

$T_{06}(h) = C_{j+1}H_j^{j+1}D(h)$

At h=0, D(h=0)=I such that $T_{06j} = H_j^j = H_j^{j+1}D(h=0)$ and at h=1, D(h=1) such that $T_{06j+1} = H_{j+1}^{j+1} = H_j^{j+1}D(h=1)$ which comprise boundary conditions.

Hence, $D(h=1) = [H_j^{j+1}]^{-1}H_{j+1}^{j+1}$

where $H_j^{j+1} = \begin{pmatrix} n^j & s^j & a^j & p^j \\ 0 & 0 & 0 & 1 \end{pmatrix}; H_{j+1}^{j+1} = \begin{pmatrix} n^{j+1} & s^{j+1} & a^{j+1} & p^{j+1} \\ 0 & 0 & 0 & 1 \end{pmatrix}$

$$\text{Now, } [H_j^{j+1}]^{-1} = \begin{pmatrix} n_x^j & n_y^j & n_z^j & -(n^Tp)^j \\ s_x^j & s_y^j & s_z^j & -(s^Tp)^j \\ a_x^j & a_y^j & a_z^j & -(a^Tp)^j \\ 0 & 0 & 0 & 1 \end{pmatrix} \equiv \begin{pmatrix} \rho_x^j & \rho_y^j & \rho_z^j & -(\rho^Tp)^j \\ 0 & 0 & 0 & 1 \end{pmatrix}$$

$$\rightarrow D(h=1) = \begin{pmatrix} \rho_x^j & \rho_y^j & \rho_z^j & -(\rho^Tp)^j \\ 0 & 0 & 0 & 1 \end{pmatrix} \begin{pmatrix} n^{j+1} & s^{j+1} & a^{j+1} & p^{j+1} \\ 0 & 0 & 0 & 1 \end{pmatrix}$$

$$= \begin{pmatrix} n_j^T n_{j+1} & n_j^T s_{j+1} & n_j^T a_{j+1} & n_j^T(p_{j+1} - p_j) \\ s_j^T n_{j+1} & s_j^T s_{j+1} & s_j^T a_{j+1} & s_j^T(p_{j+1} - p_j) \\ a_j^T n_{j+1} & a_j^T s_{j+1} & a_j^T a_{j+1} & a_j^T(p_{j+1} - p_j) \\ 0 & 0 & 0 & 1 \end{pmatrix}$$

Equivalently, this matrix represents one translation and two rotations: $D(h) = T(h)R^a(h)R^s(h)$

$$\text{where } T(h)=\begin{pmatrix}1&0&0&hx\\0&1&0&hy\\0&0&1&hz\\0&0&0&1\end{pmatrix};\ R^s(h)=\begin{pmatrix}\cos(h\varphi)&-\sin(h\varphi)&0&0\\\sin(h\varphi)&\cos(h\varphi)&0&0\\0&0&1&0\\0&0&0&1\end{pmatrix};$$

$$R^a(h)=\begin{pmatrix}\sin^2\phi[1-\cos(h\theta)]+\cos(h\theta) & -\sin\phi\cos\phi[1-\cos(h\theta)] & \cos\phi\sin(h\theta) & 0\\ -\sin\phi\cos\phi[1-\cos(h\theta)] & \cos^2[1-\cos(h\theta)]+\cos(h\theta) & \sin\phi\sin(h\theta) & 0\\ -\cos\phi\sin(h\theta) & -\sin\phi\sin(h\theta) & \cos(h\theta) & 0\\ 0 & 0 & 0 & 1\end{pmatrix}$$

$$\text{Hence, } D(h)=T(h)R^a(h)R^s(h)=\begin{pmatrix}D_{11}(h)&D_{21}(h)&D_{31}(h)&hx\\D_{12}(h)&D_{22}(h)&D_{32}(h)&hy\\D_{13}(h)&D_{23}(h)&D_{33}(h)&hz\\0&0&0&1\end{pmatrix} \qquad (4.1)$$

where

$D_{11}(h)=\cos(h\varphi)[\sin^2\phi(1-\cos(h\theta))+\cos(h\theta)]-\sin(h\varphi)[\sin\phi\cos\phi(1-\cos(h\theta))]$

$D_{12}(h)=\cos(h\varphi)[-\sin\phi\cos\phi(1-\cos(h\theta))]+\sin(h\varphi)[\cos^2\phi(1-\cos(h\theta))+\cos(h\theta)]$

$D_{13}(h)=-\cos(h\varphi)\cos\phi\sin(h\theta)-\sin(h\varphi)\sin\phi\sin(h\theta)$

$D_{21}(h)=-\sin(h\varphi)[\sin^2\varphi(1-\cos(h\theta))+\cos(h\theta)]-\cos(h\varphi)[\sin\phi\cos\phi(1-\cos(h\theta))]$

$D_{22}(h)=-\sin(h\varphi)[-\sin\phi\cos\phi(1-\cos(h\theta))]+\cos(h\varphi)[\cos^2\phi(1-\cos(h\theta))+\cos(h\theta)]$

$D_{23}(h)=\sin(h\varphi)[\cos\phi\sin(h\theta)]-\cos(h\varphi)[\sin\phi\sin(h\theta)]$

$D_{31}(h)=\cos\phi\sin(h\theta);D_{32}(h)=\sin\phi\sin(h\theta);D_{33}(h)=\cos(h\theta).$

These expressions for D(h) may be equated for h=1:

$x=n_j^T(p_{j+1}-p_j);y=s_j^T(p_{j+1}-p_j);z=a_j^T(p_{j+1}-p_j);$

$\cos\phi\sin\theta=n_j^Ta_{j+1};\sin\phi\sin\theta=s_j^Ta_{j+1};\cos\theta=a_j^Ta_{j+1};$

$$\rightarrow \tan\phi=\frac{\sin\phi\sin\theta}{\cos\phi\sin\theta}=\frac{s_j^Ta_{j+1}}{n_j^Ta_{j+1}}$$

$$\rightarrow \tan\theta=\frac{\sin\theta}{\cos\theta}=\frac{\sqrt{(\cos\phi\sin\theta)^2+(\sin\phi\sin\theta)^2}}{\cos\theta}=\frac{\sqrt{(n_j^Ta_{j+1})^2+(s_j^Ta_{j+1})^2}}{a_j^Ta_{j+1}}$$

Also, $R^s(1)=R^a(1)^{-1}T(1)^{-1}D(1)$:

$$\begin{pmatrix}\cos\varphi&-\sin\varphi&0\\\sin\varphi&\cos\varphi&0\\0&0&1\end{pmatrix}=\begin{pmatrix}s^2\phi(1-c\theta)+c\theta&-s\phi c\phi(1-c\theta)&-c\phi s\theta\\-s\phi c\phi(1-c\theta)&c^2\phi(1-c\theta)+c\theta&-s\phi s\theta\\c\phi s\theta&s\phi s\theta&c\theta\end{pmatrix}\begin{pmatrix}n_j^Tn_{j+1}&n_j^Ts_{j+1}&n_j^Ta_{j+1}\\s_j^Tn_{j+1}&s_j^Ts_{j+1}&s_j^Ta_{j+1}\\a_j^Tn_{j+1}&a_j^Ts_{j+1}&a_j^Ta_{j+1}\end{pmatrix}$$

$\rightarrow \sin\varphi=[-\sin\phi\cos\phi(1-\cos\theta)]n_j^Tn_{j+1}+s_j^Tn_{j+1}[\cos^2\phi(1-\cos\theta)+\cos\theta]+a_j^Tn_{j+1}(-\sin\phi\sin\theta)$

$\rightarrow \cos\varphi=[-\sin\phi\cos\phi(1-\cos\theta)]n_j^Ts_{j+1}+s_j^Ts_{j+1}[\cos^2\phi(1-\cos\theta)+\cos\theta]+a_j^Ts_{j+1}(-\sin\phi\sin\theta)$

$\tan\varphi=\frac{\sin\varphi}{\cos\phi}\rightarrow\varphi=\tan^{-1}(\frac{\sin\varphi}{\cos\varphi})$

This completes the computation of the drive function. It may now be used to derive the elements of the 4x4 DH matrix at any desired point along the trajectory between the initial and final points in space of the end effector. The drive transform D(h) corresponds to a translation and two rotations to move from position to position.

$$T_{06}(h)=\begin{pmatrix}n_j&s_j&a_j&p_j\\0&0&0&1\end{pmatrix}D(h)=\begin{pmatrix}n_h&s_h&a_h&p_h\\0&0&0&1\end{pmatrix} \qquad (4.2)$$

where $n_x^h=n_x^jD_{11}(h)+s_x^jD_{12}(h)+a_x^jD_{13}(h)$

$n_y^h=n_y^jD_{11}(h)+s_y^jD_{12}(h)+a_y^jD_{13}(h)$

$$n_z^h = n_z^j D_{11}(h) + s_z^j D_{12}(h) + a_z^j D_{13}(h)$$
$$s_x^h = n_x^j D_{21}(h) + s_x^j D_{22}(h) + a_x^j D_{23}(h)$$
$$s_y^h = n_y^j D_{21}(h) + s_y^j D_{22}(h) + a_y^j D_{23}(h)$$
$$s_z^h = n_z^j D_{21}(h) + s_z^j D_{22}(h) + a_z^j D_{23}(h)$$
$$a_x^h = n_x^j D_{31}(h) + s_x^j D_{32}(h) + a_x^j D_{33}(h)$$
$$a_y^h = n_y^j D_{31}(h) + s_y^j D_{32}(h) + a_y^j D_{33}(h)$$
$$a_z^h = n_z^j D_{31}(h) + s_z^j D_{32}(h) + a_z^j D_{33}(h)$$
$$p_x^h = n_x^j hx + s_x^j hy + a_x^j hz + p_x^j$$
$$p_y^h = n_y^j hx + s_y^j hy + a_y^j hz + p_y^j$$
$$p_z^h = n_z^j hx + s_z^j hy + a_z^j hz + p_z^j$$

For a 5-segment trajectory, $h = 0, \frac{1}{5}, \frac{2}{5}, \frac{3}{5}, \frac{4}{5}, 1$.

This formulation will produce constant linear and angular velocities, but at the endpoints, to avoid discontinuities, acceleration and deceleration phases are required. The time to accelerate from one velocity to another requires a time 2τ for both acceleration and deceleration assuming a symmetric constant acceleration profile. Luh & Lin (1981) pointed out that the stop at each line segment extends the execution time of the task. It is possible to initiate velocity change τ before the next point and maintain that acceleration until τ into the new motion segment, ie. a constant acceleration from $-\tau$ to τ to patch between motion segments. This generates a path of a sequence of straight line segments connected by smooth arcs. There are m segments and (m-1) intersection points denoted by H_j^j between the j=0 initial point and the j=m final point. During the execution of segment j, the position/orientation of the end effector may be either in transition from segment j-1, in segment j , or in transition to segment j+1.

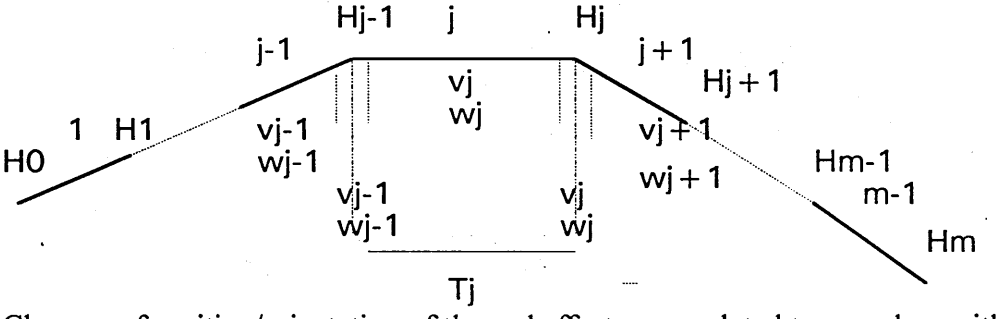

Changes of position/orientation of the end effector are related to v_j and w_j with respect to base coordinates. In the midportion of segment j, v_j and w_j are constant; in transition from segment j to j+1, $\dot{v}_j$ and $\dot{w}_j$ are nonzero constants.

The hand rests at the initial and final positions/orientations:

$$\left.\begin{matrix} p_k = p_0, p_m \\ \theta_k = 0 \end{matrix}\right) \text{ and } \left.\begin{matrix} v_k = 0 \\ w_k = 0 \end{matrix}\right) \text{ for } k<1 \text{ and } k>m \qquad (4.3)$$

For constant velocity segments (for $\tau_0 + \sum_{k=1}^{j-1} T_k + \tau_{j-1} < t < \tau_0 + \sum_{k=1}^{j} T_k - \tau_j$):

$v_j = \frac{p_j - p_{j-1}}{T_j}$

$$w_j = \left(\frac{\theta_j}{T_j}\right)\left[\frac{1}{2\sin\theta_j}\begin{pmatrix} a_j^T s_{j-1} - s_j^T a_{j-1} \\ n_j^T a_{j-1} - a_j^T n_{j-1} \\ s_j^T n_{j-1} - n_j^T s_{j-1} \end{pmatrix}\right] \quad \text{where } \theta_j = \cos^{-1}[(n_j^T n_{j-1} + s_j^T s_{j-1} + a_j^T a_{j-1})/2]$$

(4.4)

For accelerating segments (for $\tau_0 + \sum_{k=1}^{j} T_k - \tau_j < t < \tau_0 + \sum_{k=1}^{j} T_k + \tau_j$):

$$\dot{v}_j = \frac{v_{j+1} - v_j}{2\tau_j}$$

$$\dot{w}_j = \frac{w_{j+1} - w_j}{2\tau_j} \qquad (4.5)$$

The total execution time is $\tau_0 + \sum_{j=1}^{m} T_j + \tau_m$. If the the time interval $2\tau_j$ during which velocities change is too long, the path travelled by the end effector may deviate from the nominal path. Hence, a ratio may be fixed between τ_j and T_j with $\tau_{j-1} + \tau_j \leq T_j$.

Example trajectory:

Usually, 5 equal time intervals each satisfying a cubic are selected. The first 2T intervals have a nonzero second derivative. At 2T the second derivative is set to zero and a constant first derivative holds to 3T. From 3T to 5T, the path again has a nonzero second derivative. The constant rate portion in this case encompasses ⅕ of the trajectory. In reality, due to rate limitations of the actuators, short acceleration and deceleration phases at the ends of the trajectory with long constant velocity portions are more common. Maximum speed is attained by eliminating the constant rate portion in bang-bang acceleration/deceleration maneouvres, but these are not usually adopted or indeed obtainable.

For a 5-equal segment trajectory:

$$T = \tau_0 + \sum_{1}^{5} T_j + \tau_5 \rightarrow T_1 = \tfrac{T}{5} - \tau_0, T_2 = T_3 = T_4 = \tfrac{T}{5}, T_5 = \tfrac{T}{5} - \tau_5$$

In such a five-segment trajectory, the first trajectory segment is the guarded departure move, so arbitrarily $\tau_0 = 0.5T_1$; similarly, the last trajectory segment is the guarded approach move, so again arbitrarily $\tau_5 = 0.5T_5$ such that $\tau_0 = \tau_5$. This defines the guarded move at half speed. It is also desirable to accelerate and decelerate the end effector uniformly to the desired speed so $\tau_2 = \tau_3 = 0$ and $|\tau_1| = |\tau_4| = 0.5T$.

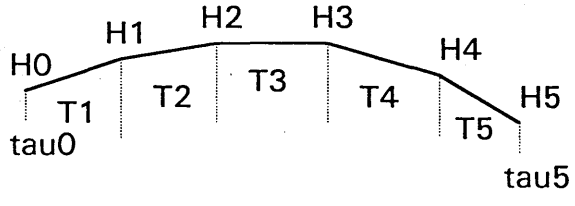

For T=0:

$$v_{j=0} = 0$$

$$w_{j=0} = 0$$

For $0 < t < 2\tau_0$:

$$\dot{v}_{j=0} = \frac{v_{j=1}}{2\tau_0}$$

$$\dot{w}_{j=0} = \frac{w_{j=1}}{2\tau_0}$$

For $2\tau_0 < t < \tau_0 + T_1 - \tau_1$:

$$v_{j=1} = \frac{p_{j=1} - p_{j=0}}{T_1}$$

$$w_{j=1} = \frac{\theta_{j=1}}{T_1}\left(\frac{1}{2\sin\theta_{j=1}}\begin{bmatrix} a_{j=1}^T s_{j=0} - s_{j=1}^T a_{j=0} \\ n_{j=1}^T a_{j=0} - a_{j=1}^T n_{j=0} \\ s_{j=1}^T n_{j=0} - n_{j=1}^T s_{j=0} \end{bmatrix}\right)$$

For $\tau_0 + T_1 - \tau_1 < t < \tau_0 + T_1 + \tau_1$:

$$\dot{v}_{j=1} = \frac{v_{j=2} - v_{j=1}}{2\tau_1} \qquad \text{with} \qquad < v_{j=1} >= \frac{v_{j=2} - v_{j=1}}{2}$$

$$\dot{w}_{j=1} = \frac{w_{j=2} - w_{j=1}}{2\tau_2} \qquad < w_{j=1} >= \frac{w_{j=2} - w_{j=1}}{2}$$

at point H_1.

For $\tau_0 + T_1 + \tau_1 < t < \tau_0 + T_1 + T_2$:

$$v_{j=2} = \frac{p_{j=2} - p_{j=1}}{T_2}$$

$$w_{j=2} = \frac{\theta_{j=2}}{T_2}\left(\frac{1}{2\sin\theta_{j=2}}\begin{bmatrix} a_{j=2}^T s_1 + s_{j=2}^T a_1 \\ n_{j=2}^T a_{j=1} - a_{j=2}^T n_{j=1} \\ s_{j=2}^T n_{j=1} - n_{j=2}^T s_{j=1} \end{bmatrix}\right)$$

For $\tau_0 + T_1 + T_2 < t < \tau_0 + T_1 + T_2 + T_3$:

$$v_{j=3} = v_{j=2} \qquad \text{since} \qquad \dot{v}_{j=2} = 0$$

$$w_{j=3} = w_{j=2} \qquad \dot{w}_{j=2} = 0$$

For $\tau_0 + T_1 + T_2 + T_3 < t < \tau_0 + T_1 + T_2 + T_3 + T_4 - \tau_4$:

$$v_{j=4} = v_{j=3} \qquad \text{since} \qquad \dot{v}_{j=3} = 0$$

$$w_{j=4} = w_{j=3} \qquad \dot{w}_3 = 0$$

For $\tau_0 + T_1 + T_2 + T_3 + T_4 - \tau_4 < t < \tau_0 + T_1 + T_2 + T_3 + T_4 + \tau_4$:

$$\dot{v}_{j=4} = \frac{v_{j=5} - v_{j=4}}{2\tau_4} \qquad \text{with} \qquad < v_{j=4} >= \frac{v_{j=5} - v_{j=4}}{2}$$

$$\dot{w}_{j=4} = \frac{w_{j=5} - w_{j=4}}{2\tau_4} \qquad < w_{j=4} >= \frac{w_{j=5} - w_{j=4}}{2}$$

at point H_4.

For $\tau_0 + T_1 + T_2 + T_3 + T_4 + \tau_4 < t < \tau_0 + T_1 + T_2 + T_3 + T_4 + T_5 - \tau_5$:

$$v_{j=5} = \frac{p_{j=5} - p_{j=4}}{T_5}$$

$$w_{j=5} = \frac{\theta_{j=5}}{T_5}\left(\frac{1}{2\sin\theta_{j=5}}\begin{bmatrix} a_{j=5}^T s_{j=4} - s_{j=5}^T a_{j=4} \\ n_{j=5}^T a_{j=4} - a_{j=5}^T n_{j=4} \\ s_{j=5}^T n_{j=4} - n_{j=5}^T s_{j=4} \end{bmatrix}\right)$$

For $\tau_0 + T_1 + T_2 + T_3 + T_4 + T_5 - \tau_5 < t < \tau_0 + T_1 + T_2 + T_3 + T_4 + T_5 + \tau_5$:

$$\dot{v}_{j=5} = \frac{-v_{j=5}}{2\tau_5}$$

$$\dot{w}_{j=5} = \frac{-w_{j=5}}{2\tau_5}$$

For t=T:

$$v_{j=6} = 0$$

$$w_{j=6} = 0$$

4.2 JOINT TRAJECTORY GENERATION

These methods of cartesian straight line trajectory generation do not allow for actuator limits in their formulation. Actuator torques, accelerations, and velocities at each joint provide constraints to the trajectory yet the path is constained in cartesian coordinates, eg. the Unimate PUMA 560/600 can exert a maximum of 22Nm at each of its joints. The manipulator is a highly coupled nonlinear mechanical system, so it is difficult to convert joint torques at the actuators to hand level equivalents. They cannot be converted to cartesian constraints by Jacobian transforms since they are only valid only on a point-to-point basis and invalid for continuous paths. Hence, actuator constraints must be applied at joint level. Acuator limits are usually set at reduced torque bands to allow for model error and disturbances. Furthermore, measured variables for feedback are joint rather than cartesian variables, ie. θ_i and $\dot{\theta}_i$.

For any trajectory, four points are usually specified:
(i) initial point with zero velocity and acceleration but with specified position;
(ii) lift off point out along normal vector to the surface from the initial point with continuous motion;
(iii) set down point into along the normal vector to the surface to the final point with continuous motion;
(iv) final position with zero velocity and acceleration.
At each of these 4 positions, velocity and acceleration are continuous over the time interval $[0,T_j]$. Joint solutions to m cartesian knot points are computed and it is necessary to interpolate between each joints' knot points. For a 6 DOF robot manipulator, there are 6 joints and so 6 approximate interpolation functions between each cartesian knot point. At joint level, a 7 DOF polynomial function may be used to fit the 4 knot points with their position, velocity and acceleration boundary conditions. However, such a polynomial is time-consuming to calculate and tends to exhibit "wandering" from the nominal trajectory and overshoot the trajectory terminal point. Such high degree polynomials involve high computational burden [Luh & Lin 1984]. The trajectory alternatively may be divided into segments to allow lower degree polynomials to be patched together. The spline curve is a polynomial of degree k with continuity in its derivative of order k-1 at its interpolation points generated to fit those points. The commonest methods of trajectory segmentation are the 4-3-4 and 5-cubic trajectories. The 4-3-4 three segment trajectory have the first segment modelled as a quartic polynomial from the initial to lift off points, the second segment by a cubic polynomial from lift off to set down point, and the third trajectory element by a cubic polynomial from the set down point to the final point. The 5-cubic trajectory has 5 segments all modelled by piecewise smooth cubic spline polynomials linking 6 knot points, ie. 2 additional points must be generated [Lin et al 1983]. The first and second derivative representing joint velocities and accelerations are continuous. In fact, the cubic is the lowest degree polynomial that allows continuity in velocity and acceleration. The cubic polynomial approximates to the cartesian straight line trajectory over a wide range of sampling rates and tracks the straight line path better than the quartic at joint level. Cubic splines may be fitted for the entire trajectory and do not require smoothing at the end points of motion segments. Lin & Chang (1983)

suggested that if cartesian knot points are sequentially generated in real-time whereby only a few knot points are known at any one time, the X-spline function which requires only local knot point information for curve fitting, may be more suitable. X-splines are generalisations of the cubic spline and requires only 2 or 3 knot points. However, it requires relaxation of the continuity condition of joint acceleration, and discontinuity of the second derivative can cause acceleration jumps at the knot points. This can only be overcome by introducing more knot points, defeating the original purpose of the X-spline technique. It is questionable if there is indeed any advantage at all, since only 6 set points are required for cubic splines and the target will normally be tracked so that the first and final knot points will be known. The remaining 4 intermediate points are generated sequentially in turn. Once the first derivative has been calculated, the rest follow rapidly from the cartesian straight line trajector generator. Hence, the 5-segment cubic joint trajectory technique appears to have substantial advantages over the others.

The inverse kinematics at each update point are calculated at intervals along the cartesian trajectory to provide a set of joint knot points - interpolation occurs at joint level between the joint knot points using polynomial functions of degree n or less: the closeness to a straight line depends on the resolution of segmentation. The cubic polynomial results in minimum jerk to reduce the possibility of structural excitation [Lumia & Wavering 1989]. Lin et al (1983) proposed a generalised cubic polynomial method for n knot points for N joints, ie. n-2 interpolation points between initial and final knot points joined by n-1 cubic polynomial segments, $Q_j(t)$ to allow jerk, acceleration and velocity constraints of the actuators to be applied at joint level. The cubic polynomials all satisfy required displacement, velocity and acceleration at each knot point and generate continuous displacement, velocity and acceleration over the complete time interval $[t_0,t_n]$. It requires a large number of knot points to be computed offline barring sensor-based real-time control. For real-time operation, trajcetory generation must require only a few knot points. Chand & Doty (1985) intoduced a means of generating cubic spline trajectories online by using a limited look-ahead of 4 points on the trajectory with an error restriction of <0.5%. As noted above, the cubic spline polynomial technique requires 6 knot points and this is highly compatible with the cartesian methods as well as overcoming some of the more undesirable effects of excessive computation. Lin et al's (1983) generalised cubic interpolation method is thus adapted to the 5 segment trajectory:

Normalised time between knot points= $\tau = \frac{t_{j+1}-t}{T_j}$ where $T_j = t_{j+1} - t_j$ and $t_j \le t \le t_{j+1}$.

$\rightarrow \frac{d\tau}{dt} = \frac{1}{T_j}$

The cubic polynomial is: $Q_j(\tau) = a_{j3}\tau^3 + a_{j2}\tau^2 + a_{j1}\tau + a_{j0}$ (cubic polynomial)

$$Q_j'(\tau) = 3a_{j3}\tau^2 + 2a_{j2}\tau + a_{j1} \text{ (parabolic polynomial)}$$

$$Q_j''(\tau) = 6a_{j3}\tau + 2a_{j2} \text{ (linear straight line)}$$

Now, $\frac{dQ_j(\tau)}{d\tau} = \left(\frac{dQ_j(\tau)}{dt}\right)\frac{dt}{d\tau} = T_j\left(\frac{dQ_j(\tau)}{dt}\right)$

$$\frac{d^2Q_j(\tau)}{d\tau^2} = \frac{d}{dt}\left(\frac{dQ_j(\tau)}{d\tau}\right) = \left(\frac{d^2Q_j(\tau)}{dt^2}\right)\frac{d^2t}{d\tau^2} = T_j^2\frac{d^2Q_j(\tau)}{dt^2}$$

Hence, $\dot{\theta}_j = \frac{Q_j'(\tau)}{T_j} = \frac{3a_{j3}\tau^2+2a_{j2}\tau+a_{j1}}{T_j}$

$$\ddot{\theta}_j = \frac{Q_j''(\tau)}{T_j^2} = \frac{6a_{j3}\tau+2a_{j2}}{T_j^2}$$

At $\tau = 0 \equiv t = t_j$:

$$Q_j(0) = a_{j0} = \theta_j$$

$$\dot{\theta}_j = \frac{Q_j'(0)}{T_j} = \frac{a_{j1}}{T_j} \rightarrow a_{j1} = \dot{\theta}_j T_j$$

$$\ddot{\theta}_j = \frac{Q_j''(0)}{T_j^2} = \frac{2a_{j2}}{T_j^2} \rightarrow a_{j2} = \tfrac{1}{2}\ddot{\theta}_j T_j^2$$

At $\tau = 1 \equiv t = t_j$:

$$Q_j(1) = \theta_{j+1} = a_{j3} + a_{j2} + a_{j1} + a_{j0} = a_{j3} + \left(\frac{\ddot{\theta}_j T_j^2}{2}\right) + \dot{\theta}_j T_j + \theta_j$$

$$\rightarrow a_{j3} = (\theta_{j+1} - \theta_j) - \left(\tfrac{1}{2}\ddot{\theta}_j T_j^2\right) - \dot{\theta}_j T_j$$

$$\rightarrow Q_j(\tau) = \left[(\theta_{j+1} - \theta_j) - \left(\tfrac{1}{2}\ddot{\theta}_j T_j^2\right) - \dot{\theta}_j T_j\right]\tau^3 + \left[\tfrac{1}{2}\ddot{\theta}_j T_j^2\right]\tau^2 + \left[\dot{\theta}_j T_j\right]\tau + \theta_j$$

$$\dot{\theta}_{j+1} = \frac{Q_j'(1)}{T_j} = \frac{3a_{j3} + 2a_{j2} + a_{j1}}{T_j} = \frac{3(\theta_{j+1} - \theta_j)}{T_j} - 2\dot{\theta}_j - \tfrac{1}{2}\ddot{\theta}_j T_j$$

$$\ddot{\theta}_{j+1} = \frac{Q_j''(1)}{T_j^2} = \frac{6a_{j3} + 2a_{j2}}{T_j^2} = \frac{6(\theta_{j+1} - \theta_j)}{T_j^2} - 2\ddot{\theta}_j - \frac{6\dot{\theta}_j}{T_j}$$

Continuous velocity and acceleration between j and j+1 are obtained from the boundary conditions:

$$\dot{\theta}_{j+1} = \frac{Q_{j+1}'(0)}{T_{j+1}} = \frac{a_{j+1,1}}{T_{j+1}} = \frac{Q_j'(1)}{T_j} \quad \text{and} \quad \ddot{\theta}_{j+1} = \frac{Q_{j+1}''}{T_{j+1}} = \frac{2a_{j+1,2}}{T_{j+1}^2} = \frac{Q_j''(1)}{T_j^2}$$

For a 5 segment trajectory:

First trajectory segment:

$$Q_1(\tau) = a_{13}\tau^3 + a_{12}\tau^2 + a_{11}\tau + a_{10} \rightarrow Q_1(0) = a_{10} = \theta_0$$

$$\dot{\theta}_0 = \frac{Q_1'(0)}{T_1} = \frac{a_{11}}{T_1} \rightarrow a_{11} = \dot{\theta}_0 T_1$$

$$\ddot{\theta}_0 = \frac{Q_1''(0)}{T_1^2} = \frac{2a_{12}}{T_1^2} \rightarrow a_{12} = \tfrac{1}{2}\ddot{\theta}_0 T_1^2$$

$$Q_1(1) = a_{13} + \tfrac{1}{2}\ddot{\theta}_0 T_1^2 + \dot{\theta}_0 T_1 + \theta_0 = \theta_1$$

$$\rightarrow a_{13} = (\theta_1 - \theta_0) - \tfrac{1}{2}\ddot{\theta}_0 T_1^2 - \dot{\theta}_0 T_1 \quad \text{where } \dot{\theta}_0 = \ddot{\theta}_0 = 0 \text{ initially}$$

ie. the first trajectory segment polynomial:

$$Q_1(\tau) = (\theta_1 - \theta_0)\tau^3 + \theta_0 \text{ with } \dot{\theta}_1 = \frac{Q_1'(1)}{T_1} = \frac{3(\theta_1 - \theta_0)}{T_1} \text{ and } \ddot{\theta}_1 = \frac{Q_1''(1)}{T_1^2} = \frac{6(\theta_1 - \theta_0)}{T_1^2}$$

Second trajectory segment:

$$Q_2(\tau) = a_{23}\tau^3 + a_{22}\tau^2 + a_{21}\tau + a_{20} \rightarrow Q_2(0) = a_{20} = \theta_1$$

$$\dot{\theta}_1 = \frac{Q_2'(0)}{T_2} = \frac{a_{21}}{T_2} = \frac{Q_1'(1)}{T_1} \rightarrow a_{21} = \dot{\theta}_1 T_2$$

$$\ddot{\theta}_1 = \frac{Q_2''(0)}{T_2^2} = \frac{2a_{22}}{T_2^2} = \frac{Q_1''(1)}{T_1^2} \rightarrow a_{22} = \tfrac{1}{2}\ddot{\theta}_1 T_2^2$$

$$Q_2(1) = a_{23} + \tfrac{1}{2}\ddot{\theta}_1 T_2^2 + \dot{\theta}_1 T_2 + \theta_1 = \theta_2 \rightarrow a_{23} = (\theta_2 - \theta_1) - \tfrac{1}{2}\ddot{\theta}_1 T_2^2 - \dot{\theta}_1 T_2$$

ie. the second trajectory segment polynomial:

$$Q_2(\tau) = \left[(\theta_2 - \theta_1) - \tfrac{1}{2}\ddot{\theta}_1 T_2^2 - \dot{\theta}_1 T_2\right]\tau^3 + \left[\tfrac{1}{2}\ddot{\theta}_1 T_2^2\right]\tau^2 + \left[\dot{\theta}_1 T_2\right]\tau + \theta_1$$

with $\dot{\theta}_2 = \frac{Q_2'(1)}{T_2} = \frac{3(\theta_2 - \theta_1)}{T_2} - 2\dot{\theta}_1 - \frac{1}{2}\ddot{\theta}_1 T_2$ and $\ddot{\theta}_2 = \frac{Q_2''(1)}{T_2^2} = \frac{6(\theta_2 - \theta_1)}{T_2^2} - 2\ddot{\theta}_1 - \frac{6\dot{\theta}}{T_2}$

Third trajectory segment:

$$Q_3(\tau) = a_{33}\tau^3 + a_{32}\tau^2 + a_{31}\tau + a_{30} \rightarrow Q_3(0) = a_{30} = \theta_2$$

$$\dot{\theta}_2 = \frac{Q_3'(0)}{T_3} = \frac{a_{31}}{T_3} = \frac{Q_2'(1)}{T_2} \rightarrow a_{31} = \dot{\theta}_2 T_3$$

$$\ddot{\theta}_2 = \frac{Q_3''(0)}{T_3^2} = \frac{2a_{32}}{T_3^2} = \frac{Q_2''(1)}{T_2^2} \rightarrow a_{32} = \tfrac{1}{2}\ddot{\theta}_2 T_3^2$$

$$Q_3(1) = a_{33} + \tfrac{1}{2}\ddot{\theta}_2 T_3^2 + \dot{\theta}_2 T_3 = \theta_3 \rightarrow a_{33} = (\theta_3 - \theta_2) - \tfrac{1}{2}\ddot{\theta}_2 T_3^2 - \dot{\theta}_2 T_3$$

ie. third trajectory segment polynomial:

$$Q_3(\tau) = \left[(\theta_3 - \theta_2) - \tfrac{1}{2}\ddot{\theta}_2 T_3^2 - \dot{\theta}_2 T_3\right]\tau^3 + \left[\tfrac{1}{2}\ddot{\theta}_2 T_3^2\right]\tau^2 + \left[\dot{\theta}_2 T_3\right]\tau + \theta_2$$

with $\dot{\theta}_3 = \frac{Q_3'(1)}{T_3} = \frac{3(\theta_3 - \theta_2)}{T_3} - 2\dot{\theta}_2 - \frac{1}{2}\ddot{\theta}_2 T_3$ and $\ddot{\theta}_3 = \frac{Q_3''(1)}{T_3^2} = \frac{6(\theta_3 - \theta_2)}{T_3^2} - 2\ddot{\theta}_2 - \frac{6\dot{\theta}_2}{T_3}$

Fourth trajectory segment:

$$Q_4(\tau) = a_{43}\tau^3 + a_{42}\tau^2 + a_{41}\tau + a_{40} \rightarrow Q_4(0) = a_{40} = \theta_3$$

$$\dot{\theta}_3 = \frac{Q_4'(0)}{T_4} = \frac{a_{41}}{T_4} = \frac{Q_3'(1)}{T_3} \rightarrow a_{41} = \dot{\theta}_3 T_4$$

$$\ddot{\theta}_3 = \frac{Q_4''(0)}{T_4^2} = \frac{2a_{42}}{T_4^2} = \frac{Q_3''(1)}{T_3^2} \rightarrow a_{42} = \tfrac{1}{2}\ddot{\theta}_3 T_4^2$$

$$Q_4(1) = a_{43} + \tfrac{1}{2}\ddot{\theta}_3 T_4^2 + \dot{\theta}_3 T_4 + \theta_3 = \theta_4 \rightarrow a_{43} = (\theta_4 - \theta_3) - \tfrac{1}{2}\ddot{\theta}_3 T_4 - \dot{\theta}_3 T_4$$

ie. fourth trajectory segment polynomial:

$$Q_4(\tau) = \left[(\theta_4 - \theta_3) - \tfrac{1}{2}\ddot{\theta}_2 T_4 - \dot{\theta}_3 T_4\right]\tau^3 + \left[\tfrac{1}{2}\ddot{\theta}_3 T_4\right]\tau^2 + \left[\dot{\theta}_3 T_4\right]\tau + \theta_3$$

with $\dot{\theta}_4 = \frac{Q_4'(1)}{T_4} = \frac{3(\theta_4 - \theta_3)}{T_4} - 2\dot{\theta}_3 - \frac{1}{2}\ddot{\theta}_3 T_4$ and $\ddot{\theta}_4 = \frac{Q_4''(1)}{T_4^2} = \frac{6(\theta_4 - \theta_3)}{T_4^2} - 2\ddot{\theta}_3 - \frac{6\dot{\theta}_3}{T_4}$

Final trajectory segment:

$$Q_5(\tau) = a_{53}\tau^3 + a_{52}\tau^2 + a_{51}\tau + a_{50} \rightarrow Q_5(0) = a_{50} = \theta_4$$

$$\dot{\theta}_4 = \frac{Q_5'(0)}{T_5} = \frac{a_{51}}{T_5} = \frac{Q_4'(1)}{T_4} \rightarrow a_{51} = \dot{\theta}_4 T_5$$

$$\ddot{\theta}_4 = \frac{Q_5''(0)}{T_5^2} = \frac{2a_{52}}{T_5^2} = \frac{Q_4''(1)}{T_4^2} \rightarrow a_{52} = \tfrac{1}{2}\ddot{\theta}_4 T_5^2$$

$$Q_5(1) = a_{53} + \tfrac{1}{2}\ddot{\theta}_4 T_5^2 + \dot{\theta}_4 T_5 + \theta_4 = \theta_5 \rightarrow a_{53} = (\theta_5 - \theta_4) - \tfrac{1}{2}\ddot{\theta}_4 T_5^2 - \dot{\theta}_4 T_5$$

ie. final trajectory segment polynomial:

$$Q_5(\tau) = \left[(\theta_5 - \theta_4) - \tfrac{1}{2}\ddot{\theta}_4 T_5^2 - \dot{\theta}_4 T_5\right]\tau^3 + \left[\tfrac{1}{2}\ddot{\theta}_4 T_5^2\right]\tau^2 + \left[\dot{\theta}_4 T_5\right]\tau + \theta_4$$

with $\dot{\theta}_5 = \frac{Q_5'(1)}{T_5} = \frac{3(\theta_5 - \theta_4)}{T_5} - 2\dot{\theta}_4 - \frac{1}{2}\ddot{\theta}_4 T_5$ and $\ddot{\theta}_5 = \frac{Q_5''(1)}{T_5^2} = \frac{6(\theta_5 - \theta_4)}{T_5^2} - 2\ddot{\theta}_4 - \frac{6\dot{\theta}_4}{T_5}$

where $\dot{\theta}_5 = \ddot{\theta}_5 = 0$.

Hence, overall:

$$Q_1(\tau) = \left[(\theta_1 - \theta_0) - (\tfrac{1}{2}\ddot{\theta}_0 T_1^2) - (\dot{\theta}_0 T_1)\right]\tau^3 + \left[\tfrac{1}{2}\ddot{\theta}_0 T_1^2\right]\tau^2 + \left[\dot{\theta}_0 T_1\right]\tau + \theta_0$$

where $\dot{\theta}_0 = \ddot{\theta}_0 = 0$

$$Q_2(\tau) = \left[(\theta_2 - \theta_1) - (\tfrac{1}{2}\ddot{\theta}_1 T_2^2) - (\dot{\theta}_1 T_2)\right]\tau^3 + \left[\tfrac{1}{2}\ddot{\theta}_1 T_2^2\right]\tau^2 + \left[\dot{\theta}_1 T_2\right]\tau + \theta_1$$

$$Q_3(\tau) = \left[(\theta_3 - \theta_2) - (\tfrac{1}{2}\ddot{\theta}_2 T_3^2) - (\dot{\theta}_2 T_3)\right]\tau^3 + \left[\tfrac{1}{2}\ddot{\theta}_2 T_3^2\right]\tau^2 + \left[\dot{\theta}_2 T_3\right]\tau + \theta_2$$

$$Q_4(\tau) = \left[(\theta_4 - \theta_3) - (\tfrac{1}{2}\ddot{\theta}_3 T_4^2) - (\dot{\theta}_3 T_4)\right]\tau^3 + \left[\tfrac{1}{2}\ddot{\theta}_3 T_4^2\right]\tau^2 + \left[\dot{\theta}_3 T_4\right]\tau + \theta_3$$

$$Q_5(\tau) = \left[(\theta_5 - \theta_4) - (\tfrac{1}{2}\ddot{\theta}_4 T_5^2) - (\dot{\theta}_4 T_5)\right]\tau^3 + \left[\tfrac{1}{2}\ddot{\theta}_4 T_5^2\right]\tau^2 + \left[\dot{\theta}_4 T_5\right]\tau + \theta_4 \qquad (4.6)$$

To maximise speed, the travelling time $t_{j+1} - t_j$ should be minimised within the velocity, acceleration, jerk (rate of change of acceleration) and torque constraints (related to acceleration by $\tau_i = I_{ci}\ddot{\theta}_i$) for each joint actuator. Kawato et al (1988) stated that minimisation of torque change (ie. jerk) through the minimisation of an objective function is performed internally in the human brain and it has the form:

$C_T = \int_{t_0}^{t_f} \sum_{i=1}^{n} \left(\frac{d\tau_i}{dt}\right)^2 .dt$. This is a nonlinear optimisation problem that indirectly minimises energy. The cost function to be minimised in this case is: $T_j = \sum_{j=1}^{5} t_{j+1} - t_j$.

For each joint i=1....6:

$|Q_{ij}^{'}(\tau)| \le V_{ij}^{max}, |Q_{ij}^{''}(\tau)| \le A_{ij}^{max}, |Q_{ij}^{'''}(\tau)| \le J_{ij}^{max}$.

Maximum velocity occurs at the midpoint of the trajectory (arbitrarily if the constant velocity segment is of finite duration), maximum acceleration occurs at the midpoint of the acceleration phases (arbitrarily since the acceleration phases are constant), and maximum jerk occurs at the end points of the trajectory. If the constraints are violated, T_j must be increased by a factor λ such that $T_j^* = \lambda T_j$.

ie. $Q_{ij}^{*}(\tau) = \frac{1}{\lambda} Q_{ij}^{'}(\tau); Q_{ij}^{*''}(\tau) = \frac{1}{\lambda^2} Q_{ij}^{''}(\tau); Q_{ij}^{*'''}(\tau) = \frac{1}{\lambda^3} Q_{ij}^{'''}(\tau)$ where $\tau = \frac{t_{j+1} - t}{T_j}$.

The velocity, acceleration and jerk are reduced by $\frac{1}{\lambda}, \frac{1}{\lambda^2}, \frac{1}{\lambda^3}$ respectively to remain within actuator constraints: $\lambda = \max(1, \lambda_v, \sqrt{\lambda_a}, \sqrt[3]{\lambda_j})$ where $\lambda_v = \frac{|Q_{ij}^{'}(\tau)|}{V_j^{max}}, \lambda_a = \frac{|Q_{ij}^{''}(\tau)|}{A_j^{max}}, \lambda_j = \frac{|Q_{ij}^{'''}(\tau)|}{J_j^{max}}$.

Now, $Q_j(\tau) = a_{j3}\tau^3 + a_{j2}\tau^2 + a_{j1}\tau + a_{j0}$

Hence for each joint i,

$$Q_j^{'}(\tau) = 3a_{j3}\tau^2 + 2a_{j2}\tau + a_{j1}$$
$$= 3\left[(\theta_{j+1} - \theta_j) - (\tfrac{1}{2}\ddot{\theta}_j T_j^2) - \dot{\theta}_j T_j\right]\tau^2 + 2\left[\tfrac{1}{2}\ddot{\theta}_j T_j^2\right]\tau + \left[\dot{\theta}_j T_j\right] \le V_j^{max}$$

$$Q_j^{''}(\tau) = 6a_{j3}\tau + 2a_{j2}$$
$$= 6\left[(\theta_{j+1} - \theta_j) - (\tfrac{1}{2}\ddot{\theta}_j T_j^2) - \dot{\theta}_j T_j\right]\tau + 2\left[\tfrac{1}{2}\ddot{\theta}_j T_j^2\right] \le A_j^{max}$$

$$Q_j^{'''}(\tau) = 6a_{j3} = 6\left[(\theta_{j+1} - \theta_j) - (\tfrac{1}{2}\ddot{\theta}_j T_j^2) - \dot{\theta}_j T_j\right] \le J_j^{max} \qquad (4.7)$$

A straight forward choice of λ is 2. This resembles the "bracketing" procedure that military artillery forward observation units use in directing gunfire onto enemy targets. A series of single shots are fired and observed on the basis of which the unit aligns initially left and right and then forward or backward the gun firing coordinates by multiple halving of the miss distance to the target at each shot. Once the target has been correctly pinpointed, the salvo is then launched. The method is swift as well as effective. Indeed this is a version of the root finding bisection algorithm which is guaranteed to converge on a root if one exists.

4.3 PARALLEL PROCESSING IMPLEMENTATIONS

The need for real time trajectory generation is critical for robotics applications: robotic algorithms place extreme burdens on computational resources, necessitating the use of enhanced parallel and concurrent computing architectures. It should be noted that the $O(n^4)$ complexity of the Lagrange-Euler dynamic equations imply that parallel processing would be of limited value in reducing the computation time unless large numbers of processors can be used. Intelligent robots will select the path on the basis of sensory data necessitating on-line trajectory generation.

The Newton-Euler dynamics with their linear recursive structure may be implemented on p processors for an n link manipulator reducing their complexity to

$O(k_1(n/p)+k_2(\log_2 p))$ [Graham 1989]. They are suitable for a parallel pipelined architectural implementation. In pipelined processing, the CPU subdivides the execution of instructions into a sequence of steps which are executed by individual subsidiary hardware unit processors. It operates like an industrial assembly line simultaneously executing the same instructions on different data streams. It is used extensively in high performance computing. They are particularly suited to floating point arithmetic computations. The systolic array is a generalisation of pipelining in a multidimensional pipelined array operating under the same control unit [Kung 1982]. It comprises a two dimensional grid (eg. hexagonal or rectangular) of SIMD processor units with nearest neighbour 4-link connections. The partial results of computations are passed onto one or more adjacent processors in the grid. They are essentially optimised for a particular calculation and have a time complexity independent of N because the flow of data through the network is fixed and optimised to a constant value. Input-output is overlapped with computation and each operand is input only once and operated on many times. A hexagonal systolic array staggers the computations so that the correct partial products arrive at the correct processor at the correct time. Such architectures are well suited to matrix and vector computations such as NxN multiplication. They are extremely fast and efficient but are limited to only a few operations. Hence they offer great promise for performing Lagrange-Euler dynamics based control for robot manipulators in real-time. Speedups can be sugnificant eg. NxN matrix multiplication can be performed in time complexity O(N) rather than $O(N^2)$ as in conventional processors. For a 6 degree of freedom robot manipulator, this would require 36 processor units which for the forseeable future is not likely to be implemented on space systems. In these approaches, the number of processors required implies a heavy hardware cost and associated mass penalty.

Chapter 5

ROBOTIC CONTROL

As well as mechanism and structure, robot designs are also characterised as systems. Systems are of two types: process plant where material is processed and service networks which process information. Motor control systems in robotics are of the latter type. A robot must have the ability to change configuration and the position, velocity and acceleration of its end effector in real-time. This is a severe constraint on the control system. The control system provides the mapping between sensing of the environment and the effector actions on the environment. The environment state is successively altered by those actions invoking the need for successive sensing. ie. a perception-action cycle. In human cognition, sensory-motor cortical maps provide the means for cyclically alternating between attentional (sensory) and orienting (motor) systems during movement to direct the agent towards its target. The cycle implements comparison between the terminal motor map and a proprioceptive motor map to determine the degree of match [Grossberg 1980]. Only when the entire map plan has been executed do the proprioceptive and motor maps match thereby terminating the movement.

It is characteristic of robotics that the sensory processing required by the machine-level controller is concerned with sensory servoing rather than high level object identification. It is absolutely essential therefore for on-line control to be realised that efficient computation of the control algorithms occurs. The situation is hampered by the complex nonlinear dynamics due to the robotic manipulator's articulated structure. The majority of industrial robots are open-loop controlled but this is not sufficient for variable environments where sensory feedback is required. This necessitates closed loop control.

The objective of the robot controller is to determine the input torques required to drive the joints from an initial steady state to reach a final steady state of desired output positions with the desired output velocities and accelerations within a prescribed settling time. This requires minimising to zero the difference between the performance trajectory and the reference trajectory. This discrepancy between the observed and predicted behaviour is the error. The controller applies input torques to reduce this error between actual and desired trajectories to zero. The control law specifies the magnitude of the correction to be applied in response to the error measurements specified as the gain. If exact models of the robot dynamics were available and those models were linearised exactly, then control could be implemented using optimal control techniques, and several workers have used this approach. However, modelling errors will occur because the robot is a complex, highly nonlinear system for which complete models are not available (eg. dry coulombic friction at the joints is difficult to model). The use of high gains to render the control insensitive to parameter variations is unsuitable since this can produce instability and excitation as well as possible actuator saturation. It is a characteristic of nonlinear feedback systems that they can exhibit chaotic dynamics [Baillieul et al 1980]. Chaotic behaviour is characteristic of sensitive dependence on initial conditions, variations of which produce output behaviour that is irregular and disordered. Although random and unpredictable such

behaviours obey mathematical rules. However, chaotic output is not desirable in robotic control systems.

At each sample period, the control algorithm performs the following functions [Geshke 1983]:
(i) read sensor outputs of joint position and velocity; compute desired joint angles, velocities and accelerations using the inverse kinematic formulations;
(ii) compute the model dynamics to calculated the required input torques.

Hand control is normally performed separately from arm control since hand control can be complex if multijointed universal hands are used instead of parallel jaw grippers. The arm control problem is to calculate the joint torques to cause the manipulator to track the desired trajectory. This must be computed frequently ~kxf_{max} where f_{max} for most manipulators is 5-10Hz and k~5-8, ie. $f_{update} \sim 60Hz$.

5.1 DC MOTOR CONTROL:

Actuators at each joint provide the torques to drive the end effector through its required trajectory. The voltage-controlled dc motor is an electromechanical system whereby the mechanical part is coupled to the electrical part and it drives an inertial load. Permanent magnets give a constant magnetic field and the motor is controlled by the current in the armature coil. The system input is the applied voltage to the armature coil and the ouput is the angular position of the rotor. Internal sensors are used to provide direct information concerning the state of the manipulator joints for the control system. The motor shaft is connected to optical encoder, resolver or potentiometer sensors for position sensing and tachometer sensors for velocity sensing. The actuator dynamics affect robot manipulator performance and so must be used to derive the control gains.

If gear transmission is used, the gear ratio n is given by (for a direct drive motor, n=1):
n=(no. of teeth of input motor shaft)/(no. of teeth of output load shaft)=$\frac{N_m}{N_l} = \frac{\theta_l}{\theta_m}$
Hence, actuator displacement, $\theta_l = n\theta_m$

actuator velocity, $\dot{\theta}_l = n\dot{\theta}_m$

actuator acceleration, $\ddot{\theta}_l = n\ddot{\theta}_m$

where subscrpit "l" indicates load and subscript "m" indicates motor.
Consider a single dc motor [Luh 1983a,b; Moya & Seraji 1987].
Total torques comprise of torques on the motor and on the load: $\tau = \tau_l + \tau_m$

where $\tau_m = J_m\ddot{\theta}_m + b_m\dot{\theta}_m$ where J=moment of inertia

$\tau_l = J_l\ddot{\theta}_l + b_l\dot{\theta}_l$ b=viscous friction damping

This includes the internal torques required to overcome the inertia and the damping effects (assuming that the nonlinear static friction is negligible - typically it is ~0.02Nm). Conservation of work states that the work done by the load referred to the load shaft $\tau_l\theta_l$ is equal to the work done by the load referred to the motor shaft $\tau_l'\theta_m$. The load inertia is increased by n^2 when referenced to the motor shaft: $\tau_l' = \frac{\tau_l\theta_l}{\theta_m} = n\tau_l = n(J_l\ddot{\theta}_l + b_l\dot{\theta}_l) = n^2(J_l\ddot{\theta}_m + b_l\dot{\theta}_m)$
Hence, the torque at the motor shaft,

$\tau = \tau_m + \tau_l' = J_{eff}\ddot{\theta}_m + b_{eff}\dot{\theta}_m$ where $J_{eff} = J_m + n^2 J_l$ =effective combined inertia

$b_{eff} = b_m + n^2 b_l$ =effective viscous friction coefficient

The torque required to accelerate the inertial load is directly proportional to the armature current:

$\tau_m = K_t i$ where K_t=motor torque constant.

Apply Kirchoff's voltage law to the armature circuit to relate armature current i to the applied control voltage V_i at the terminals of the armature:

$V_i = R_i i + L_i \frac{di}{dt} + E_b$ where R_i=armature coil resistance

L_i=armature coil inductance

E_b=back EMF

The back EMF varies in proportion to the angular velocity of the motor according to Faraday's law:

$E_b = K_b \dot{\theta}_m = \frac{K_b}{n}\dot{\theta}_l$ where K_b=motor electromechanical torque constant

Armature current, $i = \frac{V_i - L_i\frac{di}{dt} - K_b\dot{\theta}_m}{R_i}$.

For a constant input voltage, the motor will rotate at a constant angular velocity such that the back EMF balances the applied voltage. The angular position output increases at a contant rate. This is characterised by the proportionality gain K_t to generate the electromagnetic torque:

$\rightarrow \tau = K_t \frac{V_i - L_i\frac{di}{dt} - K_b\dot{\theta}_m}{R_i}$

This may be equated to the earlier formulation for the motor torque:

$J_{eff}\ddot{\theta}_m + b_{eff}\dot{\theta}_m = K_t \frac{V_i - L_i\frac{di}{dt} - K_b\dot{\theta}_m}{R_i}$

The electrical time constant t=L/R is much less than the mechanical time constant, so the armature inductance may be considered as negligible.

Apply the Laplace transform such that $F(s) = \Im[f(t)] = \int_0^\infty f(t).e^{-st}.dt$ where $s = \sigma + jw$:

$T(s) = s^2 J_{eff}\theta_m(s) + sb_{eff}\theta_m(s) = K_t\left[\frac{V_i(s) - sK_b\theta_m(s)}{R_i}\right]$

Open loop transfer function, $G(s) = \frac{\Im(output)}{\Im(input)} = \frac{\theta_m(s)}{V(s)} = \frac{K_t}{s^2 R_i J_{eff} + s(R_i b_{eff} + K_t K_b)}$

$\frac{\theta_l(s)}{V(s)} = \frac{nK_t}{s^2 R_i J_{eff} + s(R_i b_{eff} + K_t K_b)} = \frac{nK}{s(T_m s + 1)}$ where K=motor torque gain constant=$\frac{K_t}{R_i b_{eff} + K_t K_b}$

T_m=motor torque time constant=$\frac{R_i J_{eff}}{R_i b_{eff} + K_t K_b}$

It is now necessary to close the open-loop control system by introducing feedback. A closed loop may be implemented such that the angular position output is fed back to cancel the input voltage to maintain a constant voltage for a constant angular position. A position controller servos the motor such that the actual angular displacements of the joint track the desired angular displacement. The error from the reference (desired) trajectory q^d is given by $|q^d - q| < e$ and for small error, e, the actual trajectory q must remain in the neighbourhood of q^d for stability. The applied voltage of the motor varies linearly with the position error defined as the difference between the desired angular displacement and the angular displacement measured by the position sensor:

$V_i = \frac{K_p e}{n} = \frac{K_p}{n}(\theta_l^d - \theta_l)$ where K_p=position feedback gain

Position feedback provides a deadbeat response to external disturbances which might deflect the manipulator. To minimise the response time and provide stability with no

overshoot, damping of flexible modes must be added by including a rate feedback proportional to the velocity error to stabilise the response particularly if K_p is large. The actual velocity of the joint is measured by a tachometer sensor:

$V_i = \frac{K_p}{n}(\theta_1^d - \theta_1) + \frac{K_v}{n}(\dot{\theta}_1^d - \dot{\theta}_1) = \frac{K_p e + K_v \dot{e}}{n}$ where K_V=velocity feedback gain

Velocity feedback is particularly important for direct drive motors due to their high inertial loads. An integrator (for PID control) is not usually included in robot motors because the velocities of robot motion are not particularly high in comparison to other applications. Substitute the feedback into the open-loop transfer function to generate the closed loop transfer function:

$$\frac{\theta_l(s)}{K_p E + sK_v E} = \frac{nK_t}{s^2 R_i J_{eff} + s(R_i b_{eff} + K_t K_b)} \rightarrow G(s) = \frac{\theta_l(s)}{E(s)} = \frac{nK_t(K_p + sK_v)}{s^2 R_i J_{eff} + s(R_i b_{eff} + K_t K_b)}$$

Substitute $E(s) = \theta_1^d - \theta_1$ to obtain the closed loop transfer function:

$$\frac{\theta_l(s)}{\theta_l^d(s)} = \frac{G(s)}{G(s)+1} = \frac{K_t(K_p + sK_v)}{s^2 R_i J_{eff} + s(R_i b_{eff} + K_t K_b + K_t K_v) + K_t K_p} \quad (5.1)$$

K_p and K_V are chosen so that e and $\dot{e}$ tend to zero exponentially: $\ddot{e} + K_v \dot{e} + K_p e = 0$. High controller gains increase the size of the neighbourhood about the operating point within which tracking errors are exponentially convergent. The transfer functions have the form $G(s) = \frac{1}{s^2 + 2\varsigma w_n + w_n^2}$ for a second order differential equation (damped linear oscillator) $\ddot{y} + 2\varsigma w_n \dot{y} + w_n^2 y = 0$ where w_n=characteristic natural frequency (typically f_n~10Hz for a manipulator; ς =damping ratio.

For $\frac{\theta_l(s)}{\theta_l^d(s)}$: $w_n = \sqrt{\frac{K_t K_p}{R_i J_{eff}}}$ and $2\varsigma w_n = \frac{R_i b_{eff} + K_t K_b + K_t K_v}{J_{eff} R_i} \rightarrow \varsigma = \frac{R_i b_{eff} + K_t K_b + K_t K_v}{2\sqrt{J_{eff} R_i K_t K_p}}$

If ς<1, we get a fast response with overshoot, ie. underdamped response. This increases the possibility of collision. If ς>1, we get overdamping with no oscillation to generate zero steady state error. If ς=1, we get critical damping with maximum speed, ie. for stability, $\varsigma \geq 1$.

Position feedback gain, $K_p = \frac{J_{eff} R_i w_n^2}{K_t} > 0$ (5.2)

Velocity feedback gain, $K_v \geq \frac{2\sqrt{J_{eff} R_i K_t K_p} - R_i b_{eff} - K_t K_b}{K_t}$ (5.3)

For a direct drive motor, since the motor is mounted in adjacent links directly, the motor inertia is that of the link mounting. Too high a position gain will increase the amplitude of oscillations. At high gain values, an effectively infinite amplitude ratio resonance peak occurs with zero input making the system become unstable. In order not to excite structural oscillations, Paul (1981) suggested that the natural damping frequency should be less than half the structural oscillation frequency: $w_n \leq 0.5 w_s$. The structural resonant frequency depends on the material stiffness and the motor inertia: $w_s = \sqrt{\frac{K_s}{J_{eff}}}$ where K_S=effective stiffness of the joint. Hence, $0 \leq K_p \leq \frac{w_s^2 J_{eff} R_i}{4K_t}$.

Similarly, $K_v \geq \frac{R_i w_s \sqrt{J_{eff}} - R_i b_{eff} - K_t K_b}{K_t}$

For direct drive motors [Asade Kanade & Takeyama 1983]:

$\frac{R_i}{K_t} = 15.88 V/Nm$ for arm motors and $\frac{R_i}{K_t} = 2.15 V/Nm$ for wrist motors,

$J_{eff} = 3.3 kgm^2$ and $b_{eff} = 1.4 N/m/s$ are typical parameters for robot motors.

5.2 COMPUTED TORQUE CONTROL:

It is possible to control each robot joint individually using a PD servo system to each joint motor. Indeed, this is the way that the majority of industrial robot manipulators are controlled. However, the dynamic interactions between the joints allow only slow speeds at the joints to keep the nonlinear coupling small. Nonlinear systems require linearisation about the operating point, in this case the desired trajectory, in the neighbourhood of which the system may be regulated by a linear control system to track the reference input. This may be accomplished by feedforward compensation to linearise the system by decoupling the system into a series of decoupled linear independent subsystems which may be controlled by PD feedback laws [Bejczy & Tarn 1986]. This computed torque technique is a nonlinear control method whereby the dynamic model of the manipulator is used to dynamically decouple the joints through precomputed nonlinear feedforward compensation to cancel the effects of the nonlinear coupling. The nonlinear coupling terms are treated as disturbance torques and fed forward into the contoller of each joint. In effect, it is an example of a MIMO system which has been decoupled into a series of SISO systems. As well as feeding forward nonlinear components to compensate for the interaction forces, it simultaneously feeds back deviations from the desired trajectory. It is a PD technique where position and velocity feedback provide corrective torques to decrease the position error and provide damping whilst employing exact multivariable linearisation about the desired trajectory through feedforward compensation to cancel out the nonlinear effects. Each joint acts as an second order oscillator with natural frequency w and damping ratio ς :

$\tau_i = \ddot{\theta}_i^d + 2\varsigma w(\dot{\theta}_i^d - \dot{\theta}) + w^2(\theta_i^d - \theta_i)$ as a single dc motor.

The motor torque generated by each dc motor has an additional disturbance torque:

$\tau = J_{eff}\ddot{\theta}_m + b_{eff}\dot{\theta}_m + D$ where D=disturbance torques.

Hence, $J_{eff}\ddot{\theta}_m + b_{eff}\dot{\theta}_m + D = K_t\frac{V_i - K_b\dot{\theta}_m}{R_i} \rightarrow R_iJ_{eff}\ddot{\theta}_l + (R_ib_{eff} + K_tK_b)\dot{\theta}_l = nK_tV_i - nR_iD$

Apply Laplace transforms with $V(s) = \frac{K_pE + sK_vE}{n}$:

$s^2R_iJ_{eff}\theta_l(s) + s[R_ib_{eff} + K_tK_b]\theta_l(s) = K_t(K_pE(s) + sK_vE(s)) - nR_iD(s)$

$\rightarrow \frac{\theta_l(s)}{E(s)} = \frac{K_t(K_p + sK_v) - nR_iD(s)}{s^2R_iJ_{eff} + s(R_ib_{eff} + K_tK_b)}$

Hence, $\theta_l(s) = \frac{K_t(K_p + sK_v)\theta_l^d(s) - nR_iD(s)}{s^2R_iJ_{eff} + s(R_ib_{eff} + K_tK_b + K_tK_v) + K_tK_p}$

System error derives from the disturbing torques:

$E(s) = \theta_l^d(s) - \theta_l(s) = \frac{[s^2J_{eff}R_i + s(R_ib_{eff} + K_tK_b)]\theta_l^d(s) + nR_iD(s)}{s^2R_iJ_{eff} + s(R_ib_{eff} + K_tK_b + K_tK_v) + K_tK_p}$ (5.4)[Fu, Gonzalez & Lee 1987]

The disturbance torques are precomputed as centrifugal/Coriolis and gravity torques and fed forward into the controller to compensate for their effects such that $D(s) = \tau_c(s) + \tau_g(s) + \tau_e(s) - \tau_{comp}(s)$ where each term respectively refers to Coriolis/centrifugal torques, gravity torques, other disturbance torques (eg. static friction or load dependent torques), and precomputed torques. The precomputed term depends on the dynamic model of the manipulator which precomputes the gravity and centrifugal/Coriolis torques and possibly the viscous friction torques at the joints. The overall computed torque control law may be represented thus for all the joints:

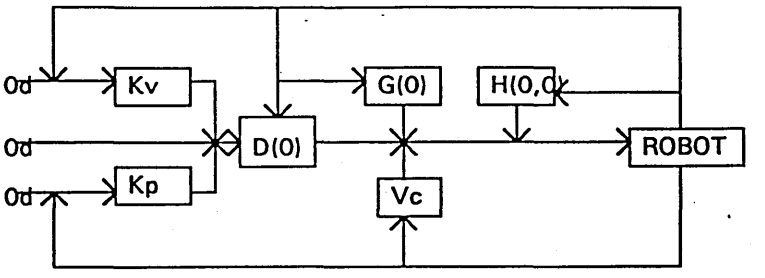

Kp = position gain
Kv = velocity gain
G(0) = gravitation torque
H(0,0) = coriolis/centrifugal torque
D(0) = inertia matrix
Vc = other disturbance torques

The steady state performance of the system is given by the error between the desired output and the actual output after transients have decayed. It is determined by the numerator behaviour of the error as s tends to zero.

A step input of $\theta_i^d(s) = \frac{A}{s}$ commands the manipulator to hold its position constant to illustrate the response to sudden disturbances:

$$e_{ss}(step) = \lim_{s\to 0} . \frac{[s^2 J_{eff} R_t + s(R_t b_{eff} + K_t K_b)]A/s + nR_t D(s)}{s^2 R_t J_{eff} + s(R_t b_{eff} + K_t K_b + K_t K_v) + K_t K_p} = \lim_{s\to 0} \frac{nR_t(\tau_c + \tau_g + \tau_e - \tau_{comp})}{s^2 R_t J_{eff} + s(R_t b_{eff} + K_t K_b + K_t K_v) + K_t K_p}$$

If $\tau_{comp}(s) = \tau_c(s) + \tau_g(s)$: $e_{ss}(step) = \frac{nR_t \tau_e(s)}{K_t K_p} = \frac{4n\tau_e(s)}{w_s^2 J_{eff}}$ where $K_p \le \frac{w_s^2 J_{eff} R_t}{4K_t}$

A ramp input of $\theta_i^d(s) = \frac{A}{s^2}$ commands the manipulator to move with constant velocity to illustrate its response to time-variable input:

$$e_{ss}(ramp) = \lim_{s\to 0} . \frac{[s^2 J_{eff} R_t + s(R_t b_{eff} + K_t K_b)]\frac{A}{s^2} + nR_t D(s)}{s^2 R_t J_{eff} + s(R_t b_{eff} + K_t K_b + K_t K_v) + K_t K_b} = \frac{(R_t b_{eff} + K_t K_b)A}{K_t K_p} + e_{ss}(step)$$

The computed torque control law for all joints has the form in terms of Lagrangian matrix coefficients (the subscript "q" indicates desired variable values):

$$\tau = D(\theta)[\ddot{\theta}^d + K_v(\dot{\theta}^d - \dot{\theta}) + K_p(\theta^d - \theta)] + H(\theta, \dot{\theta}) + G(\theta)$$

since $u = \ddot{\theta} = \ddot{\theta}^d + K_v(\dot{\theta}^d - \dot{\theta}) + K_p(\theta^d - \theta)$

where position error, $e = \theta^d - \theta$ and velocity error, $\dot{e} = \dot{\theta}^d - \dot{\theta}$ and K_v and K_p are 6x6 velocity and position feedback gain matrices.

In cartesian coordinates, $u = \ddot{\theta} = J^{-1}[\ddot{q}^d + K_v(\dot{q}^d - \dot{q}) + K_p(q^d - q) - \dot{J}\dot{\theta}]$ such that

$$\tau = D(\theta)J^{-1}[\ddot{q}^d + K_v(\dot{q}^d - \dot{q}) + K_p(q^d - q) - \dot{J}\dot{\theta}] + H(\theta, \dot{\theta}) + G(\theta).$$

$H(\theta, \dot{\theta}) + G(\theta)$ comprise the feedforward dynamics component. For the Newton-Euler equations, an equivalent recursive control law is generated by substitution of $\ddot{\theta}_i$ into the Newton-Euler equations [Fu Gonzalez & Lee 1987]:

$$\ddot{\theta}_i = \ddot{\theta}_i^d + \sum_{j=1}^{n} K_v^{ij}(\dot{\theta}_j^d - \dot{\theta}_j) + \sum_{j=1}^{n} K_p^{ij}(\theta_j^d - \theta_j) \qquad (5.5)$$

K_v^{ij} and K_p^{ij} are velocity and position feedback gains for joint i. They do not vary from task to task unless the payload varies greatly.

A Lyapunov function may be chosen similar to the normalised Hamiltonian H=KE+PE. It is a constant of motion and is correlated closely with the concept of the stability

condition being a state of minimum energy at equilibrium. The Lyapunov function chosen is based on the KE of the error with velocity replaced with velocity error:

$V = \frac{1}{2}|\dot{e}|^2 + \frac{1}{2}e^T K_p e$ where $e = \theta - \theta^d$.

$\dot{V} = \frac{\partial V}{\partial e} = \dot{e}^T \{D(\theta)^{-1}[-H(\theta,\dot{\theta}) + \tau] - \ddot{\theta}^d + K_p e\}$

The computed torque control law: $u = \tau = D(\theta)[\ddot{\theta}^d - K_p e - K_v \dot{e}] + H(\theta,\dot{\theta})$

$\rightarrow \dot{V} = -\dot{e}^T K_v \dot{e} \leq 0$

Hence, the closed loop computed torque technique is globally asymptotically stable. If K_p is large in comparison to the initial kinetic energy error $\frac{1}{2}\dot{e}^T D(\theta)\dot{e}$ the tracking error converges to zero. The initial KE error may be made zero by choosing the initial desired velocity to equate to the initial actual velocity. The computed torque scheme is stable provided robot parameters are reasonably accurately known and is robust to model errors of <5-10%. For this reason, Abdullah et al (1991) classify the computed torque technique as a robust control scheme. The robustness can be increased by using PID control laws: $u = \ddot{\theta}^d + K_p e + K_v \dot{e} + K_i \int e.dt$. Moya & Seraji (1987) have shown the computed torque method to provide perfect reference tracking for both transient as well as steady state modes. The linearisation process depends on virtual perfect modelling of the manipulator dynamics. It will become unstable for large uncertainties >10% by producing amplitude output errors in the dynamics. Inexact cancellation in the feedforward linearisation can result in the loss of stability. In fact, variable payload mass will cause deviations from the model and state measurement sensors are often corrupted with noise. Finally, all else being equal, as long as the available actuator power output is sufficient to generate the required tracking torque, the tracking position and velocity errors should remain small. However, if the available power falls short of the required output, then tracking errors may become large. Astrom (1987) classified the computed torque scheme as an example of the gain scheduling adaptive control technique because the dynamic parameters are determined by the nonlinear feedforward compensation which effectively transforms the system from a nonlinear one to a set of linear subsystems. However, it does require a priori information about the system including payload variability.

5.3 RESOLVED MOTION CONTROL:

Resolved motion control specifies all control variables in terms of cartesian end effector coordinates. The chief advantage lies in performing all kinematic control at cartesian hand level which is more suitable for task execution. One difficulty lies in the fact that sensors operate at joint level and forward transformation is required to implement feedback control introducing the possibility of inaccuracy. Resolved motion control is used in teleoperation with the human operator providing closure of the control loop. The major disadvantage is that it takes no account of the dynamics of the system unless these are explicitly included in the control system.

5.3.1 Resolved Position Control

In resolved position control, θ is specified, while $\dot{\theta}$ and $\ddot{\theta}$ are obtained numerically:

$$\begin{pmatrix} n_x & s_x & a_x & p_x \\ n_y & s_y & a_y & p_y \\ n_z & s_z & a_z & p_z \\ 0 & 0 & 0 & 1 \end{pmatrix}^{-1} \begin{pmatrix} n_x^d & s_x^d & a_x^d & p_x^d \\ n_y^d & s_y^d & a_y^d & p_y^d \\ n_z^d & s_z^d & a_z^d & p_z^d \\ 0 & 0 & 0 & 1 \end{pmatrix} = \begin{pmatrix} 1 & -\delta_z & \delta_y & dx \\ \delta_z & 1 & -\delta_x & dy \\ -\delta_y & \delta_x & 1 & dz \\ 0 & 0 & 0 & 1 \end{pmatrix}$$

$$\text{such that } e = \begin{pmatrix} dx \\ dy \\ dz \\ \delta_x \\ \delta_y \\ \delta_z \end{pmatrix} = \begin{pmatrix} n(p^d - p) \\ s(p^d - p) \\ a(p^d - p) \\ \frac{1}{2}(a.s^d - a^d.s) \\ \frac{1}{2}(n.a^d - n^d.a) \\ \frac{1}{2}(s.n^d - s^d.a) \end{pmatrix} \tag{5.6}$$

5.3.2 Resolved Rate Control

In resolved rate control, $\dot{\theta}$ is specified, θ is measured and $\ddot{\theta}$ is obtained numerically. Present and desired positions are computed by resolved position techniques and corrective cartesian rate $\dot{q}$ is calculated to reduce the position error and joint rates are obtained by inversion of the Jacobian [Whitney 1969, 1972].

$$\begin{pmatrix} n_x^d(t) & s_x^d(t) & a_x^d(t) & p_x^d(t) \\ n_y^d(t) & s_y^d(t) & a_y^d(t) & p_y^d(t) \\ n_z^d(t) & s_z^d(t) & a_z^d(t) & p_z^d(t) \\ 0 & 0 & 0 & 1 \end{pmatrix}^{-1} \begin{pmatrix} n_x^d(t+\delta t) & s_x^d(t+\delta t) & a_x^d(t+\delta t) & p_x^d(t+\delta t) \\ n_y^d(t+\delta t) & s_y^d(t+\delta t) & a_y^d(t+\delta t) & p_y^d(t+\delta t) \\ n_z^d(t+\delta t) & s_z^d(t+\delta t) & a_z^d(t+\delta t) & p_z^d(t+\delta t) \\ 0 & 0 & 0 & 1 \end{pmatrix}$$

$$= \begin{pmatrix} 1 & -w_z^d & w_y^d & v_x^d \\ w_z^d & 1 & -w_x^d & v_y^d \\ -w_y^d & w_x^d & 1 & v_z^d \\ 0 & 0 & 0 & 1 \end{pmatrix} \delta t$$

$$\text{such that } \dot{q}^d = \begin{pmatrix} v_x^d \\ v_y^d \\ v_z^d \\ w_x^d \\ w_y^d \\ w_z^d \end{pmatrix} = \begin{pmatrix} n^d(t)[p^d(t+\delta t) - p^d(t)]/\delta t \\ s^d(t)[p^d(t+\delta t) - p^d(t)]/\delta t \\ a^d(t)[p^d(t+\delta t) - p^d(t)]/\delta t \\ \frac{1}{2}[a^d(t).s^d(t+\delta t) - a^d(t+\delta t).s^d(t)]/\delta t \\ \frac{1}{2}[n^d(t).a^d(t+\delta t) - n^d(t+\delta t).a^d(t)]/\delta t \\ \frac{1}{2}[s^d(t).n^d(t+\delta t) - s^d(t+\delta t).n^d(t)]/\delta t \end{pmatrix} \tag{5.7}$$

and $\dot{e} = \dot{q}^d - \dot{q}$ with $\dot{q} = J\dot{\theta}$.

This mode of control is adopted by the Space Shuttle Remote Manipulator System and it is also being suggested for use in future Canadian space robotic systems. It is the most generally used method of control for teleoperated robots.

5.3.3 Resolved Acceleration Control

In this method, $\ddot{\theta}$ is specified while θ and $\dot{\theta}$ are measured. This method is in fact a resolved cartesian version of the computed torque technique [Luh et al 1980]:

$$\ddot{q} = \ddot{q}^d + K_v(\dot{q}^d - \dot{q}) + K_p(q^d - q)$$

where $e = \begin{pmatrix} p^d - p \\ \frac{1}{2}(n \times n^d + s \times s^d + a \times a^d) \end{pmatrix}$ and $\dot{e} = \begin{pmatrix} v^d - v \\ w^d - w \end{pmatrix}$

If no errors occur in position or velocity, $\ddot{q}$ will track $\ddot{q}^d$ such that $\ddot{e} + K_v \dot{e} + K_p e = 0$.

Now, $\ddot{\theta} = J^{-1}(\ddot{q} - \dot{J}\dot{\theta})$:

$$\rightarrow \ddot{\theta} = J^{-1}[\ddot{q}^d + K_v(\dot{q}^d - \dot{q}) + K_p(q^d - q) - \dot{J}\dot{\theta}] \qquad (5.8)$$

The input torques to each joint are determined from the computed $\ddot{\theta}$ and measured $\dot{\theta}$ and θ using the Newton-Euler equations or Langrange-Euler equations. For the Lagrange-Euler equations:

$$\tau = D(\theta)\ddot{\theta} + H(\theta, \dot{\theta}) = D(\theta)[J^{-1}(\ddot{q}^d + K_v(\dot{q}^d - \dot{q}) + K_p(q^d - q) - \dot{J}\dot{\theta})] + H(\dot{\theta}, \theta)$$

The resolved acceleration control method is computationally very intensive.

5.3.4 Resolved Motion Force Control

Resolved motion force control works well only when the load mass is much greater than the manipulator mass [Wu & Paul 1982], ie. when only negligible joint torques are required to accelerate the links, thereby restricting its validity. Although such a situation may occur for space robotics, this is rarely the case in terrestrial robotics. Furthermore, the method is approximate rather than exact.

5.4 FORCE FEEDBACK CONTROL

The motion of a robotic manipulator is performed in two distinct phases: gross motion control from initial to final position/orientations along a trajectory, and fine control where the end effector dynamically interacts with the target object. Gross motion utilises position/velocity feedback for geometric information while fine motion utilises force feedback for dynamic information [Whitney 1977]. Force control is fundamental to robotics since the fraction of time spent to complete the terminal compliant phase is comparable or greater than that to perform the gross motions. Furthermore, most robotic functions are concerned with the manipulation of objects in the world. Assembly is a basic manufacturing operation that involves the interaction of piece parts. Indeed, robot function may be regarded as a series of desired and undesired collisions with the environment. A trajectory may be divided into sequences of compliant motion joined by guarded moves. Manipulator motion is characterised by 2 basic states and transitions: (i) the manipulator controls displacement and monitors force in the force space where unpredicted forces indicate error; (ii) the manipulator controls force and monitors displacement in position space whereby any unpredicted displacement indicates error. Switching between control modes occurs on contact or release. On contact, hand forces increase until the desired force is attained and control switches from position to force control. On release, hand forces drop to zero and control switches from force to position control. Paul (1987) introduced into the computer programming language WAVE two commands to differentiate two types of force control methodologies: STOP (terminate current motion when force exceeds a

limit- this is the guarded move) and FORCE (pursue the current motions to generate a force of a given value - if zero, this corresponds to free motion). Switching between position/velocity control only and position/force control may be accomplished at each sampling period with activated touch sensors triggering the required formulation. Proximity sensing may be used to provide a smooth transition from vision to touch control. It has been suggested that inclusion of force control reduces task execution time by ~30-50% and that for space operations force control is critical [Varsi 1991].

For manipulation tasks, compliant motion through force control is absolutely essential when the position of a gripper is constrained by the task. The use of position/velocity control only will introduce substantial errors due to the unavoidable sensor and robot parameter inaccuracies. The remote centre compliance wrist assembly is a passive compliant device which is suitable only for a small class of tasks involving misaligments (ie. peg-in-hole tasks). Hence active force control using force sensors is required when the manipulator makes contact with its environment to precisely control contact forces through closed loop fine motion feedback. To include force control, the general dynamic equation has the form: $\tau = D(\theta)\ddot{\theta} + H(\theta,\dot{\theta}) + G(\theta) + J^T F_{ext}$

There are two main approaches to explicit force feedback control which close the force control loop around the position control loop [Whitney 1987]. The stiffness approach is based on the generalised spring model [Salisbury 1980]. Stiffness is the property that induces restoring forces and torques on a cantilever beam as it is deflected from a nominal position. The difference between the actual and desired effector positions are related to force errors through a stiffness matrix: $\delta f = K_s \delta q$ where δq =displacement from nominal position q_0, K_S=6x6 diagonal stiffness matrix the inverse of which is the compliance matrix (with dimensions of position/force). The generalised damper model treates forces as being in proportion to velocity errors offering adavantages of continuity [Whitney 1969, 1977]: $\delta f = K_F \delta \dot{q}$ where $\delta \dot{q}$=velocity error (v^d-v) with v=0 nominally, K_F=6x6 diagonal damping matrix, the inverse of which is the accomodation matrix (with dimensions of velocity/force). Transformation to joint level is straightforward suggesting that both methods are virtually equivalent:

$$\dot{q} = \delta q = J\dot{\theta} = J\delta\theta \rightarrow \delta f = K_s J\delta\theta = K_F J\dot{\theta}$$

$$\tau = J^T F = J^T K_s J\delta\theta = J^T K_F J\dot{\theta}$$

In both cases these explicit methods involve nullifying the contact forces and torques at the end effector by generating position/velocity modification commands. However, in general there is no one-to-one correspondence between contact forces and misalignments in assembly tasks, whereas these methods assume that there is such a linear relation between force variation and position/velocity error. Both approaches exhibit sluggish behaviour in stiff environments [Whitney 1987].

Whitney (1987) investigated the stability of force control. The manipulator interacts with its environment which behaves as a spring producing a reaction force/torque on the end effector. Both the environment and force sensors have natural frequency responses. The environment stiffness K_e is often high ~10^6N/m which produces little damping but give high natural frequency responses generating poor stability. Low stiffness environments still give K_e~10^5N/m and such enivironments are often determined by both the object stiffness K_0 and the manipulator compliance K_m:

$\frac{1}{K_e} = \frac{1}{K_o} + \frac{1}{K_m} \rightarrow K_e = \frac{K_m K_o}{K_m + K_o}$. Generally $K_o >> K_m$, hence, $K_e \sim K_m$. A system is stable if $K_e K_F \delta t < 1$ or $K_m K_F \delta t < 1$ where δt=sensor sample rate, $K_F = diag(K_f K_\tau)$ such that $K_f = R^3 K_\tau$ where R is the distance between the contact end point and the coordinate centre of freedom (usually the wrist) [Whitney 1977]. Stability requires $K_F K_e$ to be small, so to deal with stiff environments with high K_e, K_F must be small. Generally, a fixed force gain is not ideal: the value of K_F will differ depending on the contact dynamics between the manipulator and the environment. As stiffness of contact increases, so K_F should be reduced. Without a priori knowledge of the environmental stiffness, K_F should be set as low as possible, but in softer environments this will result in slower response times and so extended task completion times. Typically, $K_F = diag(0.005, 0.0001)$. At the transition point between position and force control at contact, collision energy is absorbed by the natural compliance of the system and dissipated with the possibility of destructive consequences. Force sensors are typically the least stiff parts of the manipulator and the most fragile: the Scheinmann force sensing wrist required a force overload mechanism to protect it from damage. A force sensor has a typical stiffness $K_s \sim 5x10^4 N/m$. The time constant of interaction is much less than that of the feedback controller response. The frequency of force measurement must be as high as possible for stability of the closed loop. Sensors are limited to ~1000Hz sample rates, but there is the further limitation imposed by the computation to intervals ~20ms. Hence, only resonant frequencies ~50 Hz are capable of being tracked by the controller. However, such a control sample will generate a time delay in the control loop between force measurement and feedback. The manipulator hand is supported by spring-like force sensors and the compliance of the reaction surfaces, so the hand behaves as an oscillator causing small amplitude oscillations on the force signal. This oscillation will be persistent and will arise particularly at the contact-make and contact-break phases of manipulation.

Hand natural resonant frequency $f = \frac{1}{2\pi}\sqrt{\frac{K_e + K_s}{m_{wrist}}} \approx 300Hz$ with m_{wrist}=wrist mass=0.6kg. These oscillations with durations of microseconds cannot be responded to by software control loops due to their high frequency relative to the control cycle. A low bandpass filter may overcome this if the amplitudes are low. However, for large input forces, a low bandpass filter is not capable of compensation. Wen & Murphy (1991) suggested that although derivative force feedback cannot be used since this requires gross arm motions, integral force feedback may be used as it can represent the virtual motions of compliance. An integral force feedback control law acts as a filter to counter instability. It removes bias forces by introducing a saturation nonlinearity and reduces the effective gain for large force errors making the controller stable. For good transient response and disturbance rejection in an infinitely stiff environment, the integral gain should be large, but if the environment exhibits any flexibility (ie. any real environment), the integral gain should be small. One way to reduce $K_F K_e$ is to introduce passive compliance at the wrist to reduce the effective environmental stiffness, ie. a remote centre compliance (RCC). If force/torque is applied at the compliance centre, translation/rotation of the device reduces the effective stiffness of the environment. However, the RCC is susceptible to damage if large displacements are forced upon it and it is limited to misaligments ~1mm or ~1^0. The instrumented RCC device is an RCC effectively mounted to a force/torque sensor for monitoring

displacements to prevent damage from excessive displacements. The RCC has low inertia such that contact energies are low and can be absorbed by the passive compliance. Such devices can be locked for position control to provide the required stiffness.

5.4.1 Hybrid Position/Force Control:

Hybrid position/force control is reckoned to be superior to other forms of force control enabling tasks of considerable complexity to be performed [Raibert & Craig 1981; Paul 1987]. Mason (1981) introduced the concept of C-(constraint) space to break down manipulator tasks into basic components defined by contact surfaces. Assembly operations are contrained due to contact between the workpieces and the end effector such that the number of degrees of freedom is reduced so that arbitrary motion cannot be specified. The constraint exerts a reaction force on the end effector and can generate large joint forces which need to be controlled. For each task configuration, there exists a compliance frame from which the task is best described. This compliance frame {C} may be fixed to the end effector cartesian coordinate frame or reside in the object reference cartesian coordinate frame centred at its centre of mass. The C-space is the space of n-parameters defined by the task configuration. In this C-space, there are N natural constraints which result from the geometry of the task and N orthogonal artificial constraints inposed by the desired trajectory of manipulation. Two subspaces s_f and s_c exist in the C-space. In the free subspace s_f, the configuration of the manipulator is such that no contact between the manipulator and the target object occurs. In the constrained subspace s_c, the manipulator is in contact with the object. Both subspaces are separated by the C-surface which defines the task geometry. Hence, the C-space concept identifies three separate states: free space motion, contact and force exertion. The manipulator cannot cross the C-surface into s_c - it can only lie in s_f or on the C-surface since s_c is defined by the object space. If on the C-surface, the manipulator can move over the C-surface tangentially (position controlled motion). Displacement along the normal of the C-surface changes the magnitude of the contact forces since the object generates reaction forces on the end effector (force controlled motion). Hence, natural constraints partition the DOF through position constraints normal to the C-surface and through force constraints tangential to the C-surface. Artificial constraints specify the desired position and force trajectories with force constraints along the C-surface normals and position constraints along the C-surface tangents. The direction in which the manipulator moves defines whether the degree of freedom is controlled by force feedback or position feedback. Constraint of any degrees of freedom implies force control in the constrained directions while position control is used for those directions which produce unconstrained displacement motion.

This is the concept behind the hybrid position/force control methodology where position control is applied along the cartesian C-surface tangent and force control along the cartesian C-surface normal [Raibert & Craig 1981]. The position vector is constrained in the directions complementary to the constraint direction of the force vector. The task is then characterised by motion in certain directions and the exertion of force in the remaining directions. The hybrid mode allows force feedback to produce corrective motion to compensate for position inaccuracies. It satisfies position and force trajectory constraints simultaneously. During hybrid position/force control each degree of freedom is controlled by only one loop such that both position and

force feedback loops act cooperatively to control each joint. Each joint thus contributes to the control of position and force at the end effector, ie. the end effector space is partitioned into 2 orthogonal domain components which are complementary. Central to the hybrid concept is the use of a diagonal compliance selection matrix S which selects which degrees of freedom are force-controlled and which are position-controlled. This is also the disadvantage of the scheme that the selection matrix which defines the task geometry cannot be algorithmically generated for a particular task. However, for many well-defined tasks the S matrix is well known.

$S=\text{diag}(s_1 \ldots s_n)$ where $s_j=1$ for force control; $s_j=0$ for position control.

The selection matrix is implemented thus:

$$\tau_i = \sum_{j=1}^{n} s_j \varphi_{ij} \delta f_j + (1-s_j)\pi_{ij}\delta q_j$$ where φ =force transfer function

π =position transfer function

$\delta f, \delta q$=force/position errors (5.9)

In general, additional coordinate transforms are required to define the constraint frame, but for the majority of manipulation tasks, the constraint frame may be chosen to coincide at the end effector, eg. peg-in-hole tasks are specified in end effector tip coordinates. The scheme is implemented at cartesian level, so cartesian position errors are calculated from measured joint coordinates and subtracted from the desired trajectory while cartesian force errors are obtained directly. Furthermore, Uchiyama et al (1987) stressed the need for a velocity feedback component in the hybrid scheme.

$\delta q = q^d - q = p_n^d - p_n$=position error=difference between desired and actual cartesian positions

$\dot{\delta q} = \dot{q}^d - \dot{q} = v_n^d - J\dot{\theta}$=velocity error=difference between desired and actual cartesian velocities

$\delta f = F_{ext}^d - F_{ext}$=force error=difference between desired and actual cartesian forces

The position/velocity errors are set to zero in the force controlled directions and force errors are set to zero in the position controlled directions by the selection matrix and the errors are mapped into position and force controlled subspaces.

$e_q = (I-S)\delta q$

$\dot{e}_q = (I-S)\dot{\delta q}$

$e_f = S.\delta f$

These errors are then transformed back into joint coordinates using the inverse and transposed Jacobian for use in the joint referenced control law.

$e_\theta = J^{-1}e_q$

$\dot{e}_\theta = J^{-1}\dot{e}_q$

$e_\tau = J^T e_f$

Position-controlled torque, $\tau_p = D(\theta)[\ddot{\theta}^d + K_p e_\theta + K_v \dot{e}_\theta] + H(\theta,\dot{\theta})$ (5.10)

Force controlled torque, $\tau_f = J^T F_{ext}^d + K_F e_\tau + K_{Fi}\int e_\tau . dt$ (5.11)

where K_F and K_{Fi} are 6x6 diagonal force feedback matrices and they depend on the stiffness of the environment. $J^T F_{ext}^d$ is the feedforward force component for reference tracking.

Complete hybrid position/force control law: $\tau = \tau_p + \tau_f$ (5.12)

The use of a PD type position control law in conjunction with a PI type force control law makes the hybrid control law of the PID type. The hybrid scheme exhibits a stable and accurate response to step inputs with very little overshoot in position and force trajectories [Raibert & Craig 1981]. Zheng & Paul (1985) noted that the hybrid scheme required the J^{-1} transformation to joint coordinates from cartesian coordinates which imposes a heavy computational burden. To reduce the computational load, they adapted the hybrid scheme to operate directly in joint coordinates by introducing a joint compliance matrix $C = J^{-1}SJ$. This was far more efficient and yields a control law of the form:

$$\tau = D(\theta)\{\ddot{\theta} + (I-C)[K_v(\dot{\theta}^d - \dot{\theta}) + K_p(\theta^d - \theta)]\} + H(\theta,\dot{\theta}) + \\ + J^T F_{ext}^d + (C)[K_F J^T (F_{ext}^d - F_{ext}) + K_{Fi} J^T \int (F_{ext}^d - F_{ext})dt] \quad (5.13)$$

West & Asade (1985) characterised hybrid position/force control as being based on constraints imposed by contact with the environment reducing the number of degrees of freedom similar to a closed kinematic chain. They established a 6xm contact Jacobian for such a closed kinematic chain such that $\dot{\theta} = (I - J_c^+ J_c)\dot{q}$ defines the velocity control loop and $\tau = (J_c^+ J_c)^T F_{ext}$ defines the force control loop. A diagonal selection matrix is required to select between the loops. The method is considerably more complex than the usual approach to hybrid position/force control with little apparent advantage.

Impedance control is a methodology for robotic control based on a biological paradigm [Hogan et al 1985]. Muscles behave as tunable springs by virtue of their arrangement around joints in antagonistic pairs. The elasticity of the muscle is determined by its activation level which determines their length-extension α which in turn defines the equilibrium position and stiffness of the joint. This may be modelled as a potential function of the joint angle, the negative derivative of which is the generalised force. Activation of antagonistic muscles determines the potential minimum (determined by the α ratio) and the potential minimum curvature (determined by the α sum. Displacement from the potential minimum results in a restoring torque independent of feedback. Thus all control acts through a single time-dependent potential function with the muscles themselves computing the joint torques. The function of the nervois system is to transform the desired trajectory into a sequence of joint equilibrium positions and stiffnesses determined by a global time-dependent potential function. This method of hybrid position/force (impedance) control is still under development though offers great promise.

5.4.2 Grasp Planning

Choosing a grasp configuration on a part is similar to the Findspace problem (see section 5.5) for a safe configuration amongst a set of obstacles but involves additional constraints including [Latombe 1984, Volz et al 1984]:

(i) the end effector fingers must be in contact with the grasp points on gripping;

(ii) the configuration must be reachable at both initial and destination points without interference between them;

(iii) the grasp points must be stable such that the object is immovable in the grasp.

For a good grip both contact dimensions and finger separation should be as large as feasible. If world coordinates do not coincide with the manipulator base coordinates

and a different reference frame is defined as the world reference, a relational transform is required to relate the reference and base frame coordinates.

Stability may require the centre of mass of the object (if it is small) to be located between the jaws of the end effector. Stability however is ultimately determined in the general case by a lack of slip between the fingers and the object. Parallel planar surfaces whose distance from each other is less than the maximum parallel jaw finger opening are suitable as grasp points and the internal faces of the fingers must overlap the grasp surfaces with sufficient contact area. Other possible grasp pairs include face and parallel edge, face and vertex, and parallel edges for cylinders. However, two parallel faces are the preferred legal grasp configuration. For small objects, almost all grasps are stable.

The grasp plane is defined as the plane parallel to the faces being grappled and midway between them. When approaching a grasp point, the fingers remain parallel to the grasp plane and centred about it, but otherwise free to rotate and translate in the plane. This minimises the risk of collision with the object to be grasped. The grasp plane is bounded by a rectangle whose size determines the range of motions allowed by the hand during grasping. The rectangular volume that the hand can sweep out while constrained to move in the grasp plane is the grasp volume. The motion of the hand is a translation along the free motion vector connecting the finger and object grasp points in the grasp plane without rotation. Grasping is heavily dependent on features. Features may be defined as specific geometric configurations found on the surfaces, edges or corners of a workpiece which modify or aid in achieving a given function [Vijaykumar & Arbib 1987]. Specific features of objects dictate how these objects may be assembled together. Global features include shape, length, width, height, volume, surface area, location and local features such as holes. If the origin of the coordinate object frame lies it the object's centre of mass, then local features are specified in terms of these coordinates. This allows a representation of features and the relationships between them. This is the primary problem - of identifying positions and orientations of features on objects relative to each other.

For assembly operations, certain heuristic requirements must be met:
(i) the features of the female connector must be hollow;
(ii) the dimensions of the female connector must be at least as large as the male connector.
Other heuristics may include: closeness of fit such that the difference between each pair of mating features should be small and the features should be symmetric.
eg. insertion operation:
Insert feature k of object i into feature l of object j with conditions:
(i) normal axes of feature k and feature l must be colinear and opposed;
(ii) bottom surface of insertion feature k will be against the bottom surface of containing feature l;
(iii) if insert and container are cylindrical, their cylindrical surfaces will be in contact;
(iv) centre of insertion feature k will be a distance equal to the depth of feature l away from the centre of feature l along the direction of the normal axis of feature j with respect to object coordinate frame origin.
A CAD database may be used to store the grip points in the target object. This grip list would be generated offline from geometric and topological data within the CAD

database. Selection of the grip point is generated online. Certain grip positions may be eliminated offline: grips on sets of vertices (subject to rotation) and grips on edge/vertex combinations (subject to twisting). Grip positions are ordered in terms of the quality of the grip position (ie. resilience to slippage and twisting).
The motion primitive for grasping comprises of:
(i) move the end effector to the approach position;
(ii) open the end effector jaws;
(iii) guarded move at half-speed to the grasp position;
(iv) centre the end effector on the grasp position;
(v) grasp the object with a suitable pinching force;
(vi) check slip sensors.

The peg-in-hole/screw-in-hole task is one of the commonest assembly tasks and is used as the standard for force control validation for assembly (indeed, it is fundamental to the ORU exchange operation). The compliance frame is at the tip of the tool with the z-direction defined as pointing to the hole from the tool tip coinciding with the hole axis.

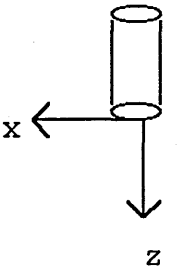

Natural constraints: $v_x = 0, f_y = 0$ $\quad w_x = 0, f_z = 0$ $\quad w_y = 0, n_z = 0$

Artificial constraints: $v_y = 0, f_x = 0$ $\quad v_z = p\alpha, n_x = 0$ $\quad w_z = \alpha, n_y = 0$

where α=rate of turn constant
p=pitch
Two degrees of freedom are position-controlled: rotation about the z-axis and translation along the z-axis, so S=(1,1,0,1,1,0). This may be implemented in a robot control language such as WAVE as:
COMPLY FORCE X 0
COMPLY FORCE Y 0
COMPLY TORQUE X 0
COMPLY TORQUE Y 0
MOVE FORCE Z UNTIL STOP FORCE Z FMAX
MOVE TORQUE Z UNTIL STOP TORQUE Z NMAX
Lateral and angular errors are corrected in response to chamfer contact forces. Wedging occurs when the peg becomes locked at the beginning of insertion such that further force will deform the peg or the hole. The insertion depth l is constrained by $l \le 2\mu r$ where μ=friction coefficient and r=peg radius. Jamming occurs when the contact forces do not correct misalignments when $\frac{nr/f_z}{\lambda \sin\theta} + \frac{f_x/f_z}{(\lambda/\lambda+1)\sin\theta} \le 1$ where $\lambda = \frac{l}{2\mu r}$.
Forces at the peg tip correspond to lateral errors which are corrected by translation and torques at the peg tip correspond to angular errors which are corrected by rotation.

5.5 OBSTACLE AVOIDANCE

For any path planning to be effective, it must deal with the problem of obstacles in its work environment and avoid those obstacles to generate collision free motion and to achieve a safe grasp point. Obstacle avoidance relies heavily on real-time sensory data. The goal is to automatically find a continuous safe path between configurations through a group of obstacles without collision. This is generally known as the piano-mover's problem and in general has a complexity of n^{2^r} where r=number of degrees of freedom of movement and n=number of moving objects [Schwartz & Sharir 1988]. It is desirable to obtain optimal collision-free solutions to the piano mover's problem. Evidently, such computational complexity is totally infeasible for real-time solution, so any practical approach needs to employ assumptions and simplifications. Henderson & Gruyen (1990) interpreted the piano mover's problem for a robot agent as essentially an egocentric problem whereby the robot must maintain certain spatial and temporal relations between itself and the world - a task that is routinely undertaken by the animal world.

The global planning methods that have been developed are of two types - the C-space approach [Lozano-Perez 1981, 1983] and the free space approach [Brooks 1983]. The problem may be broken down into two subproblems: Findspace and Findpath. Findspace is concerned with generating a safe robot configuration such that the robot does not impose on any obstacles. Essentially, this boils down to determining whether an object A can be placed inside some specified region R so that it does not collide with any of the objects B_i already in that region. Findpath is concerned with generating a safe path between a set of robot configurations to get from an initial to a final point such that all configurations are safe along the safe path. Essentially this boils down to determining how to move A from one location to another without causing collisions with objects B_j.

In the configuration space approach, the robot dimensions are reduced to a point while convex polyhedral obstacles are expanded to compensate and stored as lists of vertices. A freespace graph is constructed with arcs connecting the vertices of the expanded obstacles. Safe paths are those which do not intersect any of the obstacles. An A* algorithm based on a distance-travelled cost function will select the shortest path. A problem with this approach is that it will allow too close a proximity to the obstacles unless an error margin of additional expansion is included. This however will cause valid solutions to be lost.

The freespace method considers freeway channels between polygonal obstacles by dividing these free channels into swept-volume overlapping generalised cones. Findpath then reduces to comparing the swept volume of the object with the swept volume of free space. The problem is to find a path from the initial position to the goal position following the spines of the generalised cones and changing from cone to cone at the spine intersection points. Translations along the spines are rotation free and rotations are restricted to intercone intersection points at which all orientation changes are performed. A graph is constructed using distance travelled as a cost function for the A* algorithm search. The graph nodes represent intersection points with the arcs representing free space channels. The robot passes through the centre of these channels allowing a safe margin. The drawback with this approach is that it often generates a longer path than necessary and is not well suited to tightly constrained environments.

This essentially excludes parts mating operations which are representative of cluttered environments.

Both approaches have difficulties in three dimensions and in coping with rotational motion. However, both methods have been combined to consolidate some of the benefits of each and resolve some of the difficulties characteristic of each method. The C-space is subdivided into freeways for the hand and freeways for the arm based on constraints of the freeways for the hand. There still remains the problem that certain arrangements yield no solution restricting its use. All these approaches are hypothesise-and-test methods which lack generality and cannot be used in cluttered environments. Furthermore and more significantly, computation time remains a problem limiting its use to long-horizon time global planning only.

5.5.1 Potential Field Approach

Obstacle avoidance has traditionally been a computationally expensive capability. However, real-time obstacle avoidance may be achieved by using the artificial potential field method in the low level control laws [Khatib 1985]. Collision avoidance is fundamentally a fast response capability appropriate to real-time control, ie. it is an algorithmic process (in C or FORTRAN for example) rather than a logical process (in PROLOG or LISP for example). A path planning algorithm may be used to generate a set of critical points along a global path generated through the techniques described above[Krogh & Thorpe 1986]. These critical points act as subgoals for the potential field algorithm which implements dynamic steering using local feedback information to generate collision-free paths. The two levels of control may be executed in parallel with the path planner algorithm generating future subgoals.

In the potential field approach, the manipulator is considered to move through a field of forces whereby the goal position provides an attractive force for the end effector and obstacles generate repulsive forces at their surfaces. This will direct the end effector towards the goal but away from the obstacles. The potential field obeys the superposition principle of force summation to generate the resultant potential field. Sensors such as vision sensors provide data concerning the shape and location of obstacles.

The force field is described by: $\begin{aligned} V(q) &= V_g(q) + V_o(q) \\ F(q) &= F_g(q) + F_o(q) \end{aligned}$ where F = −gradV

F_g =attractive goal force; F_O=repulsive obstacle forces.

These forces may be incorporated directly into the control law to generate joint actuator torques to direct the end effector away from obstacles towards the goal: $\tau = J^T F(q)$ due to the artificial field of forces acting at the end effector.

For the goal point, the potential field is attractive: $V_g(q) = \frac{1}{2} K_p^{obj} (q_g - q)^2$

where K_p^{obj}=proportional gain

q_g=generalised goal position vector with respect to reference coordinates

q=end effector position vector with respect to reference coordinates

Goal force, $F_g(q) = -gradV_g = K_p^{obj}(q_g - q)$

This attains its minimum value of zero when $q=q_g$. This is a proportional control law so damping is added for stability:

$$F_g(q) = K_p^{obj}(q_g - q) + K_v^{obj} \frac{dq}{dt} \text{ such that } K_p^{obj}(q_g - q) > K_v^{obj} \dot{q}_{\max} . \qquad (5.16)$$

For the obstacles, a repulsive potential field generates a barrier at the obstacle surface which falls off rapidly away from the surface of convex polygonal objects to reduce perturbation effects:

$V_0 = \frac{1}{2}N(\frac{1}{p} - \frac{1}{p_0})^2$ if $p \le p_o$

$= 0$ if $p > p_0$.

where p_0=limiting range of potential field influence= $\frac{p}{1-\sqrt{n}v_{max}p_{max}}$

p=shortest distance from end effector to obstacle

m=shortest distance from object centre to object surface

N=potential field strength=constant

p_{max}=clearance width of end effector

v_{max}=maximum speed of end effector

Repulsive obstacle force, $F_o(x) = -\text{grad}V_o = N[\frac{1}{2}(\frac{1}{p} - \frac{1}{p_o})(\frac{1}{p})^2 \frac{dp}{dx}]$ if $p \le p_o$

$= 0$ if $p > p_0$. (5.17)

F_0 is the force inducing artificial repulsion from the surface of the obstacle. Obstacles may be described by the composition of geometric primitives such as the cylinder or ellipsoid:

$F_o = \sum_{i=1}^{n} F_{oi}$ due to the superposition property of the potential field.

Surface n-ellipsiod parallelipiped of dimensions a, b, c: $(\frac{x}{a})^{2n} + (\frac{y}{b})^{2n} + (\frac{z}{c})^{2n} = 1$

Surface n-cylinder of cross section (a,b) and length 2c: $(\frac{x}{a})^2 + (\frac{y}{b})^2 + (\frac{z}{c})^{2n} = 1$

Typically, n=4 gives a good approximation.

The potential field approach as well as being suitable for real time control is also ideally suited for the uncluttered space environment since it forms paths based on known obstacle positions rather than free space corridor generation. Collision avoidance of links and joint limit avoidance may also be achieved with this method but both require a different Jacobian to relate the required reference points to the joint torques. Kweon et al (1992) advocated the artificial potential field as a means of sensor fusion representation. Each sensor generates its own potential field model of any objects and multiple sensor data may be combined as the superposition of repellant forces in the force field.

The potential field method is prone to local minima which occur when the obstacle repulsive forces balance the goal attractive forces. These Lagrange points occur when the end effector is within range of the short range influence of the obstacle potential field and the long range attractive goal potential field such that $|F_{goal}| = |F_{obstacle}|$. These points will trap the end effector and may be avoided by using a higher level global planner (eg. C-space/freespace approaches) which derives a series of interim points along a path that avoids the local minima. The global planner works by searching for acceptable paths using a cost function based on the shortest distance, eg. A* algorithm and so tends to be slow.

5.5.2 Simulated Annealing:

Rather than using global planning to overcome the local minima problem, a simulated annealing algorithm may be used [Kirkpatrick, Gelatt & Vecchi 1983]. This technique is an optimisation method for finding the minima or maxima for functions with many independent variables such as the NP-hard travelling salesman problem. It is an

example of a contribution from pure science to practical engineering. It is based on the Metropolis algorithm which is used in statistical mechanics to numerically simulate the average behaviour of a Gibbs ensemble of many body systems (~10^{23} atoms/cm^3) in thermal equilibrium at a finite temperature. This search algorithm does not suffer from the problem of getting stuck in local minima.

Annealing involves melting the material to high temperature and then lowering the temperatue very slowly allowing a long time near the freezing point to allow the system to achieve thermal equilibrium. This generates the global ground state with a defect free highly ordered crystalline state. For optimisation problems, simulated annealing can produce solutions using effective temperature as the control variable. It allows uphill steps in the energy cost function. Solutions which yield $\delta E < 0$ are accepted, but also solutions with $\delta E > 0$. The probability of such a solution with $\delta E > 0$ is $P(\delta E) = e^{\frac{-\delta E}{k_B T}}$ and if a random number generator for 0<Rnd<1 value is less than $P(\delta E)$ the solution is retained, otherwise it is rejected. The system retains thermal equilibrium and will tend towards a Boltzmann distribution. This procedure avoids getting stuck in local minima since the stochastic component allows uphill transitions. Simulated annealing is essentially an adaptive divide-and-conquer stategy and provides an interesting model of the way that evolution by natural selection operates. Hence, it is inherently parallel offering the potential for fast computation.

5.6 DUAL MANIPULATOR CONTROL

Dual robot manipulators offer several advantages over the use of a single robot manipulator:
(i) reliability is enhanced as two arms offer redundancy;
(ii) parallel operation decreases task completion time;
(iii) some tasks explicitly require more than one manipulator.
Indeed, it is conceivable that the space environment will provide the first deployment of multiple arm robotic systems. Indeed, Adams et al (1987) noted that for the Solar Maximum main electronics box exchange, two arm parallel manipulation was essential, even if only to carry a camera. Hence any robotic freeflyer such as ATLAS must have a minimum of two arms (plus possibly a telescopic docking device). To this end this chapter covers methods for dealing with dual arm operation particularly for coordinated motion and develops techniques that are directly utilisable by the space-based dual arm kinematics formulation of Chapter 6.

5.6.1 Inter-Arm Collision Avoidance

Maimon & Nof (1985) proposed that dual arm control requires some form of coordination and introduces an Activity Controller which could be embedded in a heirarchical control structure above the level of individual robot arm servocontrollers. It could be implemented by either a central spacecraft processor or more likely a dedicated processor for dual arm coordination. This Activity Controller was divided into two parts, AC1 and AC2. AC1 provided planning of the coordination of tasks for each robot arm with respect to spatial constraints. AC2 provided planning of the synchronisation of tasks for each robot arm with respect to temporal constraints to effect collision avoidance. This highlights one of the chief difficulties in dual-arm operation - that of interarm collision. Coordinated motion of two arms may be loose such that the two arms execute independently controlled sequences of actions, or tight when both arms have a fixed relation over the motion to execute a common task. Both types of operation can generate collisions, but it is particularly susceptible in loose coordination since the arms are not maintained in fixed positions relative to each other. Furthermore, the previous section gave an indication of the difficulties inherent in obstacle avoidance particularly if the obstacle is moving.

Lee & Lee (1987) attempted to tackle the problem of inter-arm collision by representing each robot wrist as a sphere centred on the hand coordinate frame, thereby restricting their formulation to wrist collisions only (admittedly the most likely however). The use of a spherical model was motivated by the desire for minimal computation for modelling and yet allowing for rotations. They used a collision map of path length against time to generate straight line path segments and locate potential collision regions. Using a time scheduling algorithm to modify the travelling speed of the planned trajectories rather than path modification, they incorporated time delays in the trajectory generation algorithm. The main problem was that task execution time was considerably increased due to the time consuming scheduling operations. The difficulty of the planning approaches is that they are complex and cannot be performed in real-time - collision avoidance is a real-time reflexive operation and not a cognitive reasoning problem.

Collision between arms is always a possibility when the work envelopes of the two arms overlap. Mowforth & Bratko (1987) eliminated the possibility of collision using the Zambesi bridge configuration such that the manipulators were positioned so that they could not touch yet were capable of passing extended components, ie. their separation distance (taken to be in the x-direction) was the maximum extent of their combined workspaces: $h = 2 \times p_n^{\max}$ assuming both manipulators to be of the same geometry. Since the workspaces of the two robots intersect only at a point, this configuration is highly limited.

Collision may be avoided by using safety routines which halt the manipulator under certain conditions. Collision can occur between any two points on the respective manipulators but certain kinematic constraints can be imposed to effect collision avoidance. Hemami (1986) introduced the notion of software monitoring of the distances between the central axes of each link of each arm at every update step as part of an intercept driven algorithm. If the separation distance between any two links on separate manipulators falls below a prescribed value (ie. the dimensions of each arm) then the motion is halted and replanning is invoked as necessary. The number of

repetitions of this algorithm depends on the number of link segments, ie. for 3 link segments (ie. shoulder/elbow/end effector) there must be 9 repetitions at each update point.

Let t=diameter of a manipulator link, l_2=length of link 2 from shoulder to elbow, p=position vector of the specified joint of specified arm with respect to own base coordinates:
(i) No collision occurs if $p^{right}_{shoulder} - p^{left}_{shoulder} > t$ - this condition is trivially true since $p^{right}_{shoulder} - p^{left}_{shoulder} = h > t$, so this does not require computation.
(ii) No collision occurs if $p^{right}_{elbow} - p^{left}_{elbow} > t$ - this condition will always be true if $l_2 < \frac{h}{2}$.
(iii) $\left.\begin{array}{l} p^{right}_{elbow} - p^{left}_{shoulder} > t \\ p^{right}_{shoulder} - p^{left}_{elbow} > t \end{array}\right)$ - these conditions will always be true if $l_2 < h$.
Hence, by fixing $l_2 \leq \frac{h}{2}$, elbow/shoulder collisions can be avoided. For the PUMA 560/600 variant considered here, $l_2 = 0.5m \rightarrow h \geq 1.0m$.

A modification of the Zambesi bridge concept will overcome wrist collisions by allowing the robot workspaces to intersect generating a plane of intersection equidistant between the two arms at h/2. This allows a wide area for component swapping. However, the motions of each arm are restricted to their own workspace quadrants with no arm being permitted to cross the plane of workspace intersection. As no arm overlapping can occur, so neither can any collisions. The end effector positions must be repeatedly evaluated at each update step to ensure that the following condition holds at all times during loose cooperation: $p^{right}_{n(x)} \leq h/2$ and $p^{left}_{n(x)} \leq h/2$ for each end effector in the x-coordinate. This modified Zambesi bridge constraint may be relaxed during closed chain maneouvres as the maintenance of fixed position/orientation between the arms precludes the possibility of collision - in this way the Zambesi bridge configuration will not restrict large scale payload transfers by the manipulator arms.

Certain other kinematic constraints may be applied for other reasons:
(i) to enable self repair: $l_2 + l_3 \geq \frac{h}{2}$ [Wang 1987].
(ii) to enable truss walking between truss nodes: $l_2 + l_3 \geq \frac{d}{2}$ where d=truss node interval=1.67m [Xu et al 1992] - this is true for $l_2 = l_3 = 0.5m$. For the PUMA 560/600 variant considered here this gives $h \leq 2m$. Hence $1m \leq h \leq 2m$ provide the constraints on the separation distance between the two manipulators.

5.6.2 Dual Manipulator Kinematic Configuration

Hemami (1985) considered that side-mounting of two manipulators onto a platform such that the elbow or shoulder joints moved in opposition (ie. left/right configurations) offered not only an anthropomorphic configuration but better maneouverability than conventional mounting whereby the identical arms are related by a rotation and a simple translation of separation distance h. This is the configuration adopted here: a left shoulder is mounted onto the left side of the spacecraft platform mount (master arm - superscript/subscript "m") and the right shoulder configuration is mounted onto the right side of the spacecraft mount (slave arm - superscript/subscript "s"). The relationship between the two arms is the matrix H which translates h in the

+x-direction and rotates 180° about y axis of the master arm to the slave arm. H is also its own inverse [Hemami 1985,1986].

$$H = \begin{pmatrix} -1 & 0 & 0 & h \\ 0 & 1 & 0 & 0 \\ 0 & 0 & -1 & 0 \\ 0 & 0 & 0 & 1 \end{pmatrix}$$ where h=separation distance between the two manipulators.

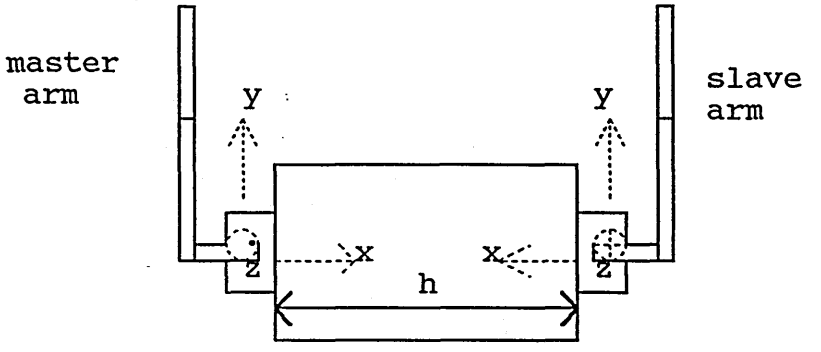

This allows specification of the kinematics of the slave arm in terms of the coordinates of the master arm, assuming that the kinematic structures of both robot manipulators are the same (except for handedness). The reference coordinate system is the base of the master arm (arbitrarily taken as the left arm).

Hence, $T_s = HT_m$ denotes the same position/orientation of the slave arm with respect to base reference coordinates where $T_m = \begin{pmatrix} n & s & a & p \\ 0 & 0 & 0 & 1 \end{pmatrix}$

Two types of control for dual manipulator configurations are possible:

(i) tasks requiring independent programming for each arm - although independent unrelated tasks may be performed by each manipulator in parallel they must be coordinated (loose coordination);

(ii) tasks requiring the two manipulators to cooperate in some fashion and require programming with respect to each other (tight coordination) - this is typical of most assembly type tasks:

(a)open chain formulation where no closed kinematic loops exist - generally the tasks will be of the main task/subsidiary role for each manipulator, but two special cases exist whereby the relative actions of the two end effectors are constrained in one or more directions [Hemami 1986; Tao, Luh & Zheng 1987]:

1. copying motion whereby each arm performs the same operation;
2. symmetric motion through a plane whereby each arm mirrors the other;

(b) closed chain formulation in which synchronisation is necessary - the arms hold a common object for spatial transfer making compliant motion necessary due to the kinematic constrants for the maintenance of constant position and orientation.

5.6.3 Open Chain Kinematic Configuration

The coordination of two arms in the open kinematic chain mode is necessary for two special case but important types of task characteristic of assembly type operations [Tao, Luh & Zheng 1987; Hemami 1986].

1/. For copied motion, only the tool point position differs between the master and slave arms - this difference is constant and serves as the task constraint:

$$\begin{pmatrix} R_s & p_s \\ 0 & 1 \end{pmatrix} = H \begin{pmatrix} R_m & p_m + b \\ 0 & 1 \end{pmatrix} = \begin{pmatrix} -n_x^m & -s_x^m & -a_x^m & -(p_x^m + b_x) + h \\ n_y^m & s_y^m & a_y^m & p_y^m + b_y \\ -n_z^m & -s_z^m & -a_z^m & -(p_z^m + b_z) \\ 0 & 0 & 0 & 1 \end{pmatrix}$$

$$\text{where } b = \begin{pmatrix} b_x \\ b_y \\ b_z \end{pmatrix} = \text{tool point bias offset} \qquad (5.18)$$

An example of where this formulation may be used is in ORU exchange by removing two bolts at once at different positions on the module or spacecraft.

2/. For symmetric motion, the position of the tool point differs only in one coordinate if the reflection occurs in the zy plane at x=d=h/2. Furthermore the z components of the **a** and **s** rotation vectors are opposed and since **n=sxa**, the x and y components of the **n** vector are also opposed for symmetric motion.

$$\begin{pmatrix} R_s & p_s \\ 0 & 1 \end{pmatrix} = H \begin{pmatrix} -n_x^m & s_x^m & a_x^m & p_x^m + 2d \\ -n_y^m & s_y^m & a_y^m & p_y^m \\ n_z^m & -s_z^m & -a_z^m & -p_z^m \\ 0 & 0 & 0 & 1 \end{pmatrix} = \begin{pmatrix} n_x^m & -s_x^m & -a_x^m & -p_x^m \\ -n_y^m & s_y^m & a_y^m & p_y^m \\ -n_z^m & s_z^m & n_z^m & -p_z^m \\ 0 & 0 & 0 & 1 \end{pmatrix} \qquad (5.19)$$

This would represent a task such as grappling - the capture operation for a space manipulator is regarded as an important elementary task for space manipulators [Umetani & Yoshida 1989]. Dual insertion tasks such as peg-in-hole operations also have this form since **n**, **s**, and p_Z are variable with p_X, p_Y and **a** fixed to allow compliance. Screwing operations are a subsidiary of insertion operations whereby the gripper orientation must change but the direction of screw turn does not, ie. $\theta_6^s = \theta_6^m$ saving a 180° rotation at the joint [Hemami 1986]:

$$\begin{pmatrix} R_s & p_s \\ 0 & 1 \end{pmatrix} = H \begin{pmatrix} n_x^m & s_x^m & a_x^m & p_x^m \\ n_y^m & s_y^m & a_y^m & p_y^m \\ n_z^m & s_z^m & -a_z^m & p_z^m \\ 0 & 0 & 0 & 1 \end{pmatrix} = \begin{pmatrix} -n_x^m & -s_x^m & -a_x^m & -p_x^m \\ n_y^m & s_y^m & a_y^m & p_y^m \\ -n_z^m & -s_z^m & a_z^m & -p_z^m \\ 0 & 0 & 0 & 1 \end{pmatrix} \qquad (5.20)$$

Both insertion and screwing operations are generic assembly tasks so these conversion are critical.

5.6.4 Closed Kinematic Chain Configuration

The closed chain configuration is a critical mode of dual arm cooperation on a single object as this is the primary purpose of using dual manipulators. For any kind of cooperative motion, an object must be accessible to both manipulators, ie. the object must extend into the workspace of both robots and/or the object must lie within the intersection of their common workspace [Uchiyama et al 1987]. The chain closure is effected by the two manipulators gripping the same object and the end effectors are separated by an offset bias. Both assembly operations and object transfer through the closed chain configuration determine that the behaviour of each robot manipulator is no longer independent of the other. The kinematic constraints alter for an open loop tree configuration which suddenly changes to a closed loop topology on target acquisition. In the closed loop configuration, the manipulators exert forces and torques

on the object to cause tension, compression or torsion in the object without affecting the motion trajectory of the object. It is desirable to minimise these forces and torques.

Tarn, Bejczy & Yun (1987, 1988) considered the closed kinematic chain case and allowed rotation between the fingers of the end effectors and the object. The closed chain formed is essentially the addition of the object as a link of a longer chain. These 2 extra degrees of freedom contributed to a total of 8 degrees of freedom to the closed chain system as a whole as defined by the Kutsbach-Grubler criterion:

n=6(m-1)-5p=8 where n=number of degrees of freedom controllable
m=number of links=14
p=number of arbitrary joints=14

Hence, 8 coordinates are required to specify this closed chain. The closed chain imposes nonholonomic constraints to the manipulator configurations implying actuator redundancy since the number of outputs (8) was less than the number of controllable inputs (12 independent torque-generating actuators), ie. the configuration of the closed chain was determined by $\theta=(\theta_1^m,...,\theta_6^m,\theta_7,\theta_8)$ where θ_7 and θ_8 represented the rotation angles between the contact surfaces of the object and the 2 end effectors (assuming no relative translation). The slave joint angles $\theta_1^s,....,\theta_6^s$ are determined by $\theta_1^m,...\theta_6^m,\theta_7,\theta_8$.

However, if the object is rigidly grasped, the Kutzbach-Grubler criterion is altered. In this case, m=12 since the last link of each arm and the payload now represent one link. They are fixed relative to each other such that θ_7 and θ_8 are invariant. The other 5 links of each arm and the mounting generate m=12. There also 12 actuators one for each manipulator joint, hence p=12 giving the number of controllable degrees of freedom to be 6. This is effectively reduces the problem of dual arm closed chain control to a holonomic problem similar to that of controlling a single manipulator. By adopting rigid grasp to form a closed kinematic chain of 12 joints and 12 links, the relative positions and orientations of the arms with respect to each other remains invariant - this is a statement of the task constraint as defined by Lim & Chyung (1987) in their resolved position control formulation for closed chain kinematics. Although the object coordinate frame is centred at the load's centre of mass and the reference coordinates are centred on the mounting centre of mass, the end effector coordinates of each arm may be found enabling inverse kinematics solution to be applied to find the joint angles.

End effector 4x4 coordinates of arm l (master or slave) with respect to its own base:

$T^l=(T_0^l)^{-1}T_{0n}^{ref}T_{n+1}^l$

where l=1 for master arm (superscript "m"), or 2 for slave arm (superscript "s")

T_{n+1}^l=constant task constraint 4x4 DH matrix

T_{0n}^{ref}=object trajectory defined by the object coordinate frame 4x4 DH matrix

T_0^l =4x4 DH matrix that maps from the centre of mass of the mount to the base of arm l

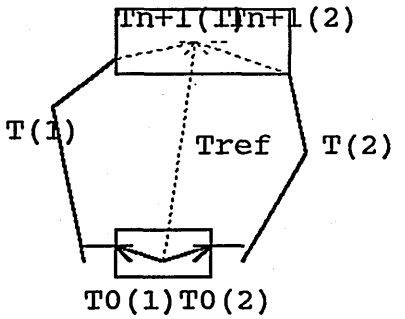

Uchiyama & Dauchez (1988) characterised T^l_{n+1} as virtual sticks fixed at each hand pointing towards the object centre of mass. This interpretation allows 4x4 matrix T^l_{n+1} to be represented as a relative position vector r^l_{n+1} without the rotational component R^l_{n+1} particularly as the relative orientation with respect to the end effectors will not change. Similarly, the 4x4 matrix T^l_0 may be represented as position vectors vectors s^l_0 with no platform attitude component R^l_0. The arm vectors are related by: $s^{l=2}_0 = Hs^{l=1}_0$.

Tao, Luh & Zheng (1987) and Zheng & Luh (1986) went a step further by deriving a set of holonomic constraints on position and orientation of the slave arm (superscript "s") to constrain the motion of the kinematic chain uniquely. The motion of the master arm (superscript "m") is planned to generate the required motion of the payload. The motion of the slave arm is then calculated to have a coordinated relation with respect to the master arm. They defined the relative position/orientation of the end effectors to be invariant whilst holding a rigid body such that [Tao Zheng & Luh 1987]:

$$T^s = H^{-1}.T^m.O$$

where $0 = \begin{pmatrix} n_{obj} & s_{obj} & a_{obj} & l_{obj} \\ 0 & 0 & 0 & 1 \end{pmatrix} = (T^s_{n+1})^{-1} T^m_{n+1}$=object 4x4 DH matrix

$$H = (T^m_0)^{-1} T^s_0$$

Since the relative positions and orientations of the end effectors are invariant in the closed chain, object matrix **O** is constant. Equivalently, the position and orientations of **O** may be decoupled $O = \begin{pmatrix} R_{obj} & l_{obj} \\ 0 & 1 \end{pmatrix}$ to yield two sets of holonomic equality constraints [Luh & Zheng 1986, Zheng 1989].

Holonomic angular constraint:

$$R_{obj} = (R^m_n)^T R^s_n = (n^m s^m a^m)^T (n^s s^m a^m) = (n_{obj} s_{obj} a_{obj}). \quad (5.21)$$

Holonomic linear constraint:

$$p^m_n + T^m_{n+1} - (p^s_n + T^s_{n+1}) = 0$$

$$\rightarrow p^m_n + R_{obj} l_{obj} - p^s_n = 0 \quad (5.22)$$

Hence, the slave arm end effector coordinates are dependent on the end effector coordinates of the master arm and the matrix R_{obj} which is constant:

$$p^s_n = p^m_n + R_{obj} l_{obj}$$

$$R^s_n = H^{-1} R^m_n R_{obj} \quad (5.23)$$

This then allows the inverse kinematic joint angles to be found for the control system.

These constraints may be extended to velocity and acceleration variables [Luh & Zheng 1986, Zheng 1989]. Both linear and angular velocities of both end effectors

must be the same at all times so that no relative motion occurs between the end effector:

$$\begin{pmatrix} v^s \\ w^s \end{pmatrix} = \begin{pmatrix} v^m \\ w^m \end{pmatrix} \rightarrow \dot{\theta}^s = (J^s)^{-1} \begin{pmatrix} v^m \\ w^m \end{pmatrix} = (J^s)^{-1} J^m \dot{\theta}^m \quad \text{and} \quad \dot{\theta}^m = (J^m)^{-1} \begin{pmatrix} v^m \\ w^m \end{pmatrix} \tag{5.24}$$

Note that in general the slave and master Jacobians will be different since they will have different configurations. Similarly, there is a similar acceleration constraint:

$$\begin{pmatrix} \dot{v}^s \\ \dot{w}^s \end{pmatrix} = \begin{pmatrix} \dot{v}^m \\ \dot{w}^m \end{pmatrix} \rightarrow J^s \ddot{\theta}^s + \dot{J}^s \dot{\theta}^s = J^m \ddot{\theta}^m + \dot{J}^m \dot{\theta}^m$$

$$\rightarrow \ddot{\theta}^m = (J^m)^{-1} \left[\begin{pmatrix} \dot{v}^m \\ \dot{w}^m \end{pmatrix} - \dot{J}^m \dot{\theta}^m \right] \text{ and } \ddot{\theta}^s = (J^s)^{-1} \left[\begin{pmatrix} \dot{v}^m \\ \dot{w}^m \end{pmatrix} - \dot{J}^s \dot{\theta}^s \right] \tag{5.25}$$

Once a closed kinematic chain is formed by the load, the load couples the dynamics of the two arms. The dynamic equations then have an additional term which represent the interaction forces. Several workers have recommended that when the closed chain configuration is adopted the individual dynamic equations of the two coordinating robots be combined to form a unified dynamic equation [Zheng 1989]. This is not desirable as this introduces computational burdens and the philosophy behind the formulation above is to decompose the dual manipulator problem into two single manipulator problems. The dynamics of each manipulator may then be considered seperately by monitoring the interaction forces and moments at the end effector applied to the object. The control of each manipulator may then be computed in parallel by dedicated microprocessors for each arm. The dynamics of the two manipulators may be represented as (using the Lagrange representation for illustration - the same arguments apply to the Newton-Euler method) [Hayati 1986, 1988]:

$$D^l(\theta^l)\ddot{\theta}^l + H^l(\theta^l, \dot{\theta}^l) + (J^l)^T F^l_{ext} = \tau^l$$

5.6.5 Closed Chain Configuration Force Control

Force control is fundamental to cooperative tasks involving more than one arm. Hayati (1986) and Alberts & Soloway (1988) employed wrist force sensors on both arms to measure interaction forces to exert desired forces of compression, tension or torsion on a rigidly held workpiece. The force controller regulated the forces and torques at each arm and the desired interaction force bias was maintained. Two approaches for closed chain control are possible: (i) the master arm is position controlled with the slave arm force controlled to provide compliance; (ii) symmetric hybrid position/force control for both arms. Master/slave architectures lose the major benefit of dual arm control in that the arms do not share the load. Tao et al (1987) proposed a master/slave configuration whereby the master arm is position controlled whilst the slave arm adopted the hybrid position/force control method with a force sensor. Seraji (1987) considered 3 approaches to dual arm control: position-position where both arms are position controlled only, position-hybrid where one arm is position controlled and the other is hybrid controlled, and hybrid-hybrid where both arms were hybrid controlled. He found that position-position control required passive compliance in order not to generate excessive forces on the load and that the position-hybrid system created fluctuations in the force profile due to vibrations in the position controlled arm. The hybrid-hybrid condition generated a smooth force profile giving the best performance. Hybrid control of both arms has been pursued as the most flexible

approach to closed chain control since arm roles may be interchanged readily. Furthermore, control can be applied to each arm independently even in the closed chain configuration provided the kinematic constraints are observed.

Uchiyama et al (1987) and Garg (1988) used hybrid velocity/force control for both arms equipped with wrist force sensors to give superior performance over position/force control. There are several ways to implement the hybrid scheme and velocity provides a natural mapping between position and force: $\dot{\theta} = J^{-1}[S.K_p(q^d - q) + (I - S)(F^d - F)]$. This may be extended for PID control. Uchiyama & Dauchez (1988) and Meier & Graf (1991) extended this hybrid scheme using as central controllers to symmetric non-master slave scheme to include the coupled kinematics of the closed chain.

Load Distribution

Carignan & Akin (1988) cited load distribution between manipulators as being particularly important for dual-manipulator freeflyer robots in space. Load distribution is a notion pertaining to both manipulators and if implemented should be implemented at a higher level than the individual controllers, eg. the Activity Controller. Orin & Oh (1981) considered the force distribution between two robot arms and a single payload. An infinite number of solutions exist due to the redundant nature of the problem (12 actuators to control 6 DOF of the payload). They applied constraints including maximum torques, maximum reaction forces and sufficient friction at the end effectors. They used a linear programming technique to minimise a cost function based on energy expenditure to minimise the power requirement within these constraints. Two criticisms have been levelled against the linear programming technique: firstly, the computation time ~10-20s for the solution precludes its use for real-time operation [Alberts & Soloway 1988]; secondly, some of the joints are deactivated at each solution - as the robot configuration changes, the joint torques are repeatedly switched on/off creating excitation of the structure [Zheng & Luh 1988].

The desired forces and moments required to move the payload may be expressed as:

$$F_{ext}^d = m_{n+1}\dot{v}_{n+1}$$

$$N_{ext}^d = I_{n+1}\dot{w}_{n+1} + w_{n+1} \times I_{n+1} w_{n+1}$$

These are the sum of the external forces/moments at the end effector [Uchiyama & Dauchez 1988; Orin & Oh 1981]:

$$F_{ext}^d = \sum_{l=1}^{2} f_{ext}^l$$

$$N_{ext}^d = \sum_{l=1}^{2} n_{ext}^l + r_{n+1}^l \times f_{ext}^l \qquad (5.26)$$

In more compact form: $F^d = H\Pi$ where $F^d = \begin{pmatrix} F_{ext}^d \\ N_{ext}^d \end{pmatrix}$,

$$H = \begin{pmatrix} I & 0 & I & 0 \\ r_{n+1}^{l=1} \times & I & r_{n+1}^{l=2} \times & I \end{pmatrix},$$

$$\Pi = \begin{pmatrix} f_{ext}^{l=1} \\ n_{ext}^{l=1} \\ f_{ext}^{l=2} \\ n_{ext}^{l=2} \end{pmatrix} \qquad (5.27)$$

[Alberts & Soloway 1988].
The H-matrix comprises the contact force map and the values of of the required forces to move the payload provide the threshold limits to the applied forces on the object.

Hayati (1986) and Alberts & Soloway (1988) defined a quadratic function of a weighting matrix W to be minimised to minimise the cartesian forces applied at the end effector to reduce the joint torques required: $Q = \Pi^T W \Pi$ where $W = diag(\alpha_1 \alpha_2 \alpha_3 \alpha_4)$, $\Pi = H^{-1} F^d$, α=weight matrix for translational and rotational components of each arm. The coefficients α_1 and α_3 relate to applied forces to each arm respectively while α_2 and α_4 relate to the applied moments to each arm respectively. The joint torques vary in proportion to motor current which in turn varies as the root of power consumption. However, although a better quadratic might be $Q = \tau^T W \tau$ representing joint space load distribution with minimum power consumption, the considerable computational overhead of such a function precludes its use [Soloway & Alberts 1989]. In any case, the cartesian forces will lead to an indirect energy minimisation through the Jacobian transpose with reduced stresses on the payload.
Using Lagrangian multplier λ:

$\tilde{Q} = \Pi^T W \Pi - \lambda^T (H\Pi - F^d)$

For mimimum $\tilde{Q}$: $\frac{\partial \tilde{Q}}{\partial \Pi} = 0 \rightarrow 2\Pi^T W - \lambda^T H = 0$

$\rightarrow \Pi^T = \frac{1}{2} W^{-1} \lambda^T H = \frac{1}{2} W^{-1} \lambda H^T$

Now $F^d = H\Pi = \frac{1}{2} HW^{-1} H^T \lambda \rightarrow \lambda = 2(HW^{-1}H^T)^{-1} F^d$

Hence, $\Pi = \frac{1}{2} W^{-1} H^T . 2(HW^{-1}H^T)^{-1} F^d = W^{-1} H^T (HW^{-1}H^T)^{-1} F^d$

This will generate the desired end effector forces and torques to be applied to the payload. Carignan & Akin (1988) considered the torque distribution between the two arms in a closed kinematic chain when both manipulators adopt the hybrid scheme. They minimised an energy cost function similar to the one above to give an optimal torque distribution. By transmitting torques through the payload, the joint torques required for motion were reduced while minimising the internal forces on the load. Zheng & Luh (1988) suggested that the load $M_{n+1} \ddot{q}$ should be distributed evenly between each manipulator to maximise the load carrying capacity (assuming identical arms), where $M_{n+1} = \begin{pmatrix} m_{n+1} I_3 & 0 \\ 0 & R_n^0 I_{cn+1} R_0^n \end{pmatrix}$ and $\ddot{q} = J\ddot{\theta} + \dot{J}\dot{\theta}$.

ie. $F_{ext}^{l=1} = F_{ext}^{l=2}$, or equivalently $\begin{pmatrix} f_{ext}^{l=1} \\ n_{ext}^{l=1} \end{pmatrix} = \begin{pmatrix} f_{ext}^{l=2} \\ n_{ext}^{l=2} \end{pmatrix} = 0.5 \begin{pmatrix} F_{ext}^d \\ N_{ext}^d \end{pmatrix}$

with $\alpha = 0.5$ for equal load-sharing.
Alberts & Soloway (1988) suggested a more general distribution of load sharing with a portion α to one manipulator and $(1-\alpha)$ to the other manipulator, ie.

$F_{ext}^{l=1} = \begin{pmatrix} f_{ext}^{l=1} \\ n_{ext}^{l=1} \end{pmatrix} = \alpha \begin{pmatrix} F_{ext}^{d} \\ N_{ext}^{d} \end{pmatrix}$ and $F_{ext}^{l=2} = \begin{pmatrix} f_{ext}^{l=2} \\ n_{ext}^{l=2} \end{pmatrix} = (1-\alpha) \begin{pmatrix} F_{ext}^{d} \\ N_{ext}^{d} \end{pmatrix}$ so that internal forces, $\mathrm{F_{int}} = \begin{pmatrix} f_{\mathrm{int}} \\ n_{\mathrm{int}} \end{pmatrix} = \begin{pmatrix} f_{ext}^{l=2} \\ n_{ext}^{l=2} \end{pmatrix} - \begin{pmatrix} f_{ext}^{l=1} \\ n_{ext}^{l=1} \end{pmatrix}$.

The weight α is selected according to the load carrying capacity of each manipulator. The generation of applied moments n_{ext}^{l} may then be penalised to have moments being generated preferably through the $r_{n+1}^{l} \times f_{ext}^{l}$ term. The weights α_2 and α_4 may be set to be K times as large as α_1 and α_3 such that K>1.

Thus far, consideration has only been given to the motion-causing components of force - internal forces and torques may build up if not controlled. These forces are generated when manipulators apply forces and torques against each other through the payload. Their sum is zero, not producing any motion but they do induce stresses in the payload.

In general: $F_{\mathrm{int}} = H^{+}\Pi + (I - H^{+}H)\Pi$ where $(I - H^{+}H)$=null space matrix

H^{+}=Moore-Penrose inverse of the contact force map

Using a PI force control law:

$$F_{\mathrm{int}} = \begin{pmatrix} f_{\mathrm{int}} \\ n_{\mathrm{int}} \end{pmatrix} = F_{\mathrm{int}}^{d} + K_f (F_{\mathrm{int}}^{d} - F_{\mathrm{int}}) + K_{fi} \int (F_{\mathrm{int}}^{d} - F_{\mathrm{int}}) dt$$

ie. $F_T = F^d + F_{\mathrm{int}}$ (5.28)

Several possibilities exist for internal force control [Kopf 1989]:

(i) Apply zero internal force criterion where $F_{\mathrm{int}}^{d} = 0$ - this is computationally the fastest approach as the remaining two approaches are computationally intensive;

(ii) Apply a minimum strain energy criterion - if the stiffness in each direction are equal, this method defaults to the zero internal force case;

(iii) Apply a minimum power criterion with weighting factor $\frac{R}{(K_t)^2}$.

Kopf (1989) found that the minimum strain method gave 1/200 the strain than the minumum power method and 1/250 the strain than the zero internal force method. However, power is required to implement the zero internal force and the mimimum power method yielded 1/9 the torque of the mimimum strain approach. This corroborates Zheng & Luh's (1988) observation that energy minimisation does not yield minimum forces exerted at the end effector. Since power is likely to be a limiting factor for space systems, good power usage is required. The power minimisation method yields as much as 9/10 the torques of the zero internal force method, a saving of only 10% at a high computational cost. In view of this and the requirement for real-time operation, the zero internal force method appears be the approach of choice.

Pittelkau (1988) stressed the need for adaptive control for load-sharing of an unknown payload and considered minimisation of internal forces which do not contribute the motion across the payload. An adaptive identifier adjusts the load sharing at each control interval according to the force feedback.

Force at each arm: $F_{ext}^{l=1} + F_{ext}^{l=2} = M_{n+1} \ddot{q}$

The load $M_{n+1}\ddot{q}$ is apportioned to each manipulator so that the forces and torques required for each manipulator can be determined. The interactive forces and torques are given by:

$F_{\text{int}}^{l=1} = \alpha M_{n+1}\ddot{q} = \alpha F_{ext}^{l=2} - (I-\alpha)F_{ext}^{l=1}$

$F_{\text{int}}^{l=2} = (I-\alpha)M_{n+1}\ddot{q} = -\alpha F_{ext}^{l=2} + (I-\alpha)F_{ext}^{l=1}$ such that $F_{\text{int}}^{l=2} + F_{\text{int}}^{l=1} = 0$

If all the diagonal components of $= diag\alpha_i$ are equal, then the respective end effector frames can be used as the task oriented frame of reference.

Performance index to be minimised with respect to α is the sum of the weighted squared joint torques: $Q = \frac{1}{2}\tau^T W \tau$

where $\tau = \begin{pmatrix} \tau_{l=1} \\ \tau_{l=2} \end{pmatrix}$=matrix of joint torques for each arm.

Now, $\frac{\partial Q}{\partial \alpha} = \left(\frac{\partial \tau}{\partial \alpha}\right)^T W \tau = 0$ and $\frac{\partial^2 Q}{\partial \alpha^2} = \left(\frac{\partial \tau}{\partial \alpha}\right)^T W \left(\frac{\partial \tau}{\partial \alpha}\right) > 0$

Now, $\frac{\partial \tau_{l=1}}{\partial \alpha} = J_{l=1}^T M_{n+1}\ddot{q} = J_{l=1}^T (F_{ext}^{l=1} + F_{ext}^{l=2})$

$\frac{\partial \tau_{l=2}}{\partial \alpha} = -J_{l=2}^T M_{n+1}\ddot{q} = -J_{l=2}^T (F_{ext}^{l=1} + F_{ext}^{l=2})$

Hence, $\frac{\partial \tau}{\partial \alpha} = \begin{pmatrix} J_{l=1}^T (F_{ext}^{l=1} + F_{ext}^{l=2}) \\ -J_{l=2}^T (F_{ext}^{l=2} + F_{ext}^{l=1}) \end{pmatrix}$ (5.30)

Newton's method may now be used to find the root α to minimise Q with seed $\alpha_0 = 0.5$:

$$\alpha_{k+1} = \alpha_k - \mu\left(\frac{\frac{\partial Q}{\partial \alpha}}{\frac{\partial^2 Q}{\partial \alpha^2}}\right) = \alpha_k - \mu\left(\frac{\left(\frac{\partial \tau}{\partial \alpha}\right)^T W \tau}{\left(\frac{\partial \tau}{\partial \alpha}\right)^T W \left(\frac{\partial \tau}{\partial \alpha}\right)}\right)$$

where $\frac{\partial \tau}{\partial \alpha}$ is given above and $0 < \mu < 1$ controls the convergence rate.

5.6.6 Dual Arm Configuration Summary

This section has considered both open chain and closed chain kinematics for dual manipulator control. The central philosophy was to enable individual robot arm servocontrollers to perform their functions independently of each other yet observing certain constraints. This has been indicated as feasible. This makes the schemes proposed as suitable for space application as indicated in the next chapter. However, for the implementation of global schemes such as load distribution, a higher level controller must be implemented to perform such tasks. This implies a hierarchical distribution of control. Suffice to state that an Activity Controller of one description or another could be used to implement this in a control framework compatible with NASREM. The approach above ensures that each arm's servocontrol is executed as low down the control hierarchy as possible to avoid computational bottlenecks and problems of differing temporal horizons higher up the control hierarchy. This section shows that the methods applicable to single arm control are applicable to dual arm control with the addition of straight forward constraints.

Chapter 6

SPACE APPLICATIONS OF ROBOTICS

This chapter is the core of the thesis. It utilises the techniques of robot control introduced in the previous chapters and modifies them for use in the control of space-based manipulators. The methodology is illustrated by applying the techniques to single manipulators initially and then expanded to apply to dual manipulator configurations as more realistic implementations of space-based freeflyer robots. It is assumed that no external forces or moments act on the total system other than those which are expressed explicitly, ie. gravity, magnetic, aerodynamic and solar pressure torques are negligible. This allows the application of the laws of linear and angular momentum which hold in an inertial frame and these provide the constraints to solve the kinematic equations. Such conservation laws are the basis of orbit raising using tethers such that if the tether is sufficiently long, the system may be modelled as a rigid dumbell of two point masses linked by a rigid massless bar suspended at the centre of mass of the system along the local vertical and lowering a mass and releasing it. The robotic freeflyer spacecraft system under consideration here comprises of a spacecraft bus mount and one or more manipulators as payload.

Linear momentum conservation law states that:

$$P = \sum_{i=0}^{n+1} m_i \dot{r}_i = \text{const} = 0 \quad \text{(arbitrarily since } \dot{P} = \sum_{i=0}^{n+1} F_{ext} = 0\text{)}$$

where P=linear momentum of the system

As a holomonic constraint, this is integrable to the equilibrium of moments principle:

$$\int_0^t \sum_{i=0}^{n+1} m_i \dot{r}_i . dt = \left[\sum_{i=0}^{n+1} m_i r_i \right]_0^t = 0$$

Angular momentum conservation states that:

$$L = \sum_{i=0}^{n+1} I_i w_i + m_i \dot{r}_i \times r_i = const = 0 \quad \text{(arbitrarily since } \dot{L} = \sum_{i=0}^{n+1} N_{ext} + \sum_{i=0}^{n+1} r \times F_{ext} = 0\text{)}$$

where L=angular momentum of the system

As a nonholonomic constraint, this is not integrable - integration of rotational velocity does not yield a unique vectorial representation of orientation since rotational motion is path dependent due to the noncommutativity of rotations. There are thus an infinite number of paths yielding a particular orientation, ie. orientation depends on the time history of motion [Nakaruma & Mukherjee 1989]. This derives from the definition of holonomy [Masutani, Mayazako & Arimoto 1989]: "A system is holonomic if and only if its motion is constrained by a set of algebraic equations involving only general angular coordinates and time. This implies that a system is holonomic if and only if a set of vector fields defining the linear space of possible velocities is completely integrable everywhere in general coordinates. Otherwise, it is nonholonomic." Hence, in this case there are more controllable states than are necessary to specify the motion of the end effector.

By decoupling the system such that linear and angular motions are treated separately, real-time control is possible and straight forward by considerably reducing the complexity of the problem. The translation effects are holonomic constraints and so linear momentum constraints may be integrated and be applied to the system through equilibrium of moments conservation to account for the translational motion of the

satellite in inertial space. The system centre of mass remains invariant in inertial space, providing unique closed form solutions for translation motion control by incorporating linear compensation into the robot kinematics formulation. These translational kinematic equations have the same form as those for a terrestrial manipulator. Hence, the linear component of the reaction effect is compensated automatically within the linear portion of the controller without the use of fuel. Fuel is a non-renewable resource, expenditure of which must be minimised as a mission constraint to maximise the satellite's operational lifetime. In fact, it has been found that fuel use is critical in the performance and flexibility of task domains and that fuel expenditure during manipulation is usually prohibitive [Marcyk & Bellazzi 1989]. Typically, the fuel expenditure to compensate for the translational motion alone of the robotic satellite would exceed the capability of cold gas thrusters by several orders of magnitude.

The angular effects are nonholonomic constraints since the attitude of the platform and the orientation of the end effector depends on the history of joint displacements because due to the noncommutativity of finite rotation sequences. Different paths of the manipulator to the same point will result in different attitudes for the spacecraft. Hence, angular momentum conservation constraints are not integrable to spacecraft attitude as a function of manipulator joint angles, and so must be applied directly. It is possible to do this straight-forwardly by employing active three axis attitude stabilisation by non-fuel expending orthogonal reaction wheels or control moment gyros to compensate for the dynamic attitude reactions based on computations of the reaction forces and moments applied at the base of the robotic manipulator. The reaction forces and torques acting on the satellite bus due to the manipulator may be calculated directly from the manipulator dynamics and be fedforward to the attitude control system. The reaction wheels are then driven to counteract the reaction forces and moments on the spacecraft mounting in conjunction with standard attitude control algorithms to maintain spacecraft attitude. Maintenance of constant attitude is desirable to enable constant remote viewing conditions. Hence all angular properties of the manipulator are identical to those of their terrestrial counterparts. The (n s a) rotational submatrix component of the 4x4 DH matrix remains unchanged from the terrestrial case since the spacecraft bus platform employs attitude control to maintain constant stabilisation of attitude.

This method avoids the dynamic singularities associated with uncontrolled attitude and allows the end effector position and orientation to be formulated as a unique function of joint angles independent of the end effector path. Indeed, it is generally considered that explicit control of attitude is essential for any docking or grappling maneouvres. All in all, this method will not exert excessive computational burdens on the spacecraft attitude and robot controllers enabling real-time operation. Apart from on-board data handling and power supply, the manipulator functions as a stand-alone system - this is more in line with the general developing preference for distributed computer systems on spacecraft. Furthermore, as well as being less computationally demanding on any single processor, this reduces the impact of any control equipment failure on the system as a whole. Finally, the method offers more favourable workspace dimensions over the free-floating mode [Vafa & Dubowsky 1987, 1990]. If satellite attitude is not controlled, the "path independent workspace" reachable by the manipulator by any path is much smaller than the "constrained workspace" available to a spacecraft employing attitude control. Dynamic singularities are characteristic of a "path

dependent workspace" (which is larger than the path independent workspace) reachable by freefloating manipulators only via certain paths [Papadopoulos & Dubowsky 1989]. The path independent workspace which does not suffer from dynamic singularities has its maximum extent when attitude control is employed, ie. when it coincides with the constrained workspace. This mode of control represents a free-flying system (ie. where a dedicated attitude control system is employed) which is a partial restriction of the more general free-floating system.

This approach is suggested by the results of Walker & Wee (1991a,b) and is a generalisation, extension and simplification of the classical approach originally formulated by Longman, Lindberg & Zedd (1986, 1987) as applied to the Shuttle Remote Manipulator System. Hence the derivations given here are original and new. The Longman/Lindberg/Zedd method was highly specific and was not conducive to a straight forward extraction of the inverse kinematics solution of manipulator joint angles. Dubowsky, Vance & Torres (1990) suggested that attitude control actuator saturation may provide a problem but Spofford & Akin (1988) suggested that this may be unlikely since manipulator motions tend to be cyclic. Certainly this will tend to be the case when employing dual manipulators. Either way environmental torque sources may be used to desaturate wheels and gyroscopes.

6.1 SPACE FREEFLYER KINEMATICS

The central concepts introduced in this chapter are represented as three theorems and proofs concerning single-manipulator freeflyer spacecraft. Later sections extend those concepts to the dual-manipluator freeflyer case. All the concepts are based on the utilisation of the robotic manipulator control algorithms of the earlier chapters.

6.1.1 Resolution Of Inertial Position:

Theorem 1 is the central core of the space robot control methodology outlined in this chapter. This is because the manipulator configuration dependency of the kinematics, dynamics and control algorithms is fundamental. The other theorems essentially follow from theorem 1.

Theorem 1: For a freeflying robotic manipulator employing dedicated attitude control of the spacecraft bus, the Denavit-Hartenberg formulation for resolved position control is given by:

$$q = \begin{pmatrix} n & s & a & p^* \\ 0 & 0 & 0 & 1 \end{pmatrix}$$

where R=(n s a) as for terrestrial manipulators, and

$$\mathrm{p}^* = \mathrm{p}^*_{cm} + \left(\frac{\mathrm{m}_0}{\mathrm{m}_T}\right)\mathrm{s}_0 + \sum_{i=1}^{n}\mathrm{R}_i\lambda_i - \left(\frac{\mathrm{m}_{n+1}}{\mathrm{m}_T}\right)\mathrm{R}_{n+1}\mathrm{r}_{n+1} \text{ where } \lambda_i = \frac{1}{\mathrm{m}_T}\left(\sum_{j=0}^{i}\mathrm{m}_j\mathrm{l}_i - \mathrm{m}_i\mathrm{r}_i\right) \quad (6.1)$$

m_0=mass of the spacecraft bus
m_T=total mass of the system

Proof: The position kinematics of a space manipulator with respect to inertial space may be given by: $p^* = r_{c0} + R_0 s_0 + \sum_{i=1}^{n} R_i^0 l_i$ (6.2)

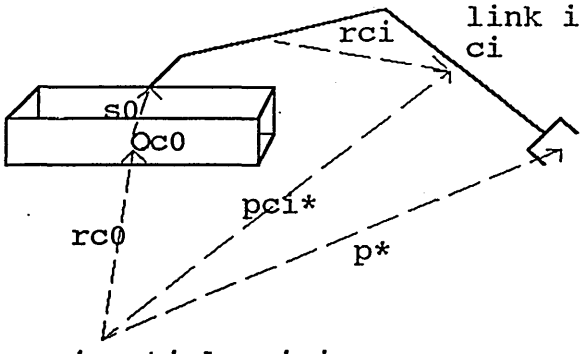

Walker & Wee (1991) used several frames between the inertial and manipulator base frames to model virtual links of zero mass, but no gain in generality is obtained by this. In general the attitude of the spacecraft platform (for roll-pitch-yaw coordinates α,β,γ):

α,β,γ):

$$R_0 = Rot(z,\gamma)Rot(y,\beta)Rot(x,\alpha) = \begin{pmatrix} c\beta c\gamma & s\alpha s\beta c\gamma - c\gamma s\gamma & c\alpha s\beta c\gamma + s\alpha s\gamma \\ c\beta s\gamma & s\alpha s\beta s\gamma + c\alpha c\gamma & c\alpha s\beta s\gamma - s\alpha c\gamma \\ -s\beta & s\alpha c\beta & c\alpha c\beta \end{pmatrix}$$

f the complete system (including the satellite bus mount, robotic manipulator and the payload) is given by [Longman, Lindberg & Zedd 1987; Lindberg, Longman & Zedd 1986]:

$$\left(\sum_{i=0}^{n+1} m_i\right) p^*_{cm} = \sum_{i=0}^{n+1} m_i p^*_{ci} \qquad \text{(equilibrium of moments)}$$

$$\text{ie. } p^*_{cm} = \sum_{i=0}^{n+1} m_i p^*_{ci} \Big/ \sum_{i=0}^{n+1} m_i \qquad (6.3)$$

The location of the system centre of mass will remain invariant in inertial space if no external forces act on the system $\sum_{i=0}^{n+1} F_i = \sum_{i=0}^{n+1} m_i \ddot{p}^*_{ci} = 0$ such that $\ddot{p}^*_{cm} = 0$, ie. this point corresponds to the "virtual ground" defined by the virtual manipulator approach [Vafa & Dubowsky 1987, 1990]. The virtual ground is the point in inertial space at which an ideal virtual kinematic chain manipulator has its base when its end effector coincides with the end effector of the actual manipulator. This virtual ground point coincides with the centre of mass of the spacecraft-manipulator system. This is to be expected since the constraints applied were the equilibrium of moments for the derivation of the kinematics of the virtual manipulator. They did not however explicitly describe the kinematics and the virtual manipulator approach is limited to non-contact situations. The system centre of mass is the point at which all the mass may be considered to be concentrated (there is no corresponding centre of inertia).

Now, $p^*_{ci} = \sum_{j=0}^{i} r_{cj}$ and $\sum_{i=0}^{n+1} m_i = m_T$ =total mass of the system

$$p^*_{cm} = \frac{1}{m_T}\left(\sum_{i=0}^{n+1} m_i \sum_{j=0}^{i} r_{cj}\right) = \frac{1}{m_T}\left(\sum_{i=0}^{n+1}\sum_{j=i}^{n+1} m_j r_{ci}\right)$$

$$= r_{c0} + \frac{1}{m_T}\sum_{i=1}^{n+1}\sum_{j=i}^{n+1} m_j r_{ci}$$

ie. $$r_{c0} = p^*_{cm} - \frac{1}{m_T}\sum_{i=1}^{n+1}\sum_{j=i}^{n+1} m_j r_{ci}$$

Substitute into (6.2):

$$p^* = p^*_{cm} + s_0 + \sum_{i=1}^{n} R_i l_i - \frac{1}{m_T}\sum_{i=1}^{n+1}\sum_{j=i}^{n+1} m_j r_{ci} \qquad (6.4)$$

Now, $r_{ci} = R_i r_i + R_{i-1} s_{i-1}$ $l_i = r_i + s_i$ so substitute into (6.4):

$$p^* = p^*_{cm} + s_0 + \sum_{i=1}^{n} R_i (r_i + s_i) - \frac{1}{m_T}\sum_{i=1}^{n+1}\sum_{j=i}^{n+1} m_j (R_i r_i + R_{i-1} s_{i-1})$$

$$= p^*_{cm} + s_0 + \sum_{i=1}^{n} R_i (r_i + s_i) - \frac{1}{m_T}\left[\sum_{i=1}^{n+1}\sum_{j=i}^{n+1} m_j (R_{i-1} r_{i-1} + R_{i-1} s_{i-1}) + \sum_{i=1}^{n+1} m_i R_i r_i\right]$$

$$= p^*_{cm} + s_0 + \sum_{i=1}^{n} R_i (r_i + s_i) - \frac{1}{m_T}\left[\sum_{i=2}^{n+1}\sum_{j=i}^{n+1} m_j R_{i-1} (r_{i-1} + s_{i-1})\right] - \frac{1}{m_T}\left[\sum_{i=1}^{n+1} m_i R_0 (r_0 + s_0) + \sum_{i=1}^{n+1} m_i R_i r_i\right]$$

$$= p^*_{cm} + \frac{m_0}{m_T} s_0 + \sum_{i=1}^{n} R_i l_i - \frac{1}{m_T}\left[\sum_{i=1}^{n+1}\sum_{j=i+1}^{n+1} m_j R_i (r_i + s_i) + \sum_{i=1}^{n+1} m_i R_i r_i\right]$$

$$= p^*_{cm} + \frac{m_0}{m_T} s_0 + \sum_{i=1}^{n} R_i l_i - \frac{1}{m_T}\left[\sum_{i=1}^{n}\sum_{j=i+1}^{n+1} m_j R_i l_i + \sum_{i=1}^{n} m_i R_i r_i\right] - \left(\frac{m_{n+1}}{m_T} R_{n+1} r_{n+1}\right)$$

ie. $$p^* = p^*_{cm} + \frac{m_0}{m_T} s_0 + \frac{1}{m_T}\sum_{i=1}^{n}\left(\sum_{j=0}^{i} m_j l_i - m_i r_i\right) R_i - \frac{m_{n+1}}{m_T} R_{n+1} r_{n+1}$$

$$p^* = p^*_{cm} + \frac{m_0}{m_T} s_0 + \sum_{i=1}^{n} R_i \lambda_i - \frac{m_{n+1}}{m_T} R_{n+1} r_{n+1} \text{ where } \lambda_i = \frac{1}{m_T}\sum_{j=0}^{i} (m_j l_i - m_i r_i) \quad \text{QED(6.1)}$$

This equation has the same form as that for an earth-based manipulator (2.2) with additional constants. Note that p^*_{cm} is constant, λ_i is a lumped kinematic/dynamic parameter constant and that the payload term is constant since the payload remains fixed relative to the end effector. No loss of generality ensues by assuming that $R_{n+1} = I_3$. The r_{n+1} corresponds to a "virtual stick" vector which points from the hand of the manipulator to the payload centre of mass which remains fixed in the target object [Uchiyama & Dauchez 1988]. This vector from the grasp point to the object's centre of mass will if large impose a large inertia matrix for the object to be manipulated. It is desirable therefore to minimise r_{n+1}. It is now necessary to find the location of the system centre of mass with respect to inertial coordinates where it remains invariant through an initialisation procedure [Longman, Lindberg & Zedd 1987; Lindberg, Longman & Zedd 1986].

$$p^*_{cm} = r_{c0} + \frac{1}{m_T}\sum_{i=1}^{n+1}\sum_{j=i}^{n+1} m_j r_{ci}$$

$$= r_{c0} + \frac{1}{m_T}\sum_{i=1}^{n+1}\sum_{j=i}^{n+1} m_j (R_i r_i + R_{i-1} s_{i-1})$$

$$= r_{c0} + \frac{1}{m_T}\sum_{i=1}^{n+1}\sum_{j=i}^{n+1} m_j R_{i-1}(r_{i-1} + s_{i-1}) + \frac{1}{m_T}\sum_{i=1}^{n+1} m_i R_i r_i$$

$$= r_{c0} + \frac{1}{m_T}\sum_{i=2}^{n+1}\sum_{j=i}^{n+1} m_j R_{i-1} l_{i-1} + \frac{1}{m_T}\left[\sum_{i=1}^{n+1} m_i l_0 + \sum_{i=1}^{n+1} m_i R_i r_i\right]$$

$$= r_{c0} + \frac{1}{m_T}\sum_{i=1}^{n+1} m_i s_0 + \frac{1}{m_T}\sum_{i=1}^{n}\sum_{j=i+1}^{n+1} m_j R_i l_i + \frac{1}{m_T}\sum_{i=1}^{n} m_i R_i r_i + \frac{m_{n+1}}{m_T} R_{n+1} r_{n+1}$$

$$= r_{c0} + \left(1 - \frac{m_0}{m_T}\right) s_0 + \frac{1}{m_T}\sum_{i=1}^{n} R_i \left(\sum_{j=i+1}^{n+1} m_j l_i + m_i r_i\right) + \frac{m_{n+1}}{m_T} R_{n+1} r_{n+1}$$

hence,

$$p^*_{cm} = r_{c0} + \left(1 - \frac{m_0}{m_T}\right) s_0 + \sum_{i=1}^{n} R_i L_i + \left(\frac{m_{n+1}}{m_T}\right) r_{n+1} \text{ where } L_i = \tfrac{1}{m_T}\sum_{j=i+1}^{n+1}(m_j l_i + m_i r_i) \qquad (6.5)$$

The robot/spacecraft system centre of mass is determined by:
(i) the vector from the inertial origin to the spacecraft centre of mass r_{c0};
(ii) the moment arm due to the fractional mass of the robot/payload to the total system centre of mass $\frac{m_{17}}{m_T}$ (for a 6-degree of freedom robot manipulator), and the fixed lever arm distance from the spacecraft centre of mass to the base of the robot arm s_0;
(iii) the kinematic structure of the manipulator and the link masses.
To find the system centre of mass with respect to inertial space, we assume arbitrarily that the local inertial reference frame initially coincides with the satellite bus centre of mass, ie. $r_{c0} = 0$, since any point fixed in the interceptor body may be regarded as inertially fixed prior to any robotic maneouvre. That point will remain fixed in inertial space as long as the task execution time is short compared with the satellite's orbital period and it may be regarded as an inertial reference for any particular payload of mass m_{n+1}. Although this choice of inertial coordinates is not strictly inertial since it moves along the orbital trajectory with the spacecraft at orbital velocity $w_{orb} = \sqrt{GM/R^3}$, it is sufficiently inertial such that spin angular momentum and orbital angular momentum may be decoupled and considered separately, ie. $L = L_{orbital} + L_{spin}$. The system centre of mass will then remain fixed in inertial space. Initialisation must be recomputed on payload acquisition or release to locate the new system centre of mass in inertial coordinates. This recomputation of the link parameters L_i involves simple recomputation of the total mass and fractional mass through adding or deleting the payload mass m_{n+1}. If the manipulator grasps an object attached to the target satellite and transfers it to the robotic spacecraft bus, the object mass is deleted from the target and added to the robotic spacecraft bus. In fact, for a zero payload or payload of known mass, the computation may be performed off line and stored in memory since m_i and l_i are all constants. Initialisation may be performed for any

arbitrary robot configuration, eg. stored ("tucked") position. Once p_{cm}^* is known, r_{c0} is defined with respect to the inertial origin for any further configuration: $r_{c0} = p_{cm}^* - \left(1 - \frac{m_0}{m_T}\right)s_0 - \sum_{i=1}^{n} R_i L_i - \frac{m_{n+1}}{m_T} r_{n+1}$, though this is not specifically required for the kinematic formulation.

An equivalent form for the forward/orientation kinematics in terms of the 4x4 DH matrix representation is:

$$x = \begin{pmatrix} I_3 & p_{cm}^* \\ 0 & 1 \end{pmatrix} \begin{pmatrix} I_3 & m_0 s_0 / m_T \\ 0 & 1 \end{pmatrix} \begin{pmatrix} n & s & a & p(\lambda) \\ 0 & 0 & 0 & 1 \end{pmatrix} \begin{pmatrix} -(m_{n+1} R_{n+1} / m_T) & -(m_{n+1} r_{n+1} / m_T) \\ 0 & 1 \end{pmatrix}$$

$$= \begin{pmatrix} n & s & a & p^* \\ 0 & 0 & 0 & 1 \end{pmatrix} \qquad (6.6)$$

This form of the DH matrix allows the computation of the drive function D of the cartesian trajectory generator algorithm as outlined in Chapter 4. The advantage of this method over Longman, Lindberg & Zedd's formulation is firstly that it is completely general and is not restricted by manipulator kinematics and that explicit calculation of r_{c0} as it varies with manipulator configuration is not required for the kinematics and terrestrial algorithms can be applied directly with little modification, ie.
(i) replacement of link parameters l_i by λ_i in the standard DH formulation; and

(ii) addition of constants $p_{cm}^* + \frac{m_0}{m_T} s_0 - \frac{m_{n+1}}{m_T} r_{n+1}$ to the DH formulation.

The inverse kinematics may be solved in the same way as that for an Earth-based manipulator to generate body-referenced joint angles which correspond to inertial cartesian coordinates by solving:

$$p_{arm}^* = \sum_{i=1}^{n-3} R_i \lambda_i = p^* - p_{cm}^* - \left(\frac{m_0}{m_T}\right) s_0 + \left(\frac{m_{n+1}}{m_T}\right) R_{n+1} r_{n+1} - \lambda_n a \qquad (6.7)$$

to find positioning joint angles. The orienting joint angles of the wrist are identical to those for an Earth-based manipulator since attitude is stabilised.

Example:

Here we consider a 6 degree of freedom manipulator with an intersecting wrist and a payload (link 7) whereby all parameters are represented by assuming that their centres of mass lie on the links' longitudinal axes as bodies of revolution. The intersecting wrist means that links 4 and 5 are fictitious. Application of equation (6.2) gives:

$p^* = r_{c0} + R_0 s_0 + R_1 l_1 + R_2 l_2 + R_3 l_3 + R_6 l_6$ since $l_5 = l_6 = 0$

Now, application of equation (6.3):

$m_T p_{cm}^* = m_0 p_{c0}^* + m_1 p_{c1}^* + m_2 p_{c2}^* + m_3 p_{c3}^* + m_6 p_{c6}^* + m_7 p_{c7}^*$ since $m_4 = m_5 = 0$

Hence, $p_{cm}^* = \frac{1}{m_T}(m_0 p_{c0}^* + m_1 p_{c1}^* + m_2 p_{c2}^* + m_3 p_{c3}^* + m_6 p_{c6}^* + m_7 p_{c7}^*)$

$= \frac{1}{m_T}[m_0 r_{c0} + m_1(r_{c0} + r_{c1}) + m_2(r_{c0} + r_{c1} + r_{c2}) + m_3(r_{c0} + r_{c1} + r_{c2} + r_{c3}) + \ldots + m_7(r_{c0} + \ldots + r_{c7})]$

$= \frac{1}{m_T}[m_T r_{c0} + m_{17} r_{c1} + m_{27} r_{c2} + m_{37} r_{c3} + m_{67} r_{c6} + m_7 r_{c7}]$ where $m_{ij} = \sum_{k=i}^{j} m_k$

Hence, $r_{c0} = p_{cm}^* - \frac{1}{m_T}[m_{17} r_{c1} + m_{27} r_{c2} + m_{37} r_{c3} + m_{67} r_{c6} + m_7 r_{c7}]$

Substitute in equation (6.2):

$p^* = p_{cm}^* - \frac{1}{m_T}[m_{17} r_{c1} + m_{27} r_{c2} + m_{37} r_{c3} + m_{67} r_{c6} + m_7 r_{c7}] + s_0 + R_1 l_1 + R_2 l_2 + R_3 l_3 + R_6 l_6$

Now, $l_i = r_i + s_i$ and $r_{ci} = R_{i-1}s_{i-1} + R_i r_i$:

$$p^* = p^*_{cm} + s_0 + R_1(r_1 + s_1) + R_2(r_2 + s_2) + R_3(r_3 + s_3) + R_6(r_6 + s_6)$$
$$-\tfrac{1}{m_T}[m_{17}(R_1 r_1 + R_0 s_0) + m_{27}(R_2 r_2 + R_1 s_1) + m_{37}(R_3 r_3 + R_2 s_2) + m_{67}(R_6 r_6 + R_3 s_3) + m_7(R_7 r_7 + R_6 s_6)]$$

Multiply out and rearrange:

$$p^* = p^*_{cm} + s_0(1 - \tfrac{m_{17}}{m_T}) + R_1[r_1(1 - \tfrac{m_{17}}{m_T}) + s_1(1 - \tfrac{m_{27}}{m_T})] + R_2[r_2(1 - \tfrac{m_{27}}{m_T}) + s_2(1 - \tfrac{m_{37}}{m_T})]$$
$$+R_3[r_3(1 - \tfrac{m_{37}}{m_T}) + s_3(1 - \tfrac{m_{67}}{m_T})] + R_6[r_6(1 - \tfrac{m_{67}}{m_T}) + s_6(1 - \tfrac{m_7}{m_T})] - \tfrac{m_7}{m_T}R_7 r_7$$
$$= p^*_{cm} + \tfrac{m_0}{m_T}s_0 + R_1(\tfrac{m_{01}}{m_T}r_1 + \tfrac{m_{01}}{m_T}s_1) + R_2(\tfrac{m_{01}}{m_T}r_2 + \tfrac{m_{02}}{m_T}s_2) + R_3(\tfrac{m_{02}}{m_T}r_3 + \tfrac{m_{03}}{m_T}s_3)$$
$$+R_6(\tfrac{m_{03}}{m_T}r_6 + \tfrac{m_{06}}{m_T}s_6) - \tfrac{m_7}{m_T}R_7 r_7$$
$$= p^*_{cm} + \tfrac{m_0}{m_T}s_0 + R_1\lambda_1 + R_2\lambda_2 + R_3\lambda_3 + R_6\lambda_6 - \tfrac{m_7}{m_T}R_7 r_7$$

where

$$\lambda_1 = \tfrac{1}{m_T}(m_{01}l_1 - m_1 r_1)$$
$$\lambda_2 = \tfrac{1}{m_T}(m_{02}l_2 - m_2 r_2)$$
$$\lambda_3 = \tfrac{1}{m_T}(m_{03}l_3 - m_3 r_3)$$
$$\lambda_6 = \tfrac{1}{m_T}(m_{06}l_6 - m_6 r_6)$$

These "kinetic variables" replace the terrestrial algorithm kinematic variables by straight substitution and the other constants added. This is now applied to the the PUMA 560/600 configuration with zero elbow offset the characteristic equation for which is given by:

$$\begin{pmatrix} p^*_x \\ p^*_y \\ p^*_z \end{pmatrix} = \begin{pmatrix} r_{c0x} \\ r_{c0y} \\ r_{c0z} \end{pmatrix} + \begin{pmatrix} s_{0x} \\ s_{0y} \\ s_{0z} \end{pmatrix} + \begin{pmatrix} p_x \\ p_y \\ p_z \end{pmatrix} \quad \text{where} \quad \begin{pmatrix} p_x \\ p_y \\ p_z \end{pmatrix} = \begin{pmatrix} -s_1 d_2 + c_1(c_2 a_2 + s_{23}d_4) + a_x d_6 \\ c_1 d_2 + s_1(c_2 a_2 + s_{23}d_4) + a_y d_6 \\ -s_2 a_2 + c_{23}d_4 + a_z d_6 \end{pmatrix}$$

By multiplying through, this can be reduced to:

$$\begin{pmatrix} p^*_x \\ p^*_y \\ p^*_z \end{pmatrix} = \begin{pmatrix} p^*_{cmx} \\ p^*_{cmy} \\ p^*_{cmz} \end{pmatrix} + \tfrac{m_0}{m_T}\begin{pmatrix} s_{0x} \\ s_{0y} \\ s_{0z} \end{pmatrix} + \begin{pmatrix} -s_1\delta_1 + c_1(c_2\alpha_2 + s_{23}\delta_4) + a_x\delta_6 \\ c_1\delta_2 + s_1(c_2\alpha_2 + s_{23}\delta_4) + a_y\delta_6 \\ -s_2\alpha_2 + c_{23}\delta_4 + a_z\delta_6 \end{pmatrix} - \tfrac{m_7}{m_T}\begin{pmatrix} x_7 \\ y_7 \\ z_7 \end{pmatrix}$$

where $\delta_2 = \left(\tfrac{m_{01}d_2 - m_1 r_1}{m_{07}}\right)$; $\alpha_2 = \left(\tfrac{m_{02}a_2 - m_2 r_2}{m_{07}}\right)$; $\delta_4 = \left(\tfrac{m_{03}d_4 - m_3 r_3}{m_{07}}\right)$; $\delta_6 = \left(\tfrac{m_{06}d_6 - m_6 r_6}{m_{07}}\right)$

This defines the forward position kinematics of a space-based PUMA-type manipulator which describe the inertial position of the end effector in terms of their joint angles. The orientation of the end effector is given by the terrestrial 3x3 rotation component of the DH matrix (as the attitude is maintained as static by feedforward compensation):

$$(nsa) = \sum_{i=0}^{n} R_i = \sum_{i=1}^{n} R_i \text{ since } R_0 = I_3.$$

The initialisation process allows the computation of p^*_{cm}:

$$p^*_{cm} = r_{c0} + \tfrac{1}{m_T}(m_{17}r_{c1} + m_{27}r_{c2} + m_{37}r_{c3} + m_{67}r_{c6} + m_7 r_{c7})$$
$$= r_{c0} + \tfrac{1}{m_T}[m_{17}(R_1 r_1 + R_0 s_0) + m_{27}(R_2 r_2 + + R_1 s_1) + m_{37}(R_3 r_3 + R_2 s_2) + m_{67}(R_6 r_6 + R_3 s_3)$$
$$+m_7(R_7 r_7 + R_6 s_6)]$$
$$= r_{c0} + \tfrac{1}{m_T}[m_{17}R_0 s_0 + R_1(m_{27}l_1 + m_1 r_1) + R_2(m_{37}l_2 + m_2 r_2) + R_3(m_{67}l_3 + m_3 r_3) + R_6(m_7 l_6 + m_6 r_6)$$
$$+m_7 R_7 r_7]$$
$$= (1 - \tfrac{m_0}{m_T})s_0 + R_1 L_1 + R_2 L_2 + R_3 L_3 + R_6 L_6 + \tfrac{m_7}{m_T}R_7 r_7 \text{ with } r_{c0} = 0$$

where $L_1 = \left(\tfrac{m_{27}l_1 + m_1 r_1}{m_T}\right)$; $L_2 = \left(\tfrac{m_{37}l_2 + m_2 r_2}{m_T}\right)$; $L_3 = \left(\tfrac{m_{67}l_3 + m_3 r_3}{m_T}\right)$; $L_6 = \left(\tfrac{m_7 l_6 + m_6 r_6}{m_T}\right)$

For the PUMA 560/600 configuration:

$$\begin{pmatrix} p^*_{cmx} \\ p^*_{cmy} \\ p^*_{cmz} \end{pmatrix} = \left(1-\frac{m_0}{m_T}\right)\begin{pmatrix} s_{0x} \\ s_{0y} \\ s_{0z} \end{pmatrix} + \begin{pmatrix} -s_1 D_2 + c_1(c_2 A_2 + s_{23} D_4) + a_x D_6 \\ c_1 D_2 + s_1(c_2 A_2 + s_{23} D_4) + a_y D_6 \\ -s_2 A_2 + c_{23} D_4 + a_z D_6 \end{pmatrix} + \frac{m_7}{m_T}\begin{pmatrix} x_7 \\ y_7 \\ z_7 \end{pmatrix}$$

where $D_2 = \left(\frac{m_{27} d_2 + m_1 r_1}{m_T}\right)$; $A_2 = \left(\frac{m_{37} a_2 + m_2 r_2}{m_T}\right)$; $D_4 = \left(\frac{m_{67} d_4 + m_3 r_3}{m_T}\right)$; $D_6 = \left(\frac{m_7 d_6 + m_6 r_6}{m_T}\right)$.

To find the inverse solution to the joint angles, a slightly modified version of the terrestrial inverse algorithm can be used. The inverse kinematics solution must generate body referenced joint angles cooresponding to the inertial position coordinates:

$$\sum_{i=1}^{n} R_i \lambda_i = p^* - p^*_{cm} - \frac{m_0}{m_T} s_0 + \frac{m_7}{m_T} R_7 r_7$$

$$\rightarrow p^*_{arm} = R_1\lambda_1 + R_2\lambda_2 + R_3\lambda_3 = p^* - p^*_{cm} - \frac{m_0}{m_T} s_0 + \frac{m_7}{m_T} r_7 - R_6\lambda_6 \text{ for } R_7 = I_3.$$

$$\begin{pmatrix} p^*_{ax} \\ p^*_{ay} \\ p^*_{az} \end{pmatrix} = \begin{pmatrix} -s_1\delta_2 + c_1(c_2\alpha_2 + s_{23}\delta_4) \\ c_1\delta_2 + s_1(c_2\alpha_2 + s_{23}\delta_4) \\ -s_2\alpha_2 + c_{23}\delta_4 \end{pmatrix} = \begin{pmatrix} p^*_x \\ p^*_y \\ p^*_z \end{pmatrix} - \begin{pmatrix} p^*_{cmx} \\ p^*_{cmy} \\ p^*_{cmz} \end{pmatrix} - \frac{m_0}{m_T}\begin{pmatrix} s_{0x} \\ s_{0y} \\ s_{0z} \end{pmatrix} + \frac{m_7}{m_T}\begin{pmatrix} x_7 \\ y_7 \\ z_7 \end{pmatrix} - \delta_6 \begin{pmatrix} a_x \\ a_y \\ a_z \end{pmatrix}$$

The first 3 joint angles determine the position in space of the arm and the final 3 joint angles for the orientation of the arm are calculated as for the terrestrial case. The inverse calculations of Chapter 2 with the appropiate substitutions to equations 2.6-2.8 may be found to be:

$$\theta_1 = \tan^{-1}\left(\frac{p^*_{ay}}{p^*_{ax}}\right) - \tan^{-1}\left(\frac{\delta_2}{\sqrt{(p^*_{ax})^2 + (p^*_{ay})^2 - \delta_2^2}}\right)$$

$$\theta_2 = \tan^{-1}\left(\frac{A}{p^*_{ax}}\right) - \tan^{-1}\left(\frac{B}{-\sqrt{A^2 + (p^*_{ax})^2 - B^2}}\right) \text{ where } A = c_1 p^*_{ax} + s_1 p^*_{ay} \text{ and } B = \frac{A^2 + (p^*_{ax})^2 + \alpha_2^2 - \delta_4^2}{2\alpha_2}$$

$$\theta_3 = \tan^{-1}\left(-\frac{A - \alpha_2 c_2}{p^*_{ax} + \alpha_2 s_2}\right) - \theta_2 \qquad (6.8)$$

The inverse kinematics solution for the positioning joint angles have precisely the same form as for an Earth-based manipulator. The orienting joint angles are identical to the fixed base case since the attitude of the spacecraft is maintained as constant:

$$\theta_4 = \tan^{-1}\left(\frac{-s_1 a_x + c_1 a_y}{c_{23}(c_1 a_x + s_1 a_y) - s_{23} a_z}\right)$$

$$\theta_5 = \tan^{-1}\left(\frac{\sqrt{(c_1 c_{23} a_x + s_1 c_{23} a_y - s_{23} a_z)^2 + (-s_1 a_x + c_1 a_y)^2}}{s_{23}(c_1 a_x + s_1 a_y) + c_{23} a_z}\right)$$

$$\theta_6 = \tan^{-1}\left(-\frac{s_{23}(c_1 s_x + s_1 s_y) + c_{23} s_z}{s_{23}(c_1 n_x + s_1 n_y) + c_{23} n_z}\right) \qquad (6.9)$$

Note that these equations are only marginally more complex than those for a terrestrial manipulator. As theorem 1 is the most fundamental and original of the theorems presented, it is illustrated by response plots which show the difference that the free flying spacecraft makes on the inverse kinematics solution of joint angles compared with a terrestrial manipulator bolted to *terra firma* for nominally the same cartesian trajectory from initial the final positions. The inverse kinematics solution of both scenarios was implemented by computer program. Only the joint angles of the first three positioning joints are shown as these indicate the different joint angles required to position the robotic hand in base coordinates (for the terrestrial manipulator) and in inertial coordinates (for the space-based manipulator). It is important to note that a cartesian trajectory defined in base coordinates (to which the manipulator position is invariant) will differ from that same cartesian trajectory defined in inertial space (with respect to which the manipulator will move).

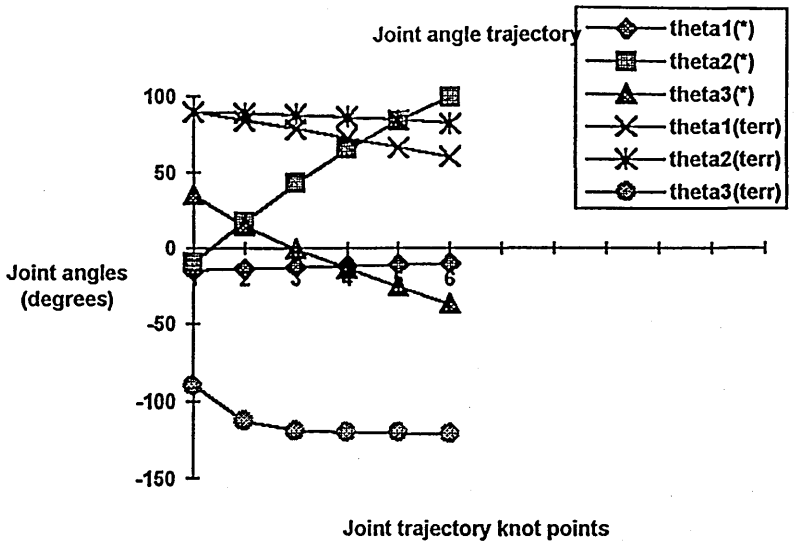

theta1(*)	-14.52	-13.34	-12.28	-11.31	-10.43	-9.64
theta2(*)	-9.36	17.79	43.21	65.3	83.68	99
theta3(*)	35.38	14.86	-0.66	-13.47	-25.32	-36.85
theta1(terr)	90	84.33	78.52	72.56	66.44	60.22
theta2(terr)	90	89.37	88.14	86.43	84.36	82.08
theta3(terr)	-90	-112.67	-118.8	-119.75	-119.84	-120.84

Legend - "*" indicates inertial space-based coordinates
"terr" indicates terrestrial base coordinates

It is evident that the joint angles required to position the end effector in inertial coordinates in space are quite different from those required to position the end effector in manipulator base coordinates on Earth Hence, any attempt to position a robotic manipulator in space without regard to the dynamics of the system will result in incorrect trajectories. Note that world coordinates as defined by the base coordinates (on Earth) and by the inertial coordinates (in space) are not the same in that the manipulator base moves with respect to inertial space (as inertial origin is defined in terms of the total system of spacecraft and manipulator), and that the cartesian trajectory defined in each will not bear direct correspondence with each other.

6.1.2 Resolution Of Inertial Velocity, Acceleration & Static Force:

Theorem 2: For a freeflying robotic manipulator employing attitude control, the extended Jacobian matrix is given by:

$$\bar{J} = \sum_{i=1}^{n}\sum_{k=1}^{i}\frac{\partial R_i}{\partial \theta_k}.\lambda_i \qquad (6.10)$$

This extended Jacobian, derived from the resolved rate kinematic control problem, may be applied in the usual manner to resolved acceleration control and resolved force control problem since they derive directly from the resolved motion rate control problem.

Proof: Differentiate (6.2) with respect to time:

$$v^* = \dot{p}^* = \dot{r}_{c0} + \dot{R}_0 s_0 + \sum_{i=1}^{n}\dot{R}_i l_i = \dot{r}_{c0} + \sum_{i=1}^{n}\dot{R}_i l_i \quad \text{where } \dot{R}_0 = 0 \qquad (6.11)$$

Now, $\dot{r}_{c0} = -\frac{1}{m_T}\sum_{i=1}^{n+1}\sum_{j=1}^{n+1} m_j \dot{r}_{ci}$ since $\dot{p}_{cm} = 0$ (6.12)

This represents the conservation of linear momentum to eliminate the platform velocity.

$\dot{r}_{ci} = \dot{R}_i r_i + \dot{R}_{i-1} s_{i-1}$

$\dot{r}_{c0} = -\frac{1}{m_T}\sum_{i=1}^{n+1}\sum_{j=i}^{n+1} m_j(\dot{R}_i r_i + \dot{R}_{i-1} s_{i-1})$

Substitute into (6.9):

$v^* = \dot{R}_0 s_0 + \sum_{i=1}^{n} \dot{R}_i(r_i + s_i) - \frac{1}{m_T}\sum_{i=1}^{n+1}\sum_{j=i}^{n+1} m_j(\dot{R}_i r_i + \dot{R}_{i-1} s_{i-1})$

Now, $\dot{R}_i^0 = \sum_{k=1}^{i} \frac{\partial R_i^0}{\partial \theta_k}\dot{\theta}_k$ and in general $\dot{R}_0 = \dot{\alpha}\frac{\partial R_0}{\partial \alpha} + \dot{\beta}\frac{\partial R_0}{\partial \beta} + \dot{\gamma}\frac{\partial R_0}{\partial \gamma} = \dot{\theta}_0 \frac{\partial R_0}{\partial \theta_0}$

Substitute:

$$v^* = \dot{\theta}_0 \frac{\partial R_0}{\partial \theta_0} s_0 + \left\{ \sum_{i=1}^{n}\sum_{k=0}^{i} \frac{\partial R_i}{\partial \theta_k} l_i - \frac{1}{m_T}\sum_{i=1}^{n+1}\sum_{j=i}^{n+1} m_j \left[\sum_{k=1}^{i} \frac{\partial R_i}{\partial \theta_k} r_i + \sum_{k=1}^{i-1} \frac{\partial R_{i-1}}{\partial \theta_k} s_{i-1} \right] \right\} \dot{\theta}_k$$

$$= \dot{\theta}_0 \frac{\partial R_0}{\partial \theta_0} s_0 + \sum_{i=1}^{n} \frac{\partial R_i}{\partial \theta_0} l_i - \frac{1}{m_T}\sum_{j=1}^{n+1} m_j \frac{\partial R_0}{\partial \theta_0} s_0 + \left\{ \sum_{i=1}^{n}\sum_{k=1}^{i} \frac{\partial R_i}{\partial \theta_k} l_i - \frac{1}{m_T}\sum_{i=1}^{n+1}\sum_{j=1}^{n+1} m_j \left[\sum_{k=1}^{i} \frac{\partial R_i}{\partial \theta_k} r_i + \sum_{k=1}^{i-1} \frac{\partial R_{i-1}}{\partial \theta_k} s_{i-1} \right] \right\} \dot{\theta}_k$$

ie. $\begin{pmatrix} v^* \\ w^* \end{pmatrix} = \bar{J}_0 \dot{\theta}_0 + \bar{J}_m \dot{\theta}_m$

where $\bar{J}_0 = \frac{\partial R_0}{\partial \theta_0} s_0 + \sum_{i=1}^{n} \frac{\partial R_i}{\partial \theta_0} l_i - \frac{1}{m_T}\sum_{j=1}^{n+1} m_j \frac{\partial R_0}{\partial \theta_0} s_0$ for $\dot{\theta}_0 = (\dot{\alpha}\dot{\beta}\dot{\gamma})^T$

$$\bar{J}_m = \sum_{i=1}^{n}\sum_{k=1}^{i} \frac{\partial R_i}{\partial \theta_k}(r_i + s_i) - \frac{1}{m_T}\sum_{i=1}^{n+1}\sum_{j=i}^{n+1} m_j \left[\sum_{k=1}^{i} \frac{\partial R_i}{\partial \theta_k} r_i + \sum_{k=1}^{i-1} \frac{\partial R_{i-1}}{\partial \theta_k} s_{i-1} \right] \text{ for } \dot{\theta}_m = (\dot{\theta}_1 \ldots \dot{\theta}_n)^T$$

These are the extended Jacobians of the spacecraft and manipulator respectively such that $v^* = (\bar{J}_0 \bar{J}_m)\begin{pmatrix} \dot{\theta}_0 \\ \dot{\theta}_m \end{pmatrix}$. Now, $(\bar{J}_0 \bar{J}_m)$ is not square and so non-invertible. However, it is possible to obtain an invertible square " generalised " Jacobian matrix.

Conservation of linear and angular momentum state:

$\sum_{i=0}^{n+1} m_i \dot{r}_i = 0$

$\sum_{i=0}^{n+1} I_i w_i + m_i r_i \times \dot{r}_i = \sum_{i=0}^{n+1} I_i w_i = 0$

For the spacecraft and manipulator:

$I_0 \dot{\theta}_0 + I_m \dot{\theta}_m = 0$ where I_0 = inertia matrix of the spacecraft

I_m = mass matrix of the manipulator

$\rightarrow \dot{\theta}_0 = -I_0^{-1} I_m \dot{\theta}_m$

Now, $v^* = \bar{J}_0 \dot{\theta}_0 + \bar{J}_m \dot{\theta}_m = \bar{J}_0(-I_0^{-1} I_m \dot{\theta}_m) + \bar{J}_m \dot{\theta}_m = (\bar{J}_m - \bar{J}_0 I_0^{-1} I_m)\dot{\theta}_m$

This represents the generalised Jacobian J^* such that $\dot{\theta} = (J^*)^{-1}\dot{x}^*$ where $J^* = (\bar{J}_m - \bar{J}_0 I_0^{-1} I_m)$ [Umetani & Yoshida 1989, Nakaruma & Mukherjee 1991]. For an

attitude controlled spacecraft, the extended manipulator Jacobian is its generalised Jacobian $J^* = (J_m - J_0 I_0^{-1} I_m) = J_m$, specifying the relation between joint velocities and end effector velocities since $J_0=0$, $w_0=0$ and $\dot{R}_0 = 0$. It may be simplified to:

$$J = \sum_{i=1}^{n}\sum_{k=1}^{i}\frac{\partial R_i}{\partial \theta_k}(r_i + s_i) - \frac{1}{m_T}\sum_{i=1}^{n+1}\sum_{j=i}^{n+1} m_j\left(\sum_{k=1}^{i-1}\frac{\partial R_{i-1}}{\partial \theta_k} r_{i-1} + \sum_{k=1}^{i-1}\frac{\partial R_{i-1}}{\partial \theta_k} s_{i-1}\right) - \frac{1}{m_T}\sum_{i=1}^{n+1}\sum_{k=1}^{i} m_i \frac{\partial R_i}{\partial \theta_k} r_i$$

$$= \sum_{i=1}^{n}\sum_{k=1}^{i}\frac{\partial R_i}{\partial \theta_k}(r_i + s_i) - \frac{1}{m_T}\sum_{i=2}^{n+1}\sum_{j=i}^{n+1} m_j\left(\sum_{k=1}^{i-1}\frac{\partial R_{i-1}}{\partial \theta_k} r_{i-1} + \sum_{k=1}^{i-1}\frac{\partial R_{i-1}}{\partial \theta_k} s_{i-1}\right) - \frac{1}{m_T}\sum_{i=1}^{n+1}\sum_{k=1}^{i} m_i \frac{\partial R_i}{\partial \theta_k} r_i$$

$$- \frac{1}{m_T}\sum_{i=1}^{n+1}\sum_{k=1}^{i} m_i \frac{\partial R_0}{\partial \theta_k}(s_0 + r_0) where R_0 = const$$

$$= \sum_{i=1}^{n}\sum_{k=1}^{i}\frac{\partial R_i}{\partial \theta_k}(r_i + s_i) - \frac{1}{m_T}\sum_{i=1}^{n+1}\sum_{j=i+1}^{n+1} m_j\left(\sum_{k=1}^{i}\frac{\partial R_i}{\partial \theta_k}(r_i + s_i)\right) - \frac{1}{m_T}\sum_{i=1}^{n+1}\sum_{k=1}^{i} m_i \frac{\partial R_i}{\partial \theta_k} r_i$$

$$= \sum_{i=1}^{n}\sum_{k=1}^{i}\frac{\partial R_i}{\partial \theta_k}(r_i + s_i) - \frac{1}{m_T}\sum_{i=1}^{n}\sum_{j=i+1}^{n+1} m_j\left(\sum_{k=1}^{i}\frac{\partial R_i}{\partial \theta_k}(r_i + s_i)\right) - \frac{1}{m_T}\sum_{i=1}^{n+1} m_i \frac{\partial R_i}{\partial \theta_k} r_i - \frac{m_{n+1}}{m_T}\sum_{i=1}^{n+1}\frac{\partial R_{n+1}}{\partial \theta_k} r_{n+1}$$

Now R_{n+1} is constant, so $\partial R_{n+1} / \partial \theta_k = 0$:

$$J = \sum_{i=1}^{n}\sum_{k=1}^{i}\frac{\partial R_i}{\partial \theta_k}\left[1 - \frac{1}{m_T}\sum_{j=i+1}^{n+1} m_j l_i\right] - \frac{1}{m_T}\sum_{i=1}^{n}\sum_{k=1}^{i} m_i \frac{\partial R_i}{\partial \theta_k} r_i$$

$$= \sum_{i=1}^{n}\sum_{k=1}^{i}\frac{\partial R_i}{\partial \theta_k}\left(\frac{1}{m_T}\sum_{j=0}^{i} m_j l_i - m_i r_i\right)$$

ie. $J = \sum_{i=1}^{n}\sum_{k=1}^{i}\frac{\partial R_i}{\partial \theta_k}\lambda_i$ where $\lambda_i = \frac{1}{m_T}\sum_{j=0}^{i}(m_j l_i - m_i r_i)$ (6.10) QED

The extended Jacobian for a freeflyer employing attitude control has the same form as that of an Earth-based manipulator with the replacement of kinematic constants l_i for dynamic constants λ_i. This is consistent with differentiating (6.1) directly:

$$v^* = \dot{p}^* = \dot{p}^*_{cm} + \frac{m_0}{m_T}\dot{s}_0 + \sum_{i=1}^{n}\dot{R}_i \lambda_i - \frac{m_{n+1}}{m_T}\dot{R}_{n+1} r_{n+1} = \sum_{i=1}^{n}\sum_{k=1}^{i}\frac{\partial R_i}{\partial \theta_k}\lambda_i \dot{\theta}_i$$

since $\dot{p}^*_{cm} = \dot{s}_0 = \dot{R}_{n+1} = 0$. Note how the extended Jacobian requires only the replacement of kinematic link parameters with kinematic-dynamic parameters and the positional constants differentiate to zero. Hence, the Jacobian may be inverted normally as with terrestrial manipulators. This is far simpler than the immensely complex fixed attitude restricted Jacobian given by: $\dot{\theta}_m = \left[J_m(I - I_m^+ I_m)\right]^+ v^*$ based on the Moore-Penrose pseudoinverse which used the inherent redundancy of the robotic manipulator spacecraft to maintain attitude [Nenchev, Umetani & Yoshida 1992].

Similar arguments for deriving the extended Jacobian above apply to other Jacobian formulations since the Jacobian is unique [Whitney 1969; Whitney 1972]. The extended Jacobian is now derived for a PUMA 560/600 manipulator adopting the

cross product formulation of the Jacobian [Whitney 1972]. The derivation begins with the dynamics formulation:

$$v = v_0 + \sum_{i=1}^{n} (z_{i-1} \times l_i)\dot{\theta}_i$$

$$w = w_0 + \sum_{i=1}^{n} z_{i-1}\dot{\theta}_i = \sum_{i=1}^{n} z_{i-1}\dot{\theta}_i$$

since $w_0 = 0$ for an attitude controlled base.

Now, $\dot{r}_{c0} = -\frac{1}{m_T}\sum_{i=1}^{n+1} m_i \dot{p}_{ci}^{*}$ where $\dot{p}_{ci}^{*} = v_{ci} = v_{i-1} + w_i \times r_i = \sum_{k=1}^{i} v_{k-1} + w_i \times r_i$

Hence, $\dot{r}_{c0} = v_0 = -\frac{1}{m_T}\sum_{i=1}^{n+1} m_i \left[\sum_{k=1}^{i} v_{k-1} + w_i \times r_i\right] = -\frac{1}{m_T}\sum_{i=1}^{n+1}\left[\sum_{i=j}^{n+1} m_j v_{i-1} + \sum_{i=1}^{n+1} m_i (w_i \times r_i)\right]$

Now, $v_i = v_{i-1} + w_i \times l_i = \sum_{k=1}^{i} w_k \times l_k$ where $w_i = \sum_{k=1}^{i} z_{k-1}\dot{\theta}_k$

$$v_i = \sum_{k=1}^{n} (z_{k-1} \times l_k)\dot{\theta}_k \rightarrow v_n = \sum_{i=1}^{n} (z_{i-1} \times l_i)\dot{\theta}_i$$

Hence, $v_0 = -\frac{1}{m_T}\sum_{i=1}^{n+1}\left[\sum_{i=j}^{n+1} m_j \sum_{i=1}^{n-1} (z_{i-1} \times l_i)\dot{\theta}_i + \sum_{i=1}^{n+1} m_i \left(\sum_{i=1}^{n+1} z_{i-1} \times r_i\right)\dot{\theta}_i\right]$

$$= -\frac{1}{m_T}\sum_{i=1}^{n+1}\left[\sum_{j=i+1}^{n+1} m_j \sum_{i=1}^{n} (z_{i-1} \times l_i)\dot{\theta}_i + m_i (z_{i-1} \times r_i)\dot{\theta}_i\right]$$

So, $v_n = \sum_{i=1}^{n} (z_{i-1} \times l_i)\dot{\theta}_i - \frac{1}{m_T}\left[\sum_{j=i+1}^{n+1} m_j \sum_{i=1}^{n} (z_{i-1} \times l_i)\dot{\theta}_i + \sum_{i=1}^{n+1} m_i (z_{i-1} \times r_i)\dot{\theta}_i\right]$

$$= \sum_{i=1}^{n} (z_{i-1} \times l_i)\dot{\theta}_i - \frac{1}{m_i}\left[\sum_{j=i+1}^{n+1} m_j \sum_{i=1}^{n} (z_{i-1} \times l_i)\dot{\theta}_i + \sum_{i=1}^{n} m_i (z_{i-1} \times r_i)\dot{\theta}_i\right]$$

where $\frac{m_{n+1}}{m_T}(z_n \times r_{n+1})\dot{\theta}_{n+1} = 0$

$$\rightarrow v_n = \sum_{i=1}^{n}\left(1 - \frac{1}{m_T}\sum_{j=i+1}^{n+1} m_j\right)(z_{i-1} \times l_i)\dot{\theta}_i - \frac{1}{m_T}\sum_{i=1}^{n} m_i (z_{i-1} \times r_i)\dot{\theta}_i$$

$$= \sum_{i=1}^{n} (z_{i-1} \times \lambda_i)\dot{\theta}_i \quad \text{where } \lambda_i = \frac{1}{m_T}\left(\sum_{j=0}^{i} m_j l_i - m_i r_i\right)$$

Hence, the cross product Jacobian is consistent with the concept of replacing kinematic link parameters with kinematic-dynamic link parameters.

For the PUMA 560/600 model:

$$\bar{J} = \begin{pmatrix} \bar{J}_{11} & \bar{J}_{21} & \bar{J}_{31} & \bar{J}_{41} & \bar{J}_{51} & \bar{J}_{61} \\ \bar{J}_{12} & \bar{J}_{22} & \bar{J}_{32} & \bar{J}_{42} & \bar{J}_{52} & \bar{J}_{62} \\ \bar{J}_{13} & \bar{J}_{23} & \bar{J}_{33} & \bar{J}_{43} & \bar{J}_{53} & \bar{J}_{63} \\ \bar{J}_{14} & \bar{J}_{24} & \bar{J}_{34} & \bar{J}_{44} & \bar{J}_{54} & \bar{J}_{64} \\ \bar{J}_{15} & \bar{J}_{25} & \bar{J}_{35} & \bar{J}_{45} & \bar{J}_{55} & \bar{J}_{56} \\ \bar{J}_{16} & \bar{J}_{26} & \bar{J}_{36} & \bar{J}_{46} & \bar{J}_{56} & \bar{J}_{66} \end{pmatrix}$$

where $\bar{J}_{11} = -s_1[\delta_6(c_{23}c_4s_5 + s_{23}c_5) + \alpha_2 c_2] - c_1(s_4s_5\delta_6 + \delta_2)$

$$\bar{J}_{12} = c_1[\delta_6(c_{23}c_4s_5 + s_{23}c_5) + \alpha_2c_2] - s_1(s_4s_5\delta_6 + \delta_2)$$
$$\bar{J}_{13} = 0; \bar{J}_{14} = 0; \bar{J}_{15} = 0; \bar{J}_{16} = 1$$
$$\bar{J}_{21} = c_1(s_4s_5\delta_6 + \delta_2)$$
$$\bar{J}_{22} = s_1(s_4s_5\delta_6 + \delta_2)$$
$$\bar{J}_{23} = -s_1[\delta_6(s_{23}c_4s_5 - c_{23}c_5) + \alpha_2s_2] - c_1[\delta_6(c_{23}c_4s_5 + s_{23}c_5) + \alpha_2c_2]$$
$$\bar{J}_{24} = -s_1; \bar{J}_{25} = c_1; \bar{J}_{26} = 0$$
$$\bar{J}_{31} = c_1s_4s_5\delta_6$$
$$\bar{J}_{32} = s_1s_4s_5\delta_6$$
$$\bar{J}_{33} = -s_1[\delta_6(s_3c_4s_5 - c_3c_5)] - c_1[\delta_6(c_3c_4s_5 + s_3c_5)]$$
$$\bar{J}_{34} = -s_1; \bar{J}_{35} = c_1; \bar{J}_{36} = 0$$
$$\bar{J}_{41} = \delta_6(s_1s_{23}c_5 - c_{23}s_4s_5)$$
$$\bar{J}_{42} = \delta_6(c_{23}c_4s_5 - c_1s_{23}c_5)$$
$$\bar{J}_{43} = \delta_6s_{23}(c_1s_4 - s_1c_4s_5)$$
$$\bar{J}_{44} = c_1s_{23}; \bar{J}_{45} = s_1s_{23}; \bar{J}_{46} = c_{23}$$
$$\bar{J}_{51} = s_{23}s_4c_5\delta_6$$
$$\bar{J}_{52} = s_{23}s_4s_5\delta_6$$
$$\bar{J}_{53} = c_5\delta_6(c_1c_{23}s_4 + s_1c_4) + s_5\delta_6(s_1c_{23}c_4 - c_1c_4)$$
$$\bar{J}_{54} = -(c_1c_{23}s_4 + s_1c_4)$$
$$\bar{J}_{55} = c_1c_4 - s_1c_{23}c_4$$
$$\bar{J}_{56} = s_{23}s_4$$
$$\bar{J}_{61} = \delta_6[s_1(c_{23}c_4s_5 + c_5s_{23}) + c_1s_4s_5]$$
$$\bar{J}_{62} = \delta_6[c_1(c_{23}c_4s_5 + s_{23}c_5) - s_1s_4s_5]$$
$$\bar{J}_{63} = 0$$
$$\bar{J}_{64} = c_1(c_{23}c_4s_5 + s_{23}c_5) - s_1s_4s_5$$
$$\bar{J}_{65} = s_1(c_{23}c_4s_5 + s_{23}c_5) + c_1s_4s_5$$
$$\bar{J}_{66} = -s_{23}c_4s_5 + c_{23}c_5$$

Hence resolved rate control is given by: $\begin{pmatrix} v^* \\ w \end{pmatrix} = \bar{J}\,\dot{\theta}_i$ with $\dot{\theta}_i = \bar{J^{-1}}\begin{pmatrix} v^* \\ w \end{pmatrix}$

Resolved acceleration control follows directly by differentation:

$$\begin{pmatrix} \dot{v}^* \\ \dot{w} \end{pmatrix} = \dot{\bar{J}}\,\ddot{\theta}_i + \bar{J}\,\dot{\theta}_i$$

with $\ddot{\theta}_i = \bar{J^{-1}}\left[\begin{pmatrix} \dot{v}^* \\ \dot{w} \end{pmatrix} - \dot{J}\,\dot{\theta}_i\right]$

Resolved force control also follows from resolved rate by virtual work arguments:

$\tau = \bar{J}^T f_{ext}$

In general, the forward kinematic solutions for a freeflyer employing dedicated attitude control have the same form as for Earth-based manipulators so that the same algorithms may be used for both forward and inverse kinematic solutions with only minor modifications. This is essentially a restatement of Papadopoulos & Dubowsky's (1990, 1991) findings for the general case of freefloating manipulators that the dynamics formulation of any terrestrial manipulators have the same form as those of space manipulators and so terrestrial robotic control algorithms such as the computed torque control law [Konigstein et al 1989], are applicable to space robotics, though their formulation was much more complex due to the constraints. The differential kinematics of freefloating systems have the same structure as those for a fixed base manipulator. By applying attitude control however, the position/orientation kinematics themselves also have this property. All these new "lumped" dynamic parameters may be precalculated offline and stored in memory with the exception of the payload parameters. The change of payload involves negligible online calculation.

6.2 SPACE ROBOT DYNAMICS FEEDFORWARD COMPENSATION:

For an attitude controlled platform with a space manipulator, the dynamic formulation includes a moving platform with a finite translational velocity $v_0 = -\frac{1}{m_T}\sum_{j=1}^{n}\sum_{i=1}^{n} m_j v_{ci}$.

Walker and Wee (1991) used a Lagragian formulation for their characterisation of space robotic problems but suggested that a recursive formulation would be more efficient. The Newton-Euler recursive formulation is better suited to the problem when employing attitude control to calculate explicitly the reaction moments applied to the spacecraft mounting by the manipulator movements - such constraint forces are eliminated in the Lagrangian approach. Nagashima & Nakaruma (1992) derived a means for calculating $(v_0 w_0)^T$ explicitly using the Newton-Euler recursive equations which reduces to the formulation above when $w_0 = 0$. Longman, Lindberg & Zedd (1986, 1987) proved a theorem specifying the feedforward component to the spacecraft attitude controller to compensate for the manipulator reaction forces on the spacecraft. When attitude control is employed, $\mathrm{w}_0 = \dot{\mathrm{w}}_0 = 0$, but v_0 and $\dot{\mathrm{v}}_0$ are finite. This requires that the robot dynamics are calculated with respect to base coordinates. This is more efficient than calculating the robot dynamics with reference to link coordinates and then transforming them to inertial coordinates as has been proposed [Nagashima & Nakaruma 1992]. Outlined here is a slightly altered version of the theorem and its proof.

Theorem 3: The feedforward signal from the robot controller to the spacecraft attitude control system enables the attitude control system to compensate for the applied moments to the spacecraft such that the total moments about the satellite centre of mass sum to zero. The feedforward dynamics component with respect to local inertial coordinates is given by:

$\mathrm{N}_r = \mathrm{N}_T + (\mathrm{p}^*_{cm} - \mathrm{r}_{c0} - \mathrm{s}_0) \times \mathrm{F}_T$

where

$$F_T = \sum_{i=1}^{n+1} F_{ci} = \sum_{i=1}^{n+1} m_i \dot{v}_{ci}$$
$$N_T = \sum_{i=1}^{n+1} N_{ci} = \sum_{i=1}^{n+1} I_i \dot{w}_i + w_i \times I_i w_i \quad (6.13)$$

Proof:

Moment on spacecraft due to manipulator movements about the coupling point at the manipulator base is given by:

$$N_T = \sum_{i=1}^{n+1} \int p_{ci} \times \ddot{p}_{ci} . dm$$

Moment about coupling point referred to inertial coordinates: $p_{ci} = p_{ci}^* - r_{c0} - s_0$

ie. $N_0 = \sum_{i=1}^{n+1} \int p_{ci} \times (\ddot{p}_{ci}^* - \ddot{r}_{c0} - \ddot{s}_0) . dm$

Now, $\ddot{s}_0 = 0$ since s_0 is invariant:

$$N_0 = \sum_{i=1}^{n+1} \int p_{ci} \times \ddot{p}_{ci}^* . dm - \sum_{i=1}^{n+1} \int p_{ci} \times \ddot{r}_{c0} . dm$$

For any inertially fixed frame of reference:

$$\int p_{ci} \times \ddot{p}_{ci}^* . dm = p_{ci} \times dF$$

ie. $N_0 = \sum_{i=1}^{n+1} p_{ci} \times dF - \sum_{i=1}^{n+1} \int p_{ci} \times \ddot{r}_{c0} . dm$

Now, $N_T = \sum_{i=1}^{n+1} N_{ci} = \sum_{i=1}^{n+1} p_{ci} \times dF$

ie. $N_0 = N_T - \sum_{i=1}^{n+1} m_i p_{ci} \times \ddot{r}_{c0}$

Centre of mass is defined by:

$$p_{cm}^* = \frac{1}{m_T} \sum_{i=0}^{n+1} m_i p_{ci}^* = \frac{1}{m_T} \sum_{i=0}^{n+1} \sum_{j=i}^{n+1} m_j r_{ci} = \frac{1}{m_T} \left(\sum_{i=0}^{n+1} m_i r_{c0} + \sum_{i=1}^{n+1} m_i s_0 + \sum_{i=1}^{n+1} m_i p_{ci} \right)$$

$$= r_{c0} + \frac{1}{m_T} \left[(m_T - m_0) s_0 + \sum_{i=1}^{n+1} m_i p_{ci} \right]$$

$$\sum_{i=1}^{n+1} m_i p_{ci} = m_T (p_{cm}^* - r_{c0}) - (m_T - m_0) s_0$$

Substitute the summation:

$$N_0 = N_T - [m_T (p_{cm}^* - r_{c0}) - (m_T - m_0) s_0] \times \ddot{r}_{c0} \quad (6.14)$$

Similarly, since no external forces are acting:

$$F_T = \sum_{i=0}^{n+1} F_{ci} = \sum_{i=0}^{n+1} m_i \ddot{p}_{ci}^* = 0 = \sum_{i=0}^{n+1} \sum_{j=i}^{n+1} m_j \ddot{r}_{ci} = \sum_{i=0}^{n+1} m_i \ddot{r}_{c0} + \sum_{i=0}^{n+1} m_i \ddot{s}_0 + \sum_{i=0}^{n+1} m_i \ddot{p}_{ci} =$$

$$m_T \ddot{r}_{c0} + \sum_{i=1}^{n+1} m_i \ddot{p}_{ci} = 0$$

Hence, $\ddot{r}_{c0} = -\frac{1}{m_T} \sum_{i=1}^{n+1} m_i \ddot{p}_{ci}$

Now, total reaction force on base of manipulator:

$$F_T = \sum_{i=1}^{n+1} m_i \ddot{p}_{ci} \rightarrow \ddot{r}_{c0} = -\frac{1}{m_T} F_T$$

Now, $F_0 = m_0 \ddot{r}_{c0} = -\left(\frac{m_0}{m_T}\right) F_T$ (6.15)

$$N_0 = N_T + [m_T(p^*_{cm} - r_{c0}) - (m_T - m_0)s_0] \times F_T / m_T \quad (6.16)$$

This gives the moments and forces on the spacecraft at the manipulator base with respect to inertial coordinates. The sum of moments about the spacecraft bus centre of mass which must be compensated by the attitude controller:

$N_r = N_0 + s_0 \times F_0$

$= N_T + [m_T(p^*_{cm} - r_{c0}) - (m_T - m_0)s_0] \times F_T / m_T - s_0 \times (m_0 / m_T).F_T$ (6.13) QED

$= N_T + (p^*_{cm} - r_{c0} - s_0) \times F_T$

This comprises the feedforward component to the attitude control system of the spacecraft that must be nullified to maintain attitude such that $w_0 = 0$. These results must be transformed to map into spacecraft body coordinates so that x, y, and z coordinates of the spacecraft and the manipulator base coincide. This is accomplished by the premultiplication matrix: $\begin{pmatrix} 0 & 1 & 0 \\ 1 & 0 & 0 \\ 0 & 0 & -1 \end{pmatrix}$.

N_{ci}, F_{ci} are calculated by the robot controller, hence N_T and F_T as their summations is trivial. However the robot controller calculates these variables in link-referenced coordinates but the attitude controller requires them in base coordinates. Recalculation in base coordinates is not trivial but only increases the complexity marginally as the algorithmic complexity of the Newton-Euler recursive method is only O(n). The other parameters p^*_{cm}, r_{c0}, s_0 are known or calculated during the kinematics formulation. Reaction moment compensation commands are the same no matter where the mounting of the reaction wheels or control moment gyros are within the spacecraft since the moment of a couple is independent of the reference point. This feedforward compensation scheme improves the stability of the satellite attitude by more than 10 times [Sato et al 1993]. Base reactions are exerted directly on the supporting space vehicle and de Silva (1991) proposed minimising the base reactions to reduce the accelerations of the base by applying a weighted quadratic function $Q = R^T W R$ where $R = (F_T N_T)^T$. However, the method is applicable to redundant manipulators only and requires finding a matrix of joint velocities and accelerations to be minimised during trajectory interpolation using the redundant degrees of freedom. This form of control is also computationally intense as well as not being applicable here. Another advantage of this scheme is that spacecraft attitude control remains referenced to the vehicle centre of mass rather than the total system centre of mass allowing the formulation of vehicle moment of inertia as constant relative to body fixed coordinates to compensate for the moments on the spacecraft - the spacecraft is likely to have a somewhat complex asymmetric shape so this is significant, (eg. due to solar arrays). The reaction moments generated will depend on the payload mass and the maximum acceleration/deceleration profile of the joint trajectory.

6.3 APPLICATION TO DUAL ARM ROBOTIC FREEFLYING SPACECRAFT

6.3.1 Dual Arm Position Kinematics:

The kinematic control equations may be adapted for two arm control in a straight forward manner to allow the use of the control techniques outlined in Chapter 5, but the formulation presented here is more generally applicable. It assumes the case of l=2 manipulator arms, but may be extended to more than 2 arms. The same assumptions that linear momentum is conserved allowing the use of the equilibrium of moments and that 3-axis feedforward stabilisation is employed are utilised.

Equilibrium of moments: $\left(m_0 + \sum_{l=1}^{2}\sum_{i=1}^{n+1} m_i^l\right) p_{cm}^* = \left(m_0 + \sum_{l=1}^{2}\sum_{i=1}^{n+1} m_i^l\right) \sum_{j=0}^{n+1} p_{cj}^l$

$$\rightarrow p_{cm}^* = r_{c0} + \frac{1}{m_T}\sum_{l=1}^{2}\sum_{i=1}^{n+1}\sum_{j=i}^{n+1} m_j^l r_{ci}^l \quad \text{where} \quad m_T = m_0 + \sum_{l=1}^{2}\sum_{i=1}^{n+1} m_i^l$$

Hence, $$r_{c0} = p_{cm}^* - \frac{1}{m_T}\sum_{l=1}^{2}\sum_{i=1}^{n+1}\sum_{j=i}^{n+1} m_j^l r_{ci}^l \qquad (6.17)$$

Now the inertial position of the end effector of arm l is given by:

$$p_l^* = r_{c0} + s_0^l + \sum_{i=1}^{n} R_i^l l_i^l$$

Substitute (6.17):

$$p_l^* = p_{cm}^* + s_0^l + \sum_{i=1}^{n} R_i^l l_i^l - \frac{1}{m_T}\sum_{l=1}^{2}\sum_{i=1}^{n+1}\sum_{j=i}^{n+1} m_j^l r_{ci}^l$$

$$= p_{cm}^* + s_0^l + \sum_{i=1}^{n} R_i^l (r_i^l + s_i^l) - \frac{1}{m_T}\sum_{l=1}^{2}\sum_{i=1}^{n+1}\sum_{j=i}^{n+1} m_i^l (R_i^l r_i^l + R_{i-1}^l s_{i-1}^l)$$

$$= p_{cm}^* + s_0^l + \sum_{i=1}^{n} R_i^l (r_i^l + s_i^l) - \frac{1}{m_T}\sum_{l=1}^{2}\sum_{i=1}^{n+1}\sum_{j=i}^{n+1} m_j^l (R_{i-1}^l r_{i-1}^l + R_{i-1}^l s_{i-1}^l) - \frac{1}{m_T}\sum_{l=1}^{2}\sum_{i=1}^{n+1} m_i^l R_i^l r_i^l$$

Now, with $r_0^l = 0$:

$$p_l^* = p_{cm}^* + s_0^l + \sum_{i=1}^{n} R_i^l (r_i^l + s_i^l) - \frac{1}{m_T}\sum_{l=1}^{2}\sum_{i=1}^{n+1}\sum_{j=i+1}^{n+1} m_j^l R_i^l (r_i^l + s_i^l) - \frac{1}{m_T}\sum_{l=1}^{2}\sum_{i=1}^{n+1} m_i^l R_i^l r_i^l$$

$$- \frac{1}{m_T}\sum_{l=1}^{2}\sum_{i=1}^{n+1} m_i^l R_0^l (r_0^l + s_0^l)$$

$$= p_{cm}^* + \left(s_0^l - \frac{1}{m_T}\sum_{l=1}^{2}\sum_{i=1}^{n+1} m_i^l s_0^l\right) + \left(\sum_{i=1}^{n} R_i^l (r_i^l + s_i^l) - \frac{1}{m_T}\sum_{i=1}^{2}\sum_{i=1}^{n}\sum_{j=i+1}^{n+1} m_j^l R_i^l (r_i^l + s_i^l)\right)$$

$$- \frac{1}{m_T}\sum_{l=1}^{2}\sum_{i=1}^{n} m_i R_i^l r_i^l - \frac{m_{n+1}}{m_T}\sum_{l=1}^{2} R_{n+1}^l r_{n+1}^l \qquad (6.18)$$

This equation now requires splitting into its component contributions from each arm l and l':

$$p_l^* = p_{cm}^* + \left(1 - \frac{m_{l n+1}^l}{m_T}\right) s_0^l - \left(\frac{m_{l n+1}^{l'}}{m_T}\right) s_0^{l'} + \left(1 - \frac{1}{m_T}\sum_{j=i+1}^{n+1} m_j^l\right)\sum_{i=1}^{n} R_i^l (r_i^l + s_i^l) - \frac{1}{m_T}\sum_{i=1}^{n}\sum_{j=i+1}^{n+1} m_j^{l'} R_i^{l'} (r_i^{l'} + s_i^{l'})$$

$$- \frac{1}{m_T}\sum_{i=1}^{n} m_i^l R_i^l r_i^l - \frac{1}{m_T}\sum_{i=1}^{n} m_i^{l'} R_i^{l'} r_i^{l'} - \frac{1}{m_T}\sum_{l=1}^{2} m_{n+1}^l R_{n+1}^l r_{n+1}^l$$

$$= p_{cm}^* + \frac{m_{0 n+1}^l}{m_T} s_0^l - \frac{m_{l n+1}^{l'}}{m_T} s_0^{l'} + \sum_{i=1}^{n} R_i^l \lambda_i - \sum_{i=1}^{n} R_i^{l'} L_i - \frac{1}{m_T}\sum_{l=1}^{2} m_{n+1}^l R_{n+1}^l r_{n+1}^l$$

where $\lambda_i = \left(\frac{1}{m_T} \sum_{i=1}^{n} \sum_{j=0}^{i} (m_j^l l_i^l + m_{1n+1}^l - m_i^l r_i^l) \right)$ and $L_i = \left(\frac{1}{m_T} \sum_{i=1}^{n} \sum_{j=i+1}^{i} (m_j^l l_i^l + m_i^l r_i^l) \right)$ (6.19)

and $s_0^{l'} = H s_0^l$

Example:

Now an illustrative example of a dual PUMA 560/600 manipulator system mounted onto a spacecraft platform is given. For generality the open loop configuration is analysed as the closed loop configuration may be regarded as an open loop system with the appropriate kinematic constraints. The formulation presented here is applied to the dual conguration of 6 degree of freedom left/right handed PUMA 560/600 manipulators with the left arm representing the master arm (superscript m) and the right arm representing the slave arm (superscript s). They are separated by a distance h in the x coordinate. The kinematic structures are assumed identical such that $m_i^m = m_i^s$ and $l_i^m = l_i^s$.

Now,

$$p_l^* = p_{cm}^* + \left(s_0^l - \frac{1}{m_T} \sum_{l}^{2} \sum_{i=1}^{n+1} m_i^l s_0^l \right) + \sum_{i=1}^{n} R_i^l l_i^l - \frac{1}{m_T} \sum_{l=1}^{2} \sum_{i=1}^{n} \sum_{j=i+1}^{n+1} m_j^l R_i^l l_i^l - \frac{1}{m_T} \sum_{l=1}^{2} \sum_{i=1}^{n} m_i^l R_i^l r_i^l - \frac{1}{m_T} \sum_{l=1}^{2} m_{n+1}^l R_{n+1}^l r_{n+1}^l$$

We assume for simplicity that the payload distribution is equal between the arms, thoough the formulation is not restricted to this assumption.

For the master arm:

$$p_m^* = p_{cm}^* + \left(1 - \frac{m_{17}}{m_T}\right) s_0^m - \frac{m_{17}}{m_T} s_0^s + \left(1 - \frac{1}{m_T} \sum_{i}^{6} \sum_{j=i+1}^{7} m_j \right) \begin{pmatrix} c_1(a_2c_2 + d_4s_{23}) - d_2s_1 + d_6a_x \\ s_1(a_2c_2 + d_4s_{23}) + d_2c_1 + d_6a_y \\ d_4c_{23} - a_2s_2 + d_6a_z \end{pmatrix}_m$$

$$- \frac{1}{m_T} \sum_{i=1}^{6} m_i \begin{pmatrix} c_1(r_2c_2 + r_3s_{23}) - r_1s_1 + r_6a_x \\ s_1(r_2c_2 + r_3s_{23}) + r_1c_1 + r_6a_y \\ r_3c_{23} - r_2s_2 + r_6a_z \end{pmatrix}_m - \frac{1}{m_T} \sum_{i=1}^{6} \sum_{j=i+1}^{7} m_j \begin{pmatrix} c_1(a_2c_2 + d_4s_{23}) - d_2s_{23} + d_6a_x \\ s_1(a_2c_2 + d_4s_{23}) + d_2c_1 + d_6a_y \\ d_4c_{23} - a_2s_2 + d_6a_z \end{pmatrix}_s$$

$$- \frac{1}{m_T} \sum_{i=1}^{n} m_i \begin{pmatrix} c_1(r_2c_2 + r_3s_{23}) - r_1s_1 + r_6a_x \\ s_1(r_2c_2 + r_3s_{23}) + r_1c_1 + r_6a_y \\ r_3c_{23} - r_2s_2 + r_6a_z \end{pmatrix}_s - \frac{1}{m_T} \left(m_7^m R_7^m r_7^m + m_7^s R_7^s r_7^s \right)$$

Multiplying the mass terms out gives:

$$p_m^* = p_{cm}^* + \left(\frac{m_{07}}{m_T}\right) s_0^m + \left(\frac{m_{17}}{m_T}\right) s_0^s + \begin{pmatrix} c_1[c_2a_2(\frac{m_{02}+m_{17}}{m_T}) + s_{23}d_4(\frac{m_{03}+m_{17}}{m_T})] - s_1d_2(\frac{m_{01}+m_{17}}{m_T}) + a_xd_6(\frac{m_{06}+m_{17}}{m_T}) \\ s_1[c_2a_2(\frac{m_{02}+m_{17}}{m_T}) + s_{23}d_4(\frac{m_{03}+m_{17}}{m_T})] + c_1d_2(\frac{m_{01}+m_{17}}{m_T}) + a_yd_6(\frac{m_{06}^m+m_{17}^s}{m_T}) \\ c_{23}d_4(\frac{m_{03}+m_{17}}{m_T}) - s_2a_2(\frac{m_{02}+m_{17}}{m_T}) + a_zd_6(\frac{m_{06}+m_{17}}{m_T}) \end{pmatrix}_m$$

$$- \begin{pmatrix} c_1[c_2r_2(\frac{m_2}{m_T}) + s_{23}r_3(\frac{m_3}{m_T})] - s_1r_1(\frac{m_1}{m_T}) + a_xr_6(\frac{m_6}{m_T}) \\ s_1[c_2r_2(\frac{m_2}{m_T}) + s_{23}r_3(\frac{m_3}{m_T})] + c_1r_1(\frac{m_1}{m_T}) + a_yr_6(\frac{m_6}{m_T}) \\ c_{23}r_3(\frac{m_3}{m_T}) - s_2r_2(\frac{m_2}{m_T}) + a_zr_6(\frac{m_6}{m_T}) \end{pmatrix}_m$$

$$- \begin{pmatrix} c_1[c_2a_2(\frac{m_{37}}{m_T}) + s_{23}d_4(\frac{m_{67}}{m_T})] - s_1d_2(\frac{m_{27}}{m_T}) + a_xd_6(\frac{m_7}{m_T}) \\ s_1[c_2a_2(\frac{m_{37}}{m_T}) + s_{23}d_4(\frac{m_{67}}{m_T})] + c_1d_2(\frac{m_{27}}{m_T}) + a_yd_6(\frac{m_7}{m_T}) \\ c_{23}d_4(\frac{m_{67}}{m_T}) - s_2a_2(\frac{m_{37}}{m_T}) + a_zd_6(\frac{m_7}{m_T}) \end{pmatrix}_s$$

$$-\begin{pmatrix} c_1[c_2r_2(\frac{m_2}{m_T})+s_{23}r_3(\frac{m_3}{m_T})]-s_1r_1(\frac{m_1}{m_T})+a_xr_6(\frac{m_6}{m_T}) \\ s_1[c_2r_2(\frac{m_2}{m_T})+s_{23}r_3(\frac{m_3}{m_T})]+c_1r_1(\frac{m_1}{m_T})+a_yr_6(\frac{m_6}{m_T}) \\ c_{23}r_3(\frac{m_3}{m_T})-s_2r_2(\frac{m_2}{m_T})+a_zr_6(\frac{m_6}{m_T}) \end{pmatrix}_s - \frac{1}{m_T}\left(m_7^m \begin{pmatrix} x_7 \\ y_7 \\ z_7 \end{pmatrix}_m + m_7^s \begin{pmatrix} x_7 \\ y_7 \\ z_7 \end{pmatrix}_s \right)$$

By grouping the common factors, the inertial position for the master arm may be found:

$$p_m^* = p_{cm}^* + \frac{m_{07}}{m_T}s_0^m + \frac{m_{17}}{m_T}s_0^s + \begin{pmatrix} c_1(c_2\alpha_2+s_{23}\delta_4)-s_1\delta_2+a_x\delta_6 \\ s_1(c_2\alpha_2+s_{23}\delta_4)+c_1\delta_2+a_y\delta_6 \\ c_{23}\delta_4-s_2\alpha_2+a_z\delta_6 \end{pmatrix}_m$$
$$-\begin{pmatrix} c_1(c_2A_2+s_{23}D_4)-s_1D_2+a_xD_6 \\ s_1(c_2\alpha_2+s_{23}D_4)+c_1D_2+a_yD_6 \\ c_{23}D_4-s_2A_2+a_zD_6 \end{pmatrix}_s - \frac{1}{m_T}\left(m_7^m \begin{pmatrix} x_7 \\ y_7 \\ z_7 \end{pmatrix}_m + m_7^s \begin{pmatrix} x_7 \\ y_7 \\ z_7 \end{pmatrix}_s \right)$$

where

$$\delta_2 = \frac{(m_{01}+m_{17})d_2-m_1r_1}{m_T} \qquad D_2 = \frac{m_{27}+m_1r_1}{m_T}$$
$$\alpha_2 = \frac{(m_{02}+m_{17})a_2-m_2r_2}{m_T} \quad \text{and} \quad A_2 = \frac{m_{37}a_2+m_2r_2}{m_T}$$
$$\delta_4 = \frac{(m_{03}+m_{17})d_4-m_3r_3}{m_T} \qquad D_4 = \frac{m_{67}d_4+m_3r_3}{m_T}$$
$$\delta_6 = \frac{(m_{06}+m_{17})d_6-m_6r_6}{m_T} \qquad D_6 = \frac{m_7d_6+m_6r_6}{m_T}$$

A similar expression may be derived for the slave arm:

$$p_s^* = p_{cm}^* + \frac{m_{07}}{m_T}s_0^s + \frac{m_{17}}{m_T}s_0^m + \begin{pmatrix} c_1(c_2\alpha_2+s_{23}\delta_4)-s_1\delta_2+a_x\delta_6 \\ s_1(c_2\alpha_2+s_{23}\delta_4)+c_1\delta_2+a_y\delta_6 \\ c_{23}\delta_4-s_2\alpha_2+a_z\delta_6 \end{pmatrix}_s$$
$$-\begin{pmatrix} c_1(c_2A_2+s_{23}D_4)-s_1D_2+a_xD_6 \\ s_1(c_2A_2+s_{23}D_4)+c_1D_2+a_yD_6 \\ c_{23}D_4-s_2A_2+a_zD_6 \end{pmatrix}_m - \frac{1}{m_T}\left(m_7^s \begin{pmatrix} x_7 \\ y_7 \\ z_7 \end{pmatrix}_s + m_7^m \begin{pmatrix} x_7 \\ y_7 \\ z_7 \end{pmatrix}_m \right)$$

This defines the forward inertial position kinematics of each end effector. Now, the geometric configuration for the dual arms was defined in Chapter 5:

$$s_0^s = Hs_0^m = \begin{pmatrix} -s_{0x}^m+h \\ s_{0y}^m \\ -s_{0z}^m \end{pmatrix} \text{ and } p_s = R_Hp_m = \begin{pmatrix} -p_x^m \\ p_y^m \\ -p_z^m \end{pmatrix}, \text{ so these equations become:}$$

$$p_m^* = p_{cm}^* + \begin{pmatrix} \frac{m_0}{m_T}s_{0x}+\frac{m_{17}}{m_T}h \\ s_{0y} \\ \frac{m_0}{m_T}s_{0z} \end{pmatrix} + \begin{pmatrix} c_1(c_2\alpha_2+s_{23}\delta_4)-s_1\delta_2+a_x\delta_6 \\ s_1(c_2\alpha_2+s_{23}\delta_4)+c_1\delta_2+a_y\delta_6 \\ c_{23}\delta_4-s_2\alpha_2+a_z\delta_6 \end{pmatrix}_m$$
$$-\begin{pmatrix} -c_1(c_2A_2+s_{23}D_4)+s_1D_2-a_xD_6 \\ s_1(c_2A_2+s_{23}D_4)+c_1D_2+a_yD_6 \\ -c_{23}D_4+s_2A_2-a_zD_6 \end{pmatrix}_s - \frac{1}{m_T}\left(m_7^m \begin{pmatrix} x_7 \\ y_7 \\ z_7 \end{pmatrix}_m + m_7^s \begin{pmatrix} -x_7 \\ y_7 \\ -z_7 \end{pmatrix}_s \right)$$

$$p_s^* = p_{cm}^* + \begin{pmatrix} -\frac{m_0}{m_T}s_{0x}+\frac{m_{07}}{m_T}h \\ s_{0y} \\ -\frac{m_0}{m_T}s_{0z} \end{pmatrix} + \begin{pmatrix} -c_1(c_2\alpha_2+s_{23}\delta_4)+s_1\delta_2-a_x\delta_6 \\ s_1(c_2\alpha_2+s_{23}\delta_4)+c_1\delta_2+a_y\delta_6 \\ -c_{23}\delta_4+s_2\alpha_2-a_z\delta_6 \end{pmatrix}_s$$

$$-\begin{pmatrix} c_1(c_2A_2+s_{23}D_4)-s_1D_2+a_xD_6 \\ s_1(c_2A_2+s_{23}D_4)+c_1D_2+a_yD_6 \\ e_{23}D_4-s_2A_2+a_zD_6 \end{pmatrix}_m - \frac{1}{m_T}\left(m_7^s \begin{pmatrix} -x_7 \\ y_7 \\ -z_7 \end{pmatrix}_s + m_7^m \begin{pmatrix} x_7 \\ y_7 \\ z_7 \end{pmatrix}_m \right)$$

The complete solution to the inertial forward kinematics requires the calculation of p_{cm}^* which may be found from:

$$\begin{pmatrix} p_{cmx}^* \\ p_{cmy}^* \\ p_{cmz}^* \end{pmatrix} = \begin{pmatrix} c_1(c_2A_2+s_{23}D_4)-s_1D_2+a_xD_6 \\ s_1(c_2A_2+s_{23}D_4)+c_1D_2+a_yD_6 \\ c_{23}D_4-s_2D_4+a_zD_6 \end{pmatrix}_m + \begin{pmatrix} -c_1(c_2A_2+s_{23}D_4)+s_1D_2-a_xD_6 \\ s_1(c_2A_2+s_{23}D_4)+c_1D_2+a_yD_6 \\ -c_{23}D_4+s_2A_2-a_zD_6 \end{pmatrix}_s$$

$$+\frac{1}{m_T}\left(m_7^m \begin{pmatrix} x_7^m \\ y_7^m \\ z_7^m \end{pmatrix} + m_7^s \begin{pmatrix} -x_7^s \\ y_7^s \\ -z_7^s \end{pmatrix} \right) + \begin{pmatrix} (1-\frac{m_0}{m_T})s_{0x} - \frac{m_{17}}{m_T}h \\ s_{0y} \\ (1-\frac{m_0}{m_T})s_{0z} \end{pmatrix} \qquad (6.20)$$

The inverse kinematics solution generates the joint angles $(\theta_1^m, \theta_2^m, \theta_3^m)$ for the master arm and $(\theta_1^s, \theta_2^s, \theta_3^s)$ for the slave arm respectively. These first 3 respective joint angles define the end effector positions for each arm. However, the kinematics of the two arms are now coupled and the equations must be solved simultaneously.

Let $\begin{pmatrix} X^m \\ Y^m \\ Z^m \end{pmatrix} = \begin{pmatrix} p_{mx}^* - p_{cmx}^* - \frac{m_0}{m_T}s_{0x} - \frac{m_{17}}{m_T}h + \frac{1}{m_T}(m_7^m x_7^m - m_7^s x_7^s) - a_x^m\delta_6 - a_x^s D_6 \\ p_{my}^* - p_{cmy}^* - s_{0y} + \frac{1}{m_T}(m_7^m y_7^m + m_7^s y_7^s) - a_y^m\delta_6 + a_y^s D_6 \\ p_{mz}^* - p_{cmz}^* - \frac{m_0}{m_T}s_{0z} + \frac{1}{m_T}(m_7^m z_7^m - m_7^s z_7^s) - a_z^m\delta_6 - a_z^m D_6 \end{pmatrix}$

$$\begin{pmatrix} X^s \\ Y^s \\ Z^s \end{pmatrix} = \begin{pmatrix} p_{sx}^* - p_{cmx}^* + \frac{m_0}{m_T}s_{0x} - \frac{m_{07}}{m_T}h + \frac{1}{m_T}(-m_7^s x_7^s + m_7^m x_7^m) + a_x^s\delta_6 + a_x^m D_6 \\ p_{sy}^* - p_{cmy}^* - s_{0y} + \frac{1}{m_T}(m_7^s y_7^s + m_7^m y_7^m) - a_y^s\delta_6 + a_y^m D_6 \\ p_{sz}^* - p_{cmz}^* + \frac{m_0}{m_T}s_{0z} + \frac{1}{m_T}(-m_7^s z_7^s + m_7^m z_7^m) + a_z^s\delta_6 + a_z^m D_6 \end{pmatrix}$$

Hence, $\begin{pmatrix} X^m \\ Y^m \\ Z^m \end{pmatrix} = \begin{pmatrix} c_1(c_2\alpha_2+s_{23}\delta_4)-s_1\delta_2 \\ s_1(c_2\alpha_2+s_{23}\delta_4)+c_1\delta_2 \\ c_{23}\delta_4-s_2\alpha_2 \end{pmatrix}_m - \begin{pmatrix} -c_1(c_2A_2+s_{23}D_4)+s_1D_2 \\ s_1(c_2A_2+s_{23}D_4)+c_1D_2 \\ -c_{23}D_4+s_2A_2 \end{pmatrix}_s$

$$\begin{pmatrix} X^s \\ Y^s \\ Z^s \end{pmatrix} = \begin{pmatrix} -c_1(c_2\alpha_2+s_{23}\delta_4)+s_1\delta_2 \\ s_1(c_2\alpha_2+s_{23}\delta_4)+c_1\delta_2 \\ -c_{23}\delta_4+s_2\alpha_2 \end{pmatrix}_s - \begin{pmatrix} c_1(c_2A_2+s_{23}D_4)-s_1D_2 \\ s_1(c_2A_2+s_{23}D_4)+c_1D_2 \\ c_{23}D_4-s_2A_2 \end{pmatrix}_m$$

These are 6 highly coupled nonlinear simultaneous equations in 6 unknowns $(\theta_1^m, \theta_2^m, \theta_3^m, \theta_1^s, \theta_2^s, \theta_3^s)$, so they may be solved numerically (eg. by Newton's method) to yield unique solutions. The two manipulator motions are coupled together such that it is not possible to control them independently without regard to each other. Note that to find the joint angles for the respective orienting wrists, terrestrial algorithms may applied to each arm independently due to the imposition of attitude control. As noted in Chapter 5 there are however, special cases whereby the motion of the slave arm is restricted by the motion of the master arm, eg. parallel copying motion, parallel symmetric motion and closed chain configurations. For these cases analytic solution are available.

A particularly relevant example of an analytic solution for a space freeflyer is the situation where the master arm grapples the satellite and remains fixed such that $(\theta_1^m, \theta_2^m, \theta_3^m)$ are specified and locked:

$$p_s^* = p_{cm}^* + \begin{pmatrix} -\frac{m_0}{m_T}s_{0x} + \frac{m_{07}}{m_T}h \\ s_{0y} \\ -\frac{m_0}{m_T}s_{0z} \end{pmatrix} - \frac{1}{m_T}\left(m_7^s \begin{pmatrix} -x_7 \\ y_7 \\ -z_7 \end{pmatrix}_s + m_7^m \begin{pmatrix} x_7 \\ y_7 \\ z_7 \end{pmatrix}_m \right)$$

$$+ \begin{pmatrix} -c_1(c_2\alpha_2 + s_{23}\delta_4) + s_1\delta_2 - a_x\delta_6 \\ s_1(c_2\alpha_2 + s_{23}\delta_4) + c_1\delta_2 + a_y\delta_6 \\ -c_{23}\delta_4 + s_2\alpha_2 - a_z\delta_6 \end{pmatrix}_s - \begin{pmatrix} c_1(c_2A_2 + s_{23}D_4) - s_1D_2 + a_xD_6 \\ s_1(c_2A_2 + s_{23}D_4) + c_1D_2 + a_yD_6 \\ c_{23}D_4 - s_2A_2 + a_zD_6 \end{pmatrix}_m$$

This gives the equation to be solved with known ($X^sY^sZ^s$) as:

$$\begin{pmatrix} X^s \\ Y^s \\ Z^s \end{pmatrix} = \begin{pmatrix} -c_1(c_2\alpha_2 + s_{23}\delta_4) + s_1\delta_2 \\ s_1(c_2\alpha_2 + s_{23}\delta_4) + c_1\delta_2 \\ -c_{23}\delta_4 + s_2\alpha_2 \end{pmatrix}_s$$

where $\begin{pmatrix} X^s \\ Y^s \\ Z^s \end{pmatrix} = \begin{pmatrix} p_{sx}^* - p_{cmx}^* + \frac{m_0}{m_T}s_{0x} - \frac{m_{07}}{m_T}h \\ p_{sy}^* - p_{cmy}^* - s_{0y} \\ p_{sz}^* - p_{cmz}^* + \frac{m_0}{m_T}s_{0z} \end{pmatrix} + \frac{1}{m_T}\left(m_7^s \begin{pmatrix} -x_7^s \\ y_7^s \\ -z_7^s \end{pmatrix} + m_7^m \begin{pmatrix} x_7^m \\ y_7^m \\ z_7^m \end{pmatrix} \right) + \begin{pmatrix} a_x\delta_6 \\ -a_y\delta_6 \\ a_z\delta_6 \end{pmatrix}$

$$+ \begin{pmatrix} c_1(c_2A_2 + s_{23}D_4) - s_1D_2 + a_xD_6 \\ s_1(c_2A_2 + s_{23}D_4) + c_1D_2 + a_yD_6 \\ c_{23}D_4 - s_2A_2 + a_zD_6 \end{pmatrix}_m$$

Unique solutions may be found for $(\theta_1^s, \theta_2^s, \theta_3^s)$ using the same inverse kinematics techniques as used for a single arm robot spacecraft:

$$\theta_1^s = \tan^{-1}\left(\frac{Y^s}{-X^s}\right) - \tan^{-1}\left(\frac{\delta_2}{\pm\sqrt{(-X^s)^2 + (Y^s)^2 - \delta_2^2}}\right)$$

$$\theta_2^s = \tan^{-1}\left(\frac{A}{-Z^s}\right) - \tan^{-1}\left(\frac{B}{\pm\sqrt{A^2 + (-Z^s)^2 - B^2}}\right) \quad \text{where } A = -c_1X^s + s_1Y^s$$

$$B = \frac{A^2 + (-Z^s)^2 + \alpha_2^2 - \delta_4^2}{2\alpha_2}$$

$$\theta_3^s = \left[\tan^{-1}\left(\frac{A - \alpha_2c_2}{-Z^s + \alpha_2s_2}\right)\right] - \theta_2^s$$

The solutions to the wrist angles proceed directly from the terrestrial manipulator algorithms.

6.3.2 Dual Arm Velocity Kinematics:

Using the same techniques as before, for the inertial velocity of each arm l where l=2:

$$v_l^* = \dot{p}_l^* = \dot{r}_{c0} + \sum_{i=1}^{n} \dot{R}_i^l l_i^l \tag{6.21}$$

Now, $\dot{r}_{c0} = -\frac{1}{m_T}\sum_{l=1}^{2}\sum_{i=1}^{n+1}\sum_{j=i}^{n+1} m_j^l \dot{r}_{ci}^l$ since $\dot{p}_{cm}^*$=0 due to the invariance of the system centre of mass.

Now, $\dot{r}_{ci} = \dot{R}_i r_i + \dot{R}_{i-1} s_{i-1}$ and $l_i = r_i + s_i$:

$$\dot{r}_{c0} = -\frac{1}{m_T}\sum_{l=1}^{2}\sum_{i=1}^{n+1}\sum_{j=i}^{n+1} m_j^l(\dot{R}_i^l r_i^l + \dot{R}_{i-1}^l s_{i-1}^l)$$

Now, substitute into (6.21):

$$v_l^* = \sum_{i=1}^{n} \dot{R}_i^l l_i^l - \frac{1}{m_T}\sum_{l=1}^{2}\sum_{i=1}^{n+1}\sum_{j=i}^{n+1} m_j^l(\dot{R}_i^l r_i^l + \dot{R}_{i-1}^l s_{i-1}^l)$$

$$= \left\{ \sum_{i=1}^{n} \sum_{k=0}^{i} \frac{\partial \mathcal{R}_i^l}{\partial \theta_k} (r_i^l + s_i^l) - \frac{1}{m_T} \sum_{l=1}^{n} \sum_{i=1}^{n+1} \sum_{j=i}^{n+1} m_j^l \left(\sum_{k=1}^{i} \frac{\partial \mathcal{R}_i^l}{\partial \theta_k} r_i^l + \sum_{k=1}^{i-1} \frac{\partial \mathcal{R}_{i-1}^l}{\partial \theta_k} s_{i-1}^l \right) \right\} \dot{\theta}_i$$

This has the form $v_l^* = \bar{J}^l \dot{\theta}_i^l$ with:

$$\bar{J}^l = \sum_{i=1}^{n} \sum_{k=0}^{i} \frac{\partial \mathcal{R}_i^l}{\partial \theta_k} (r_i^l + s_i^l) - \frac{1}{m_T} \sum_{l=1}^{2} \sum_{i=1}^{n+1} \sum_{j=i}^{n+1} m_j^l \left(\sum_{k=1}^{i-1} \frac{\partial \mathcal{R}_{i-1}^l}{\partial \theta_k} r_{i-1}^l + \sum_{k=1}^{i-1} \frac{\partial \mathcal{R}_{i-1}^l}{\partial \theta_k} s_{i-1}^l \right) - \frac{1}{m_T} \sum_{l=1}^{2} \sum_{i=1}^{n+1} \sum_{k=1}^{i} m_i^l \frac{\partial \mathcal{R}_i^l}{\partial \theta_k} r_i^l$$

Now, with $\frac{\partial \mathcal{R}_0}{\partial \theta_k} = 0$ for an attitude controlled mounting platform:

$$\bar{J}^l = \sum_{i=1}^{n} \sum_{k=0}^{i} \frac{\partial \mathcal{R}_i^l}{\partial \theta_k} (r_i^l + s_i^l) - \frac{1}{m_T} \sum_{l=1}^{2} \sum_{i=2}^{n+1} \sum_{j=i}^{n+1} m_j^l \left(\sum_{k=1}^{i-1} \frac{\partial \mathcal{R}_{i-1}^l}{\partial \theta_k} r_{i-1}^l + \sum_{k=1}^{i-1} \frac{\partial \mathcal{R}_{i-1}^l}{\partial \theta_k} s_{i-1}^l \right) - \frac{1}{m_T} \sum_{l=1}^{2} \sum_{i=1}^{n+1} \sum_{k=1}^{i} m_i^l \frac{\partial \mathcal{R}_i^l}{\partial \theta_k} r_i^l$$

$$- \frac{1}{m_T} \sum_{i=1}^{n+1} \sum_{k=1}^{i} m_i \frac{\partial \mathcal{R}_0}{\partial \theta_k} (r_0 + s_0)$$

$$= \sum_{i=1}^{n} \sum_{k=0}^{i} \frac{\partial \mathcal{R}_i^l}{\partial \theta_k} (r_i^l + s_i^l) - \frac{1}{m_T} \sum_{l=1}^{2} \sum_{i=1}^{n+1} \sum_{j=i+1}^{n+1} m_j^l \left(\sum_{k=1}^{i} \frac{\partial \mathcal{R}_i^l}{\partial \theta_k} r_i^l + \sum_{k=1}^{i} \frac{\partial \mathcal{R}_i^l}{\partial \theta_k} s_i^l \right) - \frac{1}{m_T} \sum_{l=1}^{2} \sum_{i=1}^{n+1} \sum_{k=1}^{i} m_i^l \frac{\partial \mathcal{R}_i^l}{\partial \theta_k} r_i^l$$

Now, with $\frac{\partial \mathcal{R}_{n+1}^l}{\partial \theta_k} = 0$ as the payload is invariant with respect to the end effector:

$$\bar{J}^l = \sum_{i=1}^{n} \sum_{k=0}^{i} \frac{\partial \mathcal{R}_i^l}{\partial \theta_k} (r_i^l + s_i^l) - \frac{1}{m_T} \sum_{l=1}^{2} \sum_{i=1}^{n} \sum_{j=i+1}^{n+1} m_j^l \left(\sum_{k=1}^{i} \frac{\partial \mathcal{R}_i^l}{\partial \theta_k} r_i^l + \sum_{k=1}^{i} \frac{\partial \mathcal{R}_i^l}{\partial \theta_k} s_i^l \right) - \frac{1}{m_T} \sum_{l=1}^{2} \sum_{i=1}^{n} \sum_{k=1}^{i} m_i^l \frac{\partial \mathcal{R}_i^l}{\partial \theta_k} r_i^l$$

$$- \frac{1}{m_T} \sum_{l=1}^{2} m_{n+1}^l \sum_{k=1}^{n+1} \frac{\partial \mathcal{R}_{n+1}^l}{\partial \theta_k} r_{n+1}^l$$

This may now be decomposed into the respective arm contributions l and l':

$$\bar{J}^l = \sum_{i=1}^{n} \sum_{k=1}^{i} \frac{\partial \mathcal{R}_i^l}{\partial \theta_k} \left(1 - \frac{1}{m_T} \sum_{i=1}^{n} \sum_{j=i+1}^{n+1} m_j^l (r_i^l + s_i^l) - \frac{1}{m_T} m_i^l r_i^l \right) - \sum_{i=1}^{n} \sum_{k=1}^{i} \frac{\partial \mathcal{R}_i^{l'}}{\partial \theta_k} \left(\frac{1}{m_T} \sum_{j=i+1}^{n+1} m_j^{l'} (r_i^{l'} + s_i^{l'}) + \frac{1}{m_T} m_i^{l'} r_i^{l'} \right)$$

Hence, $\bar{J}^l = \sum_{i=1}^{n} \sum_{k=1}^{i} \frac{\partial \mathcal{R}_i^l}{\partial \theta_k} \lambda_i - \sum_{i=1}^{n} \sum_{k=1}^{i} \frac{\partial \mathcal{R}_i^{l'}}{\partial \theta_k} L_i$ where $\lambda_i = \left(\frac{1}{m_T} \left[\sum_{i=1}^{n} \sum_{j=0}^{i} m_j^l l_i^l + m_{1n+1}^l - m_i^l r_i^l \right] \right)$

$$L_i = \left(\frac{1}{m_T} \left[\sum_{j=i+1}^{n+1} m_j^{l'} l_i^{l'} + m_i^{l'} r_i^{l'} \right] \right) \qquad (6.22)$$

Note that this formulation is applicable to dissimilar arms.

An equivalent derivation is given now for the cross product Jacobian with an illustrative example from the PUMA 560/600. From the cross product method for deriving the Jacobian matrix, we can calculate the Jacobian matrices of the respective manipulators for a dual arm configuration mounted onto a platform, ie. l=2 arms:

$$v_l^* = v_0 + \sum_{i=1}^{n} (z_{i-1}^l \times l_i^l) \dot{\theta}_i^l$$

$$w_l^* = \sum_{i=1}^{n} z_{i-1}^l \dot{\theta}_i^l$$

Now, $\dot{r}_{c0} = -\frac{1}{m_T} \sum_{l=1}^{2} \sum_{i=1}^{n+1} m_i^l \dot{p}_{ci}^l$ and $\dot{p}_{ci}^l = v_{ci}^l = \sum_{k=1}^{i} v_k^l + w_i^l \times (-s_i^l) = \sum_{k=1}^{i} v_{k-1}^l + w_i^l \times r_i^l$:

$$\dot{r}_{c0} = v_0 = -\frac{1}{m_T} \sum_{l=1}^{2} \sum_{i=1}^{n+1} m_i^l \left(\sum_{k=1}^{i} v_{k-1}^l + w_i^l \times r_i^l \right) = -\frac{1}{m_T} \sum_{l=1}^{2} \sum_{i=1}^{n+1} \left(\sum_{i=j}^{n+1} m_j^l v_{i-1}^l + m_i^l (w_i^l \times r_i^l) \right)$$

Now, $v_i^l = \sum_{k=1}^{i} (z_{k-1}^l \times l_k^l) \dot{\theta}_k^l$:

$$v_0 = -\frac{1}{m_T}\sum_{l=1}^{2}\sum_{i=1}^{n+1}\left(\sum_{i=j}^{n+1} m_j^l \sum_{i=1}^{n-1}(z_{i-1}^l \times l_i^l)\dot{\theta}_i^l + m_i\left(\sum_{i=1}^{n} z_{i-1}^l \times r_i^l\right)\dot{\theta}_i^l\right)$$

$$= -\frac{1}{m_T}\sum_{l=1}^{2}\sum_{i=1}^{n+1}\left(\sum_{j=i+1}^{n+1} m_j^l \sum_{i=1}^{n}(z_{i-1}^l \times l_i^l)\dot{\theta}_i^l + m_i^l(z_{i-1}^l \times r_i^l)\dot{\theta}_i^l\right)$$

Substitute:

$$v_l^* = \sum_{i=1}^{n}(z_{i-1}^l \times l_i^l)\dot{\theta}_i^l - \frac{1}{m_T}\sum_{l=1}^{2}\sum_{i=1}^{n+1}\left[\sum_{j=i+1}^{n+1} m_j^l \sum_{i=1}^{n}(z_{i-1}^l \times l_i^l)\dot{\theta}_i^l + m_i^l(z_{i-1}^l \times r_i^l)\dot{\theta}_i^l\right]$$

Now, the payload is invariant with respect to the end effector such that $\dot{\theta}_{n+1}^{l} = 0$:

$$v_i^* = \sum_{i=1}^{n}(z_{i-1}^l \times l_i^l)\dot{\theta}_i^l - \frac{1}{m_T}\sum_{l=1}^{2}\sum_{i=1}^{n}\left[\sum_{j=i+1}^{n+1} m_j^l(z_{i-1}^l \times l_i^l) + m_i^l(z_{i-1}^l \times r_i^l)\right]\dot{\theta}_i^l - \frac{m_{n+1}}{m_T}(z_n^l \times r_{n+1}^l)\dot{\theta}_{n+1}^{l}$$

Separating the expression into its two separate arm contributions l and l':

$$v_l^* = \sum_{i=1}^{n}\left[\left(1 - \frac{1}{m_T}\sum_{i=1}^{n}\sum_{j=i+1}^{n+1} m_j^l\right)(z_{i-1}^l \times l_i^l) - \left(\frac{m_i^l}{m_T}\right)(z_{i-1}^l \times r_i^l)\right]\dot{\theta}_i^l$$

$$-\frac{1}{m_T}\sum_{i=1}^{n}\left[\left(\sum_{j=i+1}^{n+1} m_j^l(z_{i-1}^l \times l_i^l) + m_i^l(z_{i-1}^l \times r_i^l)\right)\dot{\theta}_i^l\right]$$

$$= \sum_{i=1}^{n}[(z_{i-1}^l \times \lambda_i) - (z_{i-1}^l \times L_i)]\dot{\theta}_i^l \quad \text{where} \quad \lambda_i = \frac{1}{m_T}\sum_{i=1}^{n}\sum_{j=0}^{i}(m_j^l l_i^l - m_i^l r_i^l)$$

$$L_i = \frac{1}{m_T}\sum_{j=i+1}^{n+1}(m_j^l l_i^l + m_i^l r_i^l)$$

Hence, the dual configuration manipulator: $\bar{J}^l = \sum_{i=1}^{n}\left((z_{i-1}^l \times \lambda_i) - (z_{i-1}^l \times L_i)\right)$

Example: For the PUMA 560/600 configuration of dual manipulators related by the H-matrix the following extended Jacobian elements may be derived.

Master Arm Jacobian:

$$\bar{J}_{11}^{m} = \{-s_1[\delta_6(c_{23}c_4s_5 + s_{23}c_5) + s_{23}\delta_4 + \alpha_2c_2] - c_1(s_4s_5\delta_6 + \delta_2)\}_m$$
$$+\{-s_1[D_6(c_{23}c_4s_5 + s_{23}c_5) + s_{23}D_4 + A_2c_2] - c_1(s_4s_5D_6 + D_2)\}_s$$

$$\bar{J}_{12}^{m} = \{c_1[\delta_6(c_{23}c_4s_5 + s_{23}c_5) + s_{23}\delta_4 + \alpha_2c_2] - s_1(s_4s_5\delta_6 + \delta_2)\}_m$$
$$-\{c_1[D_6(c_{23}c_4s_5 + s_{23}c_5) + s_{23}D_4 + A_2c_2] - s_1(s_4s_5D_6 + D_2)\}_s$$

$$\bar{J}_{13}^{m} = 0; \bar{J}_{14}^{m} = 0; \bar{J}_{15}^{m} = 0; \bar{J}_{16}^{m} = 1$$

$$\bar{J}_{21}^{m} = \{c_1(s_4s_5\delta_6 + \delta_2)\}_m + \{c_1(s_4s_5D_6 + D_2)\}_s$$

$$\bar{J}_{22}^{m} = \{s_1(s_4s_5\delta_6 + \delta_2)\}_m - \{s_1(s_4s_5D_6 + D_2)\}_s$$

$$\bar{J}_{23}^{m} = \{-s_1[s_{23}c_4s_5\delta_6 - c_{23}(c_5\delta_6 + \delta_4) + \alpha_2s_2] - c_1[c_{23}c_4s_5\delta_6 + s_{23}(c_5\delta_6 + \delta_4) + \alpha_2c_2]\}_m$$
$$+\{-s_1[s_{23}c_4s_5D_6 - c_{23}(c_5D_6 + D_4) + A_2s_2] - c_1[c_{23}c_4s_5D_6 + s_{23}(c_5D_6 + D_4) + A_2c_2]\}_s$$

$$\bar{J}_{24}^{m} = \{-s_1\}_m; \bar{J}_{25}^{m} = \{c_1\}_m; \bar{J}_{26}^{m} = 0$$

$$\bar{J}_{31}^{m} = \{c_1s_4s_5\delta_6\}_m + \{c_1s_4s_5D_6\}_s$$

$$\bar{J}_{32}^{m} = \{s_1s_4s_5\delta_6\}_m - \{s_1s_4s_5D_6\}_s$$

$$\bar{J}^{m}_{33} = \{-s_1[s_3c_4s_5\delta_6 - c_3(c_5\delta_6 + \delta_4)] - c_1[c_3c_4s_5\delta_6 + s_3(\delta_4 + c_5\delta_6)]\}_m$$
$$+\{-s_1[s_3c_4s_5D_6 - c_3(c_5D_6 + D_4)] - c_1[c_3c_4s_5D_6 + s_3(D_4 + c_5D_6)]\}_s$$

$$\bar{J}^{m}_{34} = \{-s_1\}_m; \bar{J}^{m}_{35} = \{c_1\}_m; \bar{J}^{m}_{36} = 0$$

$$\bar{J}^{m}_{41} = \{s_1s_{23}(\delta_6c_5 + \delta_4) - \delta_6c_{23}s_4s_5\}_m + \{s_1s_{23}(D_6c_5 + D_4) - D_6c_{23}s_4s_5\}_s$$

$$\bar{J}^{m}_{42} = \{\delta_6c_{23}c_4s_5 - c_1s_{23}(\delta_6c_5 + \delta_4)\}_m - \{D_6c_{23}c_4s_5 - c_1s_{23}(D_6c_5 + D_4)\}_s$$

$$\bar{J}^{m}_{43} = \{\delta_6s_{23}(c_1s_4s_5 - s_1c_4s_5)\}_m + \{D_6s_{23}(c_1s_4s_5 - s_1c_4s_5)\}_s$$

$$\bar{J}_{44} = \{c_1s_{23}\}_m; \bar{J}^{m}_{45} = \{s_1s_{23}\}_m; \bar{J}^{m}_{46} = \{c_{23}\}_m$$

$$\bar{J}^{m}_{51} = \{s_{23}s_4c_5\delta_6\}_m + \{s_{23}s_4c_5D_6\}_s$$

$$\bar{J}^{m}_{52} = \{s_{23}s_4s_5\delta_6\}_m - \{s_{23}s_4s_5D_6\}_s$$

$$\bar{J}^{m}_{53} = \{\delta_6[c_5(c_1c_{23}s_4 + s_1c_4) + s_5(s_1c_{23}s_4 - c_1c_4)]\}_m$$
$$+\{D_6[c_5(c_1c_{23}s_4 + s_1c_4) + s_5(s_1c_{23}s_4 - c_1c_4)]\}_s$$

$$\bar{J}^{m}_{54} = \{-(c_1c_{23}s_4 + s_1c_4)\}_m; \bar{J}^{m}_{55} = \{c_1c_4 - s_1c_{23}s_4\}_m; \bar{J}^{m}_{56} = \{s_{23}s_4\}_m$$

$$\bar{J}^{m}_{61} = \{\delta_6[s_1(c_{23}c_4s_5 + c_5s_{23}) + c_1s_4s_5]\}_m + \{D_6[s_1(c_{23}c_4s_5 + c_5s_{23}) + c_1s_4s_5]\}_s$$

$$\bar{J}^{m}_{62} = \{-\delta_6[c_1(c_{23}c_4s_5 + s_{23}c_5) - s_1s_4s_5]\}_m - \{-D_6[c_1(c_{23}c_4s_5 + s_{23}c_5) - s_1s_4s_5]\}_s$$

$$\bar{J}^{m}_{63} = 0; \bar{J}^{m}_{64} = \{c_1(c_{23}c_4s_5 + s_{23}c_5) - s_1s_4s_5\}_m; \bar{J}^{m}_{65} = \{s_1(c_{23}c_4s_5 + s_{23}c_5) + c_1s_4s_5\}_m;$$

$$\bar{J}^{m}_{66} = \{-s_{23}c_4s_5 + c_{23}c_5\}_m$$

Slave Arm Jacobian:

$$\bar{J}^{s}_{11} = \{-s_1[\delta_6(c_{23}c_4s_5 + s_{23}\delta_4 + \alpha_2c_2] - c_1(s_4s_5\delta_6 + \delta_2)\}_s$$
$$+\{-s_1[D_6(c_{23}c_4s_5 + s_{23}c_5) + s_{23}D_4 + A_2c_2] - c_1(s_4s_5D_6 + D_2)\}_m$$

$$\bar{J}^{s}_{12} = \{c_1[\delta_6(c_{23}c_4s_5 + s_{23}c_5 + s_{23}\delta_4 + \alpha_2c_2] - s_1(s_4s_5\delta_6 + \delta_2)\}_s$$
$$-\{c_1[D_6(c_{23}c_4s_5 + s_{23}c_5 + s_{23}D_4 + A_2c_2] - s_1(s_4s_5D_6 + D_2)\}_m$$

$$\bar{J}^{s}_{13} = 0; \bar{J}^{s}_{14} = 0; \bar{J}^{s}_{15} = 0; \bar{J}^{s}_{16} = 1$$

$$\bar{J}^{s}_{21} = \{c_1(s_4s_5\delta_6 + \delta_2)\}_s + \{c_1(s_4s_5D_6 + D_2)\}_m$$

$$\bar{J}^{s}_{22} = \{s_1(s_4s_5\delta_6 + \delta_2)\}_s - \{s_1(s_4s_5D_6 + D_2)\}_m$$

$$\bar{J}^{s}_{23} = \{-s_1[s_{23}c_4s_5\delta_6 - c_{23}(c_5\delta_6 + \delta_4) + \alpha_2s_2] - c_1[c_{23}c_4s_5\delta_6 + s_{23}(c_5\delta_6 + \delta_4) + \alpha_2c_2]\}_s$$
$$+\{-s_1[s_{23}c_4s_5D_6 - c_{23}(c_5D_6 + D_4) + A_2s_2] - c_1[c_{23}c_4s_5D_6 + s_{23}(c_5D_6 + D_4) + A_2c_2]\}_m$$

$$\bar{J}^{s}_{24} = \{-s_1\}_s; \bar{J}^{s}_{25} = \{c_1\}_s; \bar{J}^{s}_{26} = 0$$

$$\bar{J}^{s}_{31} = \{c_1s_4s_5\delta_6\}_s + \{c_1s_4s_5D_6\}_m$$

$$\bar{J}^{s}_{32} = \{s_1s_4s_5\delta_6\}_s - \{s_1s_4s_5D_6\}_m$$

$$\bar{J}^{s}_{33} = \{-s_1[s_3c_4s_5\delta_6 - c_3(c_5\delta_6 + \delta_4)] - c_1[c_3c_4s_5\delta_6 + s_3(\delta_4 + c_5\delta_6)]\}_s$$
$$+\{-s_1[s_3c_4s_5D_6 - c_3(c_5D_6 + D_4)] - c_1[c_3c_4s_5D_6 + s_3(D_4 + c_5D_6)]\}_m$$

$$\bar{J}^{s}_{34} = \{-s_1\}_s; \bar{J}^{s}_{35} = \{c_1\}_s; \bar{J}^{s}_{36} = 0$$

$$\bar{J}^{s}_{41} = \{s_1 s_{23}(\delta_6 c_5 + \delta_4) - \delta_6 c_{23} s_4 s_5\}_s + \{s_1 s_{23}(D_6 c_5 + D_4) - D_6 c_{23} s_4 s_5\}_m$$

$$\bar{J}^{s}_{42} = \{\delta_6 c_{23} c_4 s_5 - c_1 s_{23}(\delta_6 c_5 + \delta_4)\}_s - \{D_6 c_{23} c_4 s_5 - c_1 s_{23}(D_6 c_5 + D_4)\}_m$$

$$\bar{J}^{s}_{43} = \{\delta_6 s_{23}(c_1 s_4 s_5 - s_1 c_4 s_5)\}_s + \{D_6 s_{23}(c_1 s_4 s_5 - s_1 c_4 s_5)\}_m$$

$$\bar{J}^{s}_{44} = \{c_1 s_{23}\}_s; \bar{J}^{s}_{45} = \{s_1 s_{23}\}_s; \bar{J}^{s}_{46} = \{c_{23}\}_s$$

$$\bar{J}^{s}_{51} = \{s_{23} s_4 c_5 \delta_6\}_s + \{s_{23} s_4 c_5 D_6\}_m$$

$$\bar{J}^{s}_{52} = \{s_{23} s_4 s_5 \delta_6\}_s - \{s_{23} s_4 s_5 D_6\}_m$$

$$\bar{J}^{s}_{53} = \{\delta_6 [c_5(c_1 c_{23} s_4 + s_1 c_4) + s_5(s_1 c_{23} s_4 - c_1 c_4)]\}_s$$
$$+ \{D_6 [c_5(c_1 c_{23} s_4 + s_1 c_4) + s_5(s_1 c_{23} s_4 - c_1 c_4)]\}_m$$

$$\bar{J}^{s}_{54} = \{-(c_1 c_{23} s_4 + s_1 c_4)\}_s$$

$$\bar{J}^{s}_{55} = \{c_1 c_4 - s_1 c_{23} s_4\}_s$$

$$\bar{J}^{s}_{56} = \{s_{23} s_4\}_s$$

$$\bar{J}^{s}_{61} = \{\delta_6 [s_1(c_{23} c_4 s_5 + c_5 s_{23}) + c_1 s_4 s_5]\}_s + \{D_6 [s_1(c_{23} c_4 s_5 + c_5 s_{23}) + c_1 s_4 s_5]\}_m$$

$$\bar{J}^{s}_{62} = \{-\delta_6 [c_1(c_{23} c_4 s_5 + c_5 s_{23}) - s_1 s_4 s_5]\}_s - \{-D_6 [c_1(c_{23} c_4 s_5 + c_5 s_{23}) - s_1 s_4 s_5]\}_m$$

$$\bar{J}^{s}_{63} = 0; \bar{J}^{s}_{64} = \{c_1(c_{23} c_4 s_5 + s_{23} c_5) + c_1 s_4 s_5\}_s; \bar{J}^{s}_{65} = \{s_1(c_{23} c_4 s_5 + s_{23} c_5) + c_1 s_4 s_5\}_s;$$

$$\bar{J}^{s}_{66} = \{-s_{23} c_4 s_5 + c_{23} c_5\}_s$$

6.3.3 Dual Arm Dynamic Feedforward Compensation

The dual manipulator case does not vary much from the single manipulator case since the reaction forces are merely summed at the mounting platform. Similarly if more than two manipulators are mounted. Indeed, this makes the procedure very flexible so that it may be applied to any mechanism (such as deployable arrays, extendable booms, gimballed sensors and antenna) which may be operational on the spacecraft. Such mechanisms may be treated (if they are rigid bodies) using robotics techniques such as the Newton-Euler recursive method to calculate the reaction forces and moments that they exert on the mounting spacecraft which may then be compensated by the dynamically feeding them forward to the attitude controller. For the dual arm case:

$$N_0^l = \sum_{i=1}^{n} N_{ci}^l - \sum_{i=1}^{n+1} m_i^l p_{ci}^l \times \ddot{r}_{c0}$$

Now, $$N_{SUM} = \sum_{l=1}^{2} N_0^l = \sum_{l=1}^{2} \left(\sum_{i=1}^{n} N_{ci}^l - \sum_{i=1}^{n+1} m_i^l p_{ci}^l \times \ddot{r}_{c0} \right)$$

Now, $$p_{cm}^* = \frac{1}{m_T} \sum_{l=1}^{2} \sum_{i=0}^{n+1} m_i^l p_{ci}^{*l} = \frac{1}{m_T} \sum_{l=1}^{2} \left(\sum_{i=0}^{n+1} m_i^l r_{c0}^l + \sum_{i=1}^{n+1} m_i^l s_0^l + \sum_{i=1}^{n+1} m_i^l p_{ci}^l \right)$$

$$= r_{c0} + \frac{1}{m_T} \left[\sum_{l=1}^{2} \left(m_{1n+1}^l s_0^l + \sum_{i=1}^{n+1} m_i^l p_{ci}^l \right) \right] \qquad \text{where} \quad m_T = m_0 + \sum_{l=1}^{2} \sum_{i=1}^{n+1} m_i^l$$

Hence, $$\sum_{l=1}^{2} \sum_{i=1}^{n+1} m_i^l p_{ci}^l = m_T (p_{cm}^* - r_{c0}) - \sum_{l=1}^{2} m_{1n+1}^l s_0^l$$

Substitute: $$N_{SUM} = \sum_{l=1}^{2} \left(\sum_{i=1}^{n} N_{ci}^l - [m_T (p_{cm}^* - r_{c0}) - m_{1n+1}^l s_0^l] \times \ddot{r}_{c0} \right)$$

Similarly, $F_0^l = -\left(\frac{m_0}{m_T}\right)\sum_{i=1}^{n} F_{ci}^l$, $F_{SUM} = -\left(\frac{m_0}{m_T}\right)\sum_{l=1}^{2}\sum_{i=1}^{n} F_{ci}^l$ and $\ddot{r}_{c0} = -\left(\frac{1}{m_T}\right)\sum_{l=1}^{2}\sum_{i=1}^{n} F_{ci}^l$.

The sum of moments about the centre of mass of the mounting spacecraft to be compensated by the attitude control system:

$$N_r = N_{SUM} + \sum_{l=1}^{2} s_0^l \times F_0^l$$

$$= \sum_{l=1}^{2}\left(\sum_{i=1}^{n} N_{ci}^l - \left[m_T(p_{cm}^* - r_{c0}) - (m_{1n+1}^l s_0^l)\right] \times -\frac{1}{m_T}\sum_{i-1}^{n} F_{ci}^l + s_0^l \times -\left(\frac{m_0}{m_T}\right)\sum_{i}^{n} F_{ci}^l\right)$$

$$= \sum_{l=1}^{2}\left(\sum_{i=1}^{n} N_{ci}^l + \left[p_{cm}^* - r_{c0} - s_0^l\right] \times \sum_{i=1}^{n} F_{ci}^l\right) \qquad (6.23)$$

Notice that this formulation may easily be generalised to more than two manipulators and that if l=1 it is consistent with the single arm formulation.

6.4 SUMMARY

The decoupling of orientation and translation effects in the robotic spacecraft system trades off vast amounts of complexity with little loss of flexibility - for this reason the author refers to this methodology as the "engineering" approach as opposed to a strictly mathematical approach. We have seen that the motion of the manipulator(s) will generate reaction forces and moments on the spacecraft platform at the spacecraft/manipulator coupling point(s). This will induce translational and rotational motion of the spacecraft platform in response to the manipulator movements. If no compensation is made for this effect, the robot end effector will miss its target. Feedforward thruster control introduces an unacceptable propulsive fuel overhead. The alternative solution in the literature involves the use of the generalised Jacobian and the inherent redundancy of the system does not permit closed form solutions to the inverse position kinematics problem. The generalised Jacobian has a high complexity of $O(n^2)$ imposing a major computational burden on the limited processing capability of space-rated microprocessors (currently of the 8086 class). Furthermore, the generalised Jacobian suffers from dynamic singularities in the manipulator workspace and these singularities are not unique kinematic functions but are dependent on the dynamic properties of the system and are thereby unpredictable. This is a serious limitation. The approach adopted here was to decouple the translation and rotation components of the kinematics and dynamics of the system. The system utilises a dedicated attitude control system to which the reaction moments on the spacecraft are fed forward for online compensation. The robot control system for the manipulator accounts for the translation effect of reaction forces by incorporating dynamic terms into the kinematic control algorithms as "lumped" parameters. The additional complexity of the formulation is small and utilises standard control methodologies for both spacecraft attitude and robotic manipulator control with small modifications. It has also been demonstrated that inertial control of position in space yields different joint requirements than for base control of position on Earth. Furthermore the formulation is readily extended to the dual manipulator case.

Finally, the methodology outlined is applicable generally to all spacecraft deployment mechanisms such as boom deployment and antenna deployment (barring flexibility). Coriolis forces are generated during boom deployment as the boom moves relative to the body axes and reaction moments imposed on the spacecraft may be compensated

by the feedforward compensation technique. Hence given that the dynamic properties of the deployable are known the techniques introduced in this chapter are generally applicable to all space-based actuation and deployment/pointing.

Chapter 7

SPACE SYSTEMS OVERVIEW

Consideration is now given to a potential dual manipulator robotic freeflying space robot dedicated to satellite servicing (ATLAS). Such a manipulator system may be designed around the control system outlined in the last chapter. The starting point is to assess the mission goals and constraints to generate the functional requirements to define the system and subsystems required to meet those goals within the constraints of the control system. The spacecraft configuration as a whole is dominated by the requirements of the mission payload, the selection of the launch vehicle and the mode of attitude stabilisation of which the payload is the most significant driver.

Mission Statement: Because in-orbit failures have an increasing impact on the efficiency and cost of Earth-orbiting spacecraft operations there is a need for an effective system to cope with these failures.

Primary Objectives:

(i) To detect, identify and characterise the major types of spacecraft in-orbit failures and repair those failures in near real-time at profit.

(ii) To develop a safe and effective space infastructure support system for future missions.

Secondary Objectives:

(i) To demonstrate the feasibility and actuality of large scale space debris removal.

(ii) To provide support for Space Station operations at profit or with equity.

(iii) **Hidden Agenda:** To provide a focus for Information Technology research and development in the UK and demonstrate an effective partnership between long-term government investment and short term private commercial exploitation.

Mission Characterisation:

Alternative mission concepts: In-orbit servicing by EVA astronauts from the US Space Shuttle - this is costly, hazardous and suffers from scheduling difficulties as well as being limited in orbital parameters (ie. near equatorial LEO only with $i=28.5^{o}$ and $e=0$).

Hidden Agenda: As the continuing US manned space programme is justified primarily through its in-orbit servicing capabilities it is important that the proposed system is not seen as a threat to this justification. Political negotations with NASA should be undertaken to reach an equitable arrangement without jeopardising their marketing strategy, eg. the proposed system should be Shuttle RMS compatible as a bolt-on capability to extend aid to EVA astronauts for complex in-orbit servicing in equatorial LEO and/or the system should also operate independently outside of near equatorial LEO.

Mission Architecture:

Mission orbit - testbed LEO between 200-1200km altitude at near equatorial or high inclination (polar orbit)

- evolution to a small fleet to cover GEO and other Earth applications orbits
- variable orbital requirements, variable eclipse, variable thermal environments
- variable thrusting, ie. liquid propellant

Mission attitude - variable attitude slewing with high pointing accuracy, ie. 3 axis stabilisation
- flexible solar paddles stowed during manipulation
- high stiffness structure without booms

Mission reliability - hardened electronics with distributed and functionally redundant computers
- debris protection
- distributed processing between ground and spacecraft
- evolution towards autonomy
- modular design with self repair capabilities
- logistic resupply of fuel tanks

Ground operations - minimal ground personnel for teleoperation and support in single Earth station
- extensive use of expert systems on the ground
- limited ground visibility
- TDRSS/EDRS communications link to support multiple video data rates

Mission duration - 15-20y with resupply of consumables and upgraded modules

Payload - EVA equivalence requires two 6 degree of freedom arms with a reach >1m
- extensive sensor suite including vision and tactile capabilities

Design budgets - total loaded mass ~1.5 tonnes
- manipulation peak power by regenerative fuel cells
- sufficient fuel for delta-v orbit changes over 200-1000km several times

The proposed dual-arm robotic freeflyer ATLAS (Advanced TeLerobotic Actuation System) has as its primary objective the maintenance, servicing and repair of Earth applications satellites or other satellites. Its secondary objectives are to provide assistance to astronauts both in EVA and in retrieval and rescue of spacecraft and to provide a means for large scale debris removal. A spacecraft comprises of two basic elements: the mission payload and the spacecraft bus. The payload performs the mission function while the spacecraft bus supports the payload and provides housekeeping. Typically the payload mass comprises from ~15% to 50% of the spacecraft dry mass. The payload classifies the satellite and drives the design of the spacecraft bus: the basic payload of the communications satellite is the active repeater/transponder and such satellites tend to reside in the 24h circular geosynchronous orbit at 36,000km altitude or in the highly eccentric 12h Molniya orbit inclined at 63.4^{o} where perigee rotation is nullified allowing a fixed latitude apogee for ground coverage; the basic payload of the meteorological satellite is the high resolution visual/infrared radiometer and such satellites may reside in high inclination LEO or in GEO; the basic payload of the Earth observation satellite is the multispectral scanner and such satellites reside in near polar sun-synchronous orbits between ~700-1200km altitude for a repeating ground track with orbit plane precession of 1^{o}/day to match the Earth's revolution around the Sun; the basic payload of the astronomical satellite is the imaging telescope and such satellites tend to reside in high altitude highly eccentric orbits ~800-1400km above the Earth's atmosphere. All these satellites except the astronomical satellite are Earth-oriented. Usually satellites are designed for a single specific purpose but multimission satellites are not unknown: INSAT-1 of ISRO (Indian Space Research Organisation) is an example which was launched in 1982 for

telecommunications and meteorological observation. Its payload comprised 12 C-band transponders for long distance telephone communication, 2 C-band transponders for TV broadcast, a very high resolution radiometer (VHRR) with visible/infrared sensitivity and a data channel for relaying meteorological, hydrological and oceanographic data to unmanned ground stations. It was three-axis stabilised providing a field of view to deep space for the radiative cooler of the Earth-pointing VHRR, sun-pointing for the solar arrays and Earth-pointing for the communications antenna [Agrawal 1980].

ATLAS also has a multifunctional role. It comprises many elements from more traditional spacecraft: optical and infrared imaging sensors (including star trackers) similar to those used on Earth observation and astronomical satellites, a high data rate communications antenna similar to those on telecommunications satellites, and possibly microwave tracking pulse radar similar to those used on Earth observation satellites. However it is characterised by very complex operational requirements typical of some military satelllites and resembling the variable operational environments like some interplanetary spacecraft. Indeed only interplanetary spacecraft to date have been exposed to such multiple design criteria. There are other similarities regarding mode of operation: real-time ground control versus autonomous onboard control. Only 12% of spacecraft launches are scientific exploratory probes or manned missions so such criteria are unusual in spacecraft missions generally. The majority of space missions are Earth-oriented applications tools which do not exhibit complex requirements. ATLAS is essentially a trade off between human, technical, financial and political risk. It reduces the human risk by minimising EVA requirements for in-orbit servicing. The high technical risk may be reduced by using off-the-shelf technologies and no new major terrestrial technological innovations are required for its implementation. The financial risk may be offset by launch and in-orbit insurance. Political risk is minimised since the political motive is process-oriented (ie. technology R&D) rather than results oriented. In the first instance it is a spacecraft which may be required to perform orbital transfers of payloads and equipment such as an OTV/OMV between limited orbits (Orbit Transfer/Maneouvering Vehicle). The ATLAS payload comprises of its dual manipulators and robotic support subsystems. This drives its size, its mass, its power and fuel requirements. The spacecraft bus should be modular to enable multiple payload capabilities to enhance future spacecraft operational flexibility by providing multi-orbit multi-attitude capabilities to a basic spacecraft bus. It should be designed for operations in all orbit from LEO to GEO and from equatorial to polar orbits so a single spacecraft design can serve in all Earth-applications orbits. Hence due consideration must be given to the variable environments that the spacecraft will experience.

7.1 SPACECRAFT SIZING

The first concern is that of size - the operational Space Shuttle RMS has a capability for large payloads up to 30 tonnes but has limited repeatability and dexterity. This suggests that servicing should involve a smaller sized manipulator about the same size as the human arm to replace or augment EVA operations. Assembly has been found to involve ~80% of small part (<4 kg) manipulation [Nevins & Whitney 1980], so it is likely that assembly of small objects forms a major part of the servicing process. Furthermore there has been a recent tendency for some space missions to become smaller, simpler and less costly. It provides a complementary approach to missions

which are getting larger, more complex and more expensive. The evolution of increasing complexity and size is well characterised by the evolution of GEO comsats which since SYNCOM in 1963 have been increasing in size and complexity. The spin stabilised Intelsat 1 launched in 1965 had a mass of 38kg with a power output of 40W and bandwidth of 50MHz compared with the three-axis stabilised Intelsat 5 launched in 1980 with a mass of 970kg and a power output of 1200W and bandwidth of 2300MHz. More powerful high directional antennas, increased use of spacecraft onboard processing, longer mission lifetimes and tighter tolerances on attitude and orbital drift have been responsible for this to allow increased simplicity of fixed ground based receivers for lower costs to the customer. This trend is likely to continue: the US National Satellite System is due for launch in 2000 AD and has a mass of 2 tonnes, a 32 Gbps transmission capability and a projected lifetime of 15-20y. However the same drive to lower costs and smaller ground receivers is also a key component in the trend to mobile communications by LEO smallsat constellations. Smallsats are most suited to specialised activities such as mobile communications, small scale space science, well focussed quick-response Earth observation and in-orbit technology demonstration. The UK's Space Technology Research Vehicle (STRV) is a minisatellite for in-orbit technology demonstration. They offer short design timescales ~12-18 months, low costs <$1M, low launch mass <200kg and small design teams. Small teams imply minimum bureaucracy and streamlined management structures which can cut development costs by ~40% - a useful lesson for any space project. Microsatellites exploit miniaturisation of electronic components, emplace all complexity in software and employ redundancy in only critical systems of limited reliability such as the control system and input-output devices. Operations can be supported from a user's PC as the ground station. Examples include the highly successful UoSAT series designed by the UK's Surrey Satellite Technology and the OSCAR series designed by AMSAT for radio amateurs. The major requirement for ATLAS is EVA equivalence and this dictates human-level capabilities. This offers the advantage of relatively low mass and lower costs and according to the US DoD's classification would not rank as a "major" mission (less than $1B costs).

The next question concerns the orbit at which ATLAS may reside. Equatorial LEO at altitudes less than 500km is accessible to astronauts and will be the orbit of the proposed Space Station at ~700km altitude which is likely to require extensive robotic support. Motorola is proposing its Iridium network constellation of 77 lightsats (<1000 kg) in LEO at 700-1100 km altitudes to provide 100% coverage of a worldwide personal handheld pocket sized cordless phone service by 2000 AD. LEO operation for comsats require several satellites in constellation for real time continuous coverage but LEO offers lower link attenuation (~15-20 dB) and so allows smaller user units. This will enable calls to and from anywhere in the world by satellite and create a truly "global village". This is a major step from the conventional GEO satellite system which essentially serves the existing communications network infrastructure in relaying international telephone calls and direct broadcast TV. The approach to user-oriented from network oriented services is truly global and offers telecommunications services to areas which have low density traffic and to maritime and aeronautical environments. INMARSAT's Project 21 (ie. 21st century) however is expected to utilise a mixture of such LEO systems with ever larger and more powerful GEO satellites. Hence GEO is another potential orbital regime that may benefit from robotic support as it is inaccessible to astronauts (it also poses a significant radiation

environment). High altitude equatorial orbit is favoured by science payloads which represent high cost, limited life payloads which may significantly benefit from servicing, replenishment and upgrading. The present emphasis on "Mission to Planet Earth" programmes for high inclination LEO remote sensing satellites favours operation in polar LEO. As the Eastern Test Range at Vandenburg AFB will not support Shuttle operations this orbit is inaccessible to astronauts. Near equatorial LEO operation would also serve as a testbed for any further proposals for operation of similar spacecraft in GEO or polar LEO. Hence, at the outset, the freeflyer should be designed to operate in all orbital environments but the initial test unit should serve in near equatorial LEO in support of Space Station activities though not necessarily exclusively. A major consideration that must be attended to is the projected long lifetime of the 15-20y operational period and the reliability of onboard equipment and systems. The effects of radiation, thermal vacuum and other environmental phenomena have a detrimental impact on survivability.

7.2 ROBOTIC PAYLOAD

The robot servicer subsystems constitute the payload of the spacecraft. The primary aim of the ATLAS freeflyer robot payload is to eliminate or at least reduce the requirement for EVA in-orbit servicing by providing general purpose Earth orbital operations (deployment, maintenance, repair and retrieval of spacecraft). This implies the replacement of the in situ human astronaut with an Earth based human teleoperator for EVA equivalence (perhaps evolving autonomy over time). Schenker (1988) and Elfving (1990) both stipulated that space robots for in-orbit servicing must exhibit EVA equivalence. This requirement presupposes two approximately human dimensioned arms side mounted onto the platform. The two arms offer greater efficiency in task execution than a single arm, generate larger workspaces and increase the number of configuration possibilities [Grossman et al 1985]. This is particularly critical in space since fixtures and jigs are not available in the highly demanding zero-g environment. The standard task for space robotics is generally considered to be the ORU (orbital replacement unit) exchange. There are certain tasks that cannot be performed by a single arm by virtue of their natures. Legged motion along truss structures requires two arms for a freeflyer. Handling of extended and flexible objects requires two arm manipulation. For instance a basic requirement is the need to cut through thermal insulation to get to components. Satellite grappling also implies the necessity of using dual arms since two arms can provide up to 2-5 times the force-torque capability of a single arm [Bruhm 1987]. Indeed two may be regarded as the absolute minimum number of arms required for parallel and co-ordinated task execution. Side mounting generates larger workspaces than overhead mounting, better manoeuvrability, ease of stowage and anthropomorphic configuration [Hemami 1985, 1986]. A modified Zambesi bridge configuration would eliminate the problems of inter-arm collision. For two arm control several modes of operation are possible providing great flexibility of operation [Bruhm 1987]:

(i) single arm function - in this function the second arm may be used as a stabiliser or a leg by attaching the spacecraft to the worksite;

(ii) co-ordinated arm function - parallel execution of similar multiple tasks to reduce the task completion time;

(iii) simultaneous co-operative or auxiliary actions on a single task - examples include the rigid transfer of extended or flexible objects (closed chain configuration).

In 1988 the UKAEA under contract to the DTI as part of the Advanced Robotics Initiative studied the feasibility of developing space robotic sysytems. They considered three separate systems:
(a) Internal Experiment Manipulator for use within a space station environment (this has now seen development as ESA's EMATS);
(b) Local External Manipulator fixed externally to a space station (such as RMS-derived manipulators);
(c) Satellite Servicing Vehicle (SSV) with a mobile (freeflying) capability.
They highlighted the SSV as being considerably more sophisticated than the other proposals in that it possessed two specific properties of complexity: the variable platform reference and its bi-arm dexterity. Both have been considered in this thesis. Schenker (1988) devised an evolutionary programme of task capabilities for such a concept:
(i) stationary multi-arm function for simple satellite servicing tasks;
(ii) mobile multi-arm function for simple servicing tasks (eg. grappling);
(iii) mobile multi-arm function for complex servicing tasks (eg. ORU exchange);
(iv) mobile multi-arm function for unplanned repair involving fabrication (eg. thermal blanket handling).

A symmetric control scheme should be used rather than a master/slave configuration to provide operational flexibility allowing role exchange between the arms and provide for simpler operation, eg. panel removal, tool replacement, camera positioning. Hence the two arms should have similar dimensions, masses and structures to retain symmetry. Furthermore each manipulator should be 6 degree of freedom revolute jointed structures. Revolute joints offer larger workspaces and higher flexibility of operation over prismatic joints which exhibit large inertias from the slide and require higher motive power. The prismatic structure also has a tendency to interfere with the workspace. Since the freeflyer system all ready possesses 6 degrees of freedom through the platform translation and rotation, 6 degree of freedom manipulators are sufficient. The adoption of 7 degree of freedom arms merely adds unnecessary mass to the spacecraft with no improvement in functional performance.

The baseline rendezvous operation is taken to occur from below and behind the target so the workspace must extend both in front and above the spacecraft bus mount (up being defined as the vector opposed to the thrust vector). The baseline servicing task is the ORU exchange of standard modules for logistic resupply and inspection activities. Over time the learning curve may allow more sophisticated capabilities to be included in the manipulation inventory such as construction and assembly and thermal blanket handling. Like BIAS, ATLAS should be compatible with the Shuttle RMS as a smart front end so it should incorporate a grapple fixture on the upper torso opposite to direction of the workspace. A carousel mounted between the lower propulsion system assembly and the upper main torso housing provides a dynamic tool rack for easy access. If the upper assembly is also rotatable this provides an additional degree of freedom to the system enhancing its flexibility. To provide a telerobotic capability, sensing and actuation is required with man-machine interfaces to the human operator on the ground. Force feedback and stereo vision should be supported for the human operator, ie. bilateral force reflecting hand controllers and virtual reality representation of visual information.

Following Deptovich & Houghton (1989) a design process methodology has been adopted based on robot task definition and requirements. A set of suitable performance requirements have been derived based on the functional requirements of peak torques/forces, velocities, etc and workspace. On the basis of these performance requirements the manipulator criteria may be defined. The primary task requirement centres around the assembly process. The control system should be part of an integrated architecture of sensors and actuators. The design parameters selected for ATLAS are in agreement with other analyses performed particularly ESA's BIAS system [Andre et al 1990].

Position repeatability: 0.1mm
0.1°.

Payload capability: 250kg (maximum ORU mass)

Workspace reach radius: 1.2m/1 mm resolution

Maximum end effector velocity: 1m/s (1 mm/s resolution)
30°/s (1°/s resolution)

Force/torque capability: 100N (0.5 N resolution)
100Nm (1Nm resolution)

Arm stiffness: $2x10^5$ N/m (double the lateral stiffness of the remote centre compliance device)

Power requirement: 500W peak

The inclusion of power tools would provide a force /torque capability exceeding that of the ATLAS general purpose end effector and such tools may be useful for capture operations of large satellites with the manipulator arms adopting degrees of limpness/stiffness. The system should also carry a basic tool set of power tools designed to cope with the majority of servicing tasks that are likely to be encountered and augment any force limitations of the servicer. The primary task is the ORU exchange. Much of it could be automated with the human operator providing supervisory control and dealing with more difficult tasks such as the need to cut through thermal insulation to get to components. If the manipulator arms are stiffened ATLAS may use its onboard control moment gyro attitude control system to passivate the target on capture. The inclusion of a telescopic stabiliser with an EVA handhold gripper would provide a docking fixture to allow the use of both arms for all parallel tasks. The stabiliser should be more robust than the arms with higher stiffness and force/torque capabilities ~1kN/1kNm. This would provide the ability to withstand large reaction forces from the target particularly during force control. An additional telescopic capability for the arms may extend the arm extension to near 2m by lengthening the upper and lower arm links would increase its operational capabilities but compliance could become a problem. All robotic spacecraft are fundamentally mechatronic systems which sense and respond to their environments, ie. they are integrated sensor-effector-information processing systems.

7.2.1 Sensing Subsystem:

Teleoperation incorporating a man in the control loop requires a suite of sensors for sensor feedback. Sensing enables tasks to be performed in the presence of environmental uncertainty and sensory feedback provides information for coping with that uncertainty. Such sensors should be smart with dedicated onboard processing to buffer and compress information to reduce the requirement for data rate transmission. The most important sensor is the visual imaging system. This requires closed circuit TV cameras with pan, tilt and zoom capability - CCD cameras offer better fidelity than

vidicon cameras. Vision also requires active illumination as there is little ambient lighting. For real time tracking of a dynamically changing environment, 30 frames/s are required. Typical resolution is 512x512 pixels. Two black and white cameras are superior to a single colour camera. The Lunar Rover camera had a mass of 4kg and colour CCD cameras are available with masses of less than 1kg (excluding actuator drives) although typically they are ~10-30kg including drives. The baseline chosen here is 8kg. Two stereoscopic vision cameras with illumination mounted between the arms provides a general vision capability. Each wrist should also have camera mounts with lighting units for close work. An overhead panoramic camera with a lighting unit on an extendible boom could provide an overall workspace view at different angles. Vision processing involves low level feature extraction (segmentation, edge detection, edge clustering and chain coding) which may be implemented as hardware using special purpose pipelined processing for real-time operation to aid the human operator. Low level processing can provide the information necessary on centroids, principle moments of inertia, perimeter and area of the outlined object. Low level processing allows the use of reactive control by the robot control system. CAD database models as a source of geometric information should be available to ATLAS to enable it to perform pattern recognition by template matching and to the human operator. Distance information can be derived from the stereoscopic cameras through triangulation and this could be combined redundantly with a laser radar range finder to ease the registration problem characteristic of stereovision.

Microwave radar is well established for rendezvous and docking operations in space and offer accuracies ~3m and are well suited to highly reflective metal objects. They offer the ability for coarse target acquisition and tracking. The laser rangefinder offers greater accuracy but shorter ranges. A CO_2 laser radar requires ~50-150W of power. Radar ranges for noncooperative targets (without beacons) are typically ~70 km for microwave and ~20 km for optical signals [Korf 1982]. Radar is not included in the baseline design as stereoscopic vision provides range finding for docking distances without the additional incurrred mass penalties of rangefinder radar. For closer distances proximity detectors may be used at the end effector and pressure pads for tactile information. Proximity sensors are usually light sources and photocells between the fingers of the end effector. Tactile sensors at the fingers (possibly at the elbows and distributed over the gripper itself) are usually doped silicone rubber skins whose conductance changes with pressure. A resolution of 250 points/cm^2 are available. Compliance is an absolutely essential requirement for effective manipulation. Six degree of freedom force/torque sensors may be implemented at the wrist as piezoelectric transducers with a range of 0.5-300N. Position and velocity sensors at the joints provide proprioceptive internal servocontrol information.

7.2.2 Actuation Subsystem:

Joining tasks require at least two manipulators unless a jig is available. Each manipulator has six degrees of freedom with revolute joints as a minimum for complete workspace reachability as the spacecraft offers redundant degrees of freedom of translation and attitude. The end effector should comprise of exchangeable general purpose three-fingered grasping hands and a suite of special purpose tools. The end effector should use snare wires to close the end effector evenly for soft grappling. All exchangeable components are stored in the carousel storage racks. An additional standardised ball and socket mechanism may be advantageous for docking with the

target spacecraft as a separate specialised telescopic stabiliser arm to maintain the ATLAS platform in a rigid attitude with respect to the target. The manipulator links should be constructed from carbon composite for high stiffness and strength in a truss patterned structure to minimise mass with impact protection rubber and insulated with multilayer thermal blankets to protect the interior wiring and motors. The ratio of Young's modulus to density for graphite is 7.2 compared with that of Ti with 2.45. The ROTEX manipulator was constructed in this way with grid-like carbon fibre links each of 0.2kg. Brushless direct drive dc electric motors for each joint would eliminate the need for gearing and pulleys as well as offering high torques. The joint structure should be constructed from Ti alloy for high strength. ROTEX used Ti motors of mass 1 kg. DC direct drive motors may be used with the following characteristics (similar to the direct drive robot motor): link 1 motor of 6 kg has a diameter of 50cm and a 200Nm torque capability; link 2 and 3 motors of 4kg mass have a diameter of 30 cm with 140 Nm capability; the 3 wrist motors of 3 kg have diameters of 20cm with 50Nm capabilities. Each link has the following lengths: d_2=0.25m, a_2=d_4=0.5m and d_6=0.2m+ (dependent on the tool or end effector - the remote centre compliance has a length of 0.2m while the HST power tool has a length of 0.3m). The motors contribute most to the link mass. With Ti motors and carbon fibre truss links and thermal insulation an additional 30% above motor mass is added so that link 1 has a mass of 8kg, links 2 and 3 have a mass of 6kg and the wrist has a mass of 12kg. The end effector is projected to have a mass of 6kg most of which is supplied by a 4kg 30cm diameter motor to apply over 100N applied force. These figures are consistent with the ≤2kg EVA HST power tool applied torques and the Japanese Space Station Module Arm capabilities. Inclusion of the remote centre compliance adds a negligible mass at 0.45kg. Because the joints cannot be thermally controlled through insulation alone, resistance heaters may be incorporated at the interior of each joint and inside the end effector to maintain sufficiently high temperatures for operation of the lubricant. The joint torques required should be ~100Nm.

7.2.3 Control System & Man-Machine Interface:

The man-machine interface connects the operator on the ground to the sensors and the manipulators. As a minimum the interface includes graphic displays for sensor data, stereoscopic visual imaging and a bilateral force reflecting joystick for controlling the manipulator. Sensors must also be pointed in the desired direction automatically by default with supervisory override. To cope with the time delays ~0.5s due to the GEO round trip predictive graphics are required which may be updated with sensory feedback to avoid move-and-wait strategies. The addition of speech recognition and auditory feedback would provide an additional modality for the interface. Overall control is shared between the human operator, ground-based expert systems and the spacecraft onboard processors. Low level control including the formulations outlined for dynamic control of the manipulator up to trajectory generation level which should be implemented by the spacecraft. Task planning and other higher level functions may be implemented on the ground and shared between the human and the AI systems.

The robot control system will require dedicated processors for each arm plus a higher level processor for co-ordination functions totalling a capability ~10 MIPS. The best computational architecture for various spacecraft and robotic functions are based around a distributed set of dedicated microprocessors for each subsystem or function. Each arm also has its own decentralised controller with which to perform dynamic

hybrid position/force control functions. Dedicated processors have the advantage of localisation of software changes, simple interfaces and error isolation. Transputers offer ~10 MIPS and with on-chip RAM disabled offer ~50 krad radiation hardness. This is sufficient for LEO which is characterised by ~1 krad/y environment but probably not sufficient for other orbits such as GEO. The currently space-rated microprocessor is the ESA MA31750 8086 16-bit processor based on silicon-on-sapphire technology. It offers ~1-3 MIPS processing power with a radiation hardness of 500 krad in a mass of 20kg and power requirement of 50W. Bubble memories offer robust performance. Their lack of flexibility can be overcome by using the shared central processors for dynamic resource allocation. A centralised spacecraft bus processor co-ordinates spacecraft bus functions and a co-ordinating centralised robot processor provides for manipulator arm co-ordination particularly in the closed chain configuration. Both centralised processors communicate with each other through an overall spacecraft wide processor (a hierarchical architecture). Such a hardware architecture is compatible with the NASREM software architecture which is distributed between the spacecraft and the ground. This is based on the hierarchical/distributed control architecture paradigm. All electronic systems require shielding from radiation, temperature extremes, mechanical shocks and vibration. Fault avoidance through the use of highly reliable components should be augmented with fault tolerance through protective redundancy from component to subsystem level. Three processors offers functional redundancy. The implementation of computation through software rather than hardware allows reprogrammability.

Around 25% of NASA's manpower is devoted to ground support and computing for ground support imposing heavy costs. The ATLAS system must support an evolutionary framework of the gradual adoption of spacecraft automation to reduce mission support costs. This implies the need for the implementation of robust artificial intelligence techniques for reliable autonomy. The boundary between autonomy and teleoperation is vague with many different degrees of supervisory control (telerobotics) in between. ATLAS provides excellent suitability to this evolutionary trend from teleoperation to autonomy through computer aided telerobotics by virtue of the task environment. It possesses a degree of structure yet it is subject to changeability. The communications link is also short so that the shared control can be implemented within a tight control loop. Machine intelligence requires large processing and memory capabilities so these functions would be implemented on the ground with their greater resources. Autonomy requires task level software to convert goal specifications into robot level commands. For this the planner requires a description of the objects to be manipulated, the present state of the environment, the desired state of the environment and procedures on how to achieve goals. Central to this capability is a world model which must provide geometric knowledge and dynamic knowledge of the objects involved (eg. from CAD/CAM models) and a simulation of the succession of environmental states between the initial and the goal situation in which the task is completed. Finally it must also monitor the plan execution and react to changes. These techniques are particularly applicable to repetitive and well characterised tasks such as ORU exchange. Telepresence should be the approach for more complex operations such as thermal blanket handling.

The following parameters have been adapted from the BIAS arm servicer unit to suit the ATLAS robot servicer [Andre et al 1990] - cf. Voyager 2 scientific instrument payload of 105 kg:

		MASS (kg)	POWER (W).
MANIPULATOR SYSTEM			
	Link 1:	8	50
	Link 2:	6	50
	Link 3:	6	50
	Wrist:	12	90
	End effector:	8	
	Subtotal:	40	250
	Dual arms:	80	500
PAYLOAD SUPPORT SYSTEM			
	MA31750 (x3):	20	50
	Offline memory	15	
	Camera (x5):	8	30
	(illumination)+ (drive)		30
	Subtotal	115	450
TOOL KIT of 10 items of 5kg		50	
TOTAL		245	950

7.3 SPACECRAFT BUS DESIGN BUDGET

There are three major budgets for a spacecraft [Wertz & Larson 1991]: the propellant budget, the power budget and the mass budget. There is usually a tradeoff between these budgets for any Earth applications programme though the attitude control system is particularly important in determining the spacecraft configuration and complexity. ATLAS adds the orbit control system to this trade off for its requirement for variable orbits and this introduces an extremely demanding set of requirements. The difficulties and complexity of decisions in determining the possibilities have not previously been appreciated in studies for similar systems such as the cancelled FTS. It was assumed rather glibly that the Space Station could be used as a warehouse for fuel, power raising and hardware thereby solving the problems of logistics. Furthermore the cost of transporting such items on a regular basis to the Space Station and usage of Space Station assets were not considered. Since ATLAS is a stand-alone system all these considerations must be explicitly examined. Most workers to date have considered the dynamic control problem due to the coupling of the spacecraft platform to the robot manipulators to be the major stumbling block to the realisation of a robotic freeflyer, eg. Andre et al (1990). This particular problem is tackled in the thesis as its central thrust but it appears in retrospect that the system design and spacecraft budgets may be just as difficult to resolve.

The propellant budget is determined by the delta-v requirement plus a 25% margin (10% margin, 10% contingency and 5% off-nominal performance and trapped residual fuel overhead):

Propellant mass, $m_p = m_i\left(1 - e^{-\Delta v/gI_{sp}}\right)$ where m_i=initial spacecraft mass

Δv=maneouvring requirement

g=acceleration due to gravity=9.8m/s^2.

I_{sp}=specific impulse

Typically the dry-to-propellant mass varies from 2:1 to 7:1. The power budget is determined by the payload and spacecraft by energy requirements plus a 5-25% margin. For large spacecraft this will exceed 500W and is usually apportioned: payload ~40-80%; propulsion ~0-5%; guidance, navigation and control ~5-40%; communications including telemetry, tracking and command ~5-50%; thermal control ~0-5%; power system ~5-25%; structure ~0%. The mass budget comprises the payload mass, the spacecraft bus dry mass, and the propellant mass, plus a margin of 4% and 2% for electrical and mechanical integration respectively and a 10% miscellaneous margin for design growth. The spacecraft dry mass comprises: propulsion system mass ~0.1 m_p; guidance, navigation and control mass ~65+0.022(m_i-700); mass of communication system; thermal control system mass ~0.02m_i, structural mass ~0.09m_i; and mass of the power system plus a 25% margin.

The mission may be regarded as having two modes: the dormant mode and the operational mode. The spacecraft mission is divided into three phases:
(i) launch and early orbit checkout;
(ii) operational phase - elliptical transfer orbit
- manipulation task in operational orbit
(iii) dormant phase - housekeeping or other assigned duties
The design approach adopted here is a conventional approach. Interfaces which provide functional boundaries joining separate subsystems across which energy, matter or information are transmitted are critical. Standardisation allows interdependability and cost savings. The packaging of all subsystems should provide good access for self-servicing and self-repair and maintain proximity between functional interfaces without interference.
The spacecraft bus can be divided into 6 subsystems:
(i) attitude control subsystem
(ii) propulsion subsystem
(iii) electric power subsystem
(iv) thermal control subsystem
(v) structural subsystem
(vi) telemetry, command and communications subsystem

7.3.1 Propulsion Subsystem

The initial assumption is that ATLAS has been placed into the required orbital family by the launcher and/or by dedicated kick motors. The propulsion subsystem injects the spacecraft into the desired orbit and maintains the orbital parameters within the required limits by providing thrust. ATLAS must employ a dedicated propulsion system to perform two-burn Hohmann transfers and rendezvous with targets. The manipulator arms must grapple each target and the attitude control system must passivate the complete system. ATLAS requires fuel storage and rocket engine thrusters to expel the fuel. Electric propulsion consumes a significant fraction of the spacecraft power and relates to power plant mass by $m_p = \alpha P$ where $P = \frac{1}{2}\dot{m}v_{ex}^2$ and α=specific power density=20 kg/kW. High power requirements usually imply either very large solar arrays which are undesirable during slewing maneouvres or the adoption of nuclear sources which are politically undesirable. Hence, as power may be regarded as a scarce resource the propulsion system for ATLAS will be conventional liquid bipropellant fuel-oxidiser for multiple thrusts. Resistance heaters which increase the enthalpy of combustion impose a 5% power requirement during thrusting. The

propulsion system comprises the lower section of the spacecraft. A single translational thruster provides the delta-v capability. The spherical propellant fuel tanks are mounted symmetrically around the lower assembly and are detachable for refuelling. The total mass of the propulsion system includes propellant, tankage, propellant feed lines and thrusters. Tankage and feed lines are the heaviest components other than the propellant itself and usually comprises ~10% of the propellant mass. Mounting hardware comprises ~20% of the mass of the propulsion system mass. For intercept and rendezvous a guidance radar is usually required but GPS could provide a backup system for the baseline spacecraft adopting stereovision. A two way 1000 km transfer between 200 km and 1200 km allows access to LEO spacecraft and HEO scientific spacecraft and this is the most demanding manoeuvre that ATLAS may be required to perform as dedicated spacecraft for polar orbital rendezvous and GEO rendezvous require only a very narrow range of altitudes. This two way manoeuvre requires $\Delta v = 1.06$ km/s. One such transfer plus a 50% margin implies a delta-v of 1.59 km/s. Hence ATLAS will need to be refuelled either incrementally through piggy-back launches of fuel tanks for every worst-case operation (smaller transfer changes will reduce the required refuelling rate). Further, by remaining in the target orbit after operation completion and making transfers between operational orbits, this further reduces the refuelling rate.

Total fuel fraction, $\frac{m_p}{m_i} = 1 - e^{-\Delta v / g I_{sp}}$ where $\Delta v = 1.59$ km/s

I_{sp}=425s for hydrazine resistojet systems

$\rightarrow \frac{m_p}{m_i} = 0.317$

The total spacecraft mass is 1.5 tonnes so the propellant mass is 475.6 kg allowing 1024.4 kg of useful equipment. This is a high propellant fraction of ~46.4%.

7.3.2 Attitude Control Subsystem

The attitude control subsystem maintains the spacecraft attitude in space particularly for pointing requirements. It requires sensors for attitude measurement, actuators to effect changes of attitude and a control system. Three axis stabilisation is the only viable attitude control mode using control moment gyro actuators (CMG) since reaction wheels are limited to <11 Nm torques and magnetorquers for momentum desaturation. Sensors include Earth and Sun sensors for coarse attitude determination and star sensors for accurate attitude determination in conjunction with gyroscopes. The Earth sensor is not strictly necessary for ATLAS. Star sensors may include filters to enable utilisation as sun sensors. Directional antennas, solar arrays and the robotic payload sensors all require gimballing. The antenna and the robotic sensors require two axis gimballing while the solar array requires only one axis of freedom with the orientational axis being provided by body attitude for sun tracking. Slewing and feedforward compensation of manipulator movements are the dominant requirements.

	mass (kg)	RPM (10^3)	Ang Mom Capy (Nms)	Max Output Torque (Nm)	Max gimbal rate (°/s)	Size Power Req (W)
Bendix DGCMG	253	4-12	1400-4000	237	5-30	1.1m diam
Skylab DGCMG	200	-	-	500	-	15-30W (standby) 0.2W/Nm (torque)

Fig 7.1 Typical double gimbal control moment gyroscopes

Torque $\tau = \frac{1}{2}\frac{w^2 I}{\theta}$ provides an attitude change of angle θ where w=angular velocity. Reaction wheel size is determined by the amount of angular momentum to be absorbed but the CMG size is determined by its torque capability $\tau = h \times w$ where h=angular momentum, w=angular rate limited by the gimbal drive ~2 rad/s usually [Heimel & Schultz 1985].

The mass of a reaction wheel including housing and control electronics is given by:
$m = 3.2h^{0.4}$ (kg) where $h = I_w w_w$ (Nms), w_W=wheel angular velocity, I_W=wheel inertia [Dougherty, Lebstock & Rodden 1971, Huddleston 1991].

The rotor mass of a CMG may be chosen optimally with the required reaction torques, rotor speed, moment of inertia and gimbal ring radii [Heimel & Schultz 1985]:
Rotor mass $m = \frac{2I_w}{r_a^2 + r_i^2}$ where $I_w = \frac{h}{w_w}$

r_i, r_a=inner/outer gimbal ring radii

Peak power required by motor depends on peak torque: $P_{max}(W) = 38\,\tau_{max}$

The average maximum torque exerted by a CMG is 500Nm. Typically m>40 kg with a power requirement of ~90-150W for such torques. Usually the total power includes 10% losses due to friction, etc.

	Mass (kg)	Power (W)
Earth sensor	2-3.5	2-10
Sun sensor	0.2-2	0-3
Magnetometer	0.2-1.5	0.2-1
Gyroscope	0.8-3.5	5-200
Star sensor	5-7	2-20
Processors	5-25	5-25
Reaction wheel	5+0.1xh	300W/Nm
CMG	35+0.05xh	0.1 W/Nm
Single axis actuators	4+0.03xtau	3W/Nm

Fig 7.2 Typical onboard attitude control component properties

The Honeywell GG1320 ring laser gyro package of 3 laser gyros and 3 accelerometers (the 150x125mm Miniaturised Inertial Measurement Unit) has a mass of 2.5kg and a power requirement of 25W. A strapdown system requires in addition a star tracker and other scanners which are available at 500g. The attitude control system will utilise two gimballed star trackers which may also be used as sun sensors with filters, 2 CMG's for functional redundancy and 3 magnetometers. A typical onboard spacecraft computer has 150 kword memory (with a 25% margin) and a 400kbps processor speed (with a 30% margin). The computational power is limited as only the 8086 processor is space qualified. The MA31750A (MAS281) computer is an 8086 CMOS/SOS architecture with 1.5μ feature sizes offering 3MIPS and 128k ROM and a maskable 48k ROM with 8087 or 6800 coprocessors. It has 1Mrad radiation hardness for a 10y life in GEO. Its mass is 20kg and has a 50W power requirement. A 10^9 bit magnetic bubble memory offers offline storage in a mass of 12kg. The Raytheon fault tolerant computer offers 0.25 MIPS and 600 kbyte memory in a package of 23kg mass and a power requirement of 25W. The SARDS (Spacecraft Attitude Real-time Determination System) is a multiprocessor distributed architecture of MIMO design with 16-bit CPU's arranged as 6 microprocessor boards with 8 coprocessors each in a 50.3x48.3x18.0cm box for recursive Kalman filtering which can be performed on just 3 of the processors [Gary 1987].

7.3.3 Electric Power Subsystem

The electric power subsystem provides and regulates the energy raising for all spacecraft functions. It comprises a power source, power storage and power conversion units. ERS-1 (Earth Resources Satellite) was ESA's Earth Observation flagship for oceanic observation launched into a sun-synchronous slightly retrograde polar orbit (i=98.5^o) in 1991 at a mean altitude of 785 km with a design lifetime of 2y. It was the first European spacecraft to use active microwave devices for Earth observation. Such microwave techniques had only been used for very short missions such as Seacat in 1987 which operated for only 90 days - a massive electrical short circuit destroyed its operational capability. ERS-1's major payload, the Active Microwave Instrument operated in two modes: the SAR (synthetic aperture radar) mode with 30m resolution and the wind scatterometer mode to measure oceanic wind velocity. The SAR mode required 4.8kW of power but the spacecraft solar arrays could supply only 1.8kW. ERS-1 however used 3kW of battery power to supplement thae array power to operate the SAR for short durations ~10 minutes per orbit with battery recharging during sunlit periods of non-usage. This is the general approach adopted here.

The power system uses solar arrays and batteries to cope with nominal dormant loads. Typical housekeeping requires ~150W. Operational loads are handled by nonregenerative or regenerative fuel cells (with electrolyser at 60% efficiency). Fuel cells have an operational life of 10,000h with a specific power of 0.5kW/kg when run at ~kW power levels. Shuttle fuel cells have power outputs of 12kW. The operational lifetime of 10,000h gives over a year's continuous operation. Peak loads are expected to last less than 10d at a time offering a potential for up to 40 operational peak loads. Conventional cells have a specific mass of 35g/W while lightweight cells have a specific mass of 15g/W. The solar array is flexible and retractable for deployment during nominal dormant phases so lightweight cells are used. Solar array areal power densities are typically 0.007m^2/W. Power budget needs to account for degradation of solar arrays from beginning of life (BOL) to end of life (EOL).

Nominal power (dormant) =500 kW

Peak power (operational)=2.0 kW

Beginning of life power, $P_{BOL} = \frac{P_{EOL}}{(1-L_d)\cos\theta(1-T_e)}$ where L_d=degradation=0.22

T_e=operating temperature=0.08

θ=sun off angle=0

This gives a P_{BOL}=P_{EOL}/0.72=695.5 W

End of life power $P_{EOL} = P_{LOAD} + \frac{C_B \times V}{15h}$ where V=array voltage=1.2C_B.

This gives P_{EOL} of 500.05W. A planar array panel has a power output in proportion to its projection area to the Sun.

Array area, $A_a = \frac{P_{BOL}}{\eta \times S}$ where η=efficiency ~18% for GaAs

S=solar constant=1351 W/m^2.

For an EOL power output of 500W, array area is 2.86m^2. Two symmetric arrays of 1.43m^2 may be implemented as square arrays 1.2m on a side. Array mass $m_a = \frac{P}{\alpha}$ where α=specific performance which varies from 70W/kg at BOL to 15-45W/kg (usually 25W/kg) at EOL due to degradation from high energy particles. The German ultralow mass panel offers a specific power of 45W/kg (almost the same specific power of muscle at 50W/kg). Each panel has a mass of 6.3kg with a power output of 280W. If α=70W/kg then m_a=0.07P_{BOL}. Equivalently for 500W of EOL power

m_a=9.9kg. The adoption of deployable flexible arrays was favoured over stiffened arrays due to mass considerations. The Aristoteles mission to generate models of the Earth's gravitational and magnetic fields by remote sensing adopted the opposite approach. It required orbit raising maneouvres between mission phases. All solar arrays and booms are stiffened to prevent the buildup of undesirable vibrations. The arrays are non-rotatable being fixed with respect to the main spacecraft. The arrays are composed of two deployable paddles and a fixed body-mounted panel. The TT&C and GPS antennas are mounted at the edges of the two deployable solar arrays paddles. The approach adopted for ATLAS in using flexible deployable arrays was constrained by the need for multiple orientations of the spacecraft.

For batteries the critical parameters are battery capacity and specific performance.
Battery capacity C_B(Wh)=$\frac{P_{LOAD} \times t}{DNV\eta}$
where η=charge efficiency=0.96
D=maximum depth of discharge=50% at LEO
N=number of cells=bus voltage/cell voltage=28/1.25=23
V=bus voltage=28V dc
t=load duration (h)=0.5 at LEO
For a load of 500W the battery capacity is 0.81 Wh.
Battery specific performance of battery mass to battery capacity is 25-40 Wh/kg for NiH_2 batteries with cycle limits of 10,000. Battery mass is given by $m_B = {}^{C_B}/_{25} = 0.035kg$. A power control unit has a mass of ~0.02 kg/W of power throughput. Electronic equipment requires voltage regulation from which ~20% is dissipated so power conversion units have masses ~0.025 kg/W. Wiring and switching dissipates ~2-5% of operating power and the wiring harness comprises ~1-4% of dry mass. The batteries provide eclipse storage during dormant phases while the solar arrays slowly trickle charge the fuel cells used for operational periods.

7.3.4 Thermal Control Subsystem

The thermal control subsystem maintains the temperature of the spacecraft equipment within their specified ranges. It comprises thermal insulation and usually heat pipes to redistribute thermal energy. It may also include radiating louvres for heat rejection. The thermal control system is dominated by passive control methods and typically comprises ~2% of the spacecraft dry mass and consumes around 20W in a medium sized spacecraft which employs active thermal control.

7.3.5 Structural Subsystem

The structural subsystem provides stiff mechanical support for all the spacecraft subsystems. It must be capable of sustaining launch loads. The maximum shell radius for the Ariane standard fairing is 1.9m and the minimum spacing for the robot arm separation to eliminate elbow collision is 1.6m for 1.2m robot arms. For a monocoque cylindrical shell under compression the critical buckling stress is:
$\sigma_{cr} = \frac{0.68Et}{R}$ where R=shell radius=1.6m
t=shell thickness
E=Young's modulus=71x10^9N/m^2 for 7075 Al
Critical buckling load $F_{cr} = \sigma_{cr}A = \sigma_{cr}2\pi Rt$
The critical load must exceed accelerations in excess of 8g steady state load and 20g transient load. Ultimate design loads should be 1.25-1.5 times the load limit. Hence the ultimate design load is $F_{cr} = m_i a = 4.4 \times 10^5 N$ assuming 50% margin onto a load of

20g. This gives a shell thickness of $1.2\text{x}10^{-3}$m or 2mm. Additional mass is imposed by shielding etc. Similarly for a monocoque shell the natural frequency is given by:

$f_n = \frac{1}{2\pi}\sqrt{\frac{EI}{\mu L^3}}$ where μ=mass/unit length

ρ=density=$2.8\text{x}10^3$kg/m^3 for Al

The principle driver to the structural subsystem is the requirement for minimum mass yet providing structural stiffness for the payload and spacecraft subsystems. The primary structure typically comprises ~10-20% of the spacecraft dry mass with fasteners and fittings increasing the primary structure mass by around 10%. The electric wiring harness alone can account for as much as 10% of the spacecraft dry mass. A design margin of 25% should be included for structural growth. Equivalently the spacecraft structure typically comprises ~8-12% of the spacecraft launch mass. The dynamic properties of the spacecraft is determined by the following heuristic rule of thumb:

Moment of inertia (kgm^2) $I_s = 0.01M_s^{5/3}$.

External arrays greatly increase the moment of inertia of the spacecraft by $\sim l_a^2 m_a$ where m_a=array mass, l_a=array offset from spacecraft mass centre=$1.5l + 0.5\sqrt{\frac{A_a}{2}}$ where l=spacecraft bus diameter. The array axis moment of inertia increases however by $\sim A_a^2 m_a$. As the arrays are not deployed during manipulation the arrays will not affect the dynamic properties of the system in this phase.

7.3.6 Communications Subsystem

The communications subsystem maintains a two way data link (uplink for command and downlink for telemetry) between the spacecraft and the ground. It requires a receive/transmit antenna and a modulation system. The communication system comprises a transmitter/receiver, and additional small omnidirectional transmitter for function redundancy and an rf diplexer for the single transmit/receive antenna. The command decoder and two telemetry multiplexers for redundancy use the basic units of the command and data handling subsystem and a dedicated digital computer should be included for co-ordinating complex data processing. The requirement for a clear and continuous field of view (FOV) to the ground during real time operations implies the need for a data relay to avoid the need for a distributed network of ground stations. It is concievable that if radar was used that the antenna may be configured to perform radio transmit/recieve if the necessary electronics were incorporated (eg. Pluto flyby mission). The waveband would be allotted and controlled by the ITU within the S band for TT&C services (2-4 GHz). This also allows compatibility with TDRSS/EDRSS, the Ground Space Tracking & Data Network and the Space Shuttle Orbiter. Although this introduces a 0.5s two way time delay this is not considered problematic. The S band offers 300 kbps uplink at 2.025-2.120GHz and 1.2Mbps for the downlink at 2.2-2.3GHz. EDRS offers 150kbps uplink and 3Mbps downlink and this is the baseline relay. EDRS requires the user spacecraft to provide an EIRP (product of transmitter power and gain) of 45 dBW and a G/T of 8 dB/K.

A typical spacecraft generates 870 bits of telemetry of which 330 is from the AOCS and 280 is from the payload. Similarly a typical spacecraft receives 540 commands of which 270 is for the AOCS and 130 for the payload. Generally housekeeping telemetry varies from 100-1000bps whilst housekeeping for the payload can generate up to 10kbps to 500Mbps. The command rates rarely exceed 1 kbps though they have been known to reach up to 100 kbps. Most spacecraft require <1 kbps for command but it is

anticipated that for teleoperation ~100 kbps is more appropriate. Most of the data rate requirement however is for the downlink of telemetry data. Data rates in excess of 1 kbps require the use of high gain directional antenna. It is anticipated that data rates for the downlink will be ~36Mbps since a 512x512 pixel TV image requires ~ 63Mbps with 8 bit words at 30 frames per second (assuming no preprocessing). The frame rate may be reduced to 2 frames/s with marginal loss in quality. The use of 8 bit words allows 256 colour levels. Use of orthogonal polarisation (doubles bandwidth capacity), adaptive DPCM (reduces data rate by orders of magnitude), QPSK (which offers 1.7 b/Hz). These and other data compression techniques can reduce this the data rate to 400kbps (the RMS has a data link of 600kbps and all ESA video services are compressed to 384kbps). The advantage of voice commanding is that it requires only ~64 kbps (48 dB/s)- a typical transmitter power for an audio band is 1W. A bandwidth allocation of 36 MHz (typical of a comsat) should easily cope with 5 cameras and numerous sensor data through the use on onboard processing. Diameter of receiver $d = \frac{100\lambda}{\delta}$ where δ=beamwidth ~1° gives a ground based antenna diameter of 13.6m at 2.2 GHz. The maximum power received on Earth is limited to -148dBW/m^2/4kHz. If the satellite EIRP is 38dBW (typical of a comsat) with a transmitter gain of 28dBW the transmitter power required is 10dBW=10W (Voyager 2 transmitter power was 30W). A 28 dB high gain antenna can communicate via the S band and steer through a solid cone of $\pm 110^{o}$. It has a mass of 40 kg including drive and support assembly of which 5 kg is the antenna. It requires a nominal power of 10W. The mass of a standard S band parabolic antenna is 10kg (with a 28dB gain and 150cm diameter). A typical 10W solid state transmitter requires ~20W at the S band due to 50% efficiency. With a gain of 28dB and a bandwidth of 36MHz (typical of a comsat) such a transmitter would have a mass of 2kg and occupy 3400cm^3. High directional antennas range in size from 0.3 to 3m in diameter. The diplexer and filters for the S band antenna have masses of 2kg in total. Receivers have a size and mass of 150cm^3 and 1.8 kg typically with a power consumption of 3W. A TDRSS compatible S band transponder has a mass of 7kg and a power requirement of 4.5W and dimensions of 14x33x14cm. A typical TT&C central microcomputer will have a mass of 7.5kg and a power requirement of 27W and dimensions of 12x23x40cm.

The link budget is determined as follows assuming that S(dBW)=10log$_{10}$P(W):

$$\frac{E_b}{N_0} = \frac{PG_tG_r}{L_aR}\left(\frac{\lambda}{4\pi r}\right)^2\left(\frac{1}{k}\right)\left(\frac{G_r}{T_s}\right)$$

where $L_s = \left(\frac{\lambda}{4\pi r}\right)^2$=free space losses=195-215dB

k=Boltzmann's constant=1.38x10^{-23}J/K=228.6dBW/K/Hz

$G_r = \frac{4\pi A_e}{\lambda^2}$=receiver gain=15-65dB for a parabolic reflector

$A_e = \eta A_r \sim 0.55A_r$ for a parabolic reflector

$A_r = \frac{\pi D^2}{4}$

L_a=transmission losses due to rain, etc=0 dB

$N_0 = kT_S$=system noise

T_S=system temperature

P_t=transmitter power=10 W

G_t=transmitter gain=28 dB for a 150cm antenna

R=data rate=1.2 Mbps

B=bandwidth=36 MHz

Receiver performance and quality is dictated by the G/T ratio: $\frac{G}{T} \sim 23dB$ typically assuming an Earth station temperature of 200K (23 dBK) and an omnidirectional receiver. System noise is typically N=30dBW and GaAs device have noise temperatures of 70K.

Carrier to noise ratio of 10^{-5} may be given by: $C/N = P_t G_t \left(\frac{\lambda}{4\pi r}\right)^2 \left(\frac{G_r}{T_s}\right)\left(\frac{1}{kB}\right)$

For a 2.2 GHz waveband and antenna efficiency of 0.55, a 1.5m diameter transmitter (28 dB) the link budget for a spacecraft-Earth link:

Transmitter power	10 dBW
Transmitter gain	28 dB
EIRP	38 dBW
Free space loss	-206 dB
Receiver G/T	23dB/K
Boltzmann contribution	228.6 dB
Data rate	-60.8 dB

Hence $E_b/N_0 = EIRP + L_s + G/T + 228.6 - 10\log R = 22.8dB$

$$C/N = E_b/N_0 + 10\log R - 10\log B = 22.8 + 60.8 - 75.6 = 8\,\text{dB}$$

This margin is more than sufficient for the Earth-spacecraft link budget.

	Mass (kg)	Power (W)
TDRSS transponder	7	4.5
TT&C PCM computer	7.5	27
Antenna (incl drive)	40	0
Diplexer	2	0
Transmitter	2	20
Receiver	2	3

7.3.7 Discussion

A second design approach may utilise more advanced technologies. A Kaufman Ar ion propulsion system may adopted with regenerative fuel cells. The flexible solar array size is enlarged to cope with ion thruster power requirements. They are deployed while operating the thrusters as the thrusts will be low during orbit transfer but will be retracted during manipulation. Fuel cells power the spacecraft during the manipulation phase. Peak power requirements are now given by the thrusters.

Peak power $P = \frac{FI_{sp}}{2\eta}$ where η=0.9

I_{sp}=6000s

F=0.5N

Hence P=1.7 kW per thruster. Assuming three 30cm thrusters implies the peak power load is 5 kW for the propulsion system alone. The trend towards the use of higher performance propulsion increases the time between refuelling assuming the same propellant mass is loaded:

$\Delta v = -gI_{sp} \ln\left(1 - \frac{m_p}{m_i}\right) = 22.45$ km/s

This is sufficient for over 2 LEO-GEO two way transfers. Hence this may provide a prototypical spacecraft bus for an off-the-shelf OMV Space Tug. As pointed out by Wertz et al (1988) if such a system used low thrusts as characterised by electric propulsion the payload could deploy all its arrays, antennae, etc before operational orbit insertion to high orbit offering greater reliability for system checkout as LEO is accessible to in-orbit maintenance by astronauts. However no such limitation is

imposed by ATLAS. This design is an alternative but reliability considerations suggest that established technologies should be adopted for the spacecraft bus of ATLAS.

	MASS	POWER										
FUEL	475.6057	75		mi=	1500	kg	mdry=	1024.394	kg	mLink1=	8	kg
PROP	57.07268	0		deltav=	1590	m/s	height=	2	m	mLink2=	6	kg
COMM	60.5	54.5		g=	9.81	m/s^2				mLink3=	6	kg
POWER	81.2274	115.012		Isp=	425	s				mLinkw=	12	kg
THERMA	20.48789	25.00262		mTDRS=	7	kg	pTDRS=	4.5	W	meffector	8	kg
STRUCT	225.3668	0		TT&Cm=	7.5	kg	TT&Cp=	27	W	mcomp=	20	kg
ACS	47.5	103		Antennm=	40	kg	Antennp=	0	W	mcamera	8	kg
PAYLOA	457.5633	1369.322		Diplexm=	2	kg	Diplexp=	0	W	mtool=	5	kg
BUS	967.7604	372.5147		Transm=	2	kg	Transp=	20	W	mmemory	15	kg
TOTAL	1425.324	1741.836		Receivm=	2	kg	Receivp=	3	W	p-arm=	50	W
				Arraym=	9.931	kg	PBOL=	695.17	W	p-wrist=	30	W
PAYLOA	incl f-cell	incl CMG		Battm=	28.30616	kg	PEOL=	500.0523	W	p-comp=	50	W
				Convm=	10.00105	kg	BATTCAP	0.808747	Wh	p-camera	60	W
				Regulm=	12.50131	kg	Regulp=	100.0105	W			
				Harnesm=	20.48789	kg	Harnesp=	15.00157	W			
				Structm=	0	kg	thickness	0.001204	m			
				Loadpow=	500	W	density=	2800	kg/m3			
				Fuelcellm	8	kg						
							Frcit=	4.40E+05	N			
							Youngmo	7.1E+10				
				MIMUm=	2.5	kg	MIMUp=	25	W			
				Starsenm	7	kg	Starsenp=	20	W			
				Magnetm	1.5	kg	Magnetp=	1	W			
				Earthsem	3.5	kg	Earthsep=	10	W			
				ACcomm	23	kg	ACcomp=	25	W			
				CMGm=	68.18777	kg	CMGp=	219.6608	W	Torque=	1098.304	N
							Angmom=	2096	Nms	Whinertia	4000	
										Whspeed	0.524	rad/s

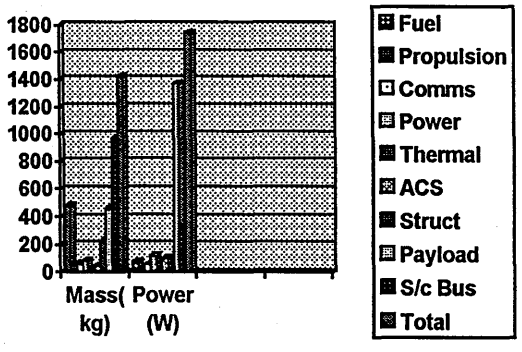

The high structural mass was estimated using a heuristic formula hence the discrepancy between the structural mass as calculated from the Euler buckling formula without accounting for spot radiation shielding and the possibility of deployable debris shielding. The figure of 225kg for a spacecraft offers a potential 1cm thick Al structure which is greatly in excess of requirements for an unmanned spacecraft defined earlier as 1.2mm. As composites may be used (at least for the secondary structure) this mass discrepancy effectively offers a substantial margin for other trade-offs. This is especially the case as spacecraft structural subsystems have negligible failure rate compared with active spacecraft systems. Note that the high power requirement of the payload includes the power requirements of the attitude control actuators which are operated for reaction moment compensation during manipulation.

We have indicated a feasible systems design for the ATLAS spacecraft on the basis of standard spacecraft technologies and standard robotic technologies both of which may advance over time. The logistics problems are still relevant but have been reduced to manageable proportions and it is this aspect on which new technologies will have an impact.

Chapter 8

CRITICAL SPACECRAFT SUBSYSTEMS

The AOCS (Attitude & Orbit Control System) is a major component of the space avionics subsystem (which also includes non-RF part of the command and data handling subsystem and power regulation and distribution) and comprises sensors, processors and actuators. It is the subsystem with which the robot control system interacts most strongly and so is considered in detail here. Its design is highly dependent on the mission profile and it is usually the most complex subsystem of the spacecraft. It is usually divided into two subcomponents: the orbital control system (OCS) and the attitude control system (ACS), of which the attitude control system is the most important. Spacecraft have traditionally been designed with attention focussed initially on structural loading with the control system being designed separately. However the spacecraft structure and its control system often interact: Explorer 1 which discovered the van Allen radiation belts became unstable when its whip antennae dissipated the spacecraft's spin energy (1958); Mariner 10 experienced roll axis instabilities due to interaction between the controller and the flexible solar array torque tubes (1973); HST encountered thermally induced vibration at the day/night terminator requiring modifications in the control system (1992). The introduction of manipulators will introduce further interactions between the spacecraft-payload structure and the control system. Any free kinematic chain without internal gyroscopic motions in space will end up spinning about its greatest moment of inertia if there is relative motion between the rigidly or elastically attached links [Pringle 1966]. Hence, any robotic manipulator will require some form of attitude control to prevent this from occurring to any spacecraft to which the manipulator is attached (the mounting spacecraft). The control system is then the central component of the robotic spacecraft design. Furthermore, the autonomy constraint on the spacecraft requires the controller to handle a large range of dynamics, and the reliability constraint on the spacecraft requires the controller to be robust to large parameter variations. For a complex spacecraft then, control is the central issue.

8.1 MISSION PROFILE

The orbit for most spacecraft is well-defined as they are usually chosen for their ground track but for a servicer spacecraft such as ATLAS the orbit will be variable. Ground coverage is not an issue for ATLAS since its application is space-oriented rather than Earth-oriented. The issue concerns ATLAS's target market. However since the Alpha Space Station will be in the 200km altitude region this may be taken as a nominal reference orbit. For an LEO to HEO transfer the delta-v requirement varies from ~0.6 to 1.5km/s depending on the precise orbit transfer. For most spacecraft the perigee burn in orbit raising is generally considered as part of the launch phase and the apogee boost is generally considered as part of the station acquisition phase both of which precede the operational orbit phase. Inclination changes cannot be effected by launchers economically so this is part of the station acquisition phase also. Although stationkeeping requires only ~200-400m/s delta-v per year, evasive maneouvres will require typically ~150-4600m/s delta-v depending on the severity of the maneouvre. For ATLAS the perigee/apogee/inclination burns form part of the in-orbit operational phase. For the ATLAS spacecraft the operational orbits are considered to vary from ~200-1200km altitude, generating a delta-v requirement of 0.53km/s for a one way

maneouvre. A two way maneouvre requires a delta-v of 1.06 km/s. ATLAS would thus require refuelling periodically with small launched payload fuel tanks.

A typical mission profile for the robotic freeflyer ATLAS consists of several phases with rendezvous and docking (RVD) required [Claudinon et al 1985]. McInnes (1992) suggested that both target and interceptor perform a cooperative rendezvous to minimise the interceptor fuel consumption. It is conceivable however that the thrusters or attitude control system of the target is inoperative (eg. Solar Max had no attitude control available). Furthermore it is likely that no gain is in fact achieved as the target's operational capability is reduced unless refuelled. Fallin (1975) considered the problem of minimising delta-v requirements for several intersatellite transfers between different orbits. It is highly unlikely that this situation of multiple missions will be required since intersatellite tranfers will be determined according to the operational priority of missions rather than according to delta-v minimisation. Tangential thrusting changes the semimajor axis, eccentricity and argument of perigee; radial thrust changes the eccentricity and argument of perigee; thrust to the poles changes the inclination, longitude of ascending node and argument of perigee. In general continuous impulse efficiency is not constant along the orbit so optimal techniques are used to calculate the thrust sequence to change the required orbit using the minimum amount of fuel.

Rendezvous may be defined as a series of maneouvres designed to bring two vehicles into close proximity to ultimately enable docking such that the two vehicles become mechanically joined. The mission profile phases are given by:

(i) Spacecraft maneouvres to rendezvous with another spacecraft demand critical timing. Orbit rendezvous and interception in space and time require phasing orbits. During the early days of the space effort orbital rendezvous and docking were performed within ~1h of orbit insertion. The wait time in the initial orbit was given by:

$t = \frac{\varphi_i - \varphi_f + 2k\pi}{w_c - w_t}$

where $\varphi_i - \varphi_f = 180 - \alpha$=phase angle between target and interceptor for rendezvous

k=number of rendezvous required

w_c=angular velocity of interceptor/chaser

w_t=angular velocity of target

α=lead angle from interceptor to target

However the single orbit chase pattern is prone to failure so 24h or 48h chase patterns have tended to become common. If the chase orbit has a smaller semimajor axis than the target orbit then it will catch up so that the target is directly above the chaser spacecraft at which point the chaser can execute its first maneouvre. The standard orbital mechanics orbit transfer between two non-intersecting orbits characterises the homing phase of the maneouvre [Chande & Newcomb 1985, Kaplan 1976]. To inject into a desired orbit from a parking orbit at least two burns are required. The two-impulse Hohmann transfer is the minimum energy maneouvre to patch between two circular concentric orbits and involves the minimum fuel expenditure in traversing a central angle of 180^o. From a circular parking orbit a perigee burn increases the initial orbit circular velocity by Δv_p to facilitate the transfer by opening the transfer ellipse tangential to and intersecting both orbits:

$\Delta v_p = \sqrt{\frac{\mu}{r_p}}\left(\sqrt{\frac{2r_a}{r_a + r_p}} - 1\right)$ from $v_p = \sqrt{\frac{\mu}{r_p}}$=perigee circular velocity

μ=GM_{Earth}.
r_p=perigee radius
r_a=apogee radius

At the apogee thrust is applied to circularise the elliptical transfer orbit by incrementing the velocity by Δv_a:

$\Delta v_a = \sqrt{\frac{\mu}{r_a}}\left(1-\sqrt{\frac{2r_p}{r_a+r_p}}\right)$ to $v_a = \sqrt{\frac{\mu}{r_a}}$=apogee circular velocity

The total velocity change is given by: $\Delta v = \Delta v_p + \Delta v_a$

The time of flight for the Hohmann transfer given by:

$\Delta t = \pi\sqrt{\frac{a^3}{\mu}}$ where a=orbit semimajor axis

For an orbital plane change the angular momentum vector must be altered by applying thrust parallel to that vector and perpendicular to the orbit plane at equatorial crossing such that the orbit precesses by angle Δi: $\Delta v_i = [2v_i \sin(\Delta i/2)]$. However such plane rotations (eg. equatorial to polar maneouvre) involve the use of much fuel (an inclination change of 1^o requires ~208m/s delta-v at LEO) so it would be desirable to use aerodynamic maneouvres for plane changes such that the lift vector is rotated out of the plane of the trajectory without or at least minimising propulsive burns. The most efficient method for plane changes while minimising fuel expenditure is to change inclination at the apogee burn circularisation maneouvre since the spacecraft velocity is lower at the apogee than at perigee:

$\Delta v = (v_i^2 + v_f^2 - 2v_i v_f \cos\Delta i)^{\frac{1}{2}}$ where v_i=initial orbit circular velocity

v_f=final orbit circular velocity

This phase of the mission profile is obstacle free and would take the freeflyer to within ~10-30km below the target and coplanar with its orbit. The double coelliptic maneouvre accomplishes this in two burns: first to within 30km and second to within 15km of the target, eg. Space Shuttle. This preliminary phasing maneouvre is analysed in geocentric inertial reference coordinates. It has been suggested that nodal regression may be utilised to reduce the delta-v requirements [Robertson et al 1988]. Nodal regression $\dot{\delta\Omega}$ varies with altitude and inclination and the resultant differential nodal regression rates between orbits may be exploited. Coplanar situations occur when the ATLAS orbit plane rotates above or below the target orbit plane. On alignment a Hohmann transfer may be executed. Similarly offsetting inclinations may be exploited particularly at near polar orbits.

Orbit rendezvous requires interception of the target spacecraft by the chaser spacecraft and this involves phasing orbits. The interceptor coasts to catch up with the target and when the line of sight is ~25^o above the interceptor's local level the final intercept maneouvre is executed either using onboard radar or optical guidance. The phasing maneouvres of the interceptor vehicle from below and behind the target to close and bring the interceptor to within ~100-500m of the target to avoid the possibility of a collision. The below and behind maneouvre will also be the relevant maneouvre if aeroassisted deorbiting is adopted. The two-impulse rendezvous motion of the chaser in the target orbital frame are given by the Clohessy-Wiltshire equations if both orbits are circular with similar semimajor axes and inclinations. They are essentially Hill's equations equated to zero, ie. no external forces are applied to the chaser spacecraft [Claudinon et al 1985]. Eccentricity may be accomodated in the equations. These and subsequent maneouvres involve the closure of the two vehicles separated by small

distances relative to the orbit dimensions with respect to geocentric inertial coordinates. Hence a non-inertial frame of reference is used fixed in the target vehicle to enable the chase vehicle maneouvres to be determined with respect to the target vehicle. A chaser spacecraft has coordinates r, θ, z with respect to a target spacecraft and the target-referenced coordinate axes rotate with orbital velocity $w_0 = \sqrt{\frac{\mu}{r_0^3}}$. This provides a set of linear constant coefficient differential equations (Clohessy-Wiltshire equations):

$$\ddot{r} - 2w_0 r_0 \dot{\theta} - 3w_0^2 r = 0$$

$$r_0 \ddot{\theta} + 2w_0 \dot{r} = 0 \qquad \text{where} \quad \begin{matrix} r = x \\ y = r_0\theta \end{matrix} \quad \text{for cartesian representation}$$

$$\ddot{z} + w_0^2 z = 0$$

The solution to these equations give the drift rates for the chaser to enable rendezvous with the target. Initial conditions provide constraints for their solution such that z_0, r_0, θ_0 are the initial coordinates of the chaser spacecraft. The solutions are given by the time rate of change of the coordinates and relative velocities:

$$z(t) = z_0 \cos w_0 t + \frac{\dot{z}_0}{w_0} \sin w_0 t$$

$$r(t) = -\left(\frac{2}{w_0} r_0 \dot{\theta}_0 + 3r_0\right)\cos w_0 t + \frac{\dot{r}_0}{w_0} \sin w_0 t + 4r_0 + \frac{2}{w_0} r_0 \dot{\theta}_0$$

$$\theta(t) = \theta_0 - \left(3\theta_0 + \frac{6w_0 r_0}{r_0}\right)t + \left(\frac{4\dot{\theta}_0}{w_0} + \frac{6r_0}{r_0}\right)\sin w_0 t + \frac{2\dot{r}_0}{w_0 r_0}\cos w_0 t - \frac{2\dot{r}_0}{w_0 r_0}$$

$$\dot{r}(t) = (2r_0 \dot{\theta}_0 + 3w_0 r_0)\sin w_0 t + \dot{r}_0 \cos w_0 t$$

$$\dot{z}(t) = -z_0 w_0 \sin w_0 t + z_0 \cos w_0 t$$

$$\dot{\theta}(t) = \left(-3\dot{\theta}_0 - \frac{6w_0 r_0}{r_0}\right) + \left(\frac{6w_0 r_0}{r_0} + 4\dot{\theta}_0\right)\cos w_0 t - \frac{2\dot{r}_0}{r_0}\sin w_0 t$$

The out of plane component δz of the chaser oscillates with the orbital period and is removed by waiting until the drift reaches z=0 and thrusting with acceleration $\ddot{z}$ such that $\dot{z} = 0$. If the chaser is below the target as is normally the case, a perigee raising maneouvre adjusts the chaser orbit. A coelliptic maneouvre at the chaser orbit apogee will allow the chaser to match the target. The terminal phase involves a two-impulse final trajectory. A closed loop terminal proportional controller reduces the range and range rate to zero to allow the transfer trajectory to be maintained. As the final closure occurs braking maneouvres reduce the residual velocity to zero near the target. Rendezvous is complete when the chaser and target are seperated by <100m with zero relative velocity. Chaser maneouvre acceleration is dominated by orbit mechanics for a rectilinear maneouvre $\ddot{r}$. The only passive stationkeeping positions are behind or in front of the target in its orbit as radial or out-of-plane differences will cause oscillations of the chaser with respect to the target. The Clohessy-Wiltshire equations describe how to reduce to zero the spacecraft relative motion assuming the impulse durations to be instaneous. The result is a series of coasting trajectories [Simmons et al 1990]. The spacecraft is now at point P_1 which is a stable standoff point on the target orbit. Stationkeeping at P_1 enables the interceptor to perform further trajectory planning prior to execution on the basis of sensor information and allows waiting for advantageous maneouvre conditions (eg. ground station visibility). Onboard trajectory

planning is required to preserve spacecraft autonomy without violating the mission constraints such as maximum time of flight, fuel efficiency, etc. The trajectory planner creates a series of intermediate states between the current state and the target state defining a planned orbit trajectory with an impulse profile of all the delta-v thrusts that need to be performed. The number of impulses should be restricted to a maximum of 4 and this will be sufficient to generate closing velocities down to 0.01ft/s. A closed loop autopilot may execute additional corrective firings if the current state strays too far outside a specified deadband around the reference trajectory. Guidance for intercept and rendezvous requires guidance radar and/or optical lidar, gyroscopic reference devices and accelerometer sensors for range, range rate, elevation and azimuth angles along the line of sight to the target.

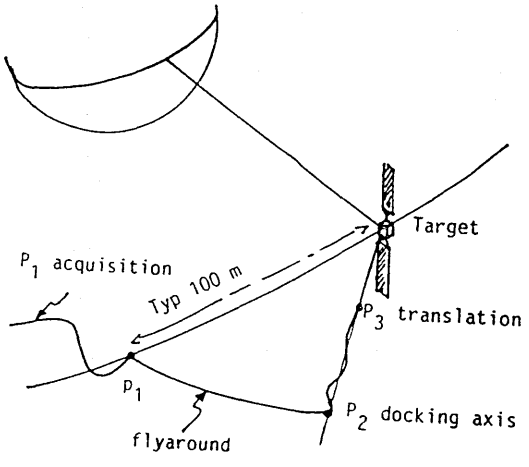

Fig 8.1 Rendezvous trajectory [from Claudinon et al 1985]

(ii) This is the final approach phase which will take the interceptor to within a few metres ~50m of the target spacecraft. It is not unusual for up to 6 correctional burns to be required to complete docking. A flyaround maneouvre from point P_1 may be required to acquire an approach corridor along the spin axis (usually the major axis of inertia). If there are no unbalanced forces on the target an arbitrary rotation of the x,y and z axes of the target may be resolved into a constant rotation about a single resultant spin axis. This spin axis will comprise the approach corridor vector. If the spin axis lies along the orbit plane then the flyaround is not necessary (unlikely). In general the spin axis lies out of the orbit plane along the orbit normal so flyaround is most likely to be necessary when dealing with spin-stabilised spacecraft. Flyaround will require complex computational facilities and position/attitude sensors to enable a trajectory profile to be calculated. After the flyaround phase, the interceptor lies at point P_2 along the selected docking axis. The motion of both bodies are virtually identical and assumed to be rectilinear with no net relative translational velocity. Active stationkeeping is required until the next maneouvre. If the target is a spinner the next maneouvre must be to spin up the interceptor to a constant angular rate. The rotation of a spin-stabilised target may be determined by visual tracking. Human reactions are too slow to track and grapple spin-stabilised spacecraft which have rotation speeds of up to 60rpm. Astronauts are generally limited to ~1rpm [Schenker

1988]. Feature matching of images and internal models gives the orientation of the target spacecraft with its grip windows. The attitude control system of the interceptor spins it up to match the rotation of the target such that their relative rotational spins are zero.

(iii) This is the final translation phase along the docking axis to point P_3. Visual inspection of the docking points by TV cameras is maintained. Trajectory control is closed loop from the range sensors and translation is performed at a predefined range/range rate profile. The last few metres is executed at constant velocity with accuracies ~2cm and 0.2^o to the point P_3. Up to this point the manipulator arms have been in a stowed configuration and once P_3 is reached the target fixtures lie within the workspace of the manipulators. The chaser spacecraft must then align its heading vector with the objects grapple vectors so that the manipulators are positioned such that they may grapple the grapple points by straight line trajectories. The arms move to the set position and then to their projected entry points to the grapple points on the target. Obstacle avoidance may be necessary if satellite appendages impose possible collision hazards. Wang (1987) proposed a grappling technique (the acquisition phase) such that the joints of the manipulators are locked and the vehicle translates in a straight line so that the manipulators intercept the object at predefined points and then grasp those points. This procedure is highly inflexible in that it comprises a standard spacecraft docking maneouvre which is expensive in fuel due to the tight constraints on docking accuracy. Furthermore it does not utilise the full potential of the manipulators in eliminating this phase of the docking maneouvre. De Peuter et al (1993) noted that limited options for mechanical grappling exist on most spacecraft due to thermal insulation covering. However they suggested that for GEO operations the nozzle of the apogee boost motor could serve as the initial grasp point for temporary attachment. A dedicated capture tool to accomodate the lack of standardisation in apoogee nozzles comprises a stinger which is inserted via the nozzle into the combustion chamber and expanded to provide a firm grasp. The capture tool then clasps to the outer ring of the nozzle to achieve greater stiffness. Unfortunately this maneouvre grasps the spacecraft at the opposite side to the payload and other subsystems which are the most likely candidates for repair. They suggested therefore that a grapple point is found subsequently (since most spacecraft are now being designed to be serviced by astronauts) or if necessary build a small lightweight truss structure of its own to use as "scaffolding".

(iv) After the rendezvous phase when the chase vehicle approaches the target the capture phase ensues comprising of a soft dock for initial alignment within the capture envelope followed by a hard dock for the final alignment and rigidising of the composite structure. Berthing may be defined as the grasping of a payload with a manipulator and maneouvering it to an active spacecraft at the berthing point for locking. Docking involves the active spacecraft flying into a docking port on a passive spacecraft such that the two are joined rigidly [AIAA 1991]. Rendezvous may be cooperative (as in Apollo-Soyuz mission) or uncooperative (as in Solar Maximum mission). Cooperative spacecraft carry transponders and lights to aid rendezvous. Mechanical interfaces for docking should be simple, highly reliable and durable. They should have emergency disconnect provisions by manual or autonomous means. Such interfaces should be in line with the centres of masses of the two objects being joined. The load capacity of the interface should be at least 1.5 times the maximum load that

the docked elements are capable of exerting. Seperation should occur with minimum tip-off dynamics. The interface should be capable of coping with lateral and angular misalignments. Several types of docking mechanism are used in spacecraft docking: (i) three point berthing ring; (ii) cone and ring docking adaptor; (iii) probe and drogue docking system. Relevent to manipulators are grapple fixtures which comprise of a pin marked to give range and orientation feedback to a vision system:

Below are listed NASA's standard tolerance levels:

Grasping tolerances:

Angular capture misalignment (pitch, yaw): $\pm 5^{o}$

Angular capture misalignment (roll): $\pm 5^{o}$

Linear misalignment (x axis, yz plane): $\pm 100mm$

Maximum linear contact velocity (along x axis): 0.3m/s

Berthing contact tolerances:

Lateral misalignment (x,y,z axes): $\pm 76mm$

Angular misalignament (roll, pitch, yaw): $\pm 1.5^{o}$

Linear velocity(x,y,z axes): $\pm 0.05m/s$

Angular velocity (roll): $\pm 0.2^{o}/s$

Angular velocity (pitch, yaw): $\pm 0.52^{o}/s$

Some of these tolerances are quite stringent and illustrate how manipulators can save fuel which would otherwise be expended in attaining such tight constraints. Manipulators are inherently capable of accomodating fine tolerances during manipulation as the rendezvous phase is required only to place the target within the manipulator workspace. This reduces the fuel penalty in achieving precise docking. It also allows the accomodation of the soft dock by incorporating most of the thrusting through orbital mechanics rather than braking thrusts and off-axis thrusts.

Manipulator grasping effectively performs the docking maneouvre culminating in the mechanical joining of the two spacecraft. As the grapple fixtures are within the work volume of the manipulators they accelerate to the speed of the predefined grapple points and make contact ensuring zero relative velocity and acceleration between them. At the actual grasp operation both position, velocity and acceleration of the manipulators must match those of the grapple points to ensure soft docking with minimised contact forces. This implies the need for a tight sensor feedback loop. If velocities and accelerations do not match within a narrow envelope slippage may occur. If the relative velocity is within a given limit perturbing forces at the end effector tip can be minimised at specific stopping distances [Krishen 1989] with the braking rule given by: $v(t) = \frac{v_p}{2}\left(1 + \cos\left[\frac{\pi t}{T_b}\right]\right)$. For very short stopping distances and minimised end effector forces the relative velocity must be <0.1ft/s (0.03m/s). At contact the wrist force/torque sensors give the contact forces. Control switches from visual/proximity guidance to the force sensors. The open loop topology of the system instanteously and discontinuously changes to the closed loop topology [Marcyk & Bellazi 1989]. The force controller reduces the speed of the grapple points to zero within a specified time frame and within maximum force constraints. This capture maneouvre is absolutely basic to any servicing operations. The discontinuous change from open loop to closed loop highlights the necessity of using a consistent unified

control methodology throughout the operation. If alternative control strategies are used the switching between them may cause instability problems.

(v) Once contact has been made there exists a single rigid body of the combined target and the robot interceptor. Thrusters and attitude control actuators on ATLAS (and/or target satellite if it is of large mass and cooperative) provide torques to passivate the complete system and suppress tumbling within a finite time sufficiently long not to exceed actuator capabilities. Ideally latching arrangements from a docking mount should be available so that after grasping the target a hard dock may be initiated between the mating parts through a standardised ball and socket (ATLAS stabiliser/target docking port). If this is not the case then one arm must retain the target spacecraft in a locked mode while the other arm performs the required manipulation tasks. The manipulators should be positioned directly opposite the work place [Adams et al 1987]. After docking the system may be translated to any desired location if necessary. Form this point on the payload acquisition/docking phase passes to the payload transfer/servicing phase [Marcyk & Bellazi 1989].

(vi) Once the manipulation and servicing tasks have been performed ATLAS must decouple from the target satellite with zero net kinetic energy. Retraction of the manipulators may accomplish this through the reverse of the soft dock/grasp. Either ATLAS or the target may reposition and reorient the target spacecraft correctly for its continued operation.

Fuel tanks should be arranged symmetrically about the vehicle thrust axis to avoid shifts in propellant distribution as fuel is consumed. The spacecraft may employ from a few to ~30 thrust units to provide a thrust ~500N sufficient for orbit transfer. One such thrust unit is the 0.4kg NASA 4.5N hydrazine thruster with a power requirement of ~5W/thruster. These thrusters may be gimballed typically to $\pm 7^{\circ}$ to align the thrust vector through the spacecraft during burns. Gimballing of thrusters allows account to be taken for changes in spacecraft mass distribution due to fuel expenditure.

8.2 ATTITUDE CONTROL SYSTEM

Attitude control is the angular momentum management system and is central to any spacecraft to maintain mission requirements. It drives the overall spacecraft design since all subsystems interface to the attitude and orbital control system and a freeflying robot interceptor is no exception. Control-structural interaction problems also occur due to appendage flexure and thermal distortion both of which it is desirable to minimise. All spacecraft are subject to disturbing torques such as aerodynamic, gravity-gradient, solar radiation pressure, magnetic torques and fuel sloshing ~10^{-4}-10^{-5}Nm which although small will induce attitude errors. The primary driver to the ACS is pointing accuracy which defines the need for control of attitude in the event of perturbations which act to change the orbital and attitude parameters of the spacecraft. The spacecraft is required to make station keeping corrections to maintain these parameters within allowable bounds. The use of onboard autonomy allows for ground station outage, but ground based control reduces the requirement for onboard electronics. The cost of the ACS comprises ~10-20% of the total satellite cost and in some cases ground control may be more cost-effective. The requirement for onboard autonomy may impose an additional ~3-8% to the total satellite cost. However, in this case for the robotic freeflyer, ground control is not a cost-effective solution. For long

mission lifetimes, onboard autonomy is preferred for cost effectiveness as the cost of ground control becomes excess to that of increased onboard hardware and complexity [Sabroff 1968]. High pointing accuracy dictates the need for inertial orientation star sensors and signal processing electronics for conversion to Earth-referenced coordinates.

A robotic freeflying spacecraft will have to move between multiple reference attitudes of operation so the spacecraft will be required to reorient itself. Such a spacecraft will comprise multiple payload segments including sensors each requiring different variable orientations. Such instruments will require gimballing with respect to the spacecraft. Multiple attitude requirements impose heavy constraints for independent pointing, eg. solar panels must be sun-oriented, directional antennae must Earth-pointing, attitude sensors require star, Earth or sun orientations, and thermal radiators must be deep space pointed. Such directional components require 2 axis degrees of freedom gimballing to provide the pointing capability. Gimballing is thus the only flexible way to cope with multiple orientation requirements.

8.2.1 Attitude Actuator Systems:

Passive systems which employ environmental torque sources for momentum control such as gravity gradient, aerodynamic and magnetic systems do not provide sufficient accuracy (limited to ~1-10^{o}) for the precision pointing required of a robotic freeflyer satellite. Gravity gradient techniques are popular for stabilisation of very large structures since they exploit the tendency of a body to align its axis of minimum inertia to the local vertical. An alternative technique for attitude stabilisation is spin stabilisation whereby the spacecraft body rotates about its principal axis of maximum inertia. The rate of precession ϖ of the angular momentum vector H obeys $\tau = \varpi \times H$ which imparts gyroscopic rigidity to the momentum bias of H giving it resistance to changes in attitude. This technique necessitates the use of omnidirectional antennae for Earth pointing communications which are characterised by zero antenna gain. Dual spin stabilisation however allows the use of an Earth-pointed antenna on a despun platform. The spacecraft rotates at a high spin rate typically ~60rpm to provide the gyroscopic stiffness while the despun platform coupled through a bearing assembly rotates at 1rev/day in the spacecraft orbit to keep the antenna Earth-pointed. All momentum bias techniques introduce an oscillating nutation mode which must be damped to reduce wobbling. For many missions, the normal to the orbit plane (pitch axis) is the direction chosen for momentum bias. For such a fixed reference trajectory, the local vertical rotates 90^{o} every quarter orbit such that yaw errors are changed to roll errors every 90^{o} and back again every 180^{o}. Both spin and dual-spin stabilisation are suitable only for spacecraft with single attitude reference trajectories during the spacecraft operational lifetime. They are totally unsuitable for a robotic freeflyer application which requires multiple attitudes and slewing during operation. The gyroscopic stiffness imparted by spinning is obviously not desirable since changes in attitude will be required during a typical robotic servicing mission. Whereas most operational spacecraft to date have adopted nominal pointing direction with fixed attitude, the robotic freeflyer will need to attain multiple attitude orientations. Hence, the freeflying robot interceptor will require active three-axis stabilisation to provide the flexibility for multiple arbitrary attitude reference trajectories involving frequent large angle slewing maneouvres about the spacecraft centre of mass. Indeed three-axis stabilisation has become the method of choice for large comsats. Three axis stabilised

spacecraft tend to be rectangular or polygonal rather than cylindrical and this offeres greater flexibility for packaging components.

However, spin stabilisation capability ~10rpm may be desirable during delta-v thrusting parallel to the spin axis during orbit insertions to maintain a stable orientation to reduce the effect of any misalignments of the thrust vector from the spacecraft centre of mass which would otherwise cause the vehicle to veer off course or tumble. In fact rather than spinning up the whole vehicle spinning up the lower section of the spacecraft and maintaining the upper section of the spacecraft despun through a bearing assembly reduces the torquing requirement. This is the dual spin configuration which provides gyroscopic stiffness from the spinning section while the despun platform is maintained stationary by counter rotation. This configuration requires nutation damping by an energy dissipation mechanism in the despun section. After the circularisation of the apogee burn the spacecraft then undergoes a typical sequence of acquisition maneouvres [Kaplan 1976]. There is an initial despin to ~1°/s. The normal means of satellite despinning following orbit injection thrusting is through the use of yo-yo's or gas thrusters. Yo-yo's are expendable masses which are attached by cords initially wrapped around the spacecraft body axis. Centrifugal forces pull them away until a split hinge enables the masses to escape carrying away the rotational kinetic energy. Yo-yo's can be used only once, and so are not suitable for multiple orbit thrusting. The initial despin is followed by dewobbling followed again by a final despin to zero. In a typical spacecraft solar panel deployment and sun acquisition is then achieved. Earth acquisition of antennae and star acquisition is then accomplished. If liquid fuel is used for thrusting, gimballing the thruster allows the use of three-axis stabilisation during thrusting. Alternatively, spin stabilisation may be employed during dormant modes between operations to reduce power consumption.

One mode of three axis stabilisation is through gas jet thrusters which exert torques by expending fuel. They are usually mounted in clusters for attitude control. Four thrusters are required to produce torque about one axis, ie. 12 thrusters are required for three-axis stabilisation: $\tau = F_{thrust} \times l$ where l=moment arm. Two pulses are required for start and stop. Cold gas thrusters can produce <1N thrust and have a low specific impulse <100s. For high impulses, hot gas systems which operate by chemical reactions use mono- or bi-propellants (eg. hydrazine derivatives) and are capable of producing $1x10^4$N thrusts. The propellant mass required for attitude change is determined by the pulse length t of the thrust and the thrust F_{thrust}: $m_p = \frac{F_{thrust} \times t}{I_{sp}}$. Limit cycling ~0.001-0.1°/s occurs due to the discrete on-off pulse mode of thrusting via the Schmitt trigger. This is a major deficiency in the accuracy of control for precise attitude maintenance. The standard NASA thruster pair has a 4.5N operating thrust with ~20,000-50,0000 total pulse rating with pulse length t~0.02-0.1s.

Thrusters should be avoided due to their excessive fuel overhead in bang-bang thrusting, particularly for multiple slewing and rapid re-orientations. The only feasible choice of three-axis control is through internal momentum transfer devices which generate internal torques and redistribute momentum within the spacecraft such as reaction wheels, momentum wheels or control moment gyros. Built-in torque motors provide momentum storage as a means of transferring momentum from one part of the spacecraft to another without changing the momentum of the vehicle as a whole. They

do not suffer from pulse effects and do not expend scarce fuel. They are a fundamental requisite for a robotic system which undergoes rapid mass and moment of inertia changes. Momentum wheel dynamics are similar to those of a dual spin system (whereby the spinning component is viewed as a large momentum wheel along the spacecraft spin axis) except that the angular momentum of the dual spin spacecraft is significantly higher than that of a three-axis stabilised spacecraft with fixed momentum wheels. Momentum wheels are nominally driven at high constant speed (~10^3 rpm) to provide momentum bias and also tend to impart a degree of gyroscopic stiffness to attitude. The speed can be increased or lowered to within 10% of nominal speed to compensate for external torques ~0.4-40Nm. Momentum bias in comparison with zero momentum bias lowers the total control torque capability before saturation occurs and introduces undesirable gyroscopic nutation. Furthermore they have the disadvantage of greater wear due to operation at constant motion. The Japanese ETS-VII will use momentum wheels however with maximum torque capability of ~1Nm with an accuracy of ~0.1^o. Reaction wheels are nominally static (zero-bias momentum) but free to rotate and they generate torques by being driven in either direction with electric motors at the required angular velocities and accelerations in response to attitude disturbances or commands. The wheels generate equal and opposite internal torques to the spacecraft in which they are rigidly mounted to counteract the external torques on the spacecraft thereby keeping the attitude fixed in inertial space. They provide a reasonably fast response ~0.1-1^o/s and good accuracy ~0.001^o. They do not suffer from the dead zone error problem inherent in thruster pulse control. However, they can suffer from jerking through low speed regimes where the wheel response tends to be nonlinear. Reaction wheels are large in volume and in mass, as well as being limited in torquing capability which is set by its inertia, ie. size and speed. However, Dougherty, Lebstock & Rodden (1971) calculated that the mass of a three-axis reaction wheel system may be less than that of a comparable momentum wheel system for high angular momentum capacities. Their big advantage is that they are simple to control since each wheel controls each vehicle reference axis degree of freedom independently. Three reaction wheels mounted orthogonally aligned along each spacecraft principle axis suffices to control spacecraft pitch, yaw and roll attitudes, though usually a fourth skewed wheel is usually included for redundancy, eg. NASA's Standard Reaction Wheel configuration. The fourth wheel is aligned equally inclined from the 3 principal axes forming a tetrahedral configuration and the fourth wheel substantially increases the momentum storage capacity of the attitude control system. The NASA Standard Reaction Wheel system has a momentum capacity of 20Nms, a torque capability of 0.5Nm, a mass of 25kg, and a power consumption of 7.5W at peak. In general, they are limited to ~300-1000Nms momentum capacity and to maximum torques of ~1Nm with the power requirement varying up to ~100W/Nm when torquing.

Both Longman et al (1987) and Marcyk & Bellazzi (1989) suggested that reaction wheels offer insufficient torque capabilities to compensate for spacecraft base reaction moments exerted by manipulator movements unless the robot manipulators are operated prohibitively slowly. Furthermore, they are insufficient for high rate slewing maneouvres at >1^o/s. The control moment gyro (CMG) is an advanced form of momentum wheel based on gyroscopic action (see Appendix 10.4). The wheel is mounted on a shaft free to rotate mounted onto gimbal bearings. It is spun at high speed mounted in either one or two gimbals fixed perpendicular to the spin axis of the

wheel and the rotor is free to rotate about the gimbal axes. Torque motors fitted to the gimbals apply control torques to displace the gimbal angles such that the inertial orientation of the momentum wheel spin axis is altered to redirect the rotor angular momentum. The torques applied at the gimbals cause a change in the angular momentum vector, the rate of change of which is proportional to the applied couple. The wheel spins at a constant rate ~10^3rpm so the direction of the angular momentum vector undergoes change with a precession of $\dot{\varpi}$ about the spin axis and a constant nutation of $\dot{\theta}$ to generate an equal and opposite reaction torque to the spacecraft thereby redistributing its angular momentum. The torque gain is such that small torques exerted about the gimbal axes produce a much larger torque on the vehicle because the gimbal torques have only to overcome the gimbal and rotor inertias which are small whereas the output torques are dependent on the rotor momentum and gimbal rate. The gimbal motors are brushless dc motors with permanent magnet rotors. Potentiometers provide gimbal feedback for torque gain compensation in the servo system. Only two double gimballed CMG's are required three-axis stabilisation. For each CMG, the constant speed flywheel is held in the inner gimbal which is coupled through a pivot which in turn is held fixed to the spacecraft [O'Connor & Morine 1969, Liska 1968]. The incorporation of fluid supports improves the accuracy and the life of the CMG by eliminating bearing friction. In fact, one double gimballed CMG allows control torques to be applied about all 3 axes through 2 degree of freedom gyrotorquing and one degree of freedom wheel speed control (like a reaction wheel or momentum wheel) [Salatun & Bainum 1983]. It is usual however to operate the CMG at constant flywheel speed for 2 degree of freedom control only. However, they can provide graceful degradation by being operated in 2 modes:

(i) CMG mode - wheel speed is constant and the spin axis is rotated by the gimbal motors for 2 degree of freedom gyrotorquing;

(ii) Reaction wheel mode - the gimbals are locked and wheel speed may be varied for single degree of freedom wheel acceleration.

The use of CMG's in Skylab (with a nominal fixed momentum of 3000Nms) for precise pointing of the ATM (a solar telescope) mounting platform demonstrated their effectiveness in controlling the station attitude to within ~1arcsec in spite of crew movements [Kaplan 1976, Chubb et al 1975]. The Skylab attitude control system comprised 3 double-gimballed CMG's each of mass 200kg oriented to each of the three vehicle axes providing 100% redundancy. Kennel (1981) recommended parallel mounting such that all outer gimbal axes are parallel. This allows identical mounting interfaces such as brackets, harnesses, etc. CMG's have excellent performance bounds generating torque capabilities ~1000 times that of reaction wheels (up to ~500Nm). They offer rapid response for high slew rates, high accuracy attitude control and superior dynamic ranges to reaction wheels. They typically require ~15-30W standby power and ~0.2W/Nm when torquing. Essentially they are rate gyroscopes which operate in reverse [Yarber et al 1966]. However, double-gimballed CMG's do suffer from limited gimbal angles and so limiting the attitude change (which is proportional to the gimbal angle deflection). Furthermore, they tend to drift as part of the angular momentum of the CMG unit resides in the gimbals due to their finite mass which causes them to move with respect to inertial space. Paradiso (1991) proposed the use of 3 single gimballed CMG's for three-axis stabilisation. Three is the minimum number required with one controllable degree of freedom per axis. These offer larger torque capabilities and high momentum capacities for lower cost, power, mass and reliability.

However, for a cluster of n single-gimballed CMG's, there exist 2^n gimbal angle singularities in the momentum space which are difficult to predict and avoid [Vadali, Oh & Walker 1989]. Due to this they require far more complex control laws than the double-gimballed type. The double-gimballed CMG only exhibits singularity in the antiparallel condition when the gimbal angle approaches $\pm 90^o$. At this singular condition, the double-gimballed CMG can no longer produce torque, but this situation is simple to monitor predict and avoid.

CMG's are much more complex to control than reaction wheels. The choice of actuator will ultimately depend on the size of the robot and the payload masses to be manipulated, though the CMG does provide a greater dynamic range of capabilities and force control will necessitate their employment over other actuators.
Example:

	Mass (kg)	RPM	Ang Mom Capacity (10^3) (Nms)	Max Output Torque(Nm)	Max Gimbal Rate (^{o}/s)	Size
Bendix DGCMG	253	4-12	1400-4000	237	5-30	1.1m diam
HST RW	48	3	<100	0.82	-	0.6m diam

All momentum transfer devices behave as momentum stores effectively transferring external momentum to the internal wheels. This will lead to eventual saturation such that the rotor spins at the maximum motor drive rate and the stored momentum has to be offloaded by momentum dumping to desaturate the internal torquers. The maximum angular momentum stored in the wheels is proportional to the area under the torque curve which is used to size the wheel. Momentum dumping is accomplished by imposing external torques on the spacecraft. In LEO, this may be accomplished by magnetorquers apart from in the plane of the magnetic equator by exerting an external torque on the spacecraft without using consumables [Kamm 1961, Burrow 1961]. Since the geographical equator and the magnetic equator do not coincide this does not preclude equatorial orbits - in such orbits the magnetic field direction varies by $\pm 120^o$. The magnetorquer generates a magnetic field derived from three orthogonal current carrying electromagnetic coils aligned along each spacecraft principal axis. The generated dipole field interacts with the Earth's local magnetic field generating a couple on the spacecraft. Since a couple is produced, magnetorquers are not sensitive to movements of the spacecraft centre of mass. They require flux gate magnetometers onboard to determine the local magnetic field magnitude and direction (at 200km, the Earth's magnetic field strength is ~0.3G) and at 200km altitude are limited to 5^o accuracy but this is sufficient for dumping (but not for attitude sensing). Magnetic flux detecting SQUIDS make highly sensitive magnetometers and magnetic gradiometers [Clarke 1989].
Torque on a current carrying coil:

$\tau = M \times B$ where B=Earth's magnetic flux
M=controllable spacecraft magnetic dipole moment

The values of B and M need to be determined. The Earth's magnetic field is a complex structure which comprises of a steady state main field and a 10% secular variable component. Periodic variations arise due to solar flux in particular. The field is confined by solar wind leading to night/day variations, seasonal variations and solar cycle variations. Similarly solar radiation ionises the upper atmosphere creating current flow which produces a solar variable field. In spite of this Earth's magnetic field may be approximately modelled as a non-rotating dipole located at the Earth's centre. The

most common magnetic field model is the tilted dipole model with the magnetic equator at 13° to the geographical equator, North magnetic pole located at 79° north latitude and 70° west longitude and South magnetic pole at 79° south latitude and 110° east longitude:

$$\begin{pmatrix} B_{north} \\ B_{east} \\ B_{vertical} \end{pmatrix} = -\left(\frac{6378km}{R_{earth}+h}\right)^3 \begin{pmatrix} -c\varphi & s\varphi c\lambda & s\varphi s\lambda \\ 0 & s\lambda & -c\lambda \\ -2s\varphi & -2c\varphi c\lambda & -2c\varphi c\lambda \end{pmatrix} \begin{pmatrix} 29900 \\ 1900nT \\ -5530 \end{pmatrix}$$

where φ=latitude

λ=longitude

R_{earth}=Earth radius

h=altitude

These coordinates must be transformed into spacecraft coordinates to determine the magnetic torques on the spaccecraft.

The controllable magnetic dipole moment, $M=p|NIA|$

where $p=(-1,0,1)^T$ =polarity

N= number of coil turns

I= current

A= coil area

Resistance, $R = \frac{Nrl}{A}$ where r= resistivity

l= perimeter length of coil per turn

Mass of the coils, $m = NlA\rho$ where ρ=density

Since power $P=I^2R$, then $M = \sqrt{\frac{Pm}{rl}}\frac{A}{l}$

For a circular geometry which provides the maximum magnetic moment, $A = \frac{\pi l^2}{4}$ and $l = \pi D$, so $M = \frac{D}{4}\sqrt{\frac{Pm}{rl}}$.

Such devices allow continous momentum dumping without fuel expenditure so that the velocity control loop can operate around a nominal constant value. The maximum momentum storage required for continuous torque input $H_m = H_0(2/\sin^2\delta\theta - 1)$ where $\delta\theta$=maximum change in field direction over a quarter orbit (eg. 90° for polar) and the momentum input $\dot{H} = 4H_0/T$ where T=orbital period. For GEO, momentum dumping must be achieved through mass expulsion thrusting. Ion propulsion may reduce the mass requirement and can be used in near continuous low thrust mode.

8.2.2 Attitude Dynamics & Control

All spacecraft attitude computations require an inertial reference. An inertial frame in the strictest sense is that which is fixed and non-accelerating with respect to the stars. In practice however, for orbital motion about the Earth a sufficient choice of inertial origin is the centre of the Earth (geocentric inertial system) with one axis x fixed along the first point of Aries (direction of the vernal equinox where the Sun is placed against the stellar background on March 21 - the vernal equinox marks the intersection of the Earth's equatorial plane and the Earth's ecliptic plane of orbit around the Sun), a second axis in the equatorial plane y and a third axis z to complete the right hand orthogonal system (in the direction of the winter solstice - the Sun's position on the first day of winter) marking the celestial sphere from the North pole. In fact the frame of reference fixed to the Earth's centre is not really inertial but rotates about the Earth's spin axis with period one day and orbits the Sun with period one year. There is no inertial frame (as shown by Einstein) since the Sun rotates around the Galactic centre

and the Galaxy is in relative motion with respect to other galaxies on a hierarchy of distance scales. However, the geocentric system is used and spherical coordinates may be used to define the position of a satellite: r=radial distance of the satellite from the geocentre; α=right ascension (angle in the equatorial plane from the vernal equinox eastwards); δ=declination (angle from the equatorial plane of the radius vector).

For the purpose of analysis, reaction wheel control is discussed here for simplicity. Although CMG's would be the actuation method of choice for ATLAS their control is much more complex than that for reaction wheels. Spacecraft dynamics with reaction wheels has the same form as for a general rigid body but with two additional coupling terms to account for nonzero wheel speeds and accelerations. The angular momentum of a rigid body with spinning wheels is the sum of the angular momentum of the rigid body and the angular momentum due to the spinning wheels. The wheels stabilise the spacecraft about any body-fixed principle axis. The total angular momentum of the system with angular momentum conservation is given by [Umetani & Yoshida 1989, Junkins & Turner 1986]:

$H = H_s + H_w + H_m = 0$ with respect to vehicle body coordinates (8.1)

where $H_s = I_s w_s$ = spacecraft angular momentum

$H_w = I_w(w_s + \Omega)$ = reaction wheel angular momentum=$H_{W1}+H_{W2}+H_{W3}$ for 3 wheels

$H_m = I_m(w_s + w_m)$ = manipulator angular momentum

I_S=inertia matrix of asymmetric spacecraft

I_m=inertia matrix of robot manipulator

ie. $H_s + H_w = -H_m$

Assuming each of three reaction wheels to be identical and each coinciding with each vehicle principle axis:

$$\begin{pmatrix} I_x^s w_x^s \\ I_y^s w_y^s \\ I_z^s w_z^s \end{pmatrix} + \begin{pmatrix} I_a^w(w_x^s + \Omega_x) \\ I_t^w w_y^s \\ I_t^w w_z^s \end{pmatrix} + \begin{pmatrix} I_t^w w_x^s \\ I_a^w(w_y^s + \Omega_y) \\ I_t^s w_z^s \end{pmatrix} + \begin{pmatrix} I_t^w w_x^s \\ I_t^w w_y^s \\ I_a^w(w_z^s + \Omega_z) \end{pmatrix} = -\begin{pmatrix} H_x^m \\ H_y^m \\ H_z^m \end{pmatrix}$$

where Ω = relative wheel speed

I_a^w = axial inertia of axisymmetric wheel = $I_Z{}^W$

I_t^w = transverse inertia of axisymmetric wheel=$I_X{}^W$=$I_Y{}^W$

Equivalently:

$$\begin{pmatrix} I_x^* w_x^s \\ I_y^* w_y^s \\ I_z^* w_z^s \end{pmatrix} + \begin{pmatrix} I_a^w \Omega_x \\ I_a^w \Omega_y \\ I_a^w \Omega_z \end{pmatrix} = -\begin{pmatrix} H_x^m \\ H_y^m \\ H_z^m \end{pmatrix} \quad (8.2)$$

where $I_i^* = (I_i^s + I_a^w + 2I_t^w)$ = composite spacecraft/wheel inertia.

(i) For an attitude controlled platform, $w_s = 0$ nominally. Differentiating with respect to time and noting that $\dot{H}_m = -N_r$:

$$\begin{pmatrix} I_a^w \dot{\Omega}_x \\ I_a^w \dot{\Omega}_y \\ I_a^w \dot{\Omega}_z \end{pmatrix} = -\begin{pmatrix} N_{rx} \\ N_{ry} \\ N_{rz} \end{pmatrix} \quad (8.3)$$

The wheel motor torque, $\tau_m^w = \frac{d}{dt}\left(I_a^w \Omega\right)$ so $\tau_m^w = -N_r$. The body-mounted wheels drive the spacecraft in a large angle slew maneouvre to counteract the applied moments from the robotic arm (assuming that the nominal desired attitude variables are zero so the measured values are the errors).

(ii) Once the feedforward component has commanded the reaction wheel torques, a feedback control law must be supplied to reduce attitude errors to zero from nominal zero attitude rates. The feedforward component may be used in conjunction with a PD feedback control law for the attitude controller, ie. attitude control and robot control schemes outlined here are both computed torque modes of control.
Similar equations are used with the angular velocity and angular acceleration values given by the attitude sensors to generate errors from nominal.
$H = H_s + H_w = 0$ where $w_s \neq 0$.

$$H = \begin{pmatrix} I_x^* w_x^s \\ I_y^* w_y^s \\ I_z^* w_z^s \end{pmatrix} + \begin{pmatrix} h_x \\ h_y \\ h_z \end{pmatrix} = 0$$

where $h_i = I_a^w \Omega$ =relative wheel momentum with respect to the spacecraft
Differentiate with respect to time according to Euler's equation of rotational motion to derive the moments associated with angular momentum changes defined by the differential of angular momentum over time:

$$\dot{H} = \dot{H}_s + \dot{H}_w = I^* \dot{w}_s + \dot{h} + w_s \times (I^* w_s + h) = I^* \dot{w}_s + w_s \times I^* w_s + I_a^w \dot{\Omega} + w_s \times I_a^w \Omega = 0$$

$$\text{where } \dot{H}_s = \begin{pmatrix} I_x^* \dot{w}_x^s + (I_z^* - I_y^*) w_y^s w_z^s \\ I_y^* \dot{w}_y^s + (I_x^* - I_z^*) w_x^s w_z^s \\ I_z^* \dot{w}_z^s + (I_y^* - I_x^*) w_x^s w_y^s \end{pmatrix} \quad \text{and } \dot{H}_w = \begin{pmatrix} \dot{h}_x + h_z w_y^s - h_y w_z^s \\ \dot{h}_y + h_x w_z^s - h_z w_x^s \\ \dot{h}_z + h_y w_x^s - h_x w_y^s \end{pmatrix} \tag{8.4}$$

These are first order Euler differential equation of the general form $N = \dot{H} = \left(\frac{dH}{dt}\right)_{body} + w \times H = I\dot{w} + w \times Iw$ which describe the external moments acting on the spacecraft in spacecraft principle axis coordinates [Agrawal 1980]. They are coupled and nonlinear and provide the body-referenced angular velocities and accelerations with which to drive reaction wheels. A strapdown optical inertial navigation system with rate gyroscopes and sensors rigidly attached to the vehicle can give angular rates with respect to the vehicle body frame, w, $\dot{w}$ from which inertial rates may be computed. Integration provides angular position values. The variation of parameters approach to attitude dynamics allows the use of the torque-free solution even when when small torques are acting on the spacecraft [Wertz 1978].
Now, wheel motor torque, $\tau_m^w = \dot{h}_w = \frac{d}{dt}\left(I_a^w (w + \Omega)\right) = I_a^w \dot{w}_s + \dot{h} = I_a^w (\dot{w}_s + \dot{\Omega})$:

$$\begin{pmatrix} \tau_x^m \\ \tau_y^m \\ \tau_z^m \end{pmatrix} = -\begin{pmatrix} (I_x^* - I_a^w) \dot{w}_x^s \\ (I_y^* - I_a^w) \dot{w}_y^s \\ (I_z^* - I_a^w) \dot{w}_z^s \end{pmatrix} + \begin{pmatrix} (I_y^* - I_z^*) w_y^s w_z^s \\ (I_z^* - I_x^*) w_z^s w_x^s \\ (I_x^* - I_y^*) w_x^s w_y^s \end{pmatrix} + \begin{pmatrix} h_y w_z^s - h_z w_y^s \\ h_z w_x^s - h_x w_z^s \\ h_x w_y^s - h_y w_x^s \end{pmatrix} \tag{8.5}$$

Now,

$$\begin{pmatrix} \dot{w}_x^s \\ \dot{w}_y^s \\ \dot{w}_z^s \end{pmatrix} = \begin{pmatrix} (I_x^* - I_a^w)^{-1}[(I_y^* - I_z^*)w_y^s w_z^s - h_z w_y^s + h_y w_z^s - u_x] \\ (I_y^* - I_a^w)^{-1}[(I_z^* - I_x^*)w_x^s w_z^s - h_x w_z^s + h_z w_x^s - u_y] \\ (I_z^* - I_a^w)^{-1}[(I_x^* - I_y^*)w_x^s w_y^s - h_y w_x^s + h_x w_y^s - u_z] \end{pmatrix} \text{ and } \begin{pmatrix} \dot{h}_x \\ \dot{h}_y \\ \dot{h}_z \end{pmatrix} = \begin{pmatrix} u_x \\ u_y \\ u_z \end{pmatrix} - I_a^w \begin{pmatrix} \dot{w}_x^s \\ \dot{w}_y^s \\ \dot{w}_z^s \end{pmatrix}$$

The wheel dynamics may now be given:

$$\begin{pmatrix} I_a^w \dot{\Omega}_x \\ I_a^w \dot{\Omega}_y \\ I_a^w \dot{\Omega}_z \end{pmatrix} = \begin{pmatrix} u_x - I_a^w \dot{w}_x^s \\ u_y - I_a^w \dot{w}_y^s \\ u_z - I_a^w \dot{w}_z^s \end{pmatrix}$$

$$= -I_a^w \begin{pmatrix} (I_x^* - I_a^w)^{-1}[(I_y^* - I_z^*)w_y^s w_z^s - h_z w_y^s + h_y w_z^s] \\ (I_y^* - I_a^w)^{-1}[(I_z^* - I_x^*)w_x^s w_y^s - h_x w_z^s + h_z w_x^s] \\ (I_z^* - I_a^w)^{-1}[(I_x^* - I_y^*)w_x^s w_y^s - h_y w_x^s + h_x w_y^s] \end{pmatrix} + \begin{pmatrix} I_x^*(I_x^* - I_a^w)^{-1} u_x \\ I_y^*(I_y^* - I_a^w)^{-1} u_y \\ I_z^*(I_z^* - I_a^w)^{-1} u_z \end{pmatrix} \quad (8.6)$$

The simplest way to transfer angular momentum from the spacecraft to the rotor for slewing is to let the wheel relative momentum increase linearly such that $\dot{h} = \text{constant}$. Euler's equations may yield analytic solutions using Jacobian elliptical functions but the usual procedure for solving Euler's equations in spacecraft attitude control systems is by applying the Runge-Kutta numerical integration method which approximates a Taylor series extrapolation of the differential equation function by evaluating the first derivative at points within the required interval. A fourth order algorithm with a fixed time step can yield solutions ~msec comparable to robotic algorithm solutions.

For the differential equation $\frac{dy}{dt} = f(y,t)$:

$y_{n+1} = y_n + \frac{h}{6}(k_1 + 2k_2 + 2k_3 + k_4)$ where $k_1 = f(y_n, t_n)$

$k_2 = f(t_n + \frac{1}{2}h, y_n + \frac{1}{2}hk_1)$

$k_3 = f(t_n + \frac{1}{2}h, y_n + \frac{1}{2}hk_2)$

$k_4 = f(t_n + h, y_n + hk_3)$

h=step size

The method is equivalent to Simpson's rule, is stable and does not require a starting procedure.

For a complete description of the rotational dynamics, a set of Euler angle representations are required to provide the body attitude with respect to inertial coordinates. One such set is the Euler angle set which denotes Z-X-Z rotation sequence wich describes the orientation of Earth-orbiting space objects relative to the Earth's equatorial plane. The inertial reference is initialised on the basis of the earth/spacecraft/star geometry. Solutions provide spacecraft attitude as a function of time. The commonest Euler set for Earth orbit operations are the roll-pitch-yaw formulations from a local vertical which relate inertial roll-pitch-yaw rates $(\dot{\alpha}, \dot{\beta}, \dot{\gamma})$ to body-referenced rates. The roll axis x lies in the direction of flight, pitch axis y is normal to the orbit plane, and the yaw axis z points towards the Earth centre:

$$w_x = \dot{\alpha}\cos\gamma\cos\beta - \dot{\beta}\sin\gamma$$

$$w_y = \dot{\alpha}\sin\gamma\cos\beta + \dot{\beta}\cos\gamma \qquad (8.7)$$

$$w_z = -\dot{\alpha}\sin\beta + \dot{\gamma}$$

Euler rates are not orthogonal so transposing the transformations do not yield the correct formulations for the inverse transformations. The classical Euler set which denotes a Z-X-Z rotation sequence becomes singular at $\theta = 0, \pm\pi$, ie. for level flight. An alternative Euler set which does not suffer from this is the aircraft Z-Y-X sequence of yaw, pitch and roll from a local vertical which only becomes singular at $\beta = \pm\frac{\pi}{2}$ corresponding to vertical flight. Since vertical flight is not usually encountered during in-orbit operations this is usually the set adopted. The roll axis X is the direction of flight, the pitch axis Y is normal to the orbit plane and the yaw axis Z is directed to the Earth's centre. This coordinate frame rotates about the pitch axis with respect to the inertially fixed coordinate frame at an angular rate of 1rev/day. It is possible to avoid singularities altogether by using the Euler 4-parameter set (similar to quaternions) which is based on Euler's principle rotation theorem that the most general displacement of a rigid body can be obtained by first translating a body parallel to an arbitrary axis then rotating the body about the axis in a single rotation. No 3-parameter set is free from singularities but the Euler set may be chosen such that orientational singularities will not be entered into or by switching between representations. Traditionally spacecraft have adopted the roll-pitch-yaw Euler convention. The vertical flight configuration is an unlikely scenario but if it did occur the representation could switch to the classical Euler set.

After the slewing acquisition stage is complete and the feedforward component has been realised, attitude errors will be small, so linearisation is permitted for the feedback part of the controller eliminating problems of singularity such that cos a~1 and sin a~a:

$$w_{0x} = \dot{\alpha} - \gamma\dot{\beta}$$

$$w_{0y} = \dot{\alpha}\gamma + \dot{\beta} \qquad (8.8)$$

$$w_{0z} = \dot{\gamma} - \beta\dot{\alpha}$$

This may be differentiated to yield:

$$\dot{w}_{0x} = \ddot{\alpha} - \dot{\beta}\dot{\gamma}$$

$$\dot{w}_{0y} = \ddot{\alpha}\gamma + \dot{\alpha}\dot{\gamma} \qquad (8.9)$$

$$\dot{w}_{0z} = -\ddot{\alpha}\beta - \dot{\alpha}\dot{\beta} + \ddot{\gamma}$$

These may be substituted into (8.6):

$$\begin{pmatrix} I_x^*(\ddot{\alpha} - w\dot{\beta}\dot{\gamma}) \\ I_y^*(\ddot{\alpha}\gamma + \dot{\alpha}\dot{\gamma}) \\ I_z^*(\ddot{\gamma} - \ddot{\alpha}\beta - \dot{\alpha}\dot{\beta}) \end{pmatrix} + \begin{pmatrix} (I_z^* - I_y^*)(\dot{\alpha}\gamma + \dot{\beta})(\dot{\gamma} - \beta\dot{\alpha}) \\ (I_x^* - I_z^*)(\dot{\alpha} - \beta\dot{\gamma})(\dot{\gamma} - \beta\dot{\alpha}) \\ (I_y^* - I_z^*)(\dot{\alpha} - \beta\dot{\gamma})(\dot{\alpha}\gamma + \dot{\beta}) \end{pmatrix}$$

$$+\begin{pmatrix} \dot{h}_x + h_z(\dot{\alpha}\gamma + \dot{\beta}) - h_y(\dot{\gamma} - \dot{\beta}\alpha) \\ \dot{h}_y + h_x(\dot{\gamma} - \dot{\beta}\alpha) - h_z(\dot{\alpha} - \dot{\beta}\gamma) \\ \dot{h}_z + h_y(\dot{\alpha} - \dot{\beta}\gamma) - h_x(\dot{\alpha}\gamma + \dot{\beta}) \end{pmatrix} = \begin{pmatrix} 0 \\ 0 \\ 0 \end{pmatrix} \qquad (8.10)$$

This is the general case and is very complex requiring control to be implemented in vehicle body coordinates. In general, a nominal reference trajectory may be selected such that the spacecraft follows a normal orbit trajectory similar to traditional spacecraft. This will be valid in the majority of cases. By assuming that the coupling terms are negligible (in the small angle limit), this allows a simplified form to be used for control in Earth-referenced inertial coordinates. Orbital motion about Earth is a rate of change of pitch causing the body referenced axes to rotate at an orbital rate of $\dot{\beta}_0 = w_{orb} = \sqrt{GM_{earth}/R^3_{earth+altitude}}$.

$$\begin{pmatrix} w_{0x} \\ w_{0y} \\ w_{0z} \end{pmatrix} = \begin{pmatrix} \dot{\alpha} \\ \dot{\beta} \\ \dot{\gamma} \end{pmatrix} + \begin{pmatrix} 1 & \gamma & -\beta \\ -\gamma & 1 & \alpha \\ \beta & -\alpha & 1 \end{pmatrix} \begin{pmatrix} 0 \\ -w_0 \\ 0 \end{pmatrix} = \begin{pmatrix} \dot{\alpha} - \gamma w_0 \\ \dot{\beta} - w_0 \\ \dot{\gamma} + \alpha w_0 \end{pmatrix}$$

This may be substituted into the Euler equations:

$$\begin{pmatrix} I_x^* \ddot{\alpha} + (I_z^* - I_y^*)(\dot{\beta} - w_0)(\dot{\gamma} + \alpha w_0) \\ I_y^* \ddot{\beta} + (I_x^* - I_z^*)(\dot{\alpha} - \gamma w_0)(\dot{\gamma} + \alpha w_0) \\ I_z^* \ddot{\gamma} + (I_y^* - I_x^*)(\dot{\alpha} - \gamma w_0)(\dot{\beta} - w_0) \end{pmatrix} + \begin{pmatrix} \dot{h}_x + h_z(\dot{\beta} - w_0) - h_y(\dot{\gamma} + \alpha w_0) \\ \dot{h}_y + h_x(\dot{\gamma} + \alpha w_0) - h_z(\dot{\alpha} - \gamma w_0) \\ \dot{h}_z + h_y(\dot{\alpha} - \gamma w_0) - h_x(\dot{\beta} - w_0) \end{pmatrix} = \begin{pmatrix} 0 \\ 0 \\ 0 \end{pmatrix} \qquad (8.11)$$

Rearranging the terms into the relevant inertial angular rates allows the use of an inertially derived PD control law of the form:

$$\begin{pmatrix} I_x^* \ddot{\alpha} + K_p \alpha + K_v \dot{\alpha} \\ I_y^* \ddot{\beta} + K_p \beta + K_v \dot{\beta} \\ I_z^* \ddot{\gamma} + K_p \gamma + K_v \dot{\gamma} \end{pmatrix} = \begin{pmatrix} 0 \\ 0 \\ 0 \end{pmatrix}$$

This completes the consideration of the attitude control system. Evidently, through the robotic feedforward compensation scheme the robot control system interacts directly with the spacecraft attitude control system. The attitude control system scheme resembles the computed torque technique in that error feedback is implemented by the attitude control system while the external effects of the robot are fedforward for compensation. Standard attitude control techniques may be employed with the proviso that reaction moment feedforward compensation is required.

Chapter 9

POLITICAL, ECONOMIC & LEGAL ENVIRONMENT

9.1 ECONOMICS OF SPACE TECHNOLOGY

The raison d'etre for a dedicated robotic spacecraft such as ATLAS was outlined earlier on the basis that spacecraft maintenance is more cost-effective than replacing spacecraft [Robertson et al 1988]. Here, the economics and legal issues involved in robotic servicing in space and more general issues are examined.

Generally, scientific/technological research comprises three categories: basic research which provides original investigation for the advancement of scientific knowledge without regard to commercial objectives; applied research which provides inverstigation for the advancement of scientific knowledge with specific commercial objectives; and development which involves the technical process of translating scientific research into commercial products or services. Technological R&D is a major component of the competitive environment in ensuring that technological development and innovation proceed at a high level. Non-inflationary economic growth and expansion requires productivity growth through technological change. The market economy is driven by widening the choice of goods to the consumer and this requires technological innovation stimulated by investment. Technological progress provides the means to dynamically revitalise mature economies. It provides the source of increased resource productivity by the application of technological knowledge to resource utilisation. This occurs through the deliberate distribution of investment resources to technological progress through R&D. Technological progress is a fundamental part of defining rational investment plans in achieving high rates of return. It has been estimated that for 1.6% economic growth a minimum capital investment of 5% of GNP is required. A GNP growth rate of 3% is generally considered the onset of strong growth.

Space programmes are pursued by governments for a multitude of reasons. National security is probably the most important motivator and always has been the primary reason - space activities are dominated by the superpowers. National image and foreign policy is the political background to the national security dimension. Space capability not only implies military capability but also denotes the importance of a nation in the international arena. Space technology was born out of World War II from military technology. Secondary motives are the opening up of commercial opportunities and the generation of tangible benefits to society. A side effect of this is stimulating advances in important technologies and assisting in social and economic development. Finally the least important motivators are scientific progress through exploration as these motives tend to be peculiar to scientists (though they represent a powerful and influential lobby).

The space industry is generally characterised by large investment requirements, political interdiction due to the military importance of space, the need for international co-operation for large projects, little prior knowledge of the risk and financial return and uncertain competition [MacArthur 1984]. This implies the need for government funding either directly or indirectly. Many of the industrial manufacturers and users are from the public sector including ground facilities. Only satellites are sufficiently

developed financially in terms of investment cost versus direct commercial return to lend themselves to the project investment approach favoured by the private sector. They are the only space systems which are characterised by adequate experience, reliability, demand, profitability and risk. The commercial development of space technologies are of different degrees and stages. Satellite communications is well established. Earth observation is in the process of commercial development while microgravity processing is in its infancy.

Funding for space activities is primarily from government through taxes with the original motivation coming from Cold War politics - the technology that puts men and satellites into orbit is the same technology as that to launch warheads on ICBM's. Almost all launch vehicles and many other space technologies (with notable exceptions such as the civilian NASA Shuttle and the civilian ESA Ariane) were developed directly from military rocket arsenals. However with the contraction of the defence industry which has traditionally been the source of advanced technology development, space activities are increasingly contributing to such development as well as providing a repository for a trained and skilled workforce. Technological advance and education has now become space technology's primary justification (swords into ploughshares). Indeed the technological returns from space investment to society are much larger than those from military research as military research is often classified and not utilisable in the public domain. Governments must play a pivotal role in nurturing the growth on new industries including investment in space infrastructure to open up new commercial space markets. Indeed space technology has been dominated by government financed agencies such as NASA and ESA which provide the market for existing aircraft manufacturers among others by providing contracts for spacecraft launch vehicles and ground systems.

Space economics is concerned with the assessment of tangible benefits (as measured by revenue) to society from space projects [Cohendet 1992]. The impact on industry may be direct or indirect. Direct effects are those that meet specific objectives of marketable services and arise out of contracts while indirect effects are based on technology transfer (spin-offs) and are derivatives applied to non-space industries. Such space spin-offs are well documented: electronic miniaturisation of computer technology and biomedical sensing motivated by the Apollo missions, ceramic materials motivated by the Shuttle heat tiles, NASTRAN finite element software package. Other less tangible benefits include the high quality label associated with space activities due to the high standards imposed by reliability requirements and sophisticated non-destructive quality control techniques. There are other possibilities such as the diffusion of highly trained expertise, closer collaboration between firms, new management and organisational structures but these are difficult to quantify (but should not be underestimated). Spin off capabilities of space investments to non-space activities depend on the nature of the technology. The UK, France and Italy have tended in the past to concentrate on structures and propulsion systems which are not generic in that they produce few indirect spin-offs (this refers specifically to spin-offs and not commercial application of the space technology) [Hertzfeld 1992]. Germany's space programmes tend to have broader scope by including electronics and power systems. It has been found that ~80% of the spin-offs from space were in electronics and instrumentation in particular. Indeed the Apollo missions are generally credited with being a strong spur to the miniaturisation of electronic components. Around 32%

of these electronics spin-offs were related to onboard equipment and around 25% were related to production and test equipment. There is usually an incubation period between the development of a product and its marketing of around 5y. Space technology is privileged like defence in that it straddles all the major fields of science on which industry is based. MBB-ERNO have established that around 50% of the technology transfer projects originate from their space departments.

There are two main methods of analysis for assessing the impact of space technology on the economy: macroeconomic analysis and microeconomic analysis. Microeconomic analysis is concerned with commercial return from an investment by analysing supply and demand through cost/benefit analysis. Macroeconomic analysis describes the relation between a nation's economy and its constituents. Both workforce and capital resources contribute to production. A critical driver to the economy is the rate of technological progress. In general it has been reckoned that technological advance contributed ~30% to US economic growth from 1930 to 1960 (of which 20% was attributed to organised R&D) but the link between formal R&D and GNP growth is indirect. Other studies have been performed with respect to NASA [Hertzfeld 1992]. The Midwest Research Institute in 1971 used a least squares regression to estimate the linear relationships between gains from past R&D to economic growth. It was estimated that between 1959 to 1969 a $30B investment would generate a return of $200B to the economy by 1987, ie. a 7:1 overall return or 33% discounted rate of return. Another 1988 study increased this overall return ratio to 9:1 and these figures were robust to increased time lags and R&D productivity reductions. The Chase Econometric Associates Study assessed the contribution of NASA to the US economy in relation to other US research expenditure. They calculated that the overall return ratio was 14:1 or a discounted rate of return of 43%. The study concluded that a sustained increase in NASA's expenditure of $1B/y from 1975 would increase the US GNP by $22B in 1984, increase workforce productivity by 1.1% and reduce unemployment by 0.4% due to 1.1 million new jobs created (at present NASA programs employ 242,000 people in 1992 of which 25,000 are government employees and 217,000 are industrial contractors). However these figures should be treated with caution since they are subject to high degrees of uncertainty. This should not however detract from the general message that it appears that R&D has a direct benefit on the economy as a source of technological advance beyond measurability through economics [Stone 1989].

9.1.1 ATLAS Cost Benefit Analysis

Recently, many space projects are required to be commercially beneficial without extensive support from governmental space agencies. All commercial applications of space technology to date and for the forseeable future will be in global services. Ordinarily technologies take ~ 20-30y to develop before they become commercially viable and only after ~30-40y do they become mature technologies. This implies massive initial state support and this has certainly been the case with satellite communications. ATLAS is deemed to be an exception to this rule such that commercial return is expected to yield after ~5-10y. This section presents a cost benefit anaylis in support of this statement.

Cost benefit analysis is a primary tool in assessing investment projects to ascertain the degree of benefits over cost achievable from the project. It is clearly desirable for

benefits to exceed costs. Since with any R & D project there are uncertainties in cost estimates, uncertainties due to the complexity of secondary benefits (eg. economic cost reduction through increased employment, stimulation to further investment and productivity, etc.) present market prices are used to value costs and primary benefits to a first approximation. Further it is not possible to transform all costs and benefits to monetary value, eg. social benefits and costs. For instance increased quality of life or hazardous pollution effects as social impacts are impossible to quantify. It is questionable if it is possible to assign monetary value to human life such as by a Pareto optimum. These are incommensurable and cannot be equated with monetary value but do have valid units of measure. Other things of value even defy any unit of measure such as national prestige which is intangible. Cost benefit analysis used in assessing the desirability or undesirability of expenditure of public funds is a branch of welfare economics. It cannot give any evaluation of the goals of a nation such as the determination to compete or dominate in high technology products. Furthermore secondary effects may be difficult to ascertain such as indirect benefits on the rest of the economy and such benefits may be enormous, larger even the direct benefits. Technology transfer to other fields is one example. Secondary costs are even more difficult because it is often not possible to ascertain the deleterious effects of a project particularly in the long term, eg. environmental degradation. Such effects cannot be included in the cost benefit analysis unless they are well defined and quantifiable.

Cost benefit analysis then is merely an economic aid to be used with other methods which are concerned with policy and priorities. The main outcome to be ascertained using cost benefit analysis is the survivability of the enterprise as evidenced by its capability for generating revenue which exceeds its costs over long periods of time. As with any investment project however benefits will show a time profile and an initial outlay of capital will be required with possible later outlays. Harmon (1982) considered space robotics for in-orbit manipulation as a highly favourable applications area of robotics for investment as it is characterised by the lowest difficulty-demand product with the potential for the highest payoffs whilst offering a marketable service as well as advancing high technology. Capital cost is defined as that required to build and manufacture a product. For space projects in general the capital cost investment tends to be large. Opportunity cost is not a real cost as such but represents what is foregone as a result of not taking advantage of a good investment quickly, ie. the loss of return due to delay. An example of this might be that other financiers may take up the investment.

Space life cycle costs are divided into three phases: RDT&E (research, development, test and evaluation), production including the production of flight units and launch costs, and finally Operations & Support. The RDT&E phase is a non-recurrent cost. The prototype approach is one where the qualification test unit is refurbished for flight as the flight unit but this increases the non-recurrent RDT&E cost by ~30% though it reduces production costs substantially as there is no dead end hardware. Furthermore even the refurbishment requirement may be eliminated by eliminating the need for a hardware model prototype altogether. Major cost reductions may be effected in reducing hardware testing through the use of computer simulations and CAD/CAM for geometric and dynamic analysis, structural analysis, control analysis, visual animated simulations. The Boeing 777 was developed with no model prototype. Further cost

cuts can be made. Since management comprises 30% of RDT&E costs such should be ruthlessly minimised through a flat management structure.

A matrix company structure is preferable to independent departments with each project or mini-projects cross-correlating with R&D, marketing, manufacturing and operations divisions. This fosters internal cross-fertilisation. Recently the concept of a firm being a learning organisation has become fashionable - this is in contradistinction from the past "downsizing" philosophy that has been prevalent in the past. Part and parcel of this is that the firm relies extensively on its intangible assets such as personnel and R&D personnel in particular. Its most valuable asset is corporate knowledge reflected in the skills, knowledge and intelligence of its employees that enable it to survive and adapt in an increasingly difficult commercial environment. The greater the mix and breadth of such corporate memory, the greater its marketability. Companies recently have failed to pass significant fractions of productivity gains to employess in higher wages. Power-sharing partnerships between unions and management is essential for the interests of the company. The means to attain this corporate knowledge is through education of the employees. As technology and working practices change, so workers need new skills, especially those that allow lean production, low waste and quality control. This provides the means of an employee/employer social contract - no employee can be guaranteed a position for life but all companies ultimately rely on their employees for success. Education generates high productivity gains and high employee morale. Furthermore, employee education is not necessarily a cost centre. Education may generate direct profit through the sale of courses. However it is through the adaptability of the employee that companies can obtain survivability in a rapidly changing and competetive environment. This stresses some of the indirect and non-tangible benefits to a technologically trained workforce with the capability to adapt and learn.

Product assurance and testing accounts for 20% each of RDT&E costs and the elimination of a non-flight prototype reduces those factors to half their values. All in all these factors should offset the 30% increase in RDT&E costs for the flight unit. Finally as this is a commercial spacecraft it is likely to be less expensive ~80% than a government built spacecraft. A heuristic method of capital cost estimation was made based on average production cost/unit mass of spacecraft. Cost estimating relationships (CER) are log-linear laws of the form: Cost, $C=AxP^{X}$ where P=parameter and x is 0.5 for RDT&E costs and 0.75 for production costs. Such were not used since their validity is suspect regarding innovative designs like ATLAS. The production cost per unit mass of a spacecraft varies from $100,000/kg for commercial spacecraft to $150,000/kg for interplanetary probes. An average gives $125,000/kg which for a 1.5 tonne spacecraft gives a total production cost of $175M in round figures. Now RDT&E costs are usually around 2 to 3 times the production costs. This would generate a total RDT&E cost of $350M. This cost however is based on a 10y technology development schedule (similar to that for a warship) which for ESA is divided into 6 phases:

Phase 0: this is the exploration study which defines the mission opportunity and initial technological requirements and typically lasts 3y.

Phase A: this is the predevelopment phase which demonstrates the mission feasibility and identifies key trade offs and typically lasts 1y.

Phase B: this is the development phase which shows flight suitability of a project through in-orbit demonstration (or in-orbit hardware simulation) and defines the detailed project design. This lasts 2 y.
Phase C: this is the qualification phase whereby flight hardware and technology is constructed and flight qualified. This lasts 3y.
Phase D: this is the launch development phase which prepares the project for launch and typically lasts around 1 y.
Phase E: this is the launch and post-launch operations phase.

This thesis in effect comprises Phase 0 and much of Phase A. In addition there is a new philosophy to space projects of minimising the development period. Hence it is quite conceivable that a 5y timeline may be projected. The short lead time from conception to launch is based on the premise that most of the technologies are essentially in place. This is necessary to ensure that costs do not soar, eg. Envisat which is one of a series of polar-orbiting environmental platforms for Earth Observation following on from ERS-1 and 2 has a lead time of 15y imposing a huge $1.5B cost. Project funding is highly dependent on the schedule since most of the cost of R&D comprises salaries. The cost of hardware is small compared to time since hardware already has skilled labour time added to its purchase price. Long projects cost more because salaries are paid for longer, interest on borrowed money is lost, and storage and maintenance costs for additional storage is incurred. By reducing the R & D phase from 6y to 2y, the RDT&E would normally last 6y. RMS, ROTEX and ETS-VI may be regarded as potential demonstrators of the feasibility of robotic systems in space but a specific Phase B technology demonstrator would be required. Particularly relevant for hardware validation of ATLAS on the ground is the existence of ESA's Docking Dynamics Test Facility mock up and their European Proximity Operations Simulator mock-up as well as their extensive robotic hardware facilities. ESA has also constructed a neutral bouyancy tank to allow neutral bouyancy simulation. The tank forms part of the IVA (Intravehicular activity) Underwater Testing Programme. The tank is 6m deep and 10m in diameter. Alternatively this could be accomplished using small satellites for in-orbit testing. UoSat is in the microsat range (~10-50 kg) and is an LEO rated spacecraft costing ~£0.5M while the STRV is a minisat (~50-500 kg) and is a GEO-rated spacecraft costing ~£5m. The 150 kg STRV is in fact designed to investigate the in-orbit performance of new advanced space technologies. By implementing a "faster, cheaper, better" philosophy this may be reduced to 5y typical of that from initial specification to beginning of production for a new automobile.

Such a business methodology can reduce the cost of spacecraft development by up to 50% - Lockheed developed the all Ti SR-71 aircraft in only 22 months [Mandell 1992]. This requires lessons to be learned from smallsat programmes in cost cutting. The programme durations are short ~1.5-2y designed by a small spacecraft team of 15-30. The NASA Discovery missions are of this nature with 36 month development schedules and $150M cost ceilings. Another example is the Clementine mission launched in 1994 as an SDI project by the US Naval Research Lab to test sensors and provide the first lunar polar maps. The design philosophy was a departure from the established spacecraft design procedures in that it utilised miniaturised sensors and electronics and lightweight structural materials. New lightweight sensor technologies included 3 ultraviolet/visible CCD cameras, 2 infrared CCD cameras cooled by Stirling cycle cryocoolers, a lidar Nd:YAG altimeter for mapping, and ring laser and fibre optic

gyroscopes within a graphite epoxy structure. Furthermore the design departed from the usual practise of using military standard components by using commercial standard lightweight components. It employed a 16 bit 10 krad (Si) radiation hardened computer with a 1.7MIPS processing power for housekeeping operations and a 20 krad (Si) radiation hardened 32-bit RISC processor with 18 MIPS processing power for image processing and onboard autonomy. A GaAs on Ge solar array provided 360W power in conjunction with high power ultralightweight nickel-hyydrogen batteries. Its orbit mass was 1690kg (dry mass of 235kg, 223kg liquid fuel, the rest being the solid rocket booster to give it the 550 m/s delta-v for lunar orbit insertion from LEO). Despite the advanced technologies used, it was developed, built and launched in 2y by a team of 55 engineers for less than $80M. It successfully completed its lunar survey of the Moon's poles in testing its sensors but was unable to perform the planned flyby of the near Earth asteroid Geographos 1620 due to a thruster sticking open on leaving lunar orbit which induced a spin and necessitated burning up most of the spacecraft's maneouvring fuel. It was then returned to a near-Earth orbit. The UK also hass experience of small, cost-effective programmes with limited resources with the UK Black Arrow satellite launcher programme [Robinson 1992, Peattie 1992]. Black Arrow was a small three-stage launcher concept with a satellite payload capability of 100kg for scientific and technological research based on the Black Knight test vehicle which began in 1964, lasted for 6y with a total budget of only £10M (at 1964 prices) and a launch team of only 50. The P1 prototype was completed in 1967 and three development flight vehicles R0, R1 and R2 were launched between 1969 and 1970. The final Black Arrow utilisation vehicle R3 comprised of two liquid propelled stages and a third solid propellant apogee motor stage. Its total mass at launch was 17.8 tonnes and its overall length and maximum diameter was 13.0m and 2.0m respectively. The Black Arrow was successfully launched from Woomera in Australia into an elliptical polar orbit of 350x850 nm at an incliniation of 82^{o} in 1971. The payload was the 66kg X-3 Prospero satellite with space technology experiments. Prospero continued to function for 18y until 1989 when the VHF receivers at the TT&C station at Lasham discontinued operation. The UK then became the 6th nation to orbit its own satellite using a national launch vehicle and payload. The addition of 4 solid rocket boosters would have increased Black Arrow's performance to 250kg into a 500km circular polar orbit. The programme was cancelled after its successful flight and this was followed by the cancellation of the Blue Streak programme which was to be used as the first stage of the ELDO Europa launch vehicle. A combination of the Blue Streak with Black Arrow upper stages would have provided the UK with a commercial GEO launcher programme a decade before the operational venue of ESA's Ariane launcher.

An additional factor enabling the realisation of a short development period is that no fundamental advances in technology are required. Such developments are one of the greatest hindrances to meeting schedule deadlines: the Space Shuttle required considerable advances in materials technology to accommodate the aerothermal environments of re-entry ~1MW/m^3 without the use of ablative materials. Major problems were encountered with the adhesive for bonding the various tile layers together until a silicone-based adhesive was developed generating huge cost overruns. Costs may be minimised by using off the shelf technology, a philosophy underlying the BMDO's DC-X SSTO prototype. DC-X (Delta Clipper eXperimental) was a successful one-third scale sub-orbital prototype testbed SSTO (single stage to orbit)

cone-shaped launcher developed under the US Ballistic Missile Defence Organisation, BMDO (formerly Strategic Defence Initiative SDI). It had a budget of only $65M but used advanced lightweight composite structures to minimise its 600 tonne mass of which only 50 tonnes was structure. This full scale version should have a payload capability of 10 tonnes to LEO and 5 tonnes to polar orbit. DC-X successfully flew to 1200ft atitude, translated 350ft and descended to its launch pad in 72s. It was built in under 2y and used F-15 inertial navigation systems, commercial GPS, sensors from the F-18 and a flight control system developed by Honeywell for airliners. It was controlled from a portable launch pad set up comprising a trailer-based Flight Operations Control Centre, the launch pad, fuel handling facilities and communications equipment. This enabled it to have a turnaround time of less than 1 week. Couple these design philosophies with the slimming of administrative costs and the elimination of non-flight hardware, a conservative estimate of RDT&E costs for ATLAS is taken as $225M. The total cost is then projected as $400M as the baseline.

The next largest cost are launch fees and launch insurance. Launch costs are estimated by the cost per unit mass to LEO:

	Max payload to LEO (kg)	Unit cost ($M)	Cost ($K/kg)
Ariane IV	17800	125	6.5
Shuttle	23000	210	8.2

Ariane IV offers the lowest cost per unit mass with ~$7000/kg (cost per unit mass to GEO increases to ~$50K/kg) . A more reliable estimate comes from the Shuttle pricing algorithm:
$190M x (spacecraft mass/(0.75xshuttle capacity))=
$190Mx(1500/0.75x23000)=$16.5M
Insurance costs are around 16-20% of the spacecraft cost so with insurance at 20% of $400M the insurance bill is $80M. This is an upper bound estimate to account for the fact that ATLAS would be a new and therefore untried risk. However ERS-1 as a new type of satellite exceeded its operational lifetime - the corollary is that new spacecraft do not necessarily suffer from reliability problems. Hence the total cost is almost $500M ($400M+launch+insurance) which is taken as the total capital investment cost over a 5y investment period from conception to launch. Funding would be given year-by-year and costs are usually heaviest in the first two years such that by the midpoint of the project ~60% of the costs have been consumed. Hence the investment funding profile is perceived to be:
Year 1: $125M - RDT&E
Year 2: $100M - RDT&E
Year 3: $50M - Production
Year 4: $50M - Production
Year 5: $175M - Launch
The next stage concerns the operational costs of running ground station staff and maintenance which can usually be equated to software costs. This covers to cost of maintaining the product and its service flow over the length of its life. Ground software costs are ~$175/line of code. Assuming 100,000 lines of ground software code this gives the ground software costs at ~$17.2M. Maintenance of this code is quantified by:
C=0.1x(SW+EQ+F)x17.2M per year where SW=software cost fraction =1
EQ=equipment cost=0.81
F=facilities cost fraction=0.18

Hence C=$3.4M per year. Additional costs are for labour priced at $130,000/y for contract staff and $90,000/y for government labour. Assuming 10 staff of each (cf. Cray Systems CLEO mobile ground station system requires 6 personnel):
Labour costs = $1.3M+$0.9M=$2.2M/y.
The total yearly operating cost is therefore $5.6M/y. In addition, in-orbit insurance at 2% of the satellite cost gives an additional $8M/y overhead (except the first year of operations which is covered by launch insurance). This totals almost $15M/y to operating costs (except during the year of launch). These costs are recurrent and run through the length of life which may be up to 20y with maintainability. Additional costs include EDRSS rental during operational periods only - dormant phases will operate through a packetised command/telemetry mode. Finally there is the necessity to refuel ATLAS periodically. Docking alone is estimated to use around 40kg of hydrazine per dock although this would be relaxed through the use of manipulators. Such refuelling may take advantage of various launch opportunities offered by launch companies for launching small payloads. NASA has its GAS (Get Away Special) programme to replace Space Shuttle balancing ballast with small <68kg payloads fixed to the payload bay wall for $50,000 (not usually deployed). NASA also has its Complex Self-Contained Payload programme for slightly larger payloads of <114 kg for $150,000. Arianespace offers its ASAP (Auxiliary Payloads) facility which can launch up to 6 microsats on Ariane VI underneath a single main satellite. There are 6 mounting points in a circle of radius 2.9m for minisatellites of less than 50 kg up to a total of 200 kg. For larger minisatellites adapter cones must be used to sandwich between the larger spacecraft. Launch costs are very low ~10% normal launch costs ~$700/kg. Hence each 200kg of fuel launched as fuel canisters would cost $140,000. Four such launches would completely refuel ATLAS at a cost of $560,000, ie. around $0.5M. Such refuelling would depend on the number of operations undertaken and across what time scales so represents a negligible cost as far as the minimalist scenario adopted here is concerned. The payload are flown on standby with no guaranteed launch date. ATLAS must also use the EDRS system during operational phases (it will use a store-and-forward strategy when dormant) which costs $30/minute (TDRSS is too expensive at $200/minute). This amounts to $0.43M for a continuous 10 day operation.The implementation of a space-based support platform as an orbital "repair shop" for highly complex operations, repairs and overhauls would be expensive both in its production and its operation. Such would provide a thermally controlled environment for the storage of ORU's, consumables, and equipment for ATLAS as well as providing a stable work area. This implies the need for dedicated subsystems including electrical power, thermal control, communications, data processing and attitude control.

Once operational, revenue will be generated and this must be maximised. Selling price is a function of perceived value of the product or service and this is increased mostly by R&D which generates product innovation. Productivity increases through R&D are usually much larger than the savings in manufacturing costs like labour [Suh 1984]. Indeed the economy is driven by new innovations. In essence cost relates to time in that all human activities take time and value is placed on that time particularly that invested in a project. ATLAS can offer in-orbit servicing capabilities at lower cost than the only other supplier of in-orbit servicing capabilities: NASA through EVA from the Space Shuttle. The US is unlikely to develop a rival robotic servicer after the cancellation of the FTS - NASA at present justifies its Space Shuttle missions on the basis of the EVA in-orbit servicing capabilities. This justification is unlikely to be used

once the Space Station becomes operational as the Shuttle would be justified as a ferry, so ATLAS should be marketed as an operational service for the repair and maintenance of space assets. Indeed ATLAS would be a considerable asset to the Space Station as it could retrieve ailing spacecraft much more cheaply and regularly than the Space Shuttle. The space market is expected to undergo rapid expansion particularly at equatorial and polar LEO over the next few decades and EVA will be limited to equatorial LEO. As a virtual monopoly ATLAS offers the possibility of simultaneous penetration and skimming pricing. This monopoly arises primarily due to the control of the service but may be maintained by virtue of the large capital investment requirement and through patent ownership. Penetration pricing is offered since the price is low in comparison to the competition to enable securing of the market, and the skimming pricing is offered since the price is high enough to recover R&D costs fairly rapidly and generate high profits. It is perceived that an average revenue of $150M per mission is appropriate. This was suggested by the Intelsat VI repair mission which cost the insurers $150M and by launch insurance costs. Other lesser satellite malfunctions requiring interdiction which have been documented support this price. BS-3A in August 1990 suffered a partial power loss and required electrical unit replacement; Superbird A in December 1990 suffered a thruster malfunction and loss of control and required unit replacement, re-orientation and refuelling; Anik E2 in April 1991 suffered antenna deployment failure and recovered 81 days later with EVA grapple assistance; these three "minor" failures involved a $200M insurance claim suggesting ~$70M costs for even minor repairs. Olympus I in May 1991 suffered control loss and recovered 2 months later when assisted and reoriented by astronauts; the UARS satellite required solar array replacement. In the space of 12 months from mid-1990 to mid-1991, four repair operations were required with a market value ~$300M for that year. Numerous other cases of transponder failure, power loss, control loss and thruster malfunction have been documented. This suggests that the $150M price tag per average operation is a reasonable price and ~$75M per simple operation. The price mechanism is a form of optimal control to maximise the profit functional between supply and demand.

The next question concerns the number of operations that may be required per year. Launch rates have been constant since the mid-1960's at ~40 launches per year of which 60% are presently military launches (which are increasing at a rate of 19% compared with commercial launches which are increasing at a rate of 2%). Geographically the spread has been: USSR ~80%, USA ~12%, others ~8%. Although the status of the Russian Space Agency seems a little more certain now than a few years ago it is likely that its launch activity will drop - it is assumed that Russian launches will cease giving ~8 launches/y. Each launch places on average ~4 satellites in orbit placing ~30 satellites per year into orbit. This is the baseline taken. In fact the launch rate is expected to increase with the advent of mobile comsats in LEO and Earth Observation satellites to polar orbit to around ~100 launches per year (each with 4 satellite payloads) so the baseline represents a highly conservative figure. Launch failure rates of ~5% as given by reliability figure for launchers suggest that 10% of the 15% satellite insurance rate are in-orbit failures such as failure during checkout, etc. Hence if 10% of satellites are expected to fail or give suboptimal performance around 3 satellites will fail in-orbit per year. This correlates well with the 1990/1991 actual failure rates in LEO alone. Of those expected 3 failures, it is assumed somewhat arbitrarily that at least one will be an average operation repairable remotely in-orbit by

ATLAS or at least two will be simple operations remotely repairable by ATLAS. Hence the total annual revenue is conservatively taken to be $150M/y. Note that this does not specifically include satellite refurbishment through refuelling and module replacement. This is specifically for repair purposes. The requirement for refuelling and updating existing space assets is likely to be a primary utilisation of ATLAS particularly for scientific satellites as they tend to be expensive yet have short lifetimes due to fuel and other limitations. Refuelling a scientific satellite represents a cost effective way of extending scientific return and is likely to be a lucrative but as yet unquantifiable source of additional revenue.

The net present discounted value for a stream of net benefits $N_0 ... N_n$ is defined from the concept of compound interest:

Compound interest value $N = P(1+r)^n \rightarrow P = \frac{N}{(1+r^n)}$

Hence [Mishan 1971, Prest & Turvey 1965, Sallaberger 1993],

$$N = N_0 + \frac{N_1}{(1+r)} + \frac{N_2}{(1+r)^2} + \ldots + \frac{N_n}{(1+r)^n} = \sum_{t=0}^{n} \frac{N_t}{(1+r)^t}$$

where P=net present value (NPV)

N=net benefit=B-C where B=benefit>0 and C=cost<0.

r=rate of discount or compound interest rate ~10%

The project is attractive if N>0 but for high risk ventures N>40% is usually required for venture capitalists. The NPV is based on the time discounted value of money in that money is worth more now than the same amount in the future since it may be invested to earn a return. The interest rate depends on the source of payment. The US Office of Management & Budget recommends a rate of 10% for government projects and 15% for private projects though Greenberg (1992) suggests that in reality 3-5% is more appropriate as this represents the real rate of return defined as the difference between yield from long term, high value securities and the inflation rate. However by assuming a partnership between government and the private sector with 51% funding from the government with r=10% while 49% funding from private sources requires r=15%. Hence the interest rate is given as r=0.51(1.01)+0.49(0.15)=0.125, ie. 12.5%. We assume here that the cost-benefit analysis is that perceived by the private investor.

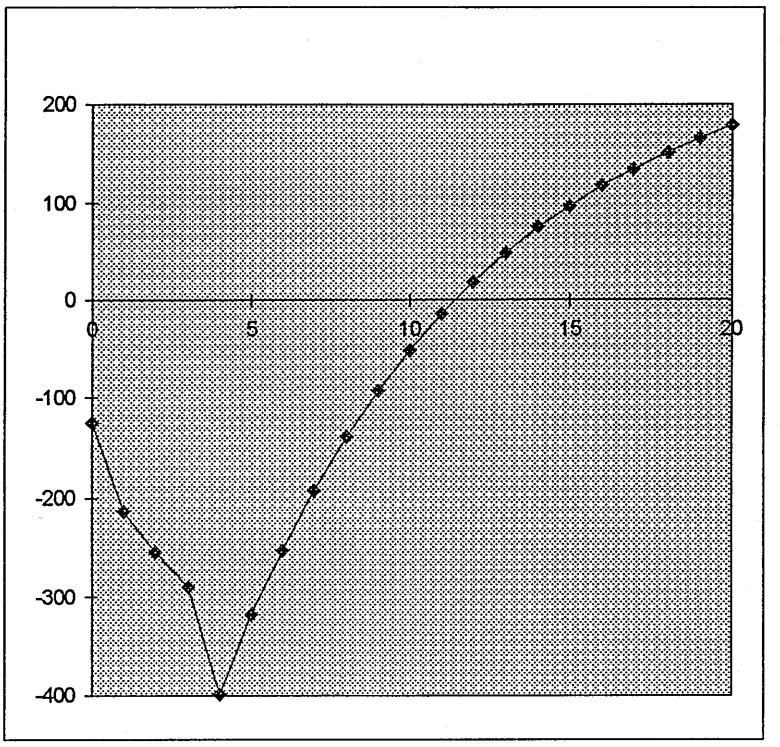

			Index	Ni	Sum
N0	-125		0	-125	-125
N1	-100		1	-88.8889	-213.889
N2	-50		2	-39.5062	-253.395
N3	-50		3	-35.1166	-288.512
N4	-175		4	-109.252	-397.763
N5	144		5	79.90977	-317.854
N6	135		6	66.59147	-251.262
N7	135		7	59.19242	-192.07
N8	135		8	52.61549	-139.454
N9	135		9	46.76932	-92.6848
N10	135		10	41.57273	-51.1121
N11	135		11	36.95354	-14.1586
N12	135		12	32.84759	18.68903
N13	135		13	29.19786	47.88689
N14	135		14	25.95365	73.84054
N15	135		15	23.06991	96.91045
N16	135		16	20.50659	117.417
N17	135		17	18.22808	135.6451
N18	135		18	16.20274	151.8479
N19	135		19	14.40243	166.2503
N20	135		20	12.80216	179.0524

The break even point is 12y after the initial investment or equivalently after 7y of operational service. After 20y from the start of the project or equivalently after 15y of operational service the ATLAS programme has generated a 45% discounted return on investment (ROI), above the 40% requirement for high risk ventures. Furthermore the high risk is offset by the insurance cover from launch throughout its operational life so

it is debatable whether the 40% ROI is a necessary qualification. A major contribution to the attractiveness of an investment like ATLAS is that the investment risk is effectively insured through the launch and in-orbit insurance and includes loss of revenue. Private financing is generally obtained through banks and venture capitalists. Bankers do not fund speculative ventures but venture capitalists have a limited time horizon - they are normally limited to a 5 y investment period after which they expect their 40% ROI. Furthermore their interest tends to be close to the stock market. Later stages of the project tend to be the attractive periods for private investors once advanced sales contracts have been obtained and sufficient assets have been created. Project financing is a technique whereby bankers lend money which is reimbursed on the basis of cash flow generated once cash flow has been established. Bank facilities such as overdraft are of dubious value due to the high interest rates in the UK. However the largest source of private investment comes from the sale of shares. Capital is a scarce resource and many projects must compete for capital investment and it is allocated on the basis of risk/reward trade-offs. Lenders expect to be repaid while investors expect to make a return. However there is no shortage of commercial funding schemes for terrestrial infrastructure projects such as dams, road and rail networks, power plant installations, bridges and so on. The French rail transport infrastructure programme required an investment of $230B over 20y (cf. Apollo programme cost $80B over 10y).

The government is the only economic entity capable of funding long term investment projects since a high proportion of national income passes through the Treasury through company profit, income and sales taxation:

Disposable income=GNP-T where GNP=C+I+G

C=consumption

I=total investment

G=government expenditure

T=total tax flow=$t.GNP+T_S$

t=tax rate

T_0=surtax. [Suh 1984]

The last decade or so has seen a major political shift in the West especially the USA and the UK to reduce the relative share of the public sector from ~40% of the national economy down to 25% with mixed success. This was the biggest political shift in the post World War II era barring the collapse in the USSR in the late 1980's [MacArthur 1984]. This shift was based on the premise that large public corporations are bureaucratic and less economically efficient than privately funded corporations as they do not employ profit maximisation. Other problems include political domination and public accountability which hinder economic efficiency. Both factors lead to tendencies towards loss-making. Bureaucratic interference in industry is harmful but overdue emphasis on the rational profit motive omits consideration of non-profit values. Individual profit maximisation is not a secure characterisation of human behaviour nor does it necessarily imply efficiency.

Governments should provide the economic and social conditions necessary to enable free enterprise to flourish. The UK government still spends almost 40% of GNP and it has a responsibility to encourage a healthy, robust economy that benefits all sectors of society. Only technological change and innovation can make the economy expand profitably and this requires long term investment. Generally a high rate of investment

promotes economic growth but low rates of investment yields low economic growth - Japan with no natural resources (requiring the import of raw materials) has achieved spectacular economic growth through its high investment rate in technology and production of manufactured goods for both domestic use and for export. The basic weakness of the free enterprise economy is that there is a propensity to save which is stronger than the inducement to invest and low interest rates are required to offset this. The public purse represents a significant fraction of the economy and only governments have the broad, long range interest to finance long term technological advancement beyond market horizons through sustained research where the costs are high and the commercial returns uncertain. The Treasury is the largest centralised institution which has the financial resources to invest heavily in R&D. Examples of investment periods prior to commercial viability include the jet engine ~14y, radar ~13y and TV ~22y. Private businesses are too susceptible to short term investment opportunities such as bonds, buyouts, share investments, etc which offer low risk. Hostile takeovers and engineered buyouts in the 1980's effectively pressurised firms to concentrate on profits and dividends before long-term investment and R&D. Furthermore privately funded research is highly localised characterised by isolationism, competitiveness and confidentiality which is detrimental to larger, national interest. Common ground between the public and private industries are not properly delineated and optimum use of resources cannot be attained. This is particularly the case for high cost research which by its nature requires cooperation between involved groups. Investors do not invest in risky technology, they invest in safe business. Firms will not invest in R&D if such benefits will be enjoyed by others. Some protection is afforded by intellectual property laws such as patents, allowing industries to gain competitive advantages. A similar situation exists with regard to skilled training of employees. The vast majority of R&D performed by private companies is financed through source funds provided by governments through contracts (eg. defence contracts). Market forces cannot generate long term technological investment programmes - this is why war is such a good stimulus to technology as rapid financial gain ceases to be the top priority and money is made available for the battlefield. Commercial rate of return is not per se sufficient to justify a decision by government to invest whereas the social rate of return demonstrates that an investment is beneficial to the economy. Increasing R&D expenditure in a market economy by government is required to increase productive efficiency. Such technological investment requires state intervention and it is the responsibility of government to invest in technology. The government must make up for the neglect of private industry by maintaining R&D innovation at optimum levels. Although ATLAS may be regarded as a space infrastructure programme, unlike terrestrial infrastructure programmes with large investment requirements ~$10B/y and very long term but low rates of return, ATLAS offers rapid high returns from high investments ~$100M/y.

The government can provide public funds at the initial stages as investment bankers to reduce the perceived risk of such space ventures and encourage private investors for stock perhaps later augmented by funds from the private lending banks. Only short term financing should be in the form of loans while longer term financing should be in the form of share sales priced on the Stock Exchange. Government finance is particularly important where the R&D component tends to be the largest fraction of the total cost as with most space projects. Space business ventures involve large capital investment, long payback periods and high risk. However uncertainty (ie.

perceived risk) may be reduced by technology demonstration programmes which otherwise effectively reduce the expected return on investment. In economic theory the reward for uncertainty bearing is profit but in actuality private investors are highly risk averse. With government funding for the demonstration programmes this reduces the initial capital burden as well as reducing the perceived risk. Furthermore, government investment is the only way to ensure commercial survivability - over 80% of technology-based business startups (especially those concerned with electronic components) fail in the first year of trading in the UK. For ATLAS the government as a 51% shareholder should invest the first $255M over the initial 3 years to open up a new market and new opportunities for private investors. In the third year stocks may be issued in the market to invite private investment. The government should have controlling interest to ensure that a significant proportion of the profits are re-invested into research rather than just churned out as dividend payments. UK companies maximise dividend payments to shareholders - all firm profits are taxed at ~35% while dividends to shareholders (comprising 33% of profit) are taxed at only 25%. In 1992, UK companies overall spent twice as much on dividend payments to shareholders than on their internal R&D compared with the top 200 international companies which spent three times as much on internal R&D than on dividend payments (some as much as 15 times). Th top 300 companies returned 4.5% of their sales revenue into R&D compared with 2.5% characteristic of British companies. The problem is to balance the dividends to shareholders to provide incentive to invest and the need for the business to reinvest in R&D, marketing and new assets.

		Index	Ni	Sum
N0	-20	0	-20	-20
N1	-50	1	-44.4444	-64.4444
N2	-175	2	-138.272	-202.716
N3	144	3	101.1358	-101.58
N4	135	4	84.27984	-17.3004
N5	135	5	74.91541	57.615
N6	135	6	66.59147	124.2065
N7	135	7	59.19242	183.3989
N8	135	8	52.61549	236.0144
N9	135	9	46.76932	282.7837
N10	135	10	41.57273	324.3564
N11	135	11	36.95354	361.31
N12	135	12	32.84759	394.1576
N13	135	13	29.19786	423.3554
N14	135	14	25.95365	449.3091
N15	135	15	23.06991	472.379
N16	135	16	20.50659	492.8856
N17	135	17	18.22808	511.1136

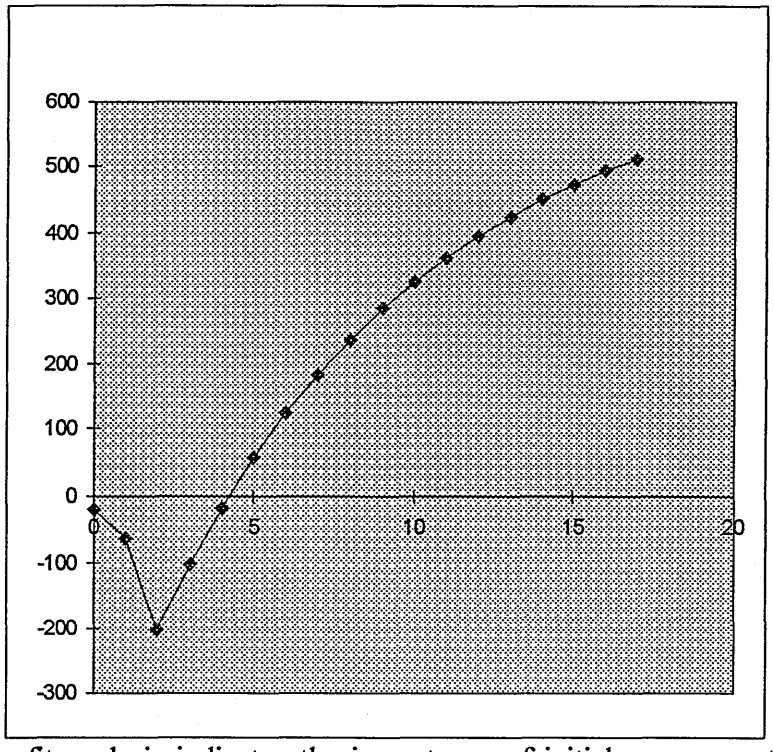

This cost benefit analysis indicates the importance of initial government investment. The payback period is within 5y (or just over 2y of operational service) just within the time horizon of venture capitalists. Furthermore the discounted ROI to the private investor after 17y (15y of operational service) is 252%. With the appropriate corporation tax rate of 35-40%, the tax returns alone on profits back to the Treasury would effectively repay the government's original investment. If the government required repayment of the investment through a government loan this would have a direct effect in reducing the likelihood of private sector investment. However it is apparent that the tax returns to the Treasury would exceed the original government outlay even when discounted eliminating any argument favouring a government loan. Albus (1990) also suggested that government financing could be achieved through selling 5y industrial development bonds and through the introduction of a savings tax. Capital raised through savings tax could be placed in industrial development funds which could be repaid with interest well above the inflation rate to the savers when the bonds mature. A savings tax would furthermore place the heaviest burden on the wealthy as a progressive surcharge on income tax. All the capital gained could be invested in state R&D programmes such as the initial ATLAS investment which would in turn create new productive capacity through the development of new technologies and industries.

Foxell (1994) suggested that the emphasis on NPV (net present value) in cost benefit analysis is one of the major reasons that UK management is bedevilled by short-termism. It can certainly kill promising long term projects since it tends to ignore cash flow after the payment period. It is the ultimate threat to long term investment. It is the accountants tool and UK management is overly accountant-biased. The best people to manage a business are those who understand the product rather than accountants. More than 50% of large company chairmen have no technical degrees. Indeed this charge may be levelled at the UK government in that few ministers have any scientific or technical background - less than 6% have technical degrees. The UK severely

under-utilises its scientific and technical expertise. In the UK almost 1% of its worforce between the ages of 25y and 35y are science graduates - 50% more than in the USA and Germany. However, only 3% of the total British workforce work in science and/or technology compared with 7% in Germany and 9% in the USA. Indeed, the UK was the only OECD country in which the number of working scientists fell between 1987 and 1991. In a technological world this is an appalling situation.

For more than one product unit of ATLAS, production costs drop per unit such that the production cost for n units=TFUxL where TFU=theoretical first unit cost and L=learning curve factor=n^b where $b = 1 - \frac{\ln(100/S)}{\ln 2}$ and S=learning curve slope. S represents the percentage reduction in cumulative average cost when the number of production units is doubled. For less than 10 units S=95% and b=0.926:

Number Of Units	Production Cost (TFUxL)	Average Cost	Unit Cost
1	1	1	1
2	1.9	0.95	0.9
3	2.77	0.92	0.87
4	3.61	0.9	0.84

Spacecraft production runs are unusual but ESA's Cluster mission is an example where 4 spacecraft are required for simultaneous in-situ investigation of the Earth's magnetosphere in almost identical, highly eccentric, polar orbits (apogee of 20 Earth radii and perigee of 4 Earth radii). They will be launched on a single Ariane V launcher into GTO necessitating a complex series of propulsive orbit maneouvres to their operational orbits. They will fly in a coordinated tetrahedral pattern. They require 4 identical sets of 11 electrical and magnetic instruments on 4 identical spacecraft. This constitutes a low production run of a custom design to be produced in the time normally allowed for one spacecraft. The need is for high quality on-time delivery. Hence Cluster occupies a situation between the one-off product typical of scientific satellites and the "mass production" run of some telecommunications satellites. At the component level however, the mass production character becomes more evident. In this case, standard off-the-shelf components are characteristic and this reduces development time and risk. Modular design allows parallel workflow and parallel integration reducing the production time. The longest period is taken for systems-level testing. These issues are relevant for any production run of ATLAS. In-orbit or ground based spares would not generate additional revenue so the cost would not be justified. However multiple units dedicated to different orbits would generate a requirement with the potential for increased earnings. Another source of potential revenue is through the sale of individual hardware units to reduce the individual cost: the sale of units to the US or NATO military offers productions runs ~1-5 items (typical aerospace production run) and so reduce the individual unit cost. Each unit could be sold at $175M minimum to recover production costs (the savings due to production of multiple units would comprise the profit) or at a higher price to regain some of the R&D costs (eg. $300M representing $125M profit per unit). The sale of such units offer large cash injections above that generated by operating the ATLAS in-orbit service. The military would benefit greatly from the sale of such units as an additional level of reliability to their present and future space systems and networks including the BMDO (formerly SDI) programme to give them flexibility of operations they could not otherwise achieve.

An important part of the success of any commercial venture depends on how well it is marketed. Marketing is the process of identifying and servicing customer needs and is one of the most important functions in any business. it involves identifying the customer, communicating the product or service to the customer, assessing the competition and assessing the product price. The space industry differs from traditional industries in that there is usually extensive government involvement, political influences which can often overshadow financial ones, emphasis on high technology, reliance on direct distribution and on public relations and trade shows rather than broadcast advertising. It is important that ATLAS is marketed in a multitude of ways and not just as a commercial enterprise.

9.1.2 ATLAS & Technology Transfer

ESA has a vigorous technology transfer (spin-off) programme. Its primary responsibility is to maintain and enhance Europe's competitiveness in all space activities and strengthen European industrial and technological standing in the world [Gibson 1989]. Technology transfer comprises a part of this mission. ESA's main purposes are enshrined in the Articles of its Constitution. Articles III, V and IX of the Paris European Space Convention (1975) which created ESA's constitution emphasises the advantages to each member state (including the UK). Article III states that member states and the Agency shall facilitate exchange of scientific and technical information. Article V states that the Agency shall place at the disposal of states its own facilities for use as requested by the member state and be approved by the Council at the cost of the user. Article IX states that if a member state wishes to realise a project not covered by ESA activities but which lies within the purposes of the Agency, the Council may decide to provide assistance to the member. Hence, a considerable body of information and resources is available to each member state.

ESA has developed a vigorous technology transfer (spin-off) programme through a consortium of agents (Spacelink Europe) which publishes an annual catalogue called TEST (Transferable European Space Technologies) [Hierronius-Leuba et al 1993]. Spacelink Europe are composed of technology brokers from France, Germany, the UK and Italy in response to Article III of the ESA Convention. As a development agency promoting technology in industry and European competitiveness, ESA's activities are complementary to those of the EC. Every year ESA files around 20 patent applications pertaining to inventions made by staff members to protect those inventions and ESA's intellectual property rights. Many of the technology transfers are software based standards including software analysis packages for process control, thermal analysis, dynamic analysis, simulation tools and an ESA standard language ESL (ESA Simulation Language). Particularly important are the general purpose image processing algorithms for use in non-optimal lighting conditions developed for Earth observation and astronomy applications. Such software is directly transferable to police and security services for number plate detection, face recognition and fingerprint analysis and to biomedical applications for imaging. One example is the biomedical application of imaging techniques developed for astronomy. Hardware developments for space application are devoted to mass reduction and miniaturisation. Numerous hardware technology transfers are listed in ESA (1993): advanced remote gas laser sensors developed to monitor gaseous oxide have been applied to monitor ground based pollution up to 2 km altitude; heat pipes developed for active thermal control in spacecraft have been applied to terrestrial heat management; robust seals have been

applied to industrial process plants to meet EC emission restrictions; life support systems developed for manned spacecraft to absorb carbon dioxide by reaction with lithium hydroxide have been applied to submarines; devices for measuring radiation dosage have been applied to the nuclear industry and to medical radiotherapy; infrared interferometric spectrometers for the measurement of atmospheric trace gases have been applied to monitor emissions from chemical plants and waste disposal facilities; space based waste treatment have been applied to medical cleanrooms for bone marrow transplant patients who have reduced immunity; radiation hardened electronics developed for space application have been applied to aircraft avionics for operation above 40,000ft where cosmic rays and secondary emissions can become significant; nanometer scale positional piezoelectric actuators developed for space based antennas, mirrors and sensors have been applied to microscopy, instrument control and interferometric sensing; shape memory alloys developed for small actuating mechanisms on spacecraft have been applied as human bone repair staples which pull bone together at body temperature; fire proofing materials developed for launchers have been applied to meet stringent fire regulations (eg. the Channel Tunnel). The Russian Space Agency RKA have expressed interest in procuring the ESA team to document their possible spin-off technologies. An ill appreciated fact is that although space rated components are often very expensive due to their high reliability in harsh environments much of the cost is in the initial design and qualification so they may be suited to commercial industrial manufacture at reasonable cost.

ATLAS is an example of a Schumpeterian model of innovation whereby new products and innovations open up new markets and better production methods. Technological progress increases productivity in two ways: product augmentation in generating new capital goods, and labour augmentation by reducing labour inputs and increasing outputs through economies of scale. Capital resource is shifted by improving its quality through greater efficiency in capital utilisation. Such technological innovation generates new products and methods which are applicable to industrial sectors beyond those for which they were developed. Limited product diversity makes firms vulnerable to recession and new developments. The corporate philosophy should be based on maximising the market/product breadth to create spin off (technology transfer) opportunities to other non-space industries. The spin-off potential is larger than the in-orbit servicing market.

Gibson (1991) specified information technology (including robotics) and advanced materials as the two most suitable space research activities that can be applied to other sectors of the economy - the USA is aware of the importance of this industry as it has invested proportionally more in IT than any other country. The European Community are also determined to develop high technology products in competition with the USA whose lead has been eroding. The EC launched its commitment to information technology in 1984 with ESPRIT (European Strategic Program for Research into Information Technology), a 10y programme to maintain European industrial competitiveness in the world market. The total budget was ~3B ECU. R&D into information technology is generally viewed as the key to the future of economies of the future.

Industrial R&D investment is particularly critical in the post Cold War era which has been characterised by massive cuts in defence spending including military R & D which

has always been the primary driver in technological developments and innovations. The space industry in general provides an important source of technological advance with the general retraction of the defence industry. For instance virtual reality (VR) is a spin-off from the defence sector to the entertainment's industry. It is an example of a development for military application which has been adapted for another commercial application. As a result it has spawned an almost cult status as "cyberspace". It is doubtful if VR would ever have been developed for the entertainment's industry in response to market forces. This illustrates the importance and the power of technology transfer. In-house software developed to support robotic operations may have significant commercial value when adapted for the leisure market.

As a key component in high technology, automation & robotics (A & R) may be regarded as a means to maintain technological leadership in the world. A & R technologies were defined to encompass the whole of computer science technologies with specific reference to: robotics, remote teleoperation, sensors, advanced control systems, knowledge-based expert systems and relational database systems, man-machine interfaces, planning systems, voice recognition and natural language understanding, computer vision, distributed processing, software engineering and validation, and autonomous systems design. Technology transfer domains for robotics and automation are numerous. Automated industrial assembly and inspection is an obvious candidate, particularly the automotive industry which dominates industrial applications. Robots can take the human worker from hazardous processes such as materials handling tasks involving die cast machines, furnaces and heavy presses whilst increasing productivity due to shorter time cycles and the reduction of work in progress. Manufacturing accounts for around 1/3 of GNP of industrial activity in a typical Western nation while services account for around 1/2 of GNP. The rest comprises the extractive industries (agriculture, mining, oil) and construction [Merchant 1985]. Services do not create primary tangible wealth as they merely increase buying power so manufacturing in reality (ie. in terms of product creation) accounts for 2/3 of wealth creation. Productivity improvement and growth generally involves innovation for new products with high growth markets and so it the the manufacturing industry (mostly defence rather than civil) which contributes to R&D expenditure rather than the services industry. This is particularly true of high quality manufacture of high cost items. Productivity growth from manufacturing is much higher ~2% than that from services at less than 1%. The importance of manufacturing industry is critical to the health of industrialised economies.

Robot have been used in the manufacturing environment to reduce the cost of manufacturing of products as well as improving their quality. Around 75% of manufacturing is in batch volume mode and so suited to automation. The repercussions on employment have been to increase the demand for skills and a shift towards services. Arguments that A&R technology destroys jobs are misplaced - Bell Laboratories found that if automatic dialling and switching had not been invented over half the population of the USA would be needed for manual switching to accommodate today's telephone traffic. Hence new and more profitable markets are opened to replace the old ones. Furthermore manufacturing productivity increases as 16% labour, 27% capital and 59% technology. The robot offers higher reliability in that it remains in the service of the employer, has higher efficiency in that the robot performs at higher speeds ~120%, offers higher quality in that the robot performs

consistently to a standard matchable by humans only after 20y training and experience. Indeed beginning with the Industrial Revolution growth in manufacturing productivity is attributable to the substitution of power driven machines and technology for human labour. Assembly, inspection and parts fabrication are the most labour intensive tasks in manufacturing (especially assembly) and the mechanisation of these tasks would have a major impact on industrial efficiency [Nevins & Whitney 1980]. The cost of labour characteristically rises very rapidly: with 80M blue collar workers in the USA and Western Europe of which 20M could be replaced on the workshop floor by robots opens up a potential market of $120B (assuming $10,000 per robot). CIM systems have the greatest impact on industrial efficiency: they reduce design costs by ~15-30%, reduce lead time by ~30-60%, increase product quality by ~200-500%, increase productivity by ~200-3500%, reduce work in progress by ~30-60% and reduce personnel costs by ~5-20%. All in all there is a several 100% improvement from a single installation [Albus 1990].

Underwater prospecting and exploration is undertaken by submersible unmanned ROV's (Remotely Operated Vehicles) and manned bathyscaphs. The freeflying mode of control presented in this thesis is also applicable to oceanic ROV's (remotely operated vehicles). Such technologies are used for oil exploration, installation and laying and repair of undersea cables and pipelines, maintenance of oil producing well-heads, inspection of offshore rigs, data collection, construction and maintenance at subsea depths beyond those reachable by divers, and seabed mining of polymetallic nodules such as manganese, cobalt, nickel, platinum and molybdenum Advances in automation and robotics may open up new industries such as ocean bed farming. The oil industry is characterised by very large companies with large resources. Their business involves making large speculative investments at high risk in the expectation of reaping high rewards. This only made possible by short timescales of return on investment and a guaranteed market. Oceanographic exploration is one of the fastest growing application areas of robotics due to their military potential for intelligence gathering and mine countermeasures. However, ROV dynamics are much more complex than those encountered by space robots due to uncertainties and nonlinearities in high density ocean currents and in the ducted propellor driven electric thrusters.

The nuclear industry requires remote and automated manipulation capabilities such as inspection, repair, maintenance and decommissioning for nuclear reactors, irradiated fuel reprocessing plants, particle accelerators and nuclear fusion research facilities. Such a manipulator performs daily maintenance of the experimental particle beam accelerator at Los Alamos National Laboratory including remote pipe fitting, line repair and welding. The UK's £2.8B Thermal Oxide Reprocessing Plant (THORP) is one plant where remote robotics is essential. THORP extracts and renews unburned plutonium and uranium by-products from fuel removed from nuclear reactor cores and separates it from the highly radioactive fission-product wastes to enable them to be used again as fuel. It serves all the UK's nuclear power fired electricity generating stations: 7 Magnox reactors, 7 AGR's and 2 PWR's and these provide ~70TWh which comprises <30% of the national grid. With the cessation of the Cold War and the dismantling of nuclear arsenals, plutonium dumps have become a major problem, eg. The Washington Hanford Nuclear Reservation. Many of the buried tanks in such sites are leaking and this requires cleaning up at great expense. This can only be achieved robotically.

Potential medical applications include leg/arm prosthetics and tele-surgery. Tele-surgery is the ultimate in human-machine interfacing with the human being the manipulation target. In minimally invasive surgery, the surgeon manipulates instruments through small ports opened in the patient. Endoscopic cameras mounted in tubular laparoscopes offer remote viewing. As the surgeon uses hi/her hands for surgery, the laparoscope is usually handled by an assistant under verbal instruction from the surgeon. Tele-manipulators may replace the assistant with control being provided by the surgeon's head movements via a 6 degree of freedom magnetic field head tracker worn by the surgeon. Tele-manipulators may also be used as surgical tool holders to guide the manual insertion of instruments particularly in critical areas such as neurosurgery. Emergency services also have much to gain from automation and robotics technology: explosives ordnance (bomb disposal), fire-fighting and chemical spillage reaction may all be enhanced by these technologies. The military may be expected to be one of the most intensive users of robotics and automation technology: the cruise missile is essentially a robot with real time adaptive capabilities. They have a strong requirement for unmanned air, land and submarine vehicles. Similar arguments may apply other industries such as chemical/pharmaceutical handling and manufacturing, telechir mining and civil construction, and automated agriculture. Even the service sector could substantially benefit from A&R technology advances: transportation safety, underwater pollution monitoring and cleanup, toxic and radioactive waste handling, security systems, hospital support, education and entertainment's and leisure industry.

Generally ATLAS provides a focus for information technology research and technology development. THe UK's total capital investment in manufacturing is £200B across 43,000 businesses employing 10 or more people (cf. £380B invested in services). The UK space industry is small ~£350M/y. Generally speaking these industries yield poor returns equating to half of that of Germany and a third that of the USA. This is primarily due to under-investment. Technology can however provide the key to revitalising UK manufacturing. The importance of information technology lies in that it has effects not just in the future of service industries but in future of the manufacturing industry as well particularly through computer integrated manufacture (CIM) [Spur 1984, 1988; Merchant 1985, 1988]. The computer comprises the central component in the modern automated factory which will provide the basis of future manufacturing industries. CIM offers variable program computer controlled manufacturing of variable products, on-line process optimisation of production control, dynamic scheduling operations control of jigs, tools, etc and dynamic co-ordination of scheduling and resources. Essentially CIM provides the interconnection between energy, material and information flows for continuous production with shorter lead times, shorter set up times, reduction in manualism and the minimisation of errors. The primary objective of CIM is the maximisation of output with respect to the input within the integrated system. Information technology has provided a new impetus for productivity increases in the factory since its inception in the 19th century. At present IT has contributed geometric processing and design through CAD and production planning through CAM and quality control through CAQ. CAM provides operational efficiency by integrating production control of CNC machines and general purpose robots. The introduction of advanced manufacturing techniques such as laser and plasma cutting and high speed grinding and milling machines offer adaptable

techniques amenable to IT planning and control. CAM allows optimisation for high processing rates for short product lifecycles. Automated machines produce high quality goods at high productivity rates with low lead times. New materials such as ceramics and synthetic materials pioneered by the aerospace industry will offer better corrosion resistance, better temperature properties, greater consistency, higher fatigue strength, better wear resistance and lower densities through the use of robotic technologies. This is particularly relevant to the phramaceutical industry which require automation of drug production for high output rates. Advanced sensors enable advanced process and standards monitoring, defect detection and failure diagnosis with on-line robotic control. The new architecture of the automated flexible manufacturing system (FMS) is based on the integrated manufacturing cell with a highly automated compact structure [Bjorke 1984]. The cell concept provides a balance between flexibility and efficiency. A multicell system will be interconnected with self drive transport vehicles on guide rails. Each cell has 5 functions overseen by a centralised cell supervisor: manufacturing, planning, preparation, supplementary functions and stocking. The cell will provide automated manufacturing, planning and stocking functions with minimal manual preparatory and supplementary functions. The cell supervisor controls and co-ordinates machine tools, robots, sequencing tasks, production processes, parts and instigate quality control. The manufacturing cell is where value is added to the raw material through processing replacing the requirement for the addition of labour, capital and energy. Indeed the cost of the raw material is only a small proportion of the total cost of the product as the majority of the cost of a product comprised labour, capital and energy [Pick & Becker 1978]. A modern factory must provide a balance between flexibility and efficiency. In mass production efficiency is maximised but at the expense of flexibility. Small lot production increases the flexibility but decreases efficiency. The need is to provide a balance between these two factors which allows frequent redesign. No longer is mass production for economies of scale the prime consideration - quality, reliability and diversity are just as important. Machine intelligence will ultimately enable the factory to adapt to new situations through expert systems. The decision making processes for the manufacturing cycle may be incorporated into expert systems which integrate, diagnose, monitor and solve problems. Maximum flexibility implies the ability for rearrangement, change in materials and machining, machining more complex geometries to increase the product range and variation, and the ability to integrate new machining technologies. This adaptability is necessary to increase the rate of change of product design and the ability to react quickly to market changes. Production will move away from the mass production principle in favour of adaptation capability to industrial standards. Bjorke (1984) suggested that a three level hierarchy of expert systems is required: task-oriented (machine level), parts-oriented (cell level) and factory oriented integrated CAD/CAM/CAQ system. Each cell is co-ordinated by the supervisory expert system. Routine and less skilled jobs would decrease in favour of higher level planning and control jobs. This is the factory of the future that will drive the manufacturing industry of the mature industrial economies. Although raw materials and energy provide the basis of world economic activity and international trade it is the manufactured product that drives it. Product utility is provided by the injection of energy and information into the raw material and this is what its value is based upon.

9.2 LEGAL ENVIRONMENT OF SPACE ACTIVITIES

All spacecraft operate within a legal environment and as such international space law provides constraints on all spacecraft. Law may be defined as a set of rules which determines the consequences of certain actions. Space law regulates the affairs and relations between states and determines the consequences of actions concerning the exploration and utilisation of outer space. However international law differs from national law in that there is no legislature which can bind all states to accept treaties and there is no executive that can force international law. However boycotts and sanctions can provide a fragmentary enforcement process and the Gulf War was an example of enforcement action under the UN charter. This was an exceptional case rather than the norm. International law is founded on two modes of introduction - treaties which are formed by negotiation and bind only signatory states, and customary law which has the status of international "common law" whereby behaviours are generally accepted through widespread practise. Customary law binds all states without exception. This is a cultural heritage from the English tradition of common law which purveys her progeny including the USA. Common law is an evolutionary process where law based on past precedent is used to establish modern approaches to problems of a similar nature in the courts. Civil law nations are based entirely on pre-emptory legislation coded in statute.

Curiously there is no strict delimitation between air and space though 100-110km altitude is generally and informally accepted. International air law is based on the absolute sovereignty of airspace above any state (Article 1 of the Chicago Convention on International Civil Aviation of 1944) whereas international space law is based on the negation of any sovereignty in space. In this way space law resembles the Law of the Seas which conform to the principle of freedom of the high seas. Similarities also exists with the Antarctic Treaty 1959 which prohibits territorial sovereignty on that continent and the basis of co-operation for scientific research. This basic principle of the nonsovereignty in space law was questioned by the Bogota Delegation of 1976 which attempted without success to claim sovereignty of equatorial orbital segments (specifically segments of equatorial GEO) as the natural resources of developing equatorial states - this objection was over-ruled on the basis of customary law that until then it had been accepted that the orbit is free for utilisation as observed since 1957.

Most space law is treaty-based in 5 treaties: the Outer Space Treaty of 1967, the Rescue Agreement of 1968, the Liability Convention of 1972, the Registration Convention of 1976, and the Moon Agreement of 1984. The Vienna Convention on the Law of Treaties (1969) defines a treaty as "... international agreement concluded between States in written form and governed by international law, whether embodied in a single instrument or in two or more related instruments and whatever its particular designation". However unlike national law there is no effective mechanism to enforce it other than out and out war. Curiously this does not seem to have invalidated treaties. All treaties are drafted through consensus by the UN General Assembly COPUOS (Committee on the Peaceful Uses of Outer Space) set up in 1959. It comprises two subcommittees: legal subcommittee and the scientific and technical subcommittee. Both operate through consensus rather than through votes. However the International Telecommunications Union (ITU) is a specialised agency of the UN which is concerned with extending and maintaining international co-operation for the use of

telecommunications while ensuring equitable access for all members. GEO is a limited natural resource and so should be shared. ITU is responsible for the regulation of satellite communications particularly with radio frequency bandwidth allocation and position allocation in GEO. The ITU operates on a "first-come first-served" basis.

The Outer Space Treaty of 1967 provides the basis for all subsequent treaties of space law, so much so that it has become a part of customary law. Hence although it has 97 ratifications and 27 signatories, it binds all states without exception. It states that outer space should be used only for the benefit of Mankind and to the benefit of all states. Exploration is free to all states without national appropriation (articles I and II). All activities in space should comply with the UN charter in the interests of international peace (defined as non-aggression thereby allowing defence) and security. This provides the guts of the Outer Space Treaty.

Offensive weapons of mass destruction are prohibited from the space environment and celestial bodies (articles III and IV). Nuclear weapons of course are banned in space by the Nuclear Test Ban Treaty of 1963 (this does not include nuclear power sources). The Outer Space Treaty does not prohibit SDI programs as they do not involve weapons of mass destruction and are classed as non-aggressive (defensive). They conform to Article 51 of the UN Charter which confers on states the right to security and self-defence. ICBM's are not included because they do not achieve full orbit. Nuclear power sources are subject to intense scrutiny under safety reviews by various nuclear and environmental agencies. The US began using RTG's with SNAP 3A in 1961 and SNAP 10A was the only US space nuclear reactor powered satellite. Containers for RTG's are designed so that they should survive re-entry and impact on Earth. In 1968 the launch of NIMBUS-81 at 300km altitude allowed the recovery of the RTG capsules without incident illustrating the plausibility of this concept of recovery. The SNAP 10A reactor was designed to be launched in subcritical mode and started up once orbit had been achieved. It presently resides in a circular polar orbit with a decay life of 4000y. The Russians regularly use nuclear reactors on their Radar Ocean Reconnaissance Satellites (RORSAT). However they produce positrons which can produce gamma rays on other spacecraft on penetration and cause interference with scientific measurements of natural phenomena.

Curiously the Agreement governing the Activities of States on the Moon and Other Celestial Bodies of 1979 which incidentally defines celestial bodies as those within the solar system only expands on the themes in the Outer Space Treaty in such a way that of the few states (8) that have ratified it none are spacefaring states. It appears that "for the benefit of Mankind" does not mean that an investor spacefaring state is obliged to relinquish commercial and economic advantage that it may have as a consequence of those space activities which is what the Moon Treaty appears to imply. By stating that the moon and natural resources are the common heritage of Mankind and that there should be equitable sharing of the benefits of those resources seems to bar commercial application. However this particular Treaty is very much open to interpretation as if the Outer Space Treaty were interpreted in a similar manner telecommunications would not be commercially possible. A similar situation occurred with the drafting of the 1988 Convention on the Regulation of Mining Activities on Antarctica to formalise a voluntary moratorium that had been observed since 1972. The Convention proposed supervised mining activities but died when the UK withdrew its support of limited

exploitation in 1990. Similarly the law of the Sea Convention of 1982 set up a Seabed Authority to control and exploit seabed resources beyond national limits. Most major national states have not signed it. It appears that when commerce is involved principles undergo major convolutions. Articles V to VIII of the Outer Space Treaty are elaborated by later treaties. Article IX states that all spacefaring states must avoid harmful contamination of both outer space and the Earth as "global commons" beyond the jurisdiction of any nation. This was tested in 1978 when Cosmos 954, a nuclear reactor powered satellite re-entered the Earth's atmosphere and contaminated parts of Canada. The USSR accepted responsibility and paid an acceptable fraction of the cost of the clean up operation. Article XI retains the UN authority by placing an obligation to report all space activities to the UN Secretary General.

Articles V to VIII of the Outer Space Treaty have been expanded upon in subsequent treaties and these treaties that have a direct impact on the nature of any robot servicing spacecraft. Article V stated that there was an obligation to assist astronauts as envoys of Mankind in the event of accident and inform the UN Secretary General of possible dangers to astronauts. Article VIII states that there is an obligation to return space objects if found to the owner state. The Treaty on the Rescue and Return of Astronauts and the Return of Objects Launched into Outer Space of 1968 (ratified by 67 nations) was more detailed. It states that astronauts and space objects found beyond the limits of the launch states must be returned to the launch state promptly. At all times the launch state retain jurisdiction over astronauts and their space objects. All astronauts as envoys of Mankind have diplomatic protection. In the event of an accident relevant states should afford all possible assistance. If a space object falls on foreign territory that foreign state should notify the launch state and the UN. Recovery must be instigated by the launch state but the recovery process falls under the jurisdiction of the foreign state. Assistance offered by the launch state may or may not be accepted. Indeed the offer of the USSR to assist the Canadian clean-up of Cosmos 954 in 1978 was refused on the grounds that the USA had all ready offered to assist, an offer which had been accepted. However the compensation to the cost must be shouldered by the launch state. The re-entry of Cosmos 954 over Canada in 1978 spread reactor debris over 124,000km^2 of the north-west region. The total cost of the cleanup cost Canada $14M of which $8M was for personnel and equipment. Canada claimed $6M but the USSR compensated $3M arguing that they could have done the clean up much cheaper. The 50% settlement has set a precedent for future situations. This treaty has considerable implications for the operation of salvage operations. Since launch states retain jurisdiction of space objects outside their state confines there is no question of gaining ownership through salvage. Evidently if salvage became commercially viable new treaties would have to come to terms with the nature of ownership and its transition as a state relinquishes control and ownership to another state. As it stands claim of ownership of spacecraft through control as salvage would constitute an act of international piracy.

Article VI of the Outer Space Treaty declares that launch states bear complete responsibility of their space activities and that private corporations must obtain from their respective states special licenses to indulge in space activities. Similarly Article VIII states that the launch state retains jurisdiction over its space objects. Again the Convention on the Registration of Objects Launched into Outer Space of 1974 makes this explicit (ratified by 37 nations). All space objects must be registered. The state of

registry which may be either the launching state or the launch-procuring state (referred to as the launch state) has jurisdiction over its space objects. The registration provides a form of identification and liability for damage. The registry implies title of the satellite to include ownership and that control of the satellite by TT&C by contractors are answerable to the owners. The register must include the spacecraft's launch date and site, orbital parameters (nodal period, inclination, apogee and perigee altitudes) and its function (article II). Military satellites circumvent this by placing their satellites in an initial orbit (reported to the UN) and then manoeuvre them to their operational orbits (not reported to the UN). This is not so unusual as military satellites have a tendency to be retasked to different orbits during their operational lifetimes. The UN Secretary General is also obliged to maintain a register to whom every state is obliged to supply the necessary information for that express purpose (articles IV and V). This has similarities to the UN Convention on the Law of the Sea 1958 whereby registration of a sea-going vessel entails the right of the vessel to use the registration state's flag as a form of identification and the Flag state has complete jurisdiction onboard its ship. Similarly the Chicago Convention on International Civil Aviation of 1944 states that aircraft have the nationality of the state where it is registered and that the registration state is responsible for all activities of the aircraft.

Article VII of the Outer Space Treaty states that the launch state is liable for damage to any state caused by a space object. The Convention on International Liability for Damage caused by Space Objects of 1972 elucidates this victim-oriented liability (ratified by 35 nations). The launch state is absolutely liable to compensate for damage caused by its space objects on Earth or in sovereign airspace to foreign states (Article II). Damage to the launch state by its own space objects is governed by its own national civil legislation (articles VII and XI). There is usually national liability legislation to public services which cause danger to private concerns regardless of fault. When damage is caused by a space object to another space object in space liability is relative according to fault established by causal link (article III). If however damage resulted from negligence, insufficient information or wilful act on the part of the claimant, liability is exonerated (article VI). Under certain conditions the national law of tort may be applied which requires a proof of negligence. Such liability must be negotiated through diplomatic channels. If diplomatic channels do not settle the issue then the matter may be referred to a claims commission comprising the claimant state, launch state and a jointly chosen chairman as arbiter who casts the decider vote (articles X, XIV-XX). Liability may be joint and several between two or more registered states according to fault (articles IV and V). Launch states may thus negotiate special agreements regarding the apportionment of liability. Hence ATLAS should include a waiver of liability clause in the contract to the customer.

The carriage of payload by launchers obliges the sponsor to pay a share of costs to the launching state. Hence interparty liability will apply. Procurement of launch establishes liability in this way. Once separation from the launcher is achieved and the payload is operational autonomously the launch-procurer becomes the flag, and so liable, state. Procurement according to section 308 of the NASA Act of 1979 requires the procurer to obtain liability insurance against damage to their property or to a third party during launch, operations or recovery. No mention is made of post-operational phases after control has been relinquished. At present there is no clear directive concerning space debris - it is possible that liability for damage may ensue by national civil legislation but

there is no legal obligation to boost into post-operational graveyard orbits and de-orbit for re-entry. This is an unclear issue but it certainly appears that if a reasonable means of clearing away debris were readily available (such as ATLAS) states may become liable for debris damage in space on the basis of negligence.

The high cost of many space activities has motivated many nations to prefer co-operative ventures. There are pro's and con's to co-operation and typically involve bargaining between co-operation and competition between economic regions of the world. The advantages of co-operation are: cost sharing, access to technology and scientific knowledge and the strengthening of relationships between nations. The disadvantages of co-operation are: loss of autonomy, an increase in the overall total cost due to increased managerial complexity, the enhancement of future competition and political difficulties in broken commitments. The USA and Japan in particular have stacked the odds against other nations in co-operative ventures. The USA has a host of intellectual property legislation favouring the US. Indeed during the development of ESA's Spacelab, US law enabled the USAF to obtain access to the European technology in Spacelab to aid in developing its own Spacelab for its own purposes without compensating ESA. US legislation acts as a considerable barrier to other nations in indulging in co-operative ventures. China has developed its space activities in isolation of other nations and both Europe and Japan (to a lesser extent) regard autonomy to act independently in certain areas of space capability as a policy objective - a policy that has led to conflicts of interest in the past in co-operative projects with the USA. To be fair to the USA, it does have the highest space expenditure and space expertise in the world (with the possible exception of the Russians) and this favours co-operative ventures in space projects for other nations. Several forms of co-operation are possible: exchange of data from separate missions (eg. weather data in the World Weather Watch); co-ordination of separate missions (eg. the Comet Halley armada encounters); increasing the mission capabilities by instrumentation from different nations (eg. Cassini-Huygens mission); joint missions (eg. Apollo/Soyuz mission); joint facility operations (eg. Space Station); new institutions (eg. Intelsat, ESA). Scientific missions such as the robotic exploration of the solar system and astronomical observation satellites have been the dominant areas of international co-operation and have been heralded as the "success story" of international co-operation. However although large space projects are amenable to co-operation, a small space project such as ATLAS is best pursued autonomously to maximise the profit return.

The UK Outer Space Act of 1986 is part of national municipal law passed in response to the 1967, 1972 and 1975 UN Conventions [BNSC 1992]. The Secretary of State for Trade & Industry is obliged to establish and maintain a register of space objects including launch, procurement of launch, the operation of space objects or any other space activity whereby licenses are granted to control space activities under UK jurisdiction. The issue of licences exonerates the UK government from all liability claims. Unlicensed operations are criminal and the Act requires that all licenses are insured for all liability. The Secretary of State grants licenses provided space operations do not jeopardise health, safety or property, does not interfere with other space activities, is consistent with UK obligations and does not impair national security. The BNSC (British National Space Centre) administers this Act as well as co-ordinating UK space activities. In the process of licensing the BNSC assesses an operator's financial and technical capacity, the nature of the mission, all aspects of

safety, orbital parameters and insurance cover and the right to impound facilities and documents. The BNSC recommends insurance for all phases of a mission from launch to operational phases to disposal. The leasing of satellite transponder capacity and the use of such capacity does not require a license. The UK government thereby fulfils its obligations and requirements:
(i) imposition of liability away from government to the space operator;
(ii) authorises and supervises non-governmental space activities and operations;
(iii) avoids potentially harmful space activities to health, safety or property;
(iv) maintains a register of space objects;
(v) conforms to national security.
The BNSC has a budget of around £150M, £100M of which comprises the UK's contribution to ESA. The BNSC was created in 1985 under the Secretary of State for Trade and Industry to provide a focus for non-military civil space activities to between the DTI, DOE, FCO, DE&S, SERC and NERC to advise the Cabinet Office. The BNSC administers the MoD's DRA space technology research centre and SERC's RAL space science research centre which offer thermal vacuum test chambers, clean rooms and a satellite control centre. The main non-ESA UK space activities are Earth observation including meteorology (46% support), telecommunications (12% support), space science (26% of support) and space technology (6% of support) with 9% funding for administration. The SERC (Science & Engineering Council) total budget is £500M (in 1992) for comparison of which £85M is allocated to the Astronomy & Planetary Science Board. Space science in the UK does rather well as it benefits through both the SERC allocation and a major portion of the UK's ESA contribution funds planetary science mission. In reality the BNSC acts as a bureaucratic stifling mechanism on space activities in the UK rather than any other function.

It is clear that legal considerations heavily govern the nature of space activities and their financial nature. For a robot servicer such as ATLAS it is clear that exoneration of liability for damage to target spacecraft must waived contractually in the same way that launch contracts pass liability to the procurer so that the procurer bears the risk. There are other important legal issues pertaining to the USA. The Buy America Act of 1933 prohibits the buying of foreign goods rather than services and imposes high tariffs on foreign goods to favour domestic goods (similar to Japan). NASA however operates a policy of not using foreign services also which are based on foreign goods. Evidently the USA's taste for free market economics is limited when it comes to protectionism. Indeed US legislation is a minefield of protectionist measures. This provides the origin of the American "not-invented-here" syndrome that afflicts foreign companies in attempting to market technologies in the USA (Concorde springs to mind). Foreign is defined such that if more than 50% of the product originates from domestic sources then it is not foreign. The DoD is an exception to this as it may buy from NATO countries , eg. the USMC operates British Harrier jump jets as their main aviation element. There are several ways to interpret this as regards ATLAS. First ATLAS offers a service which is not available within the USA unless NASA uses EVA in-orbit servicing at great expense as a comparable capability. Whether NASA could justify their cost-effectiveness is another matter but EVA in-orbit servicing is a major linchpin in their justification for manned spaceflight. In order not to alienate NASA as a potential customer it would be important for ATLAS marketeers to allow NASA to treat their utilisation of ATLAS as a co-operative venture with the UK effectively shouldering the role of the now defunct FTS in support of Space Station activities. The

second point is that the DoD have fewer restrictions as regards imports. The UK as a NATO country can export military products and/or services to the USA and the DoD is less susceptible to nationalistic protectionism and more concerned with pragmatism. The UK won the contract for the NATO communications satellite in delivering 2 off-the-shelf Skynet 4 military comsats under NATO ground control. This was the first sale of non-US military satellites to NATO winning against the US proposal of offering half the capacity of two DSCS III satellites under US control by virtue of a lower price. The Skynet 4 provides military communications for land with man-portable ground dishes, sea and air using SHF and submarines using UHF. Regarding the export of components to foreign countries from the USA, an extensive set of legislation controls exports. The Export Administration Act of 1979 requires licensing of all dual-use technical data and commodities and licensing is subject to national security, foreign policy and short supply considerations on a case-by-case basis. Three lists are used: the Industrial List of core technologies critical to Western security including dual-use technologies; the Munitions List of inherently military technologies; and the Atomic Energy List of nuclear technologies. Military technology is heavily subject to control under the Arms Export Control Act of 1976 through the issue of licenses - military technology includes dual-use items such as satellites, computer systems, rockets and technical data and services pertaining to such articles. However once again, the rules concerning the export of military technology such as spacecraft components do not apply to NATO countries [Smith 1990]. The COCOM (Co-ordinating Committee for Multilateral Export Controls) controls the export of strategic technologies which contribute to military capabilities. It is a multilateral organisation of NATO countries and is currently releasing control of computer systems and inviting republics of the former-Soviet Union to participate. Missile technology is subject to control to maintain missile non-proliferation through the multilateral Missile Technology Control Regime (comprising 18 members including the US and the UK). Missiles capable of carrying 500kg of payload to a range of 300km are defined as missiles and so include space launcher technology as well as cruise missiles.

9.2.1 Space Insurance

CT Bowring Space Projects Ltd (1993) divide insurance covers into three segments: transit and pre-launch, launch/early orbit, and in-orbit insurance segments. Transit and prelaunch covers damage to the satellite and delays from the commencement of loading operations for transit until lift-off (usually ~2-3 months). The insurance premium rates are ~0.5% of the spacecraft value. The launch/early orbit phase covers from lift-off through to commissioning to between 180 days and 360 days after launch. Commissioning involves placing the satellite in its operational configuration and orbit and subsystem function confirmation through in-orbit checkout tests. The extended period from 180-360 days included in this phase of insurance allows the satellite's function to be evaluated during eclipse. This covers infant mortality failures such as launch failure, failure of kick motors, and deployment failures being typical. This launch phase insurance premium rate is ~16-20% of the satellite cost with the cost being split with ~9-13% for launch and ~8-11% for post-separation phase. Usually the cover is for 12 months after launch (since this is only marginally more expensive than 180 day cover) to cover the total loss of satellite capability (defined as the failure of 50% of spacecraft subsystems) and/or partial loss. The purchase of full coverage policy including both the combined partial and total loss cover in the launch phase is the most cost-effective approach to space insurance. Limits are usually imposed for launch

insurance cover. The US Commercial Space Launch Act of 1988 limits launch insurance to $100M for commercial launches on expendable vehicles with a maximum return of $500M. The launch phase from lift-off to in-orbit checkout is the most expensive portion of space insurance. This launch phase insurance premium is 10-20 times greater than most terrestrial ventures and 10 times higher than airline insurance. Third party launch liability covers the satellite owner against damage to the launching organisation arising out of damage caused by the satellite. The insurance premium rate is ~0.1-0.2% of the satellite value. Usually launch manufacturers include in the launch contract a guarantee to refly the mission in the event of launch failure.

Usually insurance coverage is also required for the in-orbit operational phase of the mission particularly for communications satellites due to their commercial earning value. This will thus apply to ATLAS. In-orbit insurance covers the period from the expiration of the launch cover to 12 months and insures against subsequent loss or damage to the satellite and provides for the replacement and relaunch of the spacecraft, loss of revenue and the fulfilment of contractual obligations. Total and partial loss coverage for a healthy satellite is ~1.75-2.25% of the satellite cost but for a satellite with health anomalies this would increase to 3-4%. In-orbit insurance is a complex problem since partial in-orbit failure involves complex problems in accurate loss assessments. Different kinds of insurance payments can be given for the loss of propellant, loss of electrical power and other failures according to their severity on payload functioning and assessment of payload value. Communications satellites have the highest in-orbit insurance demand. In addition the operating company may wish to negotiate indemnities against any manufacturing defects by subcontractors (eg. the Hubble Space Telescope syndrome).

The mid 1980's involved considerable loss to underwriters due to launch vehicle failures and reduced capacity down to $100M/launch and high insurance premiums up to ~25-30% of the satellite cost. In 1986 the Challenger disaster was followed by the loss of two Titan 34D's, a Delta, an Atlas, an Ariane and a Proton. Prior to 1986 insurance premiums were ~5-6% for the Shuttle and ~8-10% for Ariane launches. The market has since stabilised with an overall capacity of $500M/y. The UK comprises 15% of the space insurance market capacity with only the US and France having higher capacities at 28% and 20% respectively. Indeed less than 10 insurance companies control over 80% of the capacity. It is evident that ATLAS may contribute significantly to offsetting insurance company losses that have tended to characterise space insurance by providing a means for inexpensive repair. This may even reduce in-orbit insurance costs and the checkout portion of launch insurance - the potential effect may be as high as 50%.

Chapter 10

COMPUTER SIMULATION PROGRAM

The simulation program was written in FORTRAN 90 and is listed in the Appendix. The program structure is sequentially linear in form rather than object designed. The only subroutine used is the numerical matrix inversion subroutine. The program linearity suits the robot control process as each calculation segment relies on preceding calculation segments in order to proceed. Furthermore this software architecture reduces reliance on processing speed in favour of memory storage as processing speed is considered the scarce commodity in space systems. The program was run in two phases: position control during a capture maneouvre and force control during passivation of the grappled target. Although hybrid position/force control was not adopted specifically (as being inappropriate for this kind of maneouvre - hybrid control is more suited to actual servicing tasks), all the elements of that control method were present less the selection matrix.

The program begins with declarations of all the variables used. The subject of simulation was a version of the ATLAS robotic servicer described in Chapter 7 and the spacecraft parameters of mass, moment of inertia, etc were taken from that chapter. The model comprised of a single arm mounted onto the satellite platform in zero gravity. The manipulator geometry was similar to that of the PUMA 560/600 with a number of modificatios as outlined in Chapter 2. The single arm formulation was used on the basis of simplicity given that the dual arm case is a straight forward extension of that formulation as outlined in Chapter 5. The additional compexity of the dual arm formulation was not expected to yield any significant insights in principle to the problem tackled in this thesis. It was assumed that the fuel had been completely expended to maximise the ratio of manipulator mass to spacecraft mass to provide maximum (worst case) reaction coupling between the robot arm and the spacecraft mount. The manipulator links were dimensioned for EVA-equivalence: the link lengths of the arm were 0.25m, 0.5m, 0.5m respectively from the manipulator base with a wrist/effector length of 0.2m. It was assumed that the links were bodies of revolution with the cylindrical axes passing through the centres of mass of each link. Again, this assumption was one of simplicity as realistic asymmetry of mass distribution was not expected to yield significant results. The target object was assumed to be a multi-modular spacecraft (MMS) attitude control module with a mass of 225kg which represents the upper mass limit to the ORU (orbital replacement unit) expected to be encountered in the satellite servicing scenario. This was precisely the modular unit that was encountered in the Solar Maximum Repair Mission of 1984. It was modelled as a rectangular box of 1.4mx1.4mx0.5m with its centre of mass lying at its centroid. The task simulated was a capture and grappling task for acquiring the target - the acquisition of a target was considered an absolutely fundamental requirement for any space robotic capability.

Once these declarations and definitions had been dealt with, a number of critical parameters were then computed particularly pertaining to the space-oriented algorithms of Chapter 6 which were used subsequently. The kinematic-dynamic link parameters $\delta_2, \alpha_2, \delta_4, \delta_6$ (in section 6.1) were calculated for use in the inverse kinematic solution section of the program. The vector s_0 from the spacecraft centre of

mass to the coordinate system of the manipulator base was derived for a cylindrical spacecraft body of radius 0.75m to give a maximum spacecraft diameter h of 1.5m (this was based on the constraint supplied in consideration of the dual arm case in Chapter 5). The moment of inertia of the ORU was estimated using a heuristic formula $I_{obj} = 0.01m^{5/2}$ [Wertz & Larson 1987]. Initialisation occurs at a default configuration defined by joint angles set at their zero values. The parameters D_2, A_2, D_4, and D_6 were then calculated (section 6.1). This allowed calculation of the system centre of mass position p^*_{cm} with respect to local inertial coordinates. This was invariant for any given payload. Evidently, recalculation of this parameter is necessary on acquiring/releasing target objects such as the ORU, eg. on switching from position control to force control during the grapple maneouvre. The importance of adopting local inertial coordinates was outlined in Chapter 6.

The robot control calculations then begin in sequence. The robot control problem is essentially that task requirements are normally specified in terms of cartesian world coordinates as an end effector trajectory while control torques for the actuators required to realise that trajectory are specified in joint level coordinates. This introduces the necessity for transforming kinematic variables of cartesian position q, cartesian velocity $\dot{q}$ and cartesian acceleration $\ddot{q}$ at the end effector into their joint equivalents. This is the fundamental problem in the robot control problem and this is highly dependent on the kinematic geometry of the manipulator. The robot control program is structured as a flow logic with each calculation segment proceeding in sequence: cartesian trajectory generation, inverse position kinematics (joint angle solution), inverse velocity kinematics (joint rate solution), inverse acceleration kinematics (joint acceleration solution), joint torque dynamics implemented with the control law, and the spacecraft reaction moments to be fed forward to the attitude control system. Hence the flow logic is a sequential and linear one:

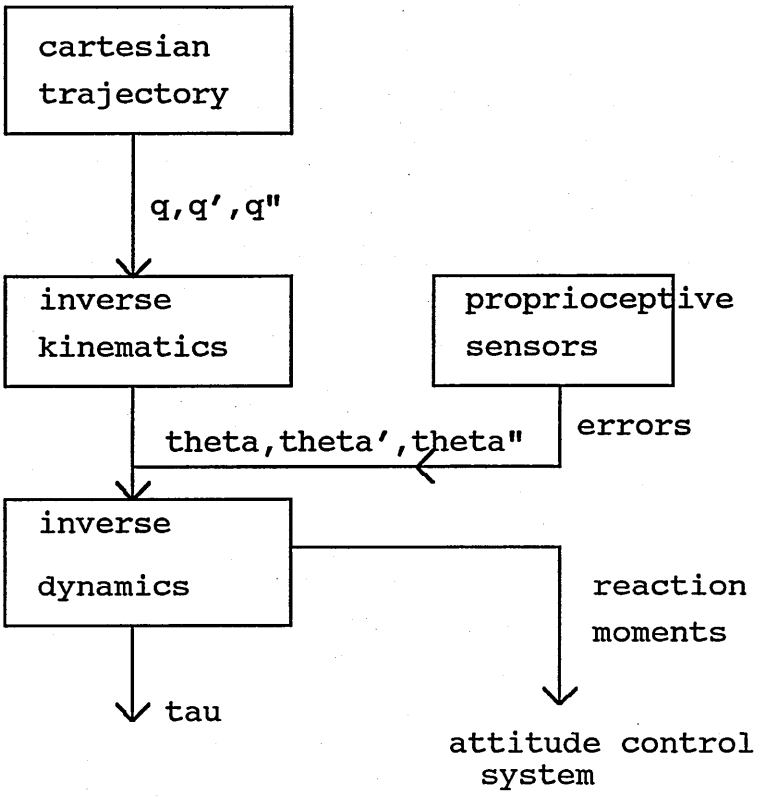

Each calculation segment is now considered in turn. Trajectory generation involves defining the trajectory of the manipulator end effector in terms of generalised cartesian position, velocity and acceleration over time. This is accomplished by describing the trajectory as a straight line path in cartesian space. The program proceeds to generate the cartesian end effector trajectory between the initial configuration and the final configuration. The initial and final configurations are defined in terms of vectorial position and roll, pitch and yaw angles in inertial space. The initial position was defined as the inertial position of the stowed configuration - note that this does not yield the stowed configuration with respect to spacecraft coordinates which are not inertial. The final position was chosen arbitrarily to lie in front of the spacecraft within the manipulator workspace. The straight line cartesian trajectory is generated to provide intermediate knot points in cartesian space along the trajectory. The 4x4 matrix drive function D(h) describes the trajectory generation in terms of a single translation and two rotations (equation 4.1). The drive function is used to derive the 4x4 DH matrix at any cartesian point along the trajectory (equation 4.2). This enables knot points to be defined along the trajectory. Usually the knot points are calculated at a rate limited by the computational capacity of the robot control processor with the rate being bounded from below by a factor of the resonant frequency of the manipulator (~60Hz). As this study does not claim to provide either the operational software for implementation on a spacecraft or its implementation on space-rated hardware, the trajectory was kept simple for illustrative purposes. The minimum number of intermediate trajectory segments is five, each equidistant in cartesian space to provide the initial point, the departure point, the approach point and the final point with acceleration/constant velocity/deceleration phases. This means 6 knot points. This is also the number of points required by the five-segment cubic spline curve fitting procedure for the joint trajectory (though joint trajectory interpolation was not adopted in the simulation on the basis of being unnecessary for illustration). The manipulator end effector started at

its initial point at rest and ended at its destination point at rest (equation 4.3). This means that the first two intervals from 0 to 2T and the last two intervals from 3T to 5T along the trajectory have non-zero second derivatives indicating acceleration/deceleration while the interval from 2T to 3T has non-zero first derivative for constant maximum velocity. The departure and approach points are characterised by instantaneous half maximum velocity values (guarded moves). The maximum end effector velocity was assumed to be 1.0m/s (see later for justification). Hence the trajectory profile follows an initial constant acceleration phase, a constant velocity phase and a constant deceleration phase (equations 4.4 and 4.5). This is a simple trajectory but sufficient for the purposes of this study.

Once the cartesian knot points are determined with their respective desired velocities and accelerations, the next segments determine solutions for finding the joint variables $\theta, \dot{\theta}, \ddot{\theta}$ equivalent to the cartesian variables $q, \dot{q}, \ddot{q}$ defined at each knot point. Hence, these program segments are embedded in a loop to be calculated recursively for each knot point. Firstly, the inverse position kinematics formulation must be employed to find the joint angles θ corresponding to each cartesian end effector position q. This is the core of the program as this and all the other kinematic variable transformations are based fundamentally on the geometric configuration of the manipulator. The kinematic configuration adopted was a generic one based on the PUMA 560/600 but with a number of modifications: zero offset at the elbow and increased link lengths for larger workspace. This manipulator has 6 revolute joints including an Euler configuration wrist to provide closed form analytic solutions to the inverse kinematics. This necessitatesd transformation of roll (R), pitch (P), and yaw (Y) coordinates of the initial and final points of the cartesian trajectory into their DH matrix equivalents of twist (n), turn (s), and tilt (a) rotation vectors:

$$n_x = \cos R \cos P$$
$$n_y = \sin R \cos P$$
$$n_z = -\sin P$$
$$s_x = \cos R \sin P \sin Y - \sin R \cos Y$$
$$s_y = \sin R \sin P \sin Y + \cos R \cos Y$$
$$s_z = \cos P \sin Y$$
$$a_x = \cos R \sin P \cos Y + \sin R \sin Y$$
$$a_y = \sin R \sin P \cos Y - \cos R \sin Y$$
$$a_z = \cos P \cos Y$$

The inverse solution may then proceed. The inverse solution finds the joint angles θ for the given generalised cartesian position coordinates q through $\theta = f^{-1}(q)$. These solutions are given by equations 2.6-2.11 as modified in Chapter 6 as equations 6.8:

$$\theta_1 = \tan^{-1}\left(\frac{\dot{p}_{ay}}{\dot{p}_{ax}}\right) - \tan^{-1}\left[\frac{\delta_2}{\pm\sqrt{(\dot{p}_{ax})^2+(\dot{p}_{ay})^2-\delta_2^2}}\right] \text{ for the left arm configuration}$$

$$\theta_2 = \tan^{-1}\left(\frac{A}{\dot{p}_{az}}\right) - \tan^{-1}\left[\frac{B}{\pm\sqrt{A^2+(\dot{p}_{az})^2-B^2}}\right] \text{ for the elbow down configuration}$$

where $A = c_1 p^*_{ax} + s_1 p^*_{ay}$

$$B = \frac{A^2 + (p^*_{ax})^2 + a_2^2 + \delta_4^2}{2a_2}$$

$$\theta_3 = \{\tan^{-1}\left[\frac{A - a_2 c_2}{p^*_{az} + a_2 s_2}\right]\} - \theta_2$$

These comprise the positioning joint angles whereas the wrist angles are given by unmodified equations from Chapter 2:

$$\theta_4 = \tan^{-1}\left(\frac{-s_1 a_x + c_1 a_y}{c_{23}(c_1 a_x + s_1 a_y) - s_{23} a_z}\right)$$

$$\theta_5 = \tan^{-1}\left[\frac{\sqrt{(c_1 c_{23} a_x + s_1 c_{23} a_y - s_{23} a_z)^2 + (-s_1 a_x + c_1 a_y)^2}}{s_{23}(c_1 a_x + s_1 a_y) + c_{23} a_z}\right]$$

$$\theta_6 = \tan^{-1} - \left(\frac{s_{23}(c_1 s_x + s_1 s_y) + c_{23} s_z}{s_{23}(c_1 n_x + s_1 n_y) + c_{23} n_z}\right)$$

where

$$\begin{pmatrix} p^*_{ax} \\ p^*_{ay} \\ p^*_{az} \end{pmatrix} = \begin{pmatrix} -s_1\delta_2 + c_1(c_2\alpha_2 + s_{23}\delta_4) \\ c_1\delta_2 + s_1(c_2\alpha_2 + s_{23}\delta_4) \\ -s_2\alpha_2 + c_{23}\delta_4 \end{pmatrix} = \begin{pmatrix} p^*_x \\ p^*_y \\ p^*_z \end{pmatrix} - \begin{pmatrix} p^*_{cmx} \\ p^*_{cmy} \\ p^*_{cmz} \end{pmatrix} - \frac{m_0}{m_T}\begin{pmatrix} s_{0x} \\ s_{0y} \\ s_{0z} \end{pmatrix} + \frac{m_7}{m_T}\begin{pmatrix} x_7 \\ y_7 \\ z_7 \end{pmatrix} - \delta_6\begin{pmatrix} a_x \\ a_y \\ a_z \end{pmatrix}$$

$$\delta_2 = \left(\frac{m_{01}d_2 - m_1 r_1}{m_{07}}\right);\ \alpha_2 = \left(\frac{m_{02}a_2 - m_2 r_2}{m_{07}}\right);\ \delta_4 = \left(\frac{m_{03}d_4 - m_3 r_3}{m_{07}}\right);\ \delta_6 = \left(\frac{m_{06}d_6 - m_6 r_6}{m_{07}}\right)$$

These equations convert end effector cartesian variables $q = \begin{pmatrix} n & s & a & p^* \\ 0 & 0 & 0 & 1 \end{pmatrix}$ as given by the 4x4 DH matrix into their equivalent respective joint coordinates $\theta_1, \ldots, \theta_6$. This portion of the program was tested to ensure that the forward and inverse kinematics were internally consistent - this was the only part of the program to be so tested as unique test data was not available for other parts of the program by virtue of the configuration-dependency of those other segments. Howver, the inverse kinematics formulation was the central part of the program.

Once the joint angles have been found, these form the basis for further calculations as they all require values for the joint angles. The next kinematic transformation is that of velocity to extract the joint rates. This involves inversion of the Jacobian matrix $J(\theta)$ such that $\dot{\theta} = J^{-1}\dot{q}$. The elements of the 6x6 Jacobian matrix J were defined using the cross product method and calculated accordingly (equation 2.15 as modified in Chapter 6 by replacing kinematic link parameters with kinemo-dynamic link parameters). The Jacobian transpose was then determined for subsequent use for force control through the formulation that defines joint torques as $\tau = J^T f_{ext}$. This transforms the end effector forces f_{ext} into their joint torque equivalents. The Jacobian matrix was then inverted using Gaussian elimination through a generic subroutine from "Numerical Recipes in FORTRAN" by William Press et al (1992). The returned inverted Jacobian allows direct computation of the joint rates corresponding to each cartesian knot velocity.

The final section of the kinematic transformations is that of acceleration to yield joint accelerations. This involved explicit use of the Jacobian derivative $\dot{J}$ - each element of the 6x6 matrix was defined analytically rather than numerically for the first time

through the cross product method (modified equation 2.24 by replacing kinematic link parameters with kinemo-dynamic link parameters). This was used in conjunction with the inverted Jacobian to determine the joint accelerations: $\ddot{\theta} = J^{-1}(\ddot{q} - \dot{J}\dot{\theta})$. This completed the inverse kinematics solution of finding the joint equivalents $\theta, \dot{\theta}, \ddot{\theta}$ of the specified cartesian end effector kinematic variables $q, \dot{q}, \ddot{q}$ defined by each cartesian trajectory knot point.

The computed torque closed loop control law was adopted as the control law for position control. It overlaid the dynamics formulation to calculate the joint torques which drive the joint motors to realise the specified end effector trajectory. Closed loop control implies the need for sensory feedback from the joint sensors which provide proprioceptive data of actual joint position and joint rate. The computed torque control scheme provided PD linear control of each joint with linearisation by feedforward compensation of the nonlinear components of the dynamics. The computed torque control law was substituted into the recursive Newton-Euler recursive equations characterising the dynamics of the manipulator: $\ddot{\theta} = \ddot{\theta}^d + K_v(\dot{\theta}^d - \dot{\theta}) + K_p(\theta^d - \theta)$ (equation 5.5). Evidently, if servo errors are zero, then $\ddot{\theta} = \ddot{\theta}^d$. The control gains for position and rate control were taken as unity and 30 respectively arbitrarily and this satisfies the constraints for stable feedback derived in Chapter 5:

$0 \le K_p \le \frac{w_s^2 J_{eff}}{4} \cdot \frac{R_i}{K_t}$ - satisfied trivially

$K_v \ge \left(\frac{R_i}{K_t}\right)(w_s \sqrt{J_{eff}} - b_{eff})$ assuming that K_b=0

where w_S=8 Hz

J_{eff}=3.3kgm^2.

b_{eff}=1.4 N/m/s

$\left(\frac{R_i}{K_t}\right)$=2.15V/Nm

These values are typical of direct drive actuators.

The closure of the control loop was enabled by modelling the joint sensor values of joint position and joint rate with a randomiser element to vary the sensor values from the calculated nominal joint trajectories randomly by up to 5%. This effectively provided modelling of inaccuracies of up to 5% which is the allowable error for which the computed torque control system remains robust and can maintain stability and reference trajectory tracking.

The dynamics formulation takes as its input the kinematic joint variables $\theta, \dot{\theta}, \ddot{\theta}$ and outputs the joint torques required to drive the joint actuators to achieve the stipulated cartesian trajectory. The formulation used was the recursive Newton-Euler method for its efficiency over other formulations. The Newton-Euler dynamics defines the forward kinematic variables of each link $w_i, \dot{w}_i, v_i, \dot{v}_i$ and these are propagated fromn the base of the manipulator to the end effector (equation 3.2). This allows the forces and moments to be calculated for each link F_{ci} and N_{ci} about each link centre of mass (equation 3.4):

$$F_{ci} = m_i \dot{v}_{ci}$$

$$N_{ci} = I_i \dot{w}_i + w_i \times (I_i w_i)$$

Each link was modelled as a body of revolution for simplicity in assuming uniform mass distribution. This was followed by the backward recursion dynamic variables f_i and n_i for each link propagated from the end effector to the base of the manipulator to enable calculation of the joint torques at each revolute joint: $\tau_i = n_i^T z_{i-1}$ (equation 3.3). This enables the manipulator control system to drive the joint motors to track the desired reference trajectory of the end effector.

The space manipulator system in addition requires the computation of the reaction moments at the base of the manipulator which induce moments on the spacecraft bus. While calculation of the joint torques are usually referred to the respective joint coordinates, reaction moment calculation for the attitude control system requires the dynamic variables F_{ci} and N_{ci} to be calculated with respect to base coordinates for summation. This is a fairly trivial calculation as it required only a few additional calculations to be performed which does not burden the algorithm. In fact the only change in the dynamics algorithm for the dual computation of F_{ci} and N_{ci} lie through the moment of inertia terms of the links. The link-referenced joint torques were not part of the simulation but are noted here as necessary to drive the robot actuators. The calculations of reaction moments are fed back to the spacecraft attitude control system for feedforward compensation, ensuring that they are transformed into spacecraft attitude coordinates defined by roll, pitch and yaw axes of the spacecraft's flight path.

This completes the position control algorithm for the robot manipulator. This provides the means to drive the joint torques through a spatial trajectory to acquire the target object. The payload during this phase was null and no external forces or torques were acting on the system. The motion of the manipulator was performed in two distinct phases: gross motion control from the initial to the final cartesian coordinates through a spatial cartesian trajectory, and fine control where the end effector dynamically interacts with the target object. Gross motion control uses the computed torque control scheme with kinematic feedback while fine control uses force feedback. The target object was the MMS AOCS module assumed to be tumbling with a dominant spin rate of 0.1 rad/s about one axis and approaching the end effector at a given velocity. Tumbling motion is in all 6 axes with values of 0.01m/s and 0.01rad/s. An approach velocity of 0.04m/s (0.1 ft/s) is typical of that encountered by the Shuttle RMS. Spacecraft rendezvous closing velocities are usually constrained to be less than 0.004m/s (0.01 ft/s). A velocity of 1m/s was defined as the maximum end effector velocity well in excess of presently conceived requirements. Hence this represents a reasonable worst-case capability. Once the object has been grappled, control switches to pure force control with external forces and moments acting on the system which are represented explicitly. For pure force control, the position trajectory is now maintained at the nominal final geometric configuration of the manipulator by the closed loop force control algorithms. Both position and force control were implemented in the same program and each was run separately by commenting out the irrelevant lines of code. Force control requires modelling the collision dynamics of the object onto the manipulator end effector. The initial force/torque at the end effector is

determined by the impact of the target ORU on the stationary end effector. The impact dynamics were modelled as external forces and moments given by (equation 3.8):

$f_{ext} = m_{obj} v_{obj} / \delta t$

$n_{ext} = I_{obj} w_{obj} / \delta t$ where δt=impulse time

The impulse time was taken to be 0.0167s representing a control bandwidth of 60Hz (as defined by the manipulator structure). The desired end effector forces/torques were taken to be 100N and 100Nm in all axes as the maximum applied forces/torques by the end effector (worst case scenario as defined in Chapter 7). The closed loop force control scheme acts to apply the end effector forces and torques on the object to passivate the object by reducing the forces/torques at the end effector to those desired. The desired joint torques to apply these end effector forces/torques are calculated using the Jacobian transpose matrix computed earlier in the program as it is the joint motors which are driven to apply the required end effector forces and torques via $\tau_f = J^T \begin{pmatrix} f_{ext} \\ n_{ext} \end{pmatrix}$. The force control law reduces the difference (force error) between the desired end effector forces/torques and the actual end effector forces/torques over the force (passivation) trajectory (modified equation 5.11):

$\tau_f = J^T F_{ext}^d + K_f J^T (F_{ext}^d - F_{ext})$ where K_f=force control gain

Evidently when the force error is zero, $\tau_f = J^T F_{ext}^d$. Note that unlike in the case of position control, these joint torques are link-referenced as they are calculated using the Jacobian transpose which relates end effector forces/torques directly to the joint torques by virtual work arguments. The passivation trajectory is clearly dependent on the force control gain. The force sensors provide the sensory feedback information f_{ext} to apply force control by reducing the force error to zero. The external forces measured by the force sensors were modelled initially by the collision dynamics and subsequently by the effect of the force feedback on the system, ie. subsequent force trajectory points were dependent on previous force trajectory points arising from the effect of the force control system on the initial impact dynamics. The impact of the object on the end effector is determined by the object's velocity of approach relative to the end effector. The difference between this impact force and the desired end effector forces defines the force error. For stability, Chapter 5 showed the constraints on the force control gain:

$K_f K_e \delta t < 1$ where δt=sample rate=0.0167s (equivalent to 60 Hz)

K_e=environment stiffness=10^4-10^5 N/m for soft-hard environments

Force sensors have a stiffness of $5x10^4$ N/m representing a median environment stiffness suggesting that K_f<0.005. Along the force trajectory, the force sensor value F_{ext} will vary and this was modelled by:

$F_{ext}^j = F_{ext}^d + K_f (F_{ext}^d - F_{ext}^{j-1})$ where j=force trajectory point

The force sensor values were assumed to vary along the force trajectory based on the previous force sensor value and the force error. This mimicked the expected variation of the sensor values as they converged to the desired end effector values.

The reaction moment dynamics fed forward to the attitude control system of the spacecraft must also incorporate the payload dynamics and this can be done using equation 3.10:

$$N_r = \sum_{i=1}^{7} N_{ci} + (p^*_{cm} - r_{c0} - s_0) \times \sum_{i=1}^{7} F_{ci}$$

where $$\begin{pmatrix} F_{c7} \\ N_{c7} \end{pmatrix} = \begin{pmatrix} f_x^0 \\ f_y^0 \\ f_z^0 \\ n_x^0 \\ n_y^0 \\ n_z^0 \end{pmatrix} = \begin{pmatrix} (a_y p^*_z - a_z p^*_y) n_x^{ext} \\ (a_z p^*_x - a_x p^*_z) n_y^{ext} \\ (a_x p^*_y - a_y p^*_x) n_z^{ext} \\ a_x f_x^{ext} \\ a_y f_y^{ext} \\ a_z f_z^{ext} \end{pmatrix}$$

The values F_{ci} and N_{ci} from i=1 to i=6 are calculated in the dynamics segment of the program and referenced to the base of the manipulator. The reaction moment trajectory is dependent on the end effector force sensor values and this will, within the restriction of the force sensor model, depend on the force control gain (in this model). It is assumed without simulation that closed loop attitude control will be accomplished by the spacecraft attitude control system and its sensors.

This completes the simulation program for the single arm ATLAS model of a robotic servicer spacecraft and its control system. The attitude control system was not specifically included as the robot control system interacts with it only through the feedforward compensation of reaction moments. Otherwise the attitude control system is no different from a standard spacecraft three axis attitude control system employing closed loop control.

The next chapter considers some of the results and case studies run with the program just outlined.

Chapter 11

RESULTS & DISCUSSION

11.1 RESULTS OF SIMULATION

The results are presented graphically at the end of this chapter. The program as described in the previous chapter is listed in the Appendix. The simulation results are shown as graphs which display certain parameters of interest concerning the trajectory of the robot arm. As mentioned in the previous chapter, the simulation proceeded through two phases: the initial capture phase to acquire the target which was purely positioned controlled, and the grapple phase to passivate the target which was purely force controlled.

We consider the first phase of position control over six trajectory knot points calculated at a rate of 60 Hz.

Figure 11.1 shows the joint angles through the trajectory. As expected the trajectory interpolation routine gives uniform straight line joint trajectories from initial to final configurations in cartesian coordinates to reflect the uniform motion of the end effector. This does not imply linear variation of the joint angles as shown.

Figure 11.2 shows the joint rates. The trajectory interpolation accelerates the end effector to maximum speed (1.0 m/s) through the first and second interpolation points and then the end effector travels at uniform velocity until the final but one interpolation point at which point the end effector decelerates to rest at the final interpolation point. The initial and final joint rates are zero as expected for the start and stop points of the end effector motion. The maximum joint rates correspond to the maximum end effector velocity at points 3 and 4 as expected. The graph clearly shows how the joints are driven at different rates to maintain straight line motion of the end effector. Note that it is not expected that the inverse velocity kinematics will yield smooth trajectories - the inverse solution (and the forward solution) is configuration dependent and the Jacobian is valid on a point by point basis only. Indeed if more points are added to the trajectory the joint velocity profile will change as the joint velocities are calculated uniquely for each velocity point.

Similar arguments apply to the inverse acceleration profile in Figure 11.3. The joint acceleration trajectory starts and ends at zero values as expected and peaks at interpolation points 2 (corresponding to acceleration of the end effector) and 5 (corresponding to deceleration of the end effector). The joint accelerations at points 3 and 4 are low during the constant end effector velocity phase as expected. They are finite however as different joint accelerations are required to maintain constant end effector velocity.

It is worth mentioning here that the initial and final values of the joint rates and joint accelerations at points 1 (start) and 6 (stop) were identical. From joint 1 to 6, both joint rate and acceleration had values at the initial point (interpolation point 1) of: 0.0006, 0.0016, -0.0068, 0.0039, 0.0049, 0.0166. Similarly, from joint 1 to 6, both joint rate and acceleration had values at the final point (interpolation point 6) of: -

0.0003, -0.0014, -0.0008, 0.0109, 0.0039, -0.0003. To two significant figures as adopted here these equate effectively to zero. However, they are finite. These are artifacts from the numerical inversion of the Jacobian as this is the only common feature of the inverse velocity kinematics and of the inverse acceleration kinematics. At the zero end effector values of velocity and acceleration, the numerical inversion yields finite values which are identical in both algorithms indicating the difficulties and errors that can arise in numerical techniques in simulation. This appears to justify emphasis on analytical methods over numerical methods, justifying the development of an analytical formulation of $\dot{J}$ in the resolution of acceleration coordinates algorithm in Chapter 2.

The joint torques as calculated in the first phase of this simulated maneouvre indicate fairly low joint torques - ~1 Nm well within the capabilities of the PUMA 560/600 joint motors (Figure 11.4). The joint torques do not start and end at zero values due to the computed torque feedback control system acting. The simulation included a random 5% error to model proprioceptive sensor feedback from the joints thereby providing small but finite torque requirements at the trajectory end points. The reaction moments are of a similar order of magnitude, but with a tendency to have greater absolute values <5 Nm, as expected from the reactive effects of simultaneously-driven multiple joints (Figure 11.5). These are large however in comparison to the typical attitude disturbance torques experienced by spacecraft ~10^{-6}-10^{-3}g. Furthermore, they are in excess of the capabilities of reaction wheels which are limited to ~1Nm torques. Once again, the control system feedback of the 5% model error provides finite values of reaction moments at the trajectory end points of start and stop. The reduced reactive effect about the x-axis is noticeable but inexplicable in view of the uniform lever arm distances of the manipulator base from the centre of mass of the spacecraft. One possibility is that the target dimensions and moment of inertia were modelled as for a cuboid. Note that the joint torques are referenced to the base of the arm coordinates and so bear no quantitative relation to the joint accelerations which are referenced to the joints. In actuality for robotic control they would have to be referred to joint coordinates by using the link-referenced Newton-Euler calculations but the interest here is in the reaction moments which require the forward recursive dynamics to be calculated with respect to the base of the arm. There is no reason why the two calculations could not be interleaved in actual implementation with little additional cost in terms of computational overhead. This completes the first phase of the trajectory.

After the first phase of the trajectory, the end effector has collided with the target object and experienced impulsive type forces. The force controller then acts to reduce those end effector forces (but without altering the end effector kinematics of zero acceleration and velocity and maintenance of the final cartesian position). The force control portion of the program was run for a number of test cases. Force control has been a much neglected consideration in the literature on space robotics and to the author's knowledge this is the first time that it has been considered in detail whilst adopting algorithms specifically modified for the space environment. Two variables were considered for the test cases: variable force control gain and object impact velocity. The smaller the force control gain, the more rapid the passivation due to the convergence of the control system to the desired end effector forces. Three values of force control gain K_f were used: 0.4, 0.25, and 0.05. Altering the force control gain thus alters the passivation trajectory over time. Object impact velocity was also varied

and given values of 0.1m/s and 1.0m/s. The value 0.1m/s is the order of magnitude typically experienced by the Shuttle RMS. There is no reason why the manipulator arm(s) have to undergo such impacts. Provided the approach velocity of the target object can be tracked, so the velocity of the end effector may be matched to that of the target object to minimise the impact forces. However we wish in this analysis to explore potential contingency situations and possible worst case type scenarios.

The desired cartesian end effector forces and torques were taken at the maximum design values at 100N and 100Nm respectively. In all cases each joint torque brackets a given value at each control point and rapidly converges to a finite value. The reaction moments similarly follow this pattern of bracketing a steady state value. These steady state joint torques and reaction moment compensation torques will be the required torques to exert 100N and 100Nm on the target by the end effector. The steady state manipulator joint torques corresponding to those desired end effector forces are 141.3Nm, -160.8Nm, -158.6Nm, -101.5Nm, 0.0, and -185.3Nm at each joint respectively from the base to the end effector. The force control trajectory converges to these values. Similarly, this generates a reaction moment on the spacecraft of $(23.0, 25.9, 79.9)^T$ Nm about the x,y and z world coordinate axes which must be compensated by the attitude control system to ensure a stable platform. The graphs by virtue of the large range of joint torque and reaction moment magnitudes encountered during passivation do not show resolution of small value torques such as thaose indicated by the desired joint torques and desired reaction moments. For this reason tables of data are included.

First we consider the variation of gain with a fixed relative approach velocity of 1.0m/s (worst case) (Figures 11.6 and 11.7) and a similar pattern was found with a relative approach velocity of 0.1m/s (Figures 11.8 and 11.10). In all cases the force trajectory over time through passivation of the target object brackets the desire joint torques required to apply the specified end effector forces/torques. The control system must reduce the difference between the impact force and the desired end effector forces (the force error). The initial joint torques corresponding to the end effector impact forces were not shown as they would be determined purely by the magnitude of the impact forces and so would be identical for a given impact velocity. Furthermore, the force control loop is assumed to be implemented immediately on activation of the force sensors.

A force control gain of 0.4 yields a passivation trajectory which oscillates about the desired joint torques for 17 trajectory points to 0.1^o accuracy and for 12 trajectory points to 1^o accuracy (Figure 11.6). A force control gain of 0.25 yields a passivation trajectory of 11 trajectory points to 0.1^o accuracy and of 9 trajectory points to 1^o accuracy (Figure 11.7). A force control gain of 0.05 yields a passivation trajectory of 6 trajectory points to 0.1^o accuracy and 5 trajectory point to 1^o accuracy (Figure 11.9). A low force control gain K_f=0.005 as suggested earlier in the text yields a passivation trajectory of only a single point, ie. passivation within the shortest time. Hence the force control gain is critical in determining the length and oscillation behaviour of the passivation trajectory over time. The first joint torque trajectory values shown are those which result from the first cycle through the force control loop. For the variable control gains, they differ for the same initial impact velocity: figure 11.6 has a maximum at 10kN (K_f=0.4), figure 11.7 has a maximum at 6kN (K_f=0.25) and figure

11.9 has a maximum at near 1.2kN (K_f=0.05). The force control gain thus determines the first joint torque trajectory values after initial impact. A high force control gain yields a high joint torque increment over the trajectory and is less effective in reducing the force error. It is this that is responsible for the passivation trajectory length. A high control gain yields higher joint torques due to the high error increment and so more trajectory points are required to bracket and converge to the desired joint torque. A low control gain on the other hand yields lower joint torques with smaller force errors and reduces the force error more rapidly to the desired values over fewer trajectory points. Hence, it is necessary to adopt low force control gains K_f~0.005 (consistent with expectations) as they rapidly reduce the force error to zero to the extent that passivation may be accomplished over a single trajectory point.

The reaction moment trajectory follows a similar pattern with force control gain variation (Figures 11.11 and 11.12 with K_f=0.25 and K_f=0.05 respectively). Higher force control gains yield longer passivation trajectories (9 trajectory points compared with 5 trajectory points to 1^o accuracy). The reaction moment trajectory shows the reaction moments from the initial impact and their subsequent passivation through the force control loop algorithm. The initial value is that corresponding to initial impact and for any given impact velocity this will be constant. Subsequent evolution of the reaction moment trajectory is then dependent on the force control loop and the effect of the force control gain on the passivation trajectory. Hence the reaction moments mirror the behaviour of the joint torque trajectory.

The next question concerns the effect of different relative approach velocities of the object to the stationary end effector. An increase from 0.1m/s to 1.0m/s approach velocity will cause an increase in the impact forces at the end effector. The initial joint torques corresponding to the impact forces are not shown - only the joint torque trajectories subsequent to impact. Figures 11.7 and 11.8 illustrate the differences in joint torque trajectory resulting from the different impact scenarios with a constant force control gain of 0.25. For 1.0 m/s impact, the first joint torque trajectory points for each joint were (-5969.2, 2200.9, 1574.6, -1343.0, -2854.8, 4706.4) Nm respectively. For 0.1 m/s impact, the first joint torque trajectory points for each joint were (-5570.0, 1350.1, 1283.7, -868.9, -2558.1, 4905.0) Nm respectively. These do not vary significantly from each other. Figures 11.9 and 11.10 show similar comparisons for a constant force control gain of 0.05 - at 1.0 m/s, the first joint torque trajectory points were (-1080.8, 311.5, 188.0, -349.8, -571.0, 793.12) Nm compared with (-1001.0, 141.4, 129.9, -255.0, -511.6, 832.8) Nm at 0.1 m/s. Both sets of results at each force control gain show that the effect of different object impact velocities on the joint torque trajectory is not large in comparison to the effect of changing the force control gains. Indeed, the force trajectory passivation endures over the same number of trajectory points for 0.1m/s and 1.0m/s effector/object relative velocities for a given control gain. This is corroborated for the two force control gains shown (K_f=0.25 for figures 11.7 and 11.8 and K_f=0.05 for figures 11.9 and 11.10) - when K_f=0.25 the joint torque trajectories at both impact velocities passivate over 9 trajectory points with similar maximum first trajectory points near 6kN; similarly, when K_f=0.05 the joint torque trajectories at both impact velocities passivate over 5 trajectory points with similar maximum first trajectory points near 1 kN. The first trajectory points vary very little. Subsequently, passivation trajectories at these different impact velocities vary even less to give similar passivation timescales. Hence, relative impact velocity is

not an important variable compared with force control gain. This emphasises the importance of low force control gain.

The reaction moment trajectories are illustrated in Figures 11.11 and 11.12 for the two impact velocities cited for each control gain. The first trajectory point represents the effect of the actual impact on the reaction moments applied to the spacecraft bus. The different approach velocities affect the reaction moments only in the approach velocity direction, ie. the y coordinate due to the impact variation in that coordinate. Once again, subsequent to impact when the force control system kicks in, this does not significantly affect the reaction moment trajectory for a given force control gain giving the same number of trajectory points.

The typical joint torques required for force control are very high ~1-10kNm with high control gains. Low control gains yield joint torques ~1kNm. These are well in excess of the capabilities of PUMA 560/600 joint torque motors. Space robotic motors offer much higher performance. Clearly this is a critical capability and this implies the need for high torque motors in conjunction with low force control gains. The reaction moments have similar orders of magnitude as the joint torques ~ kN as expected. This does illustrate the need for control moment gyro attitude control as reaction wheel control is not capable of compensation even during the slewing phase prior to passivation. Furthermore, the difference between force control and position control is evident. The implementation of force control yields very large motor torque requirements from both the manipulator joint motors and the spacecraft attitude control actuators, a factor of ~1000 greater than those imposed by pure position control. In other words, force control requirements will define the capabilities of any robotic system in space. This has been little appreciated in previous work which has been dominated by the space-based position control problem.

11.2 VALIDATION

Regarding validation, the central core of the programme is the position kinematics formulation. The inverse position kinematics yielded the correct solutions to the test case of the manipulator arm in the forward reach configuration and the "stowed" configuration. This however was for the terrestrial version of the inverse position kinematics on which this program was based but modified according to the methods presented in Chapter 6. Thes are the only test cases available. Other forward and inverse position kinematics solutions can be demonstrated to be self-consistent in the terrestrial mode. However, in the simulation, the terrestrail algorithms are modified for the space environment as presented in Chapter 6. In addition, the inverse velocity and acceleration kinematics even for terrestrial manipulators cannot be validated other than through self-consistency. The Jacobian matrix defines the forward kinematics and the inverse solution is based on inverting that matrix. Furthermore, no test case is possible as the forward and inverse solution to joint/end-effector velocity is *configuration-dependent*. Hence it will vary according to the configuration and the only standard that can be applied is that of self-consistency. The inverse solutions for joint angle rates will be self-consistent given that the Jacobian is correct and it is inverted correctly in the numerical inversion subroutine. A similar argument applies for the forward and inverse acceleration solutions.

The dynamics cannot be validated for similar reasons that they are configuration dependent and the so-called forward dynamics problem (given the joint torques what are the joint positions, rates and accelerations) is not trivial - indeed it is less well characterised than the inverse dynamics problem solved for control purposes. The lack of validity beyond self-consistency in robotics research has been a source of some criticism. However it is in the nature of the problem - the robot manipulator is a highly nonlinear system and it is complex. The only standard that is possible in simulation is self-consistency. Offsetting this somewhat are the proofs of the concepts involving space robots in Chapter 6. The single robot arm freeflyer problem is presented as a set of theorems which are then proved from the initial problem statements through a series of well defined steps. This lends the methodology proposed a degree of rigour not otherwise obtainable theoretically through simulation given that the problem statements are correct. Although the extension to the two arm case has not been presented in this way, it too could be reformulated in this fashion. Hence the problems and solutions have been presented in as rigorous manner as is possible in a theoretical thesis. The only way to really validate these control algorithms is to implement them in hardware and hardware is not always available. However this would be the next step in testing the algorithms presented here. As a spacecraft implementation would be costly the obvious choice is the implementation of hardware in neutral bouyancy conditions.

11.3 DISCUSSION

The procedure outlined in this thesis is computationally straight forward and solves the space manipulator control problem simply - consequently it may be regarded as the "engineering approach" to space robotic control since it trades off large computational overheads for a small loss of flexibility. The only advantage that the generalised Jacobian approach has over the methods presented here are that it allows the freeflyer to be maneouvred such that the inertial positioning of the end effector remains invariant whilst altering the attitude of the mounting platform. This is not, it is conjectured, a highly useful capability and that its exclusion is justified by the computational savings of the outlined method given the limited computational resources available to spacecraft. It allows the use of standard spacecraft attitude and robot control algorithms with little modification and little extra computational effort due to the ease of incorporation of the modifications. Indeed, these algorithms are applicable not just to spacecraft employing manipulators, but to all spacecraft which employ communications antennae, rigid solar panels, orientable sensors or any deployment mechanism (assuming no flexure), ie. the robotics formulation provides a generalised methodology for the dynamics and control of virtually all rigid spacecraft. Furthermore, these techniques are modifiable for application to robotic submersibles. The algorithms for the single arm formulation on which all dual arm formulations are based have undergone computer simulation using a 6 degree-of-freedom robot (PUMA 560/600) model in the performance of a grapple and passivation task as desribed in the previous chapter. This is an absolutely fundamental task which must be effected before any further, more complex manipulation can occur such as the ORU exchange task. The basic formulation was extended in the analysis to a dual arm system as a more realistic proposal (though no simulation was run) and again, the computational complexity minimisation was the prime concern. The dual-arm case introduces additional complications highlighting even more the necessity for solving control problems as low down the control hierarchy as possible, ie. at the servo level.

The dual arm case was shown to be fundamentally similar to the single arm case with the additional proviso that dynamic coupling occurs between the manipulators through the spacecraft mounting. Validation of these algorithms would require hardware implementation.

A systems design proposal was presented and it was found that if logistic factors were taken into account, the spacecraft subsystem tradeoffs were far from trivial. The specific design of the dual arm robotic interceptor presented (Advanced TeLerobotic Actuation System, ATLAS) was based on conventional technologies. The technology is thus in place to build such a system perhaps using off-the-shelf hardware and software which require very little major new technological innovation. ATLAS was proposed for service in LEO - LEO operation would provide a test bed for any such spacecraft to operate in other orbits such as GEO or polar orbits. The tradeoffs yielded a 1.5 tonne spacecraft with EVA-equivalence capable of two-way 1000km orbit changes. As always, propellant usage limits the lifetime of the spacecraft and periodic replenishment of consumables launched as piggy-back payloads would be necessary to extend the operational lifetime of the system to realistic timescales.Onboard power was another problem which required a flexible approach of using fuel cells during manipulation and deployable arrays during non-operational phases. The desirability of autonomy within the limits of space-rated microprocessor technology suggests distribution of the computational workload through a communications link sufficient to provide video data transmission. This allowed a facility for teleoperation from a ground station using EDRS for a permanent communications link during manipulation phases of the mission. The control system automatically compensates for the manipulator reactions on the spacecraft so that ground operators would not need to be retrained from terrestrial manipulators. In fact, this control compensation may be regarded as the first step towards supervised autonomy of space robotic systems. The market with an average charge of $150M per operation is estimated to potentially yield around $2B over the following 15 year operational period, representing up to a 250% discounted return on investment.

This kind of robotic system will become a baseline for further robotic and automated activities in space. General purpose manipulation represents the most varied and diverse sets of tasks that can be performed in space. A subset of this includes the servicing of scientific payloads on dedicated platforms to maintain experiments in controlled environments such as through reagent replenishment, product harvesting and product sampling. Indeed Sheskin (1985) proposed that an unmanned space platform controlled through telepresence from the ground with automated capabilities would be a lower cost alternative to a permanent manned space station. Eureka represents one such platform for microgravity experiments. The principal effect of microgravity is to reduce the importance of density differences in manufacturing such that bouyancy-driven convection is minimised. Drop towers, parabolic flights and sounding rockets are limited to microgravity durations ~seconds to ~minutes. It has been suggested that a space platform capable of mounting three Spacelab-type pallets ~1800kg for experimental payloads (especially for microgravity materials processing) would alleviate the problems of the corruption of the microgravity environment in space caused by human activity in manned missions. Pallet handling and the addition of new pallets would require manipulators. Resupply of the platform and experiment changeout may be accomplished autonomously. More immediately, the NASA

Robotic Operated Materials Processing System Project is a GAScan experiment to determine the feasibility of producing semiconductor materials autonomously.

Microgravity manufacturing of alloys, pharmaceuticals and semiconductor crystals may become one area of future commercial benefit which will rely critically on the development of robust robotics and automation technology. The future of space-based manufacturing will ultimately depend on lessons learned in general purpose manipulation tasks in zero-gravity. This commercial application would mark the start of space industrialisation and the advent of large space platforms dedicated to manufacturing controlled robotically. It has been calculated that space manufacturing could generate ~$42B/y in sales of which pharmaceutical production alone would account for $29B/y [Sepehri 1987]. Generally high product specific cost items are amenable for space-based manufacturing - the breakeven product price is $25/g for launch costs of $10/g - pharmaceuticals and semiconductor crystals presently command ~$100/g. The raw material cost of high grade silicon is $25/g compared with the processed wafer price of $250/g.

In general, space robotics research activity could provide an effective focus for broad-based technology innovation applicable to other areas of application such as undersea and battle environments to name the obvious ones as well as providing a general technology transfer medium to virtually all activities that rely on information technology and related applications.

11.4 TRAJECTORY DATA & GRAPHS

All data is taken to 2 significant figures as dictated by the sensor resolution for the forseeable future.

Fig 11.1 Joint displacement trajectory

theta1	-14.52	-13.34	-12.28	-11.31	-10.43	-9.64
theta2	-9.36	17.79	43.21	65.3	83.68	99
theta3	35.38	14.86	-0.66	-13.47	-25.32	-36.85
theta4	180	177.9	177.8	177.34	176.79	176.67
theta5	26.02	20.69	18.6	15.86	10.37	2.15
theta6	-165.48	-159.66	-154.68	-150.42	-146.54	-146.98

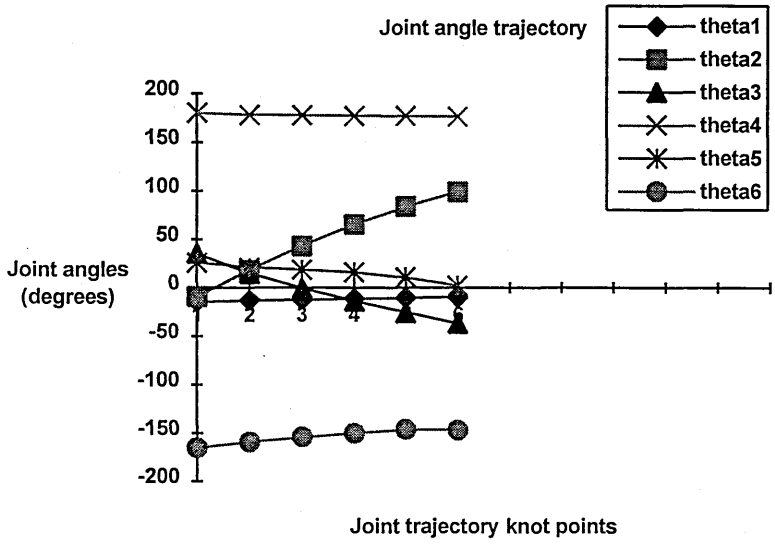

Fig 11.2 Joint rate trajectory

theta1'	0	-0.21	-1.34	0.57	0.28	0
theta2'	0	-0.8	-1.34	-5.15	-2.69	0
theta3'	-0.01	0.42	4.98	-1.52	-1.45	0
theta4'	0	2.97	6.05	12.53	8.55	0.01
theta5'	0	-0.8	4.98	-1.52	-1.45	0
theta6'	0.02	-0.21	-1.34	0.57	0.28	0

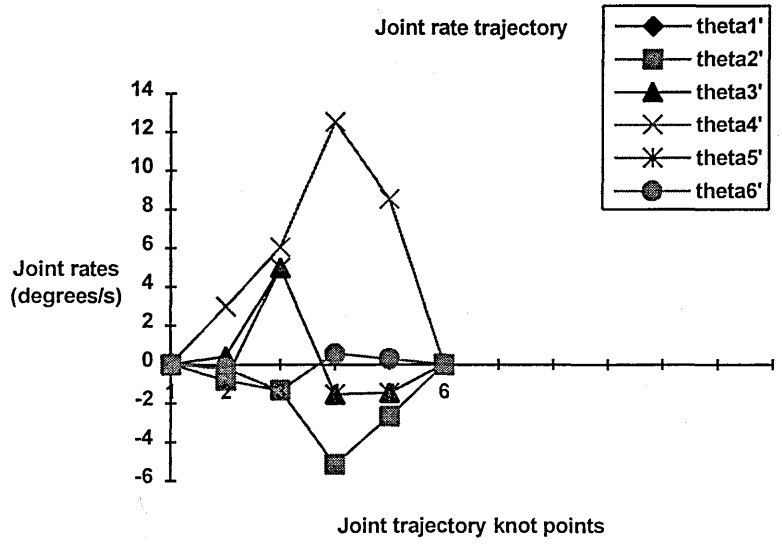

Fig. 11.3. Joint acceleration trajectory

theta1"	0	-0.53	0.24	0.02	-0.68	0
theta2'	0	-2.08	0.24	-1.5	6.17	0
theta3"	-0.01	1.05	-0.61	-0.03	3.59	0
theta4"	0	7.44	-0.25	0.85	-21	0.01
theta5"	0	-2.08	-0.61	-0.03	3.6	0
theta6"	0.02	-0.53	0.24	0.02	-0.68	0

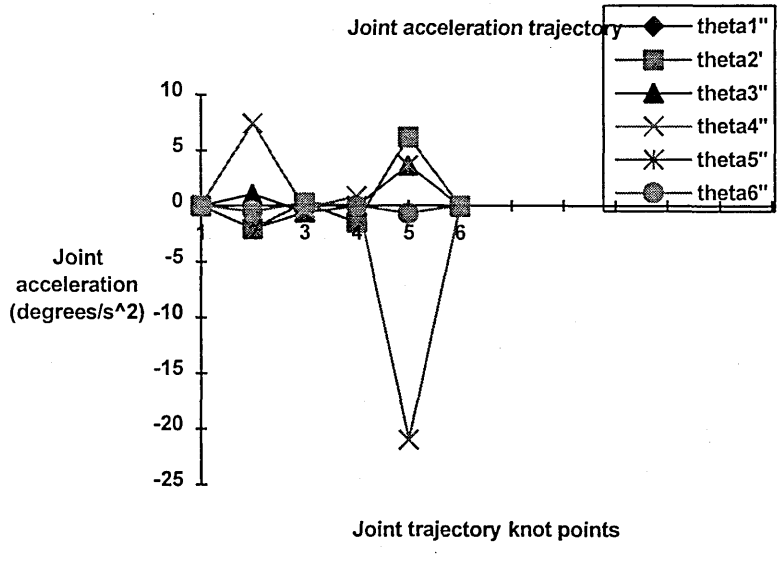

Fig 11.4 Joint torque trajectory

tau1	0.4	0.2	0.3	0.1	-0.2	-0.06
tau2	-0.16	-1.12	-0.73	-1.24	1.02	-0.97
tau3	-0.18	-0.41	-0.4	-0.47	0.88	-0.13
tau4	0.23	0.08	-0.02	-0.01	-0.35	0.24
tau5	0.03	0.04	0.05	0.06	-0.12	0.02
tau6	0.25	0.09	-0.01	0.02	-0.34	0.24

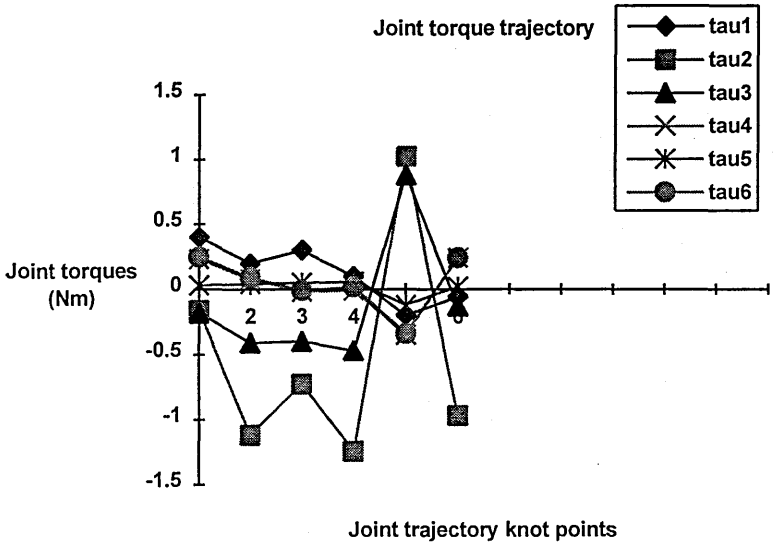

Fig 11.5 Reaction moment trajectory

nrx	0	-0.6	-0.36	-0.59	0.22	0
nry	0.14	-2.88	-1.92	-3.54	3.61	-2.06
nrz	0.64	2.41	1.89	2.63	-3.97	1.24

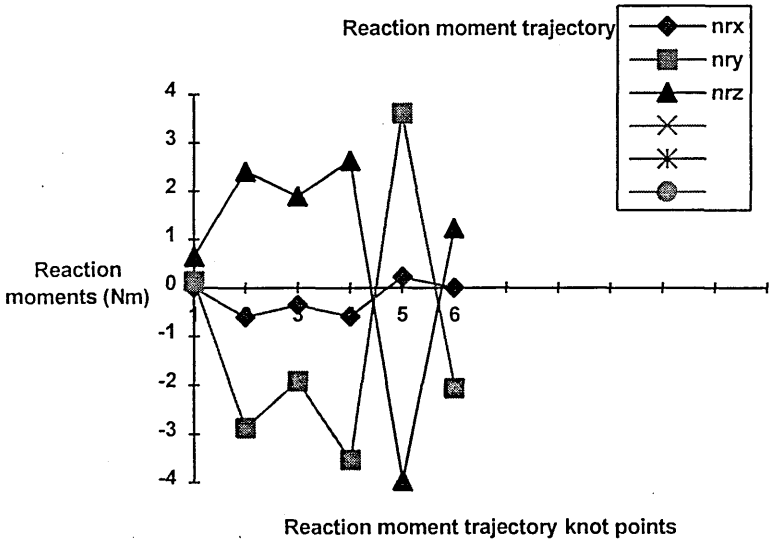

Fig 11.6 Joint torque trajectory with K_f=0.4 and v_{rel}=-1.0 m/s

tau1	-9635.43	4051.96	-1423	766.98	-109.01	241.39	101.23	157.29	134.8
	143.84	140.25	141.69						
tau2	3617.87	-1672.32	443.76	-402.63	-64.1	-199.53	-145.36	-167.03	-158.36
	-161.83	-160.4	-160.99						
tau3	2614.48	-1267.86	285.04	-336.1	-87.63	-187.02	-147.26	-163.16	-156.8
	-159.35	-158.33	-158.74						
tau4	-2087.88	693.04	-419.33	25.62	-152.36	-81.17	-109.65	-98.26	-102.81
	-100.99	-101.72	-101.43						
tau5	-4567.7	1827.08	-730.83	292.33	-116.93	46.77	-18.71	7.48	-2.99
	1.2	-0.48	0.19						
tau6	7641.36	-3315.91	1067	-686.17	15.1	-265.41	-153.2	-198.09	-180.13
	-187.31	-184.44	-185.59						

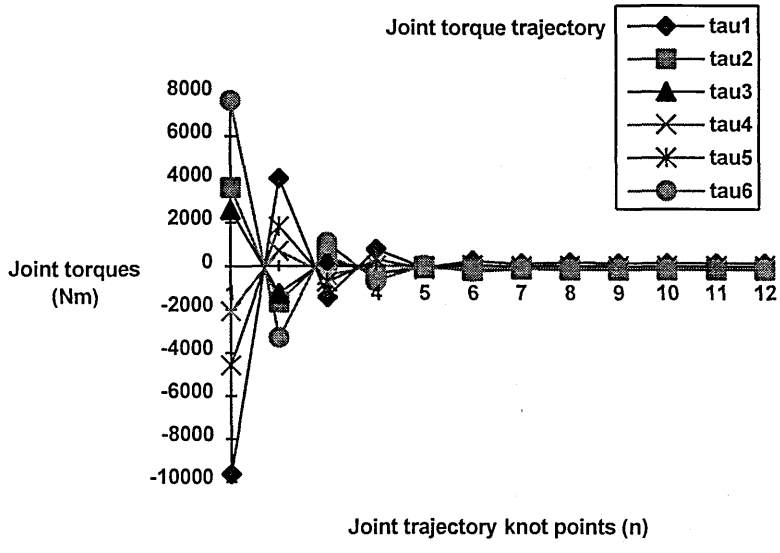

Fig 11.7 Joint torque trajectory with K_f=0.25 and v_{rel}=-1.0 m/s

tau1	-5969.17	1668.89	-240.63	236.75	117.41	147.24	139.78	141.65	141.18
tau2	2200.85	-751.26	-13.23	-197.74	-151.61	-163.14	-160.26	-160.98	-160.8
tau3	1574.57	-591.92	-50.3	-185.7	-151.85	-160.31	-158.2	-158.73	-158.59
tau4	-1342.99	208.86	-179.1	-82.11	-106.36	-100.3	-101.81	-101.44	-101.53
tau5	-2854.81	713.7	-178.43	44.61	-11.15	2.79	-0.7	0.17	-0.04
tau6	4706.38	-1408.17	120.46	-261.69	-166.15	-190.04	-184.07	-185.56	-185.19

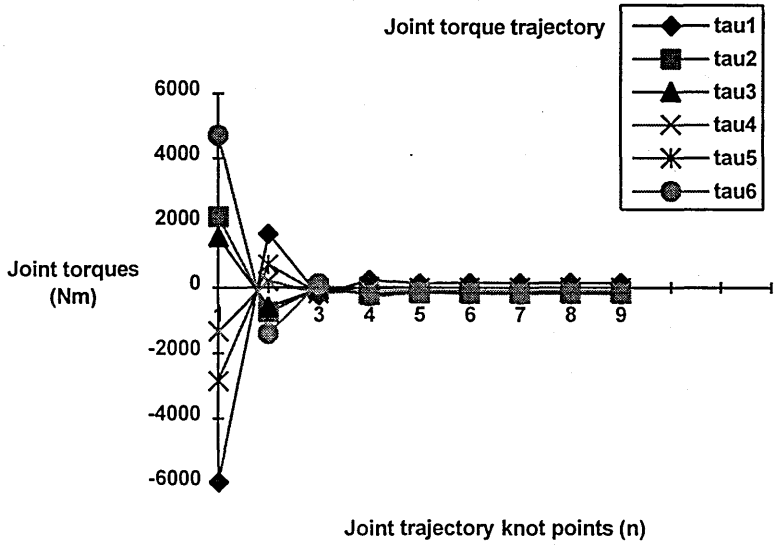

Fig 11.8 Joint torque trajectory with K_f=0.25 and v_{rel}=-0.1 m/s

tau1	-5570.04	1569.1	-215.68	230.51	118.97	146.85	139.88	141.62	141.19
tau2	1350.12	-538.58	-66.4	-184.45	-154.93	-162.31	-160.47	-160.93	-160.81
tau3	1283.71	-519.2	-68.47	-181.16	-152.99	-160.03	-158.27	-158.71	-158.6
tau4	-868.92	90.34	-149.47	-89.52	-104.51	-100.76	-101.7	-101.46	-101.52
tau5	-2558.1	639.52	-159.88	39.97	-9.99	2.5	-0.62	0.16	-0.04
tau6	4904.99	-1457.83	132.88	-264.78	-165.38	-190.23	-184.02	-185.57	-185.18

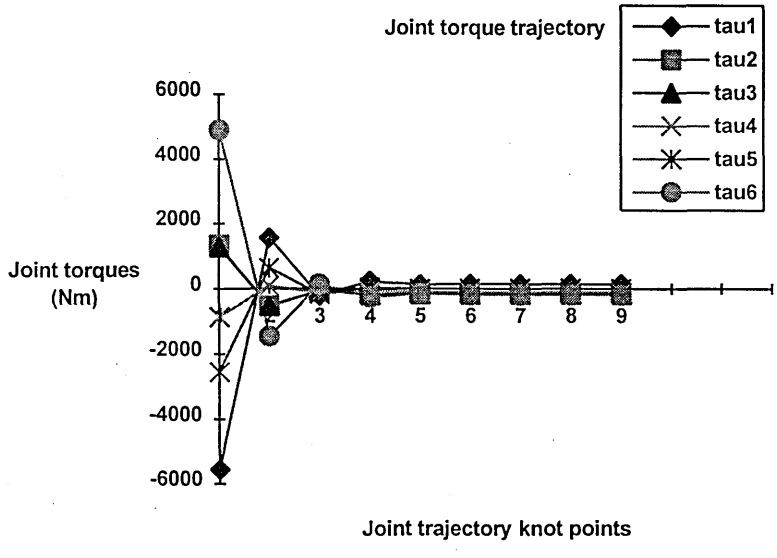

Fig 11.9 Joint torque trajectory with K_f=0.05 and v_{rel}=-1.0 m/s

tau1	-1080.81	202.38	138.22	141.43	141.27
tau2	311.5	-184.45	-159.66	-160.9	-160.83
tau3	188.02	-175.95	-157.75	-158.66	-158.62
tau4	-349.81	-89.096	-102.13	-101.48	-101.51
tau5	-570.96	28.55	-1.43	0.07	0
tau6	793.07	-234.18	-182.82	-185.38	-185.26

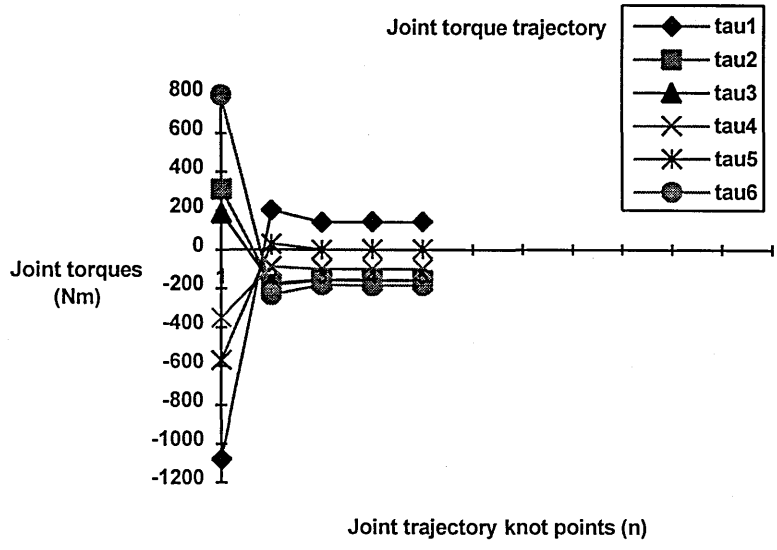

Fig 11.10 Joint trajectory with K_f=0.05 and v_{rel}=-0.1 m/s

tau1	-1000.99	198.39	138.42	141.42	141.27
tau2	141.35	-175.95	-160.08	-160.87	-160.83
tau3	129.85	-173.04	-157.9	-158.66	-158.62
tau4	-254.99	-93.84	-101.89	-101.49	-101.51
tau5	-511.62	25.58	-1.28	0.06	0
tau6	832.79	-236.17	-182.72	-185.39	-185.26

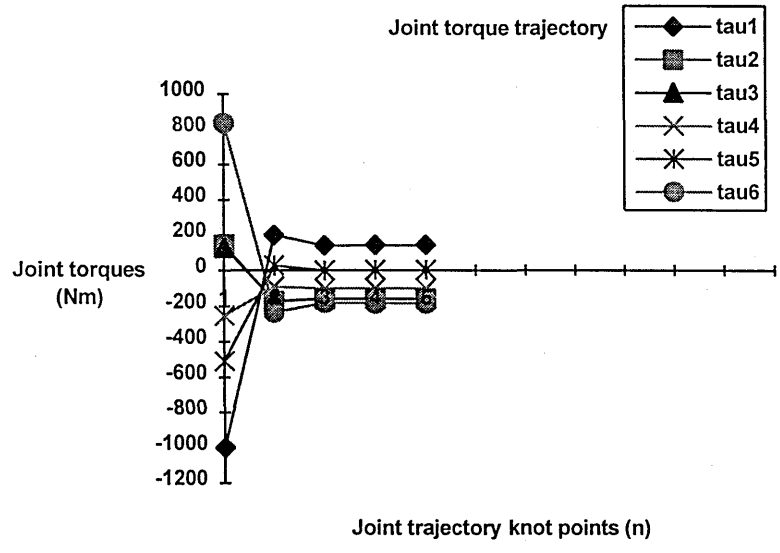

Fig 11.11 Reaction moment trajectory during force control with K_f=0.25 and v_{rel}=-1.0 m/s and v_{rel}=-0.1 m/s

nrx	1488.34	-342.42	114.57	0.12	28.73	21.58	23.37	22.92	23.03
nry(v=1.0)	-5290.79	1355.2	-306.33	109	5.16	31.12	24.63	26.26	25.85
nrz	496.33	-24.87	105.9	73.37	81.5	79.47	79.98	79.85	79.88
nry(v=0.1)	772.03	-160.52	72.6	14.26	28.85	25.2	26.11	25.88	25.94

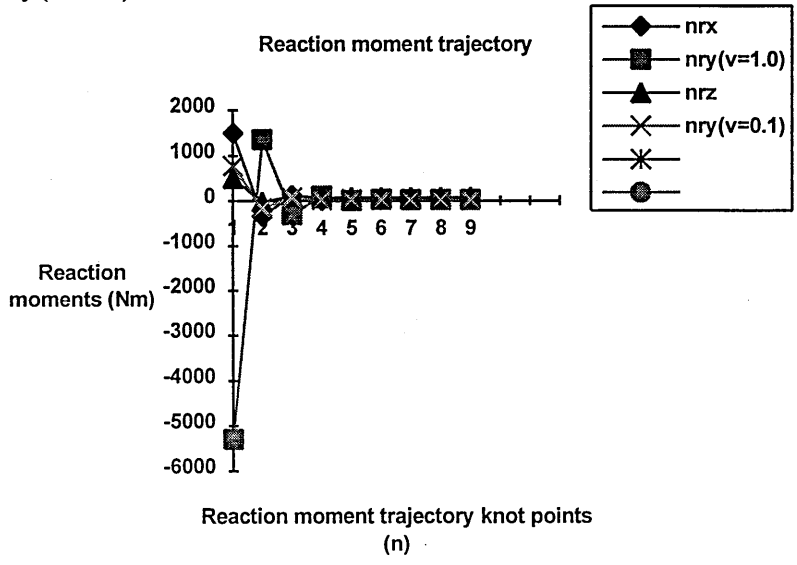

Fig 11.12 Reaction moment trajectory during force control with K_f=0.05 and v_{rel}=-1.0
m/s and v_{rel}=-0.1m/s

nrx	1488.34	-49.44	26.67	22.83	23.02
nry(v=1.0)	-5290.79	291.98	12.64	26.6	25.9
nrz	496.32	58.4	80.92	79.83	79.88
nry(v=0.1)	772.07	-11.16	27.8	25.84	25.94

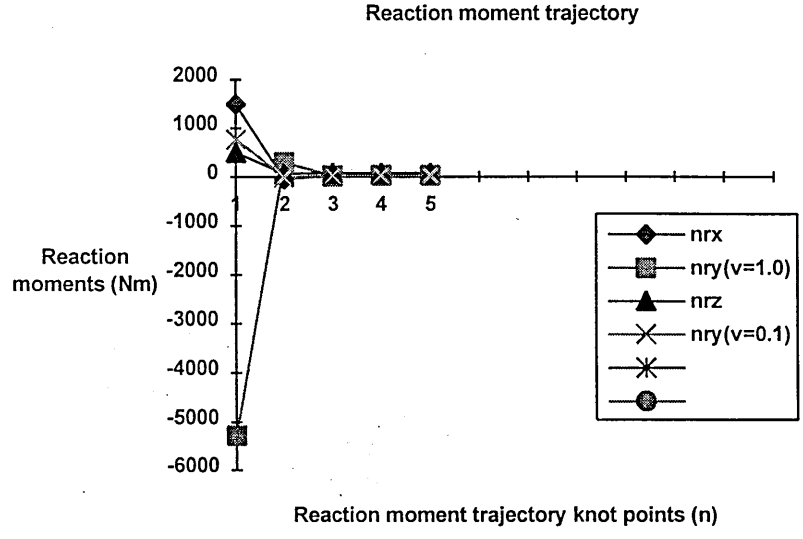

APPENDIX

ATLAS CONTROL SYSTEM FORTRAN-90 PROGRAM LISTING

Presented here is the FORTRAN-90 program listing used for the simulation of a single PUMA 560/600-type manipulator arm as described in Chapter 2 mounted onto a spacecraft bus with the parameters given in Chapter 7 utilising the algorithms presented in Chapters 2, 3, 4, 5 and 6.

```
      PROGRAM Robospace2
      INTEGER m,n
      PARAMETER (n=6,m=5)
      INTEGER i,j,k
      REAL THETA(n),DEG(n)
      REAL JAC(n,n),JACDOT(n,n),JACT(n,n)
      REAL Roll,Pitch,Yaw,t,h
      REAL nx(0:m),ny(0:m),nz(0:m),sx(0:m),sy(0:m),sz(0:m)
      REAL ax(0:m),ay(0:m),az(0:m)
      REAL epx(0:m),epy(0:m),epz(0:m),apx,apy,apz
      REAL del2,alph2,del4,del6
      REAL p06(3),p16(3),p26(3)
      REAL THETADOT(n),JRATE(n)
      REAL THETADD(n),JACCEL(n),NLACC(n)
      REAL V(0:m,3),w(0:m,3),VEL(n)
      REAL ACCEL(n),VDOT(0:m,n),maxvel
      REAL z1(3),z2(3),z3(3),z4(3),z5(3)
      REAL app3(3),app4(3),app5(3)
      REAL PI,d2,a2,d4,d6,lx(n),ly(n),lz(n)
      REAL lsx(n),lsy(n),lsz(n),radius,l(n)
      REAL Icx(n+1),Icy(n+1),Icz(n+1)
      REAL Ic0xx(n+1),Ic0yy(n+1),Ic0zz(n+1)
      REAL Ic0yx(n+1),Ic0xy(n+1),Ic0zx(n+1),Ic0xz(n+1)
      REAL Ic0zy(n+1),Ic0yz(n+1),tauf(n),taufd(n)
      PARAMETER (PI=3.14159)
      PARAMETER (del2=0.25,alph2=0.5,del4=0.5,del6=0.2)
      PARAMETER (radius=0.1)
      REAL s23,c23
      REAL A,B,C,p1,p2,Rs,rd,ACAP,TAV,mu
      REAL s2,c2,s3,c3,x4,s5,c5,s6,c6,x2,x3,y3,x5,y5
      REAL zx(0:n),zy(0:n),zz(0:n)
      REAL xx(n),xy(n),xz(n),yx(n),yy(n),yz(n)
      REAL wx(0:n+1),wy(0:n+1),wz(0:n+1)
      REAL wxdot(0:n+1),wydot(0:n+1),wzdot(0:n+1)
      REAL vxdot(0:n+1),vydot(0:n+1),vzdot(0:n+1)
      REAL vcxdot(0:n+1),vcydot(0:n+1),vczdot(0:n+1)
      REAL fcx(n+1),fcy(n+1),fcz(n+1),mass(0:n+1),mas(n)
      REAL ncx(n+1),ncy(n+1),ncz(n+1)
      REAL fx(n+1),fy(n+1),fz(n+1)
      REAL mx(n+1),my(n+1),mz(n+1)
      REAL ftx,fty,ftz,mtx,mty,mtz
      REAL Kp,Kv,r1,r2,r3,r6,ind2,ind4,ind6,ina2
      REAL tau(n),c23o,s23o,aox,aoy,aoz,epox,epoy,epoz
      REAL sox,soy,soz,x7,y7,z7,pcmx,pcmy,pcmz,mt
      REAL dx2,dx4,dx6,ax2,nrx,nry,nrz
      REAL D11h,D12h,D13h,D21h,D22h,D23h,D31h,D32h,D33h
      REAL x,y,z,phi,psi,intheta,sp,cp,st,ct
      REAL fextx,fexty,fextz,nextx,nexty,nextz
      REAL fsensx(0:m),fsensy(0:m),fsensz(0:m)
      REAL nsensx(0:m),nsensy(0:m),nsensz(0:m)
      REAL ti,vxobj,vyobj,vzobj,kf,ktau
      REAL wxobj,wyobj,wzobj
C     Given the arm and end effector cartesian positions
C     and orientations in space with respect to inertial
C     coordinates this program initially calculates the
C     joint angles to reach those cartesian coordinates
      OPEN(6,FILE="atlas25.dat")
C     ATLAS spacecraft dynamic parameters
      mass(0)=1425.0-475.0-(8.0+6.0+6.0+12.0+8.0)
      mass(1)=8.0
      mass(2)=6.0
      mass(3)=6.0
      mass(4)=0.0
      mass(5)=0.0
      mass(6)=12.0+8.0
```

```
      mass(7)=0.0
C     ORU module
C      mass(7)=225.0
      mt=mass(0)+mass(1)+mass(2)+mass(3)+mass(4)+mass(5)
     &+mass(6)+mass(7)
      r1=del2/2.0
      r2=alph2/2.0
      r3=del4/2.0
      r6=del6/2.0
      d2=((mass(0)+mass(1))*del2-mass(1)*r1)/mt
      a2=((mass(0)+mass(1)+mass(2))*alph2-mass(2)*r2)/mt
      d4=((mass(0)+mass(1)+mass(2)+mass(3))*del4-
     &mass(3)*r3)/mt
      d6=((mass(0)+mass(1)+mass(2)+mass(3)+mass(4)+mass(5)
     &+mass(6))*del6-mass(6)*r6)/mt
      sox=0.75
      soy=-0.75
      soz=-0.75
C     Dimensions of ORU module
      x7=0.0
      y7=0.0
      z7=0.0
C      x7=0.7
C      y7=0.7
C      z7=0.2
C      WRITE(*,*)d2,a2,d4,d6
C     Initialise
      THETA(1)=0.0001*PI/180.0
      THETA(2)=0.0001*PI/180.0
      THETA(3)=0.0001*PI/180.0
      THETA(4)=0.0001*PI/180.0
      THETA(5)=0.0001*PI/180.0
      THETA(6)=0.0001*PI/180.0
      dx2=((mass(2)+mass(3)+mass(4)+mass(5)+mass(6)+
     &mass(7))*del2+mass(1)*r1)/mt
      ax2=((mass(3)+mass(4)+mass(5)+mass(6)+mass(7))*alph2
     &+mass(2)*r2)/mt
      dx4=((mass(6)+mass(7))*del4+mass(3)*r3)/mt
      dx6=(mass(7)*del6+mass(6)*r6)/mt
C     Need to add these into epox,epoy,epoz
      s23o=cos(THETA(2))*sin(THETA(3))+sin(THETA(2))*cos(THETA(2))
      c23o=cos(THETA(2))*cos(THETA(3))-sin(THETA(2))*sin(THETA(3))
      aox=cos(THETA(1))*(c23o*cos(THETA(4))*cos(THETA(5))*
     &sin(THETA(5))+s23o*cos(THETA(5)))-sin(THETA(1))*
     &sin(THETA(4))*sin(THETA(5))
      aoy=sin(THETA(1))*(c23o*cos(THETA(4))*sin(THETA(5))*
     &sin(THETA(5))+s23o*cos(THETA(5)))+cos(THETA(1))*
     &sin(THETA(4))*sin(THETA(5))
      aoz=-s23o*cos(THETA(4))*sin(THETA(5))+c23o*cos(THETA(5))
      epox=-sin(THETA(1))*dx2+cos(THETA(1))*(cos(THETA(2))*ax2+
     &s23o*dx4)+aox*dx6
      epoy=cos(THETA(1))*dx2+sin(THETA(1))*(cos(THETA(2))*ax2+
     &s23o*dx4)+aoy*dx6
      epoz=-sin(THETA(2))*ax2+c23o*dx4+aoz*dx6
      pcmx=(1-mass(0)/mt)*sox+epox+(mass(7)/mt)*x7
      pcmy=(1-mass(0)/mt)*soy+epoy+(mass(7)/mt)*y7
      pcmz=(1-mass(0)/mt)*soz+epoz+(mass(7)/mt)*z7
      DO 1,k=0,1
C     Initialise
      IF(k.EQ.0)THEN
         Roll=0.00001
         Pitch=0.00001
         Yaw=0.00001
         epx(k)=-d2+0.00001
         epy(k)=d4+d6-0.00001
```

```
      epz(k)=-a2+0.00001
     Roll=45.0*PI/180.0
     Pitch=45.0*PI/180.0
     Roll=45.0*PI/180.0
     epx(k)=0.3
     epy(k)=0.7
     epz(k)=-0.5
    ELSE
       Roll=45.0*PI/180.0
       Pitch=45.0*PI/180.0
       Yaw=45.0*PI/180.0
       epx(k)=0.3
       epy(k)=0.7
       epz(k)=-0.5
    ENDIF
    Convert pitch yaw and roll angles into DH rotation
    components and calculate arm position from end
    effector position
    nx(k)=cos(Roll)*cos(Pitch)
    ny(k)=sin(Roll)*cos(Pitch)
    nz(k)=-sin(Pitch)
    sx(k)=cos(Roll)*sin(Pitch)*sin(Yaw)-
   &sin(Roll)*cos(Yaw)
    sy(k)=sin(Roll)*sin(Pitch)*sin(Yaw)+
   &cos(Roll)*cos(Yaw)
    sz(k)=cos(Pitch)*sin(Yaw)
    ax(k)=cos(Roll)*sin(Pitch)*cos(Yaw)+
   &sin(Roll)*sin(Yaw)
    ay(k)=sin(Roll)*sin(Pitch)*cos(Yaw)-
   &cos(Roll)*sin(Yaw)
    az(k)=cos(Pitch)*cos(Yaw)
    CONTINUE
    The trajectory needs to be calculated to determine the
    end effector velocities to follow the path generated
    k=0
    x=nx(k)*(epx(k+1)-epx(k))+ny(k)*(epy(k+1)-epy(k))+nz(k)*
   &(epz(k+1)-epz(k))
    y=sx(k)*(epx(k+1)-epx(k))+sy(k)*(epy(k+1)-epy(k))+sz(k)*
   &(epz(k+1)-epz(k))
    z=ax(k)*(epx(k+1)-epx(k))+ay(k)*(epx(k+1)-epy(k))+az(k)*
   &(epz(k+1)-epz(k))
    psi=ATAN(sx(k)*ax(k+1)+sy(k)*ay(k+1)+sz(k)*(k+1))
   &/(nx(k)*ax(k+1)+ny(k)*ay(k+1)+nz(k)*az(k+1))
    st=SQRT((nx(k)*ax(k+1)+ny(k)*ay(k+1)+nz(k)*az(k+1))**2
   &+(sx(k)*ax(k+1)+sy(k)*ay(k+1)+sz(k)*az(k+1))**2)
    ct=ax(k)*ax(k+1)+ay(k)*ay(k+1)+az(k)*az(k+1)
    intheta=ATAN(st/ct)
    sp=((-sin(psi)*cos(psi)*(1-cos(intheta)))*(nx(k)*nx(k+1)
   &+ny(k)*ny(k+1)+nz(k)*nz(k+1)))+((sx(k)*nx(k+1)+sy(k)
   &*ny(k+1)
   &+sz(k)*nz(k+1))*(((cos(psi))**2)*(1-cos(intheta))+
   &cos(intheta)))+((ax(k)*nx(k+1)+ay(k)*ny(k+1)+az(k)*
   &nz(k+1))*(-sin(psi)*sin(intheta)))
    cp=(-sin(psi)*cos(psi)*(1-cos(intheta)))*(nx(k)*sx(k+1)
   &+ny(k)*sy(k+1)+nz(k)*sz(k+1))+(sx(k)*sx(k+1)+sy(k)*sy(k+1)
   &+sz(k)*sz(k+1))*(((cos(psi))**2)*(1-cos(intheta))+
   &cos(intheta))+(ax(k)*sx(k+1)+ay(k)*sy(k+1)+az(k)*sz(k+1))*
   &(-sin(psi)*sin(intheta))
    phi=ATAN(sp/cp)
     DO 2 k=1,m
     nx(k)=nx(0)
     ny(k)=ny(0)
     nx(k)=nz(0)
     sx(k)=sx(0)
     sy(k)=sy(0)
```

```
C       sz(k)=sz(0)
C       ax(k)=ax(0)
C       ay(k)=ay(0)
C       az(k)=az(0)
C       epx(k)=epx(0)
C       epy(k)=epy(0)
C       epz(k)=epz(0)
       nx(5)=nx(k+1)
       ny(5)=ny(k+1)
       nz(5)=nz(k+1)
       sx(5)=sx(k+1)
       sy(5)=sy(k+1)
       sz(5)=sz(k+1)
       ax(5)=ax(k+1)
       ay(5)=ay(k+1)
       az(5)=az(k+1)
       epx(5)=epx(k+1)
       epy(5)=epy(k+1)
       epz(5)=epz(k+1)
C       WRITE(*,900)epx(0),epy(0),epz(0),ax(0),ay(0),az(0)
C       WRITE(*,900)epx(5),epy(5),epz(5),ax(5),ay(5),az(5)
C
       DO 2 j=1,m-1
       h=j/5.0
C       WRITE(*,*)h
       D11h=cos(h*phi)*(((sin(psi))**2)*(1-cos(h*intheta))
      &+cos(h*intheta))-sin(h*phi)*(sin(psi)*cos(psi)*
      &(1-cos(h*intheta)))
       D12h=cos(h*phi)*(-sin(psi)*cos(psi)*(1-cos(h*intheta)))
      &+sin(h*phi)*(((cos(psi))**2)*(1-cos(h*intheta))
      &+cos(h*intheta))
       D13h=-(cos(h*phi)*cos(psi)*sin(h*intheta))
      &-(sin(h*phi)*sin(psi)*sin(h*intheta))
       D21h=-sin(h*phi)*(((sin(phi))**2)*(1-cos(h*intheta))
      &+cos(h*intheta))-cos(h*phi)*(sin(psi)*cos(psi)*
      &(1-cos(h*intheta)))
       D22h=-sin(h*phi)*(-sin(psi)*cos(psi)*(1-cos(h*intheta)))
      &+cos(h*phi)*(((cos(psi))**2)*(1-cos(h*intheta))
      &+cos(h*intheta))
       D23h=sin(h*phi)*(cos(psi)*sin(h*intheta))
      &-cos(h*phi)*(sin(psi)*sin(h*intheta))
       D31h=cos(psi)*sin(h*intheta)
       D32h=sin(psi)*sin(h*intheta)
       D33h=cos(h*intheta)
C       WRITE(*,*)h
C       WRITE(*,900)D11h,D12h,D13h,D22h,D31h,D33h
       nx(j)=nx(0)*D11h+sx(0)*D12h+ax(0)*D13h
       ny(j)=ny(0)*D11h+sy(0)*D12h+ay(0)*D13h
       nz(j)=nz(0)*D11h+sz(0)*D12h+az(0)*D13h
       sx(j)=nx(0)*D21h+sx(0)*D22h+ax(0)*D23h
       sy(j)=ny(0)*D21h+sy(0)*D22h+ay(0)*D23h
       sz(j)=nz(0)*D21h+sz(0)*D22h+az(0)*D23h
       ax(j)=nx(0)*D31h+sx(0)*D32h+ax(0)*D33h
       ay(j)=ny(0)*D31h+sy(0)*D32h+ay(0)*D33h
       az(j)=nz(0)*D31h+sz(0)*D32h+az(0)*D33h
       epx(j)=nx(0)*h*x+sx(0)*h*y+ax(0)*h*z+epx(0)
       epy(j)=ny(0)*h*x+sy(0)*h*y+ay(0)*h*z+epy(0)
       epz(j)=nz(0)*h*x+sz(0)*h*y+ay(0)*h*z+epz(0)
C       WRITE(*,900) epx(j),epy(j),epz(j),ax(j),ay(j),az(j)
2      CONTINUE
C
       DO 5 j=0,m
       t=1.0
       IF (j.GE.2.AND.j.LT.4) THEN
       V(j,1)=(epx(5)-epx(0))/t
```

```
 V(j,2)=(epy(5)-epy(0))/t
 V(j,3)=(epz(5)-epz(0))/t
 ACAP=ACOS(0.5*(nx(0)*nx(5)+ny(0)*ny(5)+nz(0)*nz(5)
&+sx(0)*sx(5)+sy(0)*sy(5)+sz(0)*sz(5)+ax(0)*ax(5)+
&ay(0)*ay(5)+az(0)*az(5)))
 TAV=(ACAP/t)*(1/(2.0*sin(ACAP)))
 w(j,1)=TAV*(ax(3)*sx(2)-ax(2)*sx(3)+ay(3)*sy(2)
&-ay(2)*sy(3)+az(3)*sz(2)-az(2)*sz(3))
 w(j,2)=TAV*(nx(3)*ax(2)-nx(2)*ax(3)+ny(3)*ay(2)
&-ny(2)*ay(3)+nz(3)*az(2)-nz(2)*az(3))
 w(j,3)=TAV*(sx(3)*nx(2)-sx(2)*nx(3)+sy(3)*ny(2)
&-sy(2)*ny(3)+sz(3)*nz(2)-sz(2)*nz(3))
 DO 3 i=1,n
 VDOT(j,i)=0.0
 CONTINUE
 ELSE IF (j.LT.2) THEN
 V(j,1)=(epx(5)-epx(0))/(2.0*t)
 V(j,2)=(epy(5)-epy(0))/(2.0*t)
 V(j,3)=(epz(5)-epz(0))/(2.0*t)
 VDOT(j,1)=(V(j,1)-0.0)/(2.0*t/5.0)
 VDOT(j,2)=(V(j,2)-0.0)/(2.0*t/5.0)
 VDOT(j,3)=(V(j,3)-0.0)/(2.0*t/5.0)
  w(j,1)=0.5*(-nz(2)*ny(3)+ny(2)*nz(3)-sz(2)*sy(3)+sy(2)
 &*sz(3)-az(2)*ay(3)+ay(2)*az(3))/t
  w(j,2)=0.5*(nz(2)*nx(3)-nx(2)*nz(3)+sz(2)*sx(3)-sx(2)
 &*sz(3)+az(2)*ax(3)-ax(2)*az(3))/t
  w(j,3)=0.5*(-ny(2)*nx(3)+nx(2)*ny(3)-sy(2)*sx(3)+sx(2)
 &*sy(3)-ay(2)*ax(3)+ax(2)*ay(3))/t
 w(j,1)=0.5*TAV*(ax(3)*sx(2)-ax(2)*sx(3)+ay(3)*sy(2)
&-ay(2)*sy(3)+az(3)*sz(2)-az(2)*sz(3))
 w(j,2)=0.5*TAV*(nx(3)*ax(2)-nx(2)*ax(3)+ny(3)*ay(2)
&-ny(2)*ay(3)+nz(3)*az(2)-nz(2)*az(3))
 w(j,3)=0.5*TAV*(sx(3)*nx(2)-sx(2)*nx(3)+sy(3)*ny(2)
&-sy(2)*ny(3)+sz(3)*nz(2)-sz(2)*nz(3))
 VDOT(j,4)=(w(j,1)-0.0)/(2.0*t/5.0)
 VDOT(j,5)=(w(j,2)-0.0)/(2.0*t/5.0)
 VDOT(j,6)=(w(j,3)-0.0)/(2.0*t/5.0)
 ELSE
 V(j,1)=(epx(5)-epx(0))/(2.0*t)
 V(j,2)=(epy(5)-epy(0))/(2.0*t)
 V(j,3)=(epz(5)-epz(0))/(2.0*t)
 VDOT(j,1)=-(V(j,1)-0.0)/(2.0*t/5.0)
 VDOT(j,2)=-(V(j,2)-0.0)/(2.0*t/5.0)
 VDOT(j,3)=-(V(j,3)-0.0)/(2.0*t/5.0)
  w(j,1)=0.5*(-nz(2)*ny(3)+ny(2)*nz(3)-sz(2)*sy(3)+sy(2)
 &*sz(3)-az(2)*ay(3)+ay(2)*az(3))/t
  w(j,2)=0.5*(nz(2)*nx(3)-nx(2)*nz(3)+sz(2)*sx(3)-sx(2)
 &*sz(3)+az(2)*ax(3)-ax(2)*az(3))/t
  w(j,3)=0.5*(-ny(2)*nx(3)+nx(2)*ny(3)-sy(2)*sx(3)+sx(2)
 &*sy(3)-ay(2)*ax(3)+ax(2)*ay(3))/t
 w(j,1)=0.5*TAV*(ax(3)*sx(2)-ax(2)*sx(3)+ay(3)*sy(2)
&-ay(2)*sy(3)+az(3)*sz(2)-az(2)*sz(3))
 w(j,2)=0.5*TAV*(nx(3)*ax(2)-nx(2)*ax(3)+ny(3)*ay(2)
&-ny(2)*ay(3)+nz(3)*az(2)-nz(2)*az(3))
 w(j,3)=0.5*TAV*(sx(3)*nx(2)-sx(2)*nx(3)+sy(3)*ny(2)
&-sy(2)*ny(3)+sz(3)*nz(2)-sz(2)*nz(3))
 VDOT(j,4)=-(w(j,1)-0.0)/(2.0*t/5.0)
 VDOT(j,5)=-(w(j,2)-0.0)/(2.0*t/5.0)
 VDOT(j,6)=-(w(j,3)-0.0)/(2.0*t/5.0)
 ENDIF
 IF (j.EQ.0.OR.j.EQ.5) THEN
 V(j,1)=0.0001
 V(j,2)=0.0001
 V(j,3)=0.0001
 w(j,1)=0.0001
```

✓

```
      w(j,2)=0.0001
      w(j,3)=0.0001
      VDOT(j,1)=0.0001
      VDOT(j,2)=0.0001
      VDOT(j,3)=0.0001
      VDOT(j,4)=0.0001
      VDOT(j,5)=0.0001
      VDOT(j,6)=0.0001
      ENDIF
5     CONTINUE
C
      DO 300, j=0,m
C     Calculate the joint angles from the inverse kinematics
      apx=epx(j)-d6*ax(j)
      apy=epy(j)-d6*ay(j)
      apz=epz(j)-d6*az(j)
      apx=apx-pcmx-(mass(0)/mt)*sox+(mass(7)/mt)*x7
      apy=apy-pcmy-(mass(0)/mt)*soy+(mass(7)/mt)*y7
      apz=apz-pcmz-(mass(0)/mt)*soz+(mass(7)/mt)*z7
      p1=apy*SQRT(ABS(apx**2+apy**2-d2**2))-apx*d2
      p2=apx*SQRT(ABS(apx**2+apy**2-d2**2))+apy*d2
      THETA(1)=ATAN2(p1,p2)
      A=cos(THETA(1))*apx+sin(THETA(1))*apy
      B=(A**2+apz**2+a2**2-d4**2)/(2.0*a2)
      THETA(2)=2*ATAN((apz-SQRT(ABS(apz**2+A**2-B**2)))/A+B)
      x3=-(A-a2*cos(THETA(2)))
      y3=apz+a2*sin(THETA(2))
      THETA(3)=ATAN(x3/y3)-THETA(2)
      c23=cos(THETA(2))*cos(THETA(3))-sin(THETA(3))
     &*sin(THETA(2))
      s23=cos(THETA(3))*sin(THETA(2))+cos(THETA(2))
     &*sin(THETA(3))
      x4=-sin(THETA(1))*ax(j)+cos(THETA(1))*ay(j)
      y4=c23*(cos(THETA(1))*ax(j)+sin(THETA(1))
     &*ay(j))-s23*az(j)
      THETA(4)=ATAN2(x4,y4)
      s5=(cos(THETA(1))*c23*cos(THETA(4))-sin(THETA(1))
     &*sin(THETA(4)))
     &*ax(j)+(sin(THETA(1))*c23*cos(THETA(4))+cos(THETA(1))*
     &sin(THETA(4)))*ay(j)-cos(THETA(4))*s23*az(j)
      c5=cos(THETA(1))*s23*ax(j)+sin(THETA(1))*s23*ay(j)+c23*az(j)
      THETA(5)=ATAN(s5/c5)
      s6=(-sin(THETA(1))*cos(THETA(4))-cos(THETA(1))*c23*
     &sin(THETA(4)))
     &*nx(j)+(cos(THETA(1))*cos(THETA(4))-sin(THETA(1))*c23
     &*sin(THETA(4)))
     &*ny(j)+sin(THETA(4))*s23*nz(j)
      c6=(-sin(THETA(1))*cos(THETA(4))-cos(THETA(1))*c23
     &*sin(THETA(4)))
     &*sx(j)+(cos(THETA(1))*cos(THETA(4))-sin(THETA(1))*c23
     &*sin(THETA(4)))
     &*sy(j)+sin(THETA(4))*s23*sz(j)
      THETA(6)=ATAN2(s6,c6)
      DO 50,i=1,n
         DEG(i)=THETA(i)*180.0/PI
50    CONTINUE
      WRITE (*,900)DEG(1),DEG(2),DEG(3),DEG(4),DEG(5),
     &DEG(6)
C     Inverse rate kinematics formulation
C     Calculate Jacobian matrix
      JAC(1,1)=-sin(THETA(1))*(d6*(c23*cos(THETA(4))
     &*sin(THETA(5))+s23*cos(THETA(5)))+s23*d4
     &+a2*cos(THETA(2)))-cos(THETA(1))*(d6*sin(THETA(4))
     &*sin(THETA(5))+d2)
      JAC(2,1)=cos(THETA(1))*(d6*(c23*cos(THETA(4))
```

```
&*sin(THETA(5))+s23*cos(THETA(5)))+s23*d4
&+a2*cos(THETA(2)))-sin(THETA(1))*(d6*sin(THETA(4))
&*sin(THETA(5))+d2)
 JAC(3,1)=0.0
 JAC(4,1)=0.0
 JAC(5,1)=0.0
 JAC(6,1)=1.0
 JAC(1,2)=d6*cos(THETA(1))*sin(THETA(4))*sin(THETA(5))
&+d2*cos(THETA(1))
 JAC(2,2)=d6*sin(THETA(1))*sin(THETA(4))*sin(THETA(5))
&+d2*sin(THETA(1))
 JAC(3,2)=-sin(THETA(1))*(d6*s23*cos(THETA(4))
&*sin(THETA(5))-d6*c23*cos(THETA(5))-d4*c23
&+a2*sin(THETA(2)))-cos(THETA(1))*(d6*c23*cos(THETA(4))
&*sin(THETA(5))+d6*s23*cos(THETA(5))+d4*s23+
&a2*cos(THETA(2)))
 JAC(4,2)=-sin(THETA(1))
 JAC(5,2)=cos(THETA(1))
 JAC(6,2)=0.0
 JAC(1,3)=d6*cos(THETA(1))*sin(THETA(4))*sin(THETA(5))
 JAC(2,3)=d6*sin(THETA(1))*sin(THETA(4))*sin(THETA(5))
 JAC(3,3)=-sin(THETA(1))*(d6*sin(THETA(3))*cos(THETA(4))
&*sin(THETA(5))-d6*cos(THETA(3))*cos(THETA(5))
&-d4*cos(THETA(3)))-cos(THETA(1))*(d6*cos(THETA(3))
&*cos(THETA(4))*sin(THETA(5))+d6*sin(THETA(3))
&*cos(THETA(5))+d4*sin(THETA(3)))
 JAC(4,3)=-sin(THETA(1))
 JAC(5,3)=cos(THETA(1))
 JAC(6,3)=0.0
 JAC(1,4)=sin(THETA(1))*s23*(d6*cos(THETA(5))+d4)
&-d6*c23*sin(THETA(4))*sin(THETA(5))
 JAC(2,4)=d6*c23*cos(THETA(4))*sin(THETA(5))
&-cos(THETA(1))*s23*(d6*cos(THETA(5))+d4)
 JAC(3,4)=d6*cos(THETA(1))*s23*sin(THETA(4))
&*sin(THETA(5))-d6*sin(THETA(1))*s23*cos(THETA(4))
&*sin(THETA(5))
 JAC(4,4)=cos(THETA(1))*s23
 JAC(5,4)=sin(THETA(1))*s23
 JAC(6,4)=c23
 JAC(1,5)=d6*s23*sin(THETA(4))*cos(THETA(5))
 JAC(2,5)=d6*s23*sin(THETA(4))*sin(THETA(5))
 JAC(3,5)=d6*cos(THETA(1))*c23*sin(THETA(4))
&*cos(THETA(5))+d6*sin(THETA(1))*cos(THETA(4))
&*cos(THETA(5))+d6*sin(THETA(1))*c23*sin(THETA(4))
&*sin(THETA(5))-d6*cos(THETA(1))*cos(THETA(4))
&*sin(THETA(5))
 JAC(4,5)=-cos(THETA(1))*c23*sin(THETA(4))
&-sin(THETA(1))*cos(THETA(4))
 JAC(5,5)=-sin(THETA(1))*c23*sin(THETA(4))
&+cos(THETA(1))*cos(THETA(4))
 JAC(6,5)=s23*sin(THETA(4))
 JAC(1,6)=d6*(sin(THETA(1))*c23*cos(THETA(4))
&+cos(THETA(1))*sin(THETA(4)))*sin(THETA(5))+
&d6*sin(THETA(1))*s23*cos(THETA(5))
 JAC(2,6)=-d6*(cos(THETA(1))*c23*cos(THETA(4))
&-sin(THETA(1))-sin(THETA(4)))*sin(THETA(5))-
&d6*cos(THETA(1))*s23*cos(THETA(5))
 JAC(3,6)=0.0
 JAC(4,6)=(cos(THETA(1))*c23*cos(THETA(4))
&-sin(THETA(1))*sin(THETA(4)))*sin(THETA(5))
&+cos(THETA(1))*s23*cos(THETA(5))
 JAC(5,6)=(sin(THETA(1))*c23*cos(THETA(4))
&+cos(THETA(1))*sin(THETA(4)))*sin(THETA(5))
&+sin(THETA(1))*s23*cos(THETA(5))
 JAC(6,6)=-s23*cos(THETA(4))*sin(THETA(5))
```

```
     &+c23*cos(THETA(5))
C     Prior to the inversion of the Jacobian the transpose of the
C     Jacobian must be calculated for force control
C
C      JACT(1,1)=JAC(1,1)
C      JACT(1,2)=JAC(2,1)
C      JACT(1,3)=JAC(3,1)
C      JACT(1,4)=JAC(4,1)
C      JACT(1,5)=JAC(5,1)
C      JACT(1,6)=JAC(6,1)
C      JACT(2,1)=JAC(1,2)
C      JACT(2,2)=JAC(2,2)
C      JACT(2,3)=JAC(3,2)
C      JACT(2,4)=JAC(4,2)
C      JACT(2,5)=JAC(5,2)
C      JACT(2,6)=JAC(6,2)
C      JACT(3,1)=JAC(1,3)
C      JACT(3,2)=JAC(2,3)
C      JACT(3,3)=JAC(3,3)
C      JACT(3,4)=JAC(4,3)
C      JACT(3,5)=JAC(5,3)
C      JACT(3,6)=JAC(6,3)
C      JACT(4,1)=JAC(1,4)
C      JACT(4,2)=JAC(2,4)
C      JACT(4,3)=JAC(3,4)
C      JACT(4,4)=JAC(4,4)
C      JACT(4,5)=JAC(5,4)
C      JACT(4,6)=JAC(6,4)
C      JACT(5,1)=JAC(1,5)
C      JACT(5,2)=JAC(2,5)
C      JACT(5,3)=JAC(3,5)
C      JACT(5,4)=JAC(4,5)
C      JACT(5,5)=JAC(5,5)
C      JACT(5,6)=JAC(6,5)
C      JACT(6,1)=JAC(1,6)
C      JACT(6,2)=JAC(2,6)
C      JACT(6,3)=JAC(3,6)
C      JACT(6,4)=JAC(4,6)
C      JACT(6,5)=JAC(5,6)
C      JACT(6,6)=JAC(6,6)
C     To perform the inverse velocity transformations the Jacobian
C     must be inverted. This is accomplished by subroutines from
C     Numerical Recipes in Fortran by William Press et al (1992).
      VEL(1)=V(j,1)
      VEL(2)=V(j,2)
      VEL(3)=V(j,3)
      VEL(4)=w(j,1)
      VEL(5)=w(j,2)
      VEL(6)=w(j,3)
      CALL GAUSSJ(JAC,n,n,VEL,1,1)
      VEL(1)=V(j,1)
      VEL(2)=V(j,2)
      VEL(3)=V(j,3)
      VEL(4)=w(j,1)
      VEL(5)=w(j,2)
      VEL(6)=w(j,3)
      THETADOT(1)=JAC(1,1)*VEL(1)+JAC(1,2)*VEL(2)+
     &JAC(1,3)*VEL(3)+JAC(1,4)*VEL(4)+JAC(1,5)*VEL(5)
     &+JAC(1,6)*VEL(6)
      THETADOT(2)=JAC(2,1)*VEL(1)+JAC(2,2)*VEL(2)+
     &JAC(2,3)*VEL(3)+JAC(2,4)*VEL(4)+JAC(2,5)*VEL(5)
     &+JAC(2,6)*VEL(6)
      THETADOT(3)=JAC(3,1)*VEL(1)+JAC(3,2)*VEL(2)+
     &JAC(3,3)*VEL(3)+JAC(3,4)*VEL(4)+JAC(3,5)*VEL(5)
     &+JAC(3,6)*VEL(6)
```

```
      THETADOT(4)=JAC(4,1)*VEL(1)+JAC(4,2)*VEL(2)+
     &JAC(4,3)*VEL(3)+JAC(4,4)*VEL(4)+JAC(4,5)*VEL(5)
     &+JAC(4,6)*VEL(6)
      THETADOT(5)=JAC(5,1)*VEL(1)+JAC(5,2)*VEL(2)+
     &JAC(5,3)*VEL(3)+JAC(5,4)*VEL(4)+JAC(5,5)*VEL(5)
     &+JAC(5,6)*VEL(6)
      THETADOT(6)=JAC(6,1)*VEL(1)+JAC(6,2)*VEL(2)+
     &JAC(6,3)*VEL(3)+JAC(6,4)*VEL(4)+JAC(6,5)*VEL(5)
     &+JAC(6,6)*VEL(6)
      DO 55 i=1,n
      JRATE(i)=THETADOT(i)*180.0/PI
55    CONTINUE
      WRITE (*,900) JRATE(1),JRATE(2),JRATE(3),JRATE(4),
     &JRATE(5),JRATE(6)
C     Resolved acceleration is the next step
      p06(1)=cos(THETA(1))*(d6*(c23*cos(THETA(4))*sin(THETA(5))+
     &s23*cos(THETA(5)))+s23*d4+a2*cos(THETA(2)))-sin(THETA(1))*
     &(sin(THETA(4))*sin(THETA(5))*d6+d2)
      p06(2)=sin(THETA(1))*(d6*(c23*cos(THETA(4))*sin(THETA(5))+
     &s23*cos(THETA(5)))+s23*d4+a2*cos(THETA(5)))+cos(THETA(1))*
     &(sin(THETA(4))*sin(THETA(5))*d6+d2)
      p06(3)=d6*(c23*cos(THETA(5))-s23*cos(THETA(5)))+c23*d4
     &-a2*sin(THETA(2))
      p16(1)=c23*(cos(THETA(4))*sin(THETA(5))*d6)+s23*(cos(THETA(5))
     &*d6+d4)+a2*cos(THETA(2))
      p16(2)=s23*(cos(THETA(4))*sin(THETA(5))*d6)-c23*(cos(THETA(5))
     &*d6+d4)+a2*sin(THETA(2))
      p16(3)=sin(THETA(4))*sin(THETA(5))*d6+d2
      p26(1)=cos(THETA(3))*cos(THETA(4))*sin(THETA(5))*d6+
     &sin(THETA(3))*(cos(THETA(5))*d6+d4)
      p26(2)=sin(THETA(3))*cos(THETA(4))*sin(THETA(5))*d6-
     &cos(THETA(3))*(cos(THETA(5))*d6+d4)
      p26(3)=sin(THETA(4))*sin(THETA(5))*d6
      app3(1)=-sin(THETA(1))*(THETADOT(2)+THETADOT(3))+cos(THETA(1))
     &*s23*THETADOT(4)
      app3(2)=cos(THETA(1))*(THETADOT(2)+THETADOT(3))+sin(THETA(1))
     &*s23*THETADOT(4)
      app3(3)=THETADOT(1)+c23*THETADOT(4)
      z4(1)=-(cos(THETA(1))*c23*sin(THETA(4))+sin(THETA(1))
     &*cos(THETA(4)))
      z4(2)=cos(THETA(1))*cos(THETA(4))-sin(THETA(1))*c23*
     &cos(THETA(4))
      z4(3)=s23*sin(THETA(4))
      z5(1)=cos(THETA(1))*(c23*cos(THETA(4))*sin(THETA(5))+s23*
     &cos(THETA(5)))-sin(THETA(1))*sin(THETA(4))*sin(THETA(5))
      z5(2)=sin(THETA(1))*(c23*cos(THETA(4))*sin(THETA(5))+
     &s23*cos(THETA(5)))+cos(THETA(1))*sin(THETA(4))*sin(THETA(5))
      z5(3)=-s23*cos(THETA(4))*sin(THETA(5))+c23*cos(THETA(5))
      app4(1)=app3(1)+z4(1)*THETADOT(5)
      app4(2)=app3(2)+z4(2)*THETADOT(5)
      app4(3)=app3(3)+z4(3)*THETADOT(5)
      app5(1)=app4(1)+z5(1)*THETADOT(6)
      app5(2)=app4(2)+z5(2)*THETADOT(6)
      app5(3)=app4(3)+z5(3)*THETADOT(6)
      JACDOT(1,1)=-p06(1)*THETADOT(1)
      JACDOT(2,1)=-p06(2)*THETADOT(2)
      JACDOT(3,1)=0.0
      JACDOT(4,1)=0.0
      JACDOT(5,1)=0.0
      JACDOT(6,1)=0.0
      JACDOT(1,2)=-sin(THETA(1))*THETADOT(1)*(sin(THETA(4))*
     &sin(THETA(5))*d6+d2)-cos(THETA(1))*THETADOT(2)*
     &(sin(THETA(1))*THETADOT(2)*p16(2)+cos(THETA(1))*
     &THETADOT(2)*p16(1))-THETADOT(1)*
     &(sin(THETA(1))*THETADOT(2)*p16(3)+THETADOT(1)*p16(1))
```

```
 JACDOT(2,2)=cos(THETA(1))*THETADOT(1)*(sin(THETA(4))*
&sin(THETA(5))*d6+d2)-sin(THETA(1))*THETADOT(2)*
&(sin(THETA(1))*THETADOT(2)*p16(2)+cos(THETA(1))*
&THETADOT(2)*p16(1))+THETADOT(1)*
&(cos(THETA(1))*THETADOT(2)*p16(3)-THETADOT(1)*p16(2))
 JACDOT(3,2)=sin(THETA(1))*THETADOT(1)*p16(1)-cos(THETA(1))*
&THETADOT(1)*p16(2)-sin(THETA(1))*THETADOT(2)*
&(sin(THETA(1))*THETADOT(2)*p16(3)+THETADOT(1)*p16(1))-
&cos(THETA(1))*THETADOT(2)*(cos(THETA(1))*THETADOT(2)*p16(3)-
&THETADOT(1)*p16(2))
 JACDOT(4,2)=-cos(THETA(1))*THETADOT(1)
 JACDOT(5,2)=-sin(THETA(1))*THETADOT(1)
 JACDOT(6,2)=0.0
 JACDOT(1,3)=-sin(THETA(1))*THETADOT(1)*sin(THETA(4))*
&sin(THETA(5))*d6+cos(THETA(1))*(THETADOT(2)+THETADOT(3))*
&(-sin(THETA(1))*(THETADOT(2)+THETADOT(3))*p26(2)-
&cos(THETA(1))*(THETADOT(2)+THETADOT(3))*p26(1))-THETADOT(1)
&*(sin(THETA(1))*(THETADOT(2)+THETADOT(3))*p26(3)+THETADOT(1)
&*p26(1))
 JACDOT(2,3)=cos(THETA(1))*THETADOT(1)*sin(THETA(4))*
&sin(THETA(5))*d6+sin(THETA(1))*(THETADOT(2)+THETADOT(3))*
&(-sin(THETA(1))*(THETADOT(2)+THETADOT(3))*p26(2)-
&cos(THETA(1))*(THETADOT(2)+THETADOT(3))*p26(1))+THETADOT(1)*
&(cos(THETA(1))*(THETADOT(2)+THETADOT(3))*p26(3)-THETADOT(1)*
&p26(2))
 JACDOT(3,3)=-cos(THETA(1))*THETADOT(1)*p26(2)-sin(THETA(1))
&*THETADOT(1)*p26(1)-sin(THETA(1))*(THETADOT(2)+THETADOT(3))*
&(sin(THETA(1))*(THETADOT(2)+THETADOT(3))*p26(3)+THETADOT(1)*
&p26(1))-cos(THETA(1))*(THETADOT(2)+THETADOT(3))*(cos(THETA(1))
&*(THETADOT(2)+THETADOT(3))*p26(3)-THETADOT(1)*p26(2))
 JACDOT(4,3)=-cos(THETA(1))*THETADOT(1)
 JACDOT(5,3)=-sin(THETA(1))*THETADOT(1)
 JACDOT(6,3)=0.0
 JACDOT(1,4)=c23*(sin(THETA(1))*(THETADOT(2)+THETADOT(3))+
&cos(THETA(1))*THETADOT(1))*cos(THETA(5))*d6+c23*(THETADOT(2)
&+THETADOT(3))*(sin(THETA(4))*sin(THETA(5))*d6+d4)+app3(2)*
&(app3(1)*(sin(THETA(4))*sin(THETA(5))*d6+d4)-app3(2)*
&cos(THETA(4))
&*sin(THETA(5))*d6)-app3(3)*(app3(3)*cos(THETA(4))
&*sin(THETA(5))*d6
&-app3(1)*cos(THETA(5))*d6)
 JACDOT(2,4)=-c23*(cos(THETA(1))*(THETADOT(2)+THETADOT(3))-
&sin(THETA(1))*THETADOT(1))*cos(THETA(5))*d6+c23*
&(THETADOT(2)+THETADOT(3))*(cos(THETA(4))*sin(THETA(5))*d6)
&+app3(3)*(app3(2)*cos(THETA(5))*d6-app3(3)*(sin(THETA(4))
&*sin(THETA(5))*d6+d4))-app3(1)*(app3(1)*(sin(THETA(4))*
&sin(THETA(5))*d6+d4)-app3(2)*cos(THETA(4))*sin(THETA(5))*d6)
 JACDOT(3,4)=c23*(cos(THETA(1))*(THETADOT(2)+THETADOT(3))
&-sin(THETA(1))*THETADOT(1))*(sin(THETA(4))*
&sin(THETA(5))*d6+d4)
&-c23*(sin(THETA(1))*(THETADOT(2)+THETADOT(3))+cos(THETA(1))*
&THETADOT(1))*cos(THETA(4))*sin(THETA(5))*d6+app3(1)*(app3(3)*
&cos(THETA(4))*sin(THETA(5))*d6-app3(1)*cos(THETA(5))*d6)-
&app3(2)*(app3(2)*cos(THETA(5))*d6-app3(3)*(sin(THETA(4))*
&sin(THETA(5))*d6+d4))
 JACDOT(4,4)=cos(THETA(1))*c23*(THETADOT(2)+THETADOT(3))
&-sin(THETA(1))*c23*THETADOT(1)
 JACDOT(5,4)=sin(THETA(1))*c23*(THETADOT(2)+THETADOT(3))
&+cos(THETA(1))*c23*THETADOT(1)
 JACDOT(6,4)=-c23*(THETADOT(2)+THETADOT(3))
 JACDOT(1,5)=cos(THETA(5))*d6*(z4(2)*(-sin(THETA(1))*
&(THETADOT(2)+THETADOT(3))+cos(THETA(1))*c23*THETADOT(4))
&-z4(1)*(cos(THETA(1))*(THETADOT(2)+THETADOT(3))+sin(THETA(1))
&*c23*THETADOT(4)))+d6*(app4(2)*app4(2)*sin(THETA(5))
&-app4(1)*cos(THETA(5))
```

```
     &-app4(3)*app4(3)*sin(THETA(5)))
      JACDOT(2,5)=sin(THETA(5))*d6*(z4(2)*(-sin(THETA(1))*
     &(THETADOT(2)+THETADOT(3))+cos(THETA(1))*c23*THETADOT(4))
     &-z4(1)*(cos(THETA(1))*(THETADOT(2)+THETADOT(3))+sin(THETA(1))
     &*c23*THETADOT(4)))+d6*(app4(3)*app4(3)*cos(THETA(5))-app4(1)*
     &(app4(2)*sin(THETA(5))-app4(1)*cos(THETA(5))))
      JACDOT(3,5)=-cos(THETA(5))*d6*(z4(3)*(cos(THETA(1))*
     &(THETADOT(2)+THETADOT(3))+sin(THETA(1))*c23*THETADOT(4))
     &-z4(2)*(THETADOT(1)+c23*THETADOT(4)))-sin(THETA(5))*d6*
     &(z4(3)*(sin(THETA(1))*(THETADOT(2)+THETADOT(3))-
     &cos(THETA(1))*c23*THETADOT(4))+z4(1)*(-sin(THETA(1))*
     &(THETADOT(2)+THETADOT(3))+cos(THETA(1))*c23*THETADOT(4)))
     &+d6*(app4(3)*(app4(1)*sin(THETA(5))-app4(2)*cos(THETA(5))))
      JACDOT(4,5)=z4(3)*(cos(THETA(1))*(THETADOT(2)+THETADOT(3))
     &+sin(THETA(1))*c23*THETADOT(4))-z4(2)*(THETADOT(1)+
     &c23*THETADOT(4))
      JACDOT(5,5)=z4(3)*(sin(THETA(1))*(THETADOT(2)+THETADOT(3))
     &-cos(THETA(1))*c23*THETADOT(4))+z4(1)*(-sin(THETA(1))*
     &(THETADOT(2)+THETADOT(3))+cos(THETA(1))*c23*THETADOT(4))
      JACDOT(6,5)=z4(2)*(-sin(THETA(1))*(THETADOT(2)+THETADOT(3))
     &+cos(THETA(1))*c23*THETADOT(4))-z4(1)*(cos(THETA(1))*
     &(THETADOT(2)+THETADOT(3))+sin(THETA(1))*c23*THETADOT(4))
      JACDOT(1,6)=d6*(-z5(3)*(-sin(THETA(1))*(THETADOT(2)+
     &THETADOT(3))+cos(THETA(1))*c23*THETADOT(4)+z4(1)*THETADOT(5))
     &+z5(1)*(THETADOT(1)+c23*THETADOT(4)+z4(3)*THETADOT(5)))
     &+d6*app5(1)*app5(3)
      JACDOT(2,6)=-d6*(z5(3)*(cos(THETA(1))*(THETADOT(2)+
     &THETADOT(3))+sin(THETA(1))*c23*THETADOT(4)+z4(2)*THETADOT(5))
     &-z5(2)*(THETADOT(1)+c23*THETADOT(4)+z4(3)*THETADOT(5)))
     &+d6*app5(2)*app5(3)
      JACDOT(3,6)=-d6*(app5(1)*app5(1)+app5(2)*app5(2))
      JACDOT(4,6)=z5(3)*(cos(THETA(1))*(THETADOT(2)+THETADOT(3))
     &+sin(THETA(1))*c23*THETADOT(4)+z4(2)*THETADOT(5))-
     &z5(2)*(THETADOT(1)+c23*THETADOT(4)+z4(3)*THETADOT(5))
      JACDOT(5,6)=-z5(3)*(-sin(THETA(1))*(THETADOT(2)+THETADOT(3))
     &+cos(THETA(1))*c23*THETADOT(4)+z4(1)*THETADOT(5))
     &+z5(1)*(THETADOT(1)+c23*THETADOT(4)+z4(3)*THETADOT(5))
      JACDOT(6,6)=z5(2)*(-sin(THETA(1))*(THETADOT(2)+THETADOT(3))
     &+cos(THETA(1))*c23*THETADOT(4)+z4(1)*THETADOT(5))
     &-z5(1)*(cos(THETA(1))*(THETADOT(2)+THETADOT(3))
     &+sin(THETA(1))*c23*THETADOT(4)+z4(2)*THETADOT(5))
C     Initialise: set desired effector accelerations
      DO 60 i=1,n
      ACCEL(i)=VDOT(j,i)
60    CONTINUE
C
      NLACC(1)=ACCEL(1)-(JACDOT(1,1)*THETADOT(1)+JACDOT(1,2)*
     &THETADOT(2)+JACDOT(1,3)*THETADOT(3)+JACDOT(1,4)*THETADOT(4)
     &+JACDOT(1,5)*THETADOT(5)+JACDOT(1,6)*THETADOT(6))
      NLACC(2)=ACCEL(2)-(JACDOT(2,1)*THETADOT(1)+JACDOT(2,2)*
     &THETADOT(2)+JACDOT(2,3)*THETADOT(3)+JACDOT(2,4)*THETADOT(4)
     &+JACDOT(2,5)*THETADOT(5)+JACDOT(2,6)*THETADOT(6))
      NLACC(3)=ACCEL(3)-(JACDOT(3,1)*THETADOT(1)+JACDOT(3,2)*
     &THETADOT(2)+JACDOT(3,3)*THETADOT(3)+JACDOT(3,4)*THETADOT(4)
     &+JACDOT(3,5)*THETADOT(5)+JACDOT(3,6)*THETADOT(6))
      NLACC(4)=ACCEL(4)-(JACDOT(4,1)*THETADOT(1)+JACDOT(4,2)*
     &THETADOT(2)+JACDOT(4,3)*THETADOT(3)+JACDOT(4,4)*THETADOT(4)
     &+JACDOT(4,5)*THETADOT(5)+JACDOT(4,6)*THETADOT(6))
      NLACC(5)=ACCEL(5)-(JACDOT(5,1)*THETADOT(1)+JACDOT(5,2)*
     &THETADOT(2)+JACDOT(5,3)*THETADOT(3)+JACDOT(5,4)*THETADOT(4)
     &+JACDOT(5,5)*THETADOT(5)+JACDOT(5,6)*THETADOT(6))
      NLACC(6)=ACCEL(6)-(JACDOT(6,1)*THETADOT(1)+JACDOT(6,2)*
     &THETADOT(2)+JACDOT(6,3)*THETADOT(3)+JACDOT(6,4)*THETADOT(4)
     &+JACDOT(6,5)*THETADOT(5)+JACDOT(6,6)*THETADOT(6))
C
```

```
      THETADD(1)=JAC(1,1)*NLACC(1)+JAC(1,2)*NLACC(2)+JAC(1,3)*
     &NLACC(3)+JAC(1,4)*NLACC(4)+JAC(1,5)*NLACC(5)+JAC(1,6)*
     &NLACC(6)
      THETADD(2)=JAC(2,1)*NLACC(1)+JAC(2,2)*NLACC(2)+JAC(2,3)*
     &NLACC(3)+JAC(2,4)*NLACC(4)+JAC(2,5)*NLACC(5)+JAC(2,6)*
     &NLACC(6)
      THETADD(3)=JAC(3,1)*NLACC(1)+JAC(3,2)*NLACC(2)+JAC(3,3)*
     &NLACC(3)+JAC(3,4)*NLACC(4)+JAC(3,5)*NLACC(5)+JAC(3,6)*
     &NLACC(6)
      THETADD(4)=JAC(4,1)*NLACC(1)+JAC(4,2)*NLACC(2)+JAC(4,3)*
     &NLACC(3)+JAC(4,4)*NLACC(4)+JAC(4,5)*NLACC(5)+JAC(4,6)*
     &NLACC(6)
      THETADD(5)=JAC(5,1)*NLACC(1)+JAC(5,2)*NLACC(2)+JAC(5,3)*
     &NLACC(3)+JAC(5,4)*NLACC(4)+JAC(5,5)*NLACC(5)+JAC(5,6)*
     &NLACC(6)
      THETADD(6)=JAC(6,1)*NLACC(1)+JAC(6,2)*NLACC(2)+JAC(6,3)*
     &NLACC(3)+JAC(6,4)*NLACC(4)+JAC(6,5)*NLACC(5)+JAC(6,6)*
     &NLACC(6)
      DO 65 i=1,n
      JACCEL(i)=THETADD(i)*180.0/PI
65    CONTINUE
      WRITE(*,900)JACCEL(1),JACCEL(2),JACCEL(3),JACCEL(4),
     &JACCEL(5),JACCEL(6)
C
C     Computed torque control law
      Kp=1.0
      Kv=30.0
      DO 70, i=1,n
      THETADD(i)=THETADD(i)+Kp*(THETA(i)-THETA(i)*0.05*RAN(1.0)+
     &Kv*(THETADOT(i)-THETADOT(i)*0.05*RAN(1.0))
70    CONTINUE
C
C
C
C     The dynamics are calculated recursively using the Newton
C     Euler method to generate the required joint torques
C     Initialise
      zx(0)=0.0
      zy(0)=0.0
      zz(0)=1.0
      zx(1)=-sin(THETA(1))
      zy(1)=cos(THETA(1))
      zz(1)=0.0
      zx(2)=-sin(THETA(1))
      zy(2)=cos(THETA(1))
      zz(2)=0.0
      zx(3)=cos(THETA(1))*s23
      zy(3)=sin(THETA(1))*s23
      zz(3)=c23
      zx(4)=-(cos(THETA(1))*c23*sin(THETA(4))+sin(THETA(1))*
     &cos(THETA(4)))
      zy(4)=cos(THETA(1))*cos(THETA(4))-sin(THETA(1))*c23*
     &sin(THETA(4))
      zz(4)=s23*sin(THETA(4))
      zx(5)=ax(j)
      zy(5)=ay(j)
      zz(5)=az(j)
      xx(1)=cos(THETA(1))
      xy(1)=sin(THETA(1))
      xz(1)=0.0
      yx(1)=0.0
      yy(1)=0.0
      yz(1)=-1.0
      xx(2)=cos(THETA(1))*cos(THETA(2))
      xy(2)=sin(THETA(1))*cos(THETA(2))
```

```
 xz(2)=-sin(THETA(2))
 yx(2)=-cos(THETA(1))*sin(THETA(2))
 yy(2)=-sin(THETA(1))*sin(THETA(2))
 yz(2)=-cos(THETA(2))
 xx(3)=cos(THETA(1))*c23
 xy(3)=sin(THETA(1))*s23
 xz(3)=-s23
 yx(3)=-sin(THETA(1))
 yy(3)=cos(THETA(1))
 yz(3)=0.0
 xx(4)=cos(THETA(1))*c23*cos(THETA(4))
&-sin(THETA(1))*sin(THETA(4))
 xy(4)=sin(THETA(1))*c23*cos(THETA(4))
&+cos(THETA(1))*sin(THETA(4))
 xz(4)=-s23*cos(THETA(4))
 yx(4)=-cos(THETA(1))*s23
 yy(4)=-sin(THETA(1))*s23
 yz(4)=-c23
 xx(5)=cos(THETA(5))*(cos(THETA(1))*c23*cos(THETA(4))
&-sin(THETA(1))*sin(THETA(4)))-cos(THETA(1))*s23*sin(THETA(5))
 xy(5)=cos(THETA(5))*(sin(THETA(1))*c23*cos(THETA(4))
&+cos(THETA(1))*sin(THETA(4)))-sin(THETA(1))*s23*sin(THETA(5))
 xz(5)=-s23*cos(THETA(4))*cos(THETA(5))-c23*sin(THETA(5))
 yx(5)=-cos(THETA(1))*c23*sin(THETA(4))-
&sin(THETA(1))*cos(THETA(4))
 yy(5)=-sin(THETA(1))*c23*sin(THETA(4))+
&cos(THETA(1))*cos(THETA(4))
 yz(5)=s23*sin(THETA(4))
 xx(6)=nx(j)
 xy(6)=ny(j)
 xz(6)=nz(j)
 yx(6)=sx(j)
 yy(6)=sy(j)
 yz(6)=sz(j)
 zx(6)=ax(j)
 zy(6)=ay(j)
 zz(6)=az(j)
 wx(0)=0.0
 wy(0)=0.0
 wz(0)=0.0
 wxdot(0)=0.0
 wydot(0)=0.0
 wzdot(0)=0.0
 lx(1)=0.0
 ly(1)=0.0
 lz(1)=0.0
 lsx(1)=0.0
 lsy(1)=0.0
 lsz(1)=0.0
 dynamics link variables are purely kinematic
 lx(2)=alph2*cos(THETA(1))*cos(THETA(2))-sin(THETA(1))*del2
 ly(2)=alph2*sin(THETA(1))*cos(THETA(2))+cos(THETA(1))*del2
 lz(2)=-alph2*sin(THETA(2))
 lsx(2)=-0.5*(alph2*cos(THETA(1))*cos(THETA(2))
&-sin(THETA(1))*d2)
 lsy(2)=-0.5*(alph2*sin(THETA(1))*cos(THETA(2))
&+cos(THETA(1))*del2)
 lsz(2)=-0.5*(-alph2*sin(THETA(2)))
 lx(3)=0.0
 ly(3)=0.0
 lz(3)=0.0
 lsx(3)=0.0
 lsy(3)=0.0
 lsz(3)=0.0
 lx(4)=del4*cos(THETA(1))*s23
```

```
      ly(4)=del4*sin(THETA(1))*s23
      lz(4)=del4*c23
      lsx(4)=-0.5*(del4*cos(THETA(1))*s23)
      lsy(4)=-0.5*(del4*sin(THETA(1))*s23)
      lsz(4)=-0.5*(del4*c23)
      lx(5)=0.0
      ly(5)=0.0
      lz(5)=0.0
      lsx(5)=0.0
      lsy(5)=0.0
      lsz(5)=0.0
      lx(6)=del6*ax(j)
      ly(6)=del6*ay(j)
      lz(6)=del6*az(j)
      lsx(6)=-0.5*del6*ax(j)
      lsy(6)=-0.5*del6*ay(j)
      lsz(6)=-0.5*del6*az(j)
      vxdot(0)=0.0
      vydot(0)=0.0
      vzdot(0)=0.0
      vcxdot(0)=0.0
      vcydot(0)=0.0
      vczdot(0)=0.0
      mas(1)=0.0
      mas(2)=8.0+6.0
      mas(3)=0.0
      mas(4)=6.0
      mas(5)=0.0
      mas(6)=12.0+8.0
      l(1)=0.0
      l(2)=del2+alph2
      l(3)=0.0
      l(4)=del4
      l(5)=0.0
      l(6)=del2
      fx(n+1)=0.0
      fy(n+1)=0.0
      fz(n+1)=0.0
      mx(n+1)=0.0
      my(n+1)=0.0
      mz(n+1)=0.0
C     forward recursion
      DO 101 i=1,n
      wx(i)=wx(i-1)+zx(i-1)*THETADOT(i)
      wy(i)=wy(i-1)+zy(i-1)*THETADOT(i)
      wz(i)=wz(i-1)+zz(i-1)*THETADOT(i)
      wxdot(i)=wxdot(i-1)+zx(i-1)*THETADD(i)+
     &(wy(i-1)*zz(i-1)-wz(i-1)*zy(i-1))*THETADOT(i)
      wydot(i)=wydot(i-1)+zy(i-1)*THETADD(i)+
     &(wz(i-1)*zx(i-1)-wx(i-1)*zz(i-1))*THETADOT(i)
      wzdot(i)=wzdot(i-1)+zz(i-1)*THETADD(i)+
     &(wx(i-1)*zy(i-1)-wy(i-1)*zx(i-1))*THETADOT(i)
      vxdot(i)=vxdot(i-1)+(wydot(i)*lz(i)-wzdot(i)*ly(i))+
     &(wy(i)*(wx(i)*ly(i)-wy(i)*lx(i))-wz(i)*(wz(i)*lx(i)
     &-wx(i)*lz(i)))
      vydot(i)=vydot(i-1)+(wzdot(i)*lx(i)-wxdot(i)*lz(i))+
     &(wz(i)*(wy(i)*lz(i)-wz(i)*ly(i))-wx(i)*(wx(i)*ly(i)
     &-wy(i)*lx(i)))
      vzdot(i)=vzdot(i-1)+(wxdot(i)*ly(i)-wydot(i)*lx(i))+
     &(wx(i)*(wz(i)*lx(i)-wx(i)*lz(i))-wy(i)*(wy(i)*lz(i)
     &-wz(i)*ly(i)))
      vcxdot(i)=vxdot(i)+(wydot(i)*lsz(i)-wzdot(i)*lsy(i))+
     &(wy(i)*(wx(i)*lsy(i)-wy(i)*lsx(i))-wz(i)*(wz(i)*lsx(i)
     &-wx(i)*lsz(i)))
      vcydot(i)=vydot(i)+(wzdot(i)*lsx(i)-wxdot(i)*lsz(i))+
```

```
     &(wz(i)*(wy(i)*lsz(i)-wz(i)*lsy(i))-wx(i)*(wx(i)*lsy(i)
     &-wy(i)*lsx(i)))
      vczdot(i)=vzdot(i)+(wxdot(i)*lsy(i)-wydot(i)*lsx(i))+
     &(wx(i)*(wz(i)*lsx(i)-wx(i)*lsz(i))-wy(i)*(wy(i)*lsz(i)
     &-wz(i)*lsy(i)))
      Force and moment calculation
      fcx(i)=mas(i)*vcxdot(i)
      fcy(i)=mas(i)*vcydot(i)
      fcz(i)=mas(i)*vczdot(i)
      Icx(i)=0.5*mas(i)*RADIUS**2
      Icy(i)=0.5*mas(i)*RADIUS**2
      Icz(i)=0.66666*mas(i)*l(i)**2
      Ic0xx(i)=Icx(i)*xx(i)**2+Icy(i)*yx(i)**2+Icz(i)*zx(i)**2
      Ic0yy(i)=Icx(i)*xy(i)**2+Icy(i)*yy(i)**2+Icz(i)*zy(i)**2
      Ic0zz(i)=Icx(i)*xz(i)**2+Icy(i)*yz(i)**2+Icz(i)*zz(i)**2
      Ic0yx(i)=Icx(i)*xx(i)*xy(i)+Icy(i)*yx(i)*yy(i)+
     &Icz(i)*zx(i)*zy(i)
      Ic0xy(i)=Ic0yx(i)
      Ic0zx(i)=Icx(i)*xx(i)*xz(i)+Icy(i)*yx(i)*yz(i)
     &+Icz(i)*zx(i)*zz(i)
      Ic0xz(i)=Ic0zx(i)
      Ic0zy(i)=Icx(i)*xy(i)*xz(i)+Icy(i)*yy(i)*yz(i)
     &+Icz(i)*zy(i)*zz(i)
      Ic0yz(i)=Ic0zy(i)
      Ncx(i)=Ic0xx(i)*wxdot(i)+Ic0xy(i)*wydot(i)+
     &Ic0xz(i)*wzdot(i)-wz(i)*(Ic0yx(i)*wx(i)+Ic0yy(i)*wy(i)
     &+Ic0yz(i)*wz(i))+wy(i)*(Ic0zx(i)*wx(i)+Ic0zy(i)*wy(i)+
     &Ic0zz(i)*wz(i))
      Ncy(i)=Ic0yx(i)*wxdot(i)+Ic0yy(i)*wydot(i)+
     &Ic0yz(i)*wzdot(i)+wz(i)*(Ic0xx(i)*wx(i)+Ic0xy(i)*wy(i)
     &+Ic0xz(i)*wz(i))-wx(i)*(Ic0zx(i)*wx(i)+Ic0zy(i)*wy(i)+
     &Ic0zz(i)*wz(i))
      Ncz(i)=Ic0zx(i)*wxdot(i)+Ic0zy(i)*wydot(i)+
     &Ic0zz(i)*wzdot(i)-wy(i)*(Ic0xx(i)*wx(i)+Ic0xy(i)*wy(i)
     &+Ic0xz(i)*wz(i))+wx(i)*(Ic0yx(i)*wx(i)+Ic0yy(i)*wy(i)+
     &Ic0yz(i)*wz(i))
.01   CONTINUE
      model collision dynamics
       kf=0.4
       ktau=0.4
       fextx=100.0
       fexty=100.0
       fextz=100.0
       nextx=100.0
       nexty=100.0
       nextz=100.0
       mu=1.0
       ti=0.0167
       vxobj=0.01
       vyobj=-0.1
       vzobj=0.01
       wxobj=0.01
       wyobj=0.01
       wzobj=0.1
       Icx(7)=0.01*(mass(7)**(5.0/2.0))
       Icy(7)=0.01*(mass(7)**(5.0/2.0))
       Icz(7)=Icx(7)/2.0
       taufd(1)=JACT(1,1)*fextx+JACT(1,2)*fexty+JACT(1,3)*fextz+
      &JACT(1,4)*nextx+JACT(1,5)*nexty+JACT(1,6)*nextz
       taufd(2)=JACT(2,1)*fextx+JACT(2,2)*fexty+JACT(2,3)*fextz+
      &JACT(2,4)*nextx+JACT(2,5)*nexty+JACT(2,6)*nextz
       taufd(3)=JACT(3,1)*fextx+JACT(3,2)*fexty+JACT(3,3)*fextz+
      &JACT(3,4)*nextx+JACT(3,5)*nexty+JACT(3,6)*nextz
       taufd(4)=JACT(4,1)*fextx+JACT(4,2)*fexty+JACT(4,3)*fextz+
      &JACT(4,4)*nextx+JACT(4,5)*nexty+JACT(4,6)*nextz
```

```
C       tauf(5)=JACT(5,1)*fextx+JACT(5,2)*fexty+JACT(5,3)*fextz+
C      &JACT(5,4)*nextx+JACT(5,5)*nexty+JACT(5,6)*nextz
C       taufd(6)=JACT(6,1)*fextx+JACT(6,2)*fexty+JACT(6,3)*fextz+
C      &JACT(6,4)*nextx+JACT(6,5)*nexty+JACT(6,6)*nextz
C       IF (j.EQ.0) THEN
C       fsensx(0)=mass(7)*vxobj/ti
C       fsensy(0)=mass(7)*vyobj/ti
C       fsensz(0)=mass(7)*vzobj/ti
C       nsensx(0)=Icx(7)*wxobj/ti
C       nsensy(0)=Icy(7)*wyobj/ti
C       nsensz(0)=Icz(7)*wzobj/ti
C       ELSE
C       fsensx(j)=fextx+kf*(fextx-fsensx(j-1))
C       fsensy(j)=fexty+kf*(fexty-fsensy(j-1))
C       fsensz(j)=fextz+kf*(fextz-fsensz(j-1))
C       nsensx(j)=nextx+ktau*(nextx-nsensx(j-1))
C       nsensy(j)=nexty+ktau*(nexty-nsensy(j-1))
C       nsensz(j)=nextz+ktau*(nextz-nsensz(j-1))
C       ENDIF
C       tauf(1)=mu*taufd(1)+kf*((JACT(1,1)*(fextx-fsensx(j)))+
C      &(JACT(1,2)*(fexty-fsensy(j)))+
C      &(JACT(1,3)*(fextz-fsensz(j)))+
C      &(JACT(1,4)*(nextx-nsensx(j)))+
C      &(JACT(1,5)*(nexty-nsensy(j)))+
C      &(JACT(1,6)*(nextz-nsensz(j))))
C       tauf(2)=mu*taufd(2)+kf*((JACT(2,1)*(fextx-fsensx(j)))+
C      &(JACT(2,2)*(fexty-fsensy(j)))+
C      &(JACT(2,3)*(fextz-fsensz(j)))+
C      &(JACT(2,4)*(nextx-nsensx(j)))+
C      &(JACT(2,5)*(nexty-nsensy(j)))+
C      &(JACT(2,6)*(nextz-nsensz(j))))
C       tauf(3)=mu*taufd(3)+kf*((JACT(3,1)*(fextx-fsensx(j)))+
C      &(JACT(3,2)*(fexty-fsensy(j)))+
C      &(JACT(3,3)*(fextz-fsensz(j)))+
C      &(JACT(3,4)*(nextx-nsensx(j)))+
C      &(JACT(3,5)*(nexty-nsensy(j)))+
C      &(JACT(3,6)*(nextz-nsensz(j))))
C       tauf(4)=mu*taufd(4)+ktau*((JACT(4,1)*(fextx-fsensx(j)))+
C      &(JACT(4,2)*(fexty-fsensy(j)))+
C      &(JACT(4,3)*(fextz-fsensz(j)))+
C      &(JACT(4,4)*(nextx-nsensx(j)))+
C      &(JACT(4,5)*(nexty-nsensy(j)))+
C      &(JACT(4,6)*(nextz-nsensz(j))))
C       tauf(5)=mu*taufd(5)+ktau*((JACT(5,1)*(fextx-fsensx(j)))+
C      &(JACT(5,2)*(fexty-fsensy(j)))+
C      &(JACT(5,3)*(fextz-fsensz(j)))+
C      &(JACT(5,4)*(nextx-nsensx(j)))+
C      &(JACT(5,5)*(nexty-nsensy(j)))+
C      &(JACT(5,6)*(nextz-nsensz(j))))
C       tauf(6)=mu*taufd(6)+ktau*((JACT(6,1)*(fextx-fsensx(j)))+
C      &(JACT(6,2)*(fexty-fsensy(j)))+
C      &(JACT(6,3)*(fextz-fsensz(j)))+
C      &(JACT(6,4)*(nextx-nsensx(j)))+
C      &(JACT(6,5)*(nexty-nsensy(j)))+
C      &(JACT(6,6)*(nextz-nsensz(j))))
C      +KfiJT(fext(d)-fext)/ti
C       fcx(7)=(ay(j)*epz(j)-az(j)*epy(j))*nsensx(j)
C       fcy(7)=(az(j)*epx(j)-ax(j)*epz(j))*nsensy(j)
C       fcz(7)=(ax(j)*epy(j)-ay(j)*epx(j))*nsensz(j)
C       ncx(7)=ax(j)*fsensx(j)
C       ncy(7)=ay(j)*fsensy(j)
C       ncz(7)=az(j)*fsensz(j)
C       wx(7)=wx(6)
C       wy(7)=wy(6)
C       wz(7)=wz(6)
```

```
C       wxdot(7)=wxdot(6)
C       wydot(7)=wydot(6)
C       wzdot(7)=wzdot(6)
C       Ic0xx(7)=Icx(7)*xx(6)**2+Icy(7)*yx(6)**2+Icz(7)*zx(6)**2
C       Ic0yy(7)=Icx(7)*xy(6)**2+Icy(7)*yy(6)**2+Icz(7)*zy(6)**2
C       Ic0zz(7)=Icx(7)*xz(6)**2+Icy(7)*yz(6)**2+Icz(7)*zz(6)**2
C       Ic0yx(7)=Icx(7)*xx(6)*xy(6)+Icy(7)*yx(6)*yy(6)+
C      &Icz(7)*zx(6)*zy(6)
C       Ic0xy(7)=Ic0yx(7)
C       Ic0zx(7)=Icx(7)*xx(6)*xz(6)+Icy(7)*yx(6)*yz(6)
C      &+Icz(7)*zx(6)*zz(6)
C       Ic0xz(7)=Ic0zx(7)
C       Ic0zy(7)=Icx(7)*xy(6)*xz(6)+Icy(7)*yy(6)*yz(6)
C      &+Icz(7)*zy(6)*zz(6)
C       Ic0yz(7)=Ic0zy(7)
C       fcx(7)=mass(7)*vcxdot(7)
C       fcy(7)=mass(7)*vcydot(7)
C       fcz(7)=mass(7)*vczdot(7)
C       Ncx(7)=Ic0xx(7)*wxdot(7)+Ic0xy(7)*wydot(7)+
C      &Ic0xz(7)*wzdot(7)-wz(7)*(Ic0yx(7)*wx(7)+Ic0yy(7)*wy(7)
C      &+Ic0yz(7)*wz(7))+wy(7)*(Ic0zx(7)*wx(7)+Ic0zy(7)*wy(7)+
C      &Ic0zz(7)*wz(7))
C       Ncy(7)=Ic0yx(7)*wxdot(7)+Ic0yy(7)*wydot(7)+
C      &Ic0yz(7)*wzdot(7)+wz(7)*(Ic0xx(7)*wx(7)+Ic0xy(7)*wy(7)
C      &+Ic0xz(7)*wz(7))-wx(7)*(Ic0zx(7)*wx(7)+Ic0zy(7)*wy(7)+
C      &Ic0zz(7)*wz(7))
C       Ncz(7)=Ic0zx(7)*wxdot(7)+Ic0zy(7)*wydot(7)+
C      &Ic0zz(7)*wzdot(7)-wy(7)*(Ic0xx(7)*wx(7)+Ic0xy(7)*wy(7)
C      &+Ic0xz(7)*wz(7))+wx(7)*(Ic0yx(7)*wx(7)+Ic0yy(7)*wy(7)+
C      &Ic0yz(7)*wz(7))
       fcx(7)=0.0
       fcy(7)=0.0
       fcz(7)=0.0
       ncx(7)=0.0
       ncy(7)=0.0
       ncz(7)=0.0
       ftx=fcx(1)+fcx(2)+fcx(3)+fcx(4)+fcx(5)+fcx(6)+fcx(7)
       fty=fcy(1)+fcy(2)+fcy(3)+fcy(4)+fcy(5)+fcz(6)+fcy(7)
       ftz=fcz(1)+fcz(2)+fcz(3)+fcz(4)+fcz(5)+fcz(6)+fcz(7)
       mtx=ncx(1)+ncx(2)+ncx(3)+ncx(4)+ncx(5)+ncx(6)+ncx(7)
       mty=ncy(1)+ncy(2)+ncy(3)+ncy(4)+ncy(5)+ncy(6)+ncy(7)
       mtz=ncz(1)+ncz(2)+ncz(3)+ncz(4)+ncz(5)+ncz(6)+ncz(7)
       rcox=pcmx-(1-(mass(0)/mt))*sox-(-sin(THETA(1))*dx2+
      &cos(THETA(1))+(cos(THETA(2))*ax2*s23*dx4)+ax(j)*dx6)
      &-(mass(7)/mt)*x7
       rcoy=pcmy-(1-(mass(0)/mt))*soy-(cos(THETA(1))*dx2+
      &sin(THETA(1))*(cos(THETA(2))*ax2+s23*dx4)+ay(j)*dx6)
      &-(mass(7)/mt)*y7
       rcoz=pcmz-(1-(mass(0)/mt))*soz-(-sin(THETA(2))*ax2+
      &c23*d4+az(j)*dx6)-(mass(7)/mt)*z7
       nrx=mtx+((pcmy-rcoy-soy)*ftz-(pcmz-rcoz-soz)*fty)
       nry=mty+((pcmz-rcoz-soz)*ftx-(pcmx-rcox-sox)*ftz)
       nrz=mtz+((pcmx-rcox-sox)*fty-(pcmy-rcoy-soy)*ftx)
C      REACTION WHEEL COMPENSATION-applied moment defines
C      wheel torque
C      Iwax=0.1
C      wheelwx=-nrx/Iwax
C      wheelwy=-nry/Iwax
C      wheelwz=-nrz/Iwax
C      Backward recursion
       DO 125, i=n,1,-1
       fx(i)=fcx(i)+fx(i+1)
       fy(i)=fcy(i)+fy(i+1)
       fz(i)=fcz(i)+fz(i+1)
       mx(i)=ncx(i)+mx(i+1)+fz(i+1)*ly(i)-fy(i+1)*lz(i)+
```

```
     &fcz(i)*(ly(i)+lsy(i))-fcy(i)*(lz(i)+lsz(i))
      my(i)=ncy(i)+my(i+1)+fx(i+1)*lz(i)-fz(i+1)*lx(i)+
     &fcx(i)*(lz(i)+lsz(i))-fcz(i)*(lx(i)+lsx(i))
      mz(i)=ncz(i)+mz(i+1)+fy(i+1)*lx(i)-fx(i+1)*ly(i)+
     &fcy(i)*(lx(i)+lsx(i))-fcx(i)*(ly(i)+lsy(i))
      tau(i)=mx(i)*zx(i-1)+my(i)*zy(i-1)+mz(i)*zz(i-1)
125   CONTINUE
C
      WRITE(*,900)tau(1),tau(2),tau(3),tau(4),tau(5),tau(6)
C      WRITE(*,900)tauf(1),tauf(2),tauf(3),tauf(4),tauf(5),
C     &tauf(6)
      WRITE(*,*)nrx,nry,nrz
300   CONTINUE
C                                                                      *
900   FORMAT (f10.4,f10.4,f10.4,f10.4,f10.4,f10.4)
      CLOSE(6)
      STOP
      END PROGRAM Robospace2
       SUBROUTINE GAUSSJ(A,N,NP,B,M,MP)
C      Linear equation solution Ax=B by the Gauss-Jordan elimination.
C      A is the input matrix of NxN elements stored in an array of physical
C      dimensions NP by NP. B is an input matrix of MxM containing M right
C      hand side vectors stored in an array of physical dimensions NP by
C      MP.On output A is replaced by its matrix inverse and B is replaced by
C      the corresponding set of solution vectors.
       PARAMETER (NMAX=50)
       DIMENSION A(NP,NP),B(NP,MP),IPIV(NMAX),INDXR(NMAX),INDXC(NMAX)
       DO 11 J=1,N
         IPIV(J)=0
11     CONTINUE
       DO 22 I=1,N
       BIG=0.0
       DO 13 J=1,N
         IF (IPIV(J).NE.1) THEN
         DO 12 K=1,N
           IF (IPIV(K).EQ.0) THEN
             IF (ABS(A(J,K)).GE.BIG) THEN
             BIG=ABS(A(J,K))
             IROW=J
             ICOL=K
           ENDIF
         ELSE IF (IPIV(K).GT.1) THEN
         PAUSE 'singular matrix'
         ENDIF
12       CONTINUE
       ENDIF
13     CONTINUE
       IPIV(COL)=IPIV(ICOL)+1
       IF (IROW.NE.ICOL) THEN
         DO 14 L=1,N
         DUM=A(IROW,L)
         A(IROW,L)=A(ICOL,L)
14     CONTINUE
         DO 15 L=1,M
         DUM=B(IROW,L)
         B(IROW,L)=B(ICOL,L)
         B(ICOL,L)=DUM
15     CONTINUE
       ENDIF
       INDXR(I)=IROW
       INDXC(I)=ICOL
       IF (A(ICOL,ICOL).EQ.0.0) PAUSE 'singular matrix'
       PIVINV=1.0/A(ICOL,ICOL)
       A(ICOL,ICOL)=1.0
       DO 16 L=1,N
```

```
        A(ICOL,L)=A(ICOL,L)*PIVINV
5       CONTINUE
        DO 17 L=1,M
         B(ICOL,L)=B(ICOL,L)*PIVINV
7       CONTINUE
        DO 21 LL=1,N
          IF (LL.NE.ICOL) THEN
             DUM=A(LL,ICOL)
             A(LL,ICOL)=0.0
             DO 18 L=1,N
               A(LL,L)=A(LL,L)-A(ICOL,L)*DUM
8            CONTINUE
             DO 19 L=1,M
               B(LL,L)=B(LL,L)*DUM
9            CONTINUE
           ENDIF
1       CONTINUE
2       CONTINUE
        DO 24 L=N,1,-1
        IF (INDXR(L).NE.INDXC(L)) THEN
        DO 23 K=1,N
        DUM=A(K,INDXR(L))
        A(K,INDXR(L))=A(K,INDXC(L))
        A(K,INDXC(L))=DUM
3       CONTINUE
        ENDIF
4       CONTINUE
        RETURN
        END
```

ACKNOWLEDGEMENTS

This work was supported by the UK Science & Engineering Research Council with a PhD research grant. The author would like to thank his supervisors Tom Bowling and John Lewis of the College of Aeronautics at Cranfield University (formerly Institute of Technology) for their support and guidance.

REFERENCES

Adams R et al (1987) "Remote repair demonstration of Solar Maximum main electronics box" *Proc 1st European In-Orbit Operations Technology Symp* (ESA SP-272), 227-323

Agrawal B (1980) *Design of Geosynchronous Spacecraft*, Prentice-Hall

AIAA (1991) "AIAA guidelines for serviceable spacecraft grasping/berthing/docking interfaces" *ANSI/AIAA R-XXX-1991*

Alberts T & Soloway D (1988) "Force control of a multi arm robot system" *Proc IEEE Int Conf Rob & Autom*, 1490-1496

Albus J, Lumia R & McCain (1988) "Hierarchical control of intelligent machines applied to space station telerobots" *IEEE Trans Aero & Elect Syst* **24**(5), 535-541

Albus J, McCain H & Lumia R (1987) "NASA/NBS Standard Reference Model for Telerobotic Control Systems Architecture" *NASA TN-1235*

Albus J & Lumia R (1988) "Teleoperation & autonomy for space robots" *Robotics & Auton Syst* **4**, 27-33

Albus J (1984) "Robotics" in *NATO ASI F11 Robotics & Artificial Intelligence*, 65-93

Albus J (1990) "Robotics: where has it been and where is it going?" *Rob & Auton Syst* **6**,198-219

Aldridge E (1993) "International space cooperation: learning from the past; planning for the future" *Rep AIAA Wshop preprint* (Mar)

Andre G, Berger G & Elfving A (1990) "BIAS: a bi-arm servicer" *ESA Rep N7406/87/NL/MAC*

Asade H, Kanade T & Takeyama I (1983) "Control of a direct drive arm" *Trans ASME J DSMC* **105** (Sept), 136-142

Backes P & Tso K (1990) "Autonomous single arm ORU changeout - strategies, control issues and implementation" *Robot & Auton Syst* **6**, 221-241

Baillieul J (1985) "Kinematic programming alternatives for redundant manipulators" *Proc IEEE Int Conf Rob & Autom*, 722-728

Bayard D & Wen J (1987) "Simple robust control laws for robot mabnipulators: Pt II - adaptive case" *Proc Wshop on Space Telerobotics* **III**,231-243

Bejczy A & Tarn T (1986) "Robot control as a systems control problem" *IFAC Theory of Robots*, Venice, 1-3

Bejczy A (1979) "Advanced teleoperators" *Astro & Aero* (May), 20-26

Bejczy A (1980) "Sensors, controls, and man-machine interface for advanced teleoperation" *Sci* **208**, 1327-1335

BNSC (1992) "Outer Space Act 1986 and the role of the British National Space Centre" preprint

Boudreault R (1988) "Design & economics of freeflying platforms for space manufacturing" *Acta Astron* **17**(4), 415-420

Bowring Space Projects Ltd, C T (1993) "Guide to satellite insurance market and its current status" preprint

Brady M (1985) "Artificial intelligence & robotics" *Artif Intell* **26**,79-121

Bronez M, Clarke M & Quinon A (1986) "Requirements for development for a freeflying robot - ROBIN" *IEEE Int Conf Rob & Autom,* 667-672
Brooks R (1983) "Solving Findpath problems by good representation of freespace" *IEEE Trans Syst, Man & Cyber* **13**(3),190-197
Brooks T (1992) "Operator aids for telerobotic assembly and sensing in space" *Proc IEEE Int Conf Rob & Autom*, 886-891
Brown E (1994) "Space policy roundup" *Earth-Space Rev* **3** (4), 5-7
Bruhm H (1987) "Remote manipulation in orbital construction, servicing and repair missions: is one arm enough?" *Proc 1st European In-Orbit Operations Technology Symp* (ESA SP-272), 217-225
Burrow J (1961) "Momentum wheel dumping using magnetic torquers" *ARS J* (Dec), 1776-1778
Caldwell D et al (1994) "Telepresence: visual, audio and tactile feedback and control of a twin armed mobile robot" *Proc IEEE Int Conf Rob & Autom,* 244-249
Camponella (1986) "Existing satellite systems and networks" *AIAA 86-1204*
Carignan C & Akin D (1988) "Cooperative control of two arms in transport of material load in zero gravity" *IEEE J Rob & Autom* **4**(4),414-419
Chambers A & Nagel D (1985) "Pilots of the future: human or computer?" *Comm Assoc Comp Mach* **28**(11), 1187-1199
Chand S & Doty K (1985) "Online polynomial trajectories for robot manipulators" *Int J Rob Res* **4** (2),38-48
Chande E & Newcomb R (1985) " Decision tree for inflight data processing for robot spacecraft trajectory guidance" *Proc IEEE Int Conf Rob & Autom,*414-419
Clarke M (1985) "Recent advances in teleoperation: implications for the Space Station" *Proc Space Tech Conf,* Anaheim, 4.1-4.10
Claudinon B et al (1985) "Control techniques for rendezvous" *IFAC Autom Cont in Space,* Toulouse, 287-294
Cohen A & Erickson J (1985) "Future uses of machine intelligence and robotics for the Space Station & its implications for the US economy" *IEEE Trans Robot & Autom* **1**(3), 117-123
Cohendet P (1992) "Economic effects of space programs" *ISU Business & Management Lecture Notes*
Collette R & Herdan B (1977) "Design problems of spacecraft for communication missions" *Proc IEEE* **65**(3), 342-356
Colluci F (1990) "Freedom under review" *Space* **6**(6), 28-33
Cornelisse J et al (1979) "Rocket propulsion & spacecraft dynamics" *Pitman Pub Co,* London
Crowther R (1994) "Trackable debris population" *J Brit Interplan Soc* **47**, 128-133
Davis R (1987) "In-orbit and laboratory exchange of ORU's designed/not designed for servicing" *Proc 1st European In-Orbit Operations Technology Symp* (ESA SP-272), 123-126
de Peuter W (1994) "Magnetic gearing for robotics" *Preparing for the Future (ESA)* **4** (3), 1-3
de Peuter W et al (1993) "Satellite servicing in GEO by robotic service vehicle" *ESA Bull* **78**, 33-39
de Silva C (1991) "Trajectory design for robotic manipulation in space" *J Guid & Cont* **14** (3), 670-674
Delpech M & Marrette M (1985) "Feasibility of time delay computation for a space teleoperative task " *IFAC Autom Cont in Space,* Toulouse, 279-286

Denavit J & Hartenberg R (1955) "Kinematics notation for lower pair mechanisms based on matrices" *Trans ASME J Appl Mech* 77,215-221
Deptovich T & Stoughton C (1989) "General approach for manipulator system specification, design and validation" *Proc IEEE Int Conf Rob & Autom*, 1402-1407
Dougherty H et al (1971) "Attitude stabilisation of synchronous communications satellites employing narrow beam antennas" *J Space & Rock* **8**, 834-842
Dubowsky S, Vance E & Torres M (1989) "Control of space manipulators subject to spacecraft attitude control saturation limits" *Proc NASA Wshop on Space Telerobotics IV*,409-418
Dubowsky S & DesForges D (1979) "Application of model reference adaptive control to robotic manipulators" *Trans ASME J DSMC* **101** (Sept), 193-200
Elfving A (1990) "Bi-arm servicer: systems description handbook" *ESA Rep MATRA/DAS/VEL/279/89*
Elfving A (1990) "Bi-arm servicer: final report (executive summary)" *ESA Rep MATRA/DAS/VEL/285/89*
Elliott C (1992) "Space agencies & their programmes" *Smith System Eng Rep PM-92/1041/1.0*
Erickson J (1987) "Manned spacecraft automation & robotics" *Proc IEEE* **75**(3),417-426
ESA (1986) "Teleoperation control study: a final report" *ESA CR(P) 2413*
ESA (1993) "Technology from space: successful technology transfers from European space research" *ESA Cat No 1*
Fallin E (1975) "Optimal intersatellite transfers for in-orbit servicing missions" *J Space* **12** (9), 565-568
Featherstone R (1983) "Position and velocity transformations between robot end effector coordinates and joints" *Int J Rob Res* **2** (2), 35-45
Foxell C (1994) "Pendulum of industry" *Physics World* (June), 32-36
Freitas A & Gilbreath W (1980) "Advanced automation for space missions" *NASA CP-2255*
French R & Boyce B (1985) "Satellite servicing by teleoperators" *Trans ASME J Bas Eng Ind* **107** (Feb), 49-54
Fu K, Gonzalez R & Lee C (1987) "Robotics: control, sensing, vision & intelligence" MacGraw-Hill Book Co, Singapore
Garg D (1989) "Multiarm coordination and control " *ASME DSC* **15**, 27-35
Garner T & Ross A (1991) "Satellite control throughout complete lifecycle" *ESA Bull* **72**, 107-109
Gary (1987) "Spacecraft attitude real time determination system based on multiprocessor distributed architecture" *IFAC 10th Triennial World Cong* (Mar), 37-47
Geshke C (1983) "System for programming and controlling sensor-based robot manipulators" *IEEE Trans Patt Anal & Mach Intell* **5**(1),1-7
Gibson R (1989) "European community: crossroads in space" *Commision of European Communities EUR 14010*
Graham J (1989) "Special computer architectures for robotics: tutorial and survey" *IEEE Trans Rob & Autom* **5**(5),543-554
Greenberg J (1992) "Financial investment analysis" in *Space Economics* (ed. Greenberg J & Hurtzfeld H), Prog in Astron **144** (AIAA)
Grossman D et al (1985) "Value of independent robot arms" *Rob & CIM* **2** (2), 135-141

Gupta A & Roth B (1982) "Design considerations for manipulator workspace" *Trans ASME J Mech Des* **104** (Oct), 704-711
Hamman R (1985) "Design techniques for robots (space application)" *Rob & Auton Syst* **1**, 223-250
Hanson J et al (1983) "Generation and evaluation of workspaces of manipulators"*Int J Rob Res* **2** (3), 22-31
Harmon L (1982) "Automated tactile sensing" *Int J Robot Res* **1**(2),3-33
Hayati S (1986) "Hybrid position/force control of multiarm cooperating robots" *Proc IEEE Int Conf Rob & Autom*,82-89
Hayati S (1988) "Position & force control of coordinated multiple arms" *IEEE Trans Aero & Elect Syst* **24** (5), 584-590
Hedley D (1986) "Design characteristics of the Shuttle Remote Manipulator Arm" *Trans Soc Automotive Engines* **7**, 1249-1254
Heer E (1978) "New lustre for space robots and automation" *Astro & Aero* (Sept), 48-50
Heimel H & Schulz H (1985) "Large wheel actuator study: final report" *ESA CR(P)-2265*
Hein G, Stevenson S & Siro J (1976) "Cost benefit analysis of space technology" *NASA TM-X-3453*
Heironnus-Leuba A et al (1993) "Return from space - ESA's Technology Transfer programme" *ESA Bull* **74**, 46-51
Hemami A (1985) "Control & programming of two armed robots" *Proc Robots 9 Conf* **2**, 16.38-16.58
Hemami A (1986) "Collision free generation of two armed robots" *Proc Robots 10 Conf*, 3.41-3.50
Hemami A (1986) "Kinematics of two armed robots" *IEEEE J Rob & Autom* **2**(4),225-228
Hertzfeld H (1992) "Measuring returns to space research and development" in *Space Economics, Prog in Astron* **144**
Hirzinger G (1987) "Sensory feedback in robotics - state of the art in research and industry" *IFAC 10th Triennial World Cong*, (Mar), 193-206
Hirzinger G (1993) "Multisensory shared autonomy and telesensor programming - key issues in space robotics" *Rob & Auton Syst* **11**, 141-162
Ho J (1977) "Direct path method for flexible multibody spacecraft dynamics" *J Space* **14** (2), 102-110
Hogan J et al (1985) "Impedance control : an approach to manipulation - Part I-III" *ASME J Dyn Syst Meas & Cont* **107** (Mar), 1-24
Hollerbach J & Sahar G (1983) "Wrist partitioned inverse kinmematics accelerations and manipulator dynamics" *Int J Rob Res* **2** (4), 61-76
Hollerbach J (1980) "Recursive Lagrangian formulation of manipulator dynamics & comaparative study of dynamics formulation complexity" *IEEE Trans Syst, Man & Cyber* **10**(11),730-736
Hollerback J & Suh K (1987) "Redundancy resolution of manipulators through torque optimisation" *Int J Rob & Autom* **3** (4), 308-316
Holliday M (1993) "Human or robot? Technical and political considerations" *ISU Lecture Notes*, Huntsville
Hooker W & Margulies G (1965) "Dynamical attitude equations for n-body satellite" *J Astron Sci* **12** (4), 123-128

Hooker W (1970)" Set of r dynamical attitude equations for arbitrary n-body satellite with r rotational degrees of freedom"*AIAA J* **8** (7), 1205-1207
Horak D (1984) "Simplified modelling and computational scheme for manipulator dynamics" *Trans ASME J DSMC* **106,** 350-352
Huddleston M (1991) *Private communication*
Hughes P (1979) "Dynamics of a chain of flexible bodies" *J Astron Sci* **27** (4), 359-380
Iwata T et al (1991) "Dynamic control of freeflying robot for capturing maneouvres" *AIAA 91-2824-CP*
Jain A (1991) "Unified formulation of dynamics of serial link rigid multibody systems" *J Guid & Cont* **14** (3), 531-542
Jerkovsky W (1978) "Structure of multibody dynamics equations" *J Guid & Cont* **1** (3), 173-182
Johnson D & Hill J (1985) "Kalman filter approach to sensor based robot control" *IEEE J Rob & Autom* **1** (3), 159-162
Junkins J & Turner J (1986) "Optimal spacecraft rotational maneouvres" Elsevier Publications, Amsterdam
Kalaycroglu S & Jaifu S (1992) "Ground based control of space station Freedom robots" *Proc IEEE Int Conf Rob & Autom,* 2796-2798
Kamm L (1961) "Magnetorquer - a satellite orientation device" *ARS J* **31**(6), 813-815
Kane T & Levinson D (1980) "Formulation of equations of motion for complex spacecraft" *J Guid & Cont* **6** (2), 99-122
Kane T & Levinson D (1983) "Use of Kane's dynamical equations in robotics" *Int J Rob Res* **2** (3), 3-21
Kaplan M (1976) *Modern Spacecraft Dynamics & Control,* John Wiley & Son
Kawato M et al (1988) "Hierarchical neural network model for voluntary movement with applications to robotics" *IEEE Cont Syst Mag* (Apr), 8-15
Khatib O (1985) "Real time obstacle avoidance for manipulators and mobile robots" *Proc IEEE Int Conf Rob & Autom,* 500-505
Khatib O (1987) "Unified approach for motion and force control of robotic manipulators: operational space formulation" *Trans ASME J Bas Eng* (Mar), 35-45
Kirkpatrick S, Gellatt C & Vecchi M (1983) "Optimisation by simulated annealing" *Sci* **320,** 671-680
Klein C & Huang C (1983) "Review of pseudoinverse control for kinematically redundant manipulators" *IEEE Syst, Man & Cyber* **13** (3), 245-250
Klinkrad H & Jehn R (1992) "Space debris environment of the Earth" *ESA J* **16,** 1-11
Klumpp A (1976) "Singularity free extraction of quaternions from direction cosine matrix" *J Space & Rock* **13** (12), 754-755
Konigstein R et al (1989) "Computed torque control of freeflying cooperating arm robot" *Proc NASA Workshop on Space Telerobotics* **V,** 235-243
Kopf C (1989) "Dynamic two arm hybrid position/force control" *Rob & Auton Syst* **5,** 369-376
Korf R (1982) *Space Robotics* (preprint)
Kosha J & Kanade T (1988) "Experimental evalution of nonlinear feedback and feedforward control schemes for manipulators" *Int J Robot Res* 7(1),18-26
Krishen K (1987) "Advanced communication, tracking, robotic vision technology for space application" *Proc EASCON,* Washington DC, 143-153
Krishen K (1989) "Robotic vision technology and algorithms for space application" *Acta Astron* **19**(10),813-826

Kumar A & Waldron K (1981) "Workspace of a mechanical manipulator" *Trans ASME J Mech Des* **103** (3), 665-672
Latombe J (1984) "Automatic synthesis of robot programs from CAD specifications" *NATO ASI F11 Rob & Artif Intell*, 199-218
Lavery D (1994) "Perspectives on future space robots" *Aero Amer* (May),32-37
Leahy M (1990) "Model based control of industrial manipulators: experimental analysis" *J Robot Syst* 7(5),741-758
Lee B & Lee C (1987) "Collision-free motion planning of two robots" *IEEE Trans Syst, Man & Cyber* **17**(1),21-32
Lee C & Lee B (1984) "Resolved motion adaptive control for mechanical manipulators" *Trans ASME J DSMC* **106** (Jun), 134-142
Lee C & Zeigler M (1984) "Geometric approach in solving kinematics of the PUMA robot " *IEEE Trans Aero & Elect Syst* **20** (6), 695-706
Lee C (1982) "Robot arm kinematics, dynamics & control" *IEEE Comp* **15**(12),62-80
Lee T & Yang D (1983) " On the evaluation of manipulator workspaces" *Trans ASME J Mech Des* **105** (Mar), 70-77
Liegeois A (1977) "Automatic supervisory control of the configuration and behaviour of multibody mechanisms" *IEEE Trans Syst Man & Cyber* **7** (12), 868-871
Lim J & Chyung D (1987) "Resolved position control for two cooperating robot arms" *Robotica* **5,** 9-15
Lin C & Chang P (1983) "Joint trajectories of mechanical manipulators" *IEEE Trans Syst Man & Cyber* **13** (6), 1094-1102
Lin F et al (1983) "Formulation and optimisation of cubic polynomial joint trajectories for industrial robots" *IEEE Trans Autom Cont* **28** (12), 189-197
Lin Z et al (1989) "Online robot trajectory planning for catching a moving object" *Proc IEEE Int Conf Rob & Autom* 1726-1731
Lindberg R, Longman R & Zedd M (1986) "Kinematics and reaction moment compensation for spaceborne elbow manipulator" *AIAA* 86-0250
Logsden J et al (1993) "Partners in space: international cooperation in space - strategies for the new century" *CREST Project Report*
Longman R, Lindberg R & Zedd M (1987) "Satellite-mounted robot manipulators - new kinematics and reaction compensation" *Int J Robot Res* **6**(3),87-103
Longman R (1988) "Kinetics and workspace of robot mounted on satellite that is free to rotate and translate" *AIAA* 88-4097-CP
Lozano-Perez T (1981) "Automatic planning of manipulator transfer movements"*IEEE Trans Syst, Man & Cyber* **11**(10), 681-698
Lozano-Perez T (1983b) "Spatial planning: configuration space approach" *IEEE Com* **32**(2),108-120
Luh J, Walker M & Paul R (1980) "On-line computational scheme for mechanical manipulators" *Trans ASME J Dyn Syst Meas & Cont* **102** (Jun),69-76
Luh J, Walker M & Paul R(1980) "Resolved acceleration control of mechanical manipulators" *IEEE Trans Autom Cont* **25**(3), 236-241
Luh J & Lin C (1981) "Optimum path planning for mechanical manipulators" *Trans ASME J DSMC* **102** (Jun), 142-151
Luh J & Lin C (1984) "Approximate joint trajectories for control of industrial robots along cartesian paths" *IEEE Trans Syst, Man & Cyber* **14** (3), 444-450
Luh J & Zheng Y (1986) "Computation of input generalisation forces for robots with closed kinematic chain mechanisms" *IEEE J Rob & Autom* **1** (2), 95-103

Luh J (1983a) "Anatomy of industrial robots and their controls" *IEEE Trans Autom Cont* **28**(2),133-153
Luh J (1983b) "Conventional controller design for industrial robots - a tutorial" *IEEE Trans Syst, Man & Cyber* **13**(3), 298-316
Lumia R & Wavering A (1989) "Trajectory generation for space telerobots" *Proc NASA Wshop on Space Telerobots II,* 123-131
Lyall F(1992) *Space Law* preprint
MacArthur J (1984) "Space: the finance sector" *Phil Trans R Soc Lon* **A312**, 75-81
MacInnes C (1992) "Optimum orbit selection for two-vehicle rendezvous" *ESA J* **16**, 447-454
Madders K & Thiebaut W (1992) "Two Europes in one space: evolution of relations between ESA and the EC in space affairs" *J Space Law* **20** (2), 117-133
Maimon O & Nof S (1985) "Coordination of robot sharing assembly tasks" *Trans ASME J DSMC* **197**,299-307
Mandell H (1992) "CER for space programs" in *Space Economics* (ed. Greenberg J & Hertzfeld H), Prog in Astron **144**
Marcyk J & Bellazzi A (1989) "Dynamics & control of freflying inspection and maintenance vehicle with manipulators" *Proc 2nd European In-Orbit Operations Technology Symp* (ESA SP-297), 413-427
Mason M (1981) "Compliance and force control for computer-controlled manipulators" *IEEE Trans Syst Man & Cyber* **11**(6), 418-432
Masutani Y, Mujazaki F & Arimoto S (1989) "Sensory feedback control for space manipulators" *Proc IEEE Int Conf Robot & Autom*, 1346-1351
McInnes B & Lin C (1986) "Kinematics and dynamics in robotics: tutorial based upon classical concepts of vectorial mechanics" *IEEE J Rob & Autom* **2** (4), 181-187
Meier W & Graf J (1991) "Two arm robot system based on trajectory optimisation and hybrid control includinfg experimental evaluation" *IEEE Int Conf Rob & Autom*,2618-2623
Merchant M (1985) "Computer integrated manufactiuring as the basis for the factory of the future" *Rob & CIM* **3** (2), 89-99
Mishan E (1971) "Cost benefit analysis" George Allen & Unwin Ltd
Mowforth P & Bratko I (1987) "Artificial intelligence & robotics: flexibility & integration" *Robotica* **5**, 2618-2623
Moya M & Seraji H (1987) "Robot control systems: survey" *Rob & Auton Syst***3**, 329-351
Murphy S et al (1991) "Simulation of cooperating robot manipulators on a mobile platform" *IEEE Trans Rob & Autom* 7 (4), 468-477
Nagashima F & Nakaruma Y (1992) "Efficient computation scheme for the kinematics and inverse dynamics of a satellite-based manipulator" *Proc IEEE Int Conf Robot & Autom,* 905-912
Nakaruma Y & Mukherjee R (1989) "Nonholonomic path planning of space robots via bidirectional approach" *IEEE Trans Robot & Autom* 7 (4), 500-514
NASA Telerobotics Unit (1988) "Telerobotics: problems and research needs" *IEEE Trans Aero & Elect Syst* **24** (5), 542-551
Nenchev D et al (1992) "Analysis of a redundant freeflying spacecraft.manipulator system" *IEEE Trans Rob & Autom* **8** (1),1-6
Nevins J & Whitney D (1980) "Assembly research" *Automatica* **16** (6), 595-613
Nevins J (1986) "Information control aspects of sensor systems for intelligent robotics" *IFAC Robot Control,* Syroco,11-16

Nevins J et al (1987) "Integrated approach to spacecraft design for robotic servicing" *AIAA 87-1672*
Nitzan D (1985) "Development of intelligent robots: achievements and issues" *IEEE J Rob & Autom* **1**(1),3-13
Norci A & Stanley J (1989) "Adaptive human-computer inteface: literature survey and perspective" *IEEE Syst Man & Cyber* **19** (2), 399-408
Orin D & Oh S (1981) "Control of force distribution in robotic mechanisms containing closed kinematic chains" *Trans ASME J DSMC* **102**, 134-141
Orin D & Schrader W (1984) "Efficient computation of Jacobian for robotic manipulators" *Int J Robot Res* **3**(4), 66-75
Orin D et al (1979) "Kinematics and kinetics analysis of open chain linkages utilising Newton-Euler methods" *Mathem Biosci* **43**,107-130
Pan D & Sharp R (1991) "Fast motion control robot manipulators with inclusion of actuator dynamics" *Proc IMechE* **204C**(5),341-348
Papadopoulos E & Dubowsky S (1989) "On dynamic singularities in the control of free-floating manipulators" *Trans ASME J Dyn Syst & Cont* **15**,45-52 (Winter Annual Meeting)
Papadopoulos E & Dubowsky S (1990) "On the nature of control algorithms for space manipulators" *Proc IEEE Int Conf Rob & Autom*,1102-1108
Papadopoulos E & Dubowsky S (1991) "On the nature of control algorithms for freefloating manipulators" *IEEE Trans Robot & Autom* 7(6),750-758
Papadopoulos E & Dubowsky S (1991) "Coordinated manipulator /spacecraft control for space robotic systems" *Proc IEEE Int Conf Rob & Autom*, 1696-1701
Paul R, Shimano B & Meyer G (1981a) "Kinematic control equations for simple manipulators" *IEEE Trans Syst Man & Cyber* **11**(6),449-455
Paul R, Shimano B & Mayer C (1981b) "Differential kinematic control equations for simple manipulators" *IEEE Trans Syst, Man & Cyber* **11**(6), 456-460
Paul R (1979) "Manipulator cartesian path control" *IEEE Trans Syst, Man & Cyber* **9**(11),702-711
Paul R (1981) "Robot manipulators: mathematics, programming and control" MIT Press, Cambridge, Mass, USA
Paul R (1987) "Problems and research issues associated with hybrid control of force and displacement" *Proc IEEE Int Conf Robot & Autom*, 1966-1971
Peattie I (1992) "Black Arrow launch vehicle development programme" *J Brit Interplan Soc* **45**, 155-164
Pin F et al (1992) "On the design and development of a human-robot synergistic system" *Rob & Auton Syst* **10**, 161-184
Pittelkau M (1988)"Adaptive load-sharing force control for two manipulators" *Proc IEEE Int Conf Rob & Autom*,498-503
Prest A & Turvey R (1965) "Cost-benefit analysis: a survey" *Econ J* **75** (Dec), 683-735
Pringle P (1966) "On the stability of a body with connected moving parts" *AIAA J* **4**(8), 1394-1404
Pryor A (1992) private communication
PSC (Parlisamentary Space Committee) (1992)"UK space report" No 2
Raibert M & Craig J (1981) "Hybrid position/force control of manipulators" *Trans ASME J Energy Res Technol* **102** (Jun),126-133
Robertson W et al (1988) "Cost effectiveness of on-orbit servicing for large constellations" *AIAA 88-3519*

Robinson H (1992) "Genesis of Black Arrow" *J Brit Interplan Soc* **45**, 149-154
Rockoff L & Anderson D (1990) "Freeflyers for Space Station EVA operations" *Space Station Advanced Technologies, NASA SP-830,* 59-64
Rodriguez G (1989) "Kalman filtering, smoothing and recursive robot arm forward and inverse dynamics" *IEEE J Rob & Autom* **3** (6), 624-639
Roth B (1985) "Overview of advanced robotics: manipulation" *Int Conf Advanced Robotics,* 569-580
Rouse W & Cody (1987) "On the design of man-machine systems: principles, practices and prospects" *Proc IFAC 10th Tiriennial World Cong,* Munich, 281-288
Russel P & Price K (1990) "Servicing communications satellites in geostationary orbit" *AIAA* 90-0830-CP
Sabroff A (1968) "Advanced stabilisation and attitude control techniques" *J Space & Rock* **5**(12),1377-1392
Salisbury J & Craig J (1982) "Articulated hands: force control & kinematic issues" *Int J Robot Res* **1**(1), 4-17
Salisbury J (1980) "Active stiffness control of a manipulator in cartesian coordinates" *Proc IEEE Conf Dec & Cont,* 95-100
Salisbury J (1988) "Issues in human/computer control of dextrous remote hands" *IEEE Trans Aero & Elect Syst* **24** (5), 591-596
Sallaberger C (1992) "Profitability analysis" *ISU preprint*
Sanderson A, Peshkin M & Homem-De-Mollo L (1988) "Task planning for robotic manipulation in space applications" *IEEE Trans Aero & Elect Syst* **24**(5), 619-628
Sata T (1984) "View of the highly automated factory of the future" *Rob & CIM* **1**(2), 153-159
Sato T & Hirai S (1987) "Language aided robotic teleoperation system (LARTS) for advanced teleoperation" *IEEE J Rob & Autom* **3** (5), 476-481
Sato Y et al (1993) "Resolving attitude disturbance while teleoperating a space manipulator" *Proc IEEE Int Conf Rob & Autom,* 516-523
Schenker P (1988) "NASA R&D for space telerobotics" *IEEE Trans Aero & Elect Syst* **24** (5), 523-534
Schroer B (1988) "Telerobotic issues in space applications" *Rob & Auton Syst***4,** 233-244
Schwarz J & Sharir M (1988) "Survey of motion planning and related geometrical algorithms" *Artif Intell* **37,** 157-169
Sepehri M ((1987) "Resupply models for space logistics and influence on design" *AIAA 87-0657*
Seraji H (1987a) "Adaptive force and position control of manipulators" *J Rob Syst* **4**(4), 551-578
Seraji H (1987b) "Design of force/position controllers for manipulators" *AIAA 87-2267*
Shashkin T (1985) "Unmanned platform as an initial capability in space" *Proc Space Tech Conf,* Anaheim, 4.35-4.42
Shimano B & Roth B (1975) "On force sensing information and its use in controlling manipulators" *Proc 8th Int Symp Ind Robotics,* 119-126
Siedman L (1992) "Towards a policy for space robotics" *AIAA 92-1718*
Silver W (1982) "On equivalence of Lagrangian and Newton-Euler dynamics for manipulators" *Int J Robot Res* **1**(2),60-69
Simmons R et al (1990) "Six dimensional trajectory solver for autonomous proximity operations" *AIAA 90-3459-CP*

Soloway D & Alberts T(1989) "Comparison of joint space versus task force level distribution optimisation for multi-arm manipulator systems" *Proc NASA Wshop on Space telerobotics IV,* 413-443
Spofford J & Akin D (1988) "Redundancy control of freeflying telerobots" *AIAA 88-4094-CP*
Spur G (1988) "Advanced manufacturing systems" *Rob & CIM* **4**(1/2), 7-12
Stark L et al (1987) "Telerobotics: display, control and communications problems" *IEEE J Rob & Autom* **3** (1), 67-75
Sterner E (1994) "Dual use technology for near term lunar exploration: Clementine program" *J Brit Interplan Soc* **47**, 521-526
Stone B (1989) "Economic benefits of commercial space activities" *Acta Astron* **19** (9), 743-747
Stone R (1992) "VR & telepresence" *Robotica* **10**, 461-467
Suh N (1984) "Factory of the future" *Rob & CIM* **1**(1), 39-49
Syromiatnikov V (1992) "Manipulator system for module redocking on Mir orbital complex" *Proc IEEE Int Conf Rob & Autom,* 913-918
Tao J, Luh H & Zheng Y (1987) "Compliant coordination control of two moving industrial robots" *Proc 26th Conf Dec & Cont,*186-191
Tarn T, Bejczy A & Yun X (1988) "New nonlinear control algorithms for mulrtiple robot arms" *IEEE Trans Aero & Elect Syst* **24** (5), 571-582
Tarn T, Bejczy A & Yun X (1987) "Design of dynamic control of two cooperating robot arms:closed chain configuration" *Proc IEEE Int Conf Rob & Autom,* 7-13
Taylor R (1979) "Planning and execution of straight line manipulator trajectories" *IBM J Res & Dev* **23**(4),253-264
Trivedi M et al (1990) "Developing robotic systems with multiple sensors" *IEEE Trans Syst, Man & Cyber* **20**(6),1285-1301
Tsin Y & Sani A (1983) "Algorithms for workspace of a general n-R robot" *Trans ASME J Mech Des* **105** (Mar), 52-57
Uchiyama M & Dauchez P (1988) "Symmetric hybrid position/force control scheme for coordination of two robots" *Proc IEEE Int Conf Robot & Autom,* 351-356
Uchiyama M et al (1987) "Hybrid position/force control for coordination of two arm robots" *Proc IEEE Conf Rob & Autom,*1242-1247
Umetani Y & Yoshida K (1989) "Resolved motion rate control of space manipulators using a generalised Jacobian matrix" *IEEE Trans Robot & Autom* **5**(3),303-314
Vafa Z & Dubowsky S (1987) "On dynamics of manipulators in space using the virtual manipulator approach" *Proc IEEE Int Conf Rob & Autom,*579-585
Vafa Z & Dubowsky S (1990) "Kinematics and dynamics of space manipulators: the virtual manipulator approach" *Int J Robot Res* **9**(4), 3-21
Vafa Z (1990) "Space manipulator motions with no satellite attitude disturbances" *Proc IEEE Int Conf Rob & Autom,*1770-1775
van Bogart E (1986) "Aspects of space law" Kluwer Pub
Varsi G (1990) "Telerobotics for the efficient utilisation of space" *J Brit Interplan Soc* **43**, 273-280
Varsi G (1991) "Advances in space robotics" *Acta Astronaut.* **25**(4), 199-207
Vijaytamar R & Arbib M (1987) "Problem decomposition for assembly planning" *Proc IEEE Int Conf Rob & Autom,* 1361-1366
Walker M & Orin D (1982) "Efficient dynamic computer simulation of robotic mechanisms" *Trans ASME J DSMC* **104** (Sept), 205-211

Walker M & Wee L (1991) "Adaptive control of space based robot manipulator" *IEEE Trans Rob & Autom* 7(6), 828-835
Walker M & Wee L (1991) "Adaptive control strategy for space based robot manipulators" *Proc IEEE Int Conf Rob & Autom,* 1673-1680
Wang K & Lien T (1988) "Structure, design & kinematics of robot manipulators" *Robotica* **6**,299-309
Wang P (1987) "Control strategy for a dual arm maneouvrable space robot" *Proc NASA Wshop Space Telerobotics* , 256-266
Weisbin C & Montemerlo M (1992) "NASA's telerobotic research programme" *Proc IEEE Int Conf Rob & Autom*, 2653-2663
Weisel W (1989) *Spaceflight Dynamics,* MacGraw-Hill
Wen J & Murphy S (1991) "Stability analysis of position and force control for robot arms" *IEEE Trans Autom Cont* **36**(3),365-371
Wertz J & Larson W (1991) "Space mission analysis and design" Kluwer Academic Publ, London
Wertz J (1978) "Spacecraft attitude determination and control" *Reidel Pub,* Holland
Wertz J et al (1988) "Reducing the cost and risk of orbit transfer" *J Space* **25** (1), 75-80
West H & Asade H (1985) "Method for the design of hybrid/position force controllers for manipulators constrained by contact with the environment" *Proc IEEE Int Conf Rob & Autom,* 251-259
Whitney D (1969) "Resolved motion rate control of manipulators and human prostheses" *IEEE Trans Man-Mach Syst* **10**(2), 47-53
Whitney D (1972) "Mathematics of coordinated control of prosthetic arms and manipulators" *Trans ASME J Dyn Syst Meas & Cont* **122**(Dec), 303-309
Whitney D (1977) "Force feedback control of manipulators fine motions" *ASME Trans J Dyn Syst Meas & Cont* (June), 91-97
Whitney D (1987) "Historical perspective and state of the art in robot force control" *Int J Rob Res* **6** (1), 3-14
Williamson R (1992) *private communication (ECSL Workshop, INMARSAT, London)*
Winchell D (1987) "Selecting affordable levels of support from spare unit suppliers for HST orbit maintenance" *AIAA 87-0696*
Wojtalik (1987) "HST systems engineering" *IFAC 10th Triennial World Cong,* Munich, 63-68
Wu C & Paul R (1982) "Resolved motion force controlfor robot manipulators" *IEEE Trans Syst Man & Cyber***12**(3), 266-275
Xu Y (1993) "Measure of dynamic coupling of space robot system" *Proc IEEE Int Conf Rob & Autom, 615-620*
Xu Y et al (1992) "Control system of self mobile space robot manipulator" *Proc IEEE Int Conf Rob & Autom,*866-871
Yang D & Lee T (1983) "On the workspace of mechanical manipulators" *ASME J Mech Des* **105** (Mar), 62-69
Yoerger D et al (1990) "Influence of thruster dynamics on underwater vehicle behaviour" *IEEE Trans Oceanic Eng* **15**(3), 167-177
Yoshida K et al (1991) "Dual arm coordination of space freeflying robot" *Proc IEEE Int Conf Rob & Autom,* 2516-2521
Yoshida K et al (1992) "Modelling of collision dynamics for space free floating links with extended generalisation inertia tensor" *Proc IEEE Conf Rob & Autom*, 899-904

Yuh S (1990) "Modelling and control of underwater robotic vehicles " *IEEE Trans Syst Man & Cyber* **20**(6), 1475-1483
Zheng Y & Luh J (1986) "Joint torques for the control of two coordinated moving robots" *Proc IEE Int Conf Rob & Autom,* 1375-1380
Zheng Y & Luh J (1988) "Optimal load distribution for two industrial robots handling a single object" *Proc IEEE Int Conf Rob & Autom,* 344-349
Zheng Y & Paul R (1985) "Hybrid control of robot manipulators" *Proc IEEE Int Conf Rob & Autom,* 602-606
Zheng Y (1987) "Kinematics and dynamics of two industrial robots in assembly" *Proc IEEE Int Conf Rob & Autom,* 1360-1365